December 1994

Research Report UMCE 94-22

EFFECT OF TRUCK LOADING ON BRIDGES

Report submitted to
the Michigan Department of Transportation

Andrzej S. Nowak, Jeffrey A. Laman and Hani Nassif

Department of Civil and Environmental Engineering
University of Michigan
Ann Arbor, Michigan 48109-2125

RC-1433 A
EFFECT OF TRUCK LOADING ON BRIDGES

DISCLAIMER

The contents of this report reflect the views of the authors, who are responsible for the facts and the accuracy of the information presented herein. This document is disseminated under the sponsorship of the Michigan Department of Transportation and Great Lakes Center for Truck Transportation Research at the University of Michigan Transportation Research Institute, in the interest of information exchange. The Michigan Department of Transportation assumes no liability for the contents or use thereof.

Table of Contents

EXECUTIVE SUMMARY

The objective of this project is to develop a procedure for evaluation of live load spectra on Michigan bridges. Truck weights, including axle loads and spacing, are measured to determine the statistical parameters of the actual live load. Stress is measured in various components of girder bridges to determine component-specific load spectra. The deteriorating capacity of corroded steel bridges is evaluated as a function of the rate of corrosion. Evaluation procedure is developed for steel girder bridges with regard to fatigue.

The study involves experimental and analytical efforts. A live load model is developed on the basis of weigh-in-motion (WIM) measurements, truck counts, truck surveys, and statistical analysis. Evaluation procedure for corroded steel bridges is developed using sensitivity functions relating the load carrying capacity, corrosion patterns and material loss. Fatigue analysis focuses on the measurement and predictions of component live load spectra.

Field testing equipment included three data acquisition systems, portable computers, strain gages, accelerometers, a van, power generator and other items. The majority of equipment was purchased exclusively for this project. Other equipment tried and considered for use in this study included electronic theodolite, fleximeter, and the Culway System. The Culway System was developed in Australia and is based on instrumentation of concrete culverts.

A large data base of truck axle weights collected at stationary weigh stations has been provided by the Michigan Department of Transportation (MDOT). It includes results of an extensive truck weight survey carried out using truck weighing stations located on I-75 and I-94 in Michigan. The data consists of over 600,000 trucks, mostly from I-75. For each truck, the measured parameters include axle loads and axle spacing. The survey data appears biased due to truck driver's motivation to avoid the weigh scales.

Michigan State Police files were reviewed to survey the trucks which violated the weight limit regulations. The citation file covers one year and it includes over 2000 vehicles. Most of the trucks were fined for minor weight violations. The heaviest vehicles were 11 axle trucks, weighing over 200 kips. The heaviest axle loads were about 40 kips.

Very little reliable trucks weigh data is currently available to bridge researchers and designers. Past studies performed in other states did not provide reliable results due to errors in the data collection. Therefore, in this project, the major source of the actual truck loads is WIM measurements. The loads were measured on 7 bridges. WIM equipment was calibrated using trucks provided by MDOT, University of Michigan Transportation Research Institute (UMTRI) and other vehicles. The WIM data provide unbiased results because the drivers are not aware of the measurements and therefore they do not make any effort of to avoid the scales. The heaviest truck recorded in the WIM survey was about 230 kips, and the heaviest axle load was about 50 kips.

Comparisons of the truck weigh station data, citation files and WIM measurements show that the unbiased truck weights (from WIM) are 30-50% larger than the extreme values obtained at Weigh Stations. Citation data agrees well with the heaviest vehicles recorded by WIM equipment. Measurements were taken on I-94 in the vicinity of the Truck Weigh Station. When the Station was closed for repairs, the weight of heaviest trucks increased by 30-40%.

For this report, bridge load spectra are considered in terms of moments and shears. Moments and shears for various span lengths have been calculated for each truck in the data base. The results are plotted on normal probability paper. This scale allows for a better statistical analysis of the load.

Truck counts were carried out to verify ADTT and to establish the statistical parameters for multiple presence. The study was

performed on I-94 and US-23. Results of the counts indicate that right lane carries 80-90% of the truck traffic, and 65-70% of trucks are 5-axle trucks. Multiple presence was considered in-lane and side-by-side. Approximately 1-2% of trucks are followed in-lane by another truck with the headway distance less than 50 ft. and 5-10% of trucks travel side-by-side with another truck.

The measurements provided data for the analysis and verification of the theoretical model of the dynamic load on bridges. The results indicate that dynamic load (measured with the static load), decreases with increasing truck weight. Dynamic load was also considered as a function of vehicle speed and length.

Corrosion is an urgent problem, particularly in the State of Michigan. The forms of corrosion and its effect on structural behavior are discussed. In addition, a corrosion evaluation procedure is formulated and included in this report. A relationship between the loss of material (plate thickness) and load carrying capacity is established in the form of sensitivity functions. The study indicates those web stiffeners at the support are important in extending the remaining life regarding corrosion.

Fatigue cracks are another common form of deterioration. Structural behavior depends on load frequency and magnitude. Therefore, component fatigue load spectra are determined using the results of WIM measurements, truck survey data and trucks counts. The results indicate that live load effect is strongly site-specific and component-specific.

In summary, the major findings of this study is information about the actual truck weights and axle weights. The gross vehicle weight (GVW) values and average daily truck traffic (ADTT) vary from site to site. It was observed that the heaviest trucks tend to avoid the Truck Weigh Stations. Further results are presented in a Report summarizing the measurements of selected bridges in the Detroit

Area. The other Report was submitted to the Michigan DOT in November 1994.

The contents of this report reflect the views of the authors, who are responsible for the facts and the accuracy of the information presented herein. This document is disseminated under the sponsorship of the Michigan Department of Transportation and Great Lakes Center for Truck Transportation Research at the University of Michigan Transportation Research Institute, in the interest of information exchange. The Michigan Department of Transportation assumes no liability for the contents or use thereof.

Note:
Intentionally left blank

ACKNOWLEDGEMENTS

The presented study was sponsored by the Michigan Department of Transportation and Great Lakes Center for Truck Transportation Research (GLCTTR) at the University of Michigan Transportation Research Institute which is gratefully acknowledged. In particular, the authors thank the technical staff of the Michigan DOT, Leo DeFrain, Roger Till, Glen Bukoski, Charles Arnold, David Juntunen, Richard Gould and Sudakhar Kulkarni for their useful comments, discussions and support, and Thomas Gillespie, of the University of Michigan Transportation Research Institute (UMTRI) for his support.

The project team received help from other researchers, current and former students and staff of the University of Michigan. In particular, thanks are due to Professor Richard Woods, Dr. Andrej Sokolik, Sang Jin Kim, Vijay Saraf, Tadeusz Alberski, Kayleen Seaver and Chan Hee Park. They were involved in field instrumentation and measurements. Thanks are due to TestConsult (CEBTP) staff, Allen Davis and Bernie Hertlein, for the demonstration of their testing equipment (Electronic Theodolite and Fleximeter) on one of the bridges considered in this project. Robert Heywood of Queensland Technical University and James Brown of Australian Road Research Board demonstrated Culway, the weigh-in-motion system developed in Australia.

Thanks are due to the Michigan State Police for their cooperation. Traffic control was provided by the Michigan DOT, Washtenaw County, Wayne County and Monroe County.

The realization of the research program would not be possible without in kind support of the Michigan DOT and the University of Michigan. Measurements were taken using a weigh-in-motion system provided by the Michigan DOT purchased from Bridge Weighing Systems, Inc. Data acquisition equipment for the study was also purchased from the SoMat Corporation using University of Michigan

funds. For dynamic measurements a system was purchased by the University of Michigan with a special discount offered by Krenz Electronics which is gratefully acknowledged. MDOT also provided trucks for calibration of the equipment. The University of Michigan provided support for other needed equipment, including a van, power generator and technician support.

Special thanks are also due to Dr. Andrej F. Sokolik who served as a technical editor of this Report.

1. INTRODUCTION

Evaluation of bridges is an increasingly important topic in the effort to deal with the deteriorating infrastructure. There is a need for accurate and inexpensive methods to determine the actual loads, strength of the bridge, and its remaining life. Knowledge of the past and current load spectra, together with predicted future loads, is essential in the fatigue analysis. Comparison of load spectra in different locations can serve as a basis for identification of the fatigue critical components.

In the United States, about 40 percent of bridges are considered as deficient. Half of these structures are functionally obsolete (mostly inadequate clearance), and the other half do not have a sufficient strength. The major factors that have contributed to the present situation are: the age, inadequate maintenance, increasing load spectra (traffic volume and truck weights) and environmental contamination. The deficient bridges are posted, repaired or replaced. The disposition of bridges involves clear economical and safety implications. To avoid high costs of replacement or repair, the evaluation must accurately reveal the present load carrying capacity of the structure and predict loads and any further changes in the capacity (deterioration) in the applicable time span.

Observations indicate that truck loads vary from site to site. Some bridges carry heavy truck traffic (volume and magnitude) others carry lighter traffic. Furthermore, live loads are also component-specific. This means that live load effects are different for different girders in the same bridge. The objective of this study is to determine the effect of truck loads on the Michigan bridges. Therefore, the major effort is directed on the development of an efficient truck measurement technique. An approach is also developed for evaluation of the actual strength and prediction of the remaining life for existing bridges. The major directions of research are:

- determination of site-specific truck loads in Michigan,
- determination of component-specific load spectra for bridges in Michigan,
- evaluation of corroded steel girder bridges,
- evaluation of steel girder bridges with regard to fatigue.

The need for reliable truck weight data has been recognized by many State DOTs. For many years, the truck weight measurements were collected by stationary weigh scales located on major highways. However, the resulting data base seems to be biased because very heavy vehicles avoid the scales by special detours. Therefore, the Federal Highway Administration sponsored an extensive weigh-in-motion (WIM) measurement program to develop an unbiased truck weigh data base. Measurements were taken in various locations in the United States for long periods of time. Processing of the data was the objective of a special NCHRP Project 12-28(11) "Development of Site-Specific Live Load Models for Bridges". However, it turned out that the measurements were done incorrectly and most of the available results include large errors (40-50%).

Another study was carried out by researchers at the University of Colorado in 1989-90. WIM measurements were sponsored by the FHWA. They instrumented about 30 bridges in various regions of the United States. The results are not available in the FHWA standard format and therefore are difficult to compare. Therefore, in the recent calibration of the new LRFD (load and resistance factor design) code for AASHTO, NCHRP Project 12-33, the live load model is based on the Ontario truck survey. These developments pointed to an urgent need for unbiased truck data for various regions of the United States. This project provides a data base for truck loads in Michigan.

The State of Michigan allows considerably higher truck loads compared to most of the other states (over 154 kips vs. 80 kips, as shown in Fig. 1-1). In spite of that, many trucks carry loads in excess of the legal limits. This may cause an accelerated deterioration due to

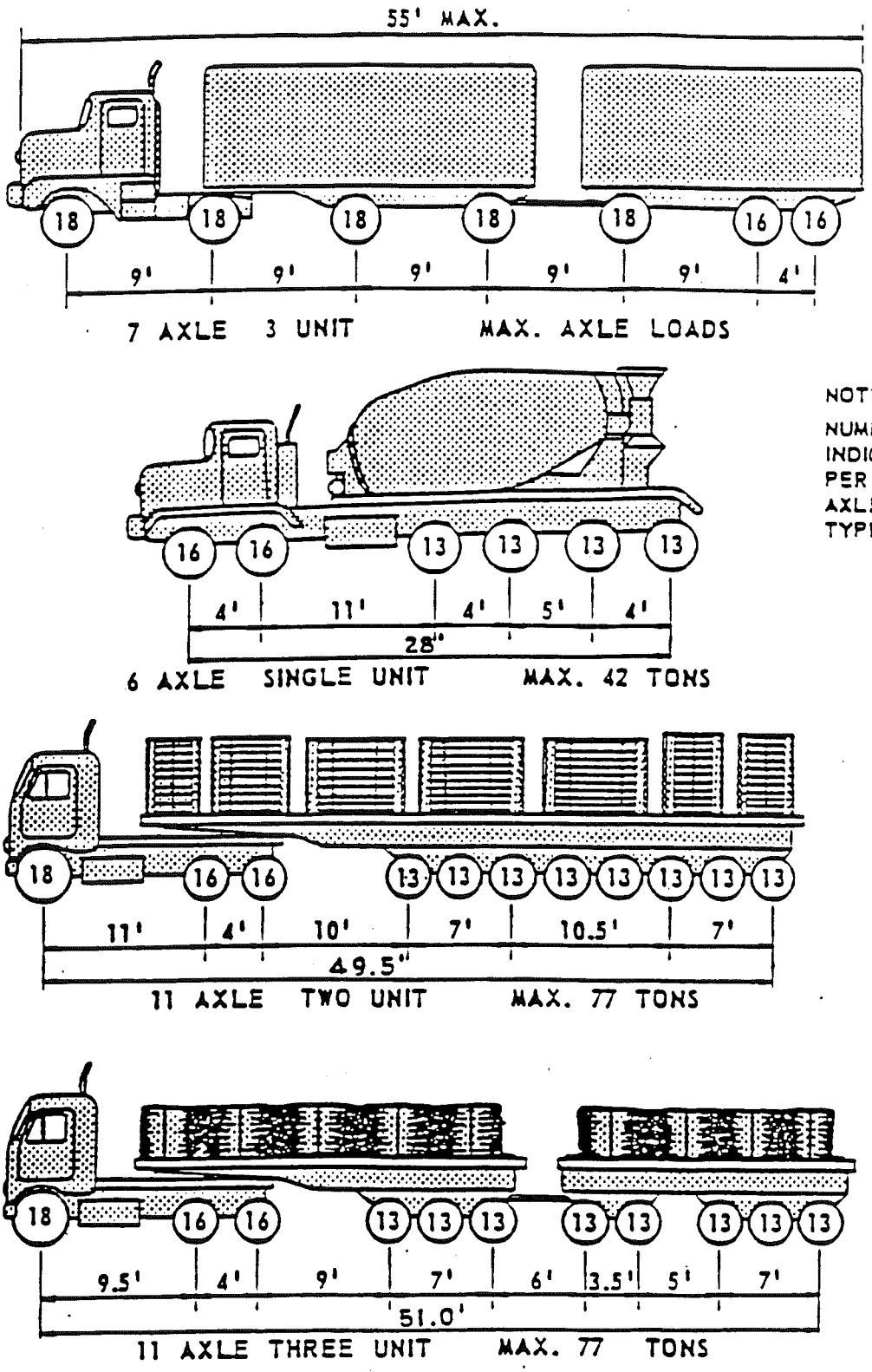

NOTE :
NUMBER IN CIRCLE INDICATES 1000 LBS PER AXLE .
AXLE SPACING IS FOR TYPICAL VEHICLES .

Fig. 1-1. Michigan Maximum Legal Loads.

fatigue. Rational evaluation criteria require a good estimate of the loads. The information concerning actual load are very important for a prediction of the remaining life and for calculation of the load carrying capacity of existing bridges. The information can further be used for the rating of bridges, prediction of the future live loads, and the development of fatigue load models. Therefore, there is a need to know the actual loads and their effect on bridges. Some observations indicate that load spectra vary from component to component. This is important in evaluation of the fatigue damage and prediction of remaining life.

In this study, the load spectra are determined on the basis of three sources:

(a) Truck counts;
(b) Truck weigh station data;
(c) Citation files;
(d) Weigh-in-motion measurements of trucks and component-specific live load stress spectra.

Truck count was carried out as a part of this project. The objective is to determine the number of trucks crossing the bridge in each direction, type of truck (number of axles) and multiple presence (more than one truck on the bridge simultaneously). Multiple presence is considered in lane and side-by-side.

Truck weigh stations are located on the major highways in Michigan. In this study, the data was provided by the Michigan DOT, from two locations. It has been observed that the truck traffic is biased, with overloaded trucks avoiding the scales by using alternative routes.

State Police citation files provide a data source on overloaded vehicles. The files covering one year were processed to determine

the distribution functions of truck weight, axle loads and load effects, such as moments and shears.

The actual truck loads are verified using weigh-in-motion measurements. A special instrumentation is used, invisible for the truck drivers. Therefore, the results can be considered as unbiased. For the measured trucks, the effect of load on the bridge is calculated in terms of stresses, moments and shears. The statistical distribution of the load effects provides a basis for the evaluation of fatigue load spectra and prediction of the extreme loads.

The statistical distribution functions can be presented in a form of a traditional histogram (frequency or cumulative). However, this approach does not allow for an efficient analysis of the extreme values (upper or lower tails) of the considered distribution. Therefore, the results are presented on the so called normal probability paper. The construction and use of the normal probability paper is presented in Appendix A.

About 10,500 or 65 percent of Michigan bridges are made of steel. Therefore, corrosion is an important consideration. In this study, the effect of corrosion is evaluated by considering various degrees of material loss (due to various rates of corrosion). Sensitivity functions are developed relating load carrying capacity with various corrosion dependent parameters (flange thickness, web thickness). The analysis indicates that web stiffeners, in particular bearing stiffeners, considerably increase the structural life.

Fatigue performance depends on strength and load spectra. An important objective of this project is to determine the actual site-specific and component-specific loads. The measurements are carried out for longer periods of time (three weeks). The resulting cumulative distribution functions are used in the fatigue analysis, based on Miner's Rule. The equivalent stresses are calculated and compared with the critical values established by material tests.

This study is divided into tasks involving analytical and experimental parts. The relevant information available in the literature is also included.

Task 1. Literature Survey

The literature was surveyed to determine the available data pertinent to the effect of truck loads on highway bridges. The covered areas include bridge loads (live load and dynamic load), weigh-in-motion studies (equipment, techniques, results, data processing), truck surveys (techniques, results, data processing), other load monitoring techniques, corrosion of steel girder bridges (types, rates, typical forms, effect on strength, prediction of remaining life), and fatigue in steel girder bridges (load spectra, fatigue-prone details, prediction of remaining life). The results of the literature survey are included in various Chapters of this report.

Task 2. Truck Count

A visual truck count was carried out on US-23 and I-94 to verify the average daily truck traffic (ADTT) and establish the statistical parameters for multiple presence (more than one truck on the bridge). Numerical simulations indicate that for two lane bridges, two side-by-side truck produce the maximum effect. The truck count also provided additional data for the statistical analysis of live load model, performed in conjunction with the development of the new LRFD code for AASHTO.

Task 3. Processing Truck Survey Data from Michigan DOT

Truck weights and configurations were obtained from MDOT. The data covers 13 month measurements (1988-89) collected by Truck Weighing Stations on I-75 and about a month on I-94. A total of over 600,000 trucks are included. The size of the data base caused special numerical problems which had to be resolved prior to data

processing. The trucks were run through influence lines to calculate the maximum moments and shears for various spans. The results are presented in a form of cumulative distribution functions.

Task 4. Processing of Citation Data

The Michigan State Police files covering one year were processed. The files include trucks which violated the State legal load limits. The statistical distribution functions were developed for gross vehicle weight (GVW) and axle loads.

Task 5. Equipment for Bridge Weigh-in-Motion

The bridge test program has been carried out using equipment available at the University of Michigan such as the Structural Engineering Laboratory, Radiation Laboratory, and computer facilities. Equipment utilized exclusively for this study includes three data acquisition systems:

(a) data acquisition system developed by the Bridge Weighing Systems, Inc. The system includes 8 channel unit for measurement of truck axle loads, speed, and other critical information).

(b) data acquisition system developed by Krenz Electronics. The system includes unit with 8 channels for dynamic load measurements (strains and/or accelerations).

(c) data acquisition system developed by SoMat Corporation. This is a very compact unit, including 8 channels, for long term strain data collection.

Additional pieces of equipment include a commercial panel van equipped for bridge testing, portable 120 volt generator, and two portable computers for data acquisition and down loading of data.

Task 6. Weigh-in-Motion Measurements

Weigh-in-Motion measurement is the major task of the project and considerable effort was concentrated on field work and data collection. Tests were conducted on seven bridges. These sites are listed below:

1. 23/HR - US-23 over the Huron River in Ann Arbor, Michigan.
   Michigan State Bridge ID: R01-81074

2. 23/SR - US-23 over the Saline River in Milan, Michigan.
   Michigan State Bridge ID: B05-58033

3. 94/JR -I-94 over Jackson Road in Ann Arbor, Michigan.
   Michigan State Bridge ID: S01-81062

4. 94/PR - I-94 over Pierce Road in Grass Lake, Michigan.
   Michigan State Bridge ID: S03-81104

5. 14/NY - M14/US-23 over the New York City Railroad in Ann Arbor, Michigan.
   Michigan State Bridge ID: R01-81103

6. WY/94 - Wyoming Road over I-94 in Detroit, Michigan.
   Michigan State Bridge ID: S36-82022

7. 75/BC - I-75 Northbound over Bay Creek Road in Luna Pier, Michigan.
   Michigan State Bridge ID: S14-58151

The truck weigh-in-motion (WIM) was performed on the first six bridges. The strain data (rainflow strain histories) was collected at six sites: 1 through 5 and 7. The WIM equipment was calibrated using trucks provided by Michigan DOT and the University of Michigan

Transportation Research Institute (UMTRI). Verification of the WIM data was also done by comparing to trucks leaving an operated weigh station along I-94.

Task 7. Processing of WIM Data

The data collected by WIM equipment was processed using the computer facilities at the University of Michigan. Programs were developed to manipulate the large quantities of truck data. The histograms of truck weight (gross vehicle weight, GVW) and axle load are shown on the normal probability paper. The measured trucks were run through influence lines to calculate the maximum moments and shears for various spans. The maximum observed values considerably exceed the design values (about three times HS-20 values). The data obtained from the WIM study is compared with the truck survey data (Truck Weighing Stations). The WIM data can be considered to be unbiased (vehicle operators are unaware of the test and are not motivated to avoid WIM measurement sites).

Task 8. Development of Fatigue Live Load Models

This task involved the development of the actual site-specific and component-specific live load from the strain measurements. The measurements were taken for extended periods of time, up to three weeks in unattended mode. The stress spectra were determined for the girders and diaphragms. Equivalent stress is calculated and compared to the critical values.

Task 9. Development of Dynamic Load Model for Bridges

The measurements performed using accelerometers and Krenz Electronics system provide a data for verification of the analytical model of dynamic load. The design dynamic load is specified as a function of span length and it is about 0.2-0.3 of static live load. Numerical simulations performed at the University of Michigan

indicated that dynamic load does not exceed 0.2 for a single truck and 0.1 for two trucks side-by-side. The analytical work was carried out in conjunction with the development of the new LRFD code for AASHTO. The actual measured dynamic loads confirmed the earlier theoretical findings.

Task 10. Development of Evaluation Procedure for Corroded Bridges

Steel girder bridges (over 60 percent of the total bridge population in Michigan) are considered for evaluation of strength loss due to corrosion. Typical corrosion patterns were observed on bridges in Michigan. Sensitivity functions, relating corrosion rate with the actual load carrying capacity, were developed for moment capacity, shear and bearing. A procedure is formulated for evaluation of corroded steel girder bridges.

Task 11. Development of Evaluation Procedure for Fatigue

The study involves the analysis of fatigue load spectra and fatigue strength. Load spectra are determined on the basis of the WIM measurements, truck survey results, and strain time histories. Load distribution factors are verified in WIM measurements and strain measurements. The load spectra are determined for individual girders and diaphragms at six bridge sites noted above. Fatigue capacity is determined using currently accepted models and structural reliability theory. The effect of variable amplitude load cycles is estimated using the rainflow algorithm and Miner's Rule.

2. TRUCK COUNT

2.1 Results of Observations

A visual truck count of trucks with number of axles in range of two to 11-axles was carried out in February 1991 to determine the number of trucks per each lane. Two locations were considered:

(a) 14/NY M14/US-23 over the New York City Railroad in Ann Arbor, Michigan, for 1 day.
Michigan State Bridge ID: R01-81 103

(b) I-94 On the Highway, about 1 mile east of Zeeb Road (about 3 miles east of Ann Arbor), for 2 days.

Trucks were counted in both directions of traffic. There are two lanes of traffic in each direction. The number of trucks was counted separately for right lane and left lane. Right and left lanes are defined according to the direction of traffic. Multiple presence (more than one truck on bridge) cases were also observed. Three cases were considered, as shown in Fig.2-1,

(a) in-lane; two trucks following each other with headway distance (from rear axle of one truck to front axle of the following truck) less than about 50 ft.

(b) side-by-side in tandem; two trucks in adjacent lanes traveling with front axles on the same line.

(c) side-by-side and behind; two trucks in adjacent lanes but one behind the other with the distance between front axles less than 50 ft.

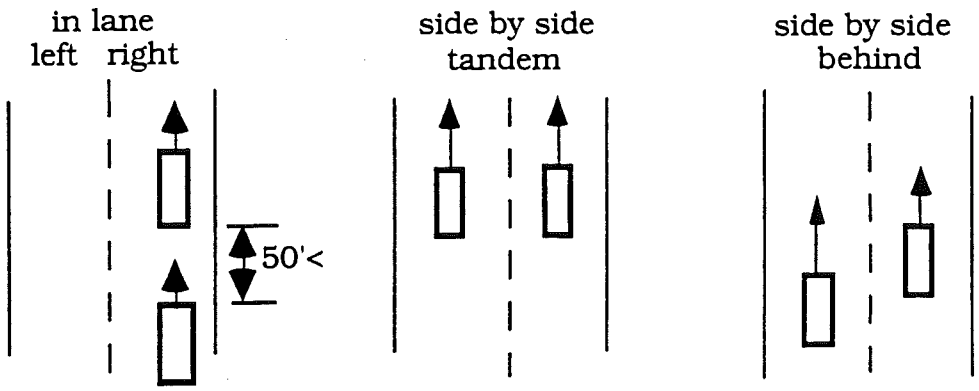

Fig. 2-1 Simultaneous Presence of Two Trucks.

The numbers of trucks are listed for the right lane (in the direction of traffic), left lane, and for simultaneous occurrence in lane, in tandem, and side-by-side with one truck being behind the other. Results of the truck count are shown in Table 2-1 for I-94 and Table 2-2 for 14/NY. In the survey on 14/NY, the number of axles was recorded for each truck. The results are shown in Table 2-3.

Table 2-1 Results of Truck Count on I-94 (West of Zeeb Road).

Hour	Eastbound					Westbound				
			Multiple presence					Multiple presence		
	right lane	left lane	in-lane	side-by-side tandem	side-by-side behind	right lane	left lane	in-lane	side-by-side tandem	side-by-side behind
09-10am	241	33	8	0	14	274	45	6	8	14
10-11am	200	24	4	4	10	236	49	2	16	12
11-12am	170	15	0	4	4	247	42	2	12	16
12-01pm	172	14	0	6	4	255	42	0	12	11
01-02pm	172	15	0	6	4	215	17	0	4	4
02-03pm	153	6	0	2	0	235	41	0	16	4
03-04pm	178	17	0	4	4	220	43	2	8	14
02-05pm	147	15	2	2	4	215	41	2	4	12
05-06pm	149	12	8	0	4	176	29	0	6	6
total	1,582	151	14	28	48	2,073	349	14	86	93

Table 2-2 Results of Truck Count on 14/NY.

Hour	Southbound/Eastbound					Northbound/Westbound				
			Multiple presence					Multiple presence		
	right lane	left lane	in-lane	side-by-side tandem	behind	right lane	left lane	in-lane	side-by-side tandem	behind
05-08am	273	63	0	14	4	222	68	0	8	6
08-09am	141	38	2	4	11	100	54	0	0	0
09-11am	317	57	8	2	15	211	114	0	8	6
11-01pm	302	52	4	2	10	208	119	0	8	10
01-03pm	302	50	2	10	10	227	94	0	10	6
03-05pm	234	65	4	4	14	194	101	0	4	4
05-06pm	116	46	0	4	12	85	51	2	0	2
total	1,685	371	24	40	76	1,247	601	2	38	34

Table 2-3 Observed Number of Axles (14/NY).

Number of Axles	Percentage of Trucks	
	Eastbound	Westbound
2	16.3	11.6
3	5.5	4.9
4	4.8	2.9
5	64.4	70.5
6	3.7	3.6
7	1.6	1.3
8	0.6	0.9
9	1.0	0.4
10	0.3	0.4
11	1.8	3.5

2.2 Multiple Presence

Structural analysis indicates that a simultaneous presence of two trucks on the bridge is critical. The percentage of in-lane and side-by-side cases (see Fig. 2-1) has been calculated and the results are shown in Table 2-4.

Table 2-4 Percentage of Multiple Truck Occurrence.

Highway	Direction	in-lane	side-by-side		
			tandem	behind	total
I-94	Eastbound	1.8	1.8	3.1	4.9
I-94	Westbound	1.3	4.1	4.5	9.6
14/NY	Eastbound	1.4	2.3	4.5	5.8
14/NY	Westbound	0.1	3.0	2.7	5.7
Total		1.6	2.9	3.8	6.7

In the recent development of a bridge live load model for the new LRFD AASHTO Code for the design of bridges, it has been found that the maximum 75 year moment and shear are caused by two trucks in adjacent lanes (side-by-side) (NCHRP Project 12-33). Therefore, there is a need for statistical data on multiple presence. The truck count results listed in Table 2-4 provide this information for I-94 and US-23. The observed percentages for multiple presence are rather consistent and they provide an indication as to what can be expected.

3. TRUCK WEIGH STATION DATA

3. 1 Data Base

Truck weighing stations data includes a very large number of trucks (over 600,000) and it represents the majority of highway traffic, but it is biased. It appears that very heavy trucks avoid the weigh stations by using alternate routes, or operate during hours when the weigh station is closed. An extensive data set was obtained from the Michigan DOT. The data covers truck survey carried out in 1987 and 1988 at truck weigh stations located on I-75 (Monroe), and in 1989 on I-94 (Grass Lake). The total number of measured trucks on I-75 is given in Table 3-1. The survey on I-94 covered the Eastbound direction only. The data base was collected in Oct./Nov. 1989 and includes 19,874 trucks.

Table 3-1. Number of Trucks in the I-75 Survey

Year	Month	North	South	Total
1987	Mar	33,092	13,766	46,858
1987	Apr.	32,898	3,874	36,772
1987	May	16,881	29,742	46,623
1987	June	32,196	17,618	49,814
1987	July	32,187	NA	32,187
1987	Aug.	51,408	NA	51,408
1987	Sep.	50,816	NA	50,816
1987	Oct.	15,815	NA	15,815
1987	Nov.	56,233	NA	56,233
1987	Dec.	5,832	30,508	36,340
1987	total	327,358	95,508	422,866
1988	Jan.	47,540	31,281	78,821
1988	Feb.	39,136	22,963	62,099
1988	Mar	48,397	16,676	65,073
1988	total	135,073	70,920	205,993
1987 and 1988		462,431	166,428	628,859

For each truck the data contains number of axles, axle loads, axle spacing, gross vehicle weight (GVW), the date of measurement and other information.

For each surveyed truck, the maximum moments and shears were calculated for various simple spans. This resulted in thousands of values for each span considered. The obtained moments and shears can be treated as random variables. The most important statistical parameter describing a random variable is the cumulative distribution function (CDF). Therefore, the CDF's are derived for the moments and shears and they are plotted using the normal probability paper. Probability paper is a special scale which has two important properties:

- any normal distribution function (CDF) is always represented by a straight line,
- any straight line represents a normal distribution function (CDF).

The vertical scale on a normal probability paper includes numbers between 0 and 1 (without 0 and 1 because these two points correspond to -/+ ∞). However, the normal probability scale is very irregular and difficult to use for computer graphics. Therefore, the it can be replaced by the inverse standard normal distribution function, which provides a convenient regular scale from - ∞ to + ∞. In structural engineering practice, the range of values is from -5 to 5. This corresponds to the probability range from 0.0001 to 0.9999. Zero (0) on the inverse normal probability scale corresponds to the probability 0.5, -1 corresponds to 0.16, 1 to 0.84, -2 to 0.02, 2 to 0.98, -3 to 0.001 and 3 to 0.999. Therefore, the intersection of zero on the inverse normal probability scale with the data points corresponds to the median. The construction and use of the normal probability paper is described in Appendix A.

3.2. Gross Vehicle Weights

The measurements were taken at Truck Weight Station on I-75 in Monroe, MI. The percentage of trucks corresponding to different

number of axles is shown in Fig. 3-1. The results are processed for both directions of traffic. Practically, there is no difference between Nortbound and Southbound traffic. The percentage of 7-axle to 11-axle trucks is so low that their are not visible in the Fig. 3-1. Detailed analysis is done in Fig. 3-2 through Fig. 3-5.

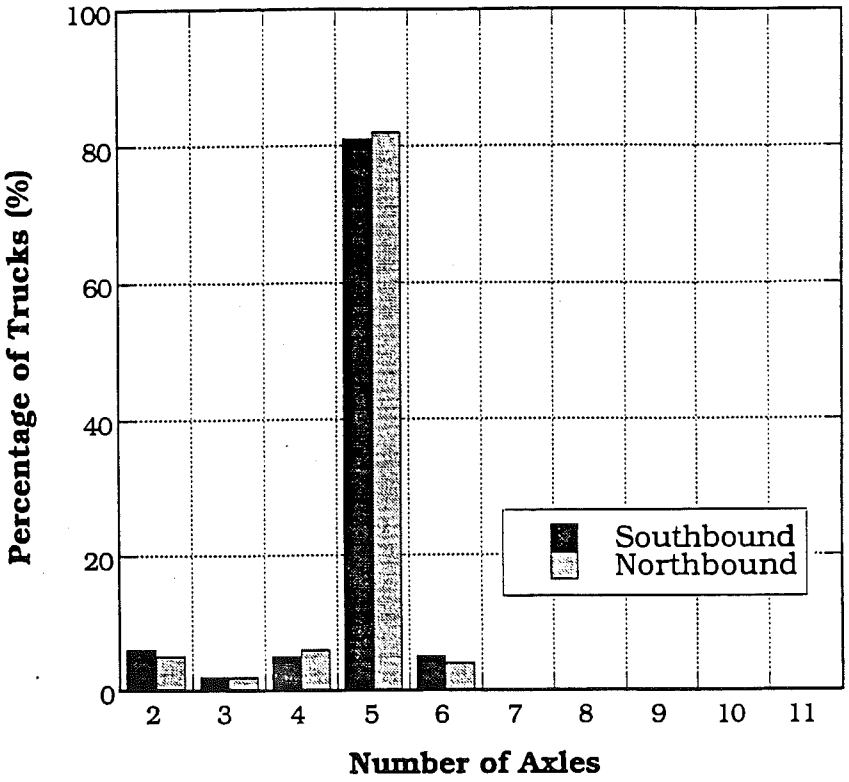

Fig. 3-1. Histogram of Truck Type (Number of Axles) for I-75.

The weights of surveyed trucks are presented in histograms. Northbound and Southbound directions are considered separately. Figure 3-2 shows gross weight histograms for I-75 Southbound in 1987. The number of trucks, is 95,508 see Table 3-1. In Fig. 3-3, the histograms are presented for I-75 Northbound in 1988. The corresponding number of trucks is 135,073. The histograms are rather similar.Review of the results indicates that most of the truck weights are within legal limits. The histograms include a full range of trucks, from empty vehicles to fully loaded ones. Therefore, some of the histograms have two humps. In particular, it is visibles in case of more than 4-axle trucks.

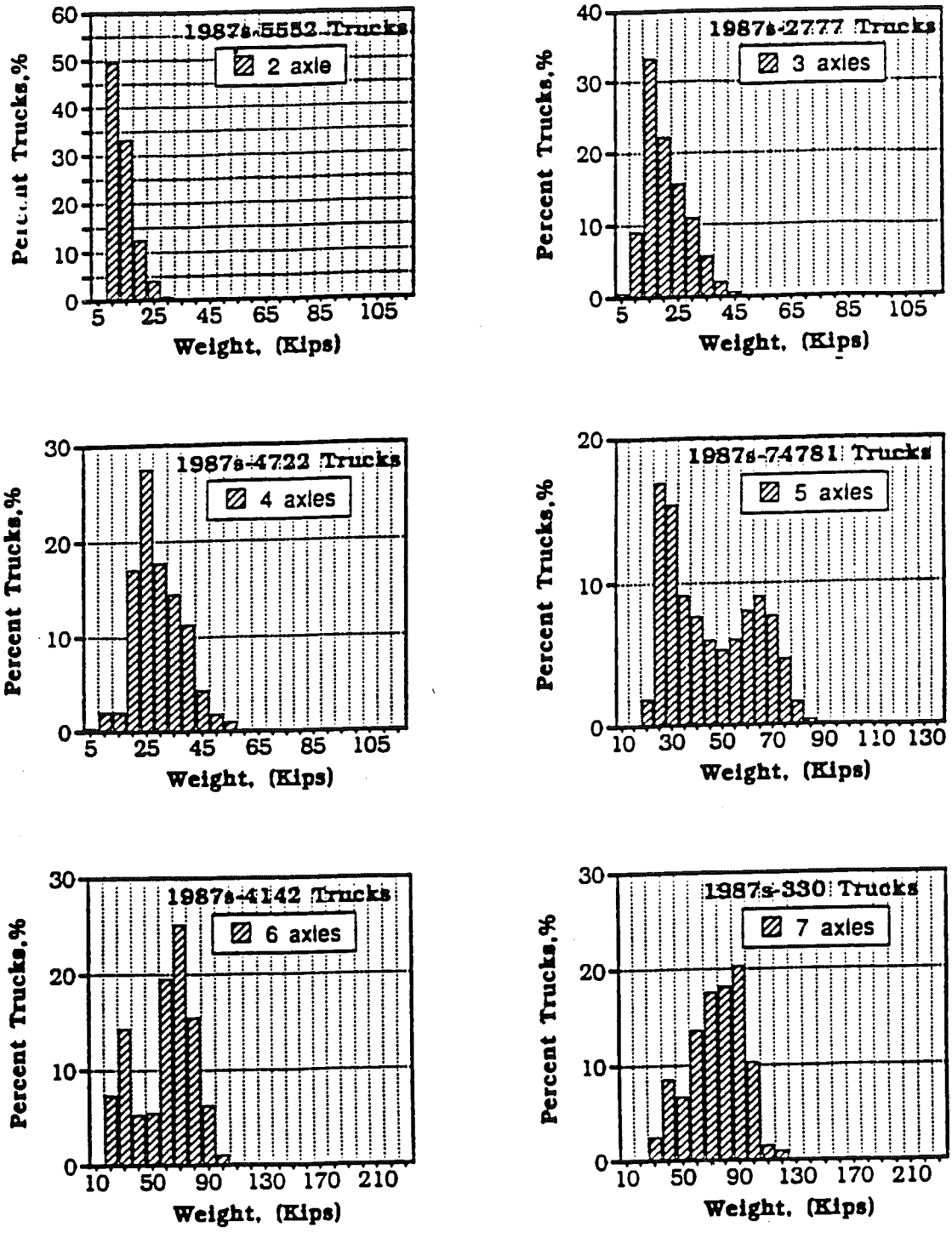

Fig. 3-2. Histograms of GVW, I-75 Southbound, Number of Axles 2-7.

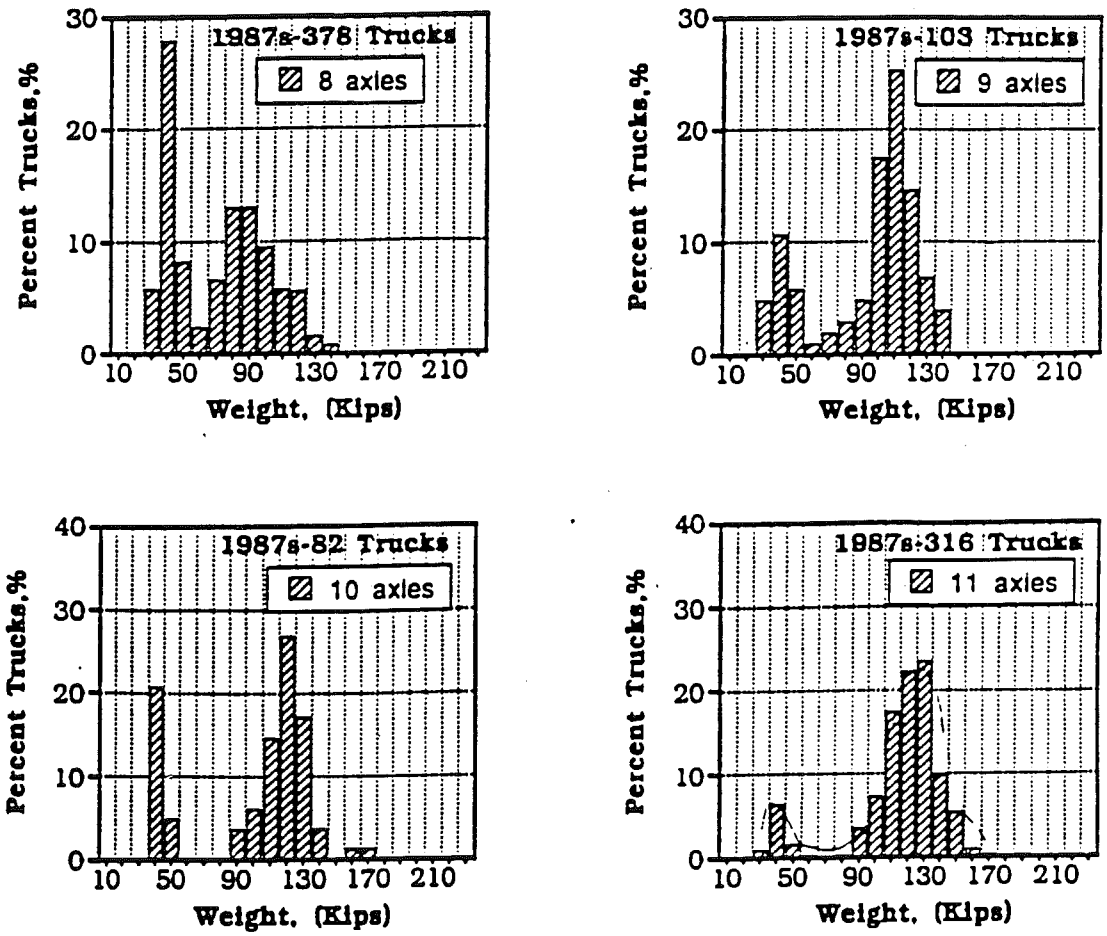

Fig. 3-3. Histograms of GVW, I-75 Southbound, Number of Axles 8-11.

3. 3 Moments Due to Surveyed Trucks

The moments and shear forces are calculated for each truck to derive the cumulative distrution function (CDF). The results are plotted on normal probability paper with the vertical scale representing the inverse standard normal distribution function.

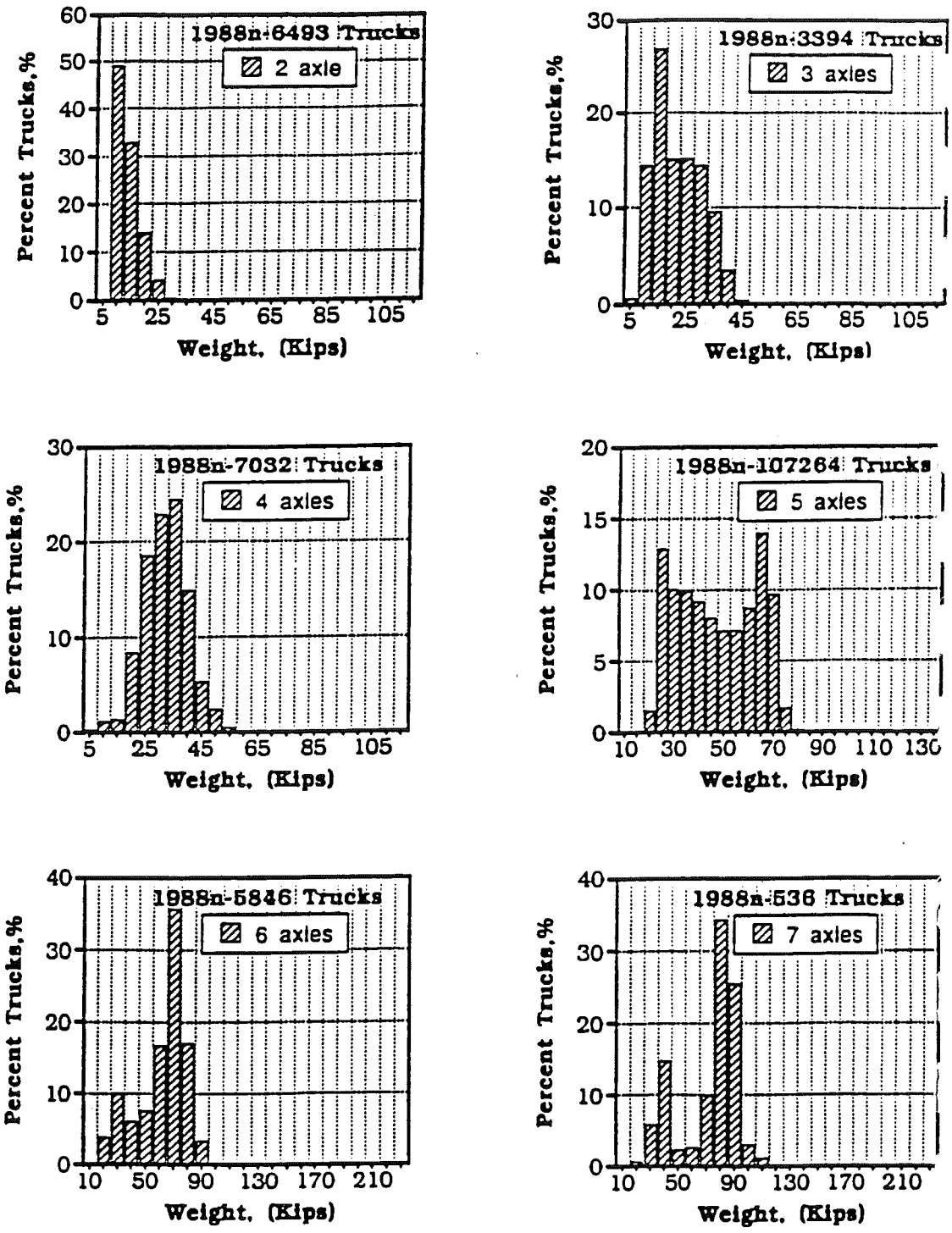

Fig. 3-4. Histograms of GVW, I-75 Northbound, Number of Axles 2-7.

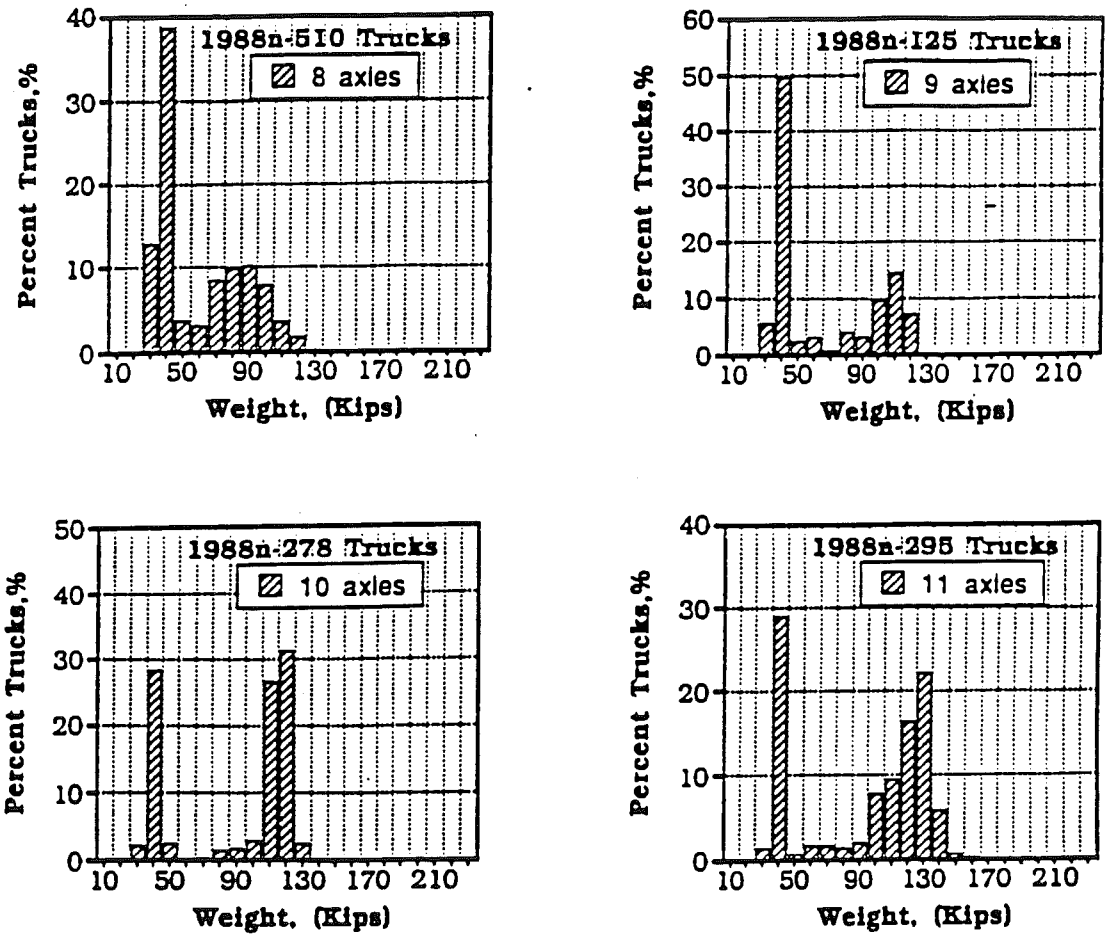

Fig. 3-5. Histograms of GVW, I-75 Northbound, Number of Axles 8-11.

For an easier comparison, the calculated moments (shears) are divided by the design HS-20 moments (shears) (AASHTO 1992) without impact. The moment (shear) ratio is plotted on the horizontal axis.

The calculated moments are presented separately for I-75 Northbound, I-75 Southbound and I-94 Eastbound. The results are shown in Fig. 3-6 through 3-12.

For Northbound traffic in 1987 and 1988, the results are shwon in Fig. 3-6 and 3-7, respectively. The irregularities (waves) in the curves indicate humps in the histogram, which corresponds to different types of trucks and whether they are fully loaded or not.

The CDF's of moments for Southbound trucks in 1987 and 1988 are shown in Fig. 3-8 and 3-9, respectively. In the Fig. 3-10, the CDF's are plotted for all the surveyed trucks on I-75 (North and South, 1987 and 1988, combined).

The moments for Eastbound traffic on I-94 are shown in Fig. 3-11. The number of trucks is considerably smaller than on I-75 (19,874 vs. 628,859), but the extreme moments corresponding to about 4 on the inverse normal probability scale are similar.

The differences in the moments corresponding to different months are presented in Fig. 3-12. The results are shown for the span of 60 ft and 10 months (March through December) in 1987 and 3 months (January through March) in 1988.

In most cases the maximum moments do not exceed twice HS-20 moments. The differences in moment values are more a function of span length than month, year, or direction of traffic.

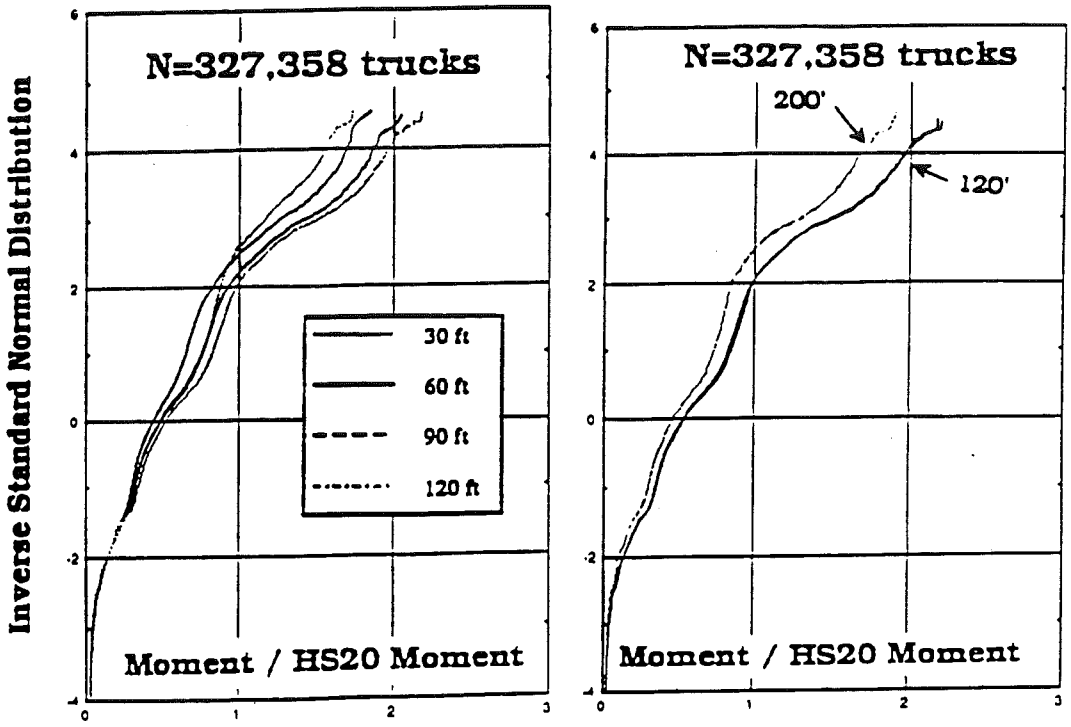

Fig. 3-6. CDF's of Moments, Weigh Station Data, I-75 North, 1987.

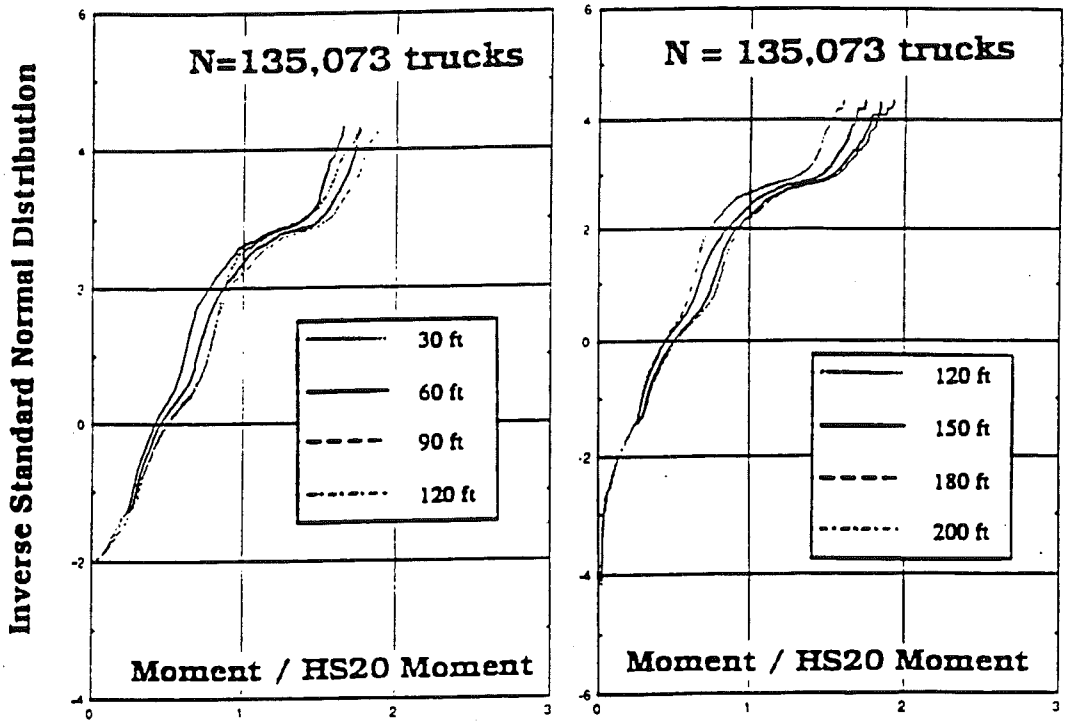

Fig. 3-7. CDF's of Moments, Weigh Station Data, I-75 North, 1988.

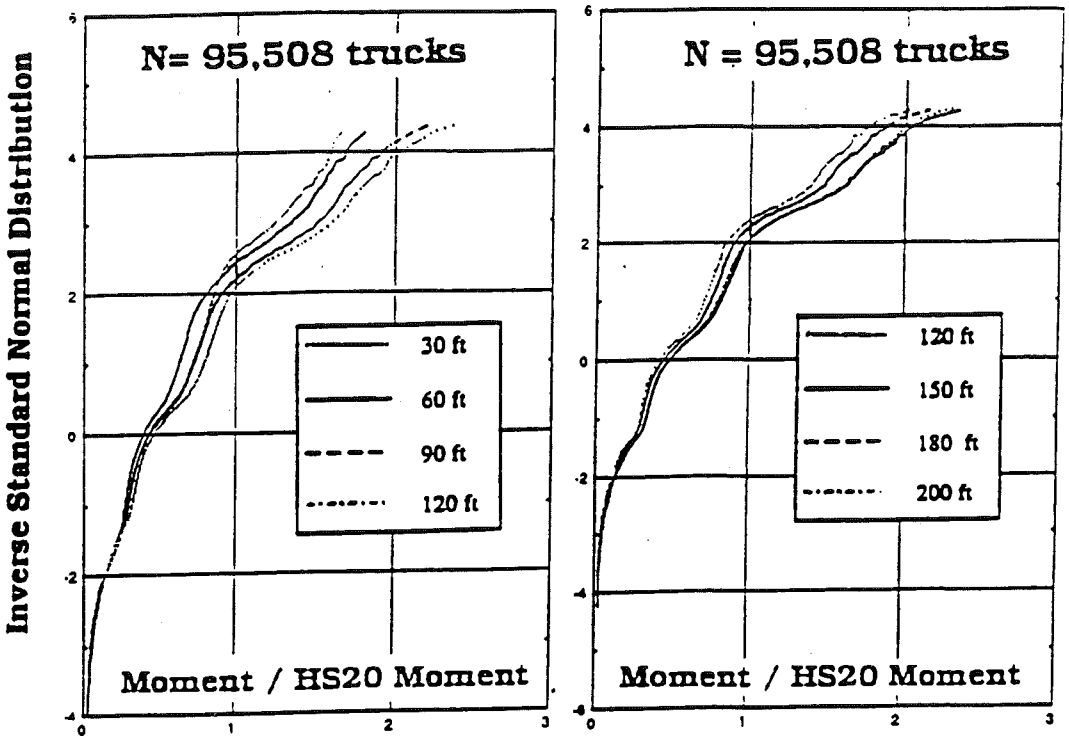

Fig. 3-8. CDF's of Moments, Weigh Station Data, I-75 South, 1987.

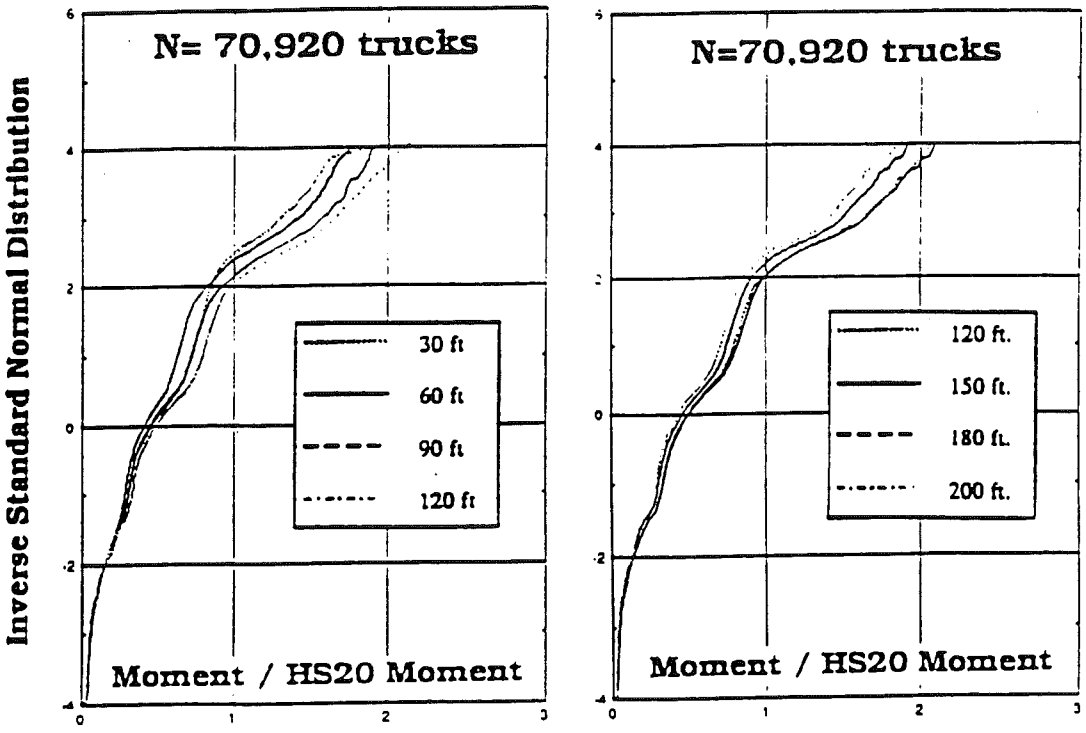

Fig. 3-9. CDF's of Moments, Weigh Station Data, I-75 South, 1988.

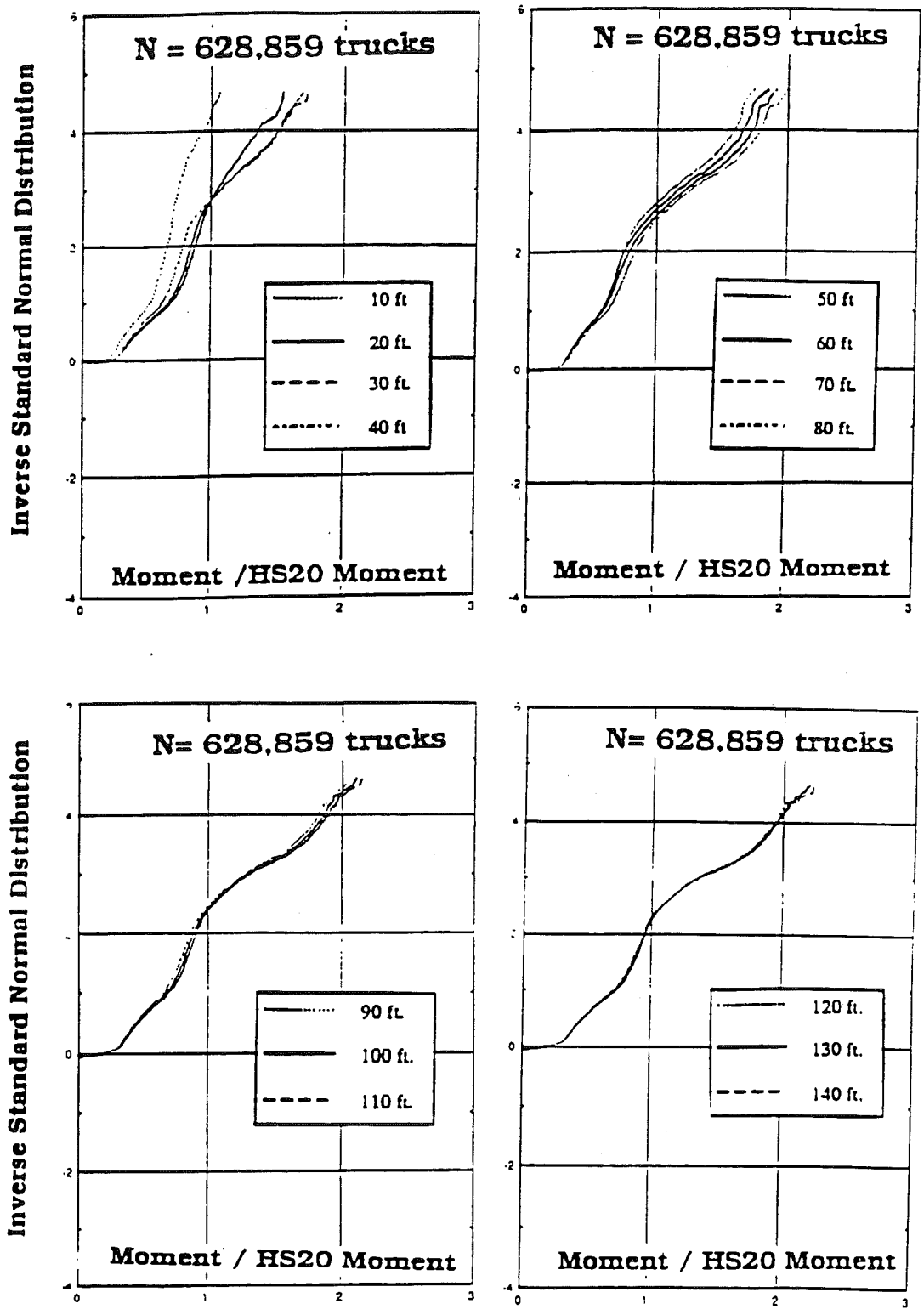

Fig. 3-10. CDF's of Moments, Weigh Station, I-75 North and South.

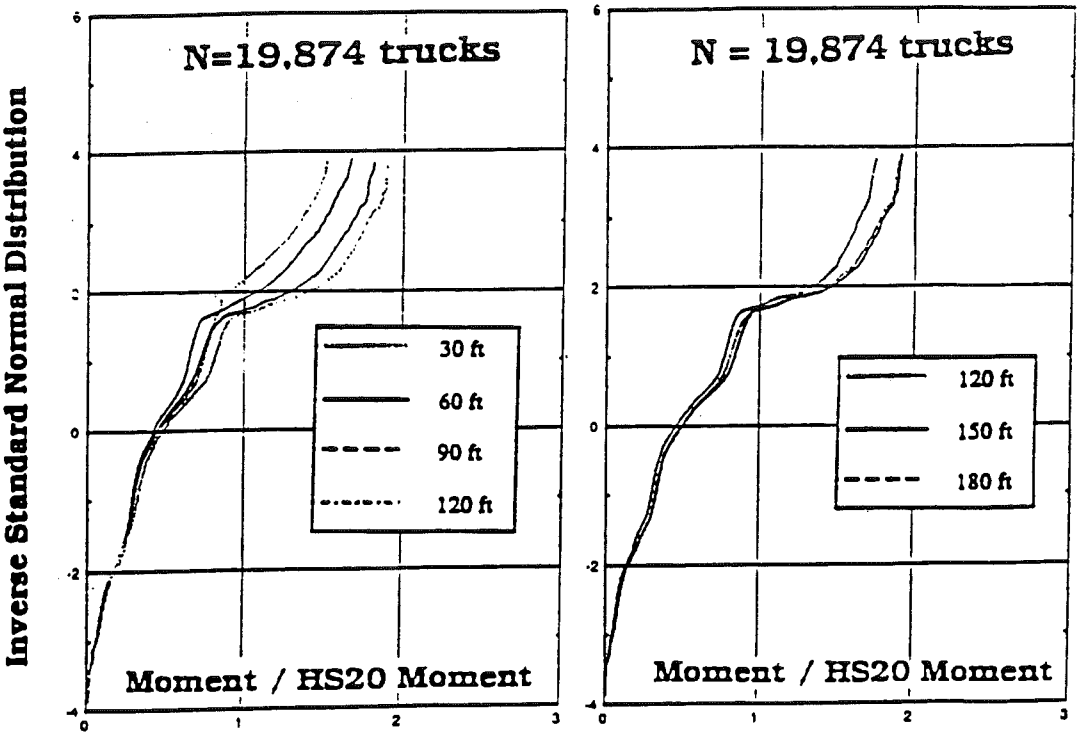

Fig. 3-11. CDF's of Moments, Weigh Station Data, I-94 East, 1989.

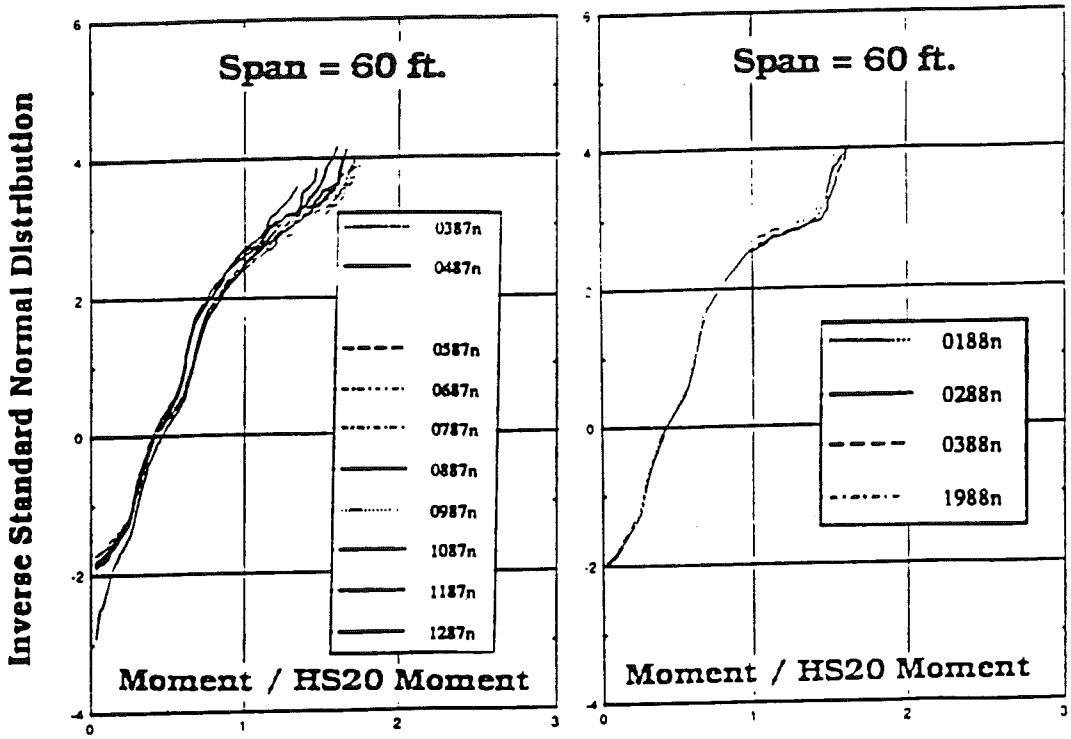

Fig. 3-12. CDF's of Moments for Different Months, Weigh Station Data.

3. 4 Shears Due to Surveyed Trucks

The calculated shears are also presented separately depending on traffic direction and year of survey, for I-75 Northbound, I-75 Southbound and I-94 Eastbound. The results are shown in Fig. 3-13 through 3-19.

For Northbound traffic in 1987 and 1988, the results are shown in Fig. 3-13 and 3-14, respectively. As in the case of moments, the irregularities (waves) in the curves indicate humps in the histogram, which corresponds to different types of trucks and whether they are fully loaded or not.

The CDF's of shears for Southbound trucks in 1987 and 1988 are shown in Fig. 3-15 and 3-16, respectively. In the Fig. 3-17, the CDF's are plotted for all the surveyed trucks on I-75 (North and South, 1987 and 1988, combined).

The shears for Eastbound traffic on I-94 are shown in Fig. 3-18. The shape of CDF's is different than for I-75 trucks. This indicates, that truck traffic is different with regard to weights, axle loads and axle spacing. However, the maximum values in Fig. 3-18, corresponding to 4 on the inverse normal probability paper, are similar to the shears calculated for I-75.

In most cases the maximum shears do not exceed twice HS-20 shears. The differences in shear values are more a function of span length than year or direction of traffic.

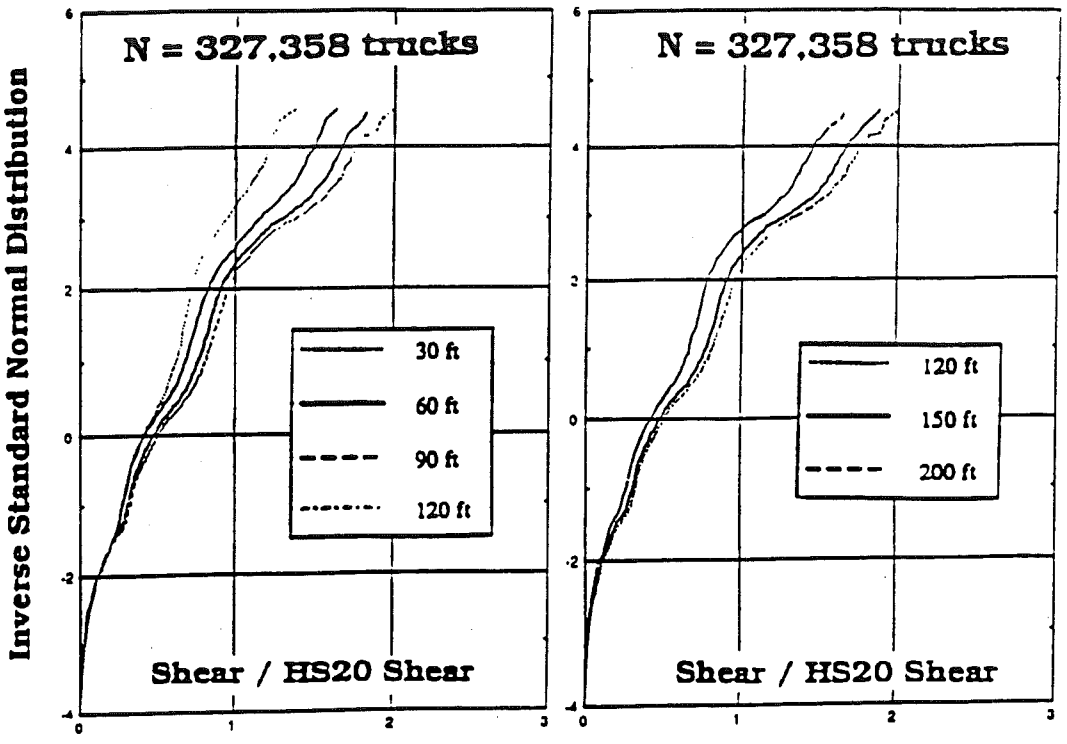

Fig. 3-13. CDF's of Shears, Weigh Station Data, I-75 North, 1987.

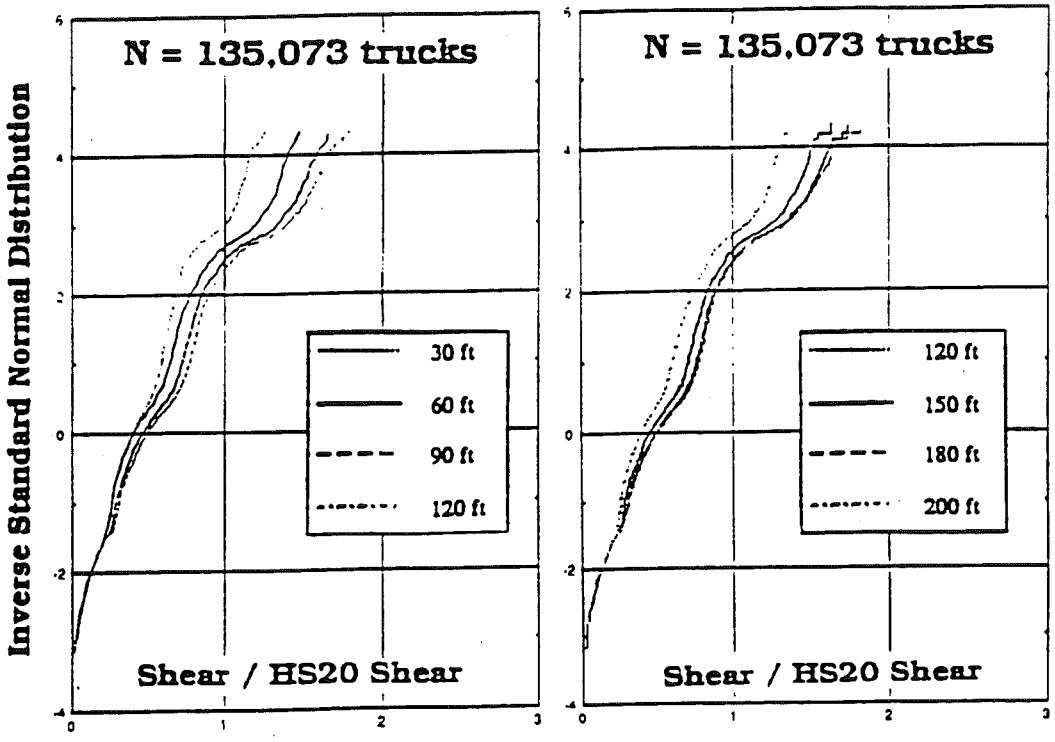

Fig. 3-14. CDF's of Shears, Weigh Station Data, I-75 North, 1988.

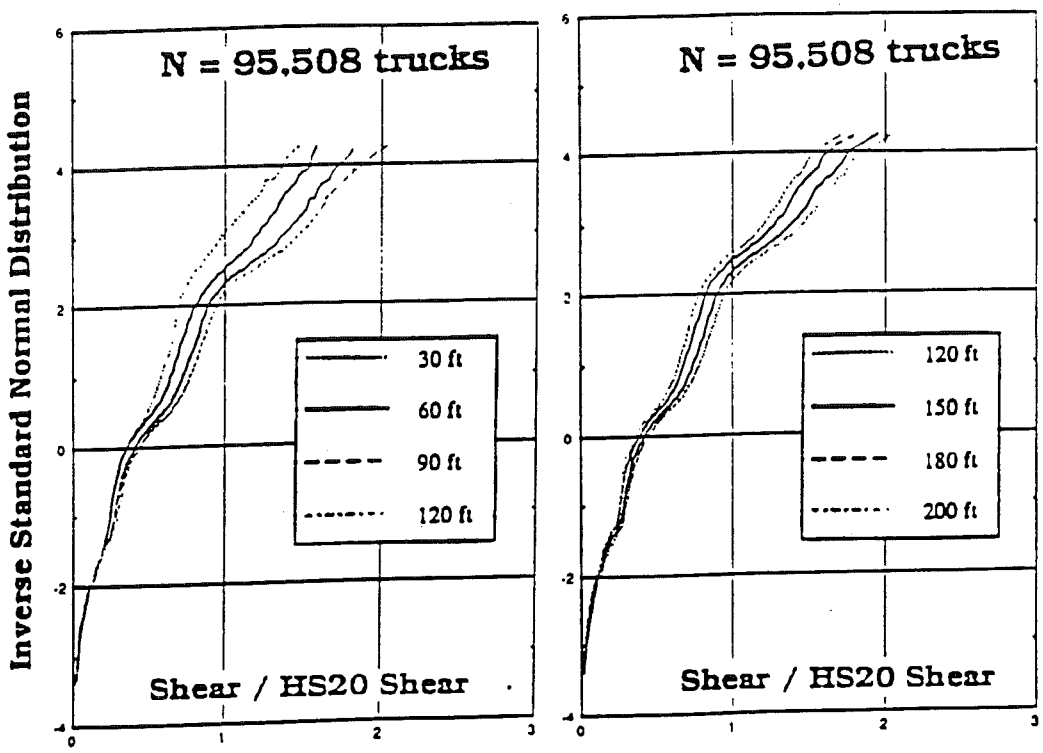

Fig. 3-15. CDF's of Shears, Weigh Station Data, I-75 South, 1987.

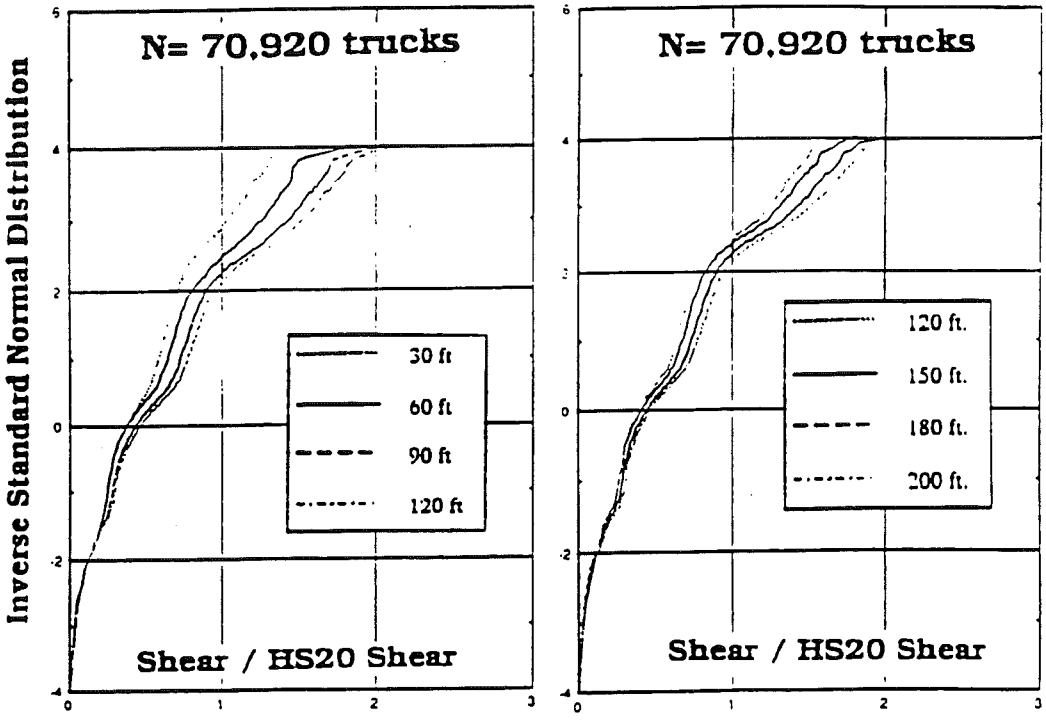

Fig. 3-16. CDF's of Shears, Weigh Station Data, I-75 South, 1988.

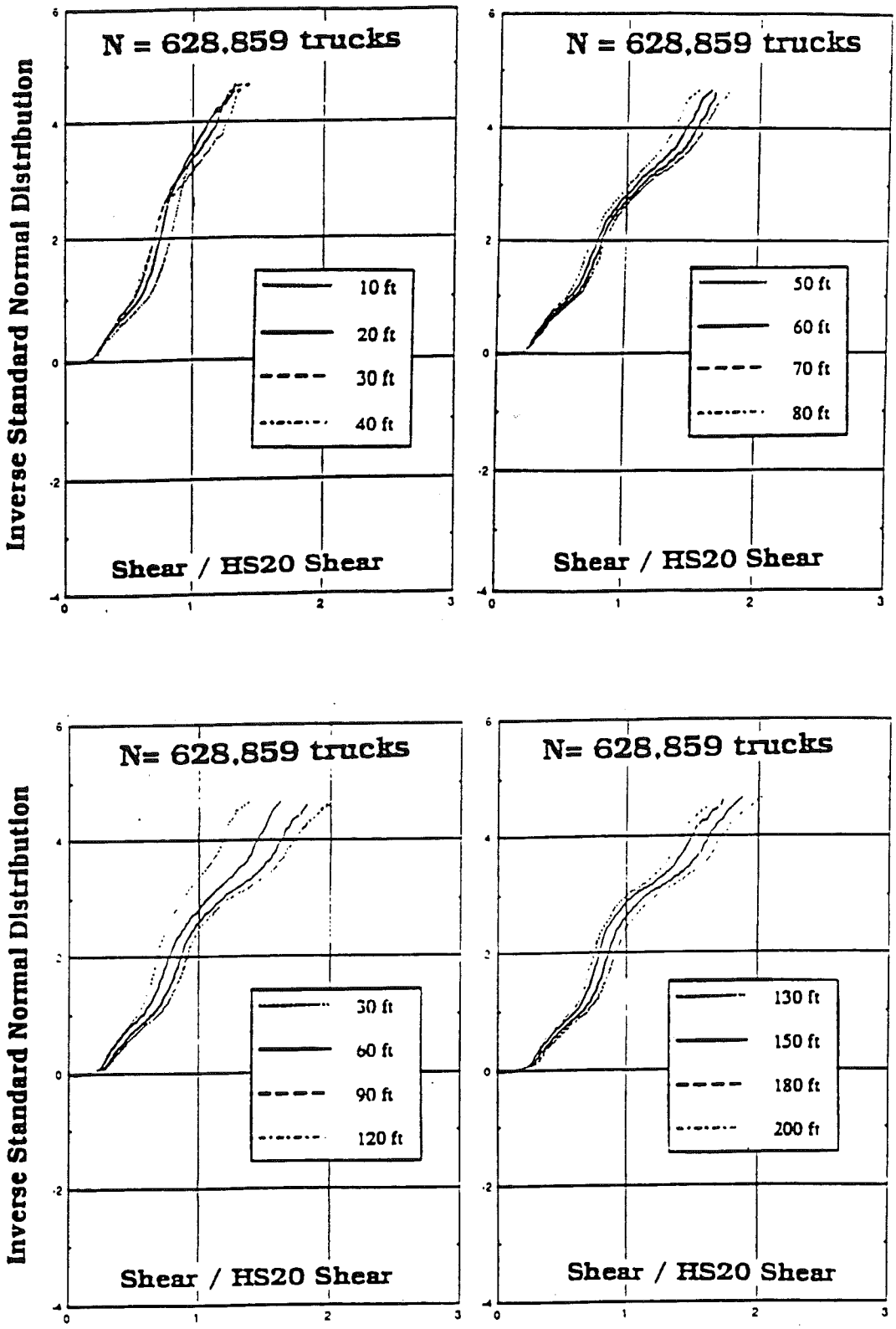

Fig. 3-17. CDF's of Shears, Weigh Station Data, I-75 North and South.

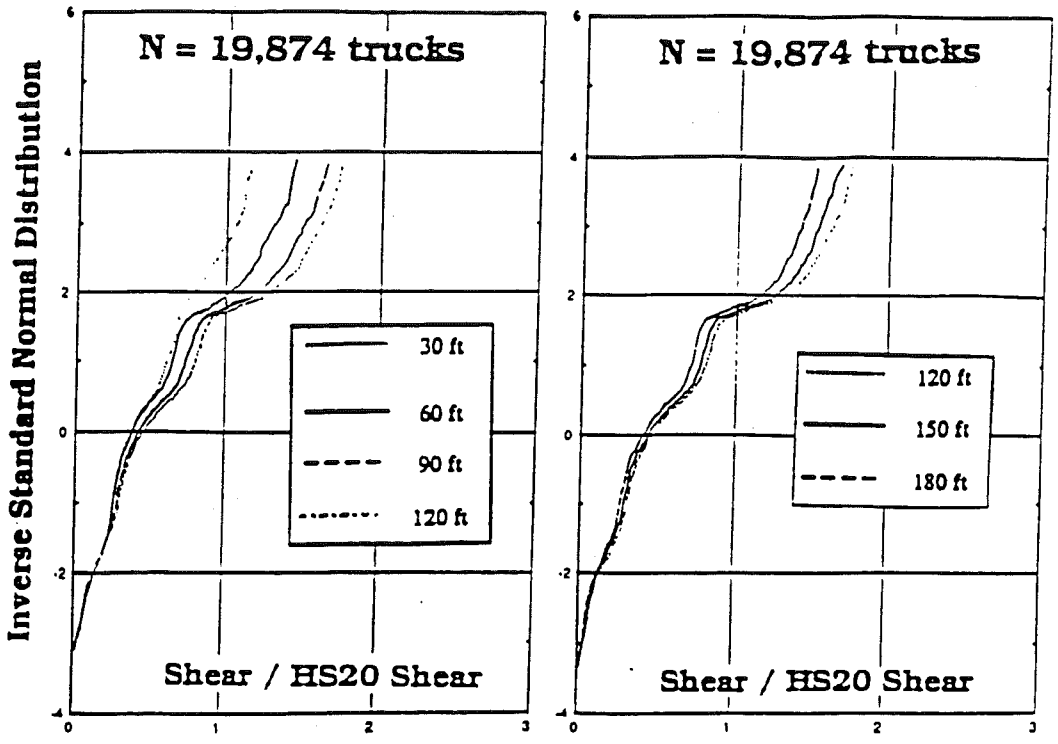

Fig. 3-18. CDF's of Shears, Weigh Station Data, I-94 East, 1989.

3. 5 Discussion of Results

In general, from the histograms of GVW, it is clear that the surveyed trucks do not exceed the Michigan legal loads. The maximum moments (shears) are in most cases less than twice HS-20 moments (shears).

The moments and shears obtained as a part of this study by field measurements and shown in Chapter 8 are considerably larger than maximum values resulting from the measurements taken at the weigh stations. This observation indicates that the truck survey data is biased because the heaviest trucks avoid the scales.

Note:

Intentionally left blank

4. CITATION DATA

Another possible source of information regarding weight and configuration of highway trucks is the citation data of overweight vehicles. This data base was provided by the Michigan State Police Motor Carrier Division. The survey covered 2,511 citations in the calendar year 1985. The data was processed in two subgroups, corresponding to half-year periods; the first one is denoted by January-May and the other by June-December.

The frequency histogram for the number of axles of citation trucks is shown in Fig. 4-1. The traffic is dominated by 5 and 6 axle trucks. The third most frequent number of axles is 11.

The frequency histogram for the gross vehicle weight (GVW) of all citation trucks is shown in Fig. 4-2. Most of GVW's are between 70 and 90 kips.

The gross vehicle weight is also represented as by cumulative distribution function (CDF). The distribution functions are plotted using normal probability paper, as described in Appendix A. The vertical scale corresponds to the probability and the actual numbers are equal to the inverse normal probability. The CDF's of the gross vehicle weight for January-May and June-December are plotted in Fig. 4-3. For the whole year, the cumulative distribution function is plotted in Fig. 4-4.

The distribution functions of axle load are shown in Fig. 4-5 and 4-6, for the first and second half year periods, respectively. For the whole year the results are shown in Fig. 4-7.

The heaviest trucks in the citation file were identified. The vehicles with GVW > 200 kips are shown in Fig. 4-8. The schematic figures of trucks with axle weight exceeding 35 kips are shown in Fig. 4-9.

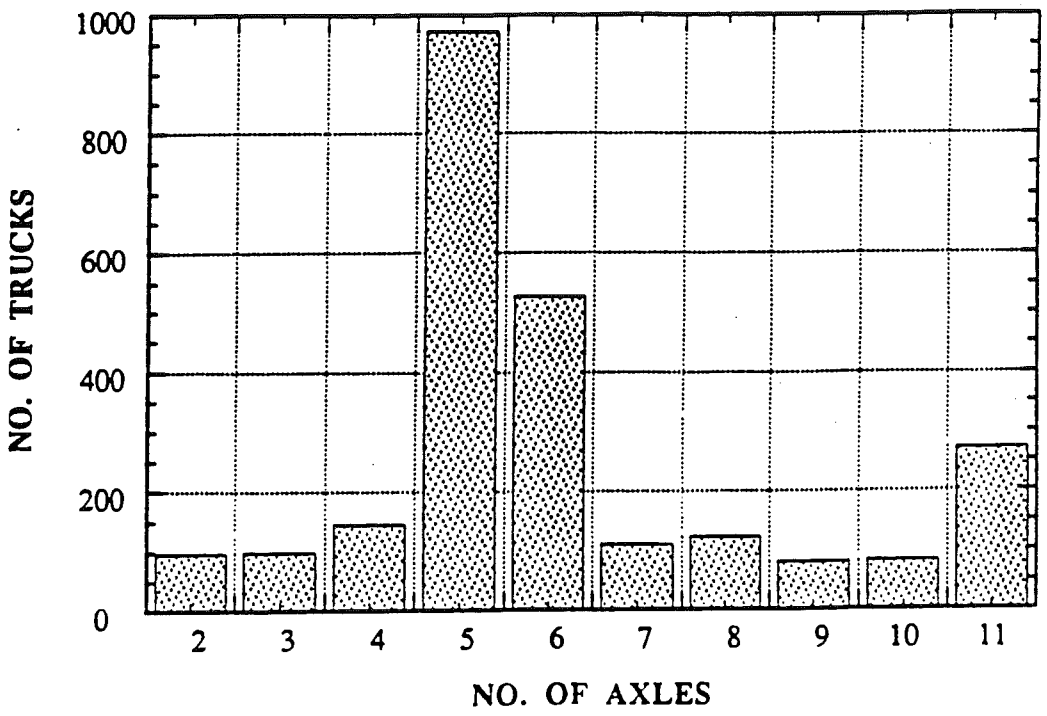

Fig. 4-1. Histogram of Number of Axles for Citation Trucks.

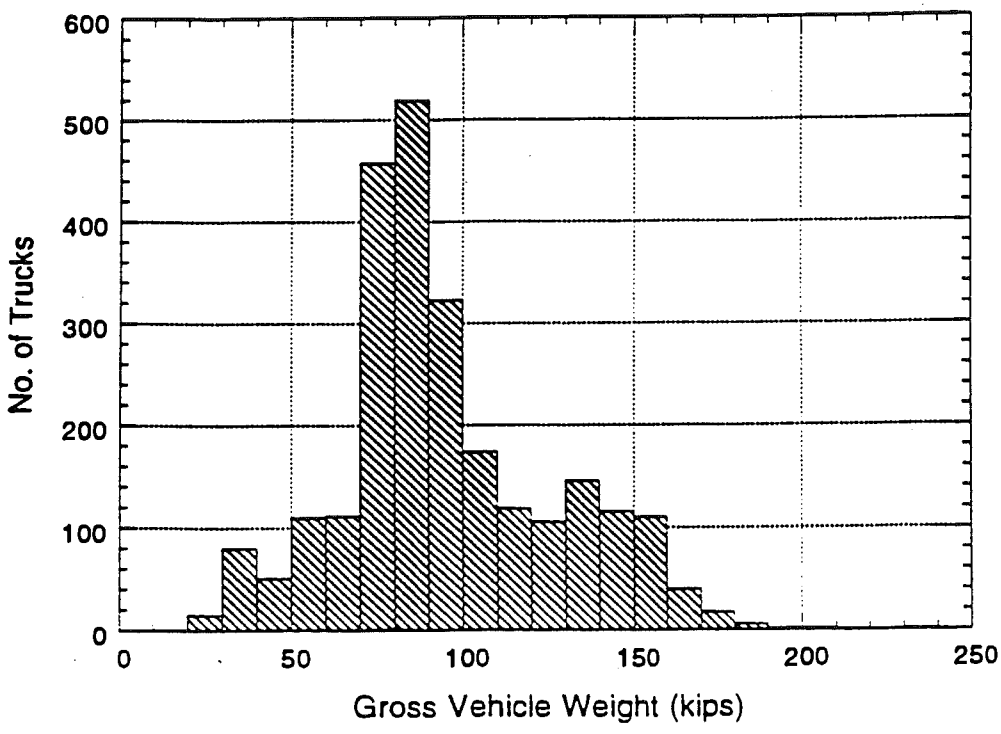

Fig. 4-2. Histogram of GVW for Citation Trucks.

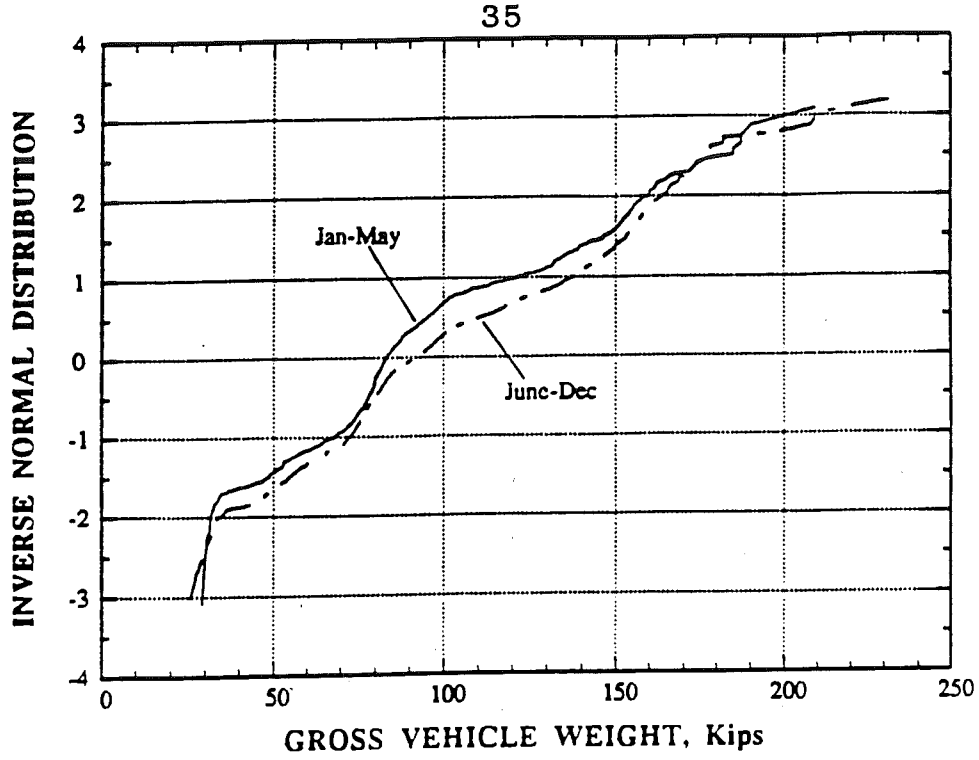

Fig. 4-3. CDF's of GVW for Half-Year Periods, Citation Data.

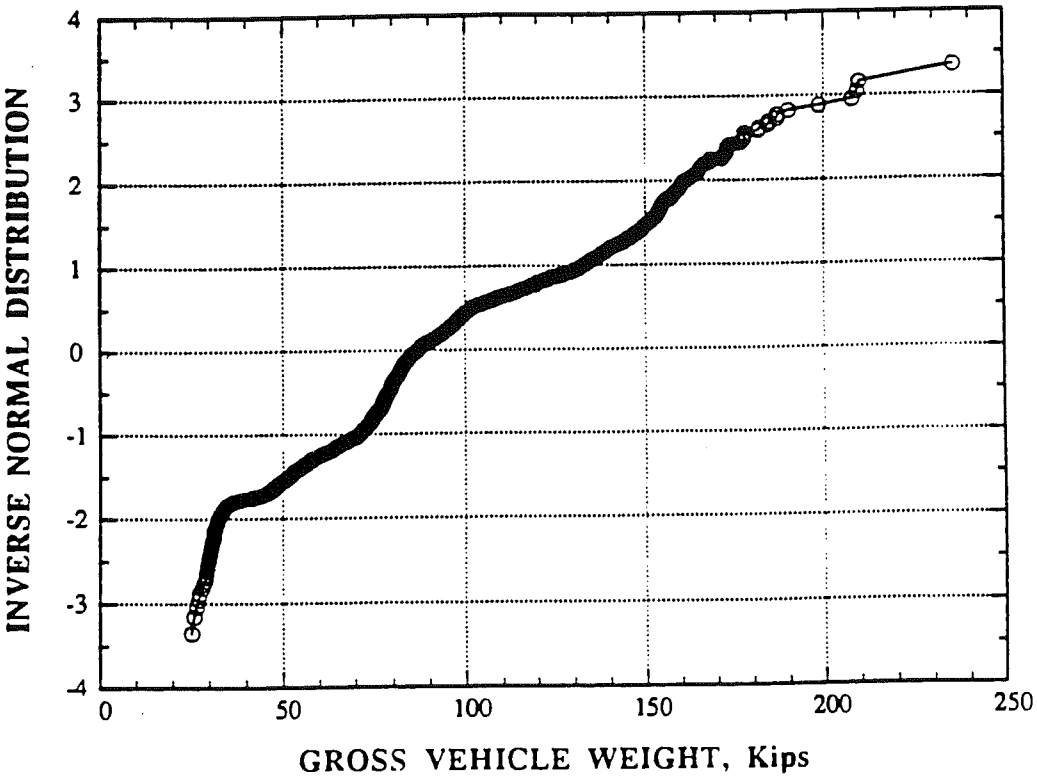

Fig. 4-4. CDF of GVW for the Whole Year, Citation Data.

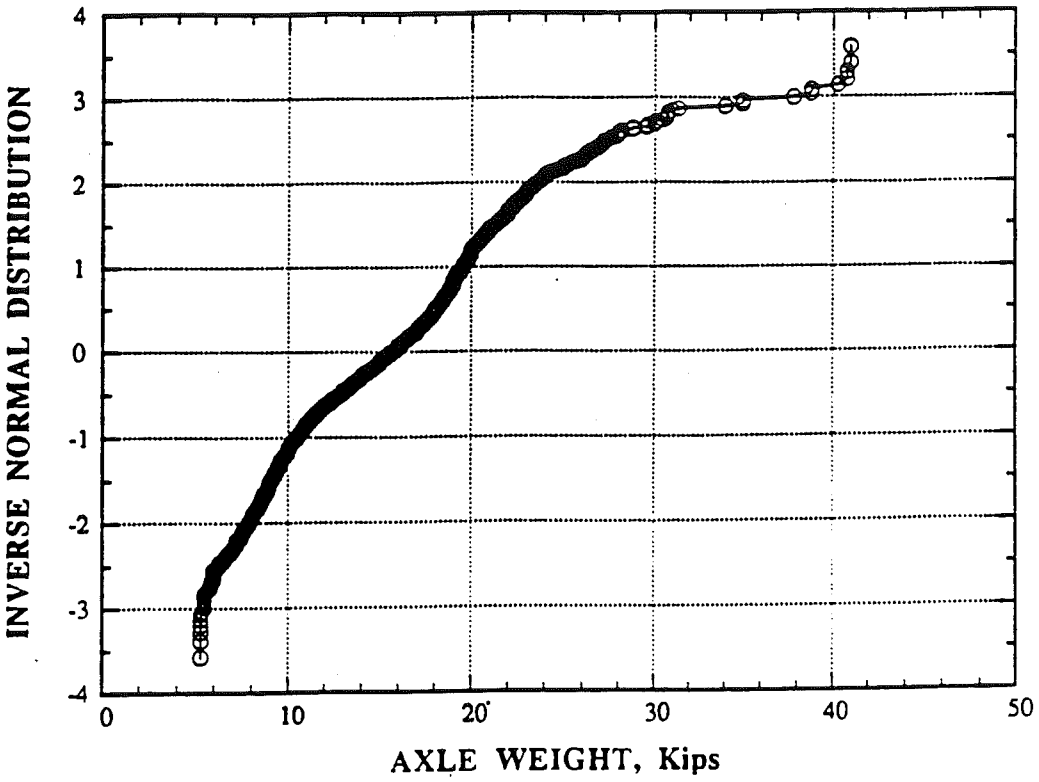

Fig. 4-5. CDF's of Axle Load for January-May, Citation Data.

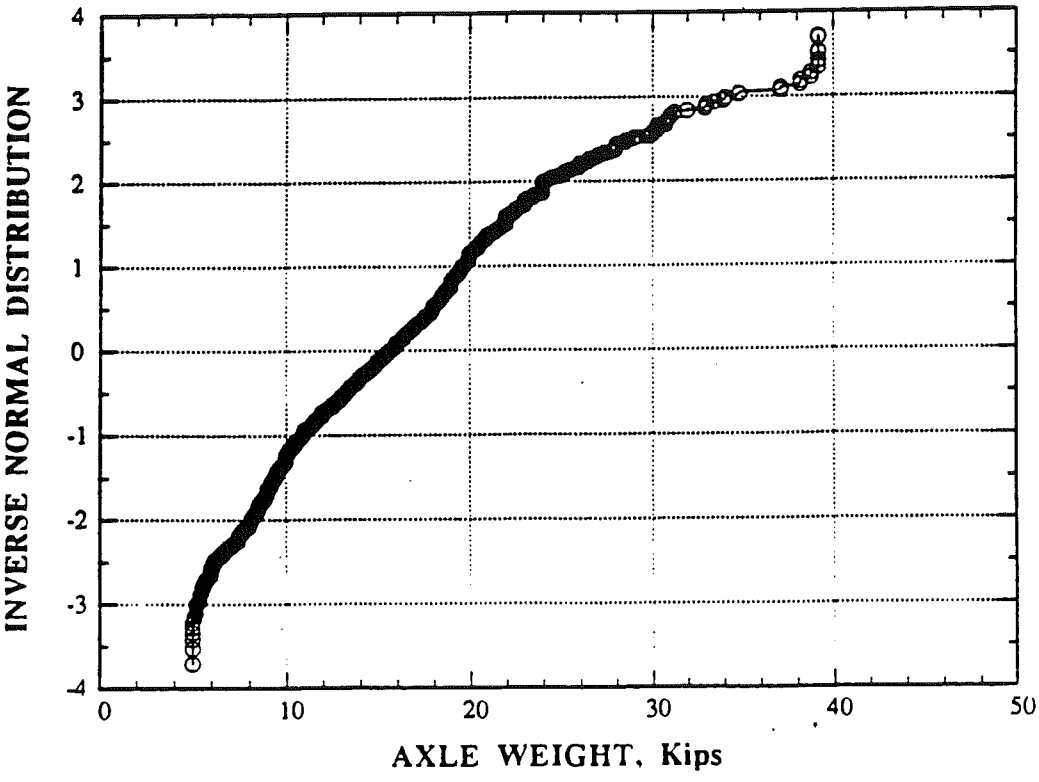

Fig. 4-6. CDF's of Axle Load for June-December, Citation Data.

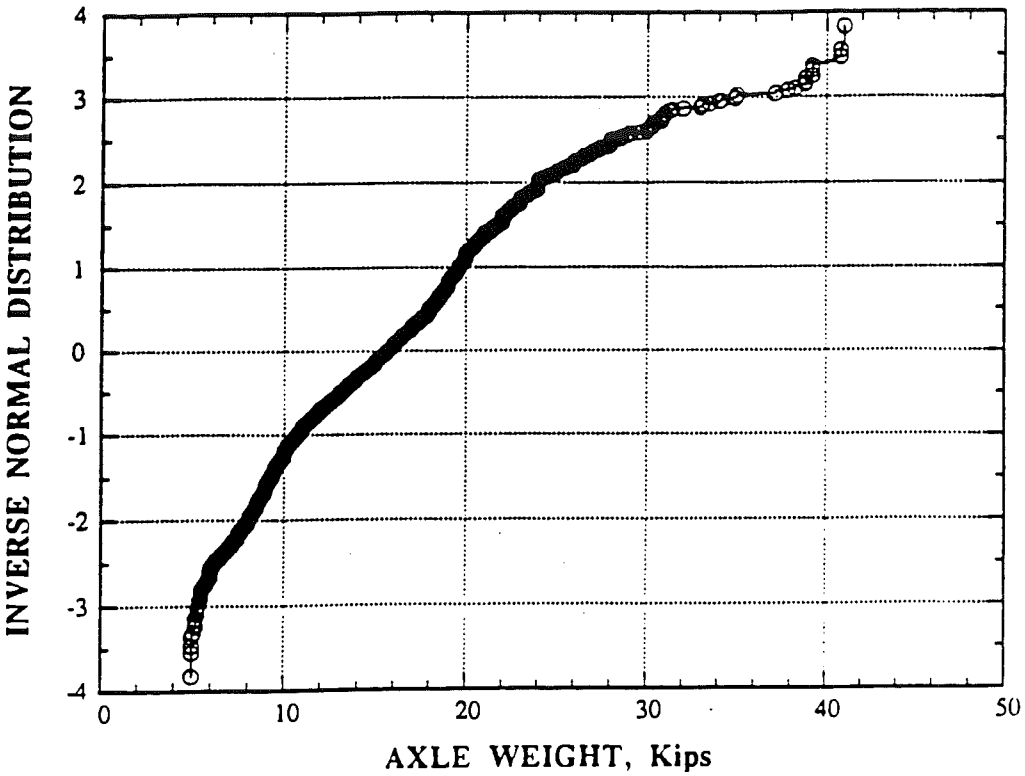

Fig. 4-7. CDF of Axle Load for the Whole Year, Citation Data.

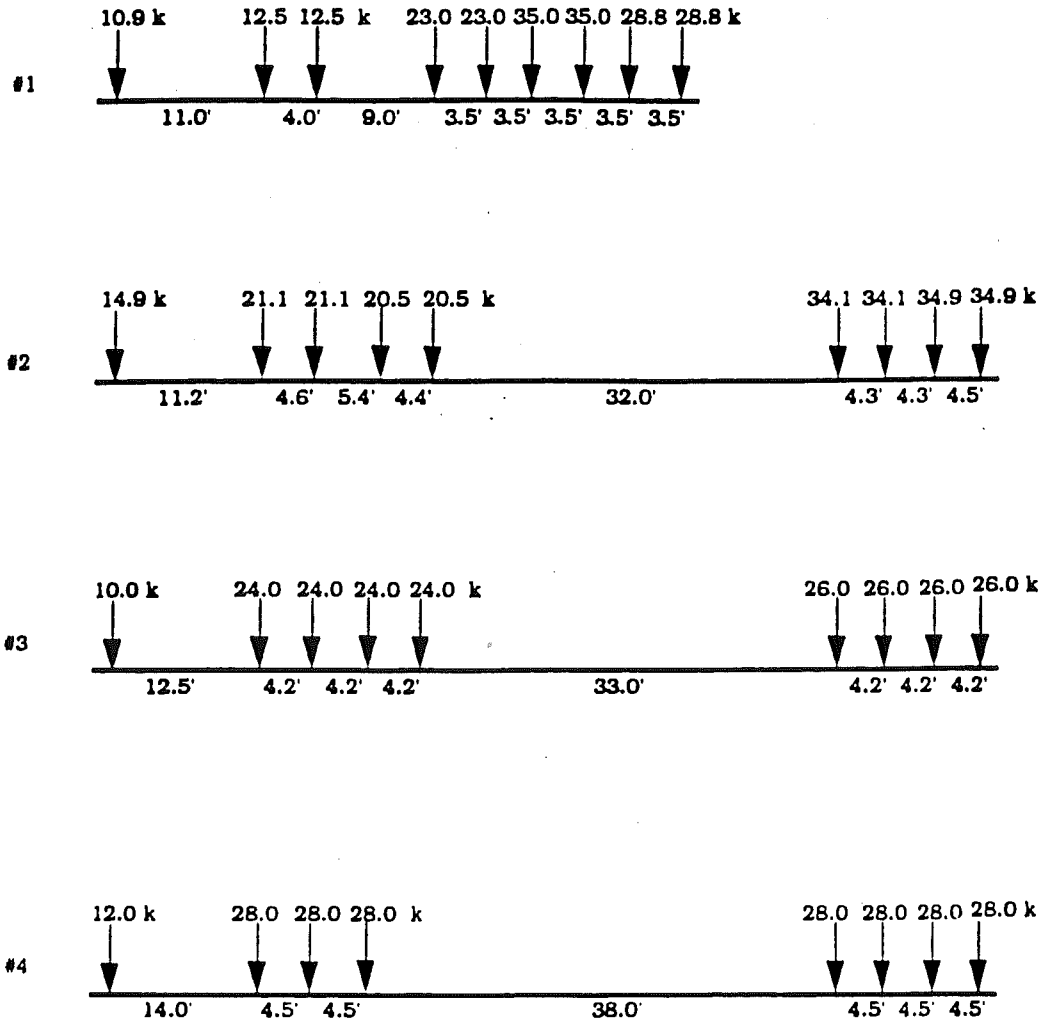

Fig. 4-8. Trucks with GVW > 200 kips, Citation Data.

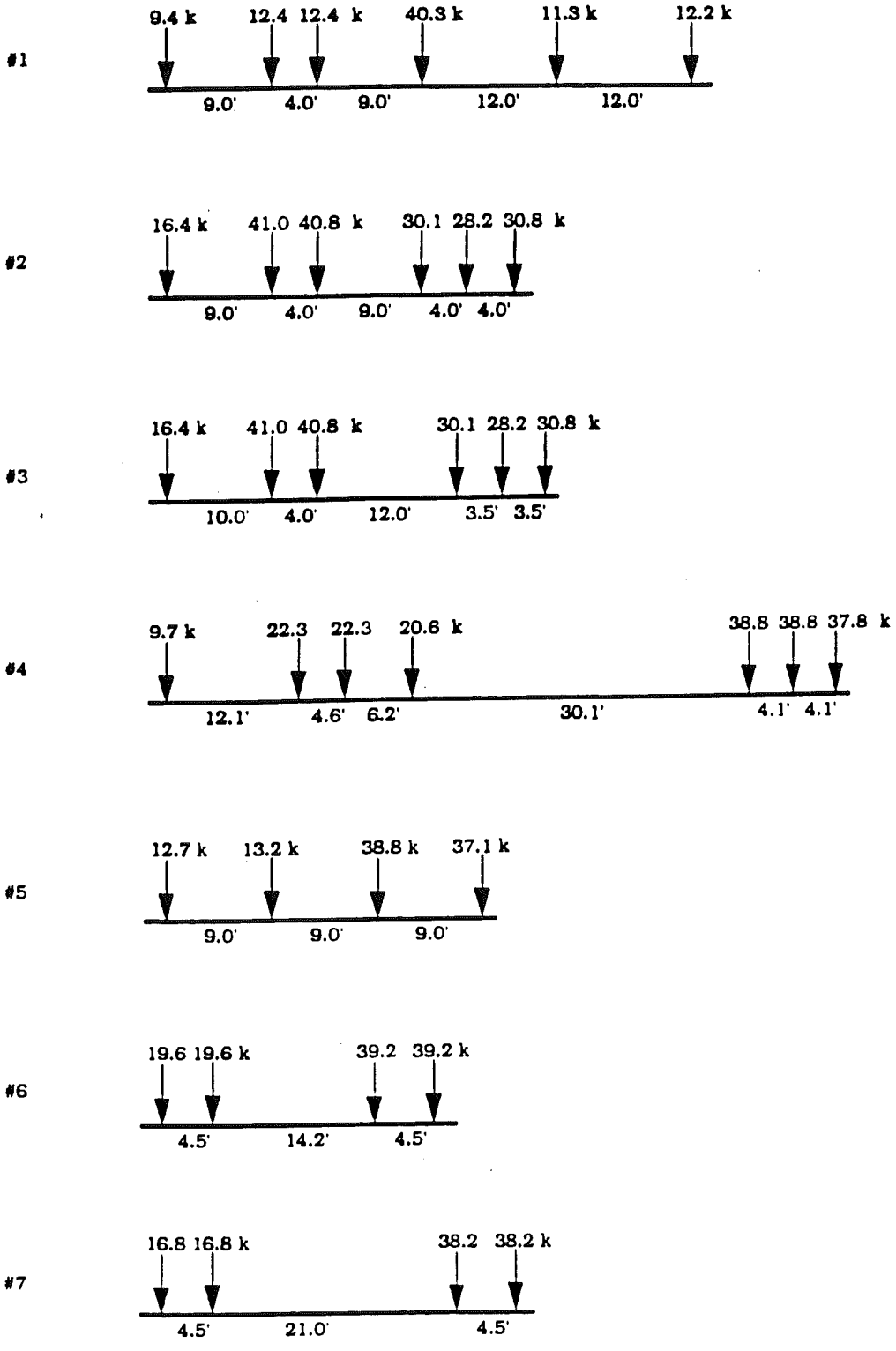

Fig. 4-9. Trucks with Axle Loads > 35 kips, Citation Data.

Note:

Intentionally left blank

5. TESTING EQUIPMENT

The testing equipment is very important in this project. The main objective is to collect data for the development of live load spectra. Several data acquisition systems were considered. Most data was collected using the Bridge Weighing System Inc. (BWS) unit specially purchased by the Michigan DOT for this project. The equipment is described in four groups including items available at the University of Michigan, equipment provided by MDOT, specially purchased equipment, and other equipment.

The system provided by MDOT was supplemented by other equipment purchased by the University of Michigan (U of M). The purchased items, by MDOT as well as by U of M, include: 8-channel data acquisition unit by Krenz Electronics, 8-channel data acquisition system by SoMat Corporation, two portable computers, power generator, van, accelerometers, strain transducers and miscellanous items such as tape switches, cables, clamps, and ladders.

5.1 Equipment Available at the University of Michigan

The computations and laboratory tests were carried out using the facilities available at the University of Michigan, and in particular at the Structural Engineering Laboratory and computer workstations.

The Structural Engineering Laboratory (SEL) was used to calibrate and adjust the testing equipment. Several state-of-the art electronic controllers and recorders are used for load and displacement control and graphical output display.

The computer facilities available to the project team include the University of Michigan Computer Aided Engineering Network (CAEN) and desktop computers. The state-of-the-art Computer Aided Engineering Network uses a variety of links to connect IBM and Apple personal computers, as well as the more powerful Apollo DN3000 and DN4000 machines, Sun, Harris, and Alliant computers. Several

computer networks including the Apollo, Ethernet, and Appletalk make it possible for the computing resources of all machines to be shared. An IBM 3090-400 is accessible from any personal computer via the Michigan Terminal System (MTS).

5.2 WIM Equipment

The WIM Data acquisition system was purchased by the Michigan DOT from the Bridge Weighing Systems, Inc. (BWS). The BWS system was designed to collect axle and gross weights on vehicles moving at highway speeds. It is based on a prediction method that was developed at the Case Western Reserve University (Moses and Ghosn, 1983). It uses instrumented bridge girders that offer several advantages over pavement scales. The measurements can be carried out in up to two traffic lanes.

The system purchased by MDOT consisted of the basic unit, 10 strain transducers, 6 cables, 2 T-boxes, and 10 tape switches. The unit is capable of handling up to 8 channels (original unit handled 6 channels and it was upgraded later) with analog front end (AFE), data processor (MVME105 computer with a mass storage device, a Citadel Datavault). In addition, a power generator and a notebook computer (to view and download data) were purchased by the Project Team. The unit required a power generator to provide AC. The main components of the system are shown in Fig. 5-1.

The data processor contains a Motorolla MVME105 processing board and one Citadel Controller card. It has a 2 Mbytes of solid state mass storage that resides on a removable cartridge (Datavault). It is also equipped with a 64 Kbytes of battery backed static Random Access Memory (RAM), that is utilized to store the WIM site parameters files. When the system is booted up those files are read by the AFE and updated to be used with the data acquisition routines. The system originally required AC current provided by a power generator. An adjustment was made to change to DC supplied by a battery.

The analog front end (AFE) system acts as a signal conditioner and amplifier with a capacity of 8 input channels. Each channel can condition and amplify signals from strain transducers. During data acquisition, the AFE maintains the strain signals at zero. The auto-balancing of the strain transducers is activated when the first axle of the vehicle crosses the first axle detector. As the truck crosses the axle detectors the speed and axle spacing are determined. When the vehicle reaches the bridge, the strain sampling is activated. As the last axle of the vehicle has exited the instrumented bridge span, the strain sampling is turned off. Data received from strain transducers is digitized and sent to the MVME105 computer where axle weights are determined by an influence line algorithm. These data do not include dynamic loads. This process takes from 1.7 to 3.0 seconds, depending on the instrumented span length, vehicle length, number of axles, and speed.

In the spring of 1992 the BWS WIM equipment was upgraded to operate on 12V DC and store data on static random access memory rather than 120V AC and the mass storage Citadel Datavault. All files are stored in SRAM capable of holding up to 20,000 truck records. Captured strain files may also be stored in SRAM with a maximum of 175 records.

The strain transducer used for the system is shown in Fig. 5-2. It is clamped to the upper or lower surface of the bottom flange of the steel bridge girder and placed in the middle third of a simple span, as shown in Fig. 5-3.

All transducers which are calibrated by company are placed on the girders at the same distance from the abutment. MDOT purchased 10 strain transducers. The University of Michigan purchased additional eight transducers. One was stolen during the measurements and another one broke. So currently the project team has 16 strain transducers.

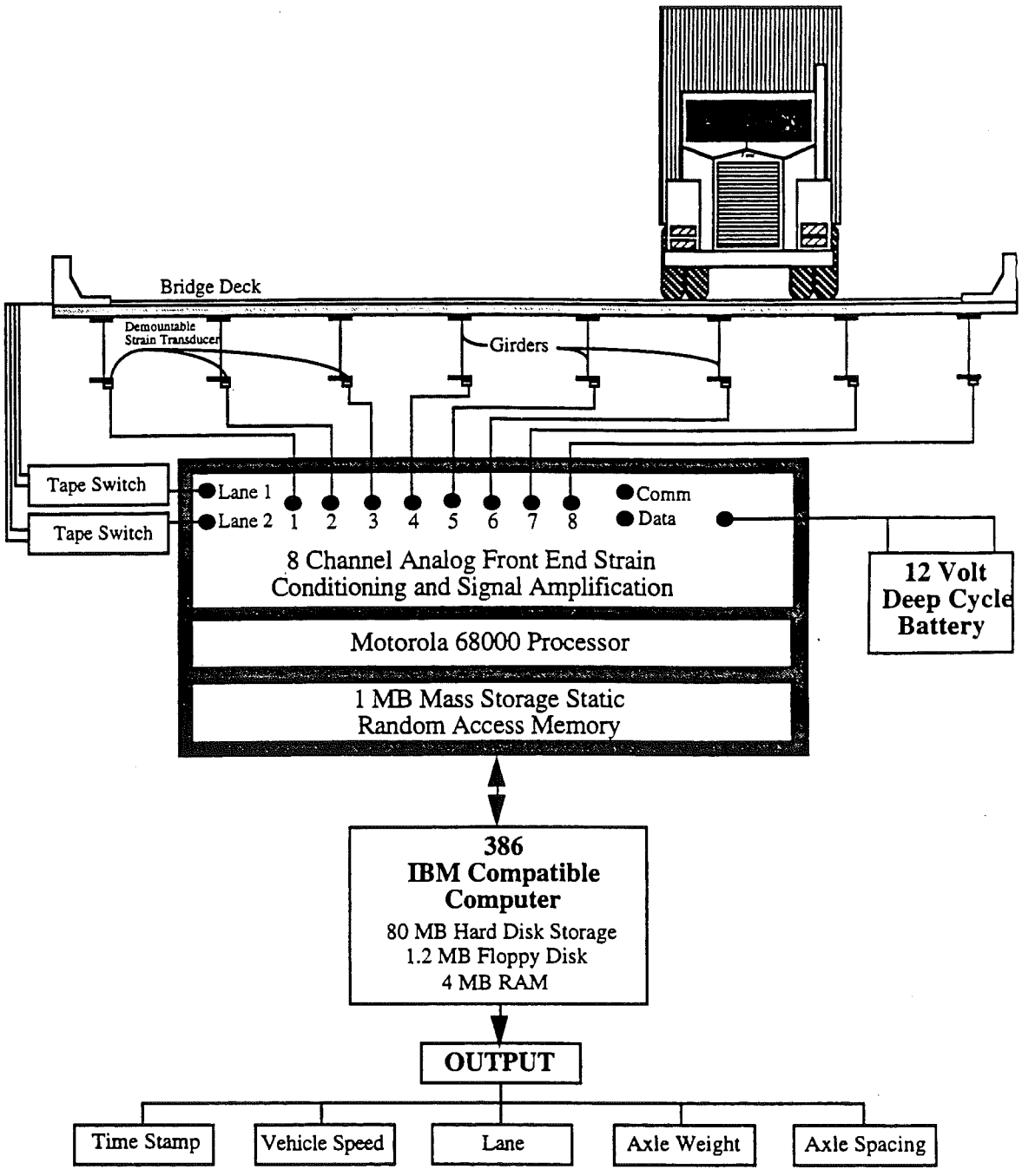

Fig. 5-1 Primary Components of the Current (BWS) Weigh-in-Motion System.

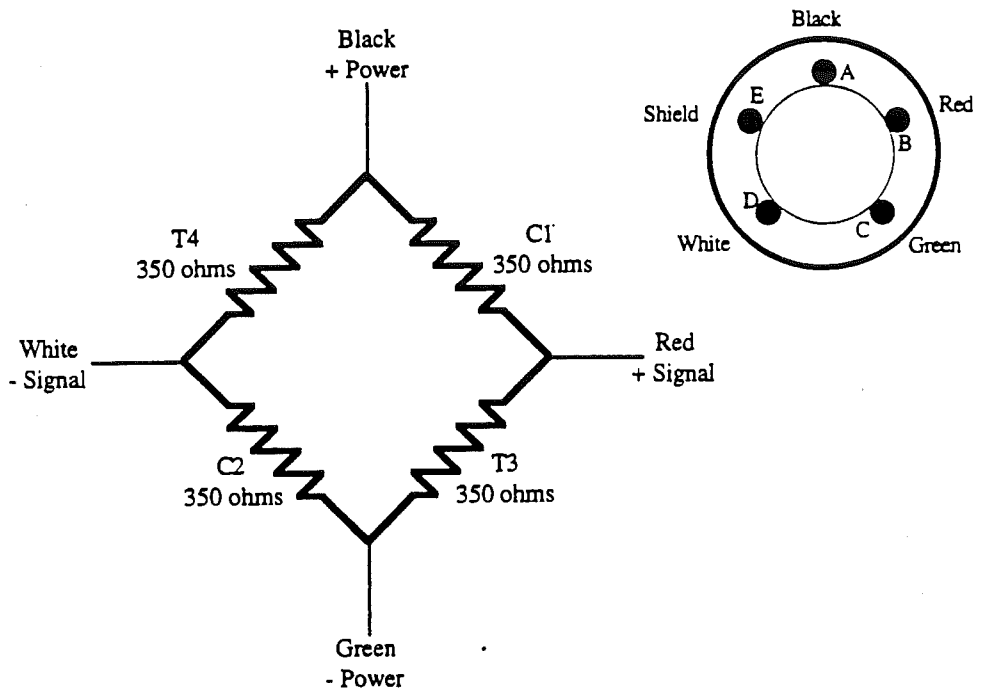

Fig. 5-2. Schematic of Strain Transducer Used in the WIM System.

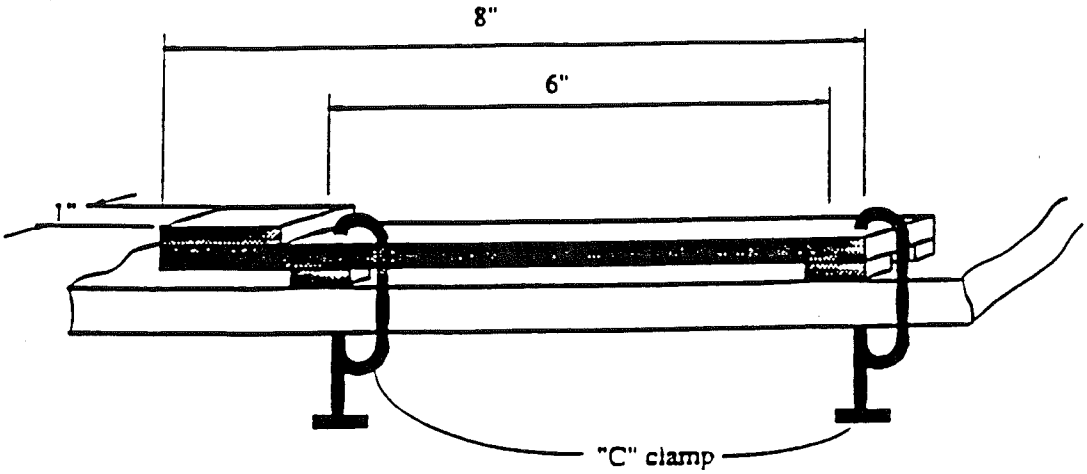

Fig. 5-3. Demountable Strain Transducer Mounted to the Lower Flange.

Tape switches consist of two metallic strips that are held out of contact in the normal condition. As a vehicle wheel passes over the tape it forces the metallic strips into contact and grounds a switch. If

a voltage is impressed across the switch, a signal is obtained at the instant the vehicle crosses the tape. This signal is fed to a computer whereby the speed, axle spacing and number of axles are determined. The tape switches are placed perpendicular to the traffic flow and used to trigger the strain data collection. All cables used to connect tape switches and strain transducer to the AFE are five pin wire cables.

The major problem with tape switches is their vulnerability to damage by moving traffic, in particular if the pavement is wet. Various alternative devices were considered. Infrared sensors were purchased by the project team to replace the tape switches. The infrared system consists of a source of infrared light beam and a reflector. Source of light is installed on the side of the road. Reflector is installed in the center of the traffic lane. However, the problem of their vulnerability to damage by moving traffic has not been resolved. The infrared system is more difficult to install and truck can easily move the reflector and interrupt the operation (light beam must be aligned).

5.3 Data Acquisition Systems by Krenz Electronics

The data acquisition unit by Krenz Electronics, transient recorder - model No.TRC 6410, is designed for a maximum of six Analog/Digital modules, each with 4 channels. The unit used in this project is operating with 8 channels with range 100mV to 20V. The sampling rate is controlled externally. The output signal can be received in several ways: analog display of the signals on an oscilloscope (serial or parallel), analog output on a x/y or y/t plotter (serial or parallel), or digital data output to computer. The unit is connected to a dedicated portable computer which serves as the means of communication. Structural response is measured by recording the accelerations (acceleratorometers are placed on lower flanges of bridge girders). The AC power is provided by a portable generator. The main components of the system are shown in Fig. 5-4.

5.4 Data Acquisition System by the SoMat Corporation

The SoMat Corporation system for Strain Gage Module is shown in Fig. 5-5. It includes a power/processor/ communication module, 1 Meg CMOS extended memory unit, and 8 strain gage signal conditioning modules. The system is designed to collect strains through 8 channels in both attended and unattended modes with range 2.1 mV to 12.5 mV. A second notebook computer is used to communicate with the SoMat system for command regarding data acquisition mode, calibration, initialization, data display, and downloading of data. The SoMat system has been configured specifically for the purpose of collecting stress/strain histories and statistical analysis for highway bridges. This is possible due to the modular component arrangement of the system.

The data acquisition system consists of five major components totaling 12 modules - eight strain transducer signal conditioning modules and four for Battery pack, Power/Communications, 1MB CMOS Extended Memory. and Model 2100 NSC 80180 Processor (see Fig. 5-5). Regulated power is supplied by a rechargeable 11.3 - 13.4 volt electrically isolated DC - DC converter. This unit powers all modules as well as providing excitation for strain transducers. Serial communications via RS 232C connector and battery backup for memory protection is provided by the Power/ Communications module. An Extended Memory Module of 1 megabyte high speed low power CMOS RAM with backup battery for data protection is included for data storage. 8 strain gage conditioning modules each provide 5 volt strain transducer excitation, internal shunt calibration resistors, and an 8 bit analog to digital converter.

Strain measurement range is ± 2.1 mV minimum and ± 12.5 mV maximum. The Processor module consists of 32 kilobytes of programmable memory and an NSC 80180 high speed processor capable of sampling data in simultaneous mode resulting in a maximum sampling rate of 3000 Hz. Communication to the PC is via RS 232C at 57600 baud. Data acquisition modes include time history,

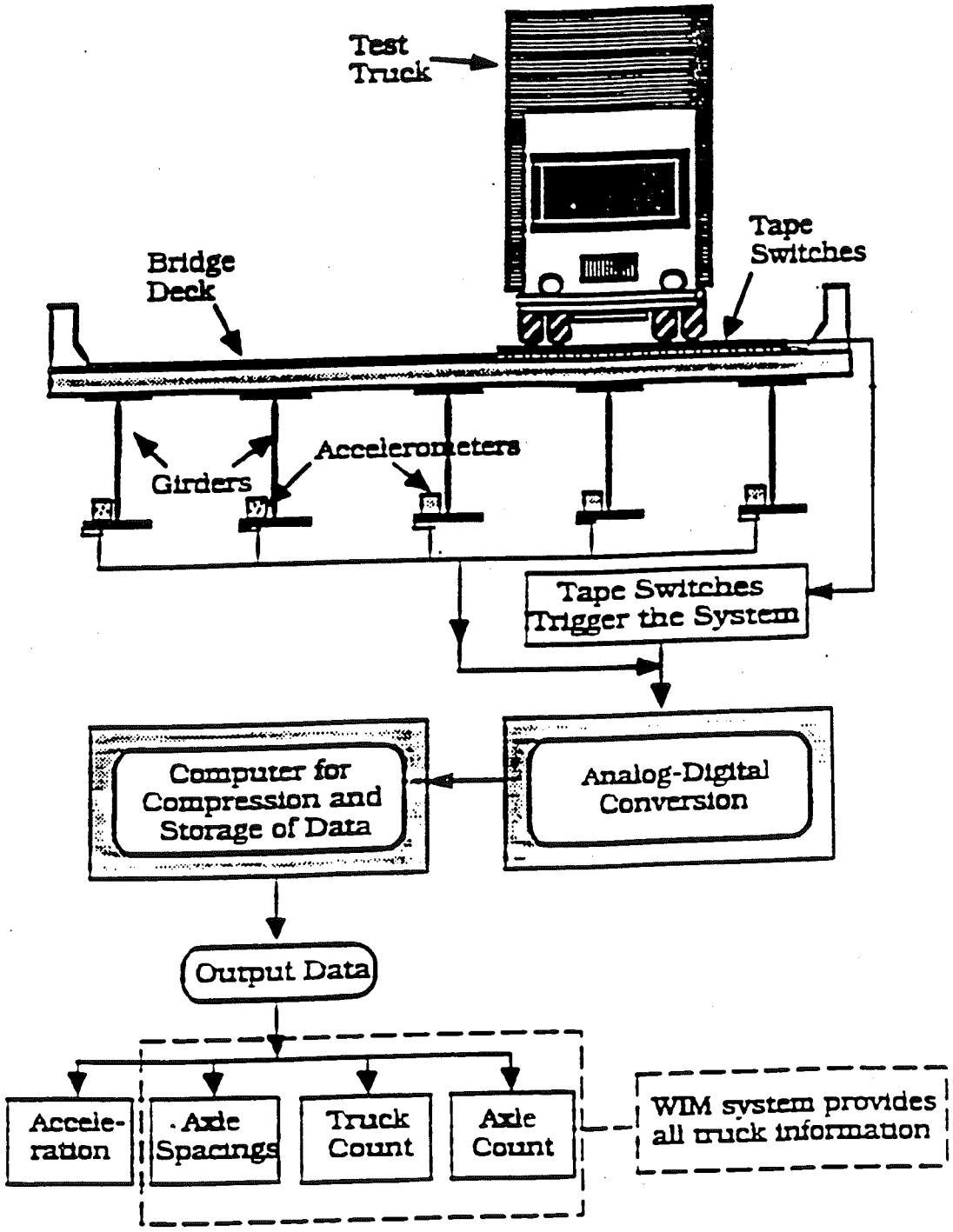

Fig. 5-4. Primary Components of the Dynamic Load Measurement System (Krenz Electronics).

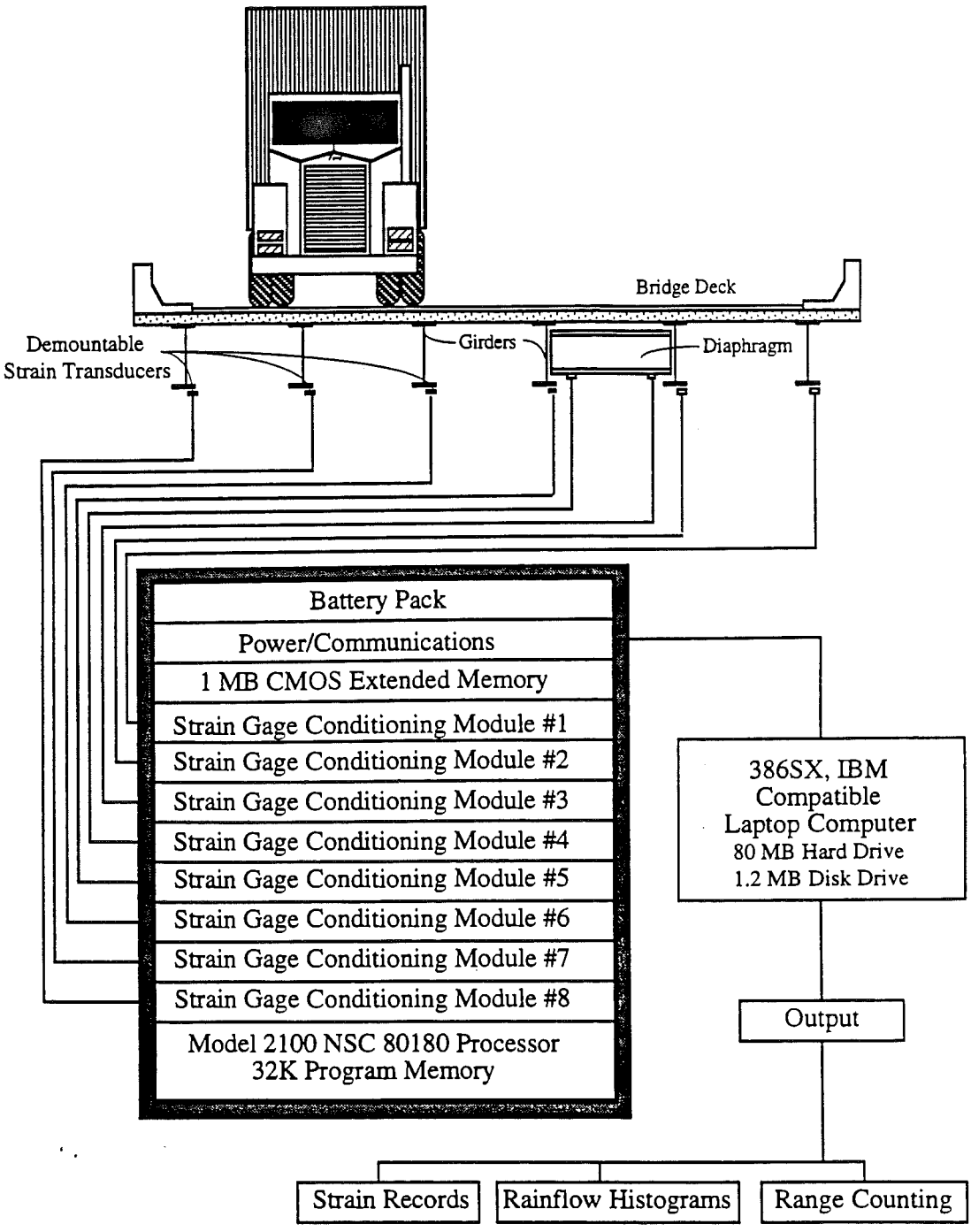

Fig. 5-5. Components of Strain Data Acquisition System by SoMat, Inc.

burst time history, sequential peak valley, time at level matrix, rainflow matrix, and peak valley matrix. Following collection, data is reviewed and downloaded to the PC hard drive for storage, processing analysis and plotting.

5. 5 Other Equipment

Bridge Weighing System, Krenz Electronics system and SoMat system are transported in the commercial van, dedicated to bridge testing.

Three other available data acquisition systems were considered in this study. Two of the reviewed systems were developed by TestConsult-CEBTP (Centre Experimentale de Recherches et d'Etudes du Batiment et des Travaux Publics, France) and the Main Roads Department in Australia. The objective of the investigation was to evaluate the efficiency of the available systems in measurement of truck loads. Because of excessive cost, these systems were not purchased for the project.

5.5.1 Electronic Theodolite

The bridge monitoring system was originally developed in France by the CEBTP. The system measured deflections of the bridge structures and uses a video camera and a target to measure deflection optically. The camera is focused on the a reflective target which is fixed to the bridge. The target is a rectangular board. The upper half of the target is white and reflective, and the lower half is black. Theodolite measures the ratio of black to white by counting the number of pixels in each half. Any vertical movement results in a change in this ratio, and it is converted into a change in output voltage. The system has no inertia, and it can respond to dynamic and static deflections. Static component can be separated from the dynamic oscillation.

An example of the results of measurements are shown in Chapter 7. The major problem with using this equipment is a high cost. One unit costs over $10,000 and it can take measurements only at one point at the time.

5.5.2 Fleximeter

The fleximeter used in this study was also provided by the CEBTP. Fleximeter is in effect a rotary potentiometer with a spring loaded return. An invar wire is wound around the shaft and attached to the bridge by a kevlar cord. A heavy steel base holds the unit down, and vertical movement of the bridge deck thus causes rotation of the shaft, varying output voltage. The use of kevlar and invar for the connection minimizes drift caused by temperature and elasticity in the system. Since this is a mechanical system, it has inertia and will thus filter out most dynamic components, following only static or quasi-static deflections.

The output from this device is recorded on a portable computer equipped with a data acquisition card. Triggering of the acquisition was taken from the tape switches used by the WIM system.

The system was not used in further work because:
- result were not more accurate than strain transducer readings
- each girder required a separate device, which would be prohibitively expensive
- operation would require one operator per girder

5.5.3 Culway

The Culway system was developed by the Main Roads Department, Western Australia, in conjunction with the Australian Road Research Board. The system uses existing road culverts as dynamic scales to measure the weight of axles as they pass over the culvert.. soil The system needs a culvert with high strata above to filter dynamic effects. It has a distinct advantage that on a relatively smooth

road, the soil will dump out most of the dynamic responses which were evident in the bridge weighing system.

Culway weighs an axle of a vehicle as it crosses a culvert, by measuring the bending strain caused by the axle load on the culvert. The basic elements of a Culway, apart from a suitably sized culvert, are data acquisition system, portable computer, strain gages and axle sensors. Four strain transducers, which are attached to the culvert roof, are constantly monitored by the data acquisition system, which responds to signals from the axle sensors. The mechanical strain amplifiers must be positioned to obtain the maximum strain reading in the culvert for any vehicle traveling in the lane being monitored. The strain measurements in the concrete culverts due to axle loading are small, in the order of 1 to 50 microstrain (1 microstrain = 0.000001 in/in). In order to produce a more powerful signal, mechanical and electronic amplification is used.

The axle sensors detect the presence of a vehicle and are located at a fixed spacing of about 30 ft, so that axle presence and number can be detected and vehicle speed computed. Those sensors are made of galvanized or stainless steel strip separated by neoprene foam tap pads, all enclosed in a waterproof cloth tape.

The micro-computer based data acquisition system is specially set up to perform the tasks required in the Culway operation. A portable computer is used to retrieve and process the results. The accuracy of system is estimated at about 10% for GVW.

The Culway system was not used in further study because:

- concrete culvert with the required parameters is difficult to find
- accuracy is not better than using strain transducer
- dynamic effects are filtered out and can not be considered.

The results of these pilot studies were supposed to be published by the Ontario Ministry of Transportation but they not done it yet.

6. SELECTED BRIDGE SITES

Bridges were selected by the Project Team in cooperation with the Michigan DOT staff. Culway system was tried on a culvert located in Ontario, Canada, with the assistance provided by the Ontario Ministry of Transportation. Important factors considered in the selection process included accessibility from the ground, availability of space to work, low dynamic effects and placement of tape switches or infrared sensors.

Seven structures were selected as are listed below together with data describing the traffic condition. There is even the annual average 24-hour traffic volumes (ADTT) and annual average 24-hour commercial traffic volumes (CADT). The data is for both directions of traffic and has been provided by MDOT-Transportation Planing Department. The location of the bridges is shown in Fig. 6-1, 6-2, 6-3, and 6-4.

1. 23/HR - US-23 over the Huron River in Ann Arbor, Michigan.
   Michigan State Bridge ID: R01-81074
   ADTT: 59,000
   CADT: 4,200 - 7.1 percent

2. 14/NY - M14/US-23 over the New York City Railroad in Ann Arbor, Michigan.
   Michigan State Bridge ID: R01-81103
   ADTT: 65,000
   CADT: 4,300 - 6.6 percent

3. 94/JR -I-94 over Jackson Road in Ann Arbor, Michigan.
   Michigan State Bridge ID: S01-81062
   ADTT: 30,000
   CADT: 4,700 - 15,7 percent

4. 94/PR - I-94 over Pierce Road in Grass Lake, Michigan.
   Michigan State Bridge ID: S03-81104
   ADTT: 37,000
   CADT: 8,400 - 22,7 percent

5. 23/SR - US-23 over the Saline River in Milan, Michigan.
   Michigan State Bridge ID: B05-58033
   ADTT: 31,000
   CADT: 4,400 - 14,2 percent

6. 75/BC - I-75 Northbound over Bay Creek Road in Luna Pier, Michigan.
   Michigan State Bridge ID: S14-58151
   ADTT: 40,000
   CADT: 11,000 - 27.5 percent

On this bridge only measurement for fatigue study was done.

7. WY/94 - Wyoming Road over I-94 in Detroit, Michigan.
   Michigan State Bridge ID: S36-82022
   ADTT: 122,000
   CADT: 410 - 0.3 percent

On this bridge only WIM was done.

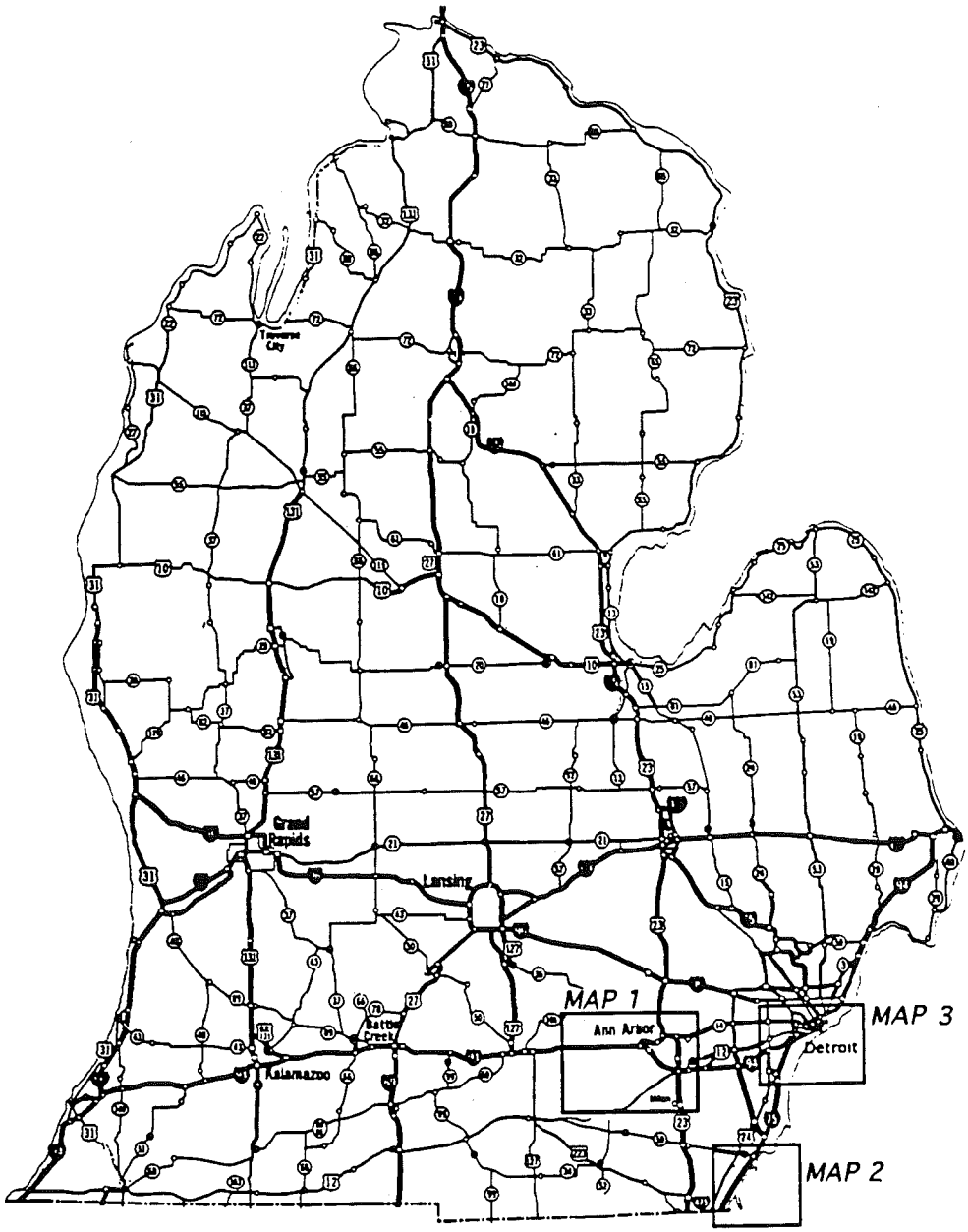

Fig. 6-1. Lower Michigan Location Map Key of Selected Bridges in Southeastern Michigan.

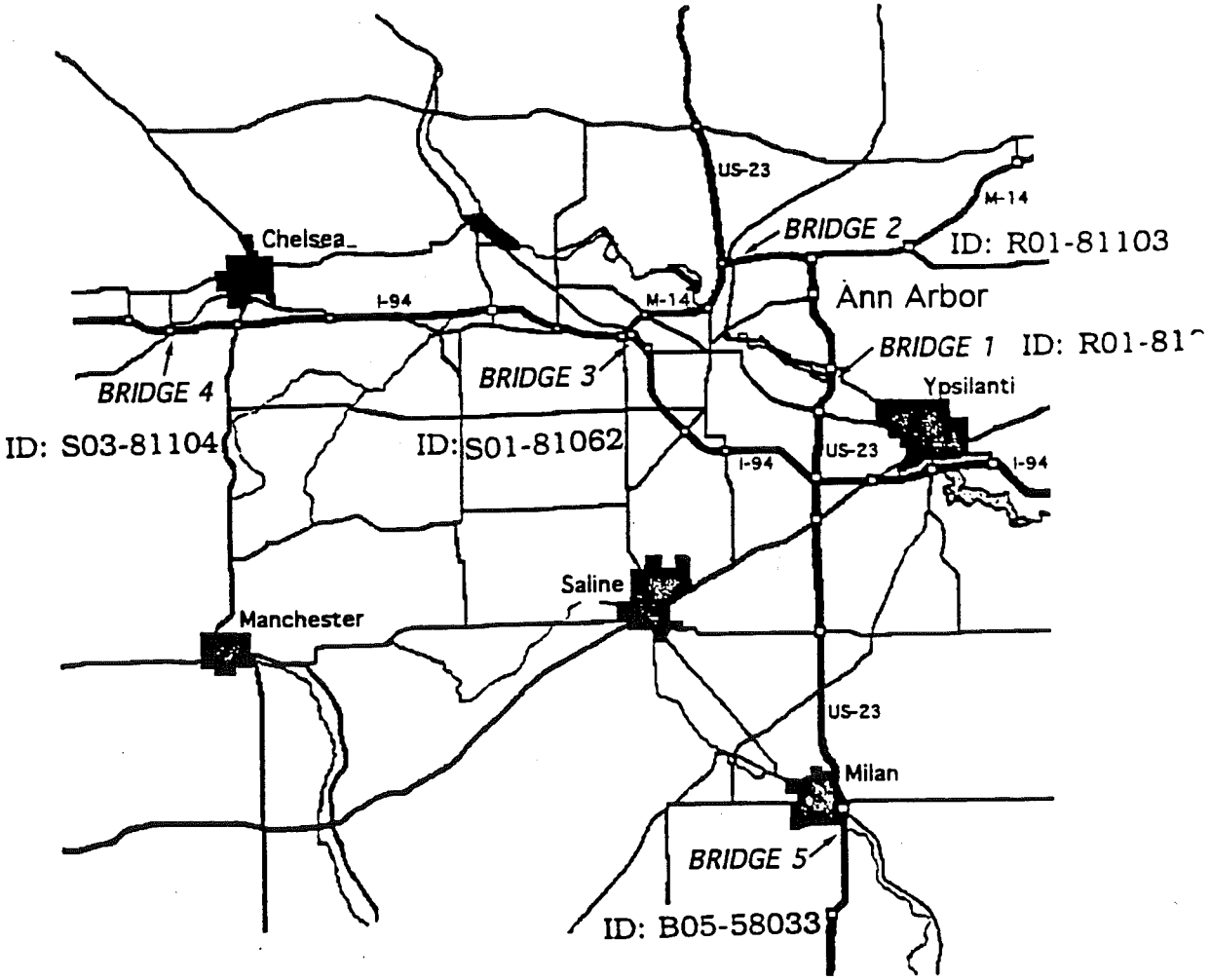

Fig. 6-2. Location Map 1 of Bridges 1-5 in Jackson and Washtenaw Counties.

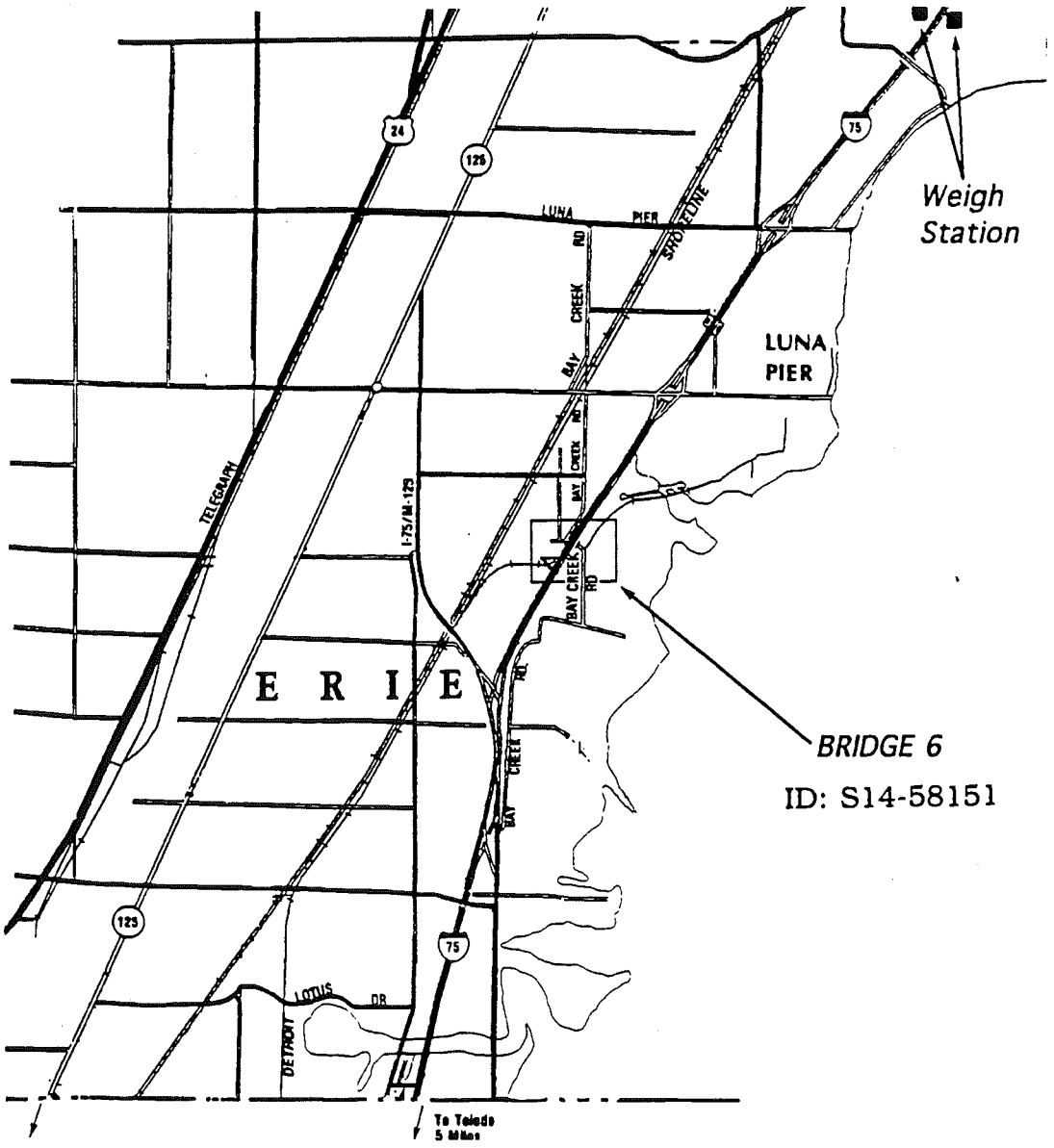

Fig. 6-3. Location Map 2 of Bridge 6 in Monroe County.

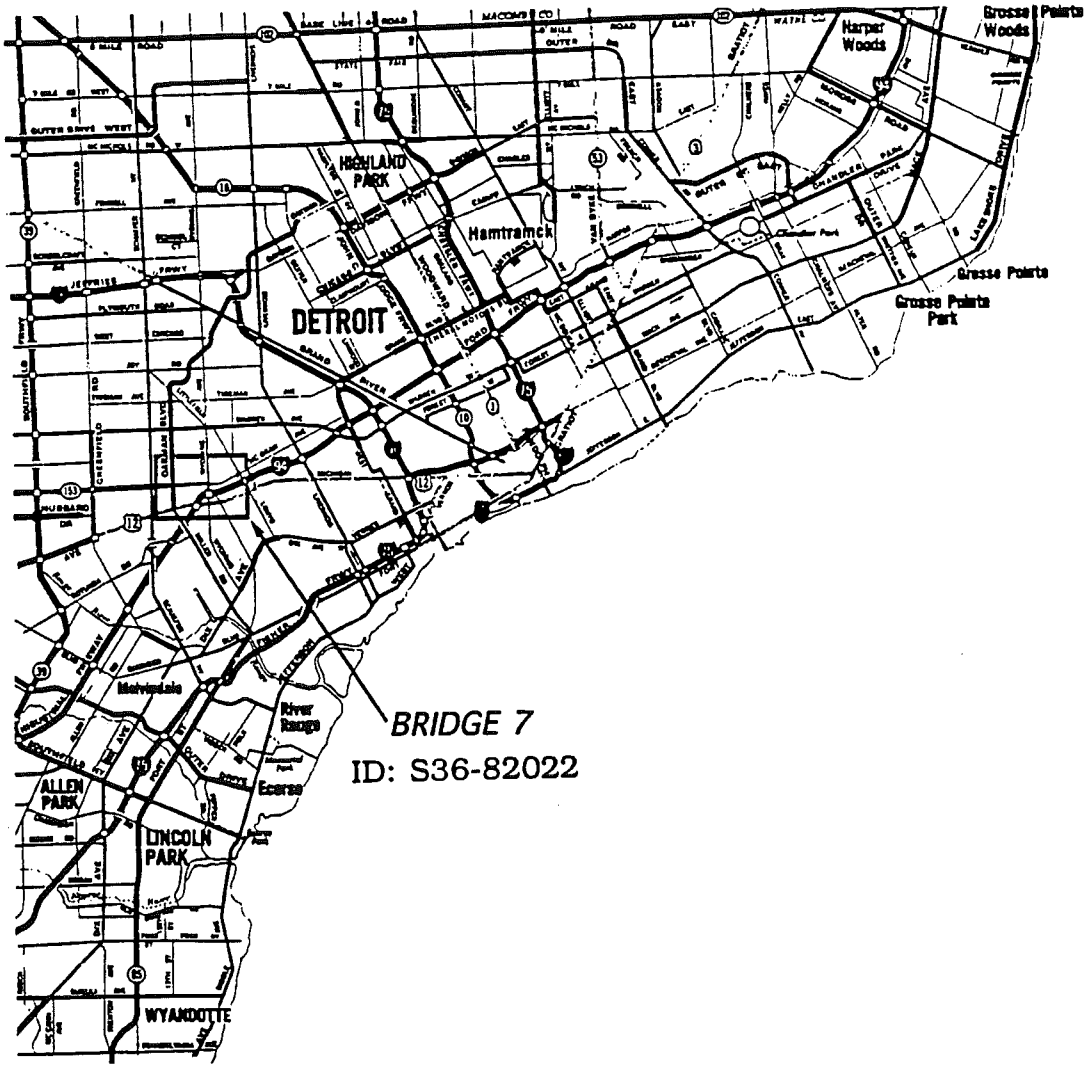

Fig. 6-4. Location Map 3 of Bridge 7 in Wayne County, Detroit Michigan.

6. 1 Bridge 1 (23/HR)

Bridge 1 (23/HR) carries Northbound traffic on US-23 over the Huron River, as shown in Fig. 6-5 and 6-6. The cross section and other details are shown in Fig. 6-7. Measurements were taken in the entrance span (in the direction of traffic). The selected span is 78'-6" long and the width is 35'-11" with a skew of 14^{o} and consists of 6 steel girders spaced at 6'-3".

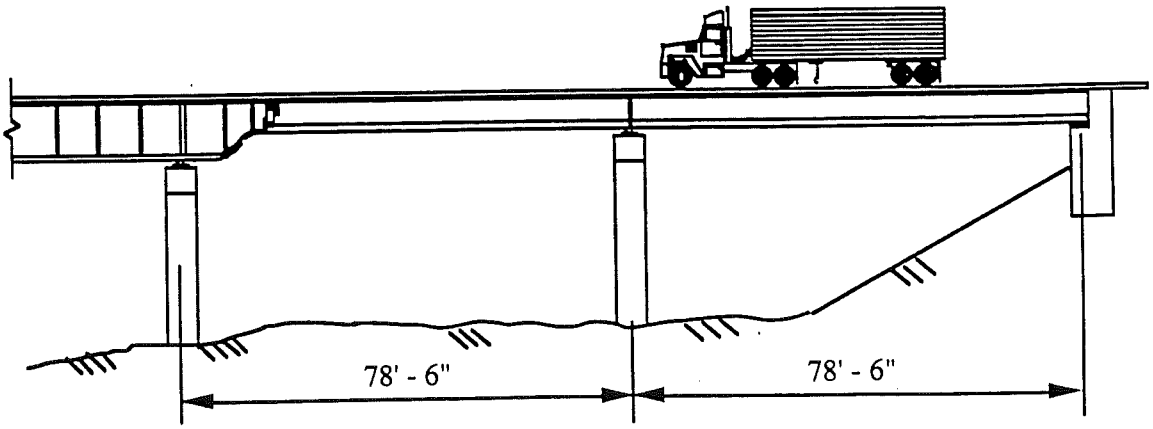

Fig 6-5. Bridge 23/HR, US-23 over the Huron River, Side Elevation.

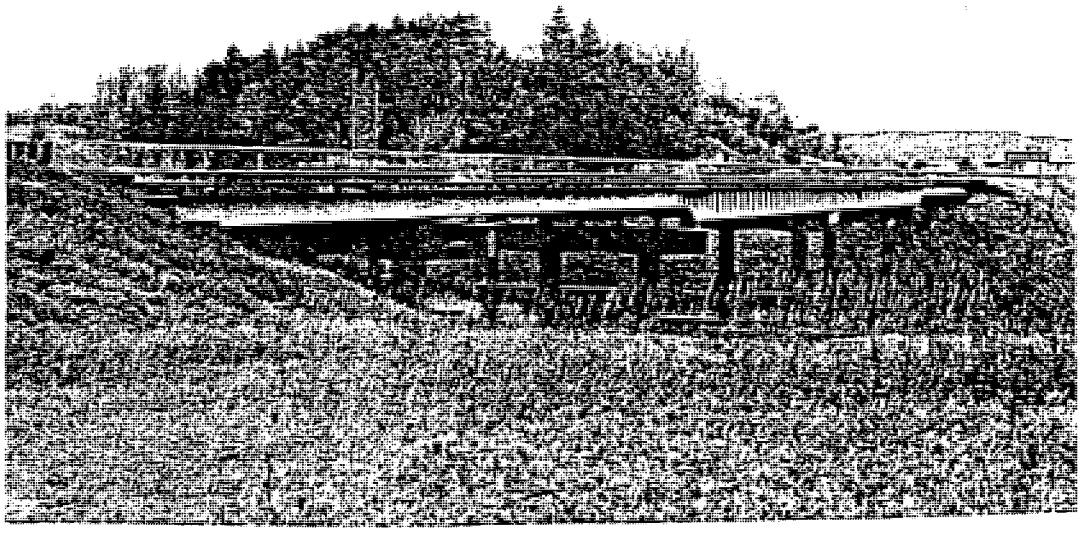

Fig. 6-6. View of Bridge 23/HR, US-23 over Huron River.

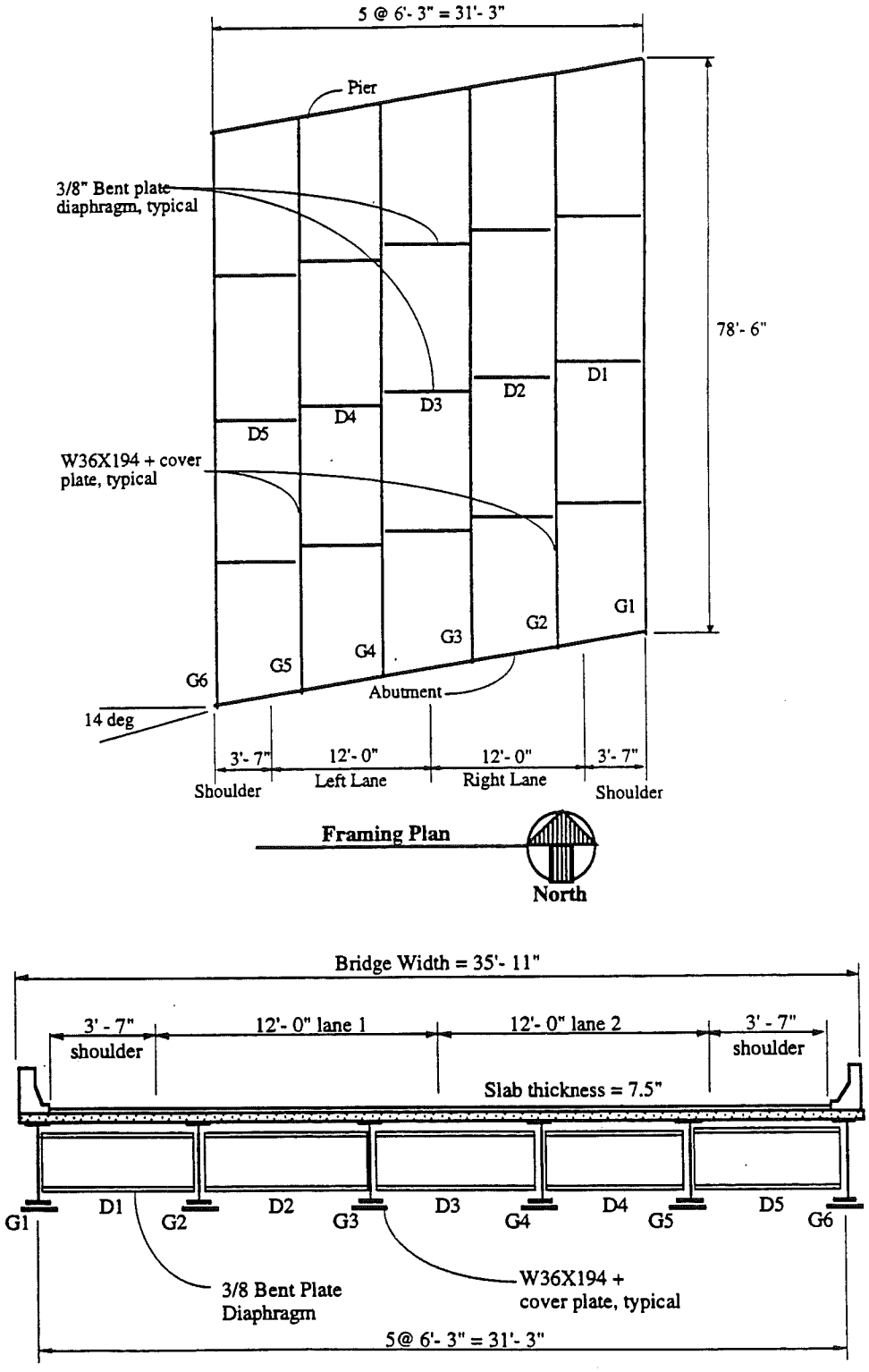

Fig. 6-7, Bridge 23/HR, US-23 over the Huron River. Plan View and Cross Section of Bridge Entrance Span.

6.2 Bridge 2 (14/NY)

Bridge 2 (14/NY), carries Southbound traffic on US-23 and Eastbound traffic on M-14 over the NYC railroad, as shown in Fig. 6-8 and 6-9. The cross section and other details are shown in Fig. 6-10. Measurements were taken in the entrance span (in the direction of traffic). The entrance span is 52'-6" long and the width is 42', with a skew of 25^{o} and consists of 8 steel girders spaced at 6' which are composite with the concrete slab.

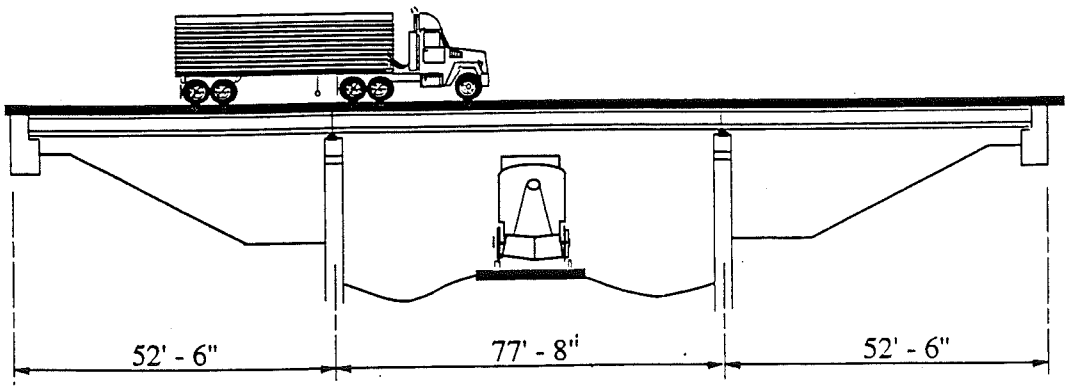

Fig 6-8. Bridge 14/NY, M14/US-23 over the NYC Railroad.
Side Elevation.

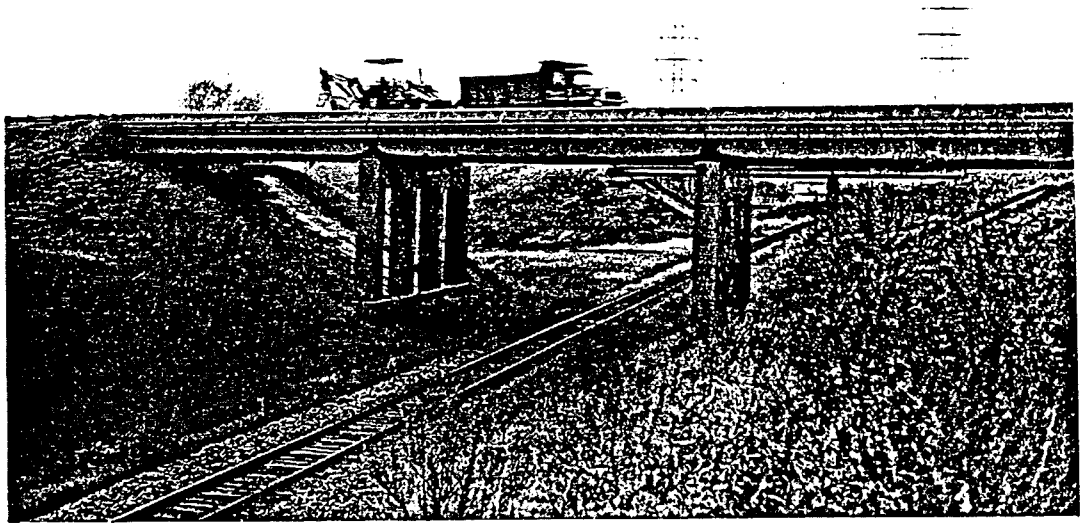

Fig. 6-9. View of Bridge 14/NY, M14/US-23 over NYC Railroad.

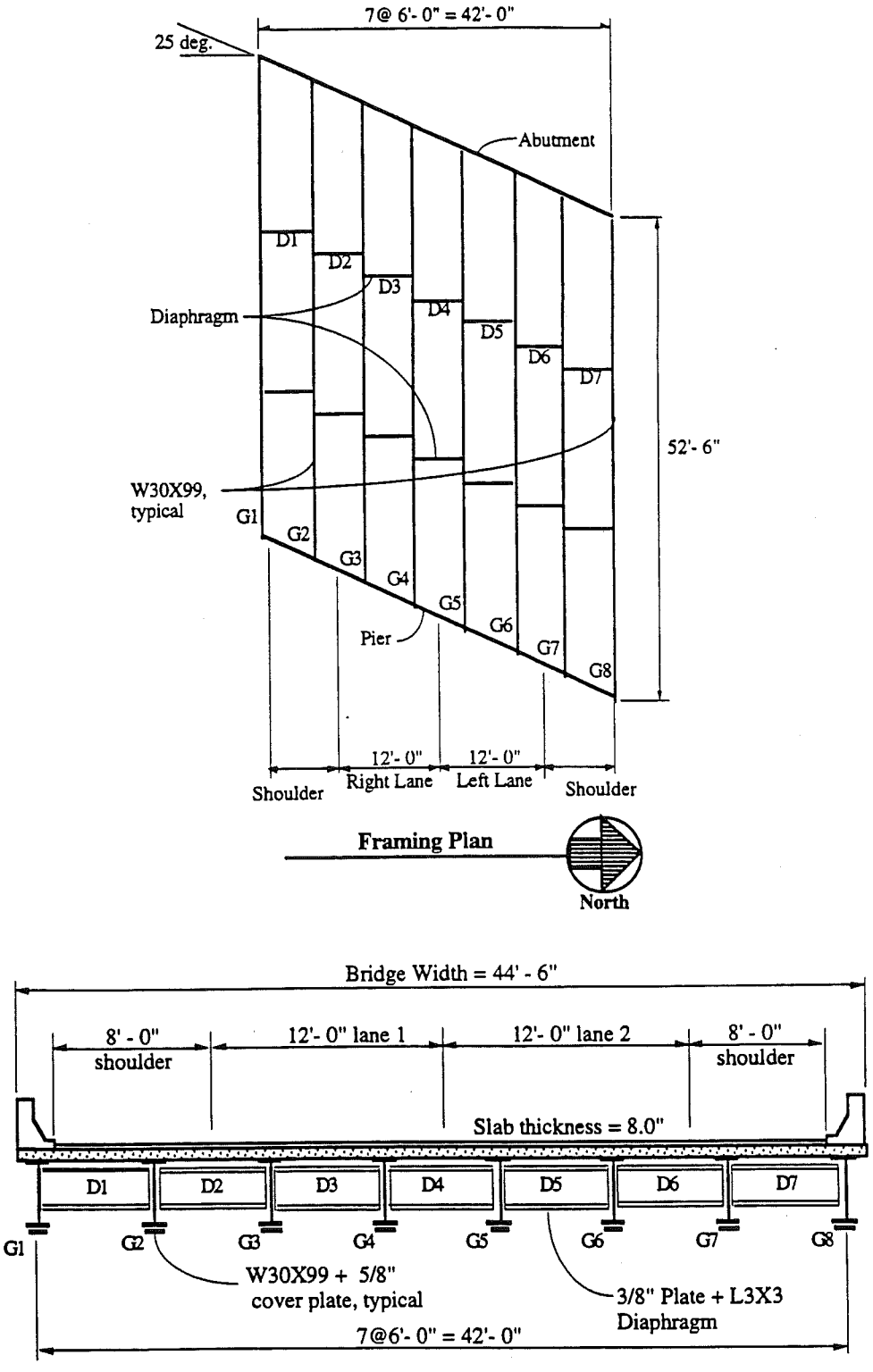

Fig. 6-10. Bridge 14/NY, M-14/US-23 over the NYC Railroad. Plan View and Cross Section of Entrance Span.

6.3 Bridge 3 (94/JR)

Bridge 3 (94/JR) carries Westbound traffic on I-94 over Jackson Road in Ann Arbor as shown in Fig. 6-11 and 6-12. The cross section and other details are shown in Fig. 6-13. Measurements were taken in the entrance span (in the direction of traffic). The selected span is 52'-6" and the width is 47"-8" with a skew of 33° and consists of 9 girders with spacings as shown in Fig. 6-13.

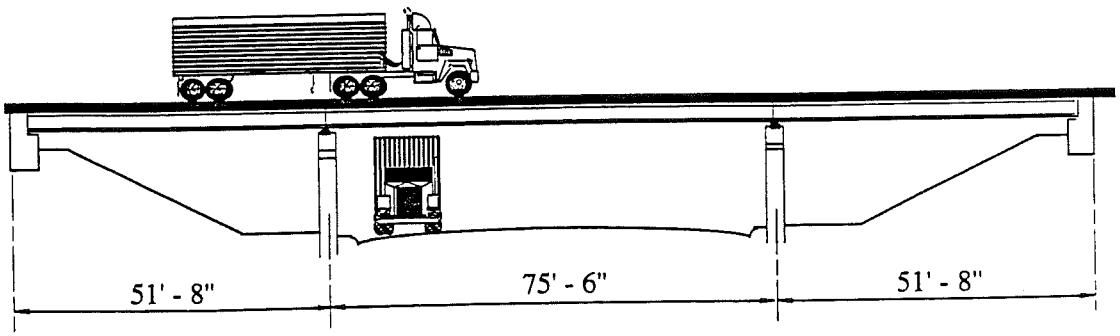

Fig 6-11. Bridge 94/JR, I-94 over Jackson Road, Side Elevation.

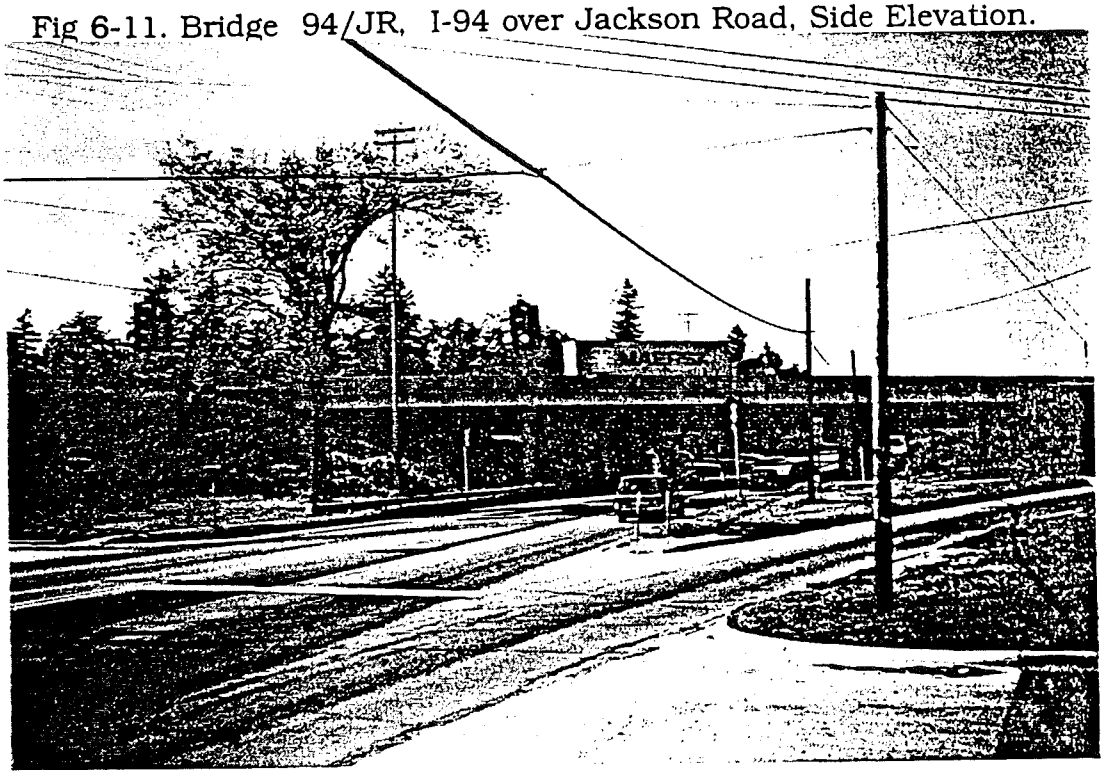

Fig. 6-12. View of Bridge 94/JR, I-94 Westbound over Jackson Road in Ann Arbor.

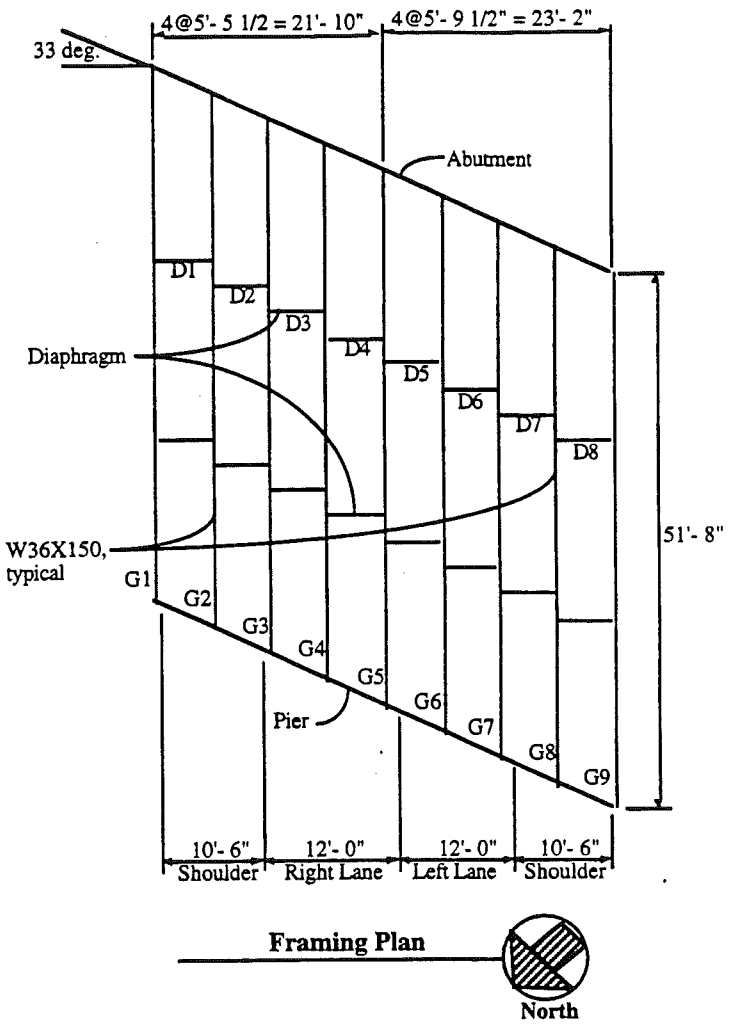

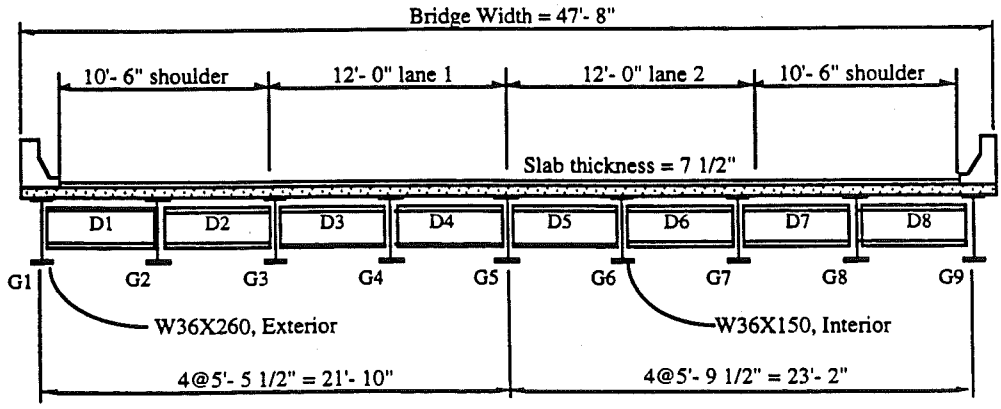

Fig. 6-13. Bridge 94/JR, I-94 over Jackson Road.
Plan View and Cross Section of Entrance Span.

6.4 Bridge 4 (94/PR)

Bridge 4 (94/PR) carries Eastbound traffic on I-94 over Pierce Road near Grass Lake, as shown in Fig. 6-14 and 6-15. The cross section and other details are shown in Fig. 6-16. Measurements were taken in the entrance span (in the direction of traffic). The selected span is 34'-6" and the width is 45' with a skew of 29^{o} consists of 10 girders spaced at 5'.

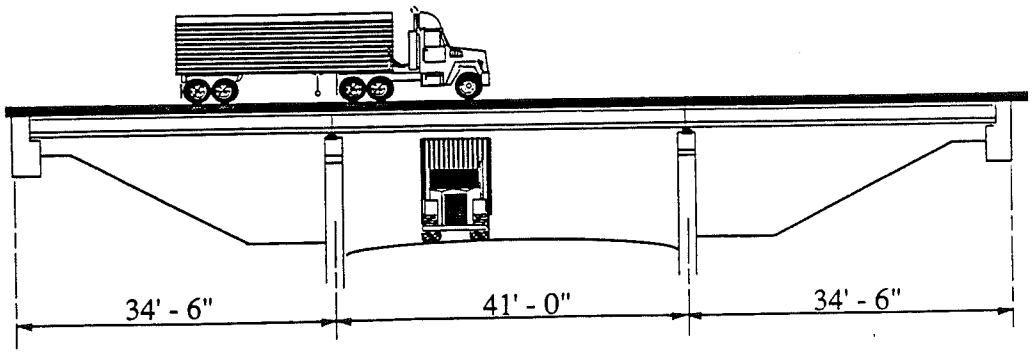

Fig 6-14. Bridge 94/PR, I-94 over Pierce Road, Side Elevation.

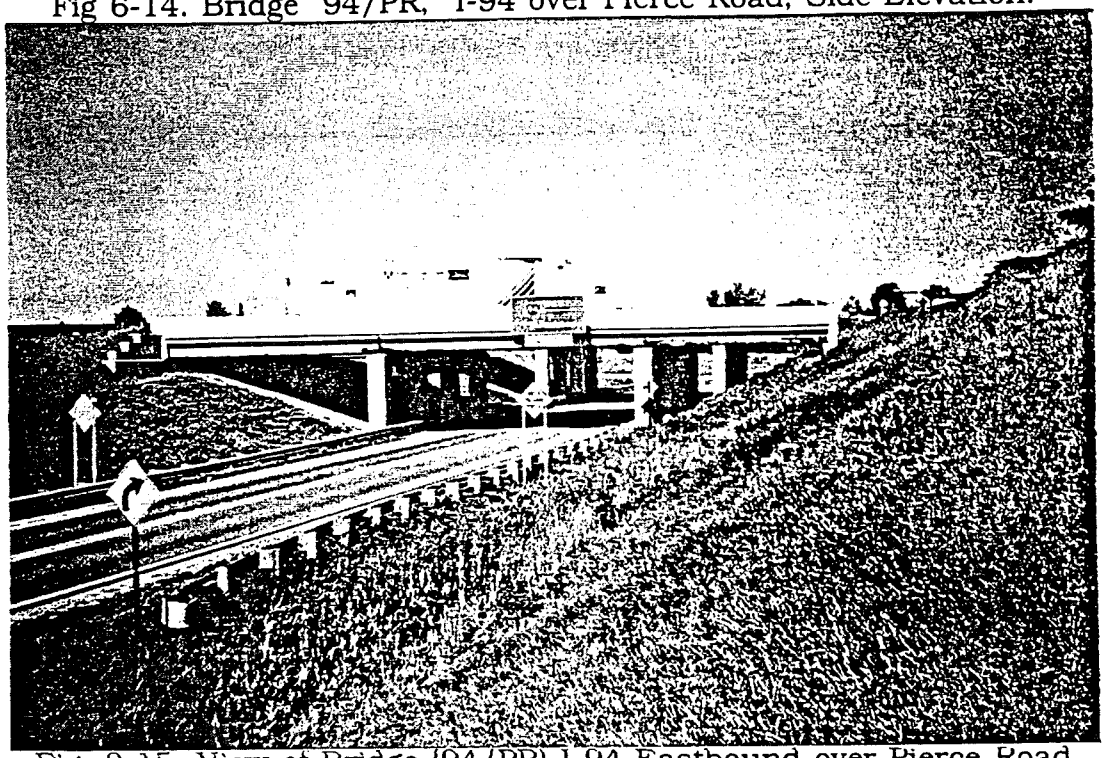

Fig. 6-15. View of Bridge (94/PR) I-94 Eastbound over Pierce Road near Grass Lake.

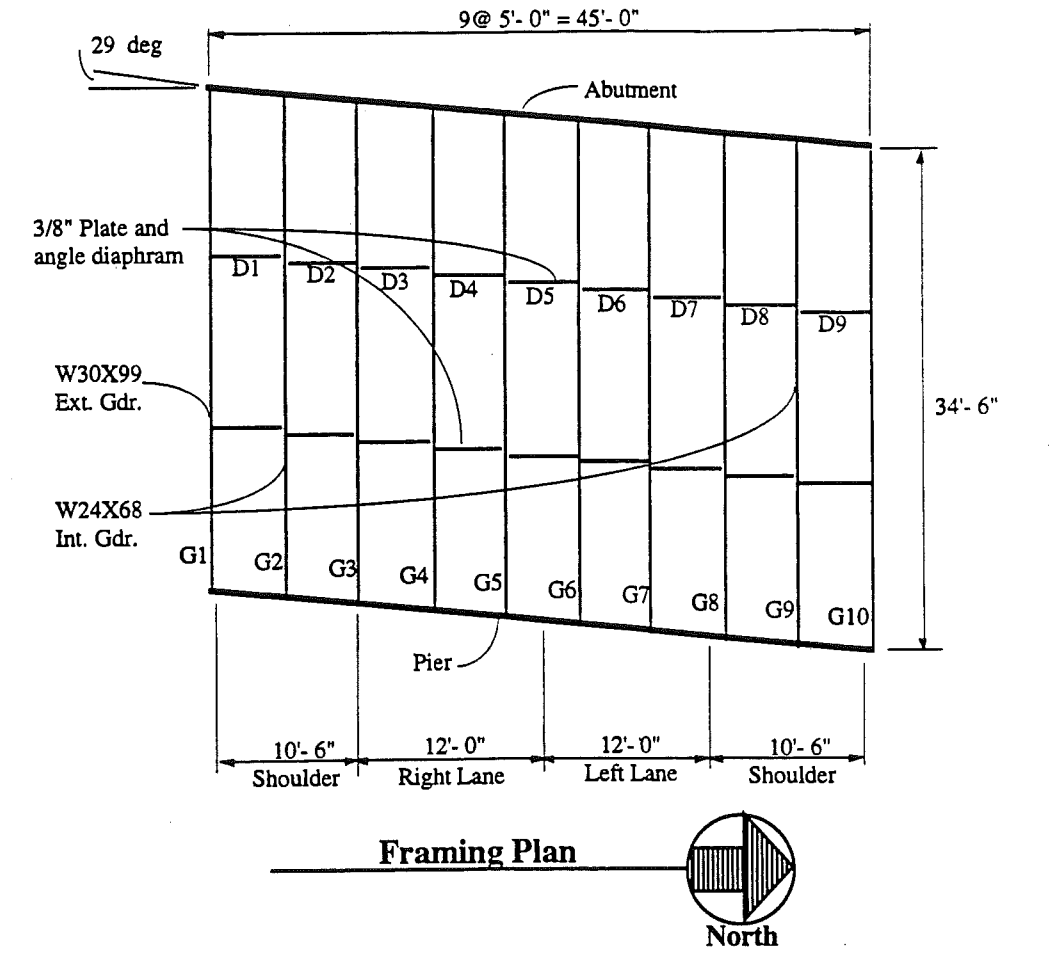

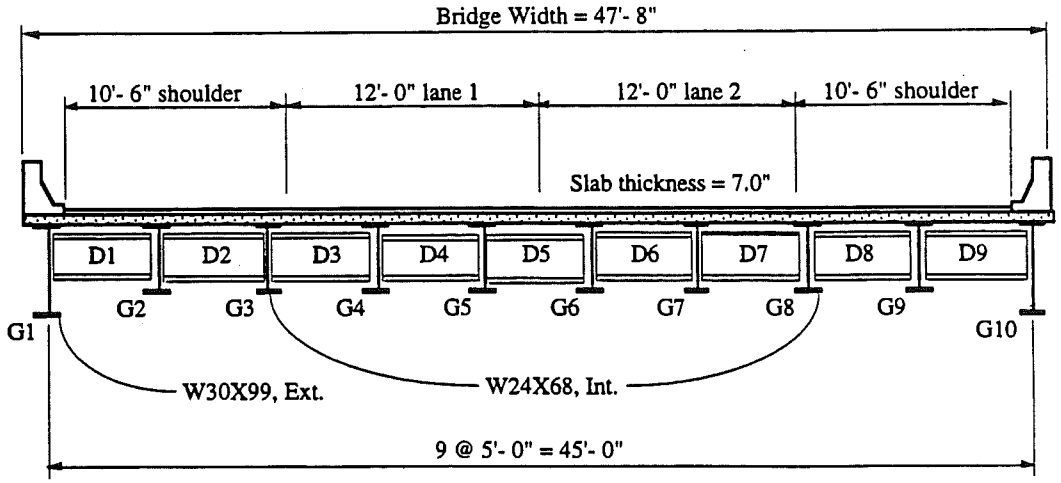

Fig. 6-16. Bridge 94/PR, I-94 over Pierce Road.
Plan View and Cross Section of Entrance Span.

6.5 Bridge 5 (23/SR)

Bridge 5 (23/SR) carries Southbound traffic on US-23 over the Saline River in Milan as shown in Fig. 6-17 and 6-18. The cross section and other details are shown in Fig. 6-19. Measurements were taken in the entrance span (in the direction of traffic). The selected span is 32'-6" and the width is 45', with a skew of 0^{o} and consists of 10 girders spaced at 5'.

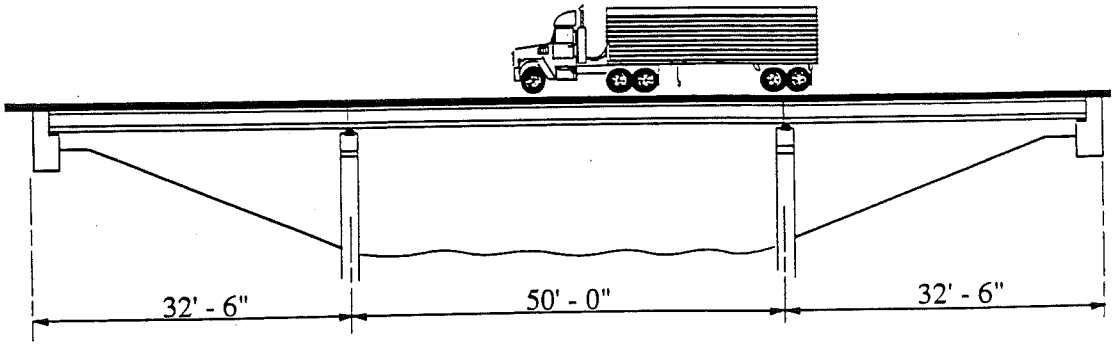

Fig 6-17. Bridge 23/SR over the Saline River. Bridge Side Elevation.

Fig. 6-18. View of Bridge 23/SR Southbound over the Saline River in Milan.

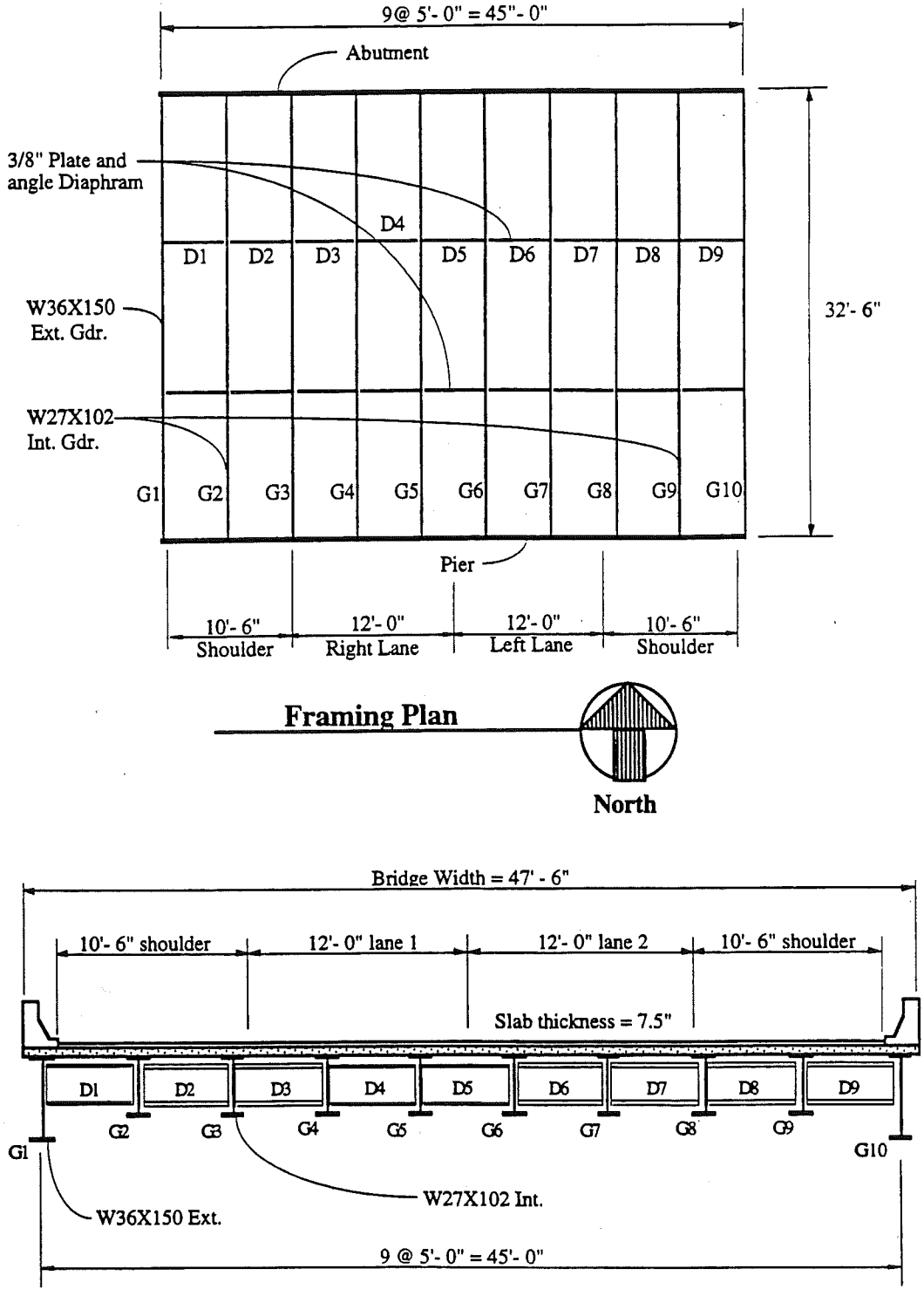

Fig. 6-19. Bridge 23/SR over the Saline River.
Plan View and Cross Section of Entrance Span.

6.6 Bridge 6 (75/BC)

Bridge (75/BC) carries Northbound traffic on I-75 over Bay Creek Road in Luna Pier as shown in Fig. 6-20 and 6-21. The cross section and other details are shown in Fig. 6-22 Measurements were taken in the entrance span (in the direction of traffic). The selected span is 35'-6" and the width is 54' with a skew of 0^{o} and consists of 10 girders spaced at 6'-0".

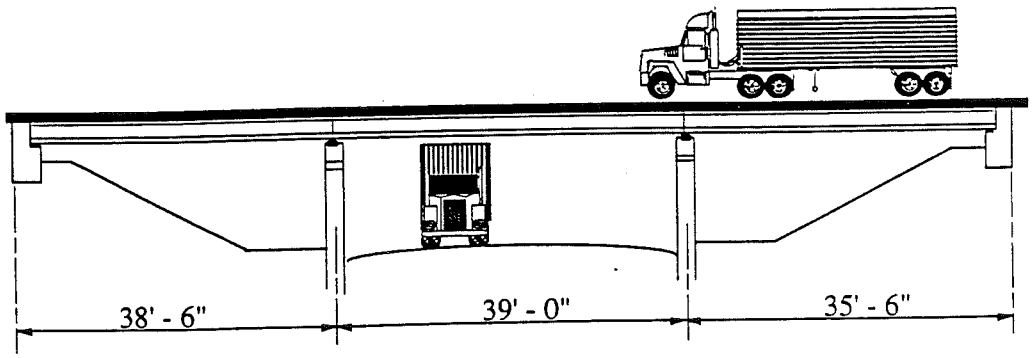

Fig. 6-20. Bridge 75/BC, I-75/Bay Creek Road Bridge Side Elevation.

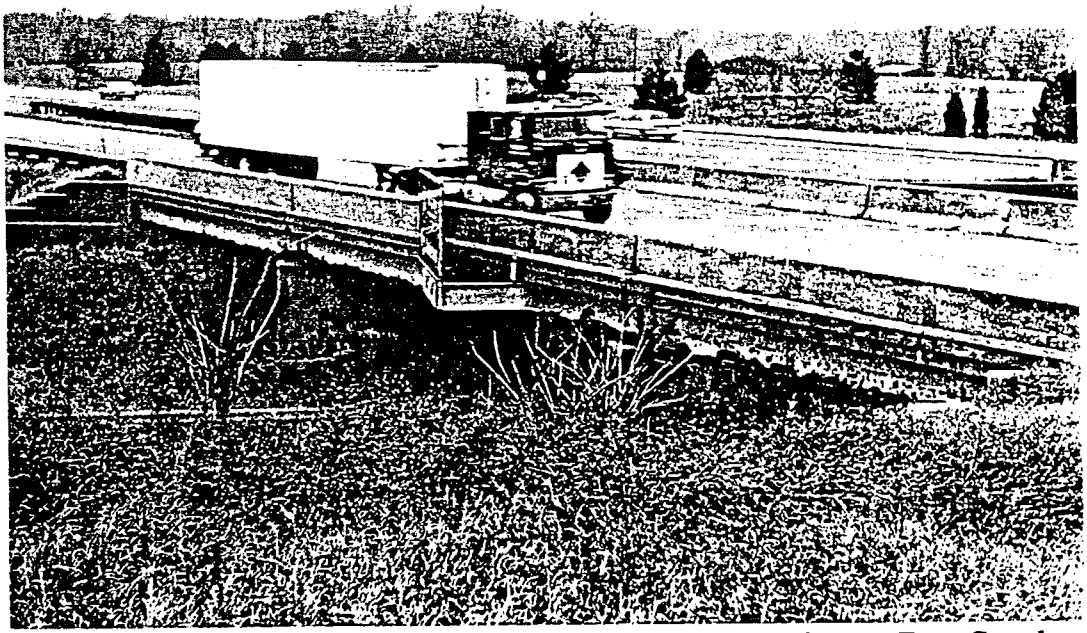

Fig. 6-21. View of Bridge 75/BC, I-75 Northbound over Bay Creek Road in Luna Pier.

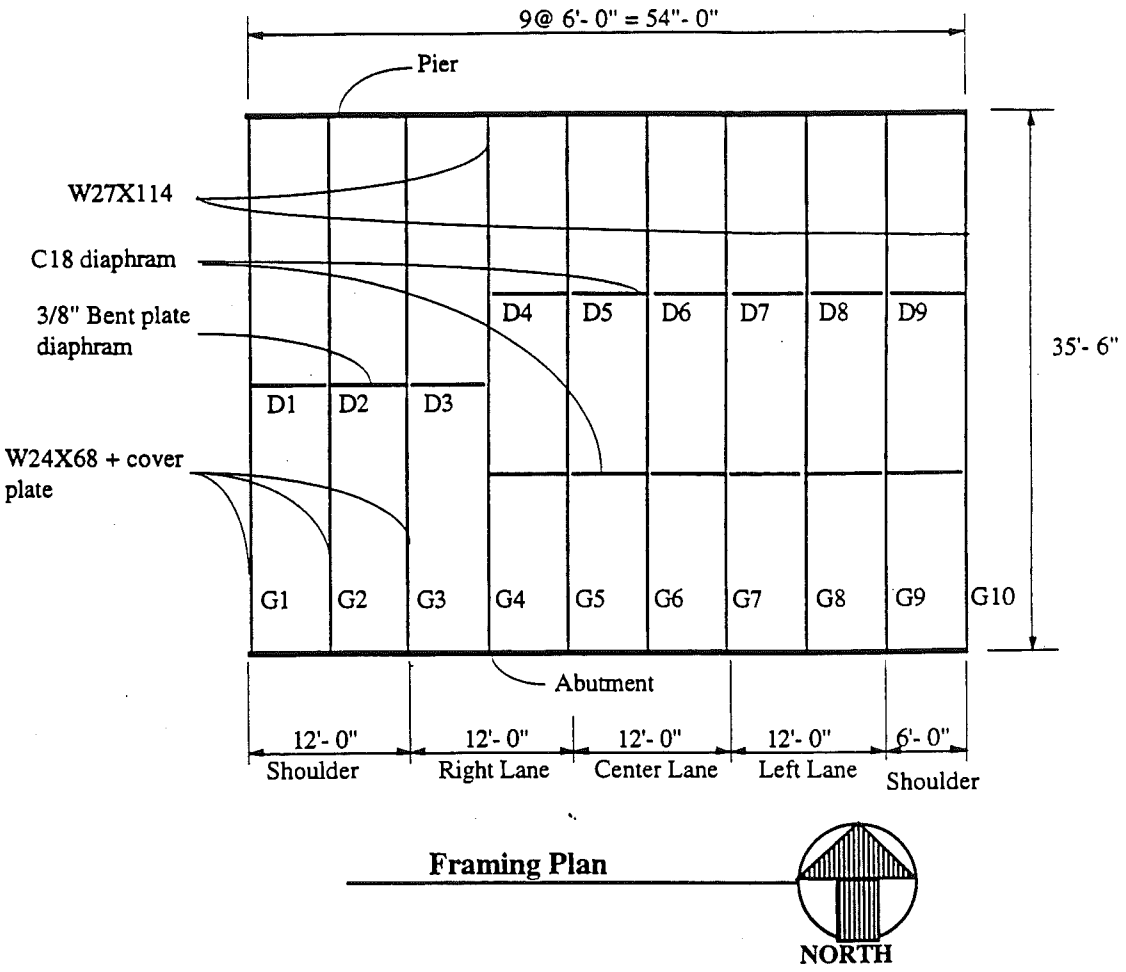

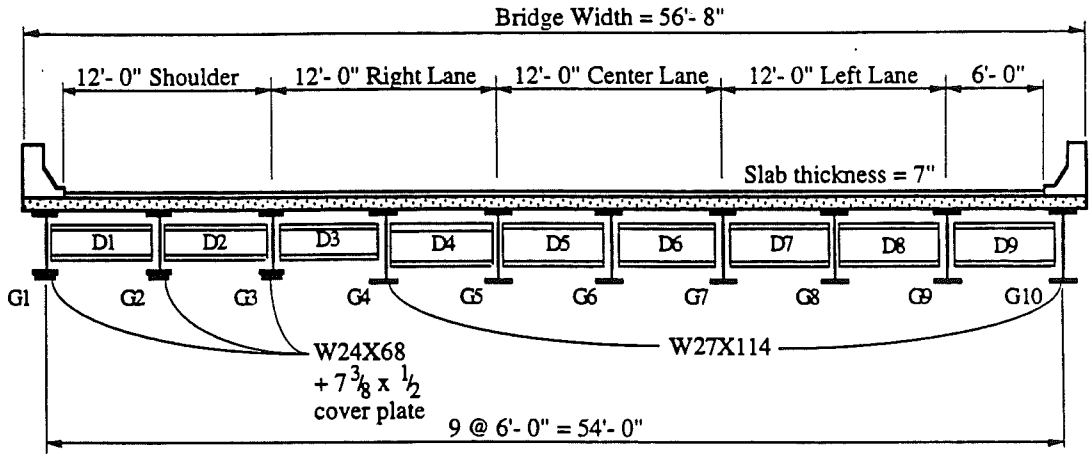

Fig. 6-22. Bridge 75/BC, I-75 over Bay Creek Road. Plan View and Cross Section.

6.7 Bridge 7 (WY/94)

Bridge (WY/94) carries Southbound traffic on Wyoming Road over I-94 in Detroit as shown in Fig. 6-23 and 6-24. The cross section and other details are shown in Fig. 6-25. Measurements were taken in the entrance span (in the direction of traffic). The selected span is 32' and the width is 41' with a skew of 18^{0} and consists of 9 girders spaced at 5'-1 1/2".

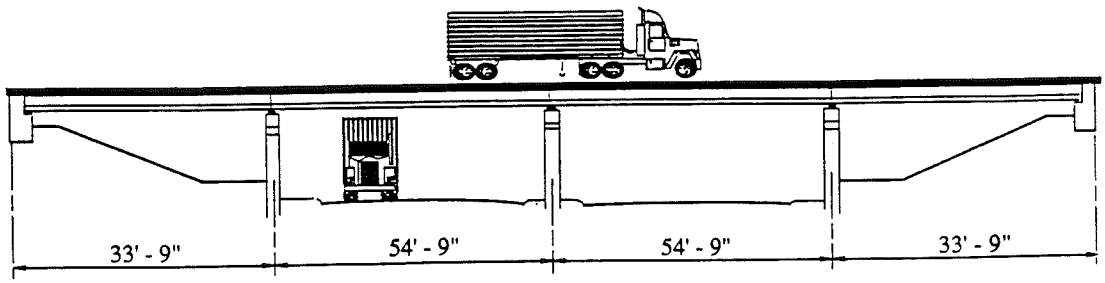

Fig 6-23. Bridge WY/94, Wyoming Road over I-94, Side Elevation.

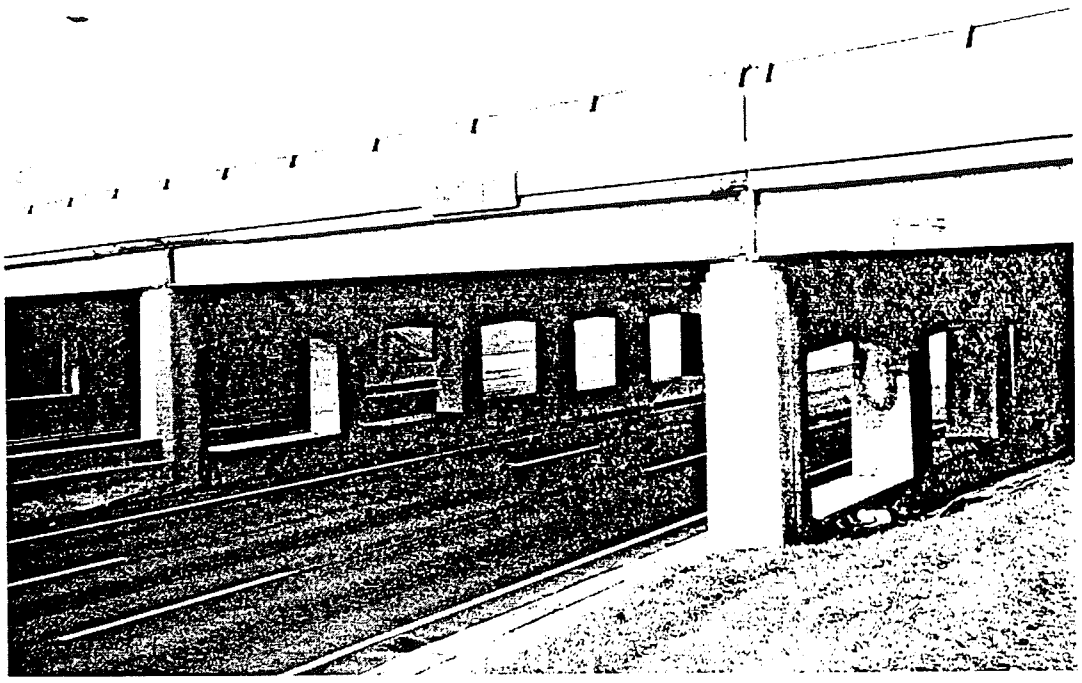

Fig. 6-24. View of Bridge WY/94, Wyoming Road Southbound over I-94 in Detroit.

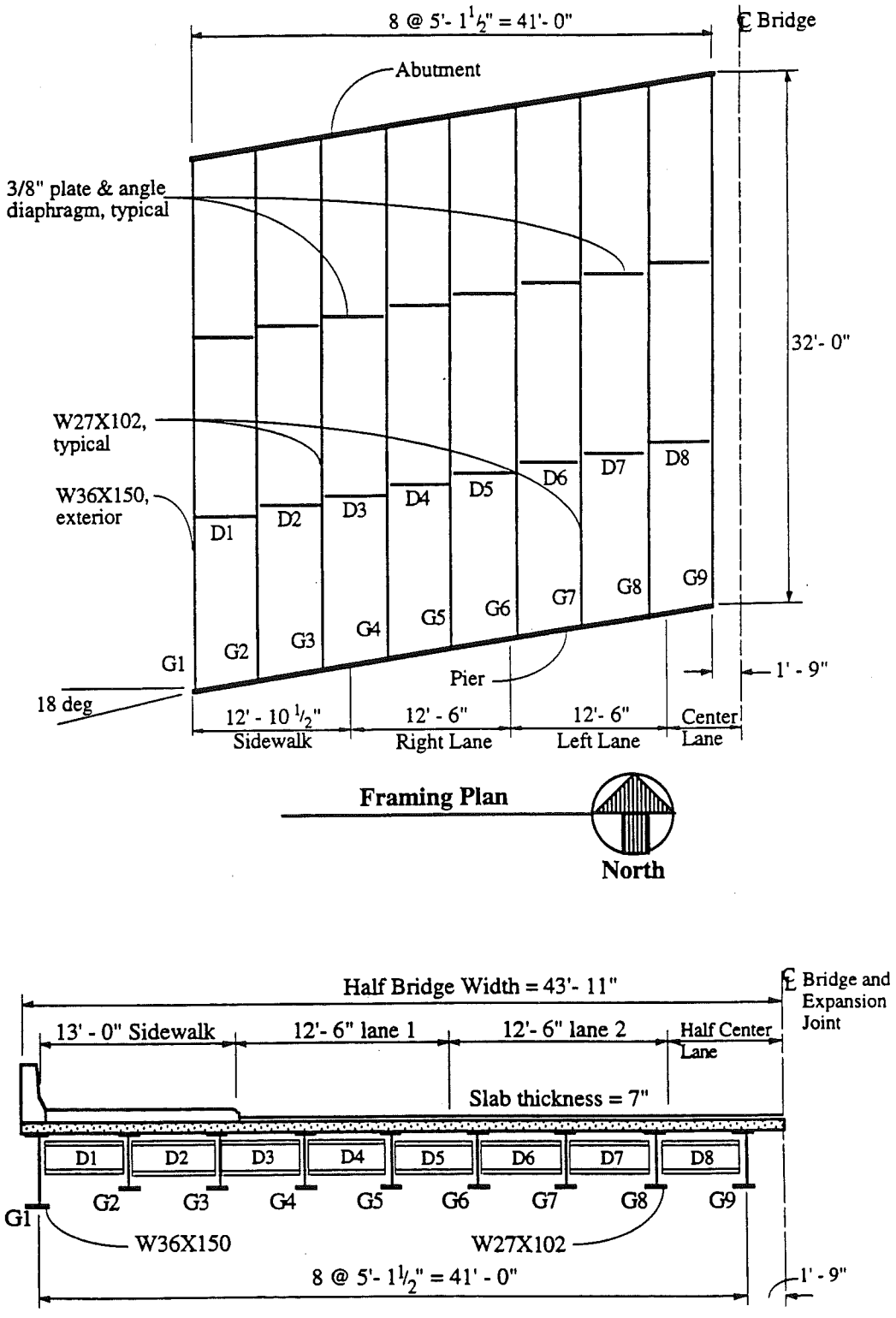

Fig. 6-25. Bridge WY/94, Wyoming Road over I-94. Plan View and Cross Section of Entrance Span.

7. CALIBRATION AND PILOT STUDY

The pilot study was conducted to evaluate the available equipment. Bridges were selected by the Project Team in cooperation with the Michigan DOT staff.

7. 1 Weigh-in-Motion using Bridge Weighing System Equipment

The objective of the pilot study was to evaluate and calibrate the equipment. A detailed description of installation procedure and operation of the WIM is described in the BWS Weigh-in-Motion (WIM) manual.

The installation procedure is summarized in steps 1 through 6:

Step 1. Installation of lane sensors.

Lane sensors(tape switches or infrared detectors) are attached to the pavement, two in each lane and perpendicular to the direction of traffic. After the sensors are installed the exact distance between sensors is measured and recorded in the system in order to calculate the speed and axle spacing. The traffic must be stopped for about 15 minutes in each lane during installation.

Step 2. Installation of demountable strain transducers.

Demountable strain transducers are attached to the lower flanges of girders using C-clamps. Access to girders is an important consideration in selecting a bridge for WIM testing. Strain transducers must be located in the middle $1/3$ of the span.

Step 3. Installation of cables.

The strain transducers are connected to the main unit using 5

shielded cables. Cables also connect the main unit with lane sensors.

Step 4. Initiation of the BWS Computer

AC power was provided by a portable gasoline powered generator. Communication with the BWS system is through a separate portable computer. All data concerning influence lines, girders, and other physical parameters are entered into the BWS computer and the system is instructed to begin weighing operation.

Step 5. Calibration.

The WIM equipment was calibrated using scale calibration trucks provided by MDOT or University of Michigan Transportation Research Institute (UMTRI) described in Section 7.1.1. The readings are verified and calibration constants are determined by running a truck with known axle loads over the bridge several times in each lane. The calibration is performed once for each tested structure. The examples of the obtained data are shown in Section 7.1.2.

Step 6. Operation.

The system is triggered when the first tire triggers the lane sensor. Strain measurements are taken at the rate of 62.5 Hz. Vehicle speed is calculated from the time delay between the first and second tape signal. Number of axles and axle distances are computed by the system and recorded. The dynamic strains sampled from each of the channels is then decomposed using preprogrammed influence lines into axle weights. A smoothing technique is used to determine the static weights from the dynamic records. Results of axle spacing and weight calculations are stored in memory for later

processing and summarization. The weighing operation results may be displayed in real time.

7.1.1 Calibration Trucks

The axle configuration of the various scale calibration trucks used for investigated bridges (see Chapter 6) are shown in Fig. 7-1 to Fig. 7-4.

The axle configuration of the Michigan DOT three axle calibration truck used for Bridge 1 on US-23 over Huron River (23/HR) is shown in Fig. 7-1.

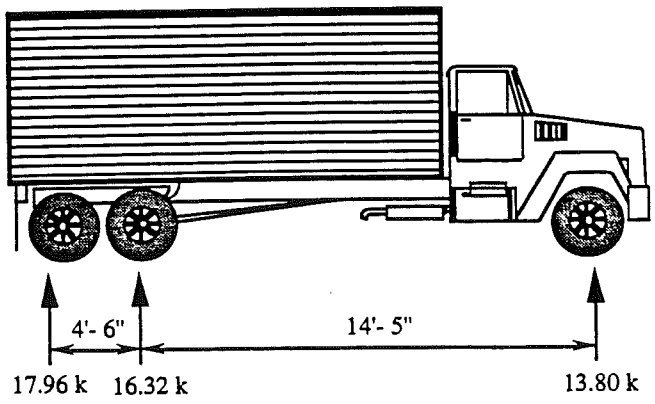

Fig. 7-1. Michigan DOT Three Axle Calibration Truck.

Calibration vehicle axle weights and spacing used at Bridge 2 on I-94 over the New York City Railroad (14/NY) are shown in Fig. 7-2. The truck used for calibration on Bridge 3 on I-94 over Jackson Road (94/JR) in Ann Arbor is shown in Fig. 7-3. The configuration of UMTRI truck used for the calibration of Bridge 5 on US-23 over the Saline River (25/SR) in Milan is shown in Fig. 7-4.

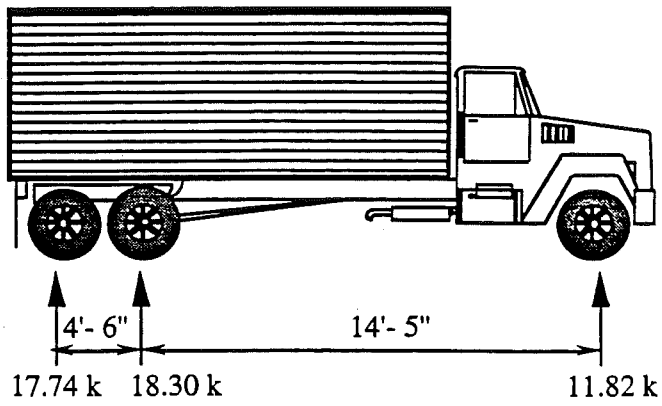

Fig. 7-2. Calibration Truck Used for Bridge 2 (14/NY).

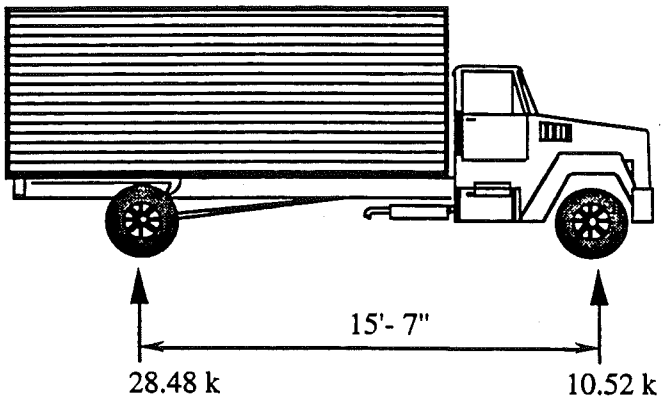

Fig. 7-3. Calibration Truck Used for Bridge 3 (94/JR).

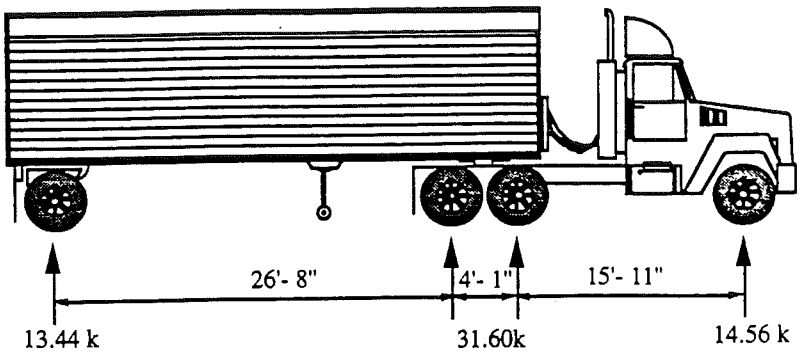

Fig. 7-4. University of Michigan Transportation Research Institute Calibration Truck.

7.1.2 Calibration Results

The results of calibration for Bridge 1 (23/HR) are presented in Table 7-1. An example of the stress vs. time results for a calibration pass on the US23 bridge over the Huron River is shown in Fig. 7-5. The sampling rate is 62.5 Hz and it is fixed by the BWS equipment. Fig. 7-5 can be used to verify the adequacy of 62.5 Hz sampling rate. The plot appears somewhat ragged and incomplete, therefore the dynamic stress/strain data, fatigue data sampled with Somat was conducted at a higher rate of 200 Hz.

The results of calibration for Bridge 3 (94/JR) are summarized in Table7-2. The calibration was verified using different calibration factors. The calibration factor for the right lane is denoted by R and for the left lane by L. The results for two different sets of calibration factors are presented in Table 7-3 and 7-4. The error in estimation of the gross vehicle weight varies from -1.8 to 5.0%, for passage of the calibration truck without any other truck on the bridge.

Results of calibration for Bridge 5 (23/SR) are shown in Table 7-5. The statistics for lane one are as follows: mean gross vehicle weight

equal to 59.9 kips, standard deviation equal to 1.21 kips, and the coefficient of variation equal to 2.0%.

Table 7-1. Calibration Results for Bridge 23/HR.

Truck Lane Posit.	Left Lane Factor	Right Lane Factor	Rear Axle, kips	Middle Axle, kips	Front Axle, kips	G.V.W. kips	Notes
Calibr. Truck.	-	-	17.96	16.32	13.80	48.08	-
Right	0.165	0.185	14.2	14.2	9.5	38	-
Right	0.165	0.185	15.5	15.5	12.1	43.1	-
Right	0.165	0.185	14.7	14.7	10.5	39.8	Good
Right	0.165	0.185	17.6	17.6	13.5	48.5	Good
Right	0.165	0.185	18.9	18.9	14.2	52	-
Right	0.165	0.185	19.2	19.2	14.3	52.7	N.Good
Right	0.165	0.185	10.9	10.9	9.3	31	Cars
Right	0.165	0.185	15.6	15.6	12.2	43.5	Cars
Right	0.165	0.185	18.6	18.6	14	51.1	Good
Right	0.165	0.185	19.7	19.7	14.6	54.1	Good
Right	0.165	0.185	16.7	16.7	12.8	46.1	Good
Left	0.165	0.185	11.5	11.5	9.7	32.8	one car
Left	0.165	0.185	16.9	16.9	13	46.9	one car
Left	0.165	0.185	17	17	13	47	Good
Left	0.165	0.185	18.2	18.2	13.7	50.1	Good
Left	0.165	0.185	17.6	17.6	13.4	48.6	Good
Left	0.165	0.185	17.2	17.2	13.1	47.6	one car
Left	0.165	0.185	16.9	16.9	13	46.8	one car

Table 7-2. Calibration Results for Bridge 94/JR.

Truck Lane Position	Left Lane Factor	Right Lane Factor	Rear Axle, kips	Front Axle, kips	Gross Weight, kips	Notes
Calibr. Truck	-	-	24.48	10.52	35.0	-
Right	0.165	0.185	24.8	13	37.9	Good
Right	0.165	0.185	24.4	13.4	37.9	Good
Right	0.165	0.185	26.2	13.6	39.8	Good
Right	0.165	0.185	23.3	13.4	36.7	Good
Right	0.165	0.185	25.5	13.5	39	Good
Right	0.165	0.185	23.7	13.7	37.4	Good
Right	0.165	0.185	25.5	13.5	39	Good
Left	0.165	0.185	24.9	14.6	39.5	Good
Left	0.165	0.185	22.9	14.2	37.1	Good
Left	0.165	0.185	24.2	14.3	38.5	Good
Left	0.165	0.185	27.9	11.6	39.5	Good
Left	0.165	0.185	25.1	14.6	39.9	Good
Left	0.165	0.185	25.6	13.1	38.7	Good
Left	0.165	0.185	27.3	12	39.3	Good
Left	0.165	0.185	25.2	14.8	40.1	Good
Left	0.165	0.185	24.6	14.1	38.8	Good
Truck	Static	Weight	28.28	10.56	39.04	

Tab. 7-3. Calibration Results on Bridge 94/JR.
UMTRI Truck, 08/13/91, Calibration Factors R=0.178, L=0.166 .

Truck Lane Position	Lane Factor	Gross Weight, kips	Gross Weight Error %	Axle Weight kips				Comments
				1	2	3	4	
Calibr. Truck	-	59.6	-	14.56	15.80	15.80	13.44	-
Right	0.178	60.9	1.0	9.6	19.5	19.5	12.2	No Trucks
Right	0.178	63.7	5.6	9.7	20.2	20.2	13.5	One Truck
Right	0.178	60.3	0.0	9.6	19.2	19.2	12.3	No Cars
Left	0.166	61.3	1.7	9.7	20.3	20.3	11.0	No Cars
Left	0.166	60.1	0.0	9.6	19.7	19.7	11.0	No Cars
Left	0.166	59.6	0.0	9.6	19.3	19.3	11.4	No Cars

Tab. 7-4. Calibration Results on Bridge 94/JR.
UMTRI Truck, 08/13/91, Calibration Factors R=0.167, L=0.181 .

Truck Lane Position	Lane Factor	Gross Weight kips	Gross Weight Error %	Axle Weight kips				Comments
				1	2	3	4	
Right	0.181	63.3	5.0	9.7	20.4	20.4	12.7	No Trucks
Right	0.181	66.2	9.8	9.8	21.2	21.2	14.1	One Truck
Right	0.181	62.7	3.9	9.7	20.1	20.1	12.8	No Cars
Left	0.167	60.9	1.0	12.3	18.9	18.9	10.9	No Cars
Left	0.167	59.7	-1.0	9.6	19.6	19.6	10.9	No Cars
Left	0.167	59.2	-1.8	9.6	19.1	19.1	11.4	No Cars

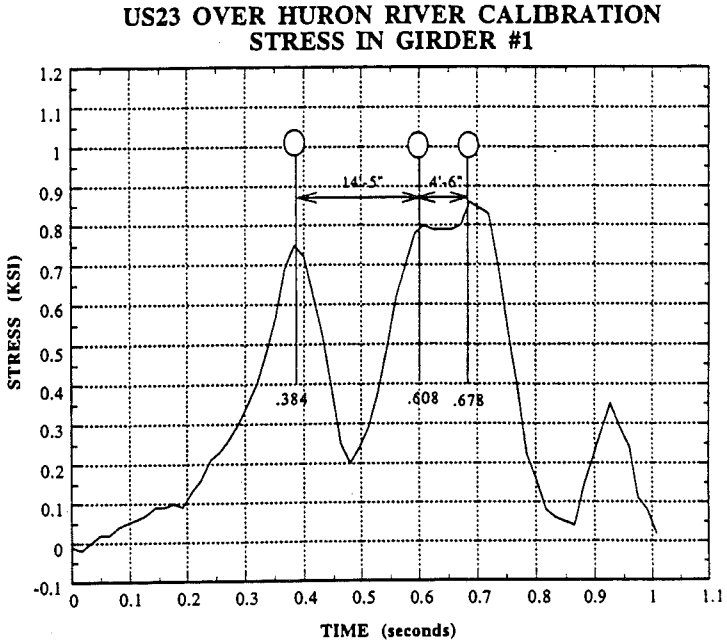

Fig. 7-5. Stress History of Girder 1, 23/HR, BWIM @ 62.5 Hz.

Table 7-5. Calibration Data for Bridge 23/SR in Milan.

Truck Lane Position	Axle Weight kips				Gross Weight kips	Lane Factor
	1	2	3	4		
Calibr. Truck	14.56	15.80	15.80	13.44	59.6	-
Right	9.2	15.7	15.7	8.8	49.4	0.1500
Right	7.7	20.9	20.9	10.2	59.7	0.1810
Right	8.1	19.3	19.3	9.9	56.8	0.1810
Right	8.2	19.9	19.9	10.4	58.5	0.1810
Left	8.4	21.1	21.1	13.2	63.7	0.1849
Left	8.4	19.9	19.9	11.8	59.9	0.1849
Left	8.5	20.3	20.3	12.0	61.2	0.1849
Left	8.8	20.1	20.1	12.2	61.1	0.1849

For lane two the calibration statistics are: mean gross vehicle weight equal to 59.6 kips, standard deviation equal to 1.35 kips, and the coefficient of variation of equal to 2.3%.

The calibration performed on Bridge 4 (94/PR) was verified using different 24 trucks. The proximity of the Truck Weigh Station in Grass Lake was used to measure vehicles which went through the stationary scales. The information from the Weigh Station was passed to the bridge site using the Michigan State Police radio. The data included axle loads and vehicle identification (type, color, plates). The calibration factors, actual GVW (from the Weigh Station) and WIM measured GVW are given in Table 7-6. Out of 24 trucks, 12 provided usable results, other data cannot be considered (because of multiple presence of other trucks or due to other errors). For the recorded 12 trucks, the axle loads obtained from the Weigh Station are listed in Table 7-7. The corresponding axle loads measured on the bridge using WIM system are shown in Fig. 7-8.

The comparison of the results indicates that the accuracy of measurements is within 13 percent for 11 axle trucks. The accuracy for 5 axle trucks varries from0.23 to 6.76 and the average is within 2.5 percent. However, the accuracy is higher for GVW than for axle loads.

7. 2 Accelerations using Krenz Electronics Data Acquisition System

The equipment was installed and used on the same bridges as the BWS system. Accelerometers were installed on top of lower flanges of the bridge girders. The results are in chapter 9.

7. 3 Strains using SoMat Data Acquisition System

The strain transducers were installed as for the BWS. The data acquisition unit is small and can be placed in a metal box on the lower flange of the girder. The system was left for one full week, with an upper limit of 3 weeks due to battery power constraints. The results of the pilot study are in chapter 11.

Tab. 7-6. Calibration Results for Bridge 94/PR.

Truck Lane Posit.	Left Lane Factor	Right Lane Factor	Truck No.	No. of Axles	SCALE G.V.W kips	BWIM G.V.W. kips	Notes G.V.W. % error
Right	0.1234	0.1253	1	10	49.40	-	Missed
Right	0.1234	0.1253	2	6	88.90	-	Missed
Right	0.1234	0.1253	3	-	-	-	Missed
Right	0.1234	0.1253	4	5	74.37	79.40	6.76
Right	0.1234	0.1253	5	5	43.00	43.10	0.23
Right	0.1234	0.1253	6	5	33.94	35.80	5.48
Right	0.1234	0.1253	7	11	128.33	-	Missed
Right	0.1234	0.1253	8	11	136.58	154.00	12.75
Right	0.1234	0.1253	9	8	132.71	127.00	-4.30
Right	0.1234	0.1253	10	5	52.22	51.00	-2.00
Right	0.1234	0.1253	11	6	82.00	-	Missed
Right	0.1234	0.1253	12	5	46.01	43.80	-4.80
Right	0.1234	0.1253	13	5	78.96	78.90	-0.08
Right	0.1234	0.1253	14	9	132.90	132.80	-0.08
Right	0.1234	0.1253	15	5	43.05	43.00	-0.12
Right	0.1234	0.1253	16	5	64.58	-	Exited
Right	0.1234	0.1253	17	5	76.20	-	Missed
Right	0.1234	0.1253	18	5	70.25	-	Missed
Right	0.1234	0.1253	19	11	119.02	-	Missed
Right	0.1234	0.1253	20	5	62.30	-	Missed
Right	0.1234	0.1253	21	7	95.20	87.60	-7.98
Left	0.1234	0.1253	22	5	74.27	74.50	0.31
Right	0.1234	0.1253	23	6	107.00	105.40	-1.50
Left	0.1234	0.1253	24	11	153.68	136.00	-11.50

Table 7-7. Axle Loads of Truck Measured at Weigh Station.

4	5	9.62	16.65	16.52	15.35	16.28	13.8	4.2	28.1	4.1											
5	5	9.54	10.66	9.82	9.23	9.06	11.4	4.3	13.7	4.1											
6	5	10.45	6.79	6.84	4.58	5.33	19.6	4.4	33.9	6.1											
8	10	9.85	19.12	18.76	10.32	13.82	14.24	13.74	12.56	11.44	12.74	3.5	4.5	11.7	3.8	3.7	3.7	3.6	3.8		
9	8	12.11	16.19	15.69	15.66	18.4	19,68	17.31	15.5	5.1	11.1	9.1	9.1	11.2	9.1						
10	5	9.6	10.78	10.44	9.2	12.21	18.8	4.4	34.6	4.0											
12	5	10.79	9.87	9.6	7.76	7.99	17.5	5	33	4.1											
14	9	12.49	16.63	16.63	24.08	12.24	11.3	11.32	11.37	17.28	14.1	4.4	10.9	12	3.7	3.8	3.8	3.9			
15	5	10.47	8.8	8.56	6.2	9.02	18.7	4.4	33.2	4.1											
21	7	9.8	18.5	18.6	9.5	10.4	11.5	16.9	13	4.4	20.6	4.2	4.0	4.1							
22	5	11.64	13.34	15.19	15.7	16.4	11.8	4.3	33.9	4.0											
23	6	11.6	22.5	21.7	16.4	17.33	17.5	20	4.6	32.9	4.3	4.2									

Table 7-8. Axle Loads of Truck Measured on the Bridge using WIM.

4	5	11.4	19.0	19.8	16.2	16.2	13.8	4.2	28.1	4.1											
5	5	9.0	10	10	8.2	8.2	11.4	4.3	13.7	4.1											
6	5	8.9	9.5	9.8	4.9	4.9	19.6	4.4	33.9	6.1											
8	10	15.4	23.4	23.4	12.5	12.5	12.5	12.5	12.5	12.5	12.3	3.5	4.5	11.7	3.8	3.7	3.7	3.6	3.8	3.8	3.8
9	8	14.2	18.4	18.4	11.3	21.7	15.2	20.5	14.3	15.5	5.1	11.1	9.1	9.1	11.2	9.1					
10	5	11.3	11	11	10.2	10.2	18.8	4.4	34.6	4.0											
12	5	10.9	10.4	10.4	7.2	7.2	17.5	5	33	4.1											
14	9	12.8	19	19	21.6	13.5	13.5	13.5	13.5	13.5	14.1	4.4	10.9	12	3.7	3.8	3.8	3.9			
15	5	9.1	11	11	7.1	7.1	18.7	4.4	33.2	4.1											
21	7	9.1	19	19	11.2	11.2	11.2	11.2	13	4.4	20.6	4.2	4.0	4.1							
22	5	9.1	17.9	17.9	16.1	16.1	11.8	4.3	33.9	4.0											
23	6	12.6	24.2	24.2	16.6	16.6	16.6	20	4.6	32.9	4.3	4.2									

7. 4 Equipment Provided by TestConsult-CEBTP (France)

The equipment was installed on Bridge 1 (23/HR). The measurements were taken using the electronic theodolite and fleximeter. The results are shown in Fig. 7-6, 7-7 and 7-8.

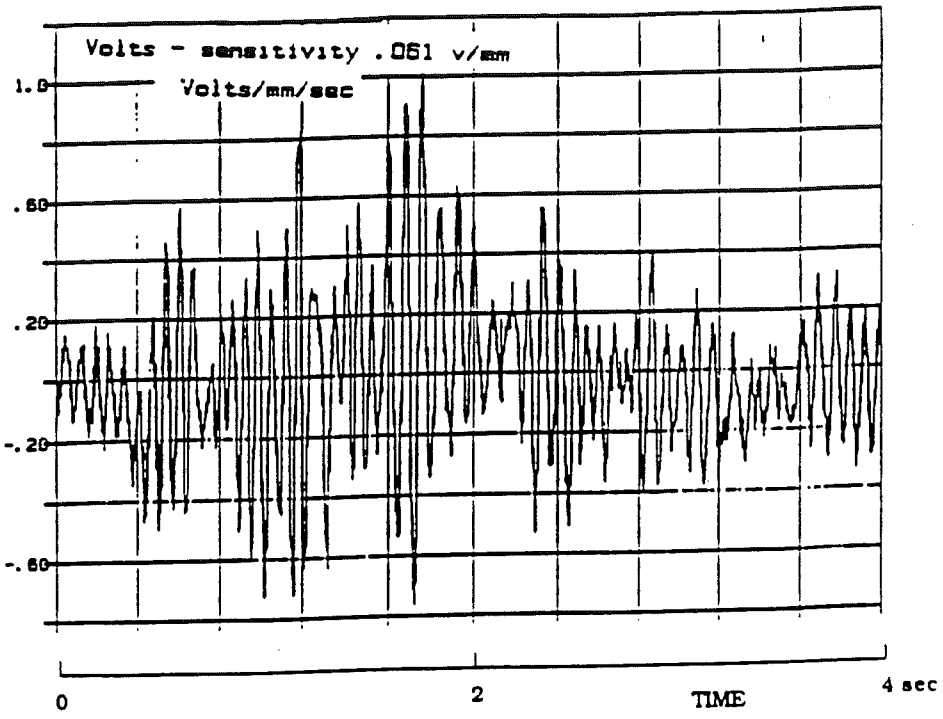

Fig. 7-6. Dynamic Response Recorded by Theodolite in Time Domain.

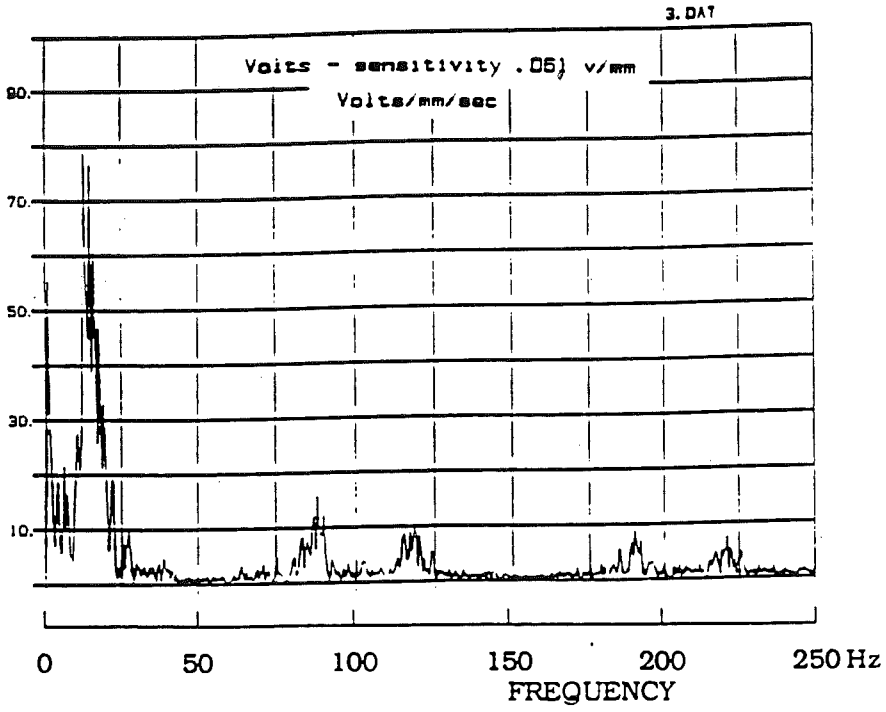

Fig. 7-7. Dynamic Response Recorded by Theodolite in Frequency Domain.

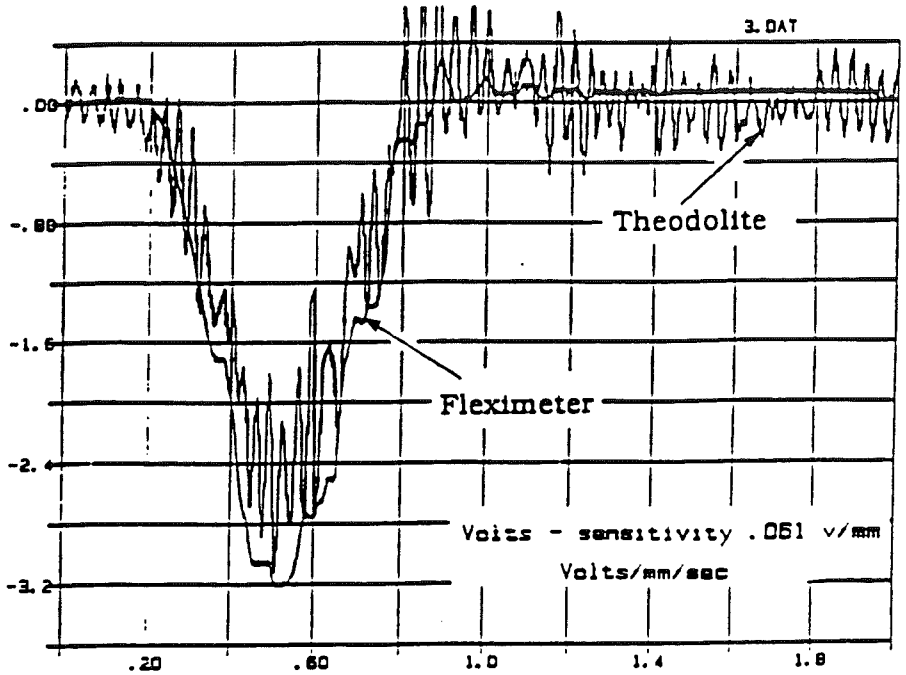

Fig. 7-8. Comparison of the Response Recorded by Theodolite and Fleximeter.

Theodolite provided very accurate results. Fleximeter filtered the dynamic portions of the response but, in general agreed with the results obtained by theodolite. However, the cost of theodolite is very high (over $10,000). Separate theodolites would be required for each point of measurement (channel).

7.5 Culway

The system was demonstrated on a culvert selected by the Ontario Ministry of Transportation. The structure is located on Highway 402 in Sarnia, Canada, near a truck weighing station equipped with static scales. All trucks that crossed the culvert were weighed at the weighing station. Also recorded were truck type, axle configuration and time of passage. Data was collected daily for a week, averaging 50-70 trucks a day. The axle weights and gross vehicle weights (GVW) were recorded and compared with the actual weights from the weighing station. Results showed a good accuracy ranging between 3 and 5 percent of GVW.

8. WEIGH-IN-MOTION MEASUREMENTS

8.1 Introduction

Truck measurements provided data for the calculation of statistical parameters including vehicle weight, truck class, and maximum, mean, median, standard deviation, coefficient of variation (COV), skewness (degree of asymmetry about the mean), and kurtosis (relative peakedness or flatness of a distribution compared to the normal distribution) of gross vehicle weights, axle weights, and moments. The considered parameters include distributions of gross vehicle weight (GVW), daily GVW distributions, distributions of GVW for five and eleven axle vehicles, axle weight distributions, front axle weight distributions, following axle weight distributions, and lane moments of all vehicles, five axle vehicles, and eleven axle vehicles for 20, 30, 60, 90, 120, and 200 foot spans. This data characterizes each site by the specific load observed at the site. A comparison between sites of the critical WIM load characteristics is also presented.

8. 2 Background

The literature was surveyed to determine the available data important for study of effect of truck loads on highway bridges.

8.2.1 Live Load

Truck data collection is important in determining both the maximum load effects and frequency distribution of heavy traffic. The data was collected for many years using several truck survey methods. Originally, the information was acquired by static weigh scales in fixed locations. The usefulness of such data was limited, because some drivers of overloaded trucks would purposefully avoid the weigh scales. The results were considered as biased, in particular, this applies to the upper tail of the gross vehicle weight histograms. However, over the past 10 years, weigh-in-motion (WIM) techniques have been developed to measure weights of moving vehicles. Trucks can now be weighed at the normal highway speed. Most importantly, weighing

operation can be conducted in a discreet manner without drivers' knowledge. During the past decade, there have been dramatic developments in the in-motion weighing technology (Bosch 1985; Cunagin 1986; Daniels et al. 1986). The WIM data provided information about various factors influencing the bridge load. This information primarily concerns vehicle weight and configuration, traffic frequency, headway distance and transverse position.

Imbsen (1987) gathered a large volume of truck weight data from the following sources:

- FHWA - 33 sites with a total of 26,613 trucks weighed;
- Wisconsin - 23 sites with a total of 72,848 trucks weighed between 1983 to 1986;
- Florida - 18 sites with a total of 71,010 trucks weighed in 1986;
- Illinois - A four-lane site was selected with a total of 49,969 trucks weighed in 1987.

The analysis was performed for the Wisconsin and Florida data. It was reported that, depending on location, 5 axle semi-trailers constitute from 54% to 89% of the truck traffic on Interstate sites, and less than 50% at urban sites. A computer program was developed to calculate the histograms and cumulative distributions of axle spacing, axle weight, gross vehicle weight and normalized moments. The analysis was carried out for each truck configuration and for a combination of various truck configurations. Table 8-1 and 8-2 summarize the results with the weight and axle spacing of a 5 axle semi-trailer configuration from two Wisconsin sites, including 2,503 and 918 trucks, respectively. Both tables summarize the mean and coefficient of variation of axle weights and spacings at two bridge sites. It is obvious that the spacing between axles can be modeled with a small variation but the axle weights involve a large variation.

Moses and Ghosn (1983) installed WIM system on 5 sites in the Cleveland area, Ohio, in 1982. A total of 1,489 trucks were weighed. Based on these field measurements, they developed a live load model.

Moses (1985) further suggested three vehicle configurations, a single body truck with 45 kips, a 5-axle semi-trailer with 67 kips and a 6-axle tractor semi-trailer with 75 kips, as representative trucks on the highway.

Nassif (1993) has reported on the analysis of the statistical data on axle weights and spacings from 1985 Michigan citation data. The results are shown in Fig. 8-3 which summarizes the mean and coefficient of variation of axle weights and spacings of Michigan Citation Data (Nassif 1993),

Table 8-1. The Statistical Parameters of Axle Weight (Imbsen 1987)

Axle Weight		Axle 1	Axle 2	Axle 3	Axle 4	Axle 5
Site 1(*)	Mean	10.2 k	9.4 k	9.4 k	20 k	20 k
	COV	15%	56%	56%	53%	53%
Site 2(**)	Mean	8.8 k	11 k	11 k	8.9 k	8.9 k
	COV	18%	43%	43%	64%	64%

Table 8-2. The Statistical Parameters of Axle Spacing (Imbsen 1987)

Axle Spacing		Spacing 1	Spacing 2	Spacing 3	Spacing 4
Site 1(*)	Mean	12.3 ft	4.3 ft	29.9 ft	4.1 ft
	COV	17%	3%	13%	5%
Site 2(**)	Mean	12.1 ft	4.3 ft	29.5 ft	4.1 ft
	COV	16%	3%	15%	4%

(*) Site 1 includes 2,503 semi-trailers

(**) Site 2 includes 918 semi-trailers

Table 8-3. The Statistical Data of Axle weights and Spacings from 1985 Michigan Citation Data

Truck Type	Percentage of Truck Population		First Axle Weight 1	First Axle Spacing 1 (*)	Tandem Weight 2 (*)	Spacing 2	Tandem Weight 3
2 Axle Truck	4 %	Mean	9.5 k	15.1 ft	23.2 k	---	---
		COV	30%	23.5%	13%	---	---
3 Axle Truck	3 %	Mean	13.5 k	15.8 k	41 k	---	---
		COV	25.8 %	26.8 %	11.5 %	---	---
4 Axle Truck	4 %	Mean	10.4 k	10.2 ft	21.7 k	16.7 ft	30.4 k
		COV	40.2 %	28.3 %	18.3 %	34 %	53.3 %
5 Axle Truck (**)	40 %	Mean	10 k	12.7	35.5 k	29.8 ft	35.1 k
		COV	13.9 %	16 %	15.7 %	18 %	18.2 %
6 Axle Truck	20 %	Mean	10.8 k	12.8 ft	36.2 k	23.2 ft	51 k
		COV	16.8 %	17.8 %	18.4 %	28.7 %	18.3 %

(*) Tandem axle is considered as one axle having total tandem weight.

(**) 5-axle type includes not only semi-trailers but all 5-axle truck configurations

8.2.2 Available Live Load Models

Three live load models are considered: the first developed for the Ontario Highway Bridge Design Code (OHBDC) 1979 edition by Nowak and Lind (1979), the second proposed by Ghosn and Moses (1984), and the third recently developed by Nowak and Hong (1991) and Nowak (1993) for the new LRFD AASHTO Code (1994).

Nowak and Lind's Model

This model was based on the 1975 Ontario truck survey data. To predict the maximum 50 year moment, the distributions of moment due to the surveyed trucks are extrapolated (Nowak and Lind, 1979). It was assumed that the upper tail of the distribution of the maximum 50 year live load, L50, is exponential (Grouni, 1978),

$$F_{L50}(x) = 1 - \exp(-x) \qquad (8\text{-}1)$$

This corresponds to a straight line on the exponential scale. Therefore, a straight line was fitted to the upper tail of the survey data. To determine the upper tail of the moment distribution, six heaviest trucks in the survey were selected. The maximum mid span bending moments were calculated for each truck, for various simple spans and continuous multiple spans.

Ghosn and Moses Model

In 1984 Ghosn and Moses developed a live load model based on the data collected from weigh-in-motion measurements (Ohio WIM data). They used a multi-dimensional stochastic process approach that utilizes bridge measurement data to obtain the maximum lifetime (50 year) distribution of live loads on multi-lane bridges. The model includes the possibility of side-by-side traffic occurrence along with sequences of trucks in each lane. The maximum 50 year live load, M_{50}, is given in the form of the following equation;

$$M_{50} = a\ m\ W^*_{.95}\ H \qquad (8\text{-}2)$$

where: a = the maximum moment effect of the standard simulation truck with a unit gross weight (a deterministic value which depends on truck configuration and span length), m = factor to account for the randomness in the axle configuration of random truck traffic, $W^*_{.95}$ = truck weigh value corresponding to the upper 5% of the gross weight histogram (i.e. 95th percentile of weight for the dominating truck type at the site), H = headway distance factor.

Nowak and Hong's Model

Nowak and Hong (1991) and Nowak (1993) developed a live load model which is based on the WIM truck data. Several assumptions were made regarding the occurrence of multiple presence in lane and side-by-side. The headway distance between trucks in the same lane was considered as speed-dependent. Three cases of correlation between the heavy trucks were considered: no correlation, partial correlation and full correlation. The actual value of the correlation coefficient depends on the location of the bridge and can be evaluated by a local truck survey. For the case of no correlation, Turkstra's rule was used to find the maximum 75 year effect of the live load. It was determined that the mean maximum 75 year moment for a two lane bridge is equal to the effect of two mean maximum 2 month trucks side-by-side. The model served as a basis for the design live load in LRFD AASHTO Code (1994). The new live load provides for a uniform bias factor for a wide range of span lengths. The results of the present study can be used in verification of the assumption about the actual truck weights, axle loads and multiple presence.

8. 3 Weigh-in-Motion Statistics

WIM statistics are presented for six bridge sites in the following tables. The bridge on I-94 over Pierce Road was subjected to study in both 1991 and 1993 for comparison of the effects of the closing of a nearby weigh station in 1993. WIM data was collected at the bridge on US-23 over the Huron River in 1991 and 1993 to study year to year differences in the data.

For brevity, the following designations have been adopted throughout the chapter:

23/HR - US-23 over the Huron River in Ann Arbor, Michigan.
Michigan State Bridge ID: R01-81074.
14/NY - M-14/US-23 over the New York City Railroad in Ann Arbor, Michigan.
Michigan State Bridge ID: R01-81103.
94/JR - I-94 over Jackson Road in Ann Arbor, Michigan.
Michigan State Bridge ID: S01-81062.
94/PR - I-94 over Pierce Road in Grass Lake, Michigan.
Michigan State Bridge ID: S03-81104.
23/SR - US-23 over the Saline River in Milan, Michigan.
Michigan State Bridge ID: B05-58033.
WY/94 - Wyoming Road over I-94 in Detroit Michigan.
Michigan State Bridge ID: S36-82022.

Table 8-4 summarizes the WIM data collection efforts by date and total number of vehicles weighed. This data includes all trucks with 2.5 kip and greater axle weights. Table 8-5 summarizes filtered WIM data of vehicles with a GVW of 15 Kips and greater, regardless of axle weight. Trucks with a GVW less than 15 kips do not have a significant affect on considerations such as fatigue. This filtered WIM data has been used for all subsequent analysis of GVW and lane moment calculations.

Federal Highway Administration (FHWA) truck class frequency vs. lane is presented in Table 8-6 through 8-8 for the sites where this information is available. Table 8-9 compares each of the four bridge sites by truck class observed. Federal Highway Administration (FHWA) axle configuration class are in the Appendix B. It can be seen from Table 8-9 that each bridge experiences a somewhat different mix of truck traffic by truck class.

GVW statistics of maximum, mean, median, standard deviation, coefficient of variation, and distribution skewness and kurtosis of all vehicles, five axle vehicles, and eleven axle vehicles at each bridge site

are presented in Tables 8-10, 8-11, and 8-12 respectively. There are distinct differences as well as similarities between bridge sites in the statistics of GVW.

Axle weight statistics of maximum, mean, median, standard deviation, coefficient of variation, and distribution skewness and kurtosis of all axles, front axles, and following axles at each bridge site are presented in Tables 8-13 to 8-15. Again, distinct differences and similarities between bridge sites can be observed. As a basis for comparison,

Table 8-4. Number of Trucks Weighed by Date and Bridge.

Bridge	Date and Number of Trucks Weighed with Axles > 2.5 kips							
23/HR	7/2/91	8/28/91	6/22/92	6/23/92				Total
	876	513	698	737				2824
23/SR	6/30/92	7/1/92	7/2/92	7/22/92	10/13/92	10/21/92	10/22/92	Total
	825	1313	1377	1075	716	797	997	7101
94/PR	8/10/91	8/11/91	6/30/93	7/1/93				Total
	625	416	1381	1570				3992
14/NY	8/21/91							Total
	1023							1023
WY/94	8/19/93	9/8/93						Total
	181	341						522
94/JR	4/26/91	5/22/91	5/23/91	6/19/91	6/20/91	8/14/91		Total
	594	2252	1456	687	1758	625		7372

Table 8-5. Trucks Weighed > 15 Kips by Date and Number.

Bridge	Date and Number of Vehicles Weighed > 15 Kips							
23/HR	7/2/91	8/28/91	6/22/92	6/23/92				Total
	658	393	382	484				1917
23/SR	6/30/92	7/1/92	7/2/92	7/22/92	10/13/92	10/21/92	10/22/92	Total
	588	854	805	651	331	483	635	4347
94/PR	8/10/91	8/11/91	6/30/93	7/1/93				Total
	312	161	1075	1264				2812
14/NY	8/21/91							Total
	769							769
WY/94	8/19/93	9/8/93						Total
	131	163						294
94/JR	4/26/91	5/22/91	5/23/91	6/19/91	6/20/91	8/14/91		Total
	344	1352	932	457	1051	419		4555

Table 8-6. Bridge (**23/HR**). Truck Class vs Lane Statistics.

Truck Class (FHWA)	Right Lane (1) (%)	Left Lane (2) (%)	Total (%)
4	3.1	1.0	4.1
5	28.6	7.1	35.7
6	3.4	0.3	3.6
7	1.7	0.3	2.0
8	10.5	1.0	11.6
9	25.3	5.7	31.0
10	1.8	0.5	2.3
11	0.1	0.1	0.1
12	0.0	0.0	0.0
13	0.1	0.0	0.1
14	7.2	2.3	9.5
Total %	81.8	18.2	100.0

Table 8-7. Bridge (**23/SR**). Truck Class vs Lane Statistics.

Truck Class (FHWA)	Right Lane (1) (%)	Left Lane (2) (%)	Total (%)
4	1.2	0.4	1.6
5	32.6	4.6	37.2
6	3.1	0.7	3.8
7	0.1	0.0	0.1
8	6.0	0.9	6.9
9	34.3	3.3	37.6
10	1.5	0.1	1.6
11	0.4	0.0	0.5
12	0.2	0.0	0.2
13	0.0	0.0	0.0
14	7.9	2.6	10.5
Total %	87.3	12.7	100.0

Table 8-8. Bridge (**WY/94**). Truck Class vs Lane Statistics.

Truck Class (FHWA)	Right Lane (1) (%)	Left Lane (2) (%)	Total (%)
4	2.9	1.2	4.1
5	19.6	32.0	51.6
6	1.8	1.8	3.6
7	0.6	0	0.6
8	0.9	2.3	3.2
9	8.8	10.3	19.1
10	2.1	1.2	3.2
11	0.0	0.0	0.0
12	0.0	0.0	0.0
13	0.0	0.0	0.0
14	6.2	8.5	14.7
Total Lane %	42.8	57.2	100.0

Table 8-9, Truck Class vs Bridge Location.

Class (FHWA)	23/HR (92) %	23/SR %	94/PR (93) %	WY/94 %
4	4.1	1.6	2.2	4.1
5	35.7	37.2	23.2	51.6
6	3.6	3.8	2.7	3.6
7	2.0	0.1	0.2	0.6
8	11.6	6.9	5.8	3.2
9	31.0	37.6	55.7	19.1
10	2.3	1.6	2.6	3.2
11	0.1	0.5	0.8	0.0
12	0.0	0.2	0.3	0.0
13	0.1	0.0	0.0	0.0
14	9.5	10.5	6.5	14.7
Lane 1	81.8	87.3		42.8
Lane 2	18.2	12.7		57.2

Table 8-10, Gross Vehicle Weight Statistics for All Vehicles > 15 kips.

Location	Maxi	Mean	Median	Std. Dev.	C.O.V.	Skewnes	Kurtosis
23/HR (92)	**170.6**	**46.6**	**40.0**	**27.4**	**0.588**	**1.760**	**4.095**
6/22/92	170.6	45.7	38.4	27.0	0.591	1.961	5.145
6/23/92	159.1	47.3	40.8	27.0	0.571	1.641	3.680
23/HR (91)	**177.7**	**52.1**	**45.6**	**29.9**	**0.574**	**1.710**	**3.645**
7/2/91	161.6	51.8	46.8	25.2	0.486	1.533	4.037
8/28/91	177.7	52.6	42.8	36.5	0.694	1.656	2.300
23/SR	**248.5**	**57.9**	**47.5**	**34.1**	**0.589**	**1.628**	**3.520**
6/30/92	185.5	52.1	42.9	28.9	0.555	1.439	2.714
7/1/92	199.1	57.2	47.2	33.7	0.589	1.586	3.151
7/2/92	214.5	56.2	45.2	33.5	0.596	1.785	4.137
7/22/92	206.6	58.5	47.0	35.6	0.609	1.709	3.452
10/13/92	225.8	61.5	48.6	38.6	0.626	1.432	2.666
10/21/92	201.5	63.1	56.4	32.4	0.513	1.070	1.762
10/22/92	248.5	59.4	49.1	35.6	0.599	1.824	4.494
94/PR (93)	**181.5**	**52.4**	**48.1**	**24.8**	**0.473**	**1.343**	**3.446**
6/30/93	170.1	51.3	47.2	23.2	0.452	1.375	3.902
7/1/93	181.5	53.7	48.8	26.0	0.484	1.312	3.064
94/PR (91)	**133.3**	**51.4**	**49.2**	**20.3**	**0.395**	**0.209**	**-.488**
8/10/91	133.3	50.2	46.5	20.1	0.400	0.463	0.0960
8/11/91	87.0	53.6	55.9	20.4	0.381	-0.265	-1.215
14/NY	**267.9**	**54.1**	**45.6**	**35.8**	**0.662**	**2.366**	**8.411**
WY/94	**177.3**	**42.9**	**35.6**	**27.0**	**0.629**	**1.983**	**4.855**
8/19/93	131.0	38.1	29.2	24.0	0.630	1.877	3.826
9/8/93	177.3	46.0	38.2	28.4	0.617	1.992	4.836
94/JR	**235.7**	**53.7**	**41.0**	**35.3**	**0.657**	**2.165**	**5.722**
4/26/91	212.5	54.9	42.1	40.9	0.745	2.081	4.435
5/22/91	235.7	54.5	42.4	33.7	0.618	2.026	5.628
5/23/91	223.7	56.0	40.8	39.2	0.700	2.006	4.363
6/19/91	218.7	53.1	41.2	32.5	0.612	2.101	5.651
6/20/91	232.8	51.4	39.3	33.0	0.642	2.344	6.991
8/14/91	228.9	52.0	41.6	34.3	0.660	2.507	7.340

Table 8-11. Gross Vehicle Weight (Kips) Statistics for 5 Axle Vehicles.

Location	Max	Mean	Median	Std. Dev.	C.O.V.	Skewnes	Kurtosis
23/HR (92)	**90.0**	**49.5**	**47.9**	**16.1**	**0.325**	**0.232**	**-0.926**
6/22/92	82.5	47.0	44.5	15.1	0.321	0.273	-0.899
6/23/92	90.0	50.5	48.9	16.4	0.325	0.171	-0.981
23/HR (91)	**137.7**	**52.6**	**50.3**	**17.3**	**0.329**	**0.357**	**-0.305**
7/2/91	87.9	53.7	51.2	16.2	0.302	0.149	-1.222
8/28/91	137.7	50.1	48.2	19.4	0.387	0.755	0.864
23/SR	**131.5**	**59.2**	**52.2**	**23.1**	**0.390**	**0.619**	**-0.785**
6/30/92	99.3	52.6	45.4	20.8	0.395	0.455	-1.190
7/1/92	108.9	57.9	49.2	22.4	0.387	0.576	-1.068
7/2/92	118.2	57.4	48.8	22.5	0.392	0.771	-0.570
7/22/92	118.5	57.6	50.8	22.2	0.385	0.658	-0.834
10/13/92	131.5	66.1	58.9	26.7	0.404	0.496	-1.075
10/21/92	124.1	67.2	62.5	24.2	0.360	0.298	-1.191
10/22/92	117.0	61.4	54.8	21.8	0.355	0.698	-0.698
94/PR (93)	**117.0**	**54.6**	**51.9**	**17.0**	**0.311**	**0.291**	**-0.874**
6/30/93	105.8	53.1	50.2	16.3	0.307	0.279	-1.036
7/1/93	117.0	55.8	52.7	18.0	0.323	0.255	-0.992
94/PR (91)	**89.3**	**56.5**	**55.7**	**16.8**	**0.297**	**-0.0226**	**-1.270**
8/10/91	89.3	54.1	52.2	16.7	0.309	0.183	-1.149
8/11/91	87.0	61.1	65.8	16.0	0.262	-0.417	-1.147
14/NY	**131.6**	**55.2**	**50.2**	**22.8**	**0.413**	**0.773**	**0.151**
WY/94	**89.5**	**42.8**	**37.4**	**16.6**	**0.388**	**0.833**	**-0.0730**
8/19/93	88.8	42.7	31.6	20.1	0.471	0.713	-0.838
9/8/93	89.5	42.9	38.3	14.2	0.331	1.092	0.727
94/JR	**115.4**	**51.4**	**42.9**	**20.8**	**0.405**	**0.808**	**-0.501**
4/26/91	92.3	51.9	46.1	19.7	0.380	0.417	-1.147
5/22/91	113.3	53.6	46.1	21.7	0.405	0.648	-0.786
5/23/91	115.4	52.2	42.5	21.8	0.418	0.854	-0.434
6/19/91	106.6	50.7	42.5	20.4	0.402	0.825	-0.505
6/20/91	110.6	49.4	40.3	20.0	0.405	1.008	-0.114
8/14/91	92.7	47.4	41.2	17.7	0.373	0.846	-0.438

Table 8-12. Gross Vehicle Weight (Kips) Statistics for 11 AxleVehicles.

Location	Max	Mean	Median	Std. Dev.	C.O.V.	Skewnes	Kurtosis
23/HR (92)	**170.6**	**137.5**	**142.7**	**31.0**	**0.225**	**-2.300**	**4.502**
6/22/92	170.6	140.7	146.5	33.2	0.236	-2.593	5.682
6/23/92	159.1	129.4	141.3	37.3	0.288	-1.621	1.215
23/HR (91)	**177.7**	**148.3**	**154.1**	**21.7**	**0.146**	**-2.744**	**8.976**
7/2/91	161.6	142.7	153.7	30.1	0.211	-2.360	4.382
8/28/91	177.7	151.3	156.1	15.7	0.104	-1.572	4.400
23/SR	**248.5**	**103.2**	**60.3**	**62.4**	**0.605**	**0.514**	**-1.495**
6/30/92	185.5	83.0	49.3	54.2	0.653	0.710	-1.369
7/1/92	199.1	92.2	56.1	57.6	0.625	0.781	-1.271
7/2/92	214.5	93.3	60.9	56.2	0.602	0.961	-0.826
7/22/92	206.6	120.7	151.2	65.2	0.540	-0.0325	-1.902
10/13/92	225.8	154.8	190.0	70.8	0.457	-0.643	-1.444
10/21/92	201.5	113.2	121.1	61.1	0.540	0.0942	-1.680
10/22/92	248.5	129.3	139.3	66.6	0.515	0.0562	-1.546
94/PR (93)	**181.5**	**136.1**	**150.2**	**39.0**	**0.284**	**-1.396**	**0.482**
6/30/93	170.1	121.1	141.0	45.8	0.378	-0.657	-1.313
7/1/93	181.5	150.3	155.0	24.8	0.165	-2.812	9.262
14/NY	**267.9**	**171.3**	**173.1**	**74.0**	**0.432**	**-0.316**	**-0.984**
WY/94	**177.3**	**83.5**	**61.5**	**44.2**	**0.529**	**0.672**	**-0.944**
8/19/93	131.0	73.5	45.5	43.9	0.597	0.448	-1.595
9/8/93	177.3	88.9	62.9	45.2	0.508	0.772	-0.955
94/JR	**235.7**	**149.7**	**172.4**	**59.3**	**0.396**	**-0.594**	**-1.243**
4/26/91	212.5	185.1	182.3	18.5	0.100	-0.323	-0.744
5/22/91	235.7	150.4	173.6	59.6	0.396	-0.465	-1.390
5/23/91	223.7	160.8	173.8	58.1	0.361	-0.928	-0.686
6/19/91	218.7	144.4	164.0	53.8	0.373	-0.733	-0.831
6/20/91	232.8	136.2	159.8	63.2	0.464	-0.180	-0.655
8/14/91	228.9	121.6	74.1	69.4	0.571	0.210	-1.774

Table 8-13. Axle Weight (Kips) Statistics for All Axles.

Location	Max	Mean	Median	Std. Dev.	C.O.V.	Skewnes	Kurtosis
23/HR (92)	44.9	10.84	9.7	4.49	0.414	1.450	3.348
23/HR (91)	58.7	11.30	10.5	4.33	0.383	1.442	5.787
23/SR	40.8	12.31	10.8	5.58	0.453	1.016	0.707
94/PR (93)	54.3	11.38	10.5	4.13	0.363	1.066	3.313
94/PR (91)	27.3	11.30	10.65	3.89	0.344	0.528	-0.257
14/NY	44.6	12.24	10.80	5.68	0.464	1.387	2.548
WY/94	31.8	10.22	9.6	3.88	0.380	1.141	2.315
94/JR	52.5	11.73	10.1	5.15	0.439	1.440	3.840

Table 8-14 Front Axle Weight (Kips) Statistics.

Location	Max	Mean	Median	Std. Dev.	C.O.V.	Skewnes	Kurtosis
23/HR (92)	19.6	8.80	8.7	2.14	0.243	1.070	3.152
23/HR (91)	19.1	9.50	9.4	2.08	0.219	0.465	1.248
23/SR	19.9	9.30	9.2	2.04	0.219	0.504	1.080
94/PR (93)	20.8	9.71	9.7	1.68	0.173	0.0978	1.747
94/PR (91)	13.2	9.71	9.9	1.58	0.163	-0.725	0.677
14/NY	23.5	9.48	9.4	2.10	0.222	0.999	3.888
WY/94	18.8	9.18	9.0	2.09	0.228	0.513	1.258
94/JR	23.0	9.28	8.90	2.11	0.227	0.812	1.999

Table 8-15. Following Axle Weight (kips) Statistics.

Location	Max	Mean	Median	Std. Dev.	C.O.V.	Skewnes	Kurtosis
23/HR (92)	44.9	11.57	10.9	4.87	0.421	1.171	2.281
23/HR (91)	58.7	11.86	11.4	4.68	0.395	1.211	4.670
23/SR	40.8	13.24	12.2	5.98	0.452	0.698	0.0173
94/PR (93)	54.3	11.87	11.4	4.50	0.379	0.802	2.346
94/PR (91)	27.3	11.76	11.55	4.23	0.360	0.276	-0.726
14/NY	44.6	13.16	12.4	6.17	0.469	1.055	1.458
WY/94	31.8	10.63	10.4	4.32	0.406	0.915	1.315
94/JR	52.5	12.55	11.3	5.60	0.446	1.136	2.707

8. 4 US-23 over the Huron River (23/HR) in Ann Arbor, Michigan

Fig. 8-1 and 8-2 are the histograms of gross vehicle weight (GVW) for all trucks measured on 23/HR in 1991 and 1992 respectively. Vehicles weighing less than 15 kips are excluded from the histograms. The distribution shapes of Fig. 8-1 and 8-2 are essentially the same with some minor differences at specific range levels, indicating that there is little change in the traffic over a one year period. The cumulative distribution functions (CDFs) - see more in Appendix A - of 1991 and 1992 GVW in Fig. 8-5 can be readily compared and similarity in shape observed, supporting the same conclusion. Results of the individual day measurements are presented in Fig. 8-7 for 6/22/92 and 6/23/92. The day to day CDFs are very similar in shape and average GVW with only a slight difference at the upper tail of the distribution. Fig. 8-8 presents day to day CDFs for 7/2/91 and 8/28/91 indicating a more pronounced difference between the two days of data. Due to the data not being collected on consecutive days, the CDFs will exhibit a slightly different distribution. From the Table 8-10 the heaviest vehicle observed in 1991 weighed 177.7 kips and 170.6 kips in 1992 with a mean GVW of 52.1 and 46.6 kips respectively.

Fig. 8-3 and 8-4 are the histograms of 5 and 11 axle vehicle GVW. Differences between 1991 and 1992 data are more pronounced for a given vehicle type, however a similar trend in the distributions is evident. Also apparent is the much higher GVW for 11 axle vehicles as compared to the 5 axle vehicles. CDFs for 5 and 11 axle trucks are plotted in Fig. 8-6. Each circle or square represents one truck in the data file. The CDFs exhibit a consistent shape between 1991 and 1992 except for one very heavy 5 axle vehicle weighed in 1991. It is apparent from the distribution of Fig. 8-6 that the northbound 23/HR is predominantly carrying loaded 11 axle trucks, resulting in a very high mean GVW for 11 axle vehicles. The 1992 and 1991 mean 5 axle vehicle GVWs are 49.5 kips and 52.6 kips. The 1992 and 1991 mean 11 axle vehicle GVW's are 137.5 kips and 148.3 kips (Tables 8-11 and 8-12). For comparison of the daily distributions of 5 and 11 axle

vehicles, the CDFs for both days are plotted in Fig. 8-9 and 8-10. There is little day to day variation in the distributions for 5 and 11 axle vehicles.

Potentially more important for fatigue cycles and the distribution of moments for a given bridge are the axle weights and spacing for the trucks passing over the bridge. Fig. 8-11 through 8-19 present the axle weight distributions of the vehicles discussed above. All distributions include axles with weights greater than 5000 pounds.

Fig. 8-11 to 8-16 are the 1992 and 1991 axle weight histograms of all vehicles axles for 23/HR. The corresponding CDFs are presented in Fig. 8-17, 8-18, and 8-19. Front and following axle weight histograms of Fig. 8-13 through 8-16 indicate a significant difference in both variation and magnitudes. Front axle weight has a much smaller variation than the following axle weight as observed in the graphs and from Table 8-13 through 8-15. As observed from the CDFs of Fig. 8-18 and 8-19 the 1992 and 1991 mean front axle weights are 8.80 kips and 9.50 kips with a maximum of 19.6 kips and 19.1 kips. The 1992 and 1991 following axle means are 11.57 kips and 11.86 kips with a maximum of 44.9 kips and 58.7 kips. The higher variation in the following axle weights is readily apparent from the CDF comparison. The 1992 and 1991 maximum axle weight observed at 23/HR is 44.9 kips and 58.7 kips with means of 10.84 kips and 11.30 kips respectively. As is the case with GVW, there is very little daily variation in the vehicle axle weights.

Of greater interest is the effect of the GVW, axle weight and axle spacing. The effect of these parameters can be determined by the lane moment caused by the truck. Fig. 8-20 through 8-35 present lane moments for various simply supported spans. Each truck in the data base is analytically driven across the bridge to determine the maximum static bending moment per lane for various simple span lengths. The CDFs of the lane moments for spans of 20, 30, 60, 90, 120, and 200 feet are then determined. As a point of reference the

lane moments are presented in terms of the truck lane moment to HS20 moment.

Fig. 8-20 through 8-23 plot the CDF's for moment effect of all trucks with GVW greater than 15 kips for 1992 and 1991. The mean of lane moment to HS20 moment is approximately 0.5 to 0.6 for all spans for both 1992 and 1991. The maximum 1992 lane moment to HS20 moment varies from 1.862 for a 200 ft. span to 2.385 for a 30 ft. span. For 1991 the maximum lane moment to HS20 moment varies from 1.872 for a 20 ft. span to 2.267 for a 120 ft. span. As or the GVW data, a comparison is made between 5 and 11 vehicles for both 1992 and 1991. Fig. 8-24 through 8-27 present 5 and 11 axle vehicle CDF's for simple spans of 20, 30, 60, 90, 120, and 200 ft. As a comparison of vehicle type for a given span, 5, 11, and all vehicle moment CDF's are plotted in Fig. 8-28 and 8-29 for a 60 ft simple span. The significant observation to be made from these graphs is that 11 axle vehicles induce the largest moments in the bridge

Fig. 8-30 through 8-35 compare the lane moment ratios for 1992 and 1991 by span. It can be observed that there is little practical yearly difference in moment effect caused by the heavier (>15 kip) vehicles, with some minor differences at the upper tail of the distributions.

Also important for fatigue is correlation of GVW to moment effect. This is again highly dependent on axle weight and axle spacing, and span length. Fig. 8-36 through 8-47 present scatter plots of lane moment vs. GVW for 20, 30, 60, 90, 120, and 200 foot spans. It can be observed from these figures that correlation between lane moment and GVW is not good for the shorter spans, but by 200 feet becomes nearly directly correlated. Fig. 8-36 through 8-47 consider only the static effect of the vehicles, however, there are many factors which affect the impact factor to be applied to the moment.

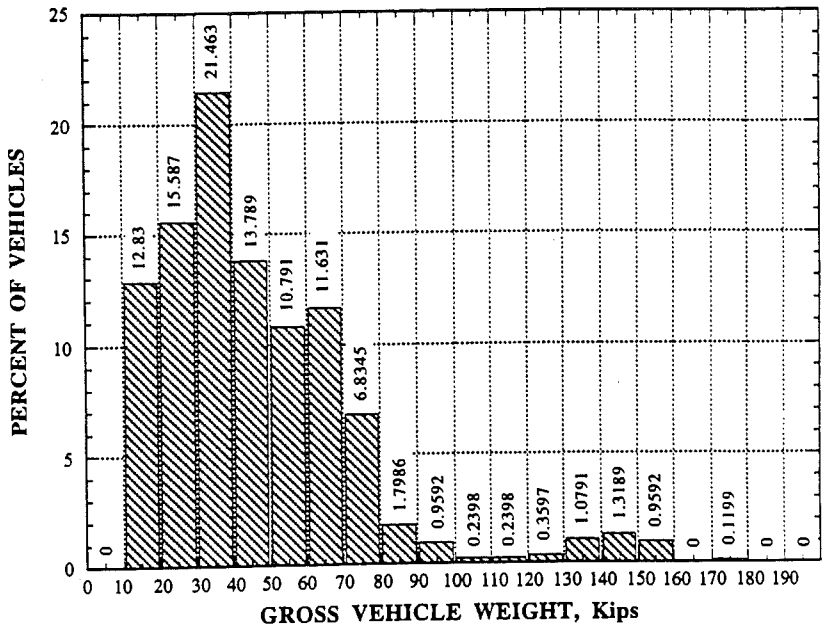

Fig. 8-1. US-23/HR, 1992, NB, GVW Histogram - Veh > 15 Kips.

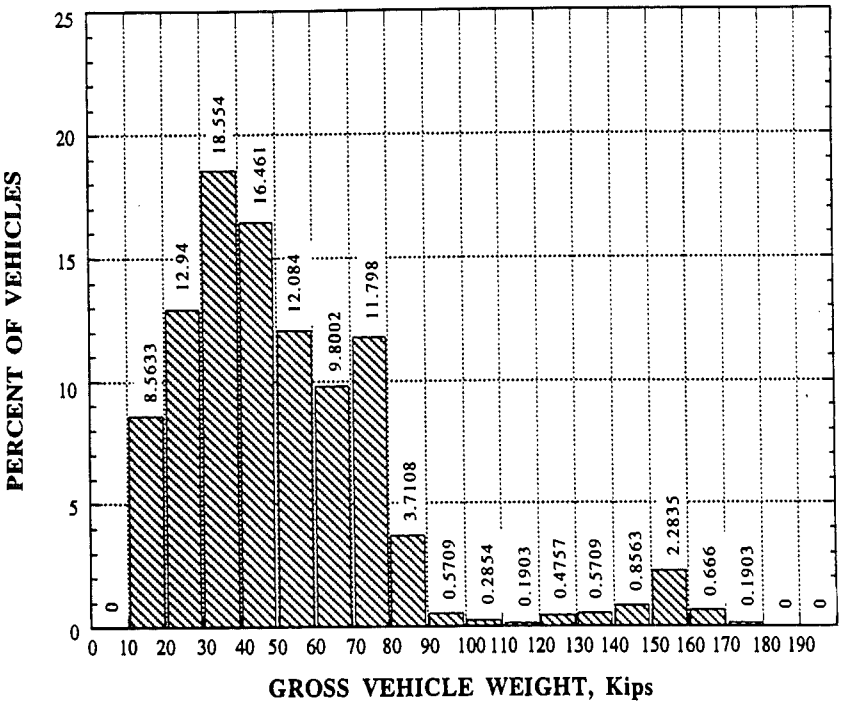

Fig. 8-2. US-23/HR, 1991, NB, GVW Histogram - Veh > 15 Kips.

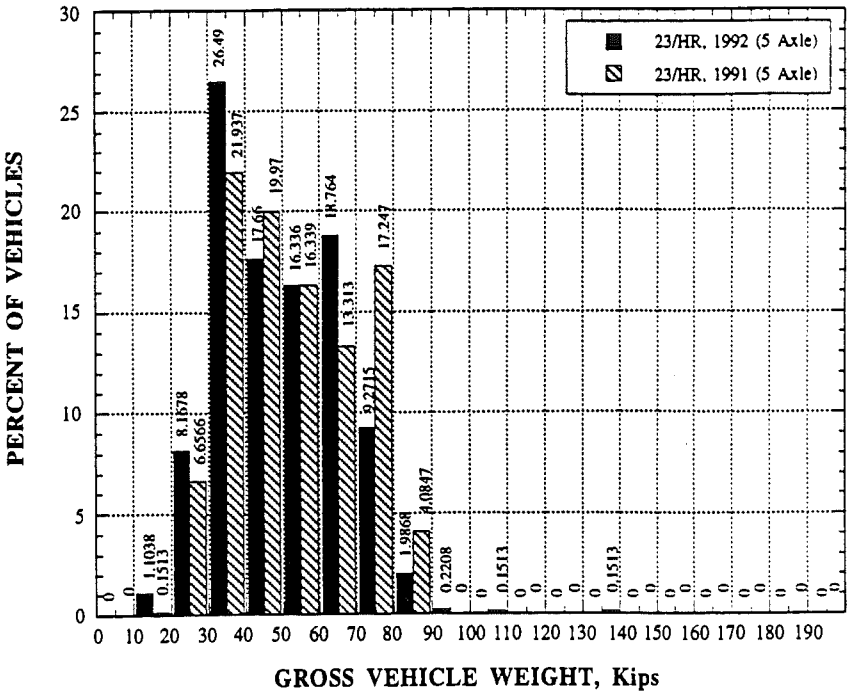

Fig. 8-3. US-23/HR. 1991, 1992, 5 Axle GVW > 15 Kips Histogram.

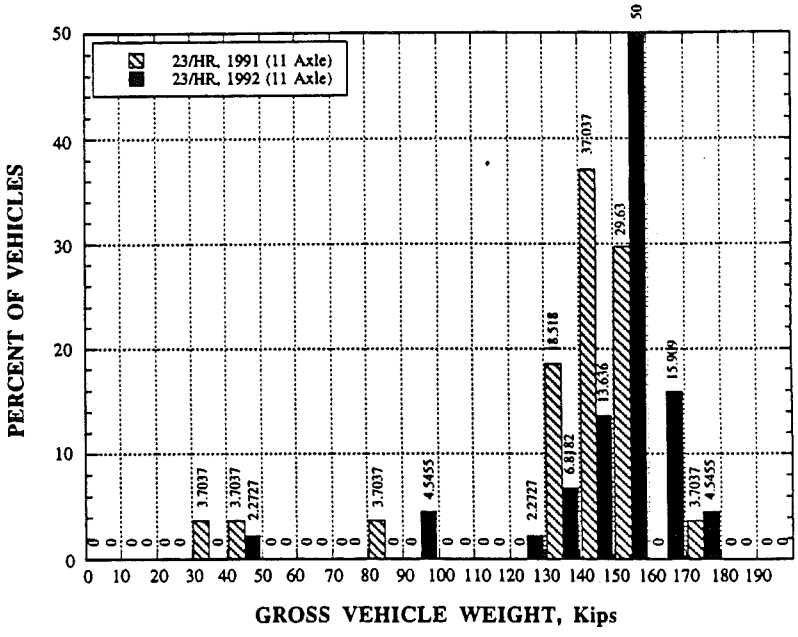

Fig. 8-4. US-23/HR. 1991, 1992, 11 Axle GVW>15 Kips Histogram.

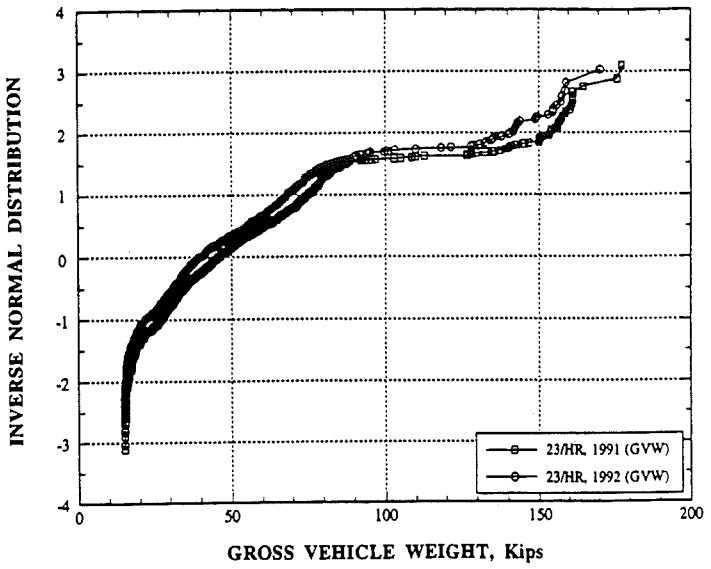

Fig. 8-5. 23/HR, 1991, 1992, NB, GVW CDF - Veh > 15 Kips.

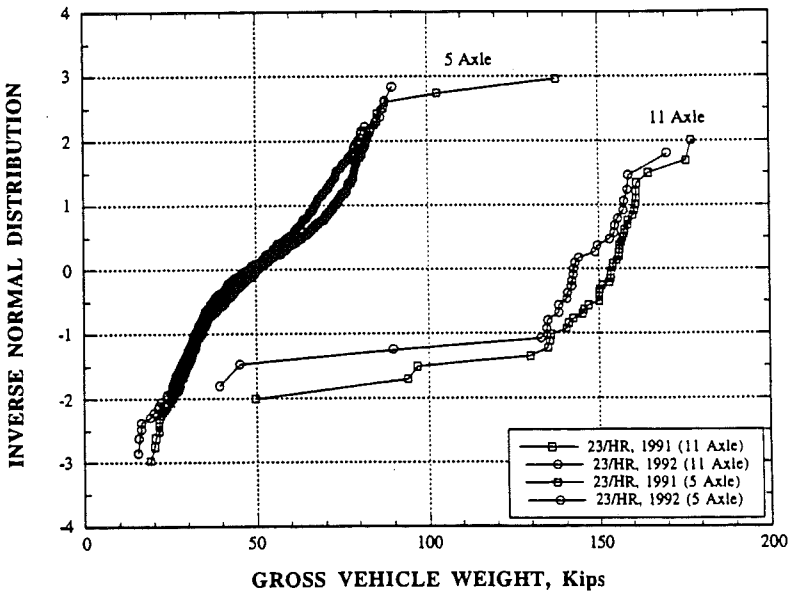

Fig. 8-6. 23/HR, 1991, 1992, 5 & 11 Axle GVW CDF -Veh>15 Kips.

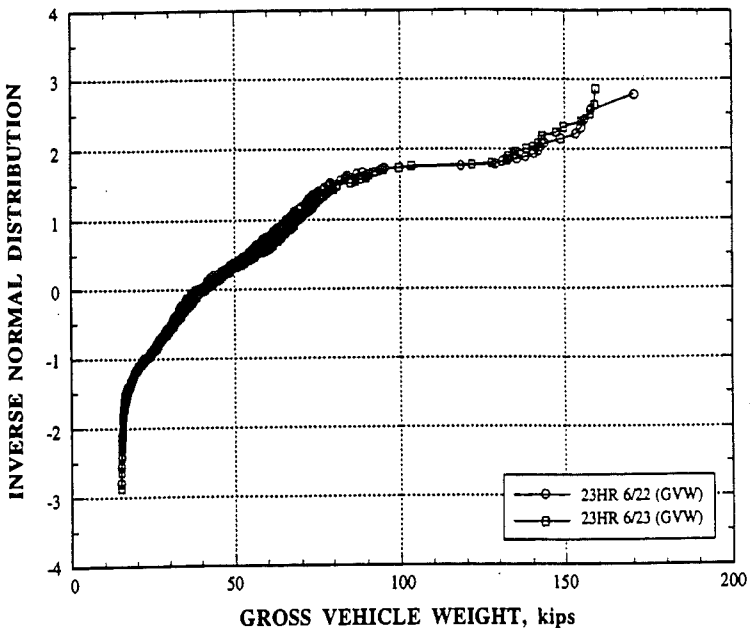

Fig. 8-7. US-23/HR, 1992, Daily GVW CDF - Veh.>15 Kips.

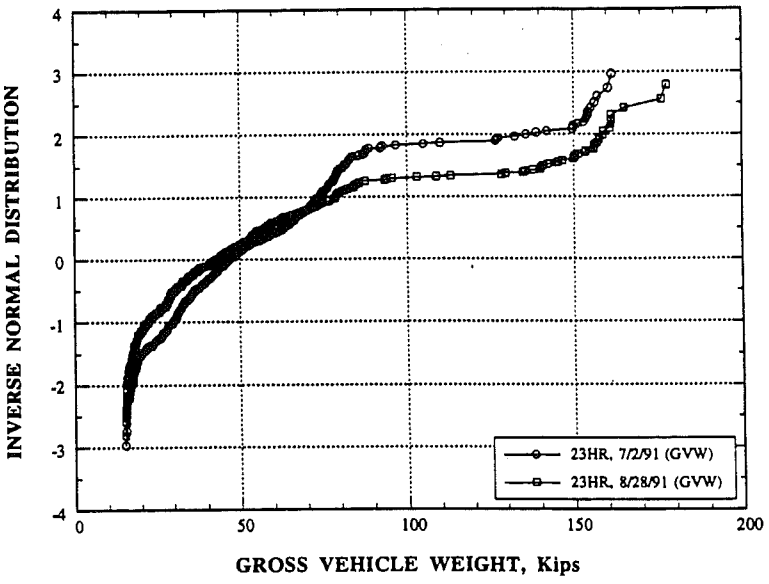

Fig. 8-8. 23/HR, 1991 Daily, GVW CDF - Veh.>15 Kips.

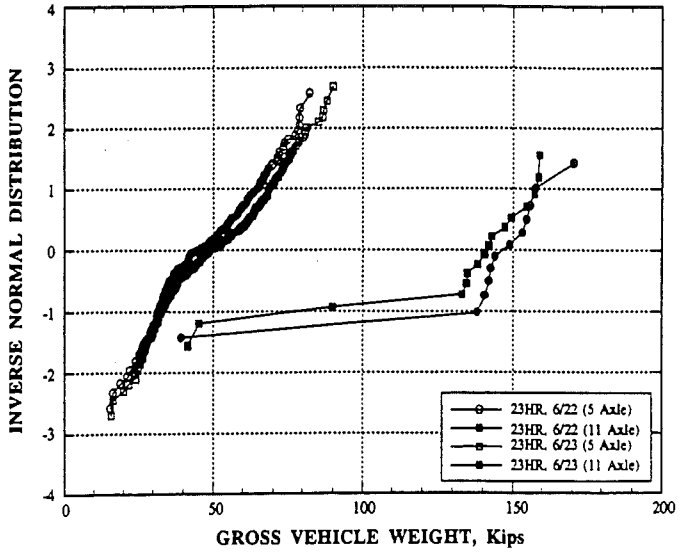

Fig. 8-9. 23/HR, 1992 Daily, 5 and 11 Axle GVW > 15 Kips CDF

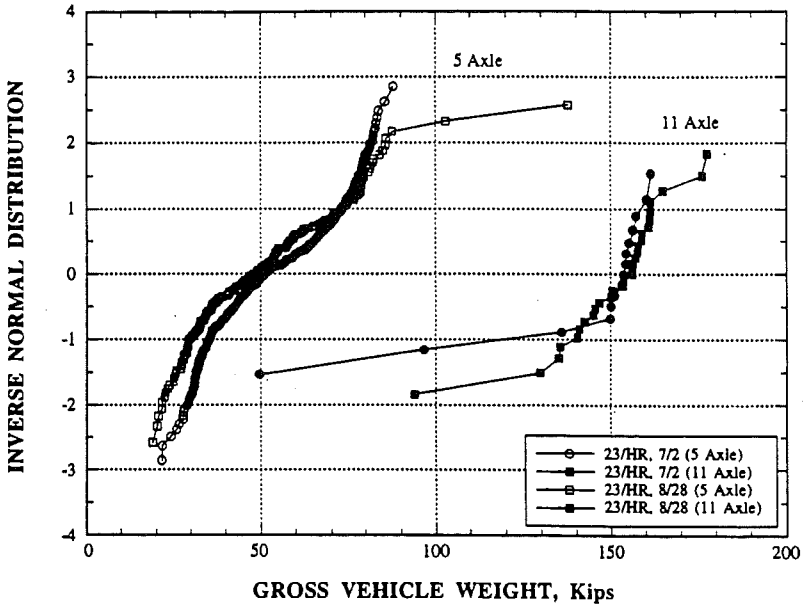

Fig. 8-10. 23/HR, 1991 Daily, 5 and 11 Axle GVW > 15 Kips CDF.

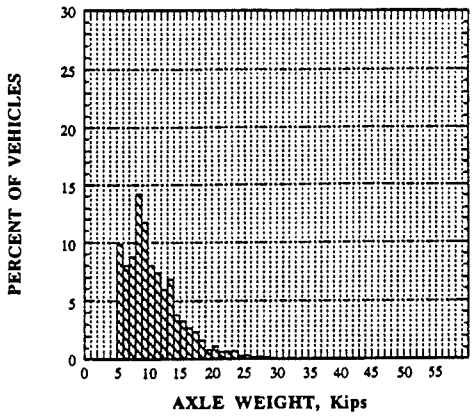

Fig. 8-11. 23/HR 1992 Axle Weight

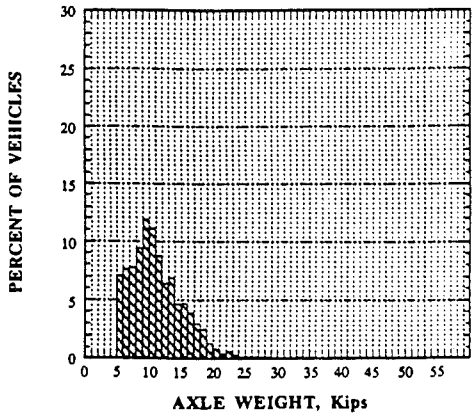

Fig. 8-12. 23/HR 1991 Axle Weight

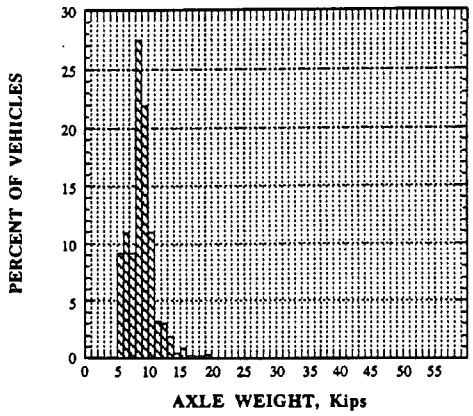

Fig. 8-13. 23/HR 1992 Front Axle Wt.

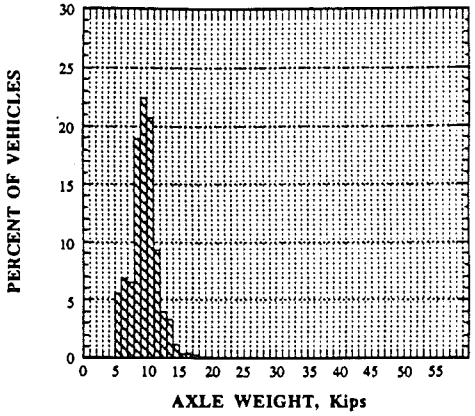

Fig. 8-14. 23/HR 1991 Front Axle Wt.

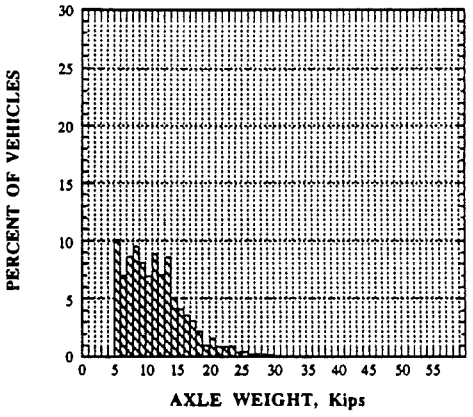

Fig. 8-15. 23/HR 1992 Following Axle Wt.

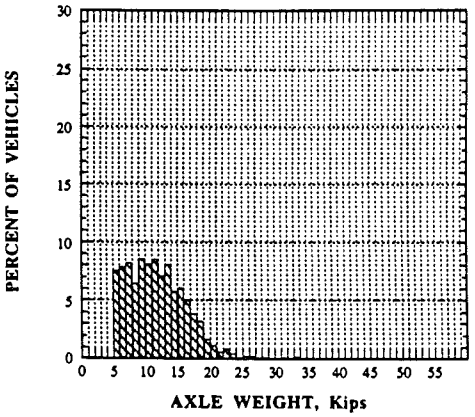

Fig. 8-16. 23/HR 1991 Following Axle Wt.

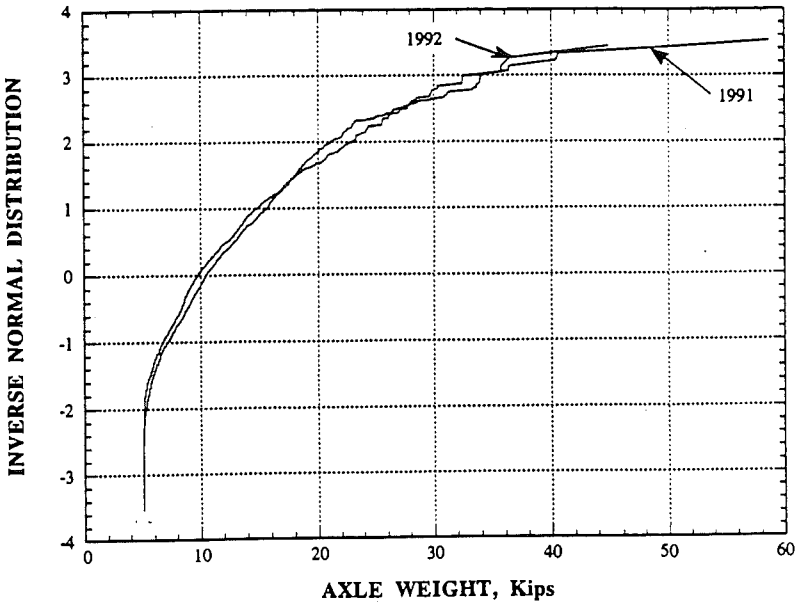

Fig. 8-17. 23/HR, 1991, 1992, Axle Weight CDF- All Axles > 5 Kips.

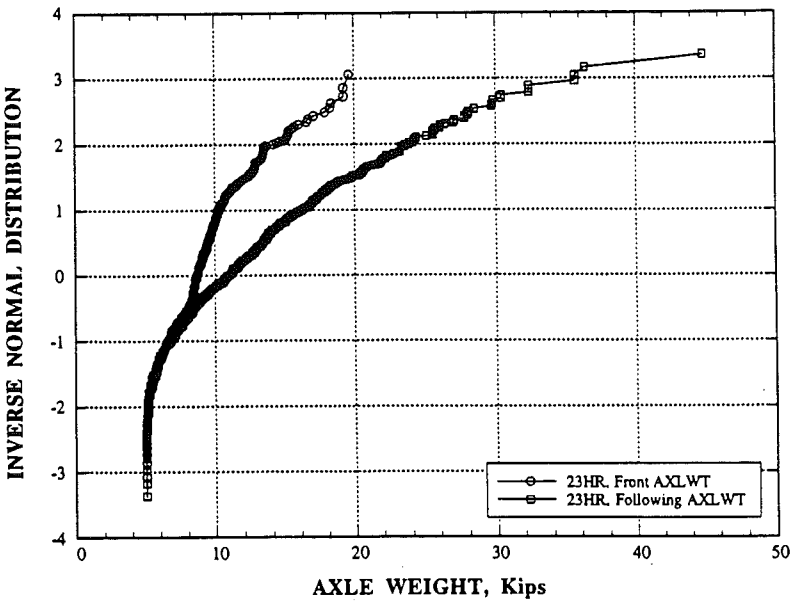

Fig. 8-18. 23/HR, 1992 ,Front and Following Axle Weight CDF.

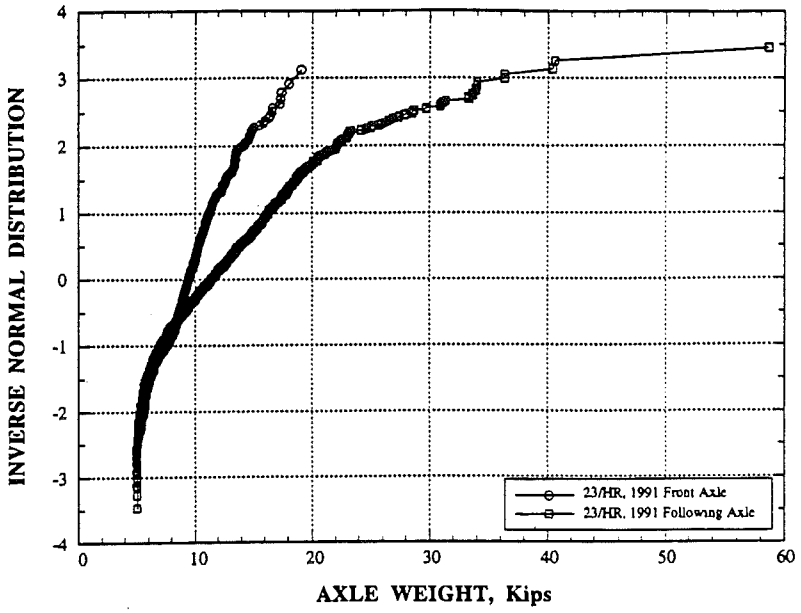

Fig. 8-19. 23/HR, 1991, Front and Following Axle Weight CDF.

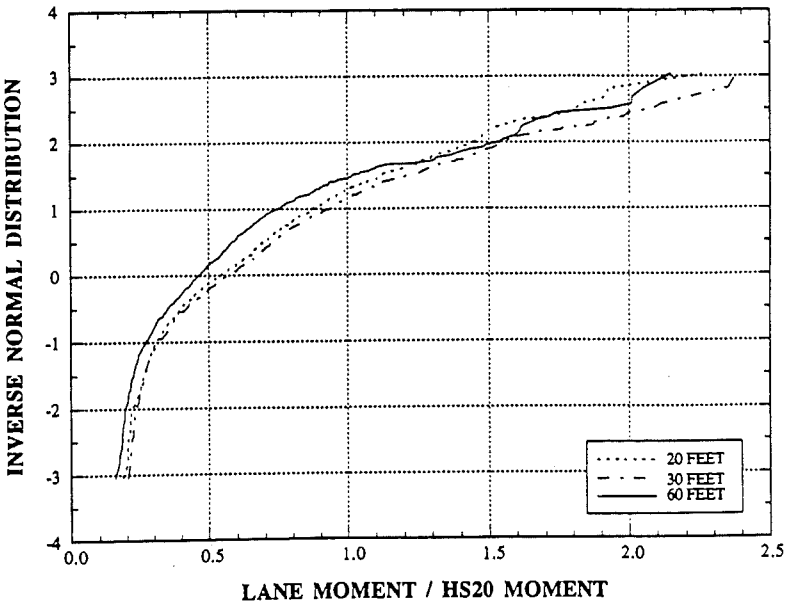

Fig. 8-20. 23/HR, Lane Moment CDF, 20, 30, & 60 Ft, 1992.

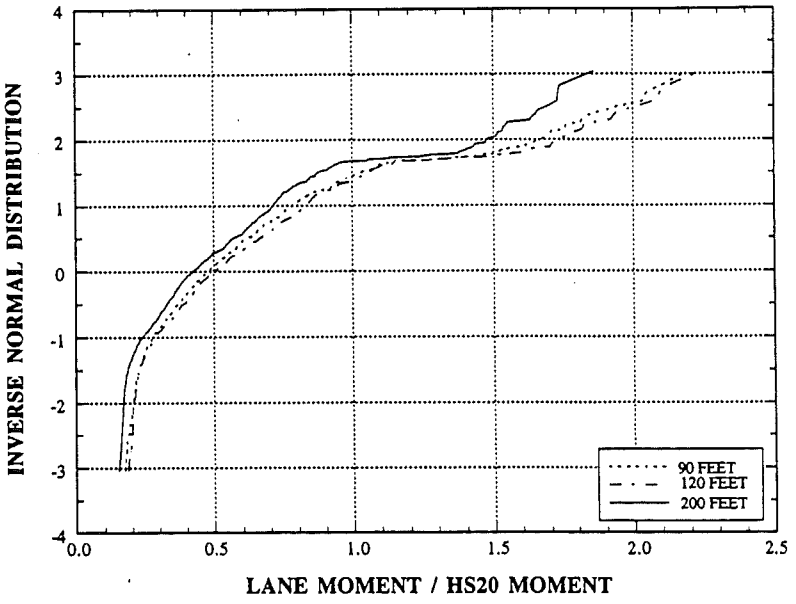

Fig. 8-21. 23/HR, Lane Moment CDF, 90, 120, & 200 Ft, 1992.

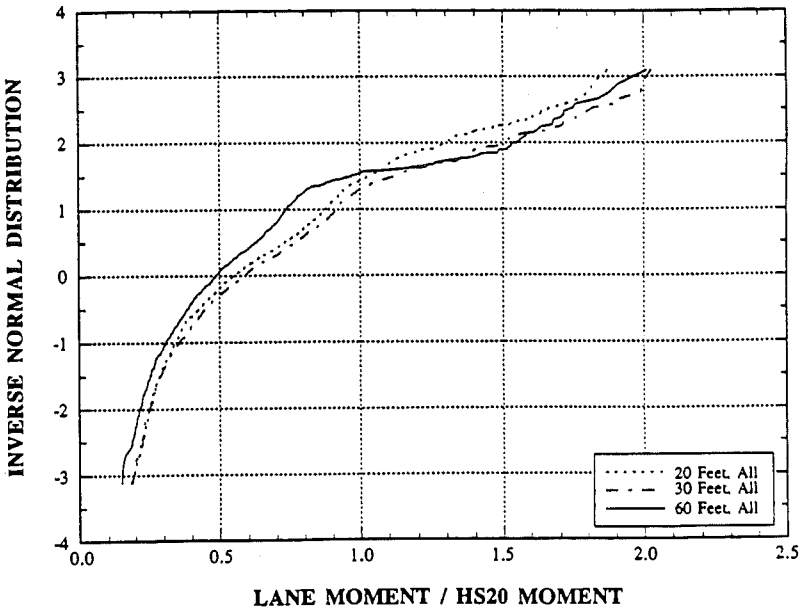

Fig. 8-22. 23/HR. Lane Moment CDF, 20, 30, & 60 Ft, 1991.

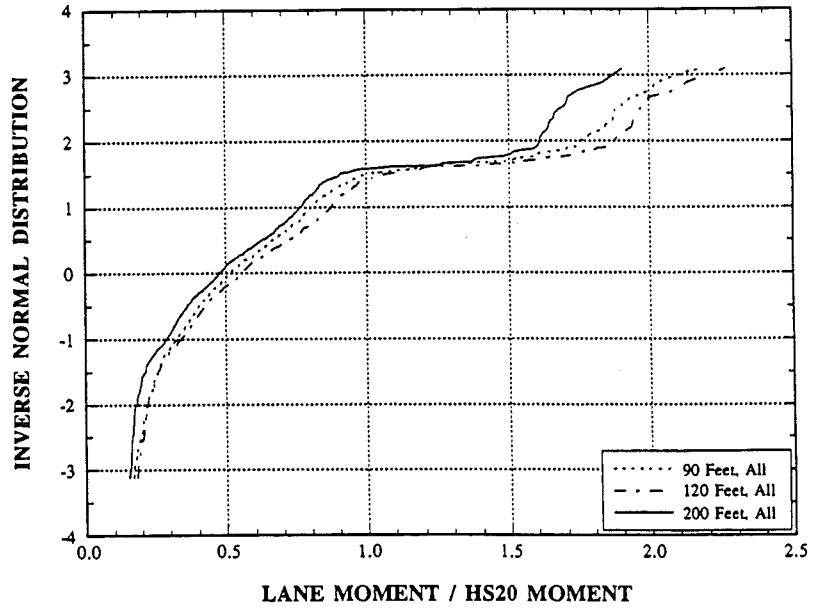

Fig. 8-23. 23/HR, Lane Moment CDF, 90, 120, & 200 Ft, 1991.

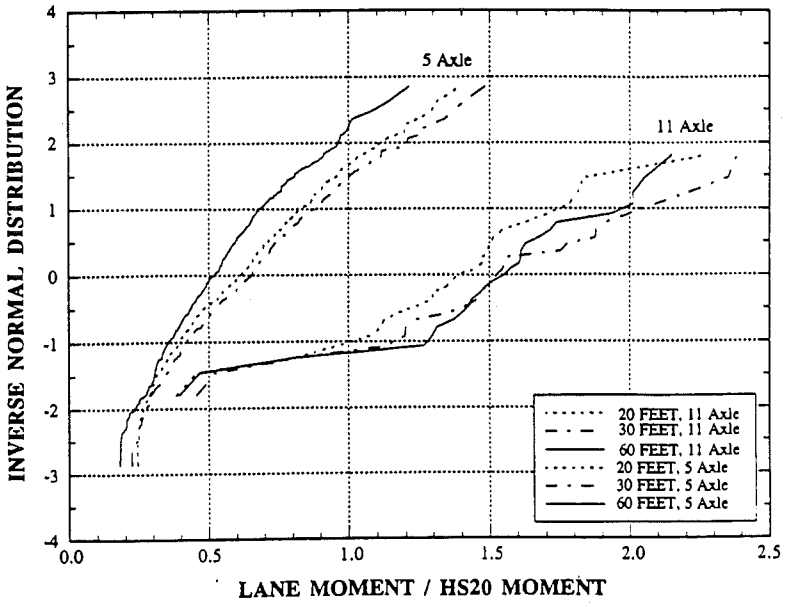

Fig. 8-24. 23/HR, 5 & 11 Axle Lane Mom. CDF, 20, 30, & 60 Ft, 1992.

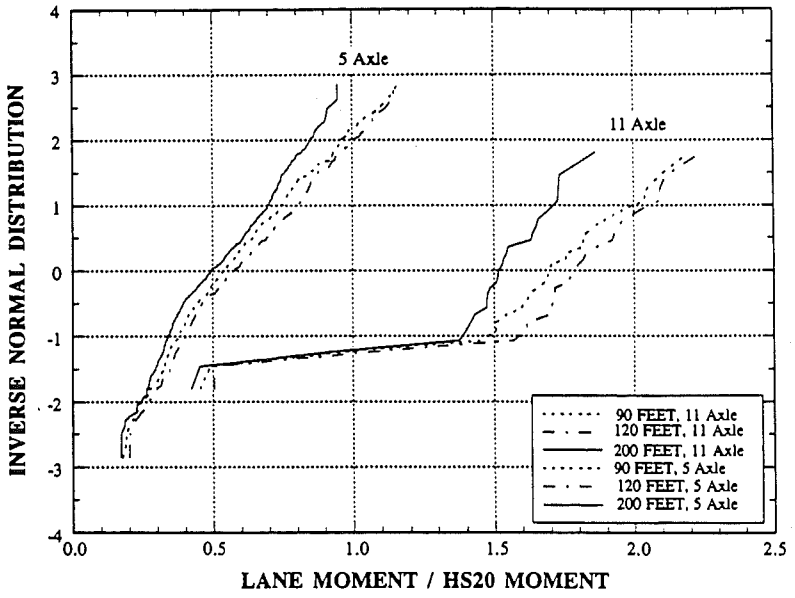

Fig. 8-25. 23/HR, 5 & 11 Axle Lane Mom. CDF, 90, 120, & 200 Ft, 1992.

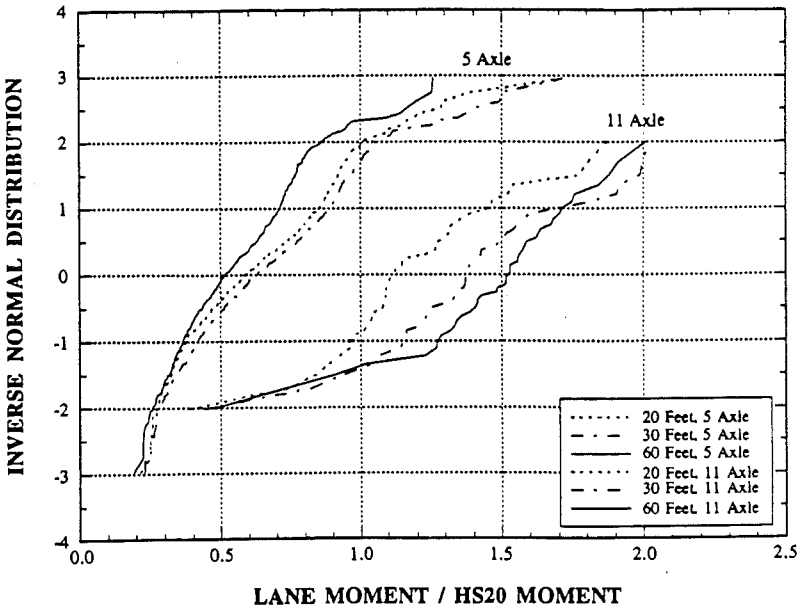

Fig. 8-26. 23/HR, 5 & 11 Axle Lane Moment CDF, 20, 30, & 60 Ft, 1991.

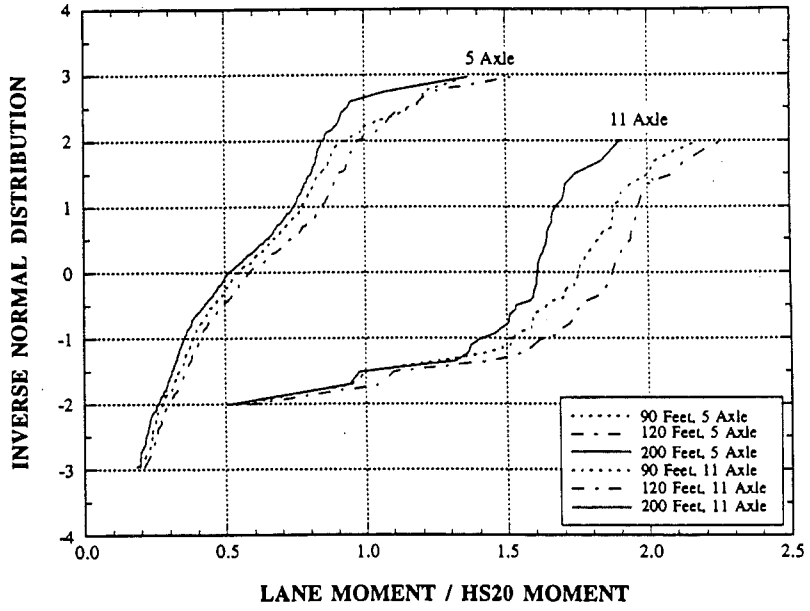

Fig. 8-27. 23/HR, 5 & 11 Axle Lane Mom. CDF, 90, 120, & 200 Ft, 1991.

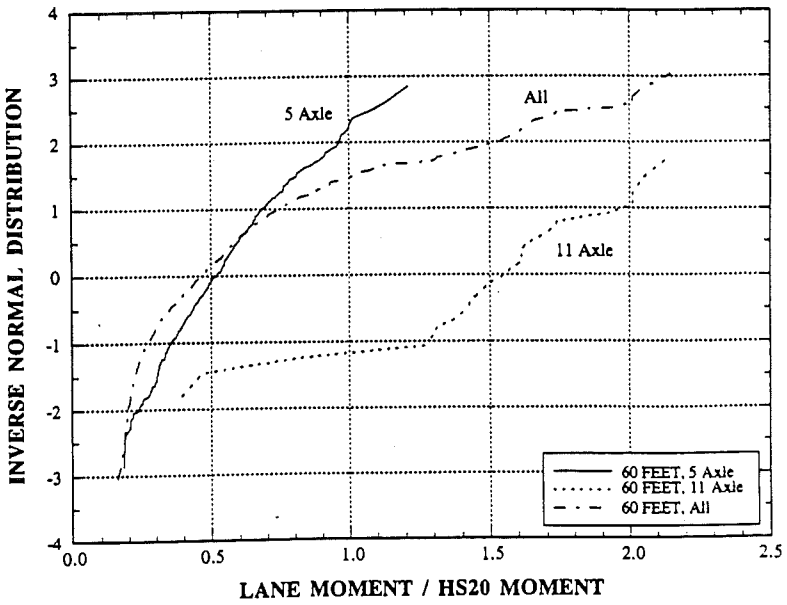

Fig. 8-28. 23/HR, 5, 11 & All Axle Lane Moment CDF, 60 Ft, 1992.

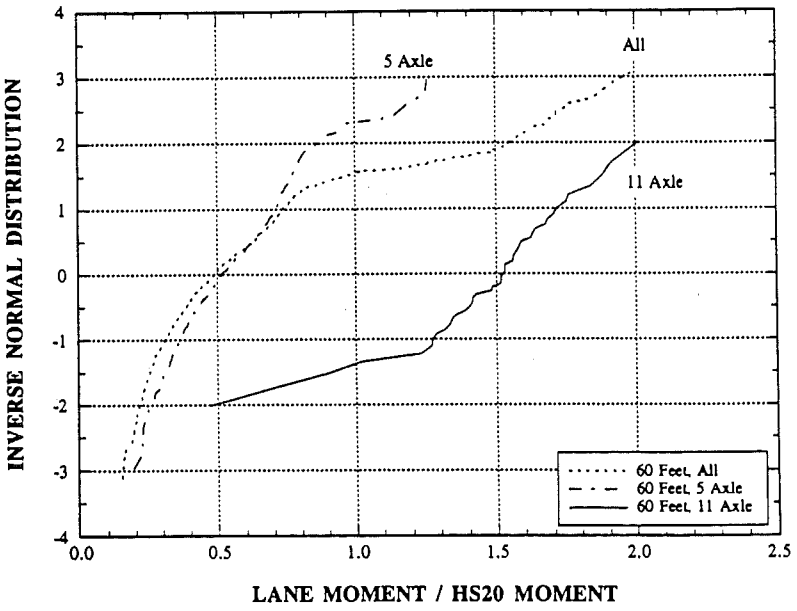

Fig. 8-29, US-23/Huron Rr 5, 11 & All Axle Lane Mom CDF, 60 Ft, 1991.

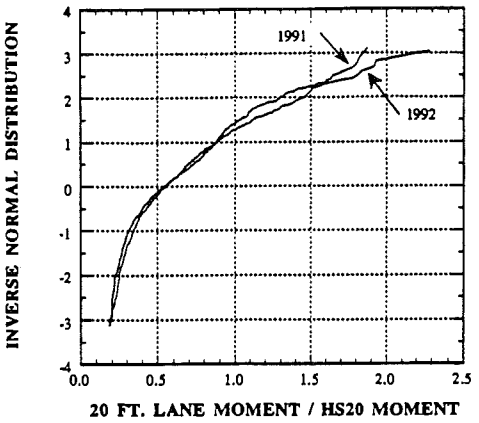

Fig. 8-30, 23/HR. 20 Ft. Moment

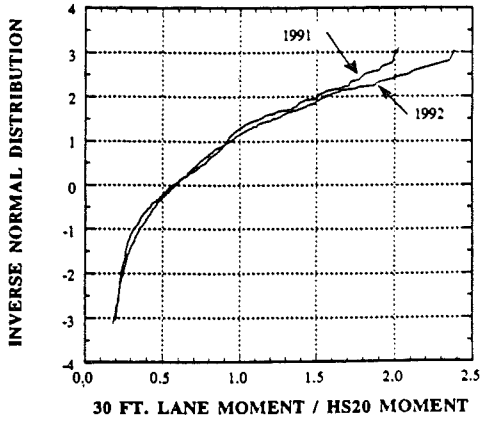

Fig. 8-31. US-23/HR. 30 Ft. Moment

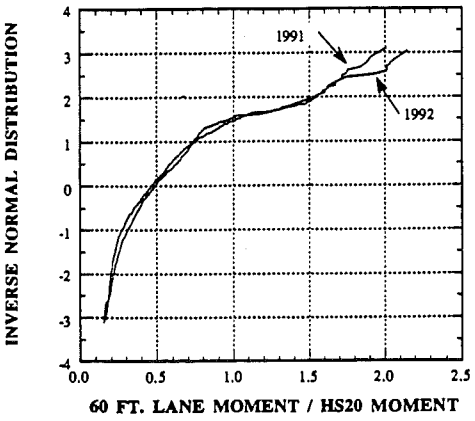

Fig. 8-32. 23/HR. 60 Ft. Moment

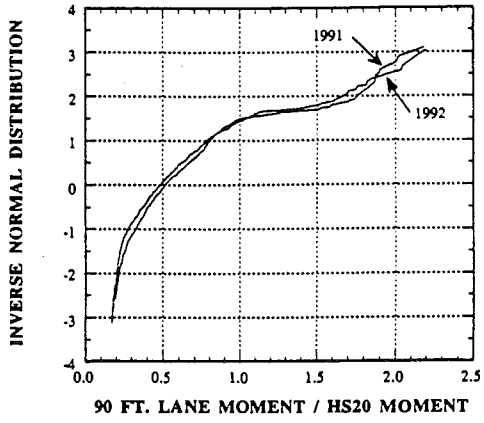

Fig. 8-33, 23/HR. 90 Ft. Moment

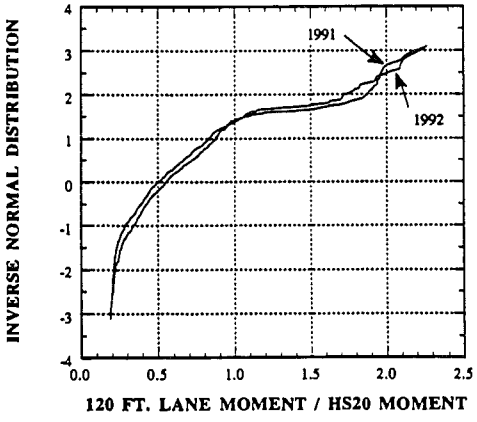

Fig. 8-34. US-23/HR. 120 Ft. Moment

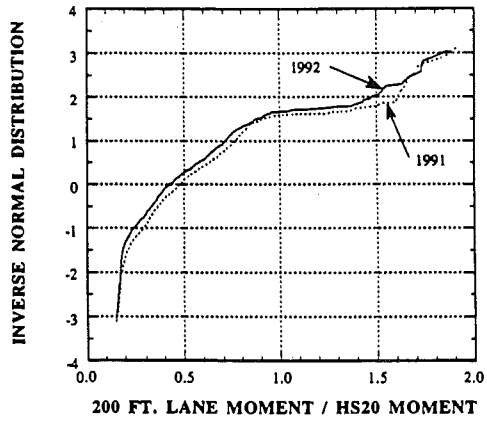

Fig. 8-35.23/HR. 200 Ft.Moment

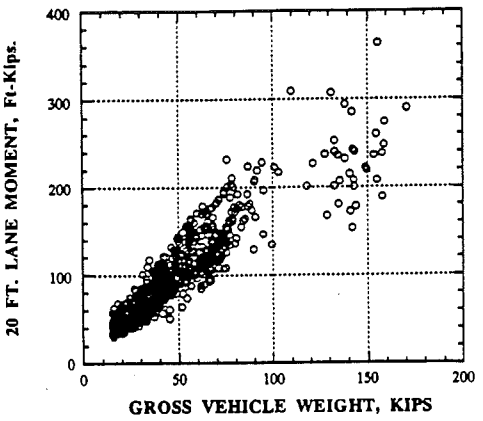

Fig. 8-36. 23/HR(92) Mom v GVW, 20 Ft.

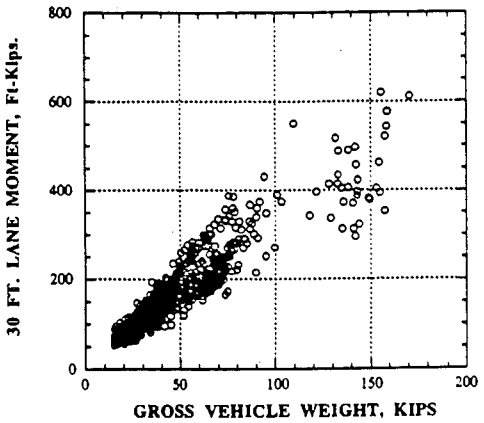

Fig. 8-37. 23/HR(92) Mom v GVW, 30 Ft.

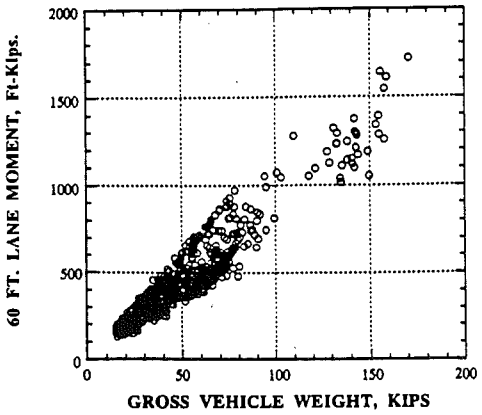

Fig. 8-38. 23/HR(92) Mom v GVW, 60 Ft.

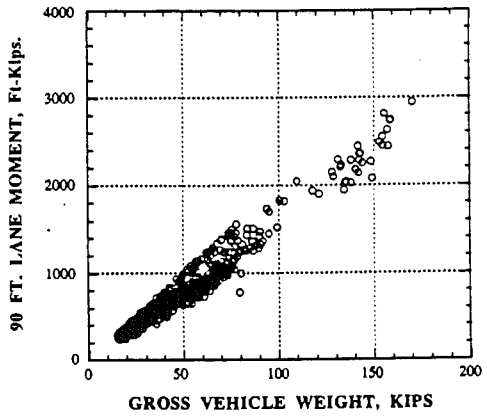

Fig. 8-39. 23HR(92) Mom vGVW, 90 Ft.

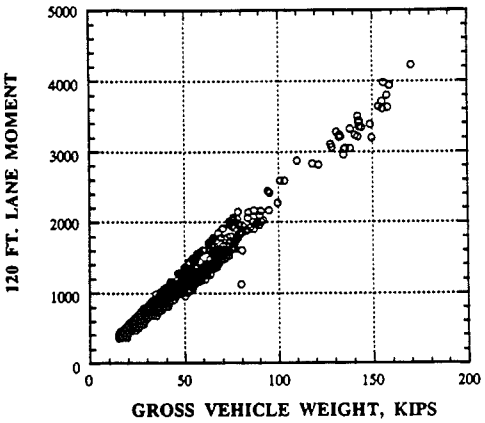

Fig. 8-40. 23HR(92) Mom v GVW, 120 Ft.

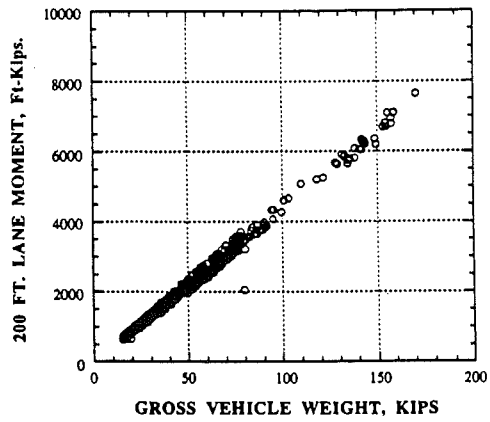

Fig. 8-41. 23HR(92) Mom v GVW, 200 Ft.

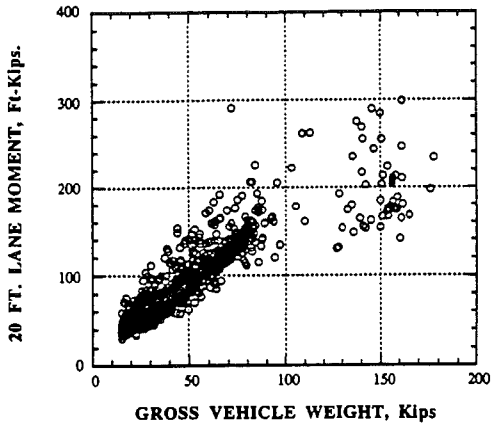

Fig. 8-42. 23HR(91) Mom v GVW, 20 Ft.

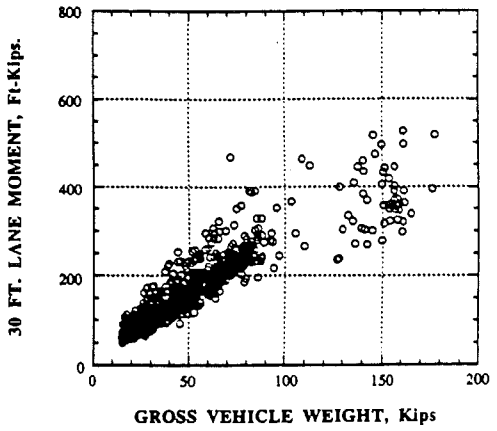

Fig. 8-43. 23HR(91) Mom v GVW, 30 Ft.

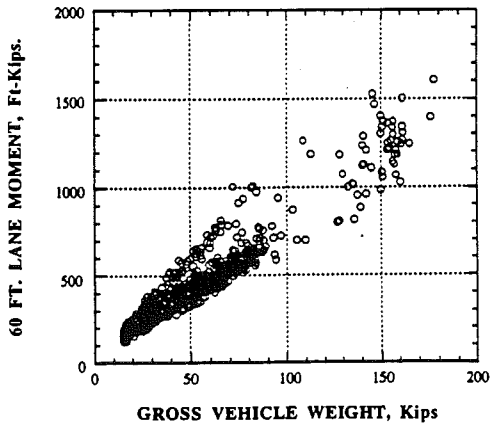

Fig. 8-44. 23HR(91) Mom v GVW, 60 Ft.

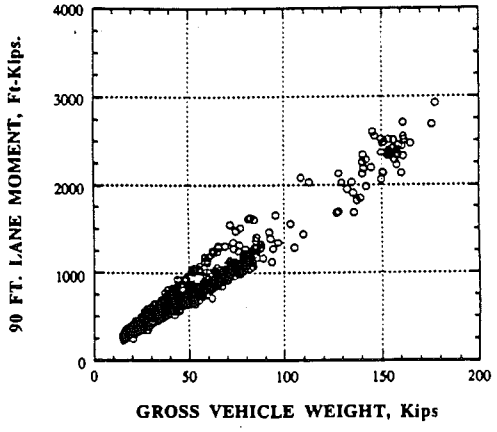

Fig. 8-45. 23HR(91) Mom v GVW, 90 Ft.

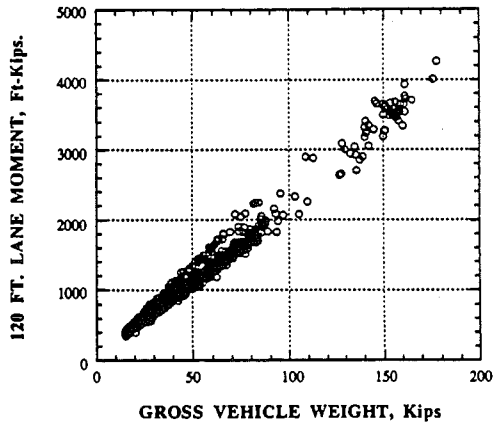

Fig. 8-46. 23HR(91) Mom v GVW, 120 Ft.

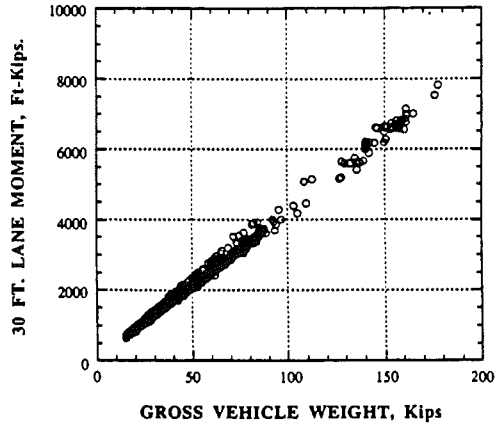

Fig. 8-47. 23HR(91) Mom v GVW, 200 Ft.

8. 5 M-14 over N.Y.C. Railroad (14/NY) in Ann Arbor, Michigan

Fig. 8-48 is the histogram of gross vehicle weight (GVW) for all trucks measured on 14/NY. Vehicles weighing less than 15 kips are excluded from the histogram. The corresponding cumulative distribution function (CDF) of GVW for all trucks is shown in Fig. 8-49. Each circle represents one truck in the data file. From the Table 8-10 the heaviest vehicle observed weighed 267.9 kips and the mean GVW for all trucks is 54.1 kips.

Fig. 8-50 is the histogram of all 5-axle vehicles and Fig. 8-51 is the histogram of all 11-axle vehicles. The corresponding CDFs of the five and 11-axle vehicles are shown in Fig. 8-52. The CDFs of Fig. 8-52 again clearly indicate that the heaviest vehicles are 11-axle trucks. It is apparent from the distributions of Fig. 8-52, with each square and circle indicating a truck, that eastbound 14/NY is carrying an approximately log normal distribution of five-axle vehicles. The database contains just 15 passing 11-axle vehicles, which was not a sufficient number to observe a general trend. The mean five-axle vehicle GVW is 55.2 kips with a maximum GVW of 131.6 kips. The mean 11-axle vehicle GVW is 171.3 kips with a maximum GVW of 267.9 kips (Tables 8-11 and 8-12).

Potentially more important for fatigue cycles and the distribution of moments for a given bridge are the axle weights and spacing for the trucks passing over the bridge. Figs 8-53 through 8-56 present the distributions of the axle weights of the vehicles discussed above. All distributions include axles with weights greater than 5,000 pounds.

Fig. 8-53 is the axle weight histogram of all vehicle axles observed and the corresponding CDF is presented in Fig. 8-54. The maximum axle weight observed at 14/NY was 48,6 kips with a mean of 12.24 kips. As is the case with GVW, there is very little daily variation in the vehicle axle weights with some differences at the upper tail of the distribution. The front and following axle weight histograms of Fig. 8-55 indicate a significant difference in both variation and magnitudes. As observed from the CDFs of Fig. 8-56 the mean front axle weight is 9.48 kips with a

maximum of 23.5 kips while the following axle mean is 13.16 kips with a maximum of 48.6 kips. The higher variation in the following axle weights is readily apparent from the CDF comparison.

Of greater interest is the effect of the GVW, axle weight and axle spacing on the bridge structure and components. The effect of these parameters can be determined in part by the lane moment caused by the vehicles crossing the bridge. Each truck in the data base is analytically driven across the bridge to determine the maximum bending moment per lane for various simple span lengths. The CDFs of the lane moments for simple spans of 20, 30, 60, 90, 120, and 200 feet are then determined. As a point of reference the lane moments are presented in terms of the truck lane moment to HS20 moment.

Fig. 8-57 and 8-58 plot the CDFs for lane moment effect of all trucks with GVW greater than 15 kips for 14/NY. The mean of lane moment to HS20 moment is approximately 0.5 to 0.6 for the spans. The maximum ratio of lane moment to HS20 moment varies from 2.3 for a 20 ft. span to 3.3 for a 120 ft. span. Similar to the GVW data, a comparison is made between 5 and 11 axle moments. Fig. 8-59 and 8-60 present 5 and 11 axle vehicle CDFs for simple spans of 20, 30, 60, 90, 120, and 200 ft. As a comparison of vehicle type for a given span, 5, 11, and all vehicle moment CDFs are plotted for a 60 ft simple span in Fig. 8-61.

Also important for fatigue is correlation of GVW to moment effect. This again is highly dependent on axle weight and axle spacing, and span length. Fig. 8-62 through 8-67 present scatter plots of lane moment vs. GVW for 20, 30, 60, 90, 120, and 200 foot simple spans. It can be observed from the Fig.s that correlation between lane moment and GVW is not good for the shorter spans, but by 200 feet becomes nearly directly correlated. It must be noted that Fig. 8-62 through 8-67 consider only the static effect of the vehicles, however, there are many factors which affect the impact factor to be applied to the moment.

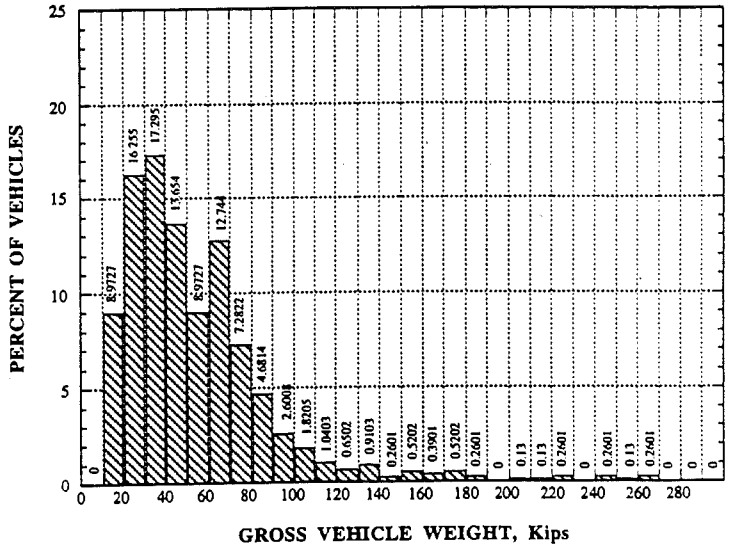

Fig. 8-48. 14/NY, EB, GVW Histogram - Vehicles > 15 Kips.

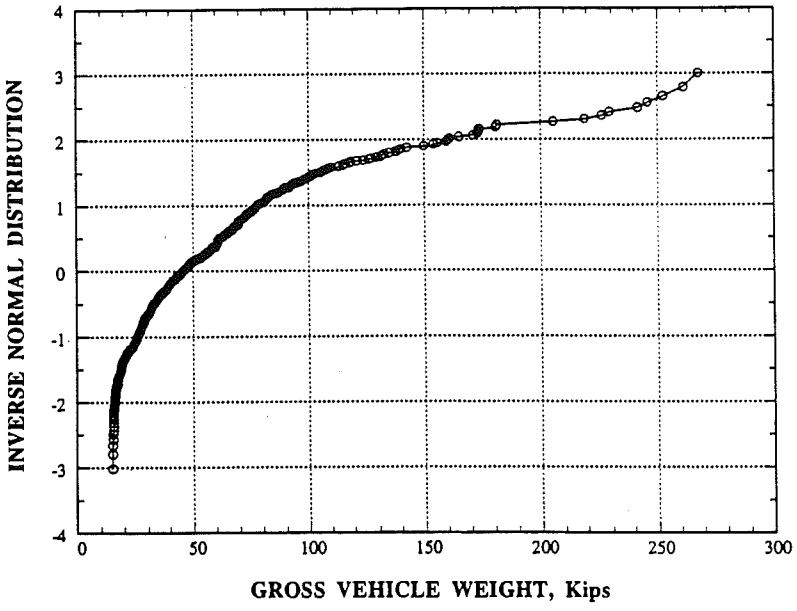

Fig. 8-49. 14/NY, EB, GVW CDF - Vehicles > 15 Kips.

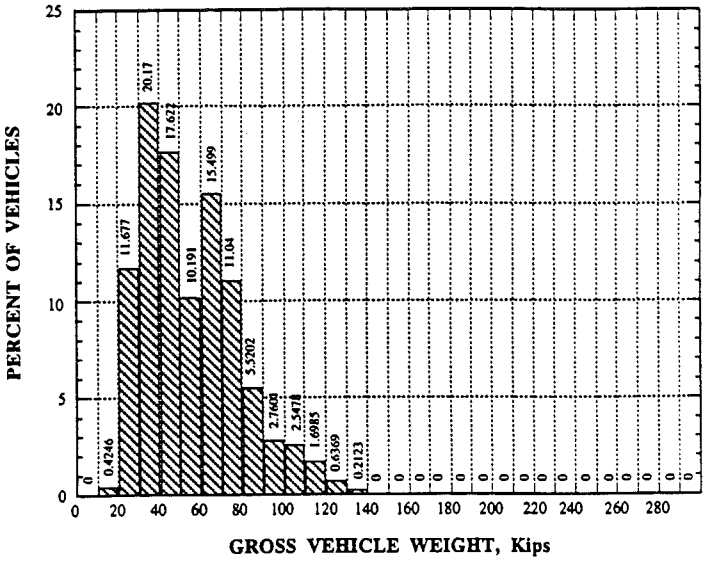

Fig. 8-50. M-14/New York RR EB 5 Axle GVW - Veh > 15 Kips Histogram.

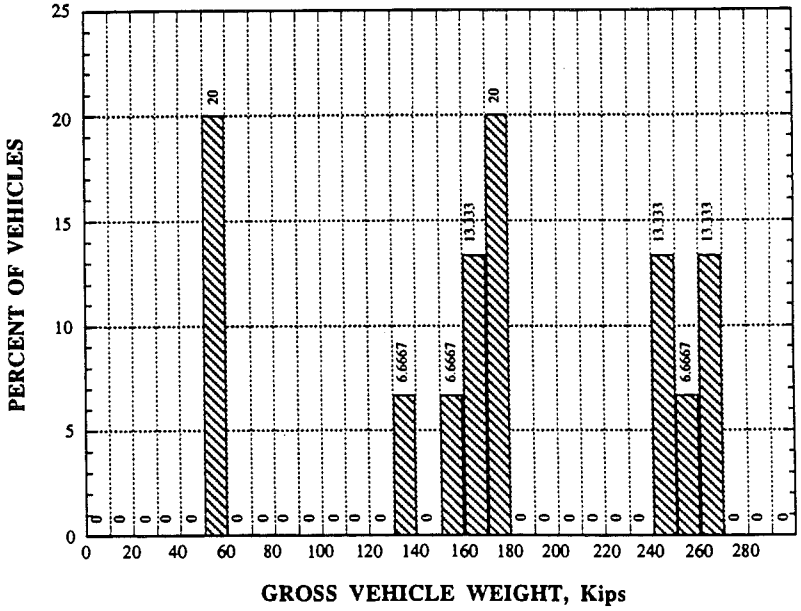

Fig. 8-51. 14/NY, EB, 11 Axle GVW - Vehicles > 15 Kips Histogram.

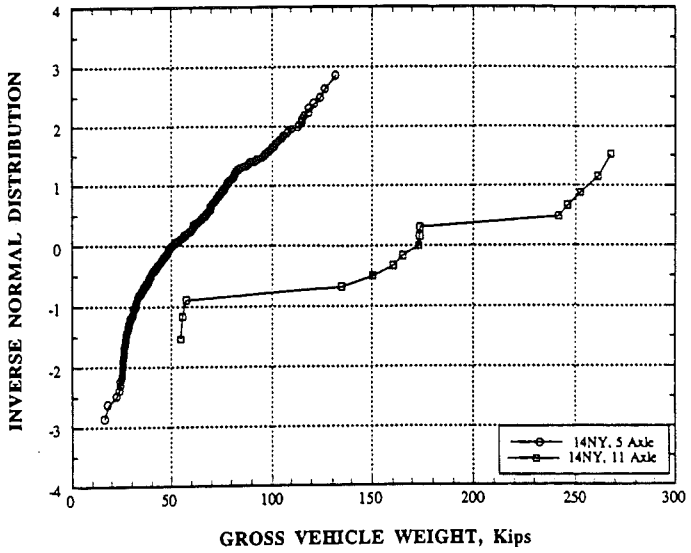

Fig. 8-52. 14/NY, EB, 5 & 11 Axle GVW CDF - Veh > 15 Kips.

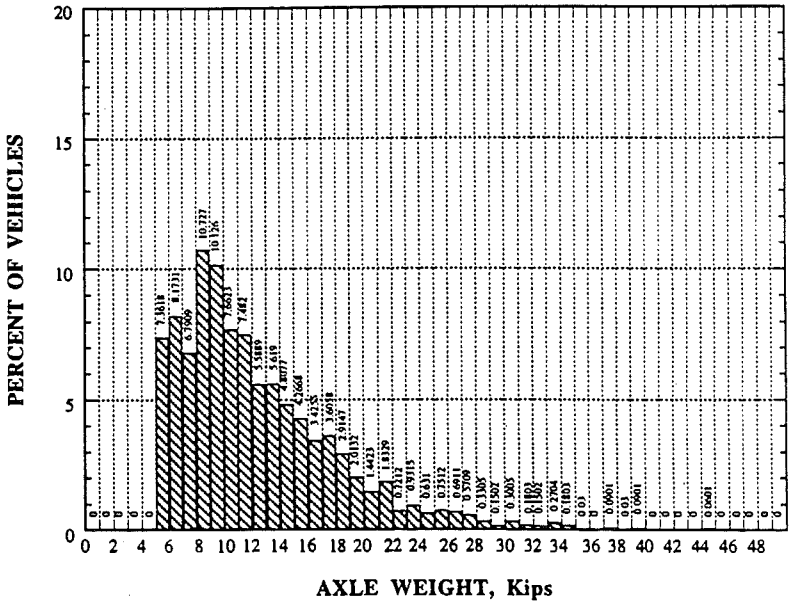

Fig. 8-53. 14/NY, EB, Axle Weight Histogram - All Axles > 5 Kips.

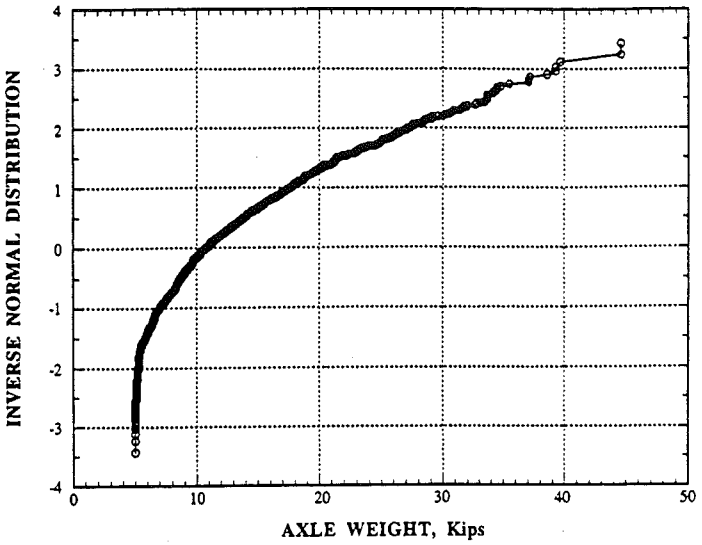

Fig. 8-54. 14/NY, EB, Axle Weight CDF - All Axles > 5 Kips.

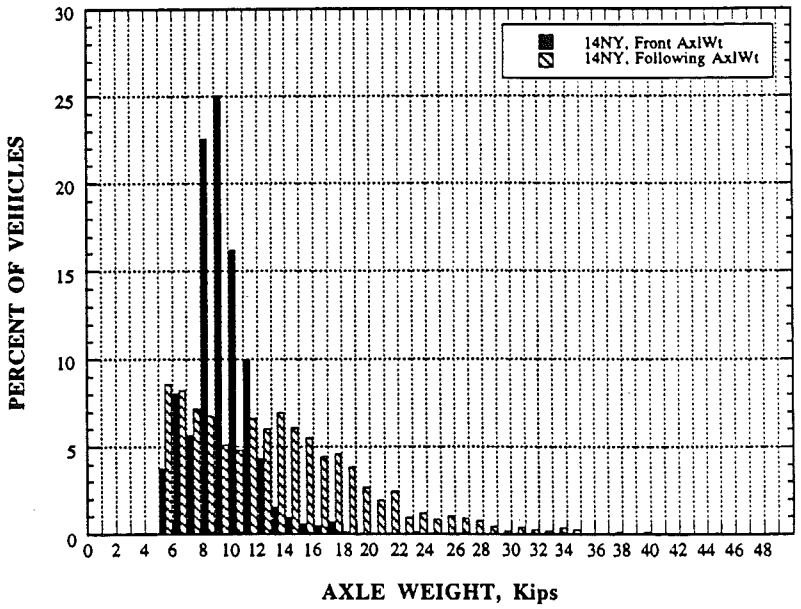

Fig. 8-55. 14/NY, EB, Front and Following Axle Weight Histogram.

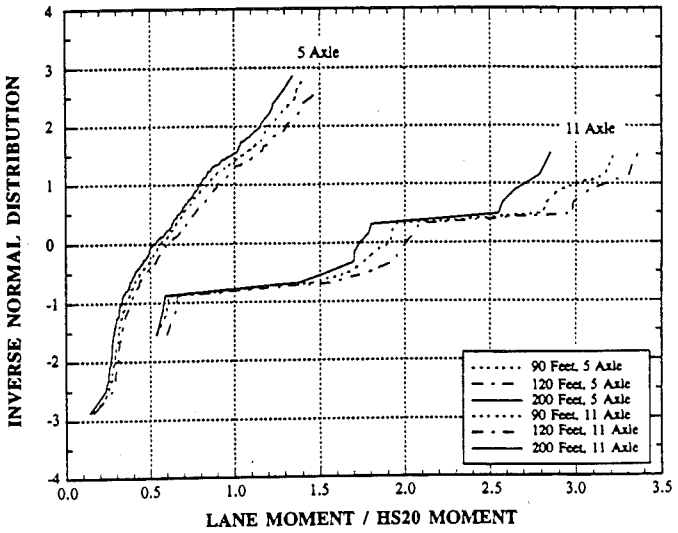

Fig. 8-60. 14/NY, EB 5 & 11 Axle Lane Moment CDF, 90, 120, & 200 Ft.

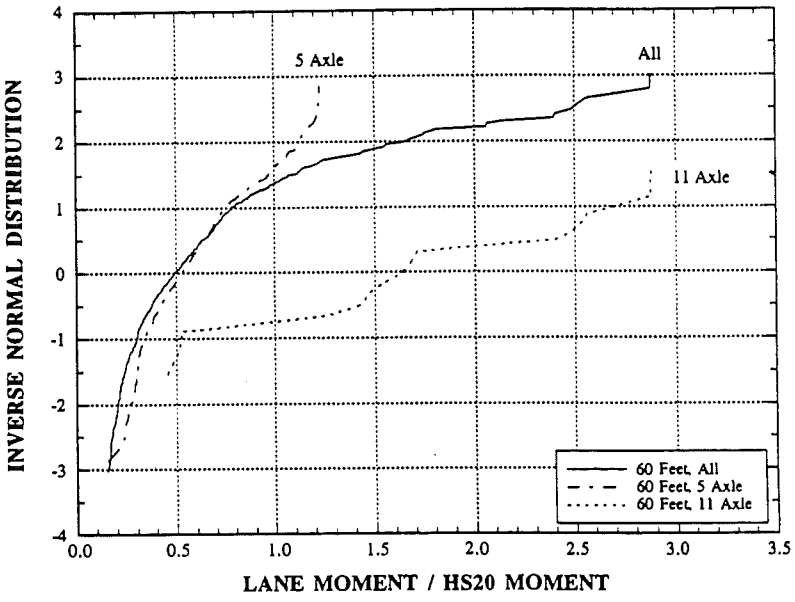

Fig. 8-61. 14/NY, EB, 5 & 11 and All Axle Lane Moment CDF, 60 Ft.

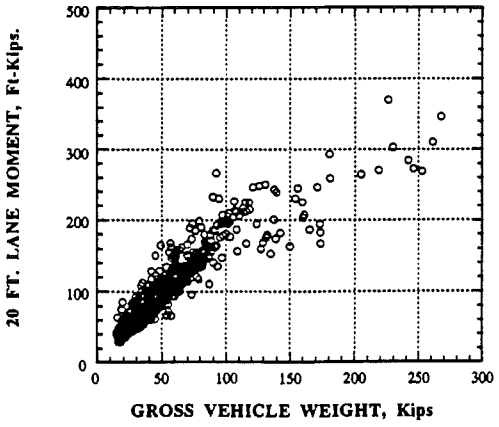

Fig. 8-62. 14/NY Mom. vs GVW, 20 Ft.

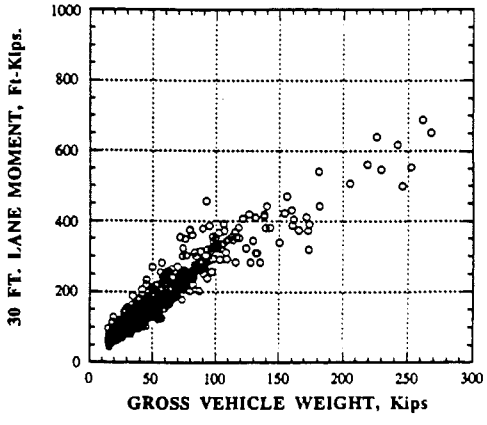

Fig. 8-63. 14/NY Mom. vs GVW, 30 Ft.

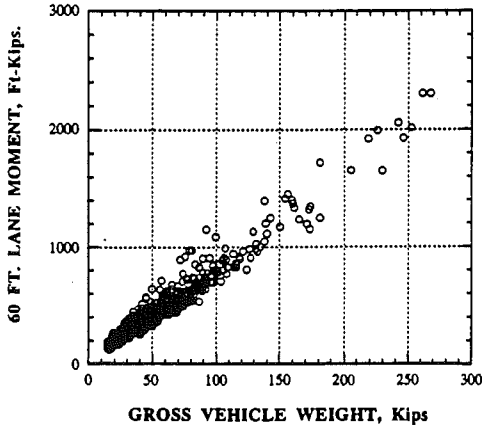

Fig. 8-64. 14/NY Moment vS GVW, 60 Ft.

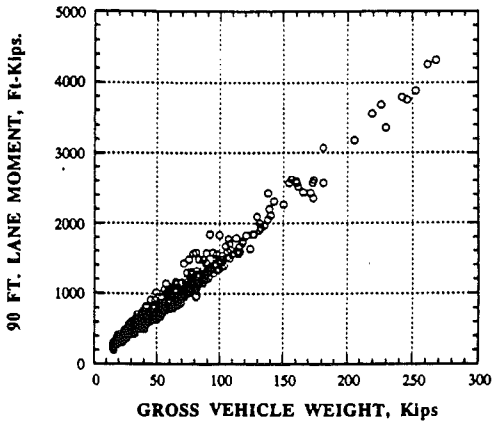

Fig. 8-65. 14/NY Moment vs GVW, 90 Ft.

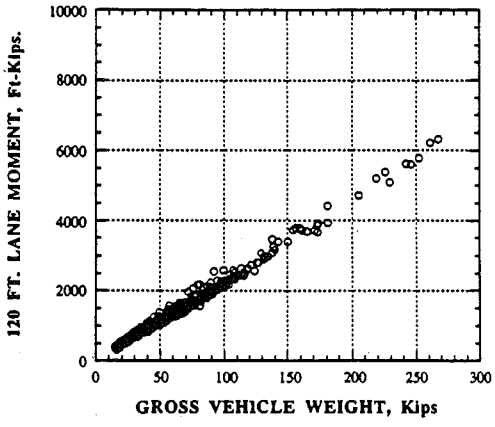

Fig. 8-66. 14/NY Moment vs GVW, 120 Ft.

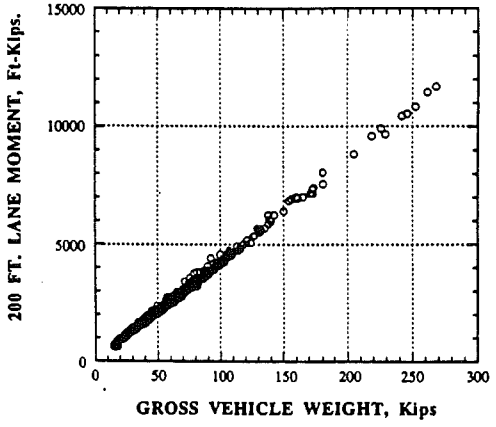

Fig. 8-67. 14/NY Moment vs GVW, 200 Ft.

8. 6 I-94 over Jackson Road (94/JR) in Ann Arbor, Michigan

Fig. 8-68 is the histogram of gross vehicle weight (GVW) for all trucks measured on 94/JR. Vehicles weighing less than 15 kips are excluded from the histogram. The corresponding cumulative distribution function (CDF) of GVW for all trucks is shown in Fig. 8-69. Each circle represents one truck in the data file. From Table 8-10 the heaviest vehicle observed weighed 235.7 kips and the mean GVW for all trucks is 53.7 kips. Results of the individual day measurements are presented in Fig. 8-70 for 4/26/91, 5/22/91, 5/23/91, 6/19/91, 6/20/91, and 8/14/91. The day to day CDFs demonstrate a similar trend and average GVW with minor differences at the upper tails of the distributions.

Fig. 8-71 is the histogram of all 5 axle vehicles and Fig. 8-72 is the histogram of all 11 axle vehicles. The coressponding CDFs of the 5 and 11 axle vehicles are shown in Fig. 8-73. The CDFs of Fig. 8-73 clearly indicate that the much heavier vehicles are 11 axle trucks. It is apparent from the distributions of Fig. 8-73, with each square and circle indicating a truck, that westbound 94/JR is carrying an approximately equal number of loaded and empty 5 axle vehicles and a higher percentage of loaded than unloaded 11 axle vehicles. The mean 5 axle vehicle GVW is 51.4 kips with a maximum GVW of 115.4 kips. The mean 11 axle vehicle GVW is 149.7 kips with a maximum GVW of 235.7 kips. (Tables 8-11 and 8-12). For comparison of the daily distribution of 5 and 11 axle vehicles, the CDFs for all days are plotted in Fig. 8-74 and 8-75 respectively.

Fig. 8-76 is the axle weight histogram of all vehicle axles observed and the corresponding CDF is presented in Fig. 8-77. The maximum axle weight observed at 94/JR is 52.5 kips with a mean of 11.73 kips. As is the case with GVW, there is very little daily variation in the vehicle axle weights with some differences at the upper tail of the distribution. The front and following axle weight histograms of Fig. 8-78 indicate a significant difference in both variation and magnitudes. As observed from the CDF's of Fig. 8-79, the mean front axle weight is 9.28 kips with a maximum of 23.0 kips while the following axle mean is 12.55 kips with

a maximum of 52.5 kips. The higher variation in the following axle weights is readily apparent from the CDF comparison.

Fig. 8-80 and 8-81 plot the CDF's for lane moment effect of all trucks with GVW greater than 15 kips for 94/JR. The mean of lane moment to HS20 moment is approximately 0.4 tro 0.6 for each of the spans. The maximum ratio of lane moment to HS20 moment varies from 2.5 for a 20 ft. span to 3.0 for a 120 ft. span. Similar to the GVW data, a comparison is made between 5 and 11 axle moments. Fig. 8-82 and 8-83 present 5 and 11 axle vehicle CDFs for simple spans of 20, 30, 60, 90, 120, and 200 ft. As a comparison of vehicle type for a given span, 5, 11, and all vehicle moment CDFs are plotted for a 60 ft simple span in Fig. 8-84.

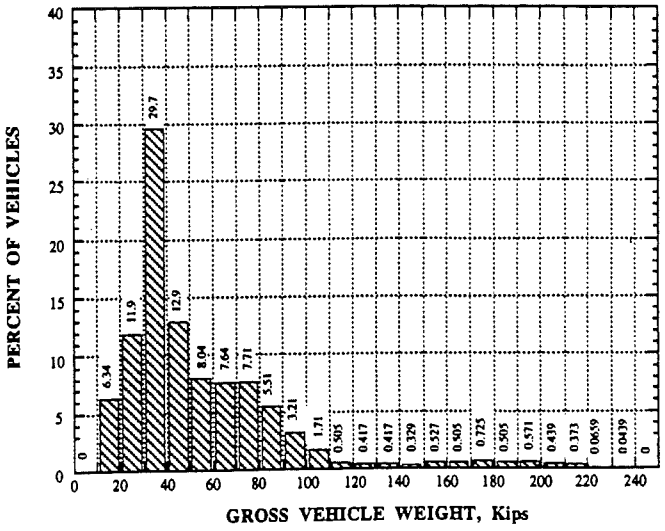

Fig. 8-68. 94/JR, WB, GVW Histogram - Veh icles > 15 Kips.

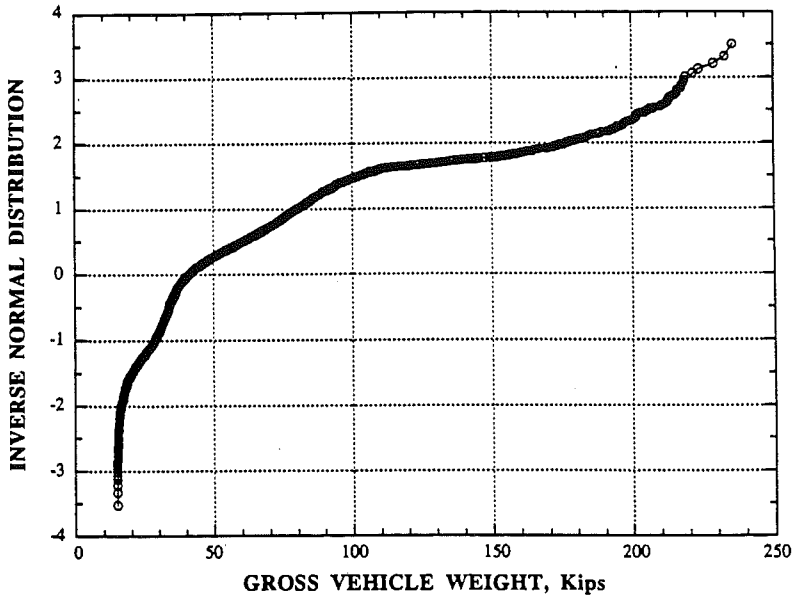

Fig. 8-69. 94/JR, WB, GVW DCDF- Vehicles > 15 Kips.

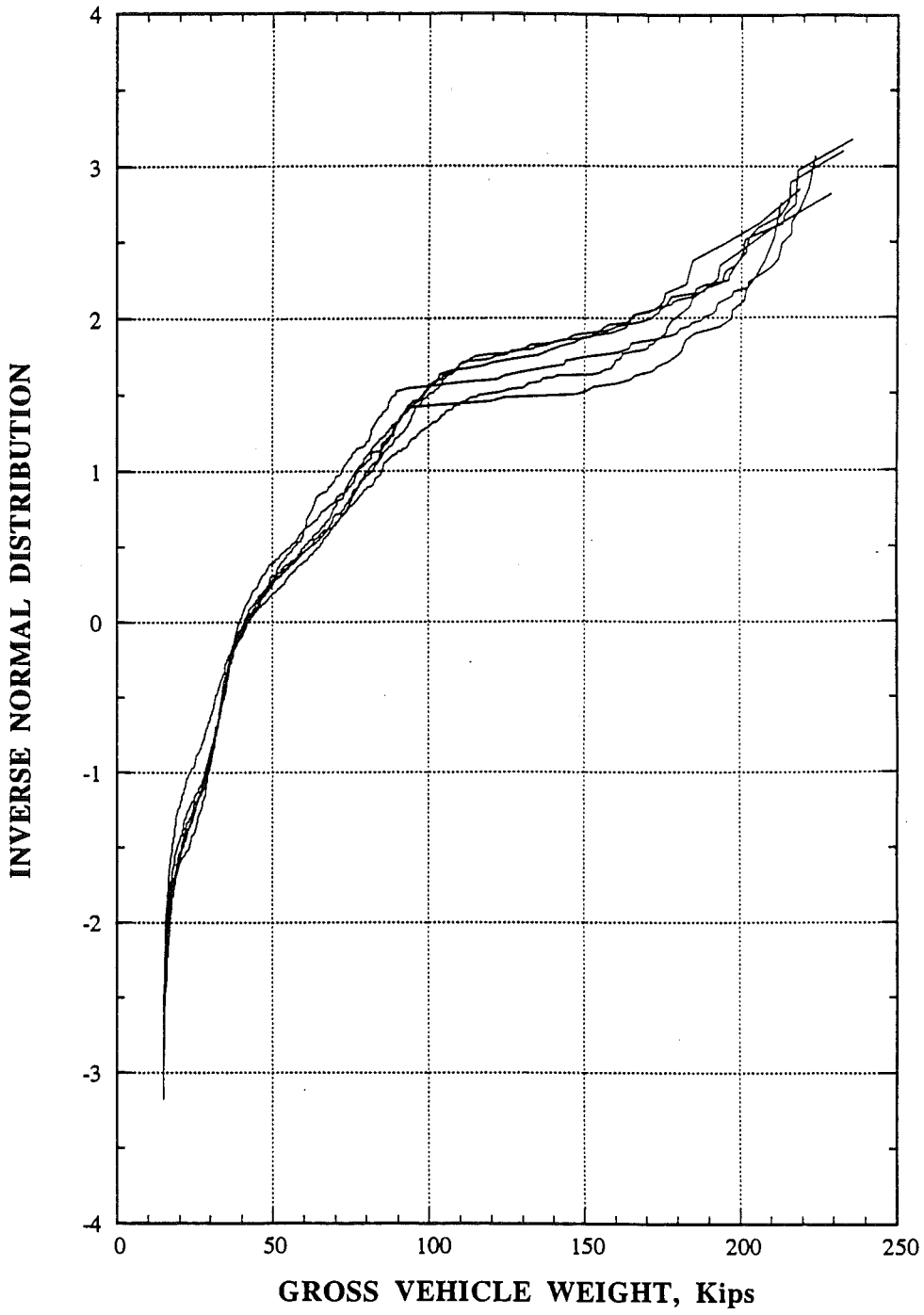

Fig. 8-70. I-94/Jackson Rd WB, Daily GVW CDF - Veh > 15 Kips.

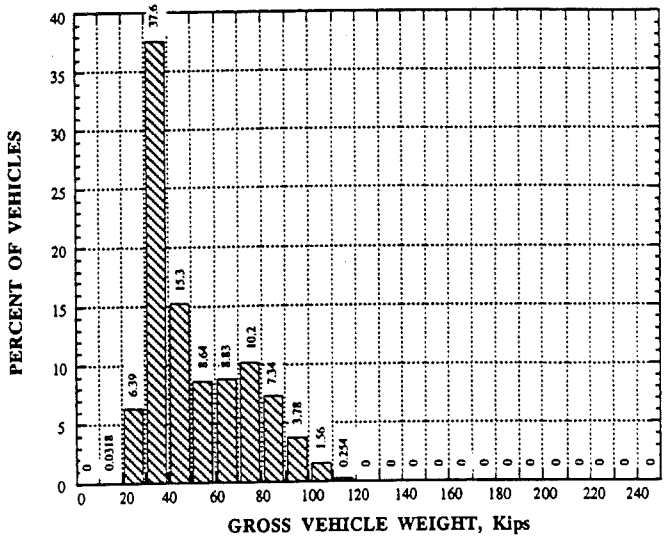

Fig. 8-71. 94/JR, WB, 5 Axle GVW - Vehicles > 15 Kips Histogram.

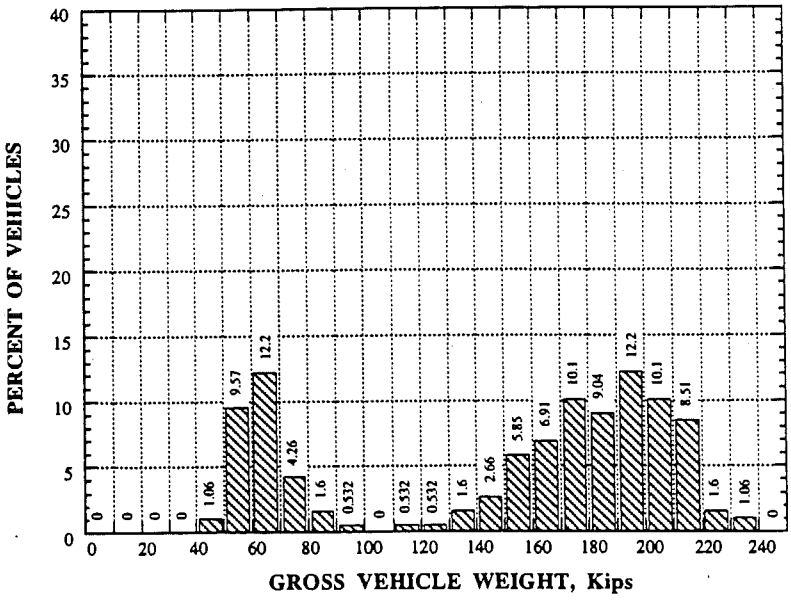

Fig. 8-72. 94/JR, WB, 11 Axle GVW - Vehicles > 15 Kips Histogram.

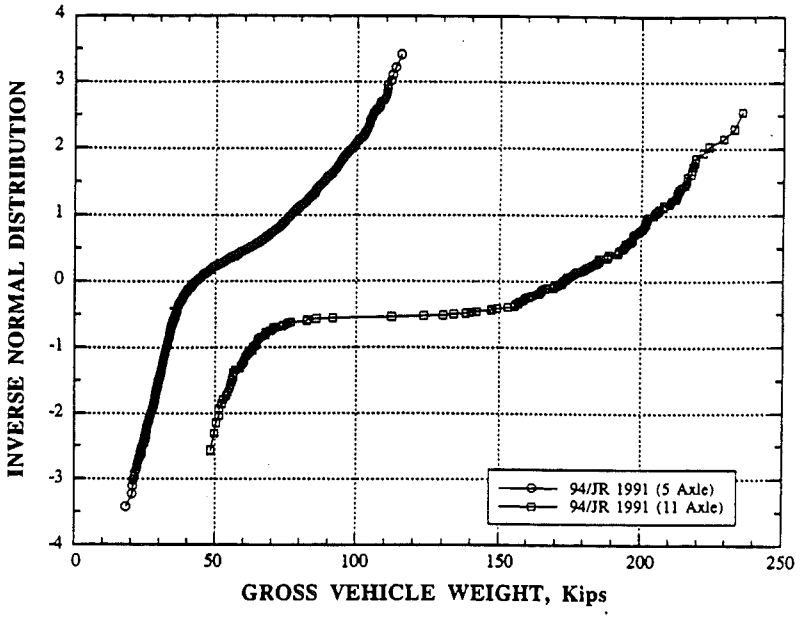

Fig. 8-73. 94/JR, WB, 5 & 11 Axle GVW CDF - Veh icles > 15 Kips.

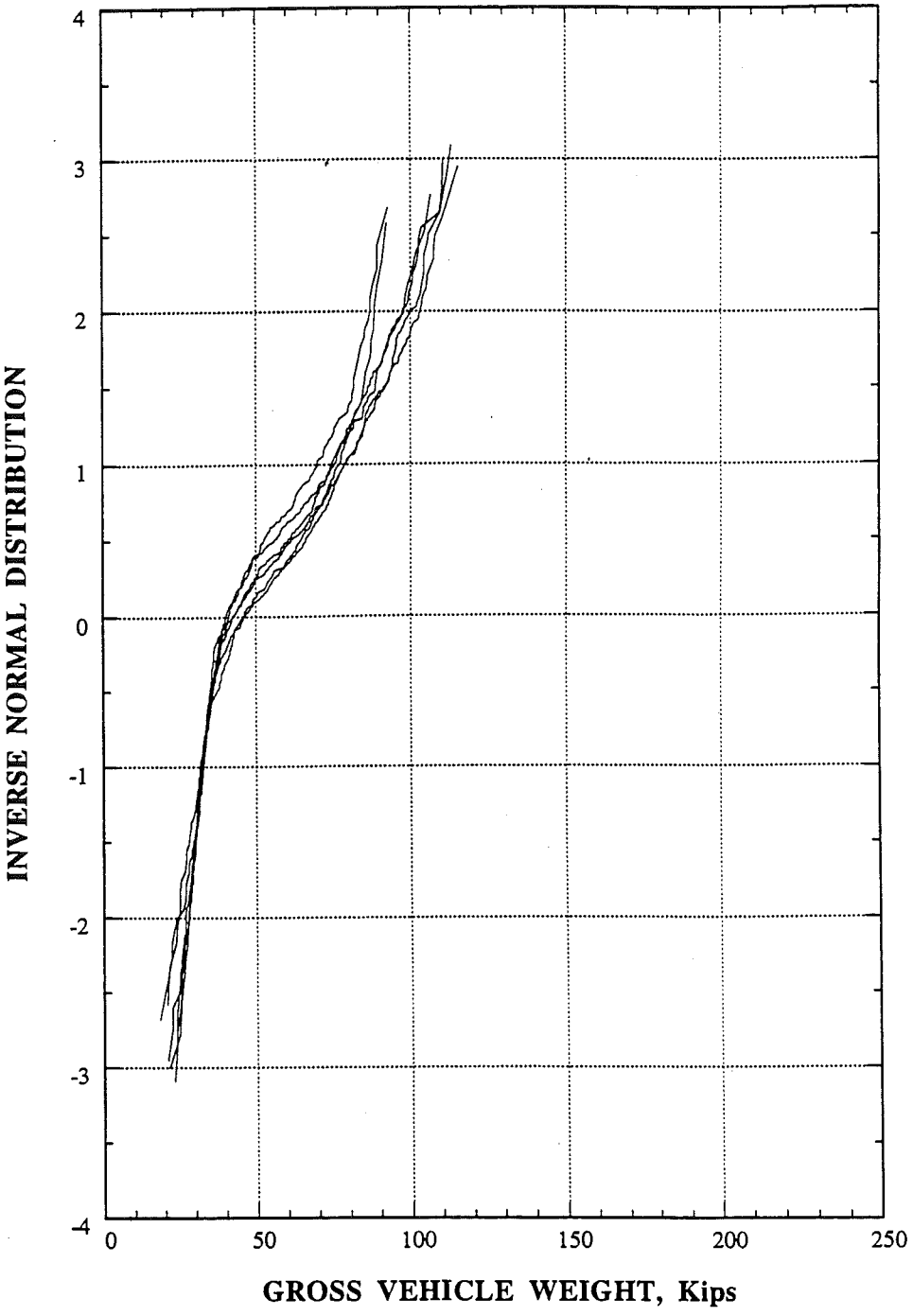

Fig. 8-74. 94/JR, Daily 5 Axle GVW CDF - Vehicles > 15 Kips.

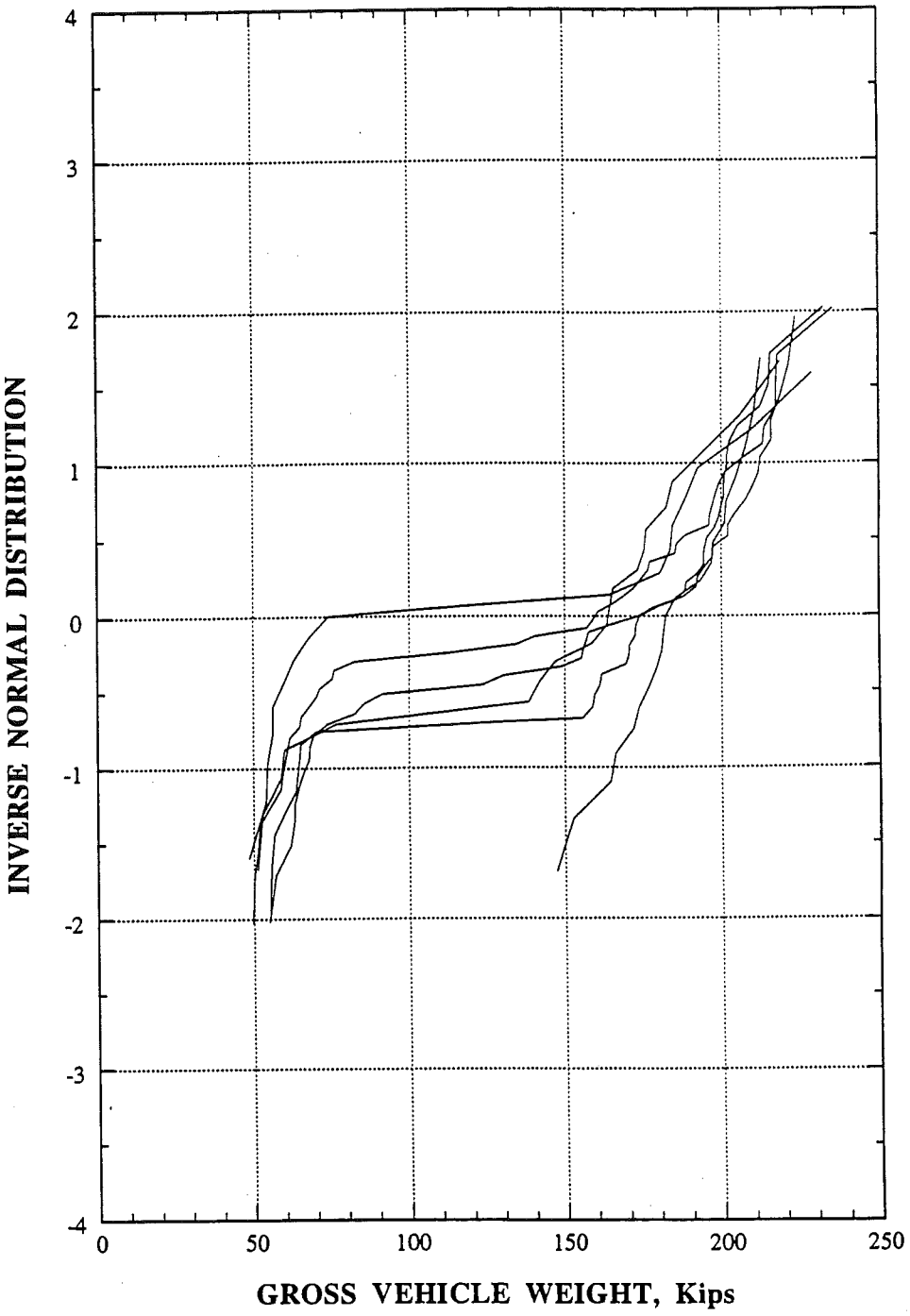

Fig. 8-75. 94/JR, Daily 11 Axle GVW CDF - Vehicles > 15 Kips.

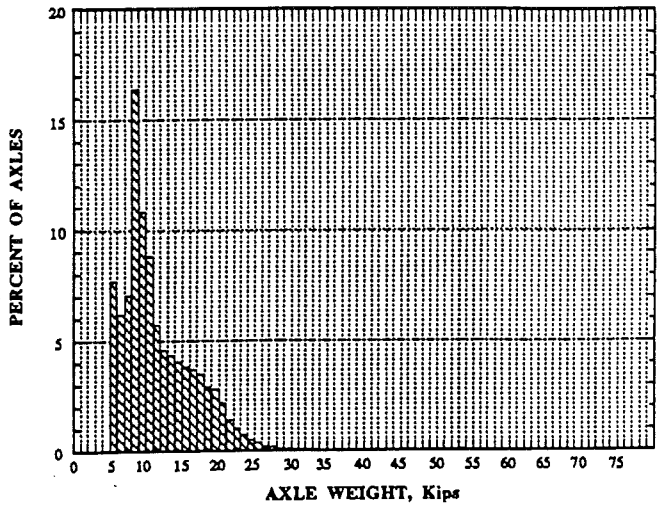

Fig. 8-76. 94/JR, WB, Axle Weight Histogram - All Axles > 5 Kips

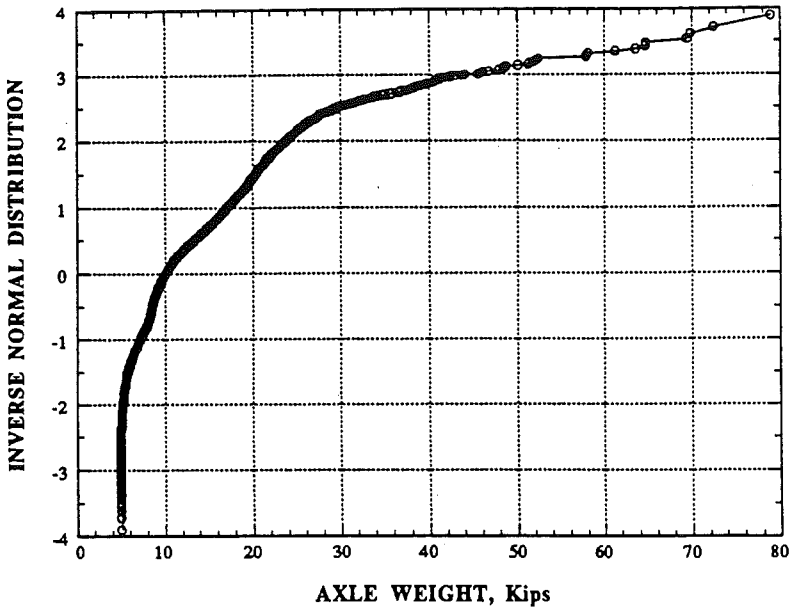

Fig. 8-77. 94/JR, WB, Axle Weight CDF - All Axles > 5 Kips.

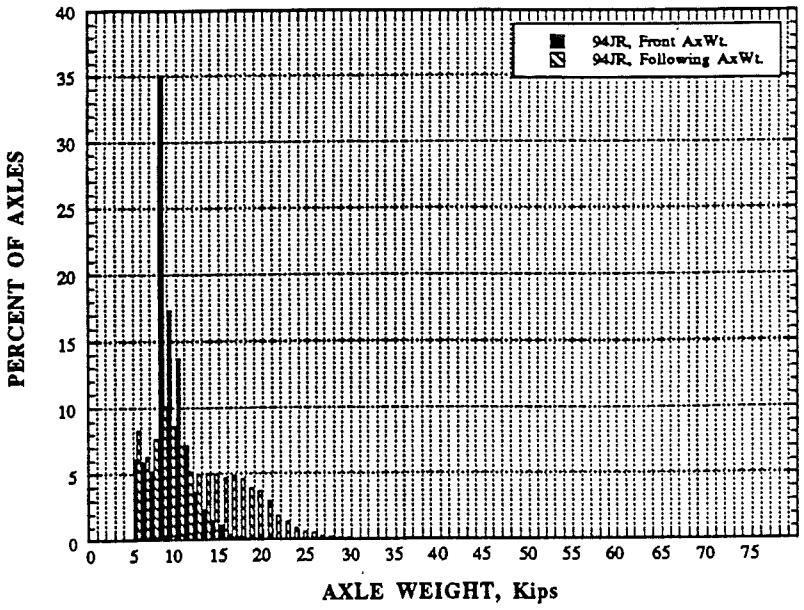

Fig. 8-78. 94/JR, Front and Following Axle Weight Histogram.

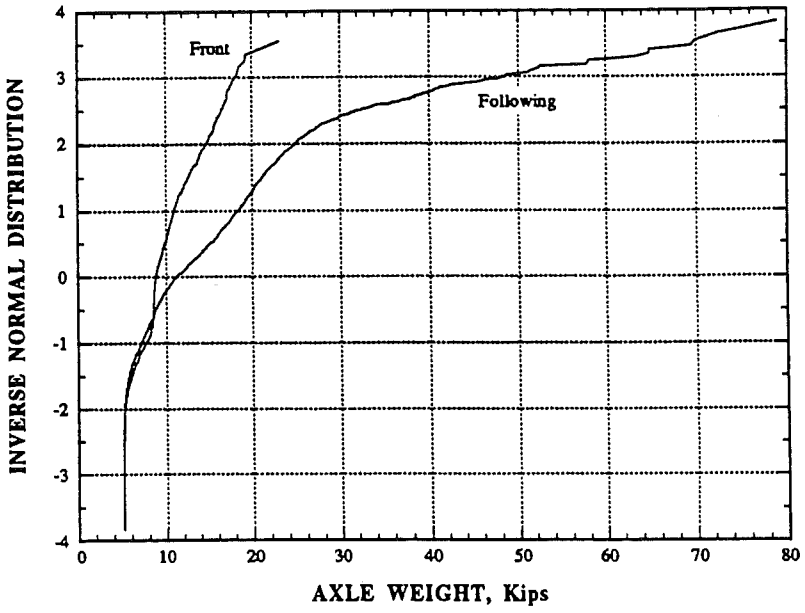

Fig. 8-79. 94/JR, Front and Following Axle Weight CDF.

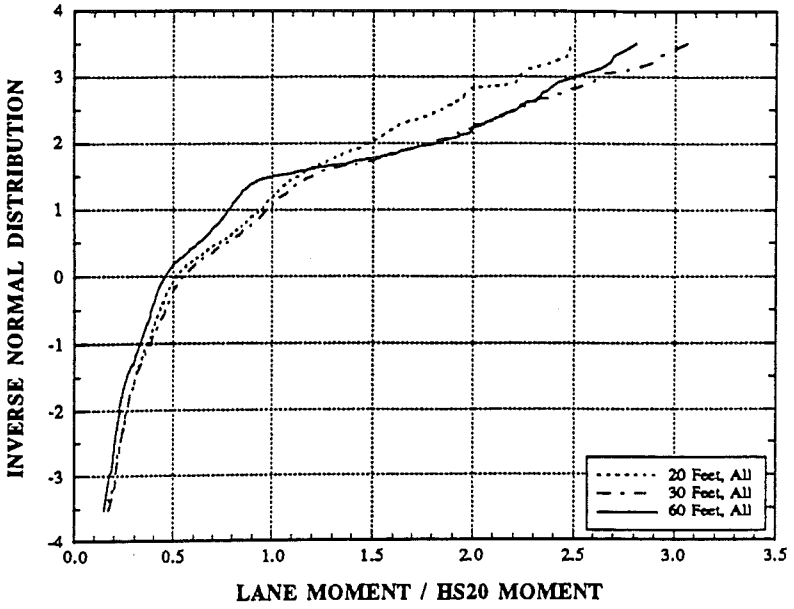

Fig. 8-80. 94/JR Lane Moment CDF, 20, 30, & 60 Ft.

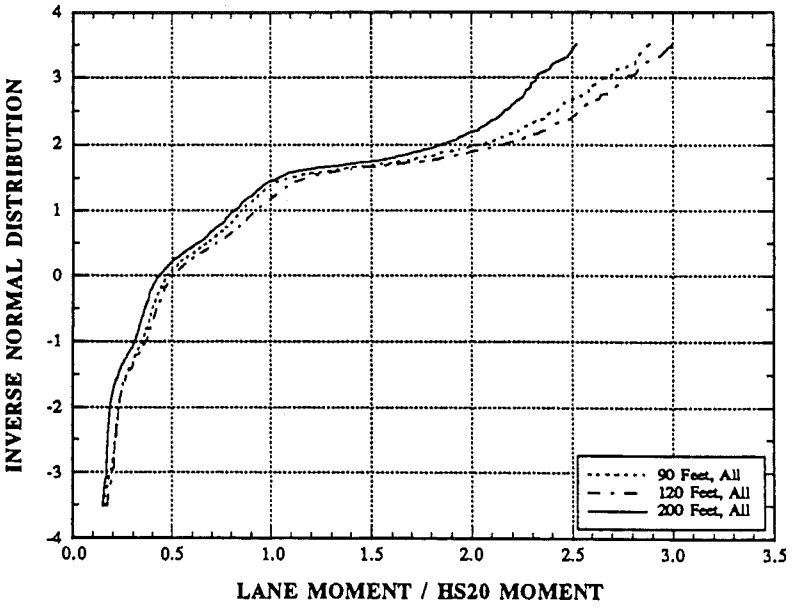

Fig. 8-81. 94/JR, Lane Moment CDF, 90, 120, & 200 Ft.

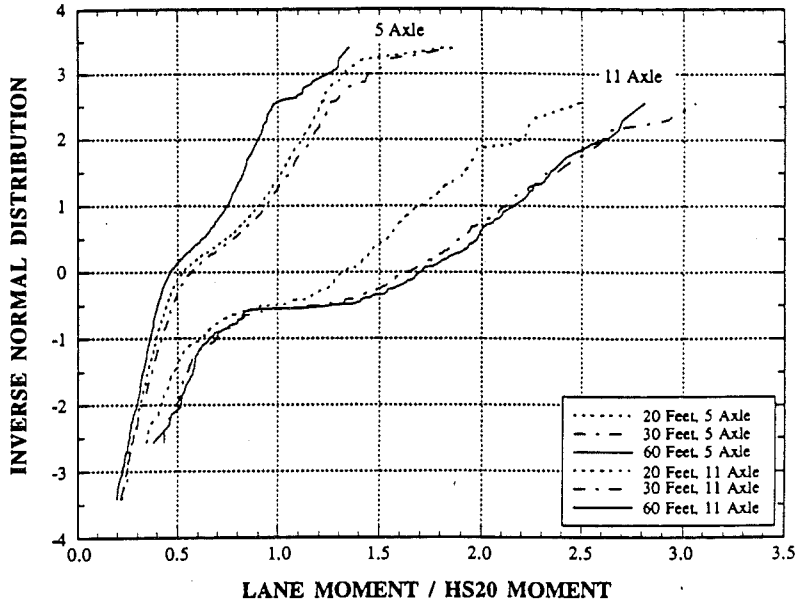

Fig. 8-82. 94/JR, 5 & 11 Axle Lane Moment CDF, 20, 30, & 60 Ft.

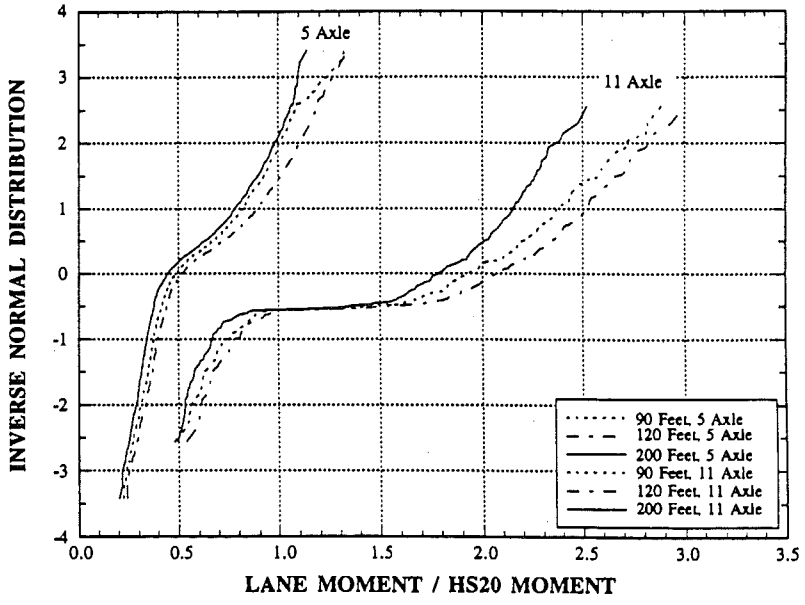

Fig. 8-83. 94/JR, 5 & 11 Axle Lane Moment CDF, 90, 120, & 200 Ft.

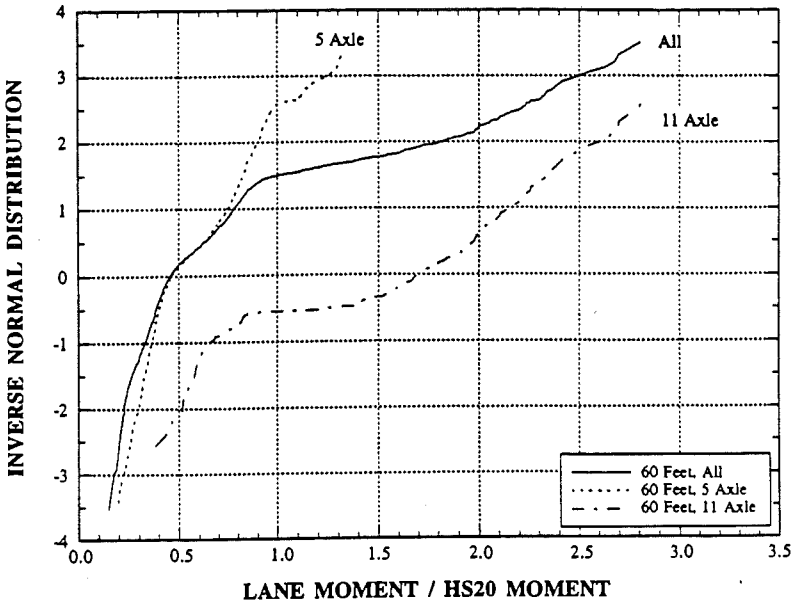

Fig.8-84. 94/JR, 5, 11 and All Axle Lane Moment CDF, 60 Ft.

8.7 US-23 over the Saline River (23/SR) in Milan, Michigan

The histogram of gross vehicle weight (GVW) for all trucks measured on 23/SR in presented in Fig. 8-85. Vehicles weighing less than 15 kips are excluded from the histogram. The cumulative distribution function (CDF) of GVW for all trucks observed and measured on 23/SR is shown in Fig. 8-86. Each circle represents one truck in the data file. From the Table 8-10 the heaviest vehicle observed weighed 248.5 kips with a mean GVW of 57.9 kips. Results of the individual day measurements are presented in Fig. 8-87 for 6/30/92, 7/1/92, 7/2/92, 7/22/92, 10/13/92, 10/21/92, and 10/22/92. The day to day CDFs demonstrate a similar trend and average GVW with the largest difference at the upper tail of the distribution.

Fig. 8-88 is the histogram of all 23/SR 5 axle vehicles; Fig. 8-89 is the histogram of all 11 axle vehicles. The histogram of 11 axle vehicles exhibits a bimodal distribution, indicating loaded and unloaded vehicles. This distinction is not apparent in Fig. 8-88 for the 5 axle vehicles. The CDFs of the 5 and 11 axle vehicles are shown in Fig. 8-90 which clearly shows that the much heavier vehicles are the 11 axle trucks. It can also be observed from the distributions of Fig. 8-90, with each square and circle indicating a truck, that southbound 23/SR is carrying an approximately equal number of loaded and empty 5 and 11 axle trucks. The mean 5 axle vehicle GVW is 59.2 kips and for 11 axle vehicles 103.2 kips (Tables 8-11 and 8-12). For comparison of the daily distribution of 5 and 11 axle vehicles, the CDFs for all days are plotted in Fig. 8-91 and 8-92 respectively.

Potentially more important for fatigue cycles and the distribution of moments for a given bridge will be the axle weights and spacing for the trucks passing over the bridge. Fig. 8-93 through 8-96 present the distributions of the axle weights of the vehicles discussed above. All distributions include axles with weights greater than 5,000 pounds.

Fig. 8-93 is the axle weight histogram of all vehicles axles observed on 23/SR and the corresponding CDF is presented in Fig. 8-94. The

maximum axle weight observed at 23/SR is 40.8 kips with a mean of 12.31 kips. As is the case with GVW, there is very little daily variation in the vehicle axle weights with some differences at the upper tail of the distribution. The front and following axle weight histograms of Fig. 8-96 indicate a significant difference in both variation and magnitudes of the two axle types. As observed from the Table 8-14, the mean front axle weight is 9.3 kips with a maximum of 19.9 kips while the mean following axle weight is 13.24 kips with a maximum of 40.8 kips. The higher variation in the following axle weights is readily apparent from the CDF comparison.

Of even greater interest is the effect of the GVW, axle weight and axle spacing on the bridge structure and components. The effect of these parameters can be determined in part by the lane moment caused by the truck. Each truck in the data base is analytically driven across the bridge to determine the maximum bending moment per lane for various simple span lengths. The CDFs of the lane moments for spans of 20, 30, 60, 90, 120, and 200 feet are then determined. As a point of reference the lane moments are presented in terms of the truck lane moment to HS20 moment.

Fig. 8-97 and 8-98 present the CDFs for lane moment effect of all trucks with GVW greater than 15 kips for 23/SR. The mean of lane moment to HS20 moment ranges from 0.6 to 0.70 for each of the spans. The maximum ratio of lane moment to HS20 moment varies from 2.043 for a 20 ft. span to 3.104 for a 120 ft. span. Similar to the GVW data, a comparison is made between lane moments produced by 5 and 11 axle vehicles. Fig. 8-99 and 8-100 present lane moment CDF's for 5 and 11 axle vehicles. The simple spans considered are 20, 30, 60, 90, 120, and 200 ft. As a comparison of vehicle type for a given span, 5, 11, and all vehicle lane moment CDF's are plotted for a 60 ft simple span in Fig. 8-101.

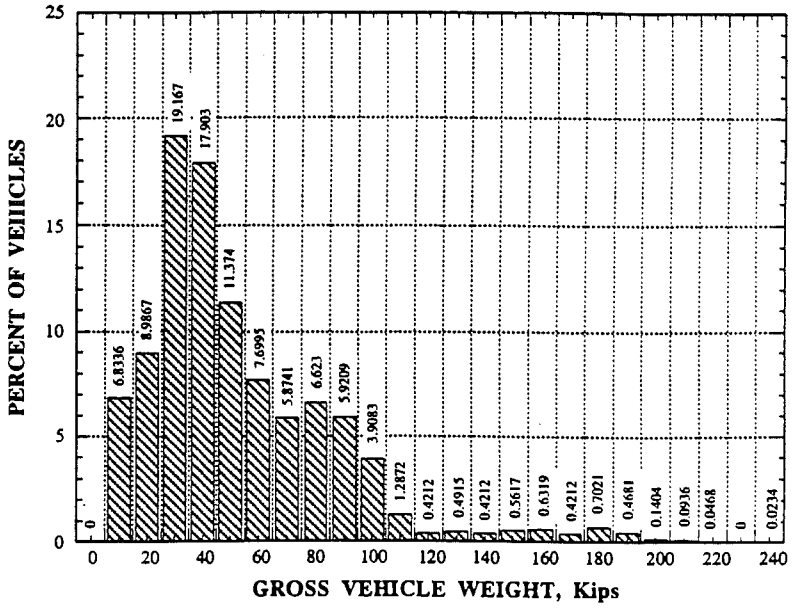

Fig. 8-85. 23/SR, SB, GVW Histogram - Vehicles > 15 Kips.

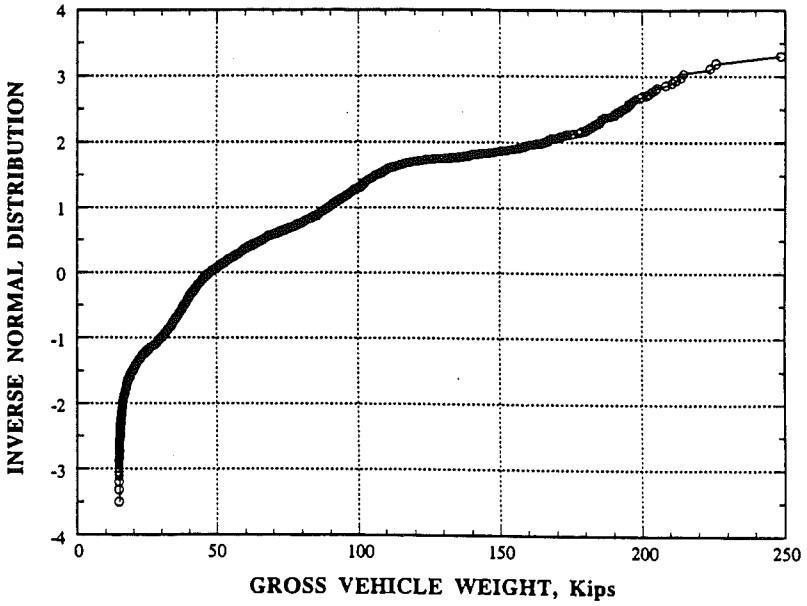

Fig. 8-86. 23/SR, SB, GVW CDF - Vehicles > 15 Kips.

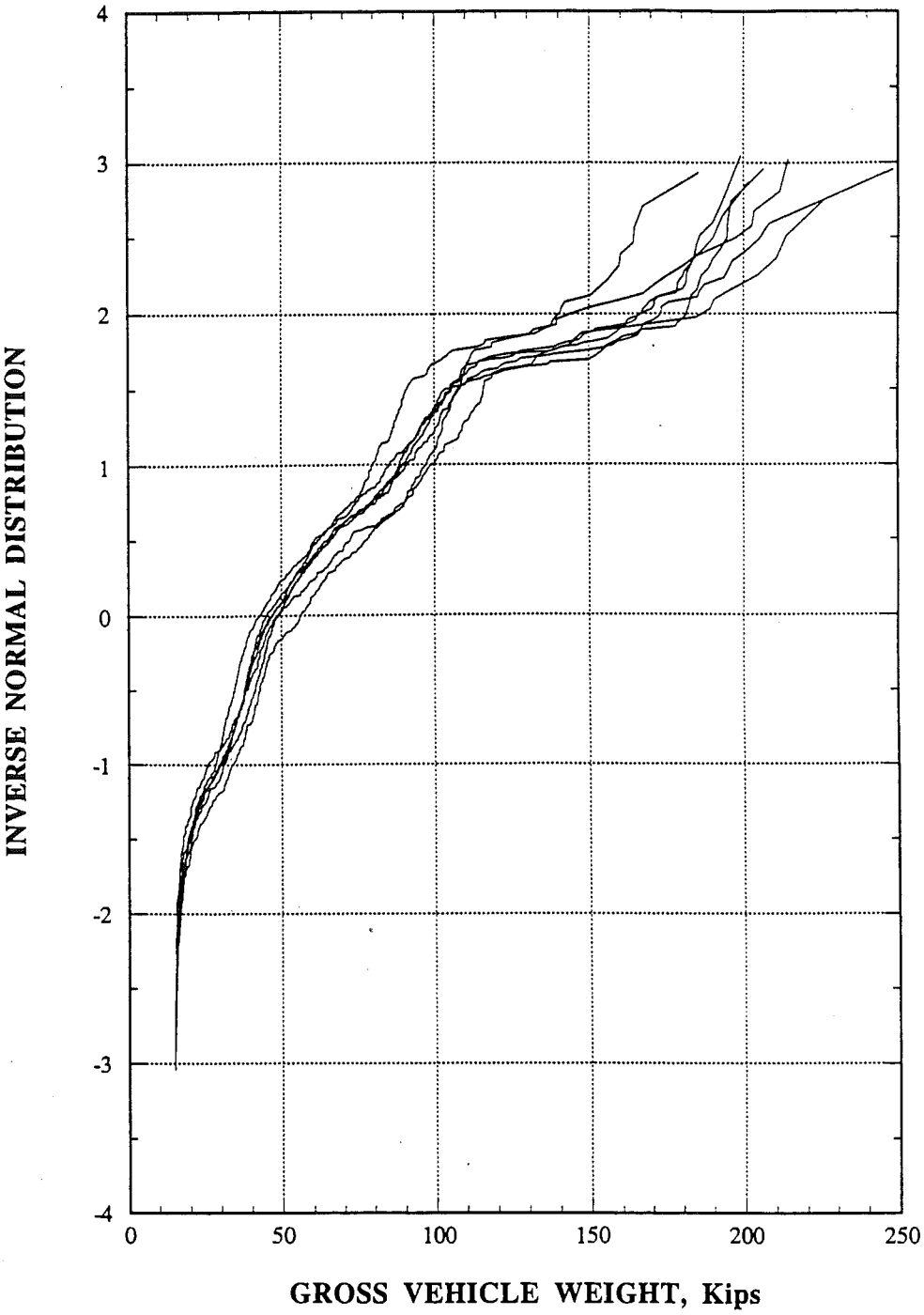

Fig. 8-87. 23/SR, SB, Daily GVW CDF - Vehicles > 15 Kips.

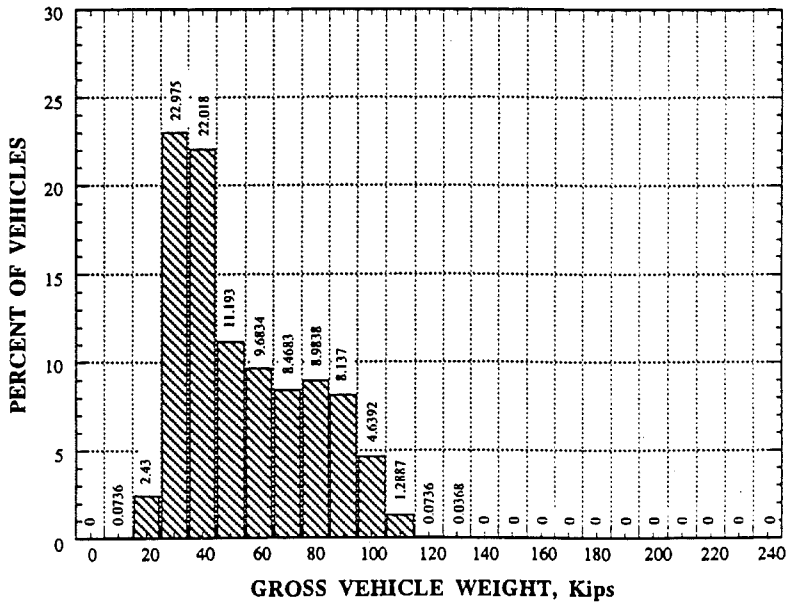

Fig. 8-88. 23/SR, SB, 5 Axle GVW > 15 Kips Histogram.

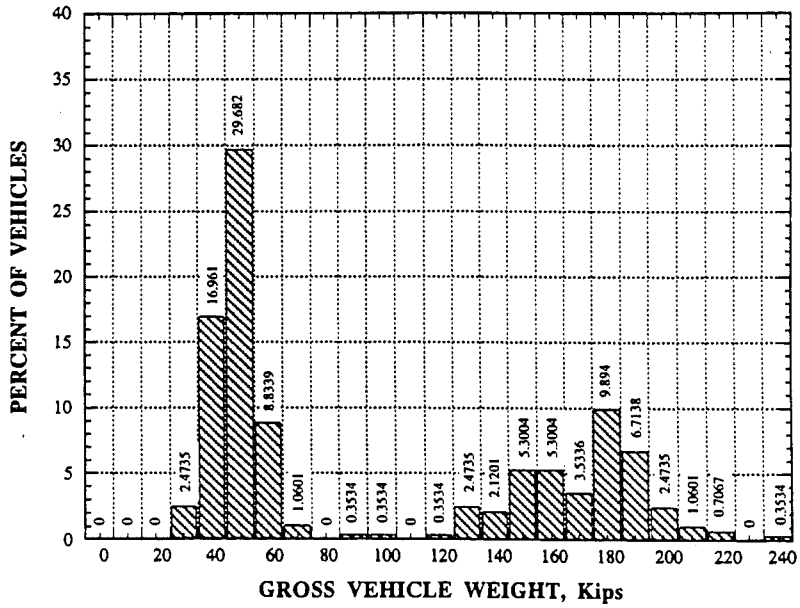

Fig. 8-89. 23/SR, SB, 11 Axle GVW > 15 Kips Histogram.

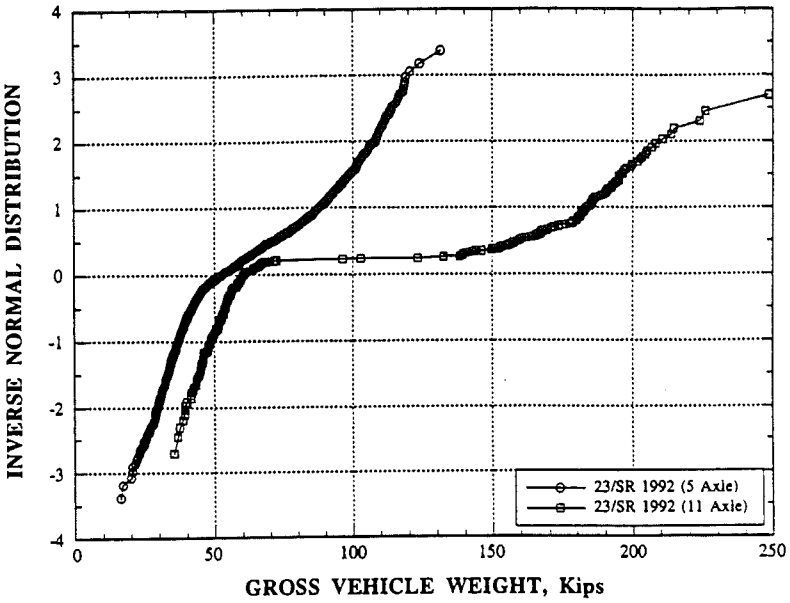

Fig. 8-90 US23/SR, SB, 5 and 11 Axle GVW CDF> 15 Kips Distributions.

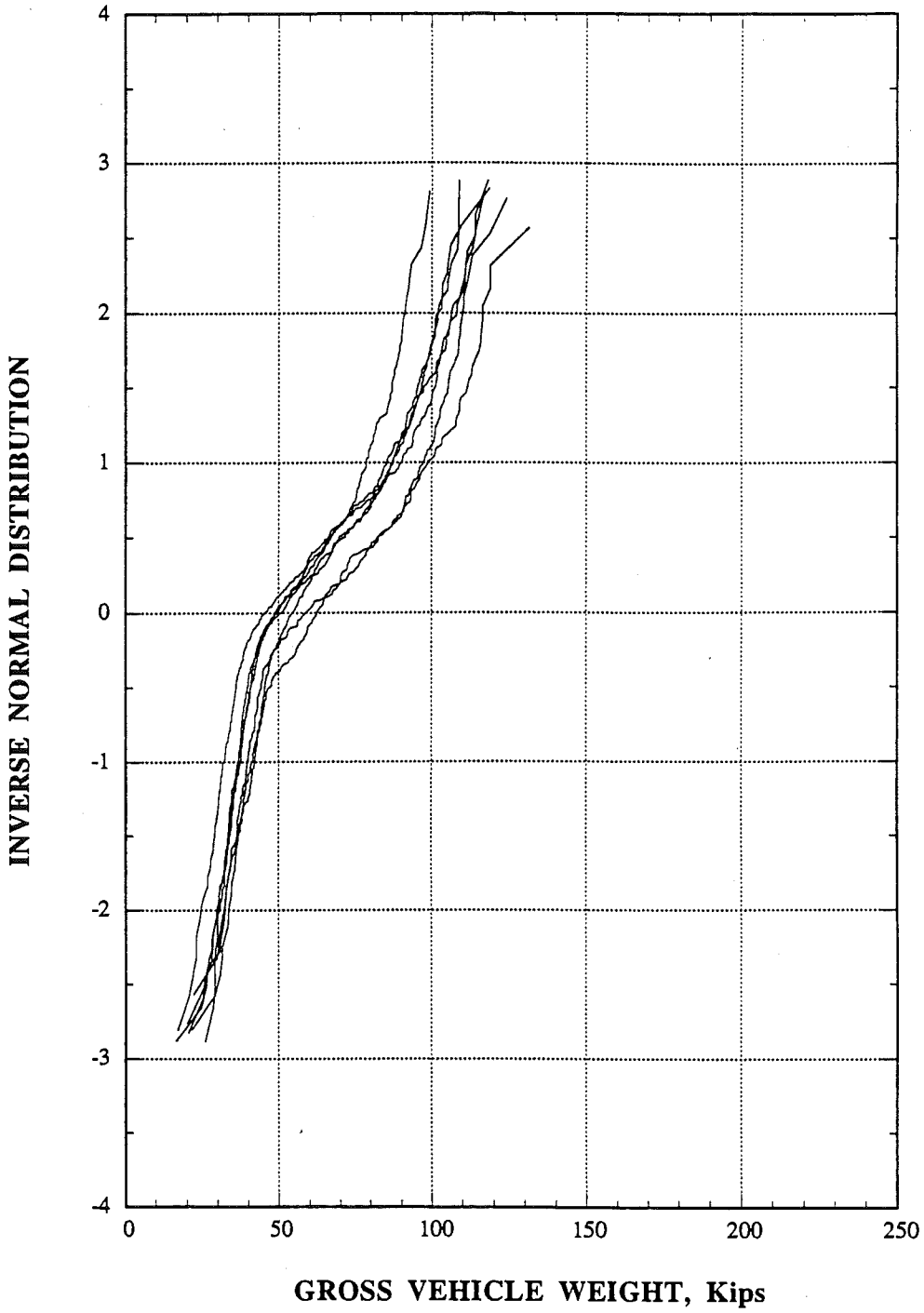

Fig. 8-91 23/SR, SB, 5 Axle Daily GVW CDF > 15 Kips Distributions.

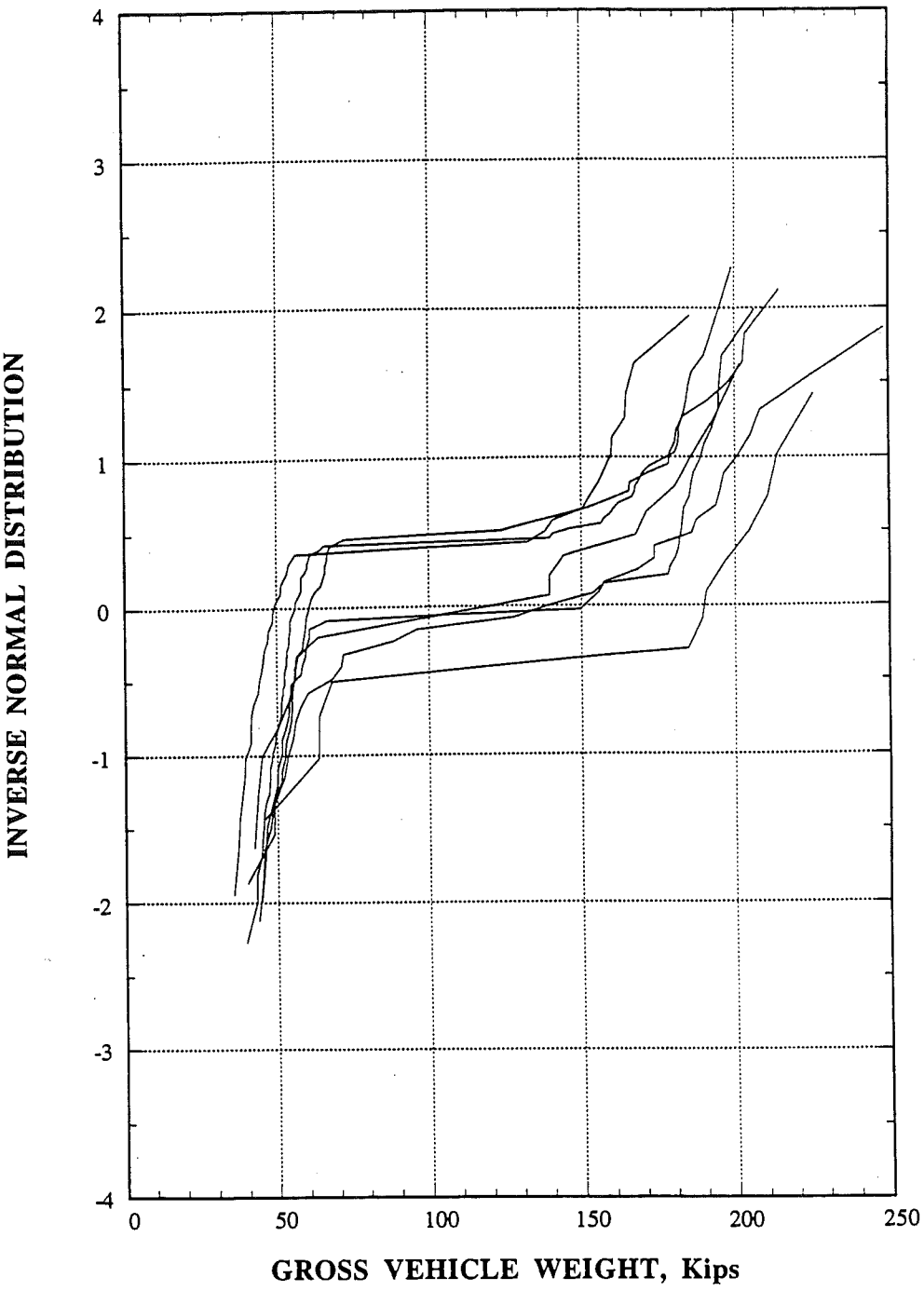

Fig. 8-92. 23/SR, SB, 11 Axle Daily GVW CDF > 15 Kips Distributions.

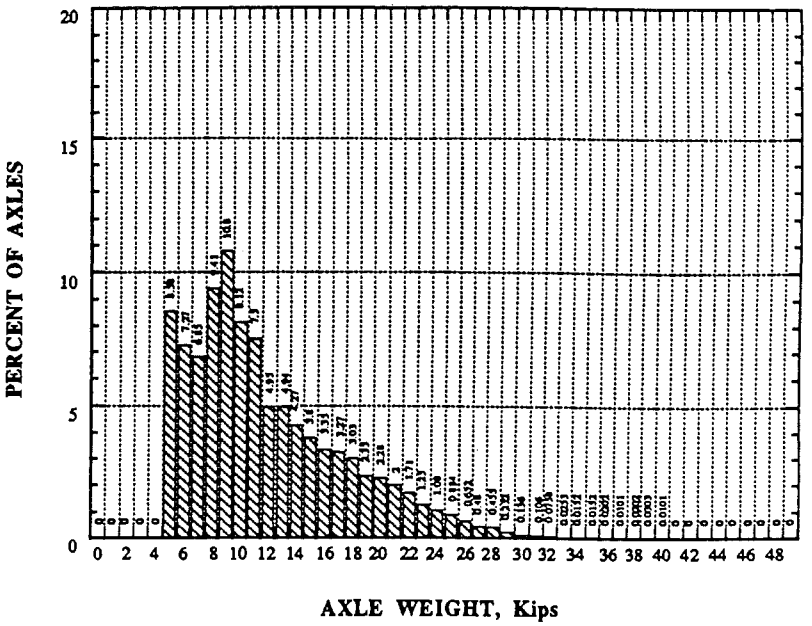

Fig. 8-93. 23/SR, Axle Weight Histogram - Axles > 5 Kips.

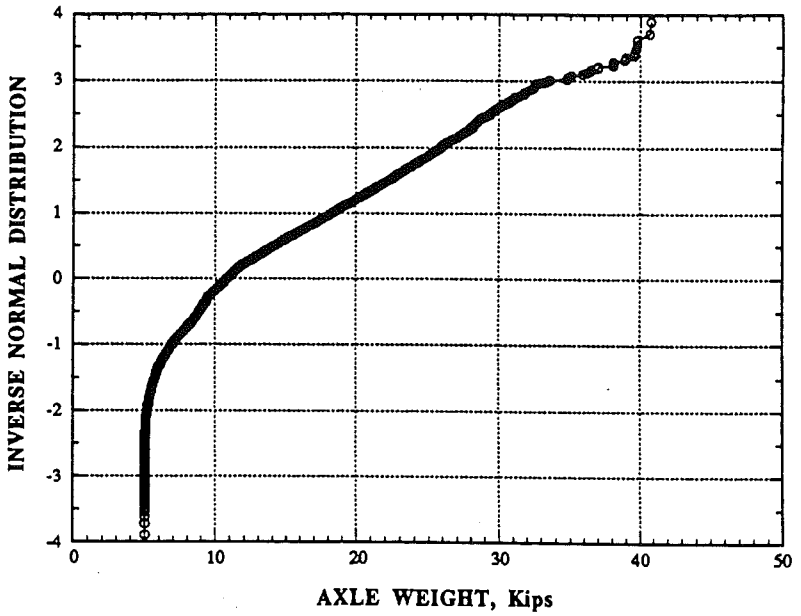

Fig. 8-94. 23/SR, Axle Weight CDF - Axles > 5 Kips.

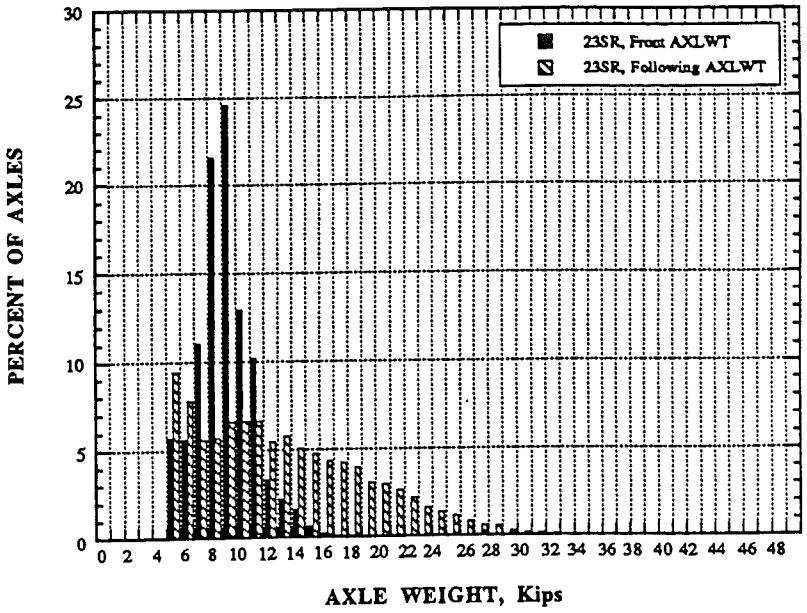

Fig. 8-95. 23/SR, Front & Following Axle Weight Histogram.

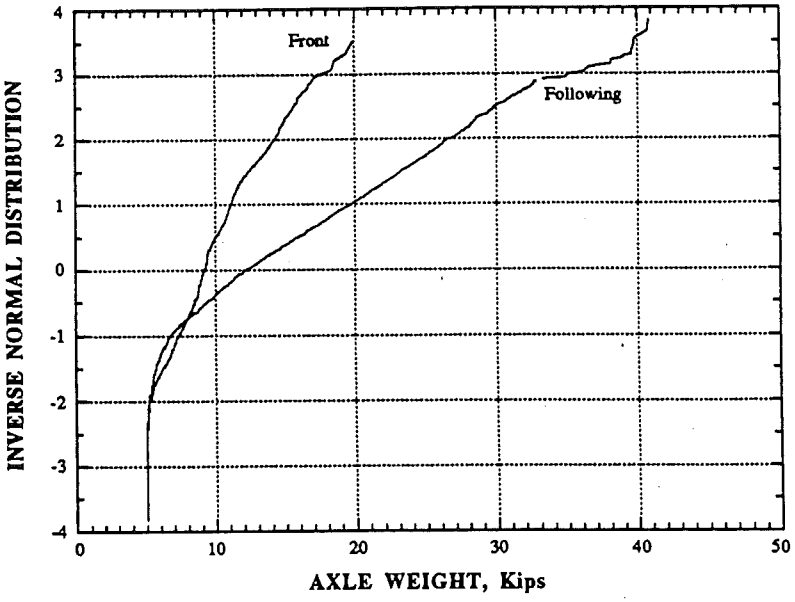

Fig. 8-96. 23/SR, Front & Following Axle Weight CDF

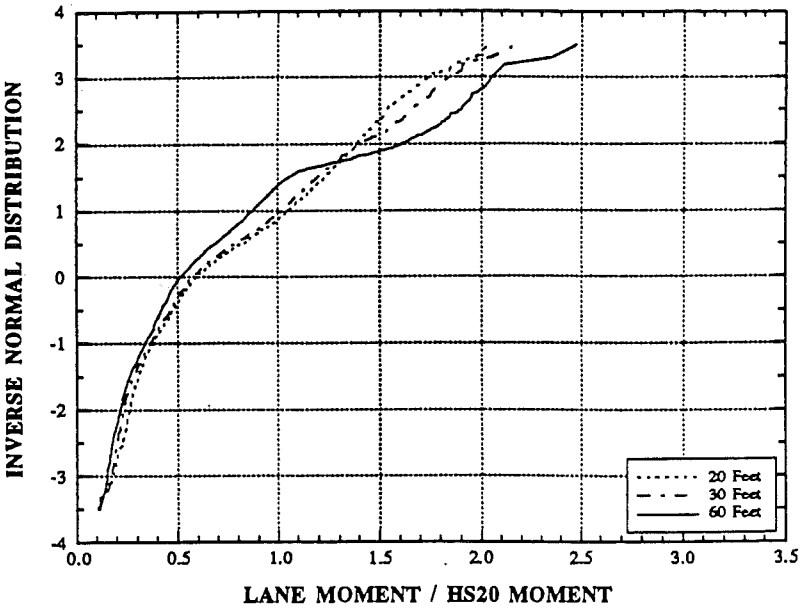

Fig. 8-97. 23/SR, Lane Moment CDF, 20, 30, & 60 Feet.

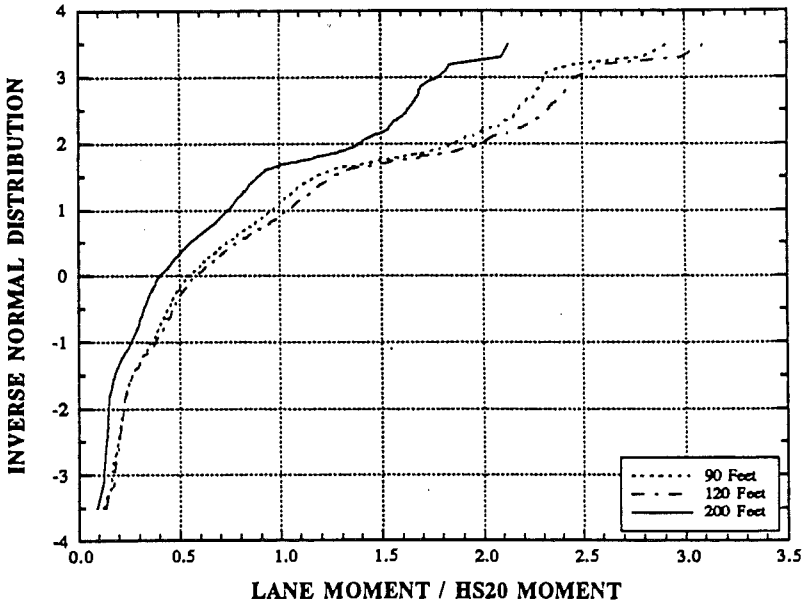

Fig. 8-98. 23/SR, ane Moment CDF, 90, 120, & 200 Feet.

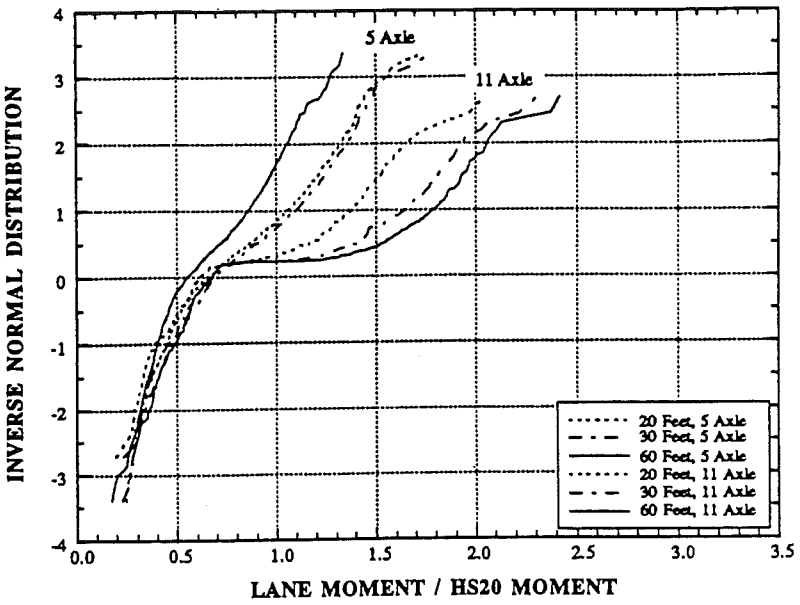

Fig. 8-99. 23/SR, 5 & 11 Axle Lane Mom CDF, 20, 30, & 60 Feet.

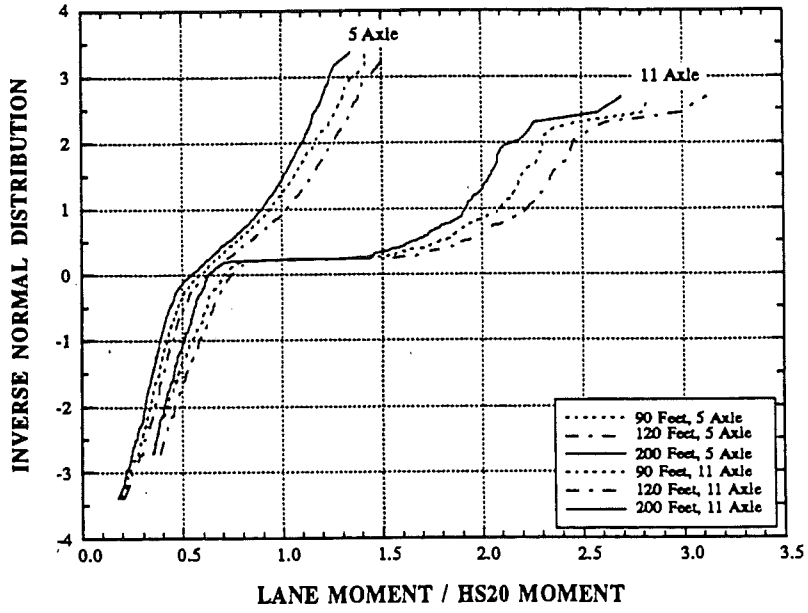

Fig. 8-100. 23/SR, 5 & 11 Axle Lane Mom CDF, 90, 120, & 200 Feet.

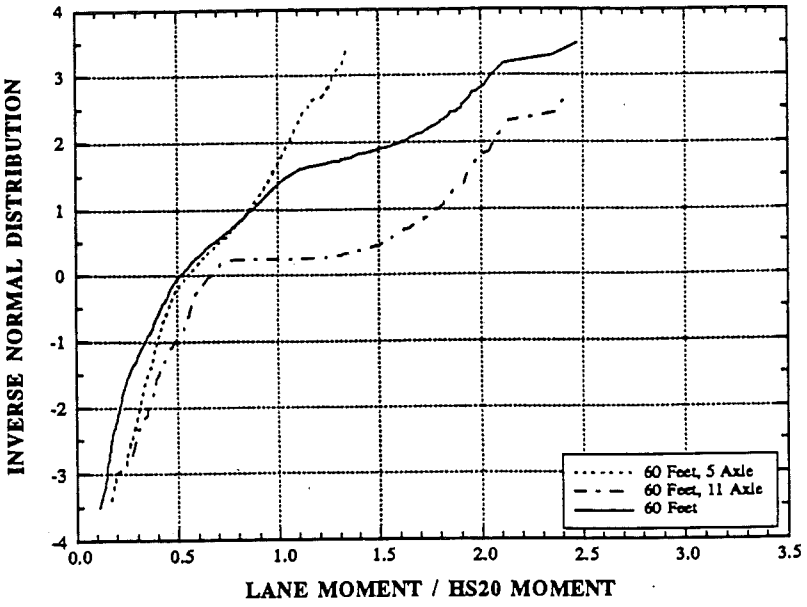

Fig. 8-101. 23/SR, 5, 11, & All Axle Lane Mom CDF, 60 Feet.

8.8 I-94 over Pierce Road (94/PR) in Grass Lake, Michigan

Truck weight data was collected on I-94 at the Pierce Road bridge during two different conditions which affected the results significantly. Data collection in 1991 took place while the Michigan State Police weigh station was in operation. Data colection in 1993 took place while the weigh station was closed for renovation. Fig. 8-102 and 8-103 are the histograms of gross vehicle weight (GVW) for all trucks measured on 94/PR in 1993 and 1991 respectively. Vehicles weighing less than 15 kips are excluded from the histograms. The distribution shapes of Fig. 8-102 and 8-103 are similar, however, subtle differences can be observed at specific range levels, indicating that there are differences in the traffic. The cumulative distribution functions (CDFs) of 1993 and 1991 GVW in Fig. 8-104 can be readily compared and differences in shape observed, particularly at the upper tail, supporting the observation.

Results of the individual day measurements are presented in Fig. 8-107 for 6/30/93 and 7/1/93. The day to day CDF's are very similar in shape and average GVW with only a slight difference at the upper tail of the distribution. Fig. 8-108 presents day to day CDF's for 8/10/91 and 8/11/91 indicating a more pronounced difference between the two days of data. From the graphs and from table 8-8, the heaviest vehicle observed in 1993 weighed 181.5 kips and 133.3 kips in 1991 with a mean GVW of 52.4 and 51.4 kips respectively.

Fig. 8-105 is the histogram of 5 axle vehicle GVW. Differences between 1993 and 1991 data are small and a similar trend in the distributions is evident. Apparent is the much higher percentage (24.9%) of 5 axle vehicles at the 70 to 80 kip range in 1991 over the percentage (16.7%) in 1993. It is apparent from the distribution of Fig. 8-105 that the eastbound 94/PR is carrying a population of loaded and unloaded 5 axle trucks, resulting in a slightly bimodal distribution, especially for the 1991 data. The 1993 and 1991 mean 5 axle vehicle GVW's are 54.6 kips and 56.5 kips (Tables 8-11).

Potentially more important for fatigue cycles and the distribution of moments for a given bridge are the axle weights and spacing for the trucks passing over the bridge. Fig. 8-109 through 8-117 present the axle weight distributions of the vehicles discussed above. All distributions include axles with weights greater than 5000 pounds.

Fig. 8-109 to 8-114 are 1993 and 1991 axle weight histograms of all vehicles axles for 94/PR. The corresponding CDF's are presented in Fig. 8-115, 8-116, and 8-117. Front and following axle weight histograms of Fig. 8-111 through 8-114 indicate a significant difference in both variation and magnitudes. Front axle weight has a much smaller variation than the following axle weight as observed in the graphs and from Table 8-13 through 8-15. As observed from the CDF's of Fig. 8-116 and 8-117 the 1993 and 1991 mean front axle weights are 9.71 kips and 9.71 kips with a maximum of 20.8 kips and 13.2 kips. The 1993 and 1991 following axle means are 11.87 kips and 11.76 kips with a maximum of 54.3 kips and 27.3 kips for 1993 and 1991.. Maximum axle weight observed was 54.3 kips and 27.3 kips for 1993 and 1991. Mean axle weights were 11.38 kips and 11.30 respectively. As is the case with GVW, there is very little daily variation in the vehicle axle weights.

Of greater interest is the effect of the GVW, axle weight and axle spacing. The effect of these parameters can be determined by the lane moment caused by the truck. Fig. 8-118 through 8-133 present lane moments for various simply supported spans. Each truck in the data base is analytically driven across the bridge to determine the maximum bending moment per lane for various simple span lengths. The CDF's of the lane moments for spans of 20, 30, 60, 90, 120, and 200 feet are then determined. As a point of reference the lane moments are presented in terms of the truck lane moment to HS20 moment.

Fig. 8-118 through 8-127 plot the CDF's for moment effect of all trucks with GVW greater than 15 kips for 1993 and 1991. The mean of lane moment to HS20 moment is approximately 0.5 to 0.6 for each

of the spans for both 1993 and 1991 as seen in Fig. 8-118, 8-119, 8-120, and 8-121. The maximum 1993 lane moment to HS20 moment varies from 1.680 for a 20 ft. span to 2.169 for a 120 ft. span. For the 1991 data the maximum lane moment to HS20 moment varies from 1.12 for a 20 ft. span to 1.65 for a 120 ft. span. A comparison is made between 5 and 11 vehicles for both 1993 and 1991. Fig. 8-122 through 8-125 present 5 and 11 axle vehicle CDF's for simple spans of 20, 30, 60, 90, 120, and 200 ft. As a comparison of vehicle type for a given span, 5, 11, and all vehicle moment CDF's are plotted in Fig. 8-126 and 8-127 for a 60 ft simple span. The significant observation to be made from these graphs is that 11 axle vehicles induce the largest lane moments in the bridge.

Fig. 8-128 through 8-133 compare the lane moment ratio CDF's for 1993 and 1991 by span. It can be observed that there are pronounced differences in moment effect at the upper tail of the distribution between the data collected while the nearby weigh station was in operation in 1991 and when the station was closed during 1993 data collection. The lane moments produced while the weigh station was open are considerably larger.

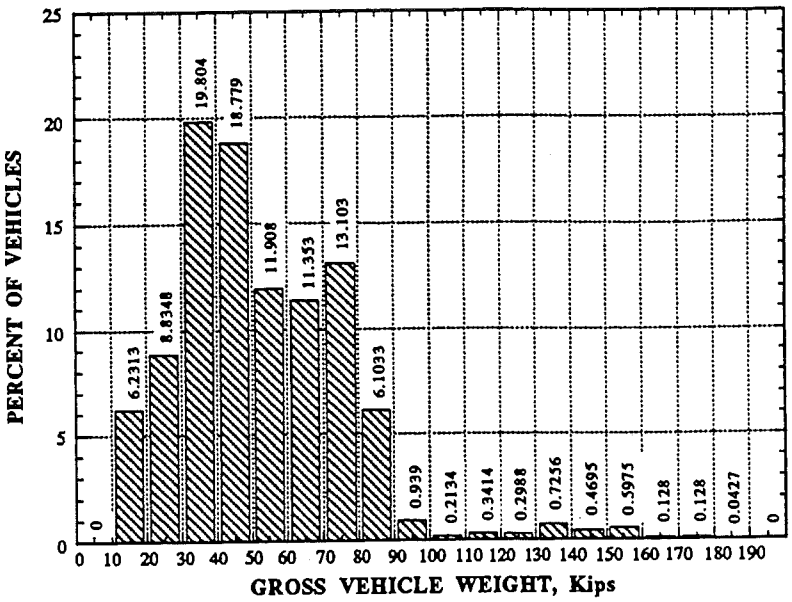

Fig. 8-102. 94/PR, 1993 GVW Histogram - Vehicles > 15 Kips.

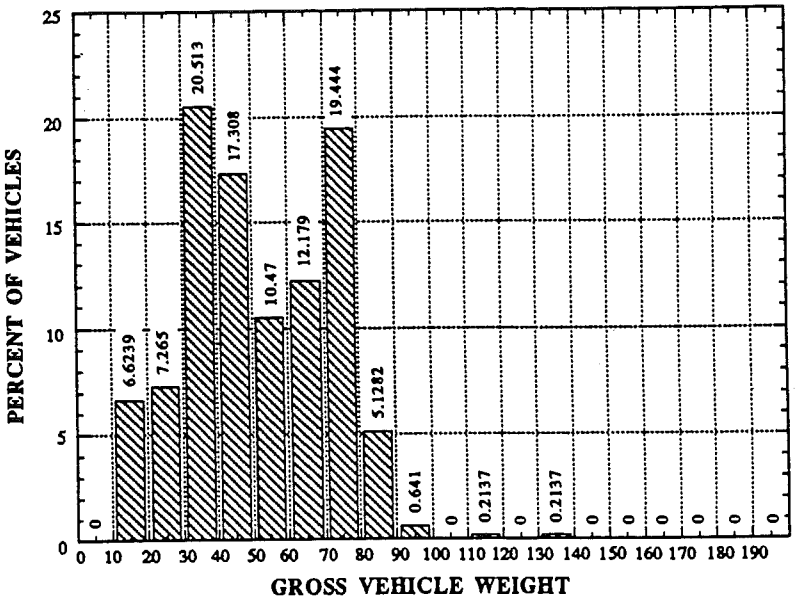

Fig. 8-103. 94/PR, 1991 GVW Histogram - Vehicles > 15 Kips.

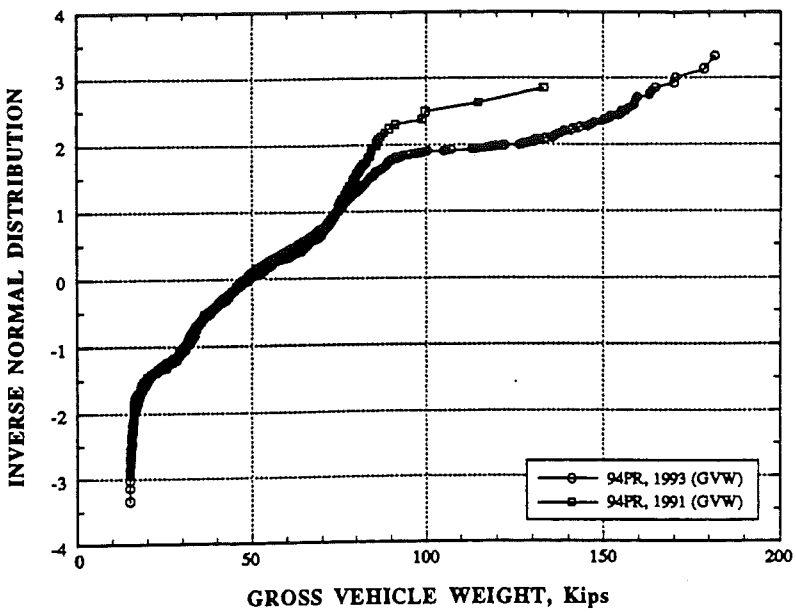

Fig. 8-104. 94/PR, 1991, 93 GVW CDF - Vehicles > 15 Kips.

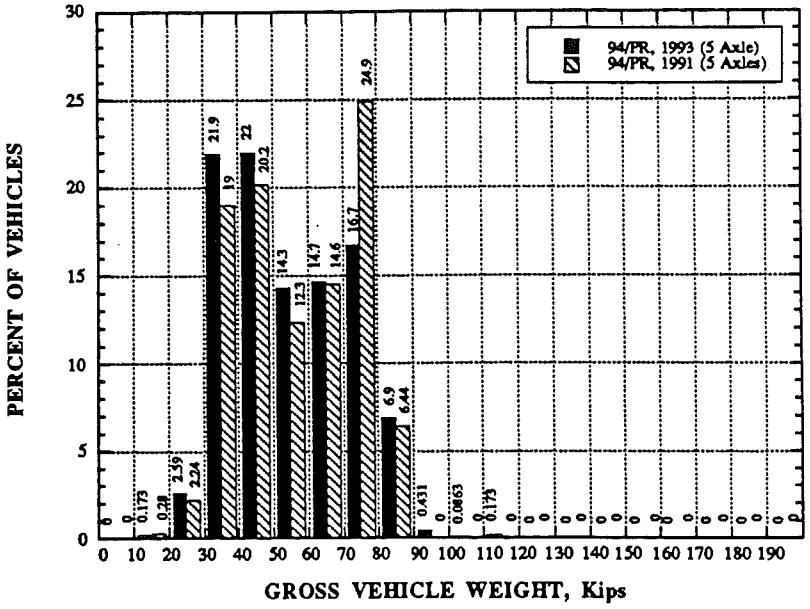

Fig. 8-105. 94/PR, 1991,3 EB, 5 Axle GVW > 15 Kips Histogram.

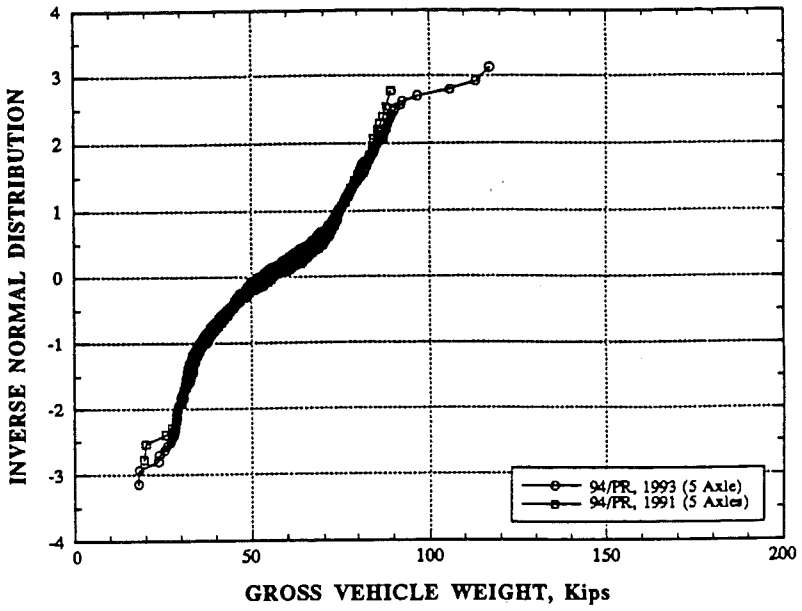

Fig. 8-106. I-94/PR, 1991, 1993, EB 5 Axle GVW CDF - Vehicles> 15 Kips.

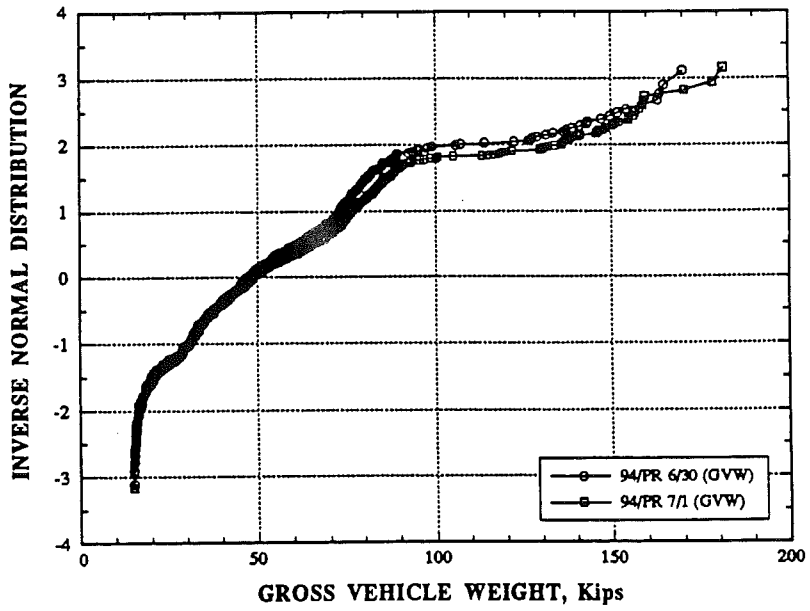

Fig. 8-107. 94/PR, EB, 1993 Daily GVW CDF - Vehicles > 15 Kips.

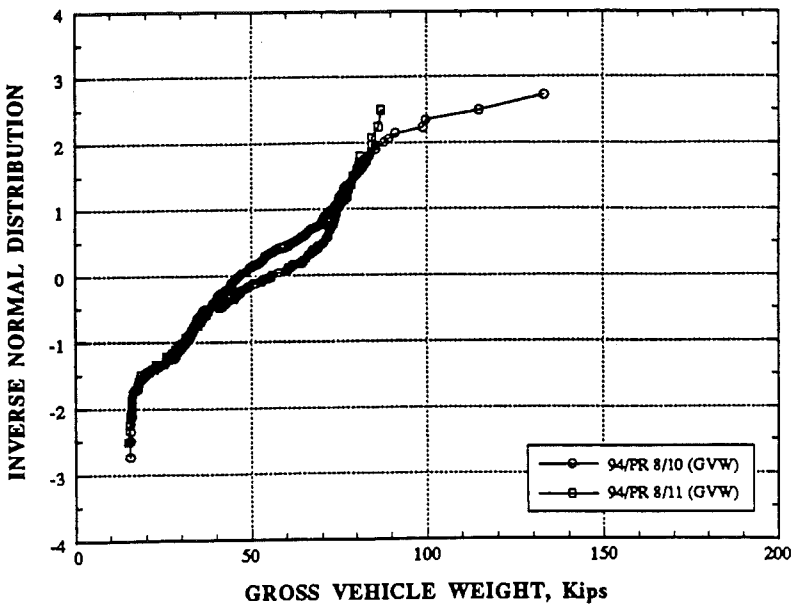

Fig. 8-108. 94/PR, EB, 1991 Daily GVW CDF - Vehicles > 15 Kips.

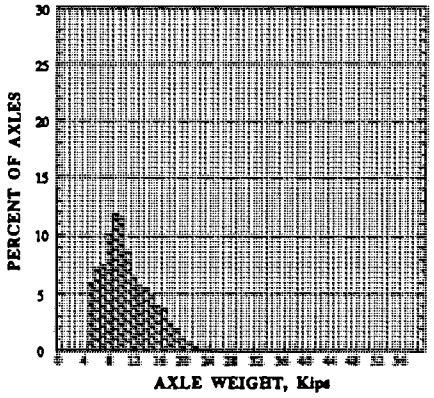

Fig. 8-109. I-94/PR 1993 Axle Weight.

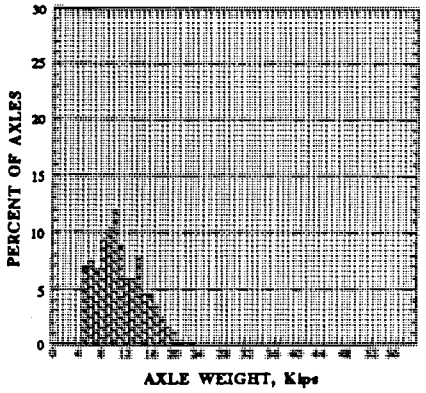

Fig. 8-110. I-94/PR 1991 Axle Weight.

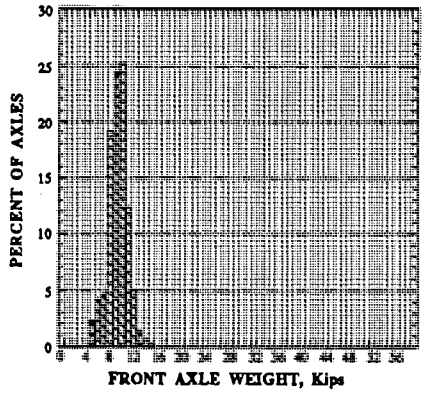

Fig. 8-111. I-94/PR 1993 Front Axle Wt.

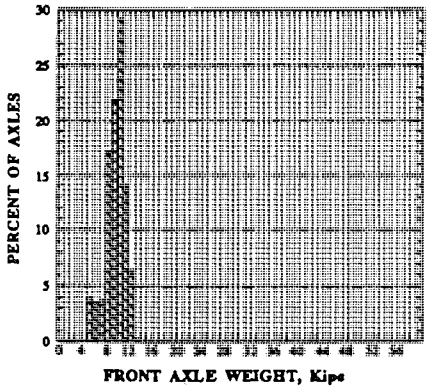

Fig. 8-112 I-94/PR 1991 Front Axle Wt.

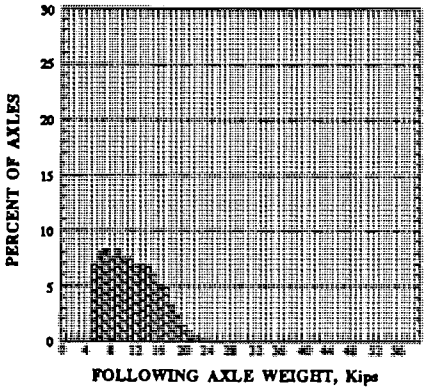

Fig. 8-113. I-94/PR 1993 Foll'g Axle Wt.

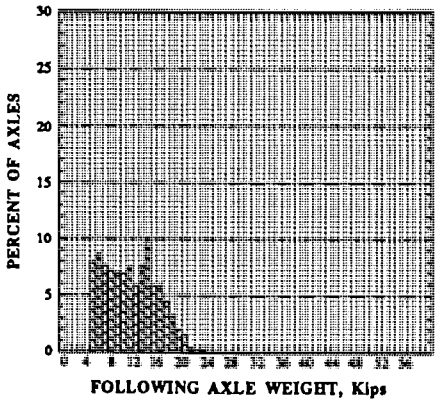

Fig. 8-114. I-94/PR 1991 Foll'g Axle Wt.

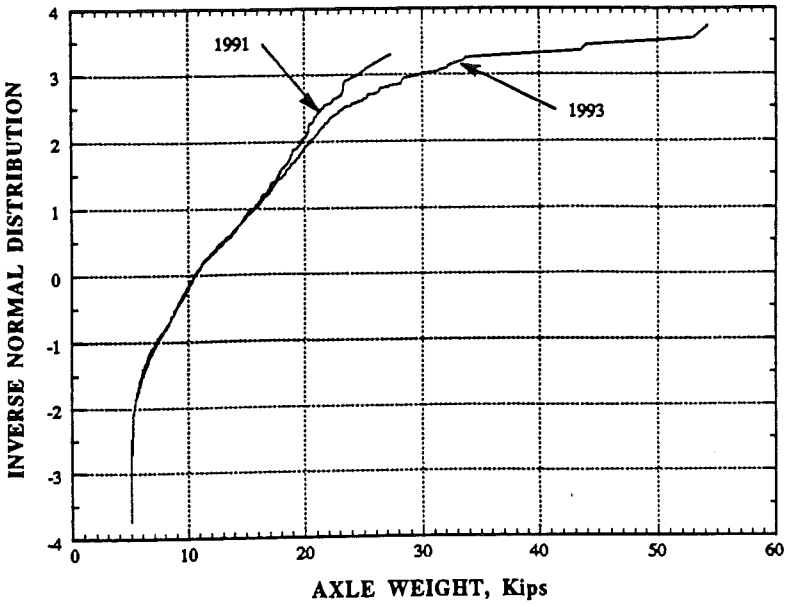

Fig.8-115. 94/PR,.1991, 1993, Axle Weight CDF - Axles > 5 Kips.

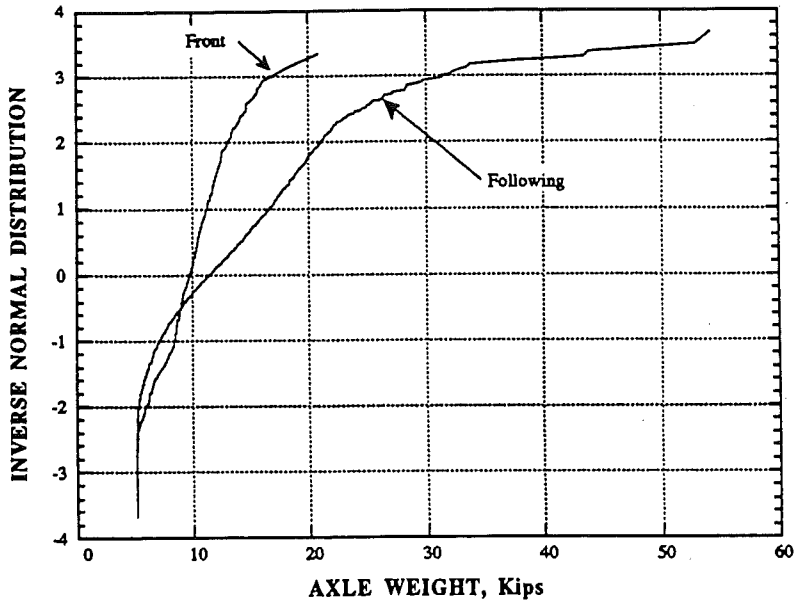

Fig. 8-116. 94/PR, 1993, Front & Following Axle Weight CDF.

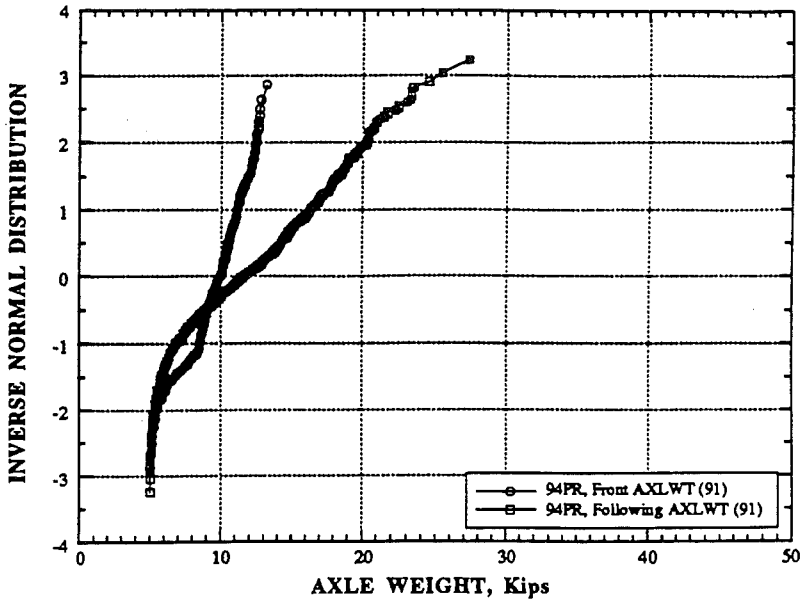

Fig. 8-117. 94/PR, 1991, Front & Following Axle Weight CDF

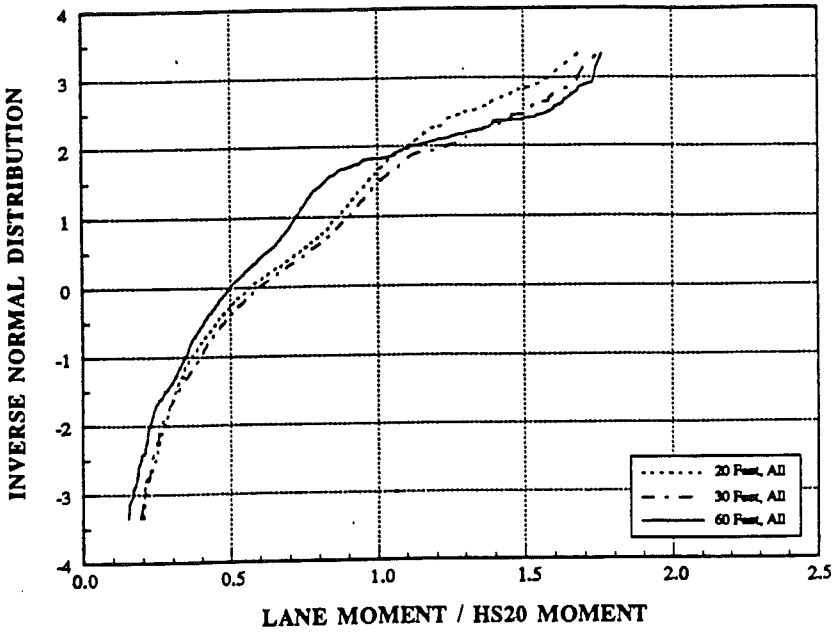

Fig. 8-118. 94/PR, Lane Moment CDF, 20, 30, and 60 Ft. - 1993.

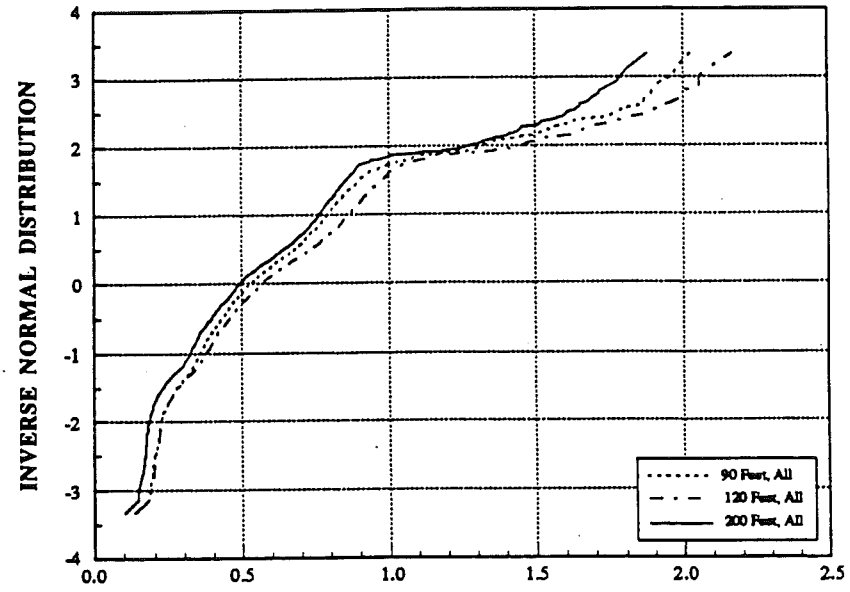

Fig. 8-119. 94/PR, Lane Moment CDF, 90, 120, and 200 Ft. - 1993.

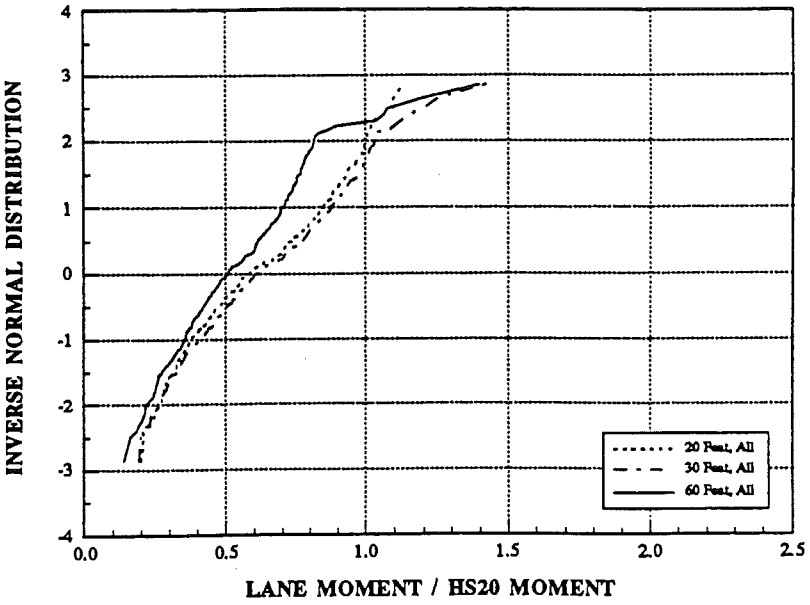

Fig. 8-120. 94/PR, Lane Moment CDF, 20, 30, and 60 Ft. - 1991.

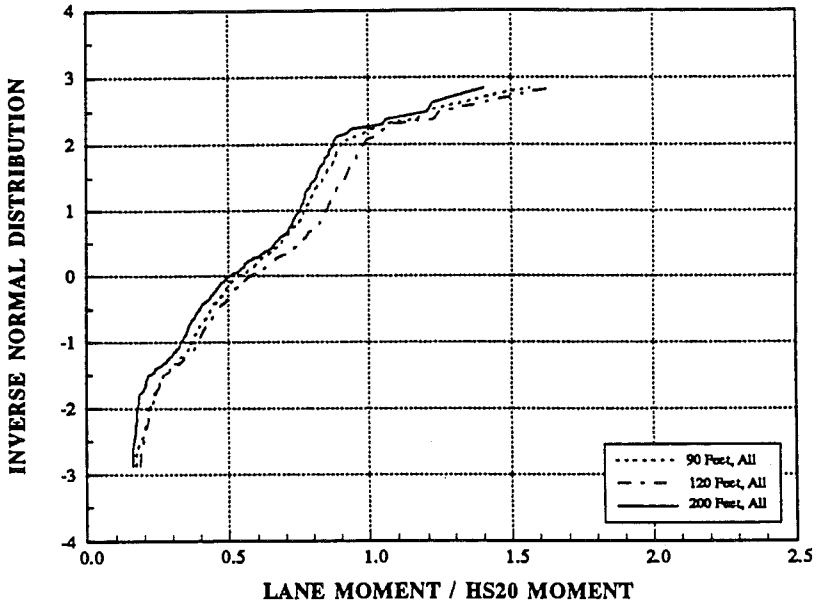

Fig. 8-121. 94/PR, Lane Moment CDF, 90, 120, and 200 Ft. - 1991.

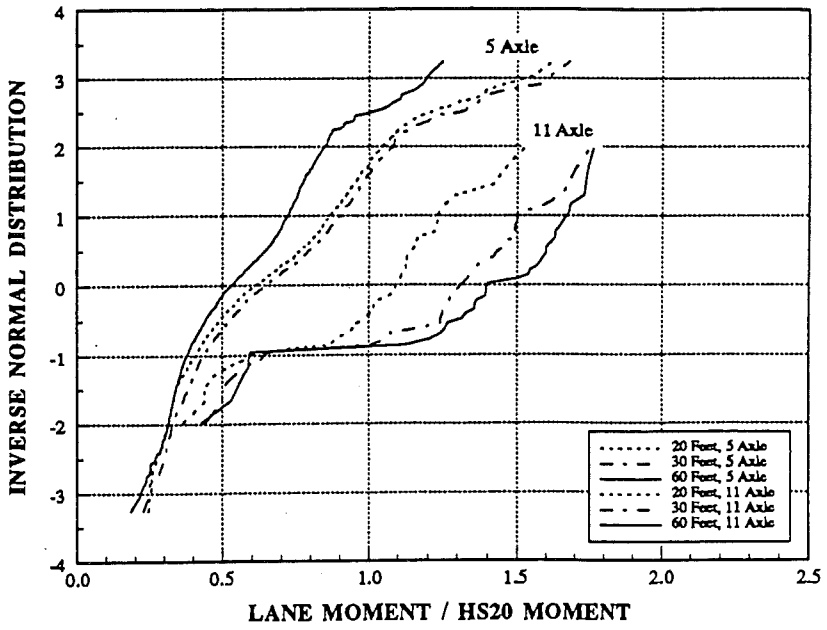

Fig. 8-122. 94/PR, 5 & 11 Axle Veh Lane Mom CDF, 20, 30, & 60 Ft, 1993.

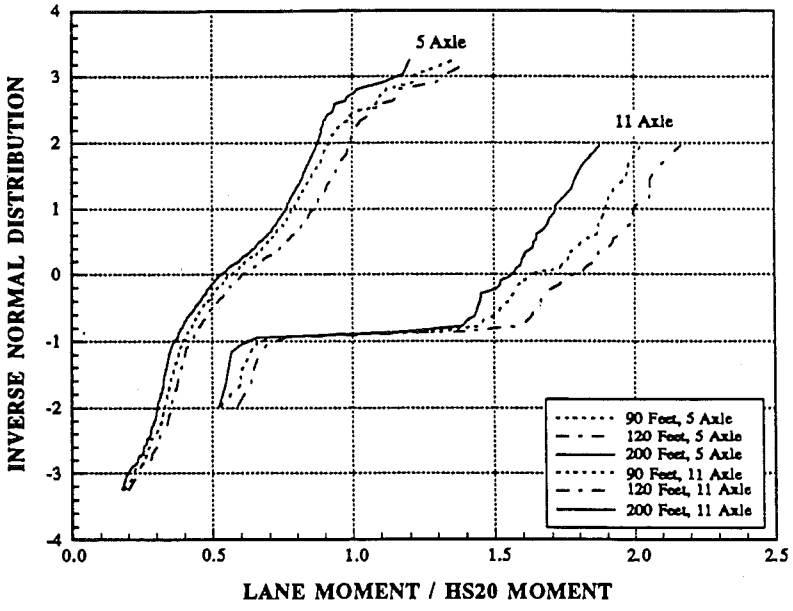

Fig. 8-123. 94/PR, 5 & 11 Axle Vehicles Lane Moment CDF, 90, 120, & 200 Ft, 1993.

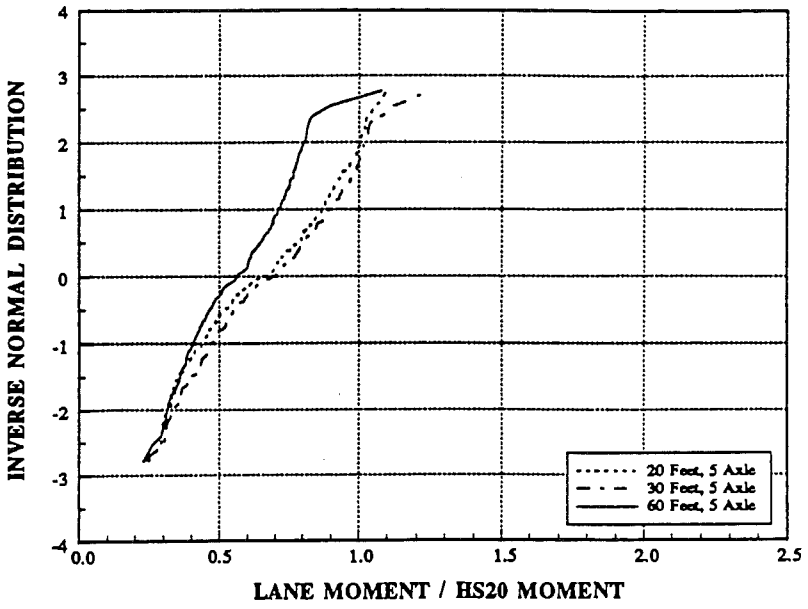

Fig. 8-124. 94/PR, 5 Axle Vehicles Lane Mom CDF, 20, 30, & 60 Ft - 1991.

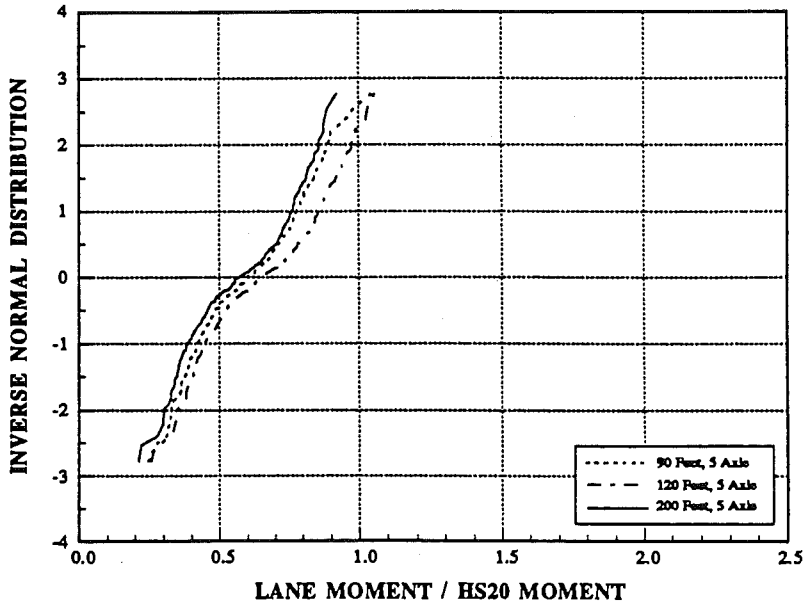

Fig. 8-125. 94/PR, 5 Axle Veh. Lane Moment CDF, 90, 120, & 200 Ft - 1991.

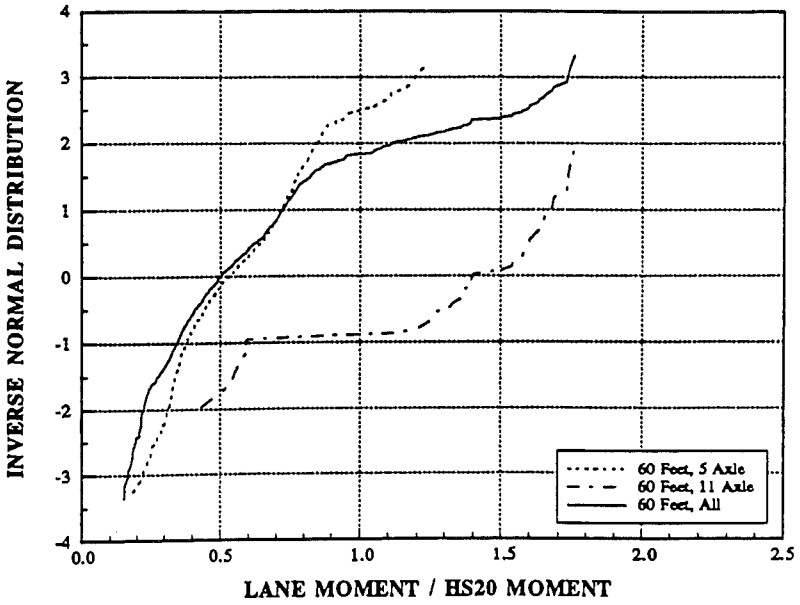

Fig. 8-126. 94/PR, All, 11 & 5 Axle Vehicles Lane Moment CDF, 60 Ft - 1993.

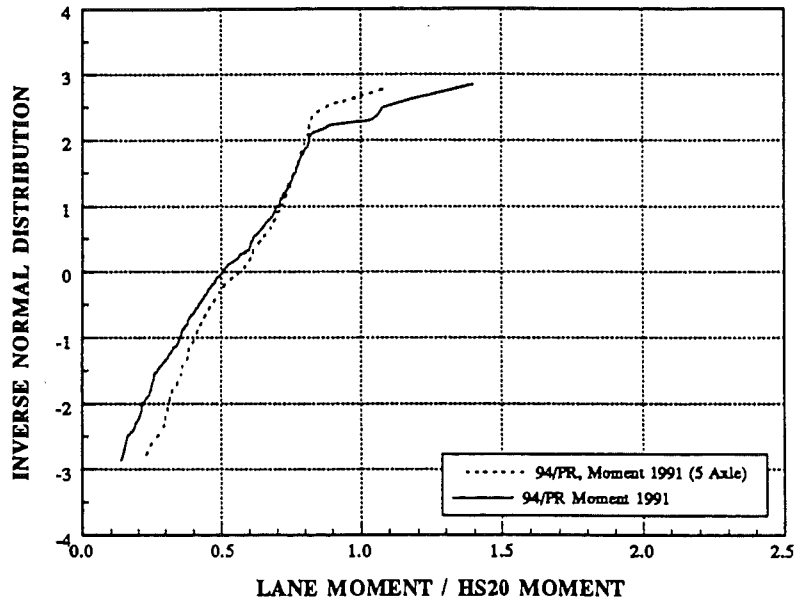

Fig. 8-127. 94/PR, All & 5 Axle Vehicles Lane Moment CDF, 60 Ft - 1991.

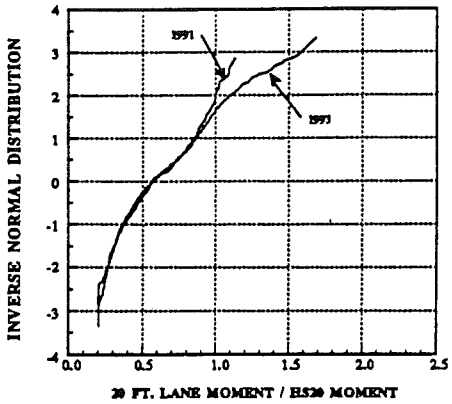

Fig. 8-128. I-94/Pierce Rd, 20 Ft Moment.

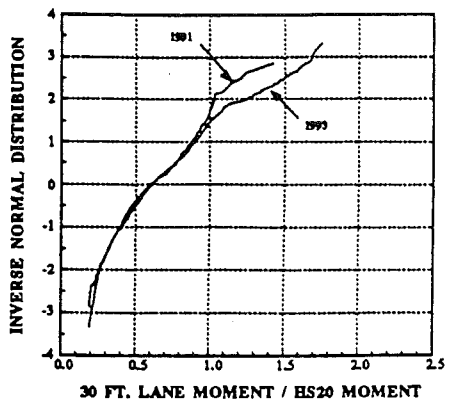

Fig. 8-129 I-94/Pierce Rd, 30 Ft Moment.

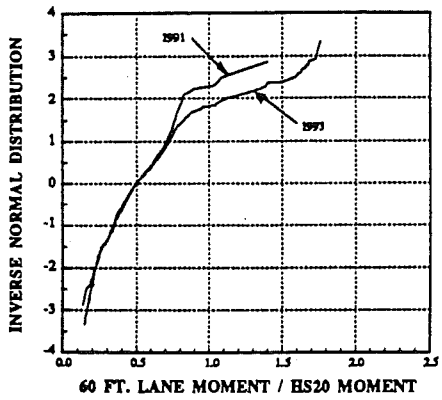

Fig. 8-130. I-94/Pierce Rd, 60 Ft Moment.

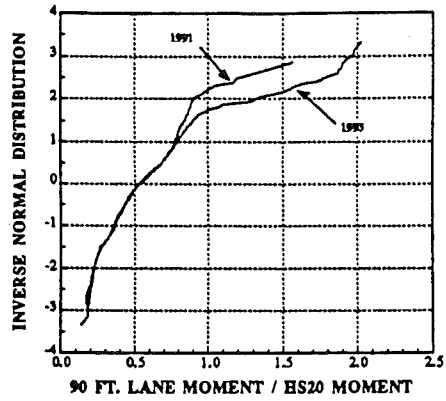

Fig. 8-131 I-94/Pierce Rd, 90 Ft Moment.

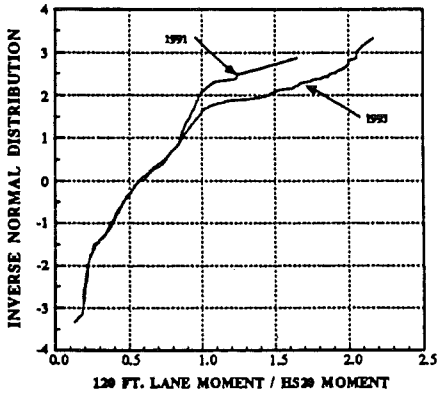

Fig. 8-132. I-94/Pierce Rd, 120 Ft Moment.

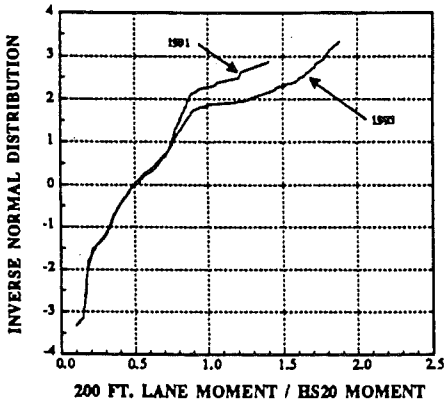

Fig. 8-133. I-94/Pierce Rd, 200 Ft Moment.

8.9 Wyoming Road over I-94 (WY/94), Detroit Michigan

Fig. 8-134 is the histogram of gross vehicle weight (GVW) for all trucks measured on WY/94. Vehicles weighing less than 15 kips are excluded from the histogram. The corresponding cumulative distribution function (CDF) of GVW for all trucks observed and measured on WY/94 is shown in Fig. 8-135. Each circle represents one truck in the data file. From THE Table 8-10 the heaviest vehicle observed weighed 177.3 kips with a mean GVW of 42.9 kips. Results of the individual day measurements are presented in Fig. 8-136 for 8/19/93 and 9/8/93. The day to day CDFs demonstrate a similar trend and average GVW with the largest difference at the upper tail of the distribution. Some of the difference may be attributed to the fact that the data was not collected on consecutive days.

Fig. 8-137 a histogram of all 5 axle vehicles; Fig. 8-138 is a histogram of all WY/94 11 axle vehicles. The corresponding CDFs of the 5 and 11 axle vehicles are shown in Fig. 8-139. The CDFs of Fig. 8-139 clearly show that the heaviest vehicles are the 11 axle trucks. The 5 axle vehicle mean GVW was 42.8 kips and for 11 axle vehicles 83.5 kips. Maximum 5 and 11 axle GVW was 89.5 kips and 177.3 kips respectively (Tables 8-11 and 8-12). For comparison of the daily distributions of 5 and 11 axle vehicles, the CDFs for both days are plotted in Fig. 8-140.

Potentially more important for fatigue cycles and the statistical distribution of lane moments for a given bridge will be the axle weights and spacing for the trucks passing over the bridge. Fig. 8-141 through 8-145 present the distributions of the axle weights of the vehicles discussed above. All distributions include axles with weights greater than 5000 pounds.

Fig. 8-141 is the axle weight histogram of all vehicles axles on WY/94. The corresponding CDF is presented in Fig. 8-142 and the daily CDFs are shown in Fig. 8-143. The maximum axle weight observed at WY/94 was 31.8 kips with a mean of 10.22 kips. As in the case with GVW, there is very little daily variation in the vehicle axle weights with

some differences at the upper tail of the distribution. The front and following axle weight histograms of Fig. 8-144 indicate a significant difference in both variation and magnitudes. As observed from the CDFs of Fig. 8-145 the mean front axle weight is 9.18 kips with a maximum of 18.8 kips while the following axle mean was 10.63 kips with a maximum of 31.8 kips. The higher variation in the following axle weights is readily apparent from the CDF comparison in Fig. 8-145.

Of greater interest is the effect of the GVW, axle weight and axle spacing. The effect of these parameters can be determined by the lane moment caused by the truck. Each truck in the data base is analytically driven across the bridge to determine the maximum bending moment per lane for various simple span lengths. The CDFs of the lane moments for spans of 20, 30, 60, 90, 120, and 200 feet are then determined. As a point of reference the lane moments are presented in terms of the truck lane moment to HS20 moment.

Fig. 8-146 and 8-147 plot the CDFs for moment effect of all trucks with GVW greater than 15 kips for WY/94. The mean of lane moment to HS20 moment is approximately 0.3 to 0.5 for the spans shown. The maximum ratio of lane moment to HS20 moment varies from 1.35 for a 20 ft. span to 2.2 for a 120 ft. span. Similar to the GVW data, a comparison is made between 5 and 11 axle moments. Fig. 8-148 and 8-149 present 5 and 11 axle vehicle lane moment CDFs for simple spans of 20, 30, 60, 90, 120, and 200 ft. As a comparison of vehicle type for a given span, 5, 11, and all vehicle moment CDFs are plotted for a 60 ft simple span in Fig. 8-150.

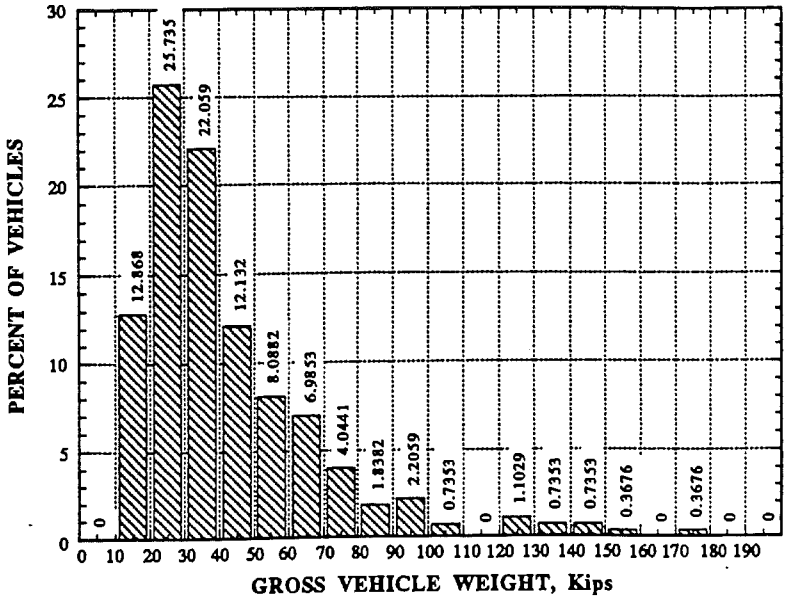

Fig. 8-134. WY/94 GVW Histogram - Vehicles > 15 Kips.

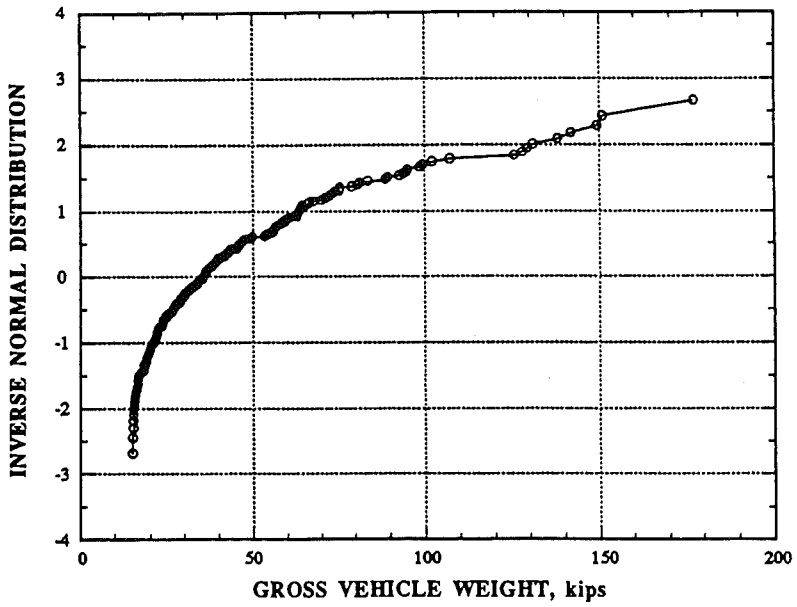

Fig. 8-135. WY/94 GVW CDF, - Vehicles > 15 Kips.

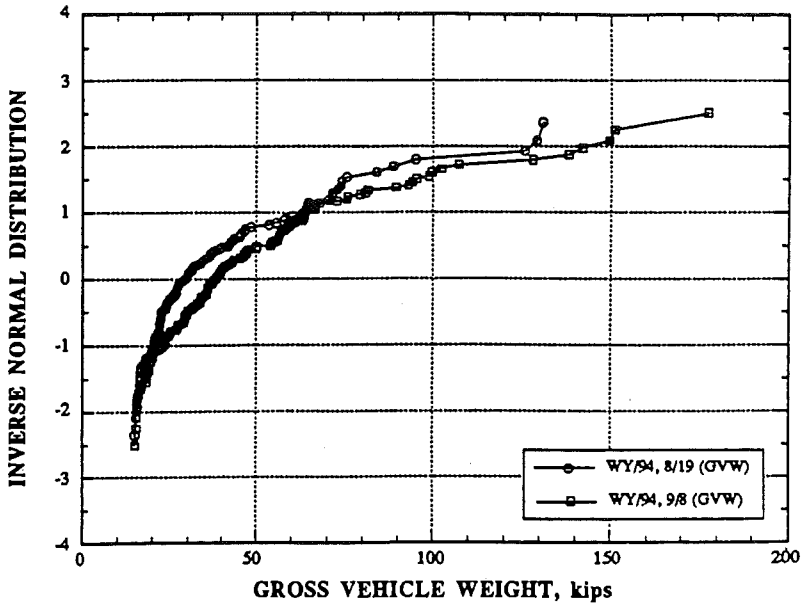

Fig. 8-136. WY/94 Daily GVW CDF - All Veh.icles > 15 Kips.

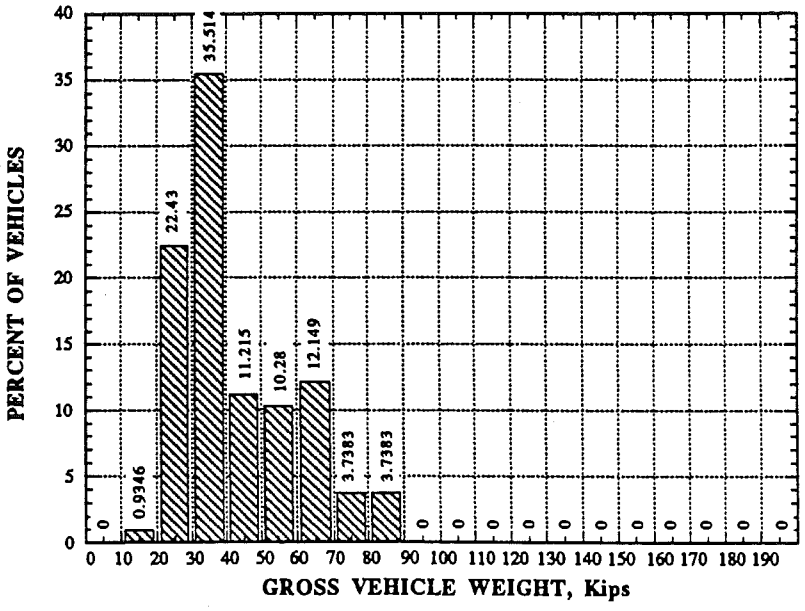

Fig. 8-137. WY/94 5 Axle GVW > 15 Kips Histogram.

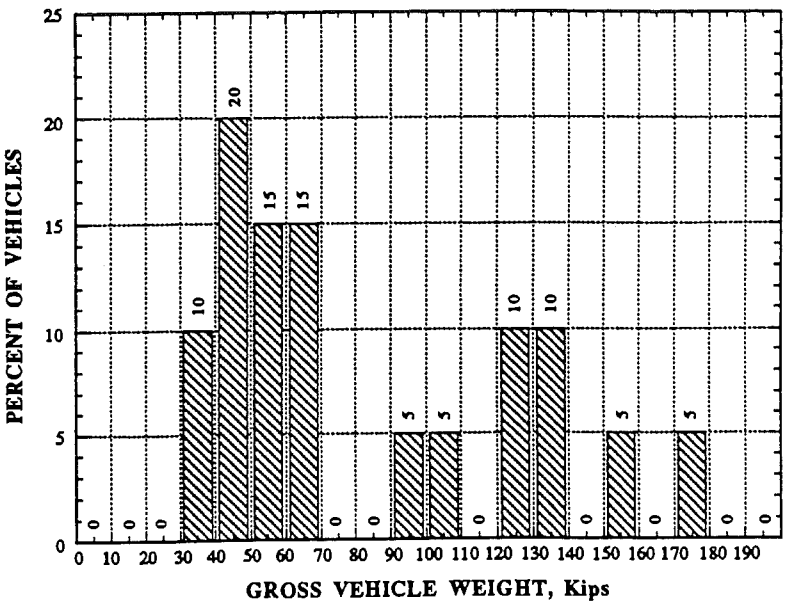

Fig. 8-138. WY/94 11 Axle GVW > 15 Kips Histogram.

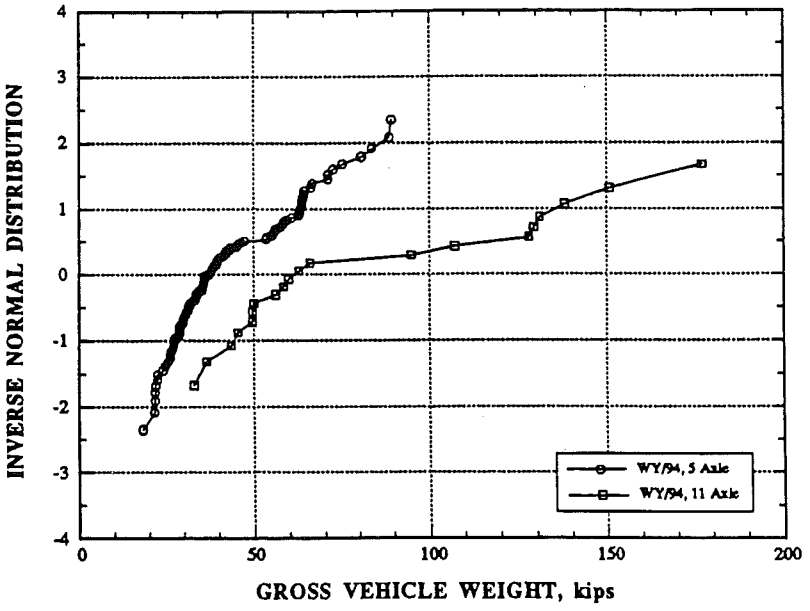

Fig. 8-139 WY/94, 5 and 11 Axle GVW > 15 Kips CDF.

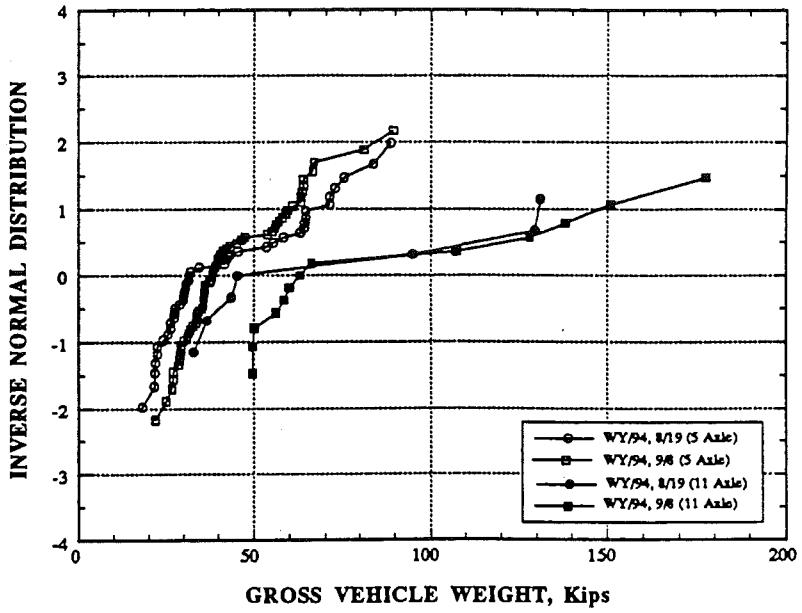

Fig. 8-140. WY/94, Daily 5 and 11 Axle GVW > 15 Kips CDF.

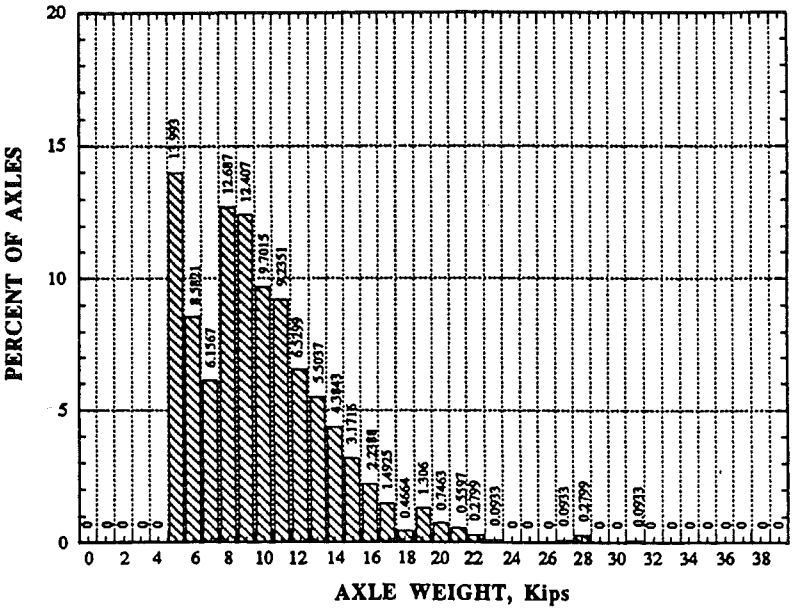

Fig. 8-141. WY/94, Axle Weight Histogram - All Axles > 5 Kips.

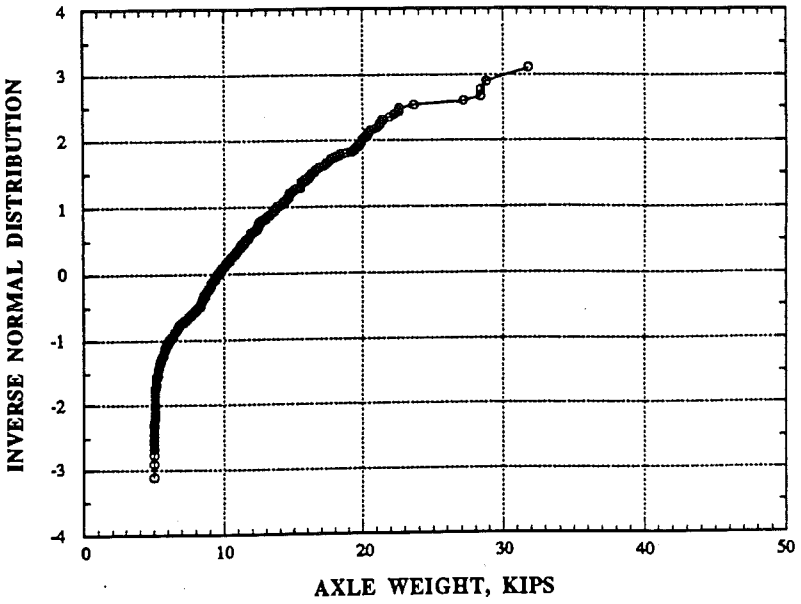

Fig. 8-142. WY/94, Axle Weight CDF - All Axles > 5 Kips.

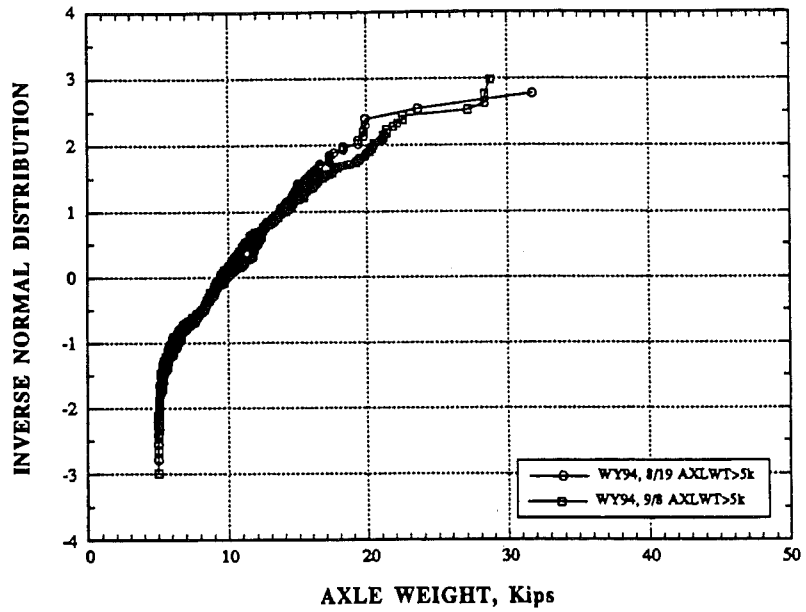

Fig. 8-143. WY/94 Daily Axle Weight CDF.- Axles > 5 Kips.

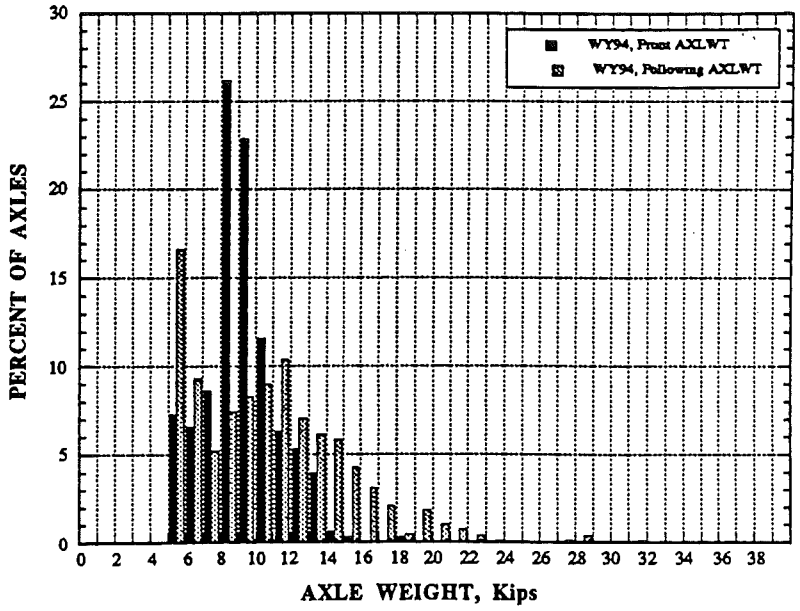

Fig. 8-144. WY/94, Front and Following Axle Weight Histogram.

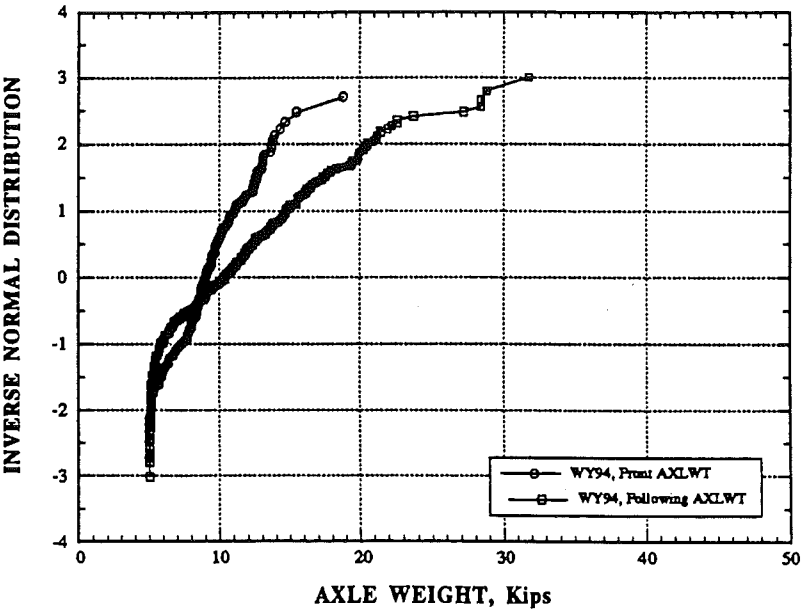

Fig. 8-145. WY/94, Front and Following Axle Weight CDF.

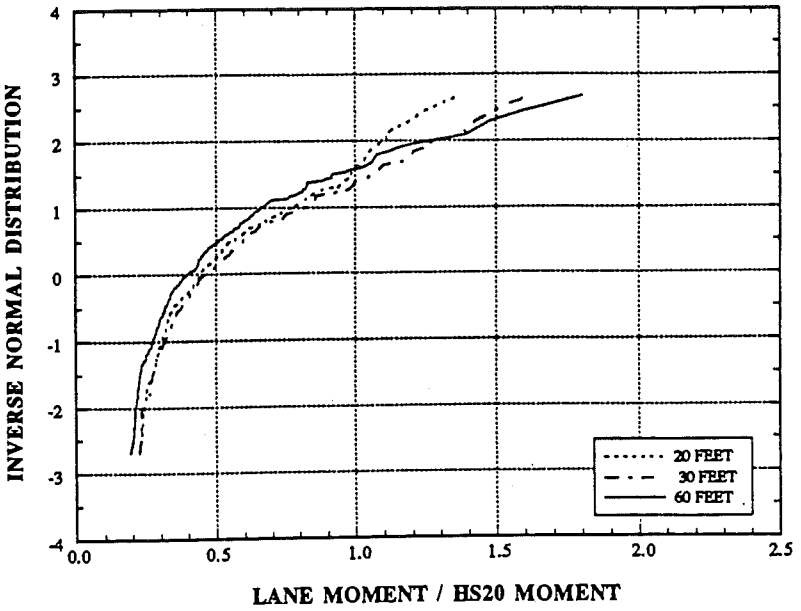

Fig. 8-146. WY/94 Lane Moment CDF, 20, 30, and 60 Feet.

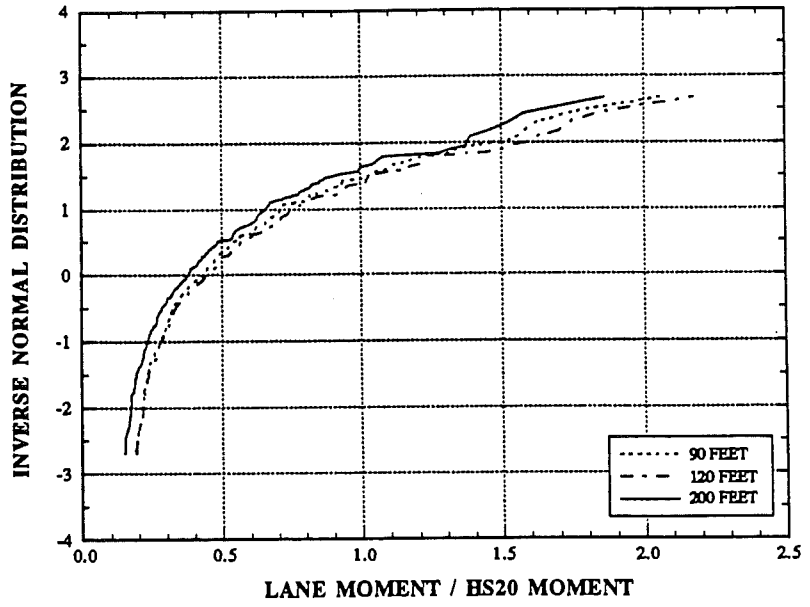

Fig. 8-147. WY/94 Lane Moment CDF, 90, 120, and 200 Feet.

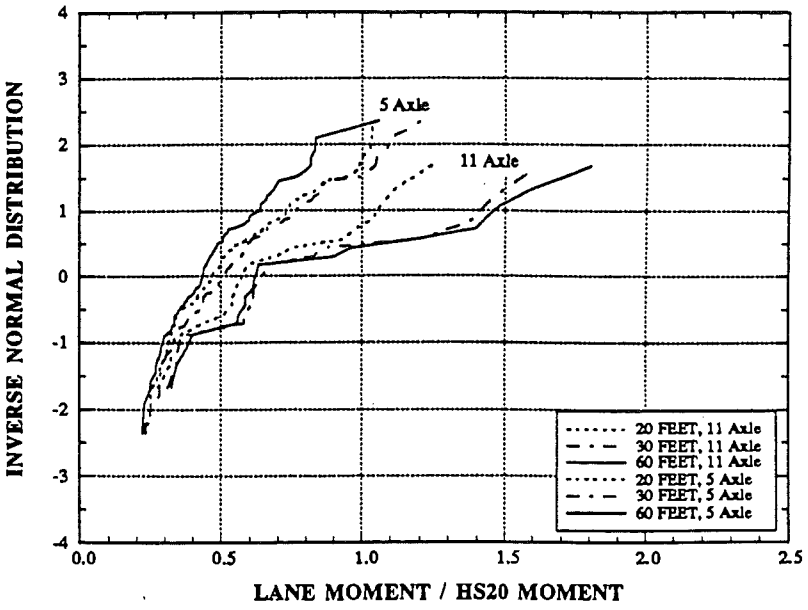

Fig. 8-148. WY/94, 5 and 11 Axle Lane Moment CDF, 20, 30, and 60 Ft.

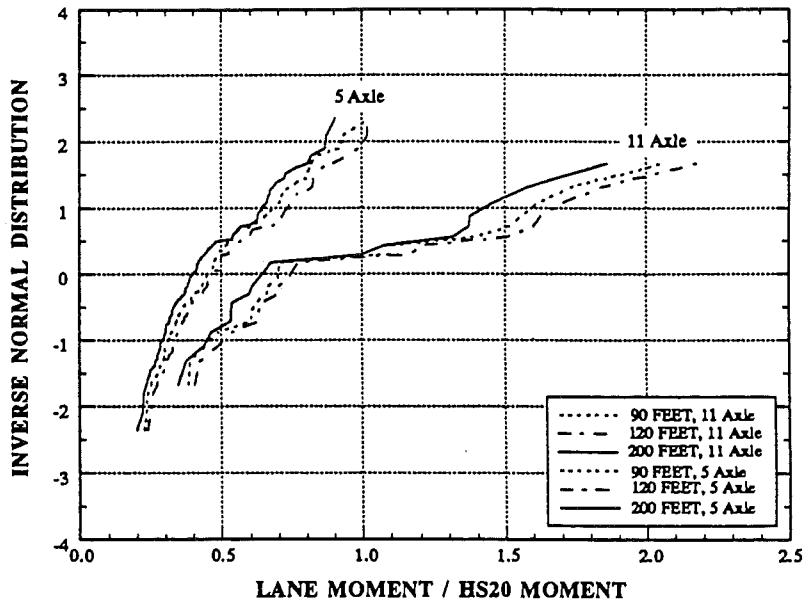

Fig. 8-149. WY/94, 5 and 11 Axle Lane Mom CDF, 90, 120, and 200 Ft.

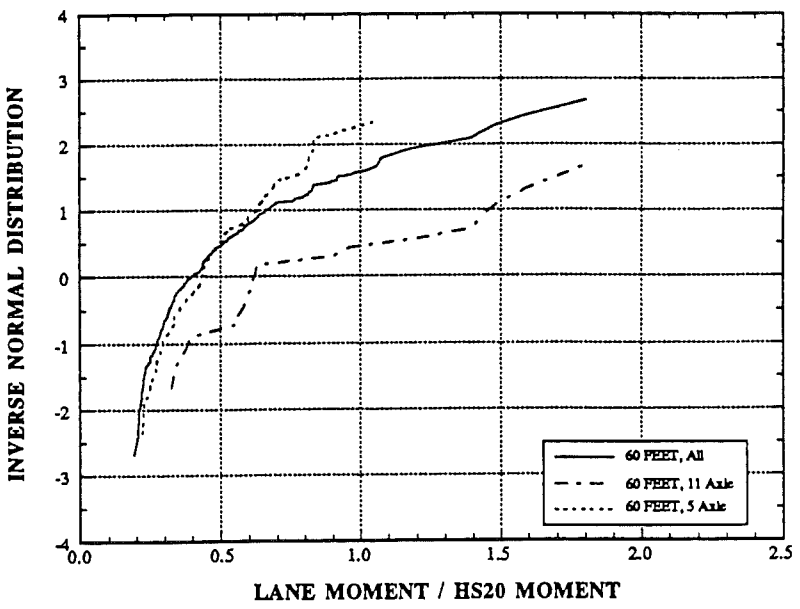

Fig. 8-150. WY/94, 5, 11, and All Axle Lane Moment CDF, 60 Ft.

8.10 Summary and Conclusions

Truck data collection is important in determining both the maximum load effects and frequency distribution of heavy traffic. The results of weight-in-motion measurements carried out during this project provided data for the calculation of statistical parameters. They include vehicle weight, truck class, and maximum, mean, median, standard deviation, coefficient of variation, skewness, and kurtosis of gross vehicle weights, axle weights, and moments. The considered parameters include distributions of gross vehicle weight (GVW), daily GVW distributions, distributions of GVW for five and eleven axle vehicles, and lane moments of all vehicles, five axle vehicles, and eleven axle vehicles for 20, 30, 60, 90, 120, and 200 foot spans.

The heaviest vehicles (GVW) are 11 axle trucks with coils of steel, gravel, or asphalt.

The measurements taken nearby of Truck Weigh Station indicate that truck weights are within the legal limits. However, on bridges further away from Weigh Stations, truck weights often exceed the legal limits. The observation was also confirmed by measurements on I-94 over Pierce Road when the Weigh Station was open and closed. This observation confirms that overloaded trucks avoid the scales.

The effect of heavy trucks is larger for longer spans. Moments and shear forces are calculated for the measured trucks.

Live load varies depending on location. The difference is not only in ADTT, but also in magnitude (truck weights). The heaviest traffic occurs on bridges that are not located close to the Truck Weigh Station.

9. DYNAMIC LOAD MODEL

9.1 Introduction

The dynamic load is an important component of bridge loads. It is time-variant, random in nature and it depends on the vehicle type, vehicle weight, axle configuration, bridge span length, road roughness and transverse position of truck on the bridge. An example of the actual bridge response for a vehicle traveling at a highway speed is shown in Fig. 9-1. For comparison, also shown is an equivalent static response, which represents the same vehicle traveling at crawling speed.

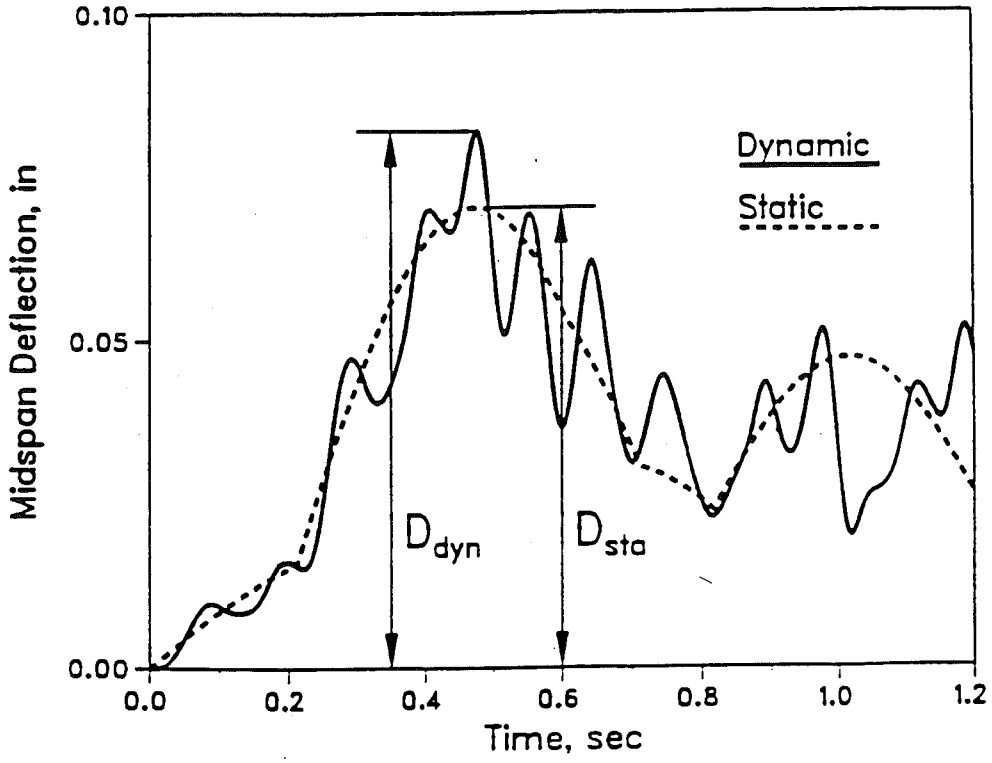

Fig. 1. Bridge Dynamic and Static Response Under Truck Load.

The dynamic load is usually considered as an equivalent static live load and it is expressed in terms of a dynamic load factor (DLF). There are different definitions for DLF as summarized by Bakht and Pinjarkar (1989) in their state-of-the-art report on dynamic testing of

bridges. In this study, DLF is taken as the ratio of dynamic and static responses (Billing 1982),

$$DLF = D_{dyn} / D_{stat} \qquad (9\text{-}1)$$

where: D_{dyn} = the maximum dynamic response (e.g. stress, strain or deflection) measured from the test data, $D_{dyn} = D_{total} - D_{stat}$; D_{total} = total response; and D_{stat} = the maximum static response obtained from the filtered dynamic response.

The measurement of static load spectra is described in Chapter 8. An accurate dynamic load model is required for the development of rational criteria for the design and evaluation of bridges. Yet, the available data is insufficient and unclear. Analytical simulation procedures provided a basis for calculation of design provisions (Hwang and Nowak 1991). However, there is a need for field verification of the results. Therefore, the objective of this study is to determine the dynamic load factor based on the field measurement data. The work is carried out on selected steel girder bridges. The obtained results are compared with DLF's calculated on the basis of the analytically simulated model (Hwang and Nowak 1991).

9.2 Dynamic Load in Design Codes

In bridge design codes, the dynamic load is specified as an equivalent static live load. The actual values vary from one document to another. Code provisions are compared for AASHTO (1992), LRFD AASHTO (1993), Ontario Highway Bridge Design Code (OHBDC 1979, 1983 and 1993) and Swiss Code (SIA 1988).

In the current AASHTO (1992), DLF is specified as function of span length only,

$$DLF = \frac{50}{125 + L} \qquad (9\text{-}2)$$

where L = span length in feet (1 ft = 0.305 m). However, the maximum value of DLF is 0.30.

In the new LRFD AASHTO Code (1994), live load is specified as a combination of HS20 truck (AASHTO 1992) and uniformly distributed load of 640 lb/ft (9.8 kN/m). DLF is equal to 0.33 of the truck effect, with no dynamic load applied to the uniform loading.

In the first two editions of the Ontario code (OHBDC 1979 and 1983), and in the Swiss Code (SIA 1988), DLF was specified as a function of the natural frequency of vibration for the bridge. The maximum DLF of 0.4 (0.45 in OHBDC 1979) corresponded to the frequencies between about 2 and 4 Hz. In the new edition of Swiss Code (Cantieni 1992) the maximum value DLF of 0.4 to 0.8 corresponded to the frequences between two and four Hz. The design provisions reflect the results of tests performed by Billing (1984) and Cantieni (1992). In the third edition of the Ontario code (OHBDC 1993), DLF is equal to 0.25 for all spans, except those governed by a single axle or a tandem, based on the simulations performed by Hwang and Nowak (1991).

9.3 Previous Studies

The available data on dynamic load in bridges is rather limited (Paultre et al. 1992). Some measurements were taken by the Ontario Ministry of Transportation (Billing 1984). A total of 27 bridges were tested. The structural types included prestressed concrete (girders and slabs), steel girders (rolled sections, plate girders and box girders), steel trusses and rigid frames. Data were recorded for test vehicles and actual traffic. The mean values of DFL are about 0.05 to 0.10 for prestressed concrete AASHTO type girders and 0.08-0.20 for steel girders. The maximum observed values exceed 0.5 and some of the coefficients of variation are over 1.0. However, the correlation between DLF and truck weight is not available. On the other hand, it is expected that the largest DLF's correspond to lighter trucks. Considerable differences in DLF are observed for otherwise very

similar structures which indicates the importance of factors such as surface condition.

Cantieni (1983) tested 226 bridges in Switzerland, mostly prestressed concrete. With the exception of 11 bridges, all were loaded with the same vehicle, under the same load, and with the same tire pressure, thus minimizing the variability due to truck dynamics. The effect of local unevenness in the pavement on the dynamic load was also investigated. The study showed that the dynamic fraction of the load was as high as 0.7 for bridges with fundamental natural frequency between two and four Hz. However, as in the Ontario data (Billing 1984), the static and dynamic loads were recorded separately, so that it is not possible now to determine the degree of correlation. It is also expected that the high values of DLF are associated with lighter vehicles.

Ghosn and Moses (1984) considered the dynamic load as an integral part of the live load model. To account for the dynamic load effect they multiplied the live load by a factor 1.11. This value falls in the middle range of the data obtained by Billing (1984).

O'Connor and Pritchard (1985) found that the dynamic load is vehicle dependent and it varies with the suspension geometry. They carried their tests on a short span composite steel and concrete bridge in Australia. The results indicate that as the weight of the vehicle increases, the dynamic load decreases. Also, O'Connor and Chan (1988) collected strain data and, using those records, they determined DLF's ranging from -0.08 to +1.32. As in the previous studies, the extreme values are associated with light trucks. Negative values of DLF indicate a strong domination of dynamic response over the static response (large vibrations with extreme values with opposite sign than static deflection).

Most of the theoretical studies on vibration of beams under moving loads concentrated on modeling only one of the parameters, either the vehicle, bridge, or surface roughness. The vehicle was

modeled as a constant force (Wu and Dai 1987), one degree-of-freedom system (Blejwas et al. 1979), two degrees-of-freedom system (Genin and Chung 1979), or more realistic complex systems (Gupta 1980). The bridge was modeled as either a continuous or discrete system. Honda, Kobori and Yamada (1986) treated the bridge as a simple beam with only bending moments in the longitudinal direction. Discrete models can be in the form of simple beams, simple beams with torsional degree-of-freedom, and orthotropic plates. The surface roughness was modeled using the so-called artificial bump on the approach method (Gupta 1980), the simple sinusoidal bridge surface model (Blejwas et al. 1979), and random processes together with Fourier series (Honda, Kobori and Yamada 1980). Further, multiple truck presence and eccentric loading were studied by Hikosaka et al. (1978) and Gupta (1980), respectively.

More recently, Huang et. al (1992) studied the variation of the DLF for six multigirder continuous bridges under moving loads. Their analysis used a grillage beam system model for the bridge, road roughness model, and a nonlinear vehicle model.

The development of a new LRFD (load and resistance factor design) code required a verification of the load model. In particular, there was a need for confirmation of the observation that the dynamic load factor decreases for heavier trucks and for multiple truck occurrence. Therefore, a computer procedure was developed by Hwang and Nowak (1991) for simulation of the dynamic bridge behavior. The dynamic load was determined as a function of three major parameters: road surface roughness, bridge dynamics (frequency of vibration) and vehicle dynamics (suspension system). Bridge was modeled as a prismatic beam. Dynamic parameters of trucks were based on the available data. Road roughness was generated using the actual measurement records. The DLF was calculated in terms of deflections. It was found that the dynamic deflection is almost a constant, while static deflection is proportional to truck weight. Therefore, DLF decreases for heavier trucks. For example, for 3 axle trucks with gross vehicle weight (GVW) approaching 300 kN (70

concrete girder bridge. The simulations were carried out for single trucks and two trucks side-by-side. For two trucks, the DLF was smaller by about 50 percent compared to DLF for single trucks, as shown in Fig. 9-5.

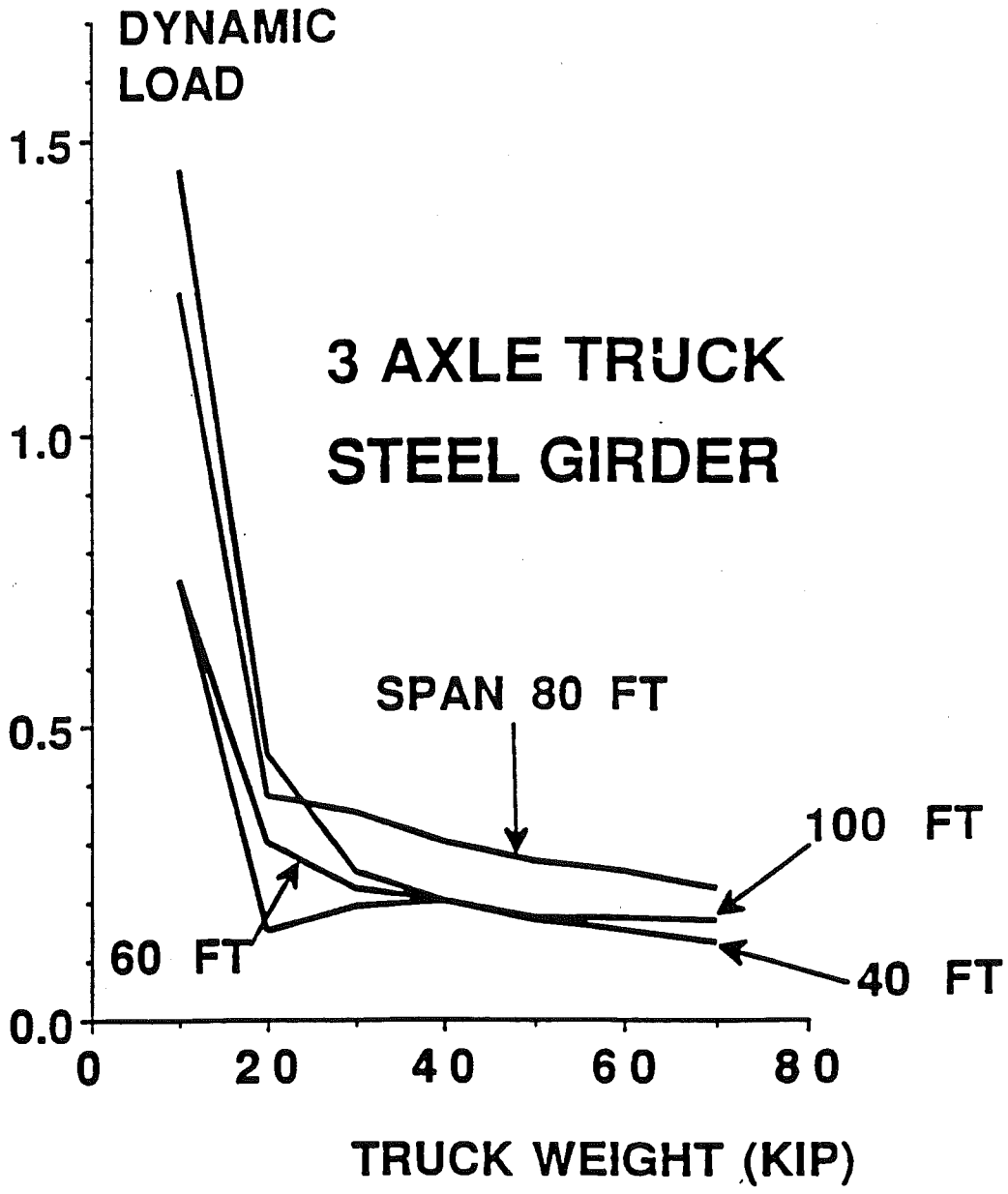

Fig. 9-2. Simulated DLF vs. 3 Axle Truck GVW on Steel Girder Bridge.

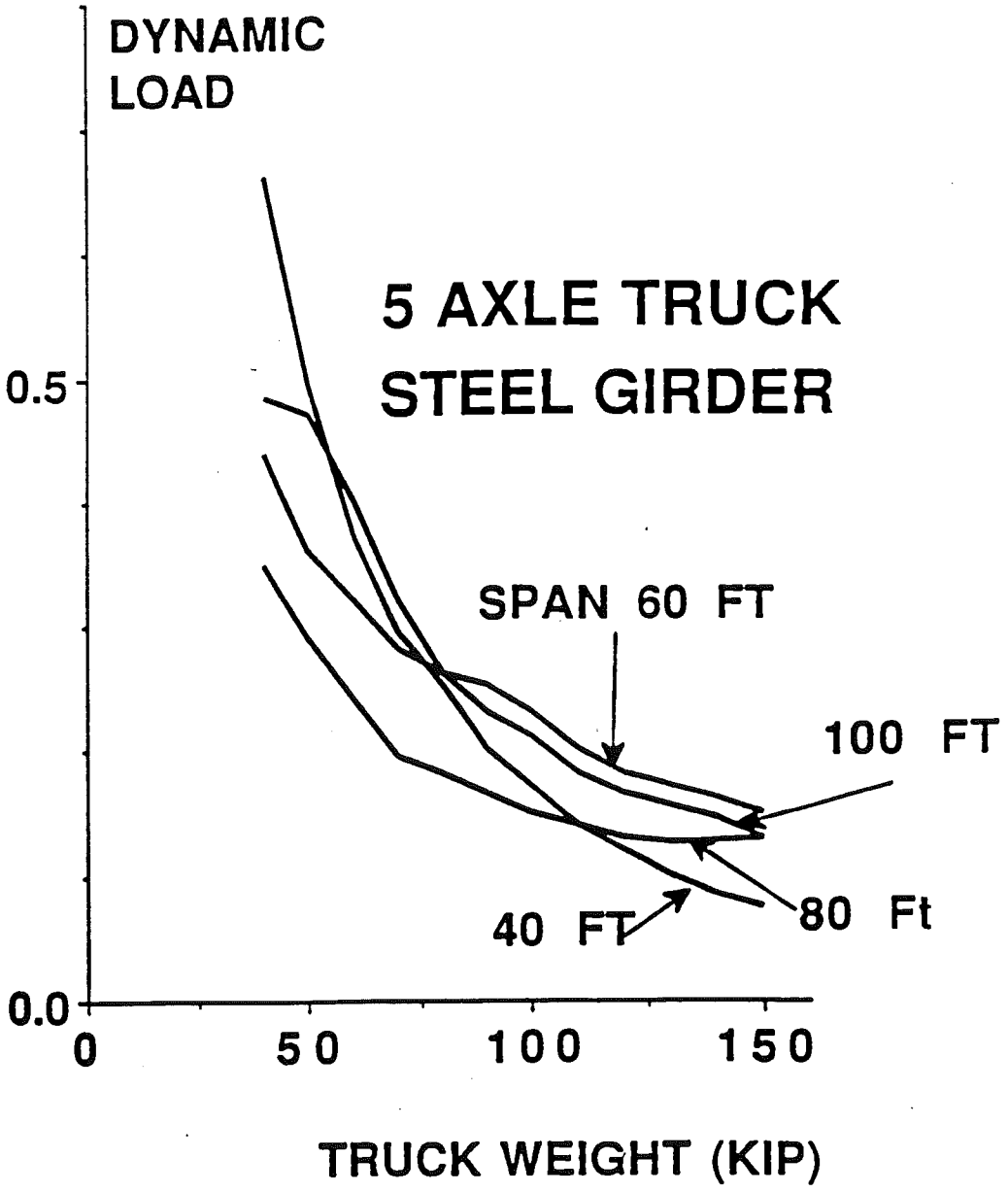

Fig. 9-3. Simulated DLF vs. 5 Axle Truck GVW on Steel Girder Bridge.

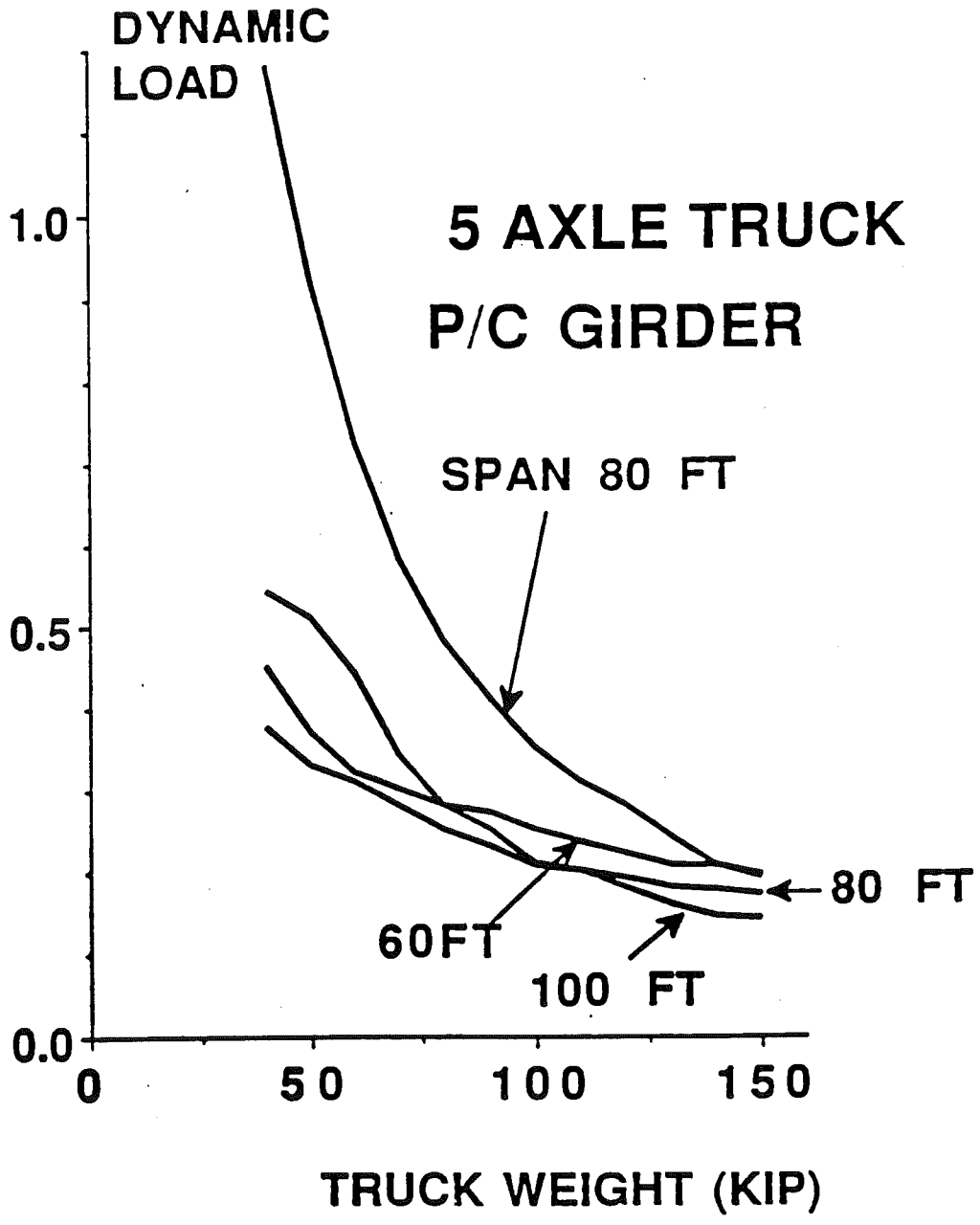

Fig. 9-4. Simulated DLF vs. 5 Axle Truck GVW on P/C Girder Bridge.

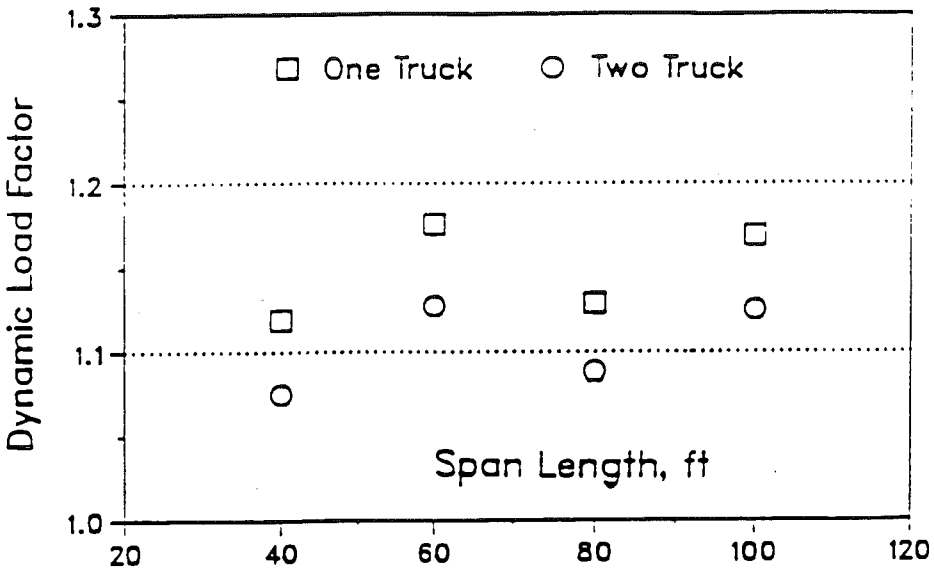

Fig. 9-5. Simulated DLF vs. Span Length for a Single Truck and Two Trucks Side-by-Side.

9.4 Experimental Program

The purpose of the experimental program is to measure the dynamic load amplification in steel girder bridges. Corresponding truck weights, in particular axle loads and axle spacings, are also recorded. The measurements are taken simultaneously by two systems: the WIM System (truck information and girder strains) and the Dynamic System (accelerations) described in Chapter 5. The purpose of the WIM system by BWS is to measure and record all relevant truck information in addition to the strain response in each girder. The strain gages are placed on lower flanges close to the position of the maximum moment. The Dynamic System, developed by Krenz Electronics, is set up to measure accelerations simultaneously, and at the same location, as the strain gages. Both systems are triggered by special tape switches, pasted to the pavement. The same tape switches are used to determine the truck speed, number of axles and axle spacings.

Four out of seven bridges listed in Chapter 6 are selected for tests. The span lengths vary from 9 to 24 m (30-80 ft). The same

procedure is used for all bridges, however, with a different equipment setup. The location of the accelerometers is dictated by the bridge geometry, number of girders, width of shoulder, span length, and the transverse position of truck traffic.

All selected structures are multi-simple-span bridges with steel girders and concrete slabs. The basic design parameters include span length, girder spacing, slab thickness, and skewness. The basic parameters of the selected bridges are given in Table 9-1.

Table 9-1. Parameters of the Tested Bridges.

Bridge No.	Location	Span (m) [Ft]	No. of Girders	Girder Spacing (m) [Ft]	Slab Thickness (mm) [Ft]	Bridge Width (m) [Ft]	Skew
1	US-23/ Huron River	24.5 [80.38]	6	1.90 [6.23]	190 [0.62]	11.0 [36.09]	14°
2	M-14/ N.Y.C. Rail Road	16.0 [52.50]	8	1.85 [6.07]	200 [0.66]	12.8 [42.00]	25°
3	I-94/ Jackson Road	16.0 [52.50]	9	1.70 [5.58]	190 [0.62]	14.5 [47.57]	25°
4	I-94/ Pierce Road	10.5 [34.45]	10	1.70 [5.58]	175 [0.57]	13.7 [44.95]	29°

The strain gages are attached to bottom flanges of girders. The equipment is calibrated using trucks with known axle weights and spacings. The measurements are carried out for several days at each location.

A computer program is developed for the automated data processing. Each data file contained data from 6 or 8 channels. Every two channels represent the time and acceleration records collected

from each girder. Each record represents the passage of a truck over the bridge, in either right or left lane. The data capturing starts when the truck is about 20 ft (6 m) from the first tape switch in either lane. The data capture mode is on until the time elapsed is equal to the preset time interval. The preset time interval depends on the span length, average truck speed and the distance of the first tape switch from the beginning of the bridge.

The tape switch signal is used to trigger the system, and start collecting data from the accelerometers and strain transducers. However, this synchronization works for bridges with traffic intensity not higher than normal. On bridges with trucks of certain characteristics (e.g. heavy, 11 axles), the manual trigger permits a better control of the data acquisition system.

The deflections are calculated by integrating the acceleration records using the Fast Fourier Transform (FFT) technique (Paz 1985; Press et al. 1988). The FFT procedure is utilized assuming that the measured acceleration-time (or strain-time data) can be represented as the sum of all contributions from all mode shapes. FFT is also used to determine the dominant frequencies as well as the cutoff frequency in the frequency domain. The cutoff frequency is best estimated, for each individual bridge, by minimizing the error in estimating the energy under the power spectrum plot in frequency domain. The equivalent static response is determined by eliminating the contribution of all modes above the cutoff frequency. The dynamic and equivalent static response are then plotted and compared to determine the DLF. The same procedure was applied for both deflection and strain measurements.

The measurements provided data on truck weights, axle loads, axle configurations and vehicle speeds. The histograms of GVW are shown in Fig. 9-6 through 9-9 for bridges 1 through 4, respectively.

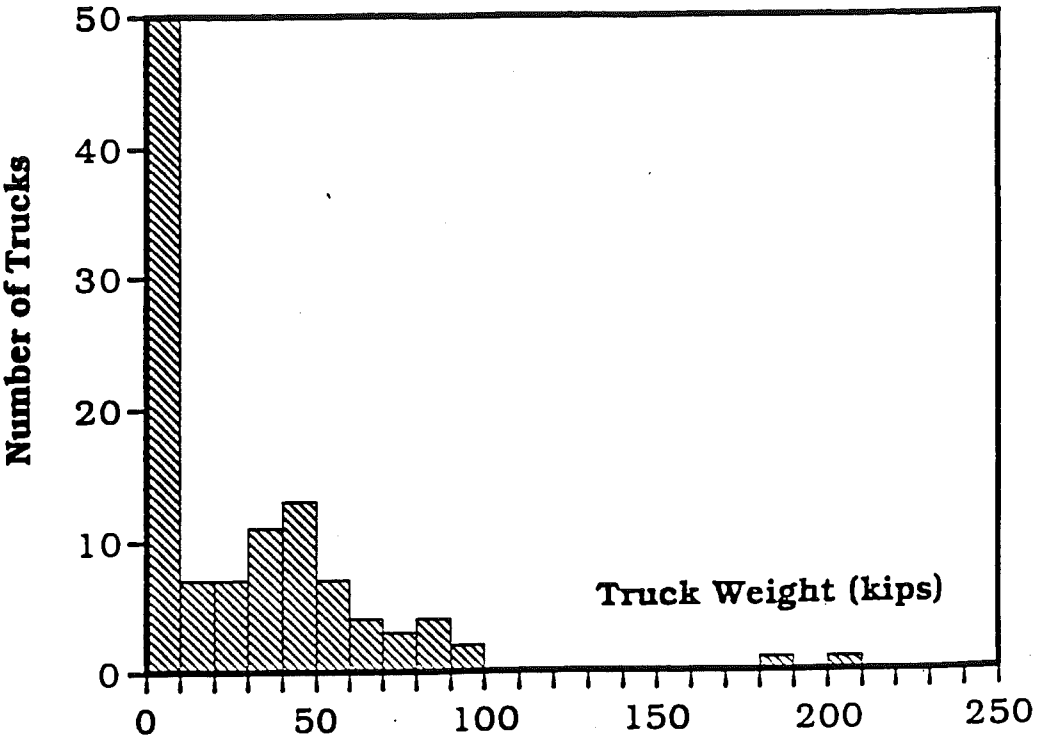

Fig. 9-6. Histogram of GVW for Bridge 1, 23/HR.

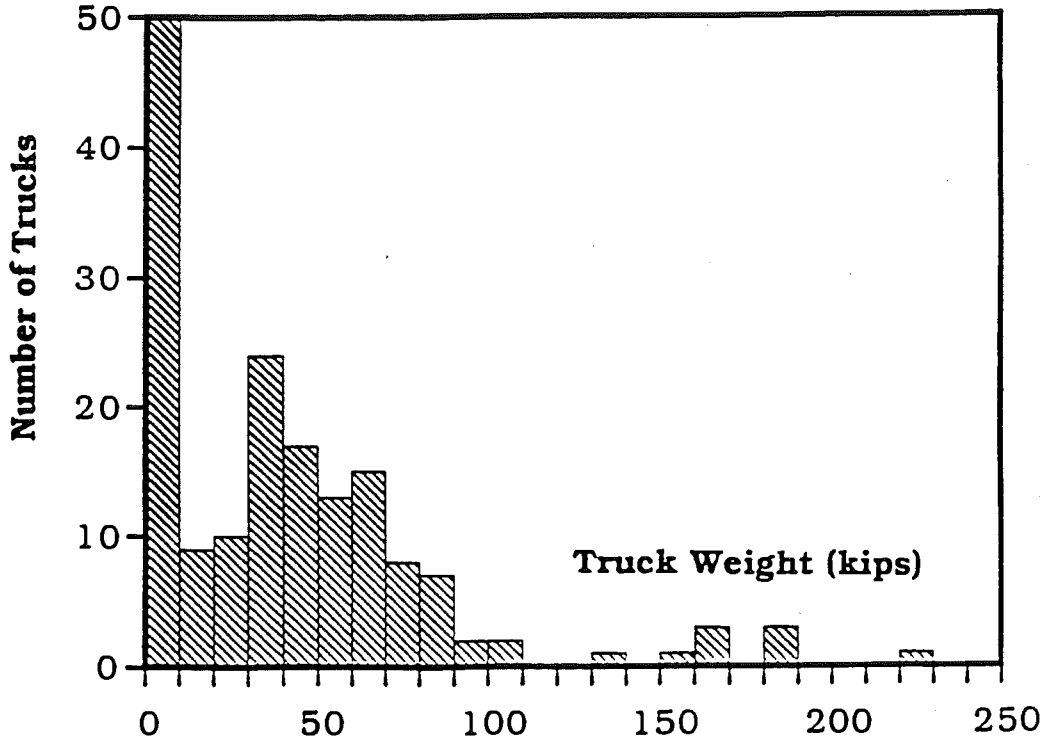

Fig. 9-7. Histogram of GVW for Bridge 2, 14/NY.

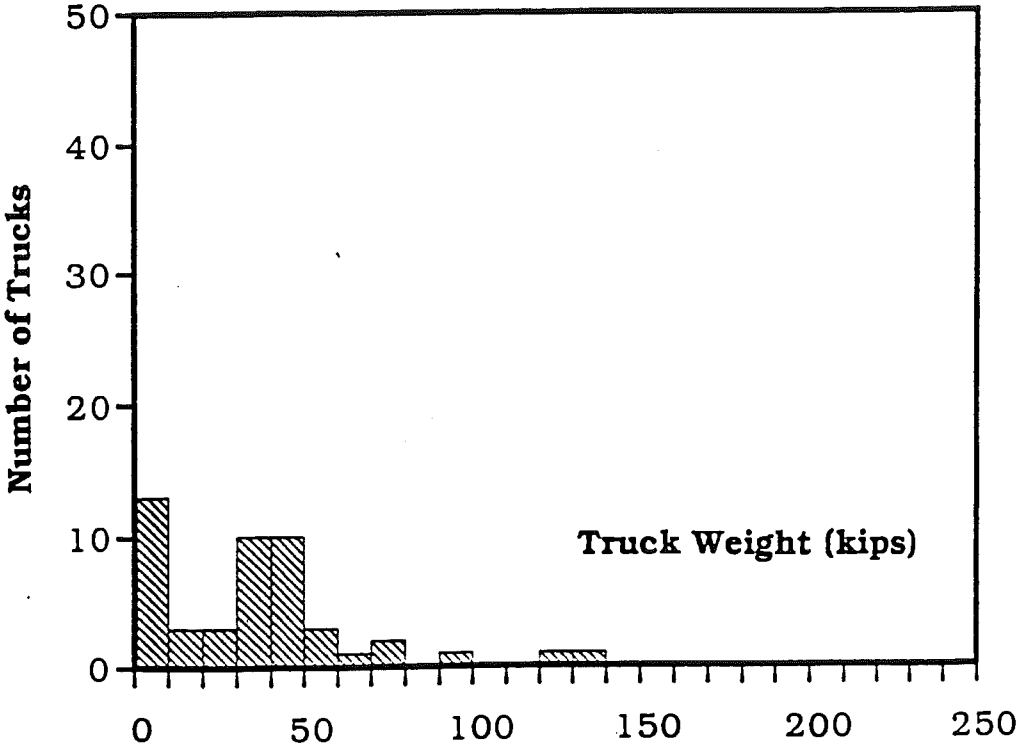

Fig. 9-8. Histogram of GVW for Bridge 3, 94/JR.

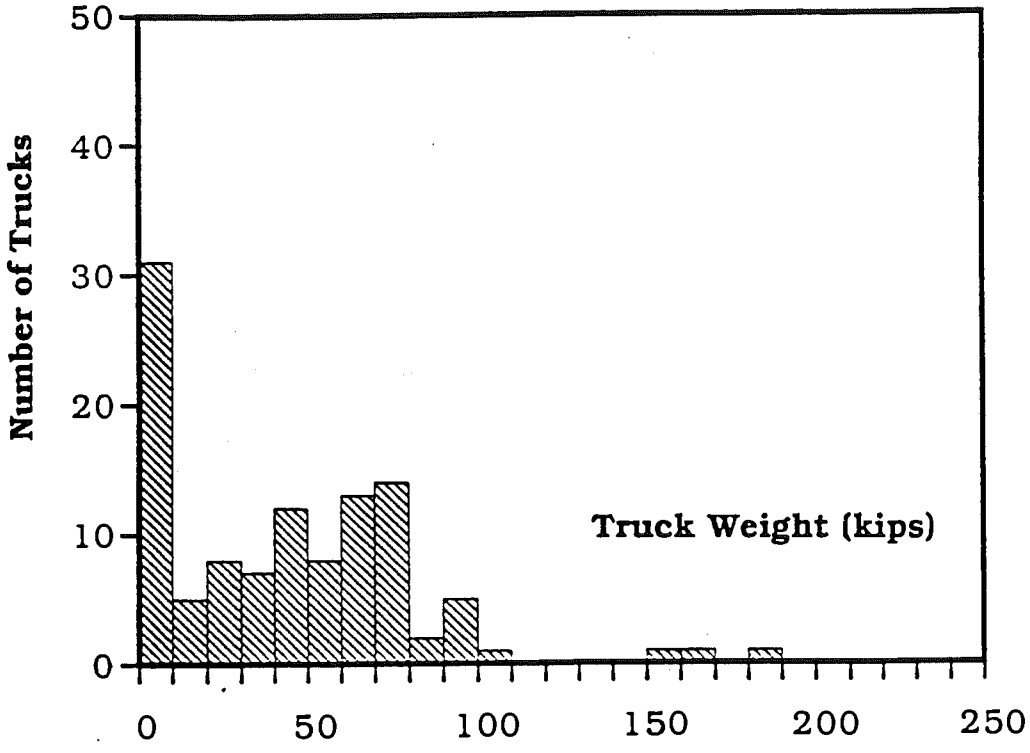

Fig. 9-9. Histogram of GVW for Bridge 4, 94/PR.

Most of the trucks traveled at about 60 mph (90 km/h). The truck traffic was a mixture of mostly 5 axle vehicles with few very heavy 11 axle trucks.

9.5 Measured Dynamic Load

The measurements are carried out on four bridges listed in Table 9-1. Static and dynamic stress is determined for each girder. The resulting dynamic load factors (DLF) are plotted vs. GVW of the corresponding vehicles in Fig. 9-10 through 9-13. The results are shown for the third girder (most loaded girder in the considered bridges).

In general, DLF decreases with GVW. However, the DLF is the ratio of dynamic and static deflection or stress, and static response varies from girder to girder, depending on positions of the girder and truck.

The statistical cumulative distribution function (CDF) of the static response (deflection or stress) are developed from the measurements. It is convenient to plot the CDF's on the normal probability paper (Appendix A). In this study the normal probability scale is replaced with the inverse normal scale, Φ^{-1} (p), where Φ^{-1} is the inverse normal probability function and p is probability. For any x_i, equal to the measured value of stress or deflection, the corresponding inverse normal value (on the vertical scale) is equal to $\Phi^{-1}(p_i)$, where p_i is the probability of x_i being exceeded.

The static stress values are determined for each girder. The CDF's for static stress are plotted on the normal probability paper. For each bridge, the results are presented for the first (exterior) and third (most loaded) girders. For each value of static stress, the corresponding dynamic stress is also plotted. The results are shown in Fig. 9-14 through 9-21, for bridges 1 to 4, respectively. For each bridge, the results are shown for girders 1 and 3.

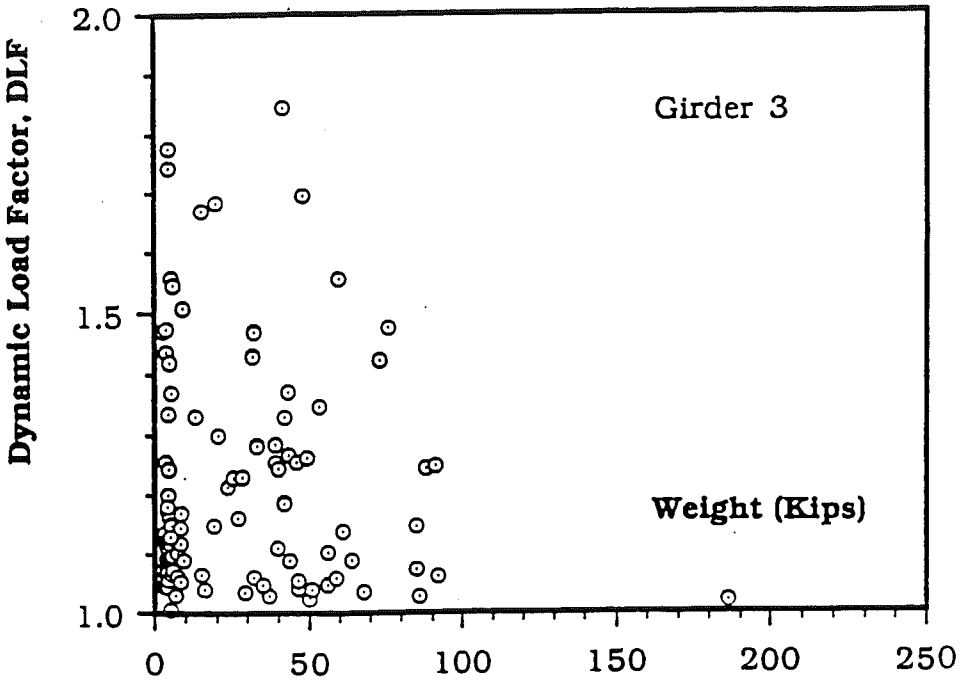

Fig. 9-10. DLF vs. Truck GVW for Bridge 1, 23/HR.

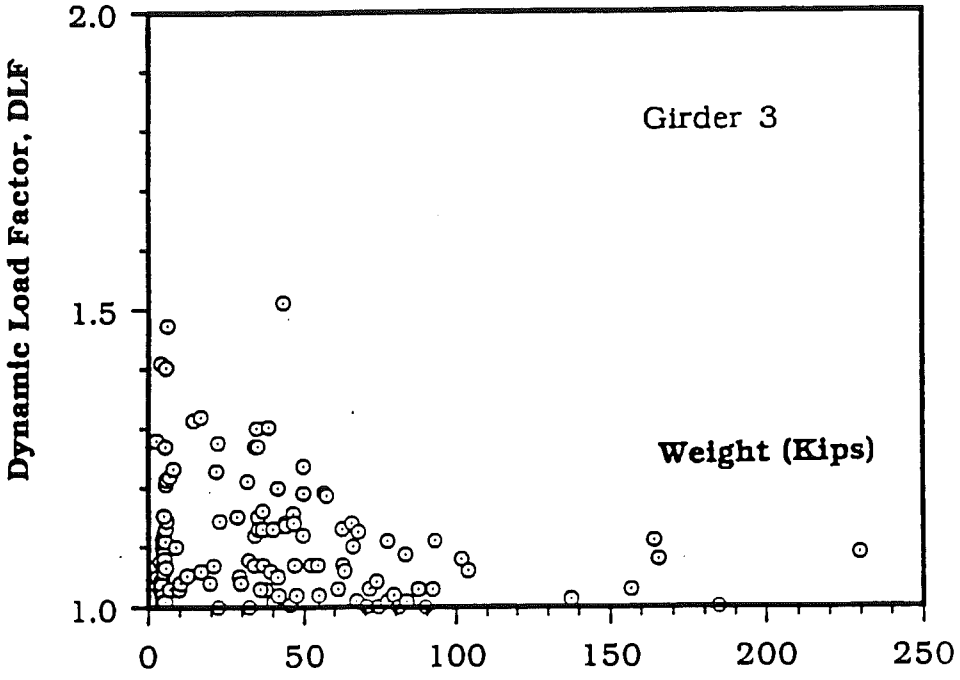

Fig. 9-11. DLF vs. Truck GVW for Bridge 2, 14/NY.

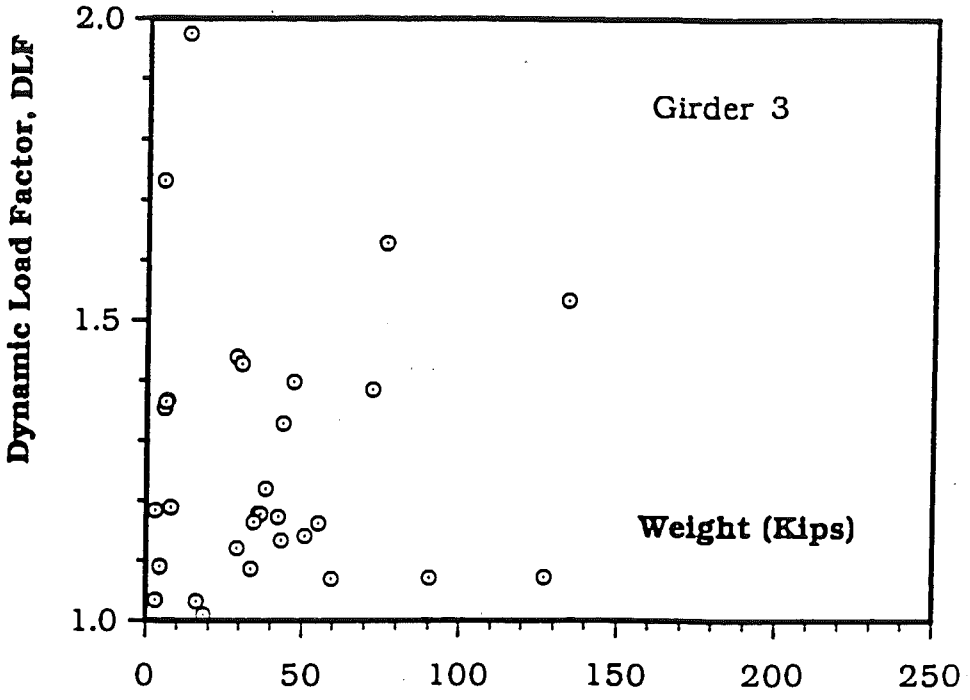

Fig. 9-12. DLF vs. Truck GVW for Bridge 3, 94/JR.

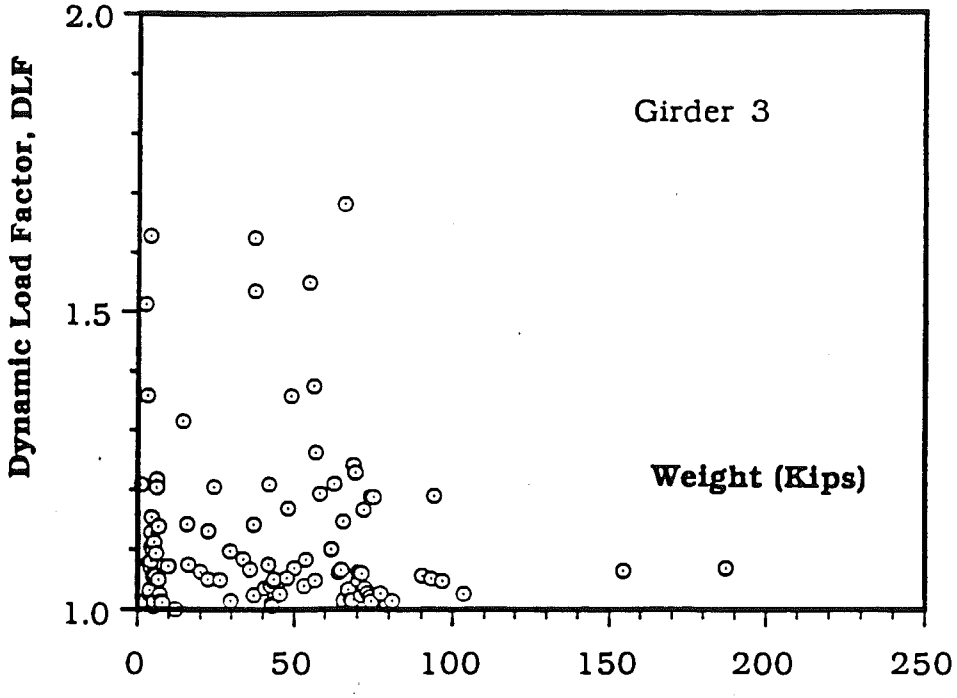

Fig. 9- 13. DLF vs. Truck GVW for Bridge 4, 94/PR.

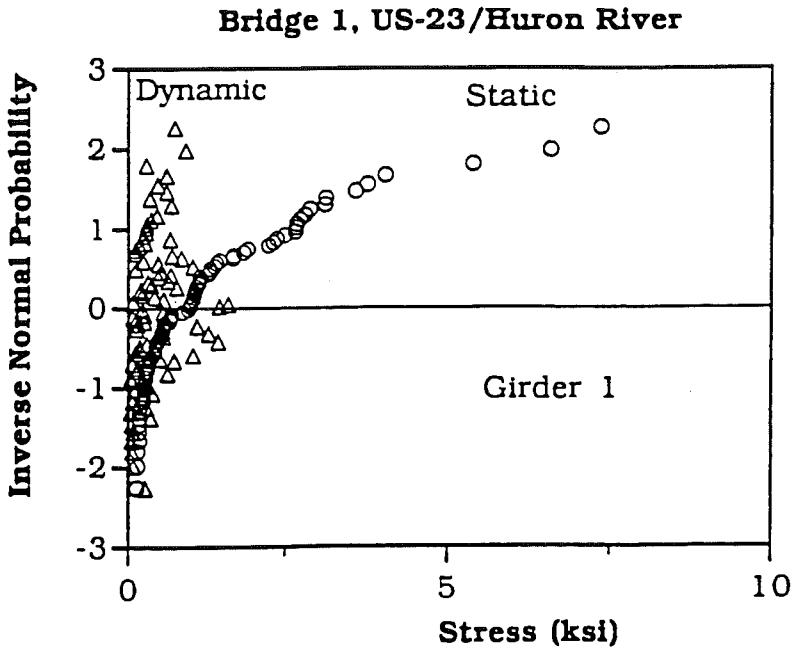

Fig. 9-14. CDF of Static Stress and Corresponding Dynamic Stress for Girder 1, Bridge 1.

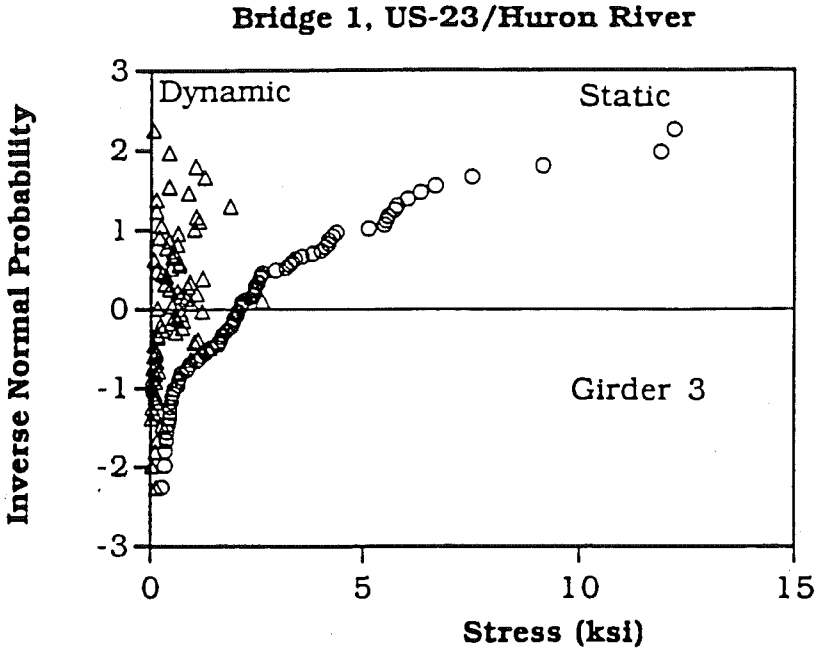

Fig. 9-15. CDF of Static Stress and Corresponding Dynamic Stress for Girder 3, Bridge 1.

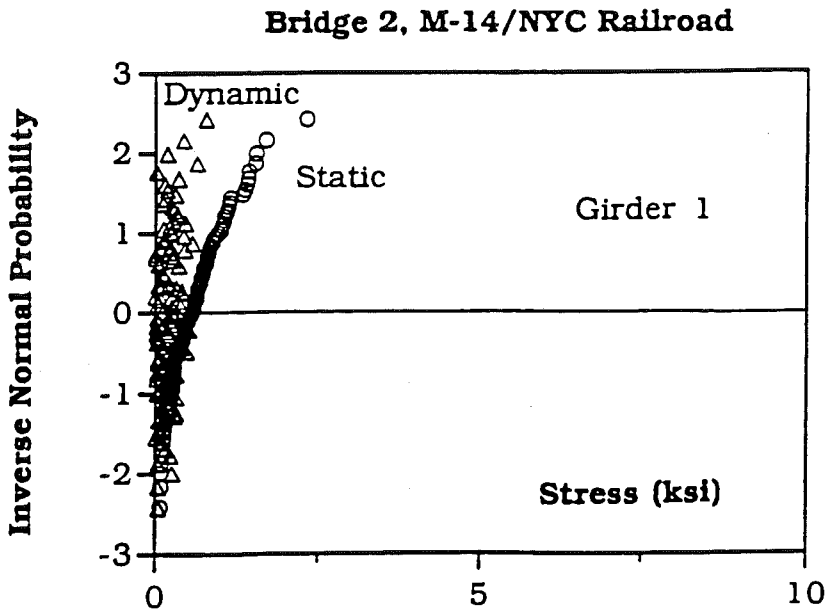

Fig. 9-16. CDF of Static Stress and Corresponding Dynamic Stress for Girder 1, Bridge 2.

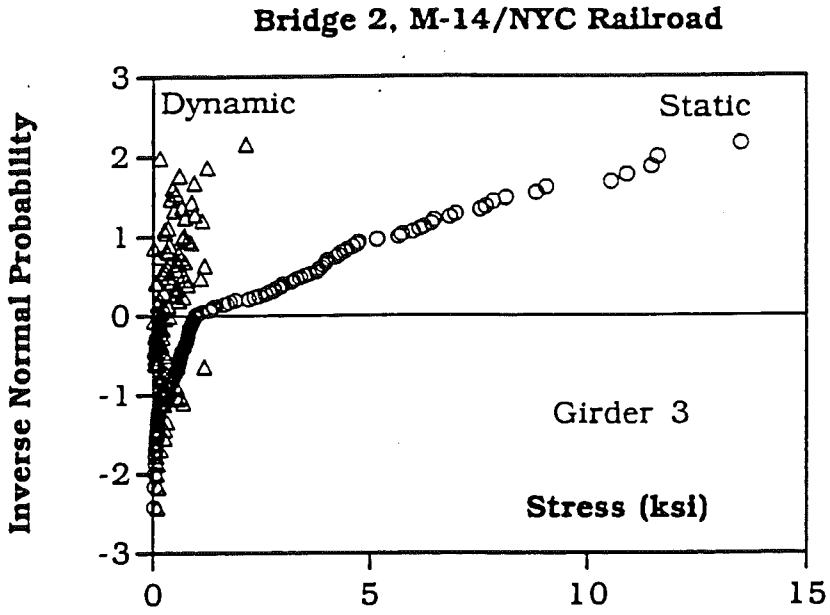

Fig. 9-17. CDF of Static Stress and Corresponding Dynamic Stress for Girder 3, Bridge 2.

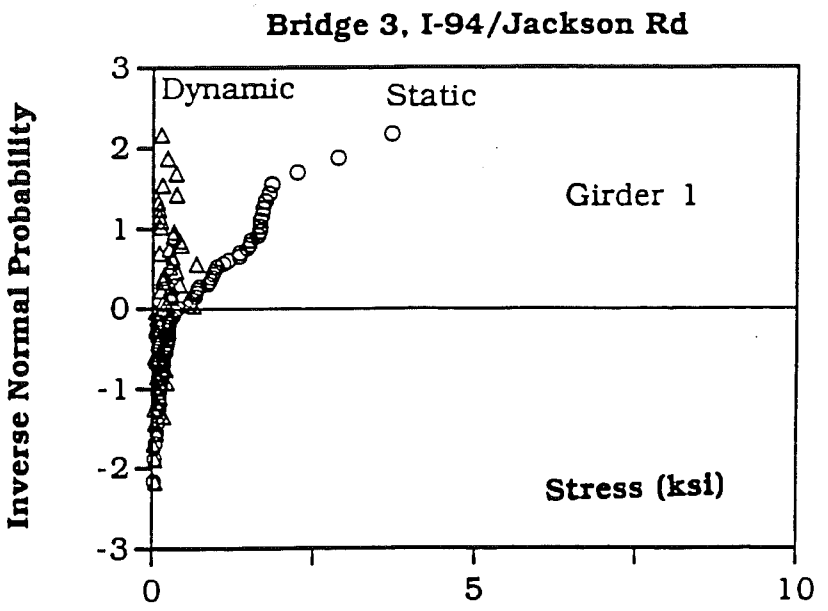

Fig. 9-18. CDF of Static Stress and Corresponding Dynamic Stress for Girder 1, Bridge 3.

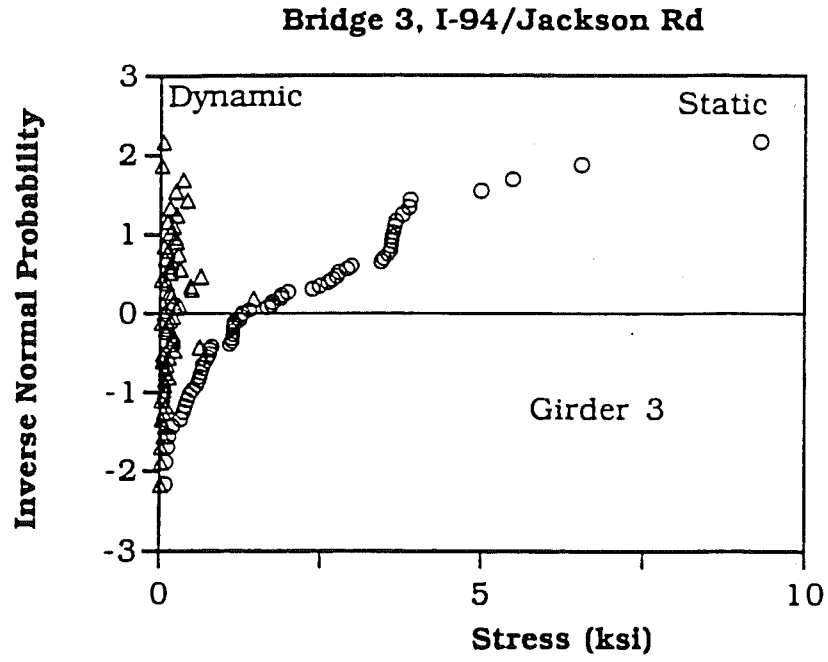

Fig. 9-19. CDF of Static Stress and Corresponding Dynamic Stress for Girder 3, Bridge 3.

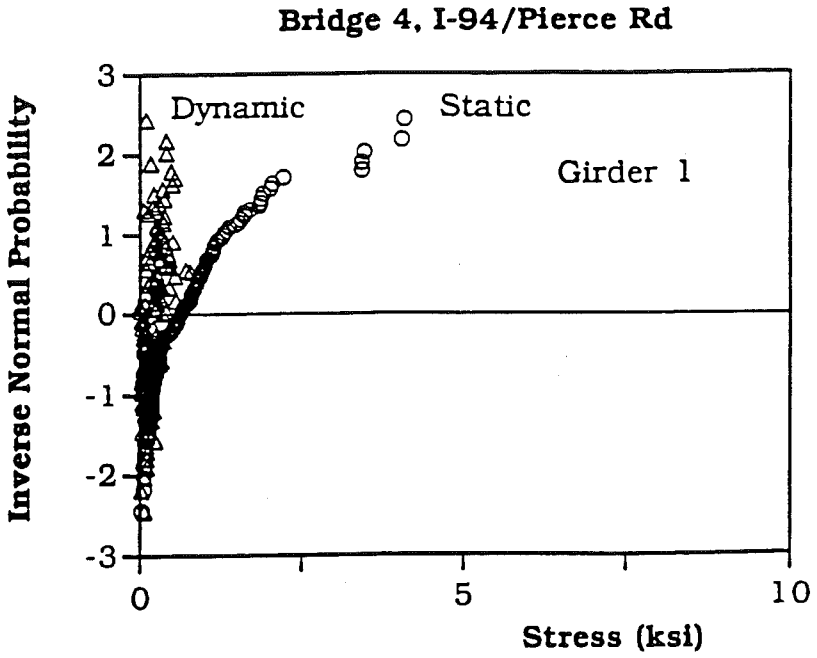

Fig. 9-20. CDF of Static Stress and Corresponding Dynamic Stress for Girder 1, Bridge 4.

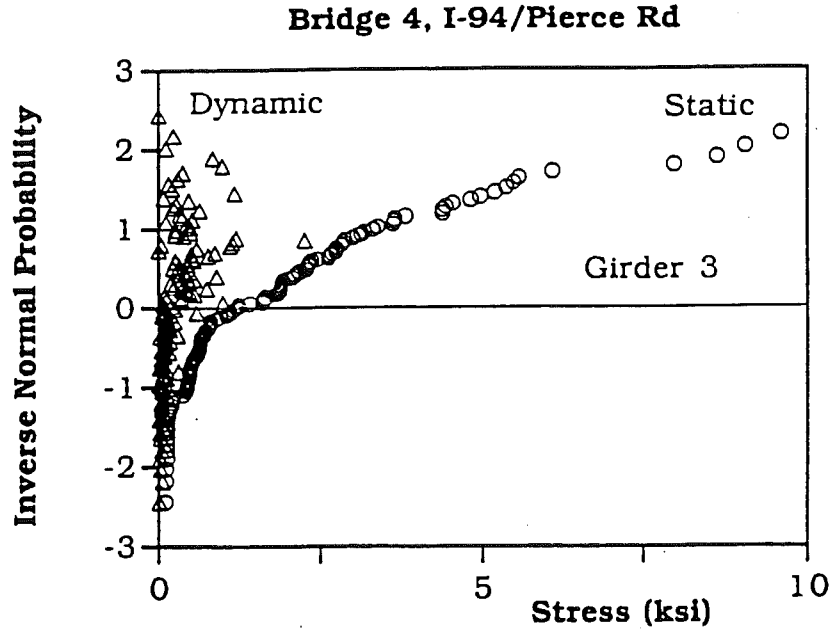

Fig. 9-21. CDF of Static Stress and Corresponding Dynamic Stress for Girder 3, Bridge 4.

Static and dynamic stress is determined for each girder. The resulting dynamic load factors (DLF) are plotted vs. the static stress in each girder in Fig. 9-22 through 9-25. The results are shown for a maximum of eight girders limited by the number of available data acquisition channels.

In general, DLF decreases as the static stress in each girder increases. However, the DLF is the ratio of dynamic and static stress, and static response varies from girder to girder, depending on the positions of the girder and truck. The variation in DLF with respect to static stress in each girder is shown in Fig. 9-22 through 9-25. It is shown that the exterior girders exhibit very small static stress (almost negligible), while the interior girders have much larger static stresses.

In general, the static stress is proportional to truck weight. However, the dynamic stress is practically independent of truck weight. Therefore, the dynamic load factor, DLF, decreases with static stress or truck weight. The variation of DLF with truck parameters is shown in Fig. 9-26 through 9-27. Results for each bridge are shown corresponding to the most loaded interior girder. It is observed that the DLF decreases as the GVW increases. It is also observed that among all types of vehicles (excluding light weight 2 axle vehicles), 5 axle trucks cause the largest DLF values as shown in Fig. 9-26. Additionally, the DLF decreases with an increase in truck speed as shown in Fig. 9-27.

In general, the static stress is proportional to truck weight. However, the dynamic stress is practically independent of truck weight. Therefore, the dynamic load factor, DLF, decreases with truck weight.

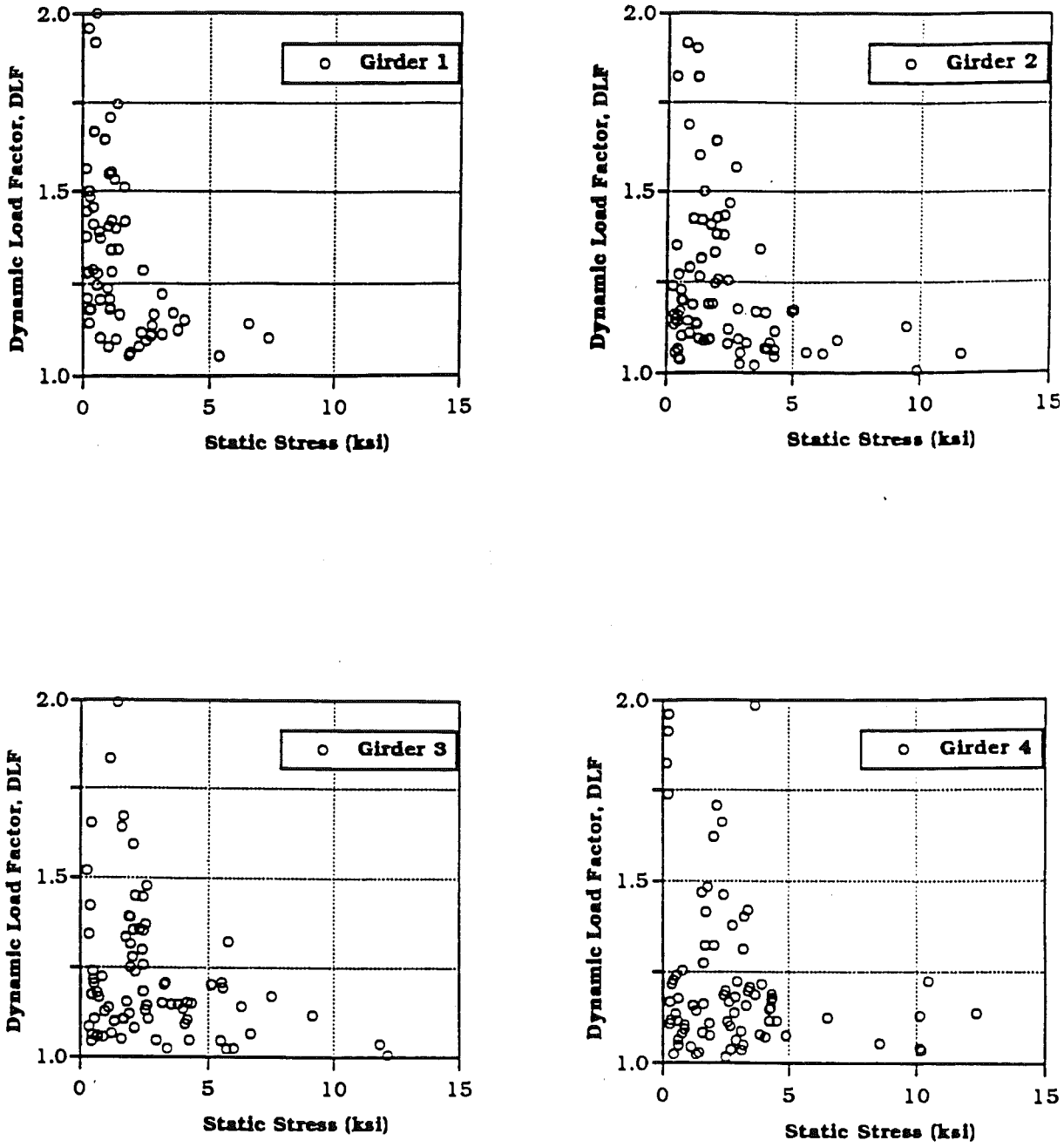

Fig. 9-22. Dynamic Load Factor (DLF) vs. Static Stress for Girders 1-6, Bridge 1.

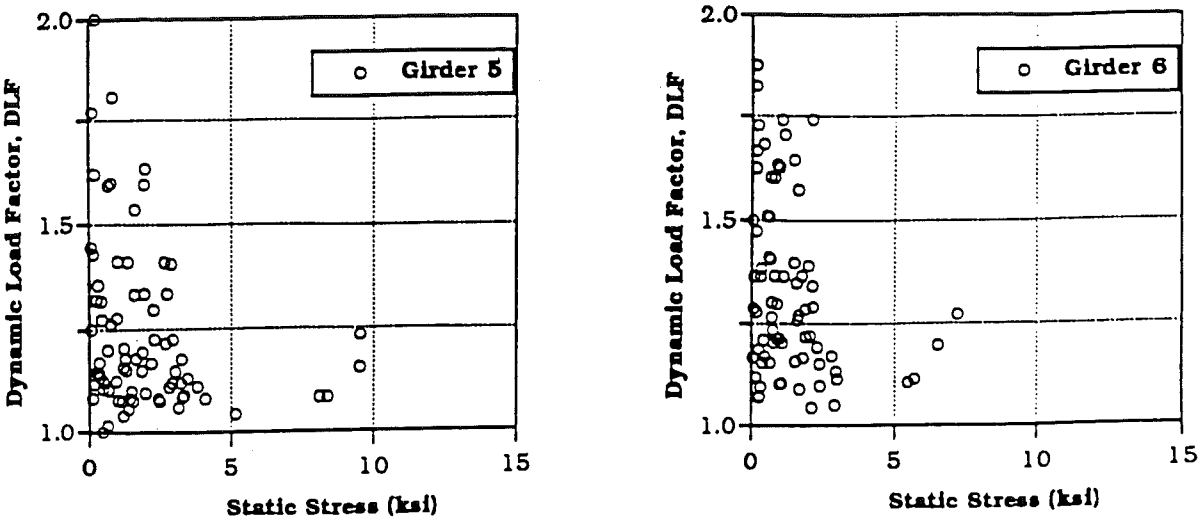

Fig. 9-22 (continued). Dynamic Load Factor (DLF) vs. Static Stress for Girders 1-6, Bridge 1.

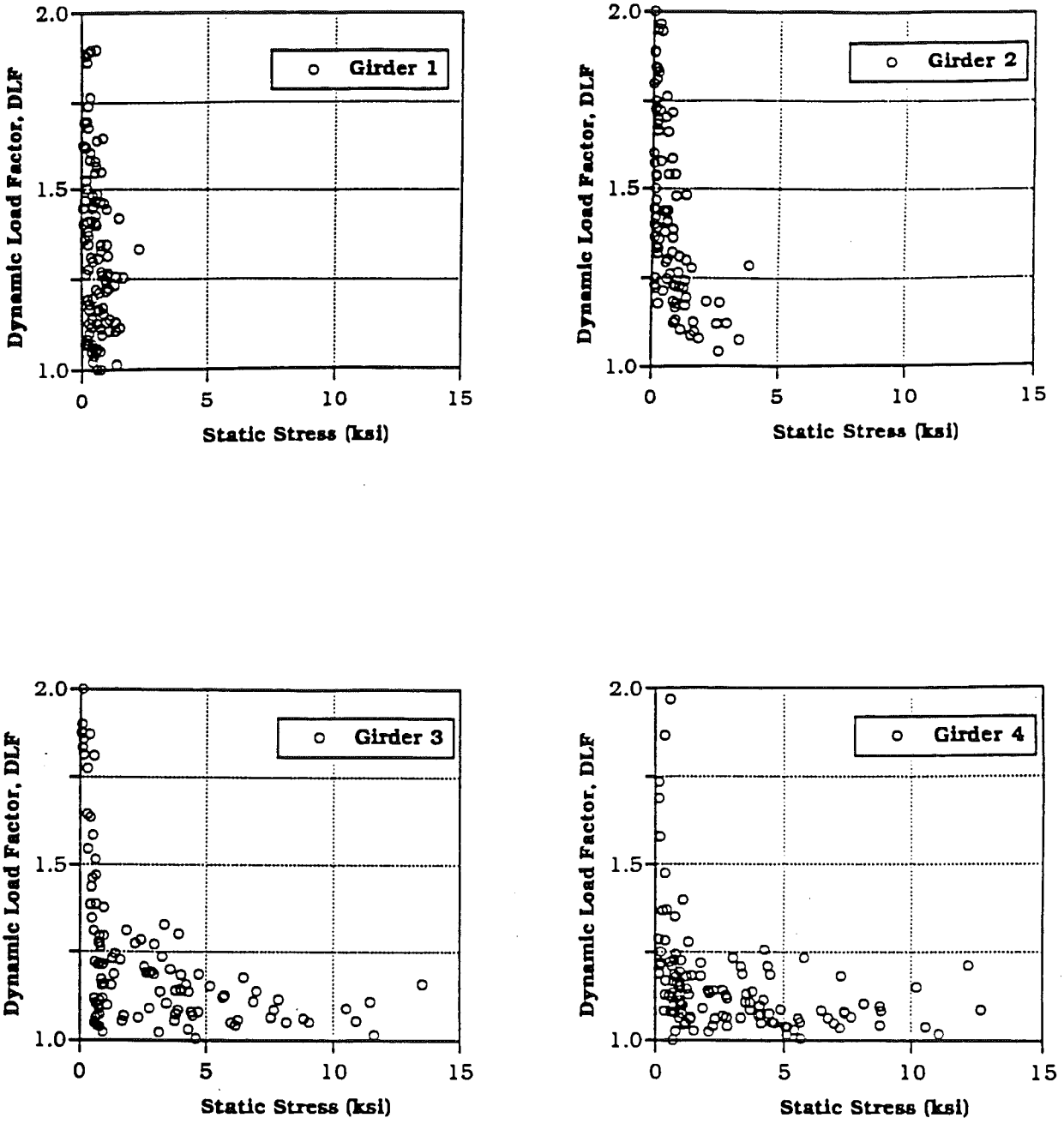

Fig. 9-23. Dynamic Load Factor (DLF) vs. Static Stress for Girders 1-8, Bridge 2.

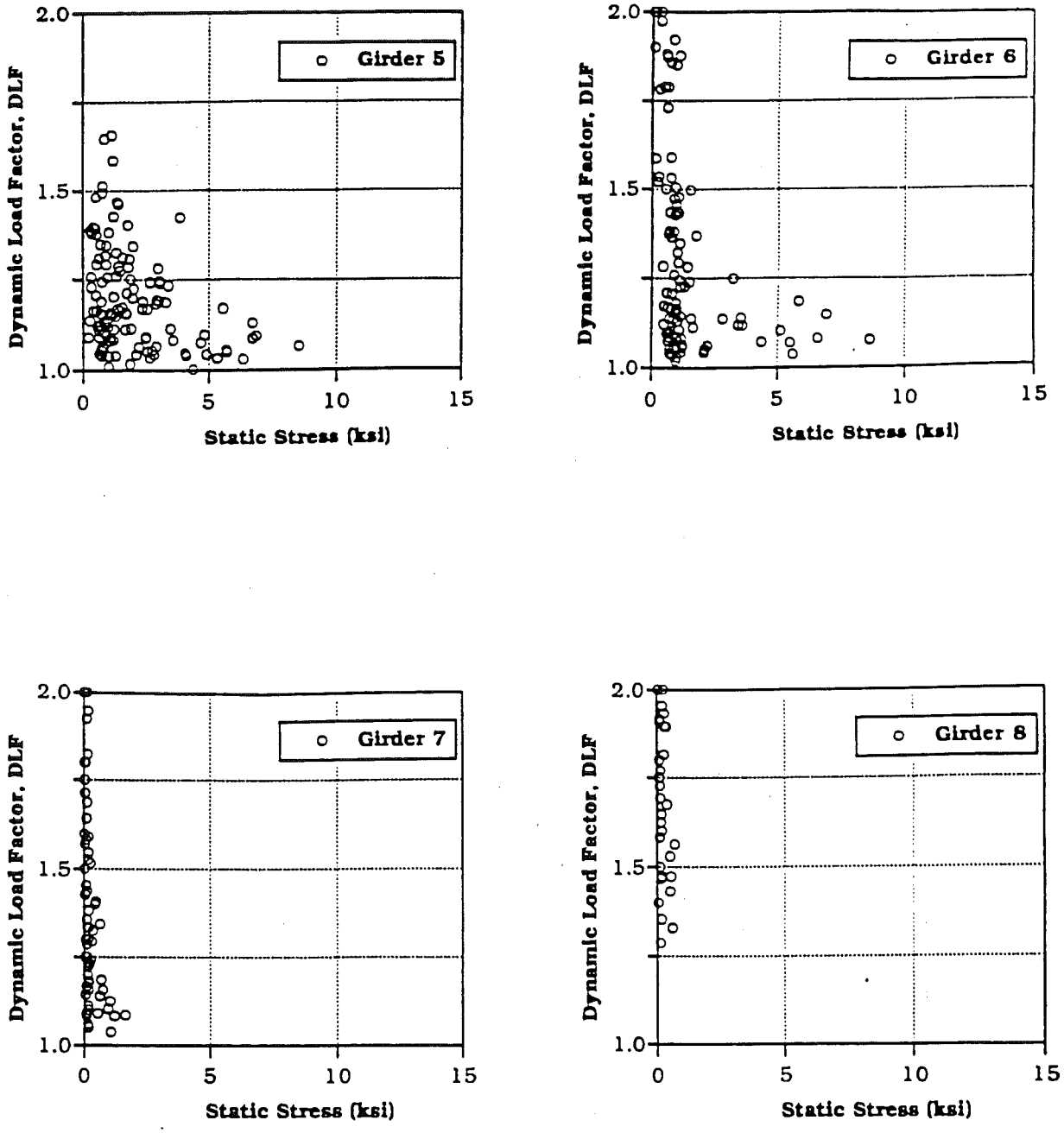

Fig. 9-23 (continued). Dynamic Load Factor (DLF) vs. Static Stress for Girders 1-8, Bridge 2.

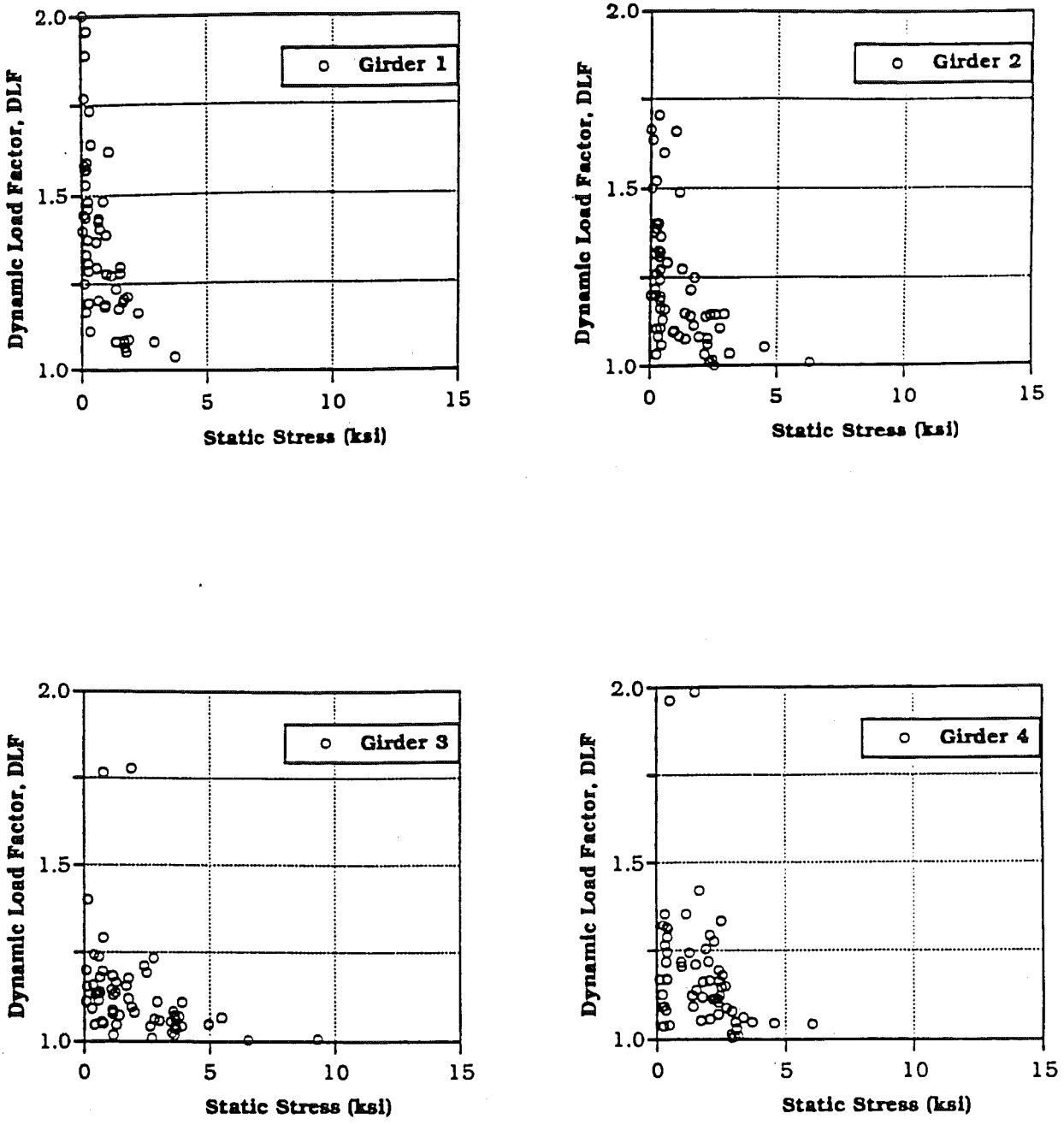

Fig. 9-24. Dynamic Load Factor (DLF) vs. Static Stress for Girders 2-9, Bridge 3.

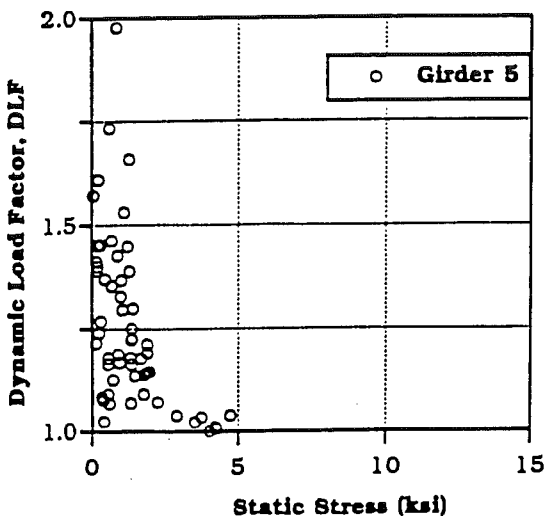

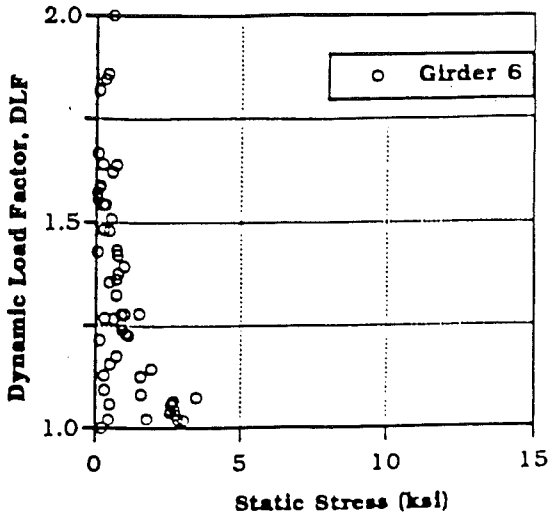

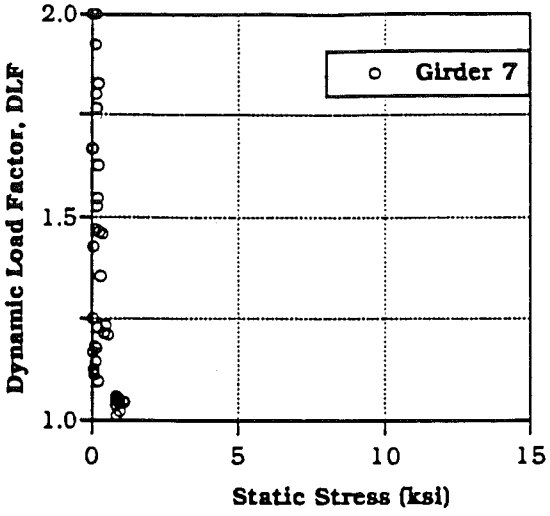

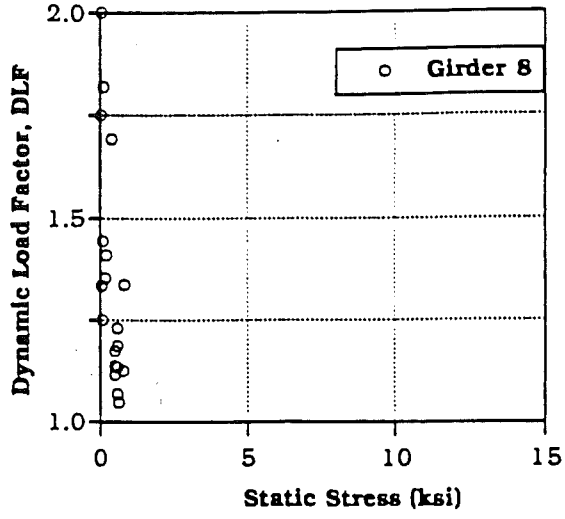

Fig. 9-24 (continued). Dynamic Load Factor (DLF) vs. Static Stress for Girders 2-9, Bridge 3.

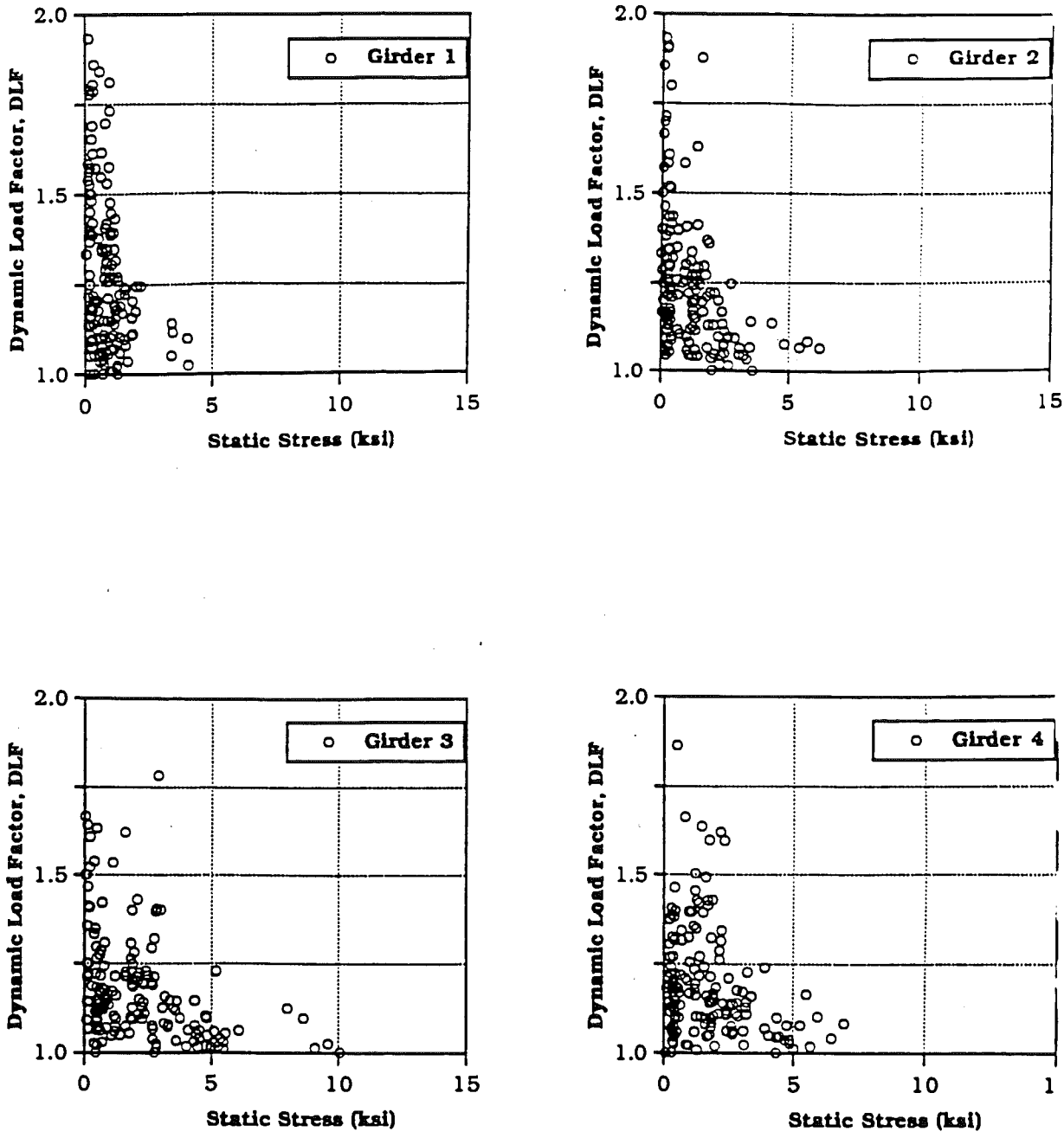

Fig. 9-25. Dynamic Load Factor (DLF) vs. Static Stress for Girders 2-10, Bridge 4.

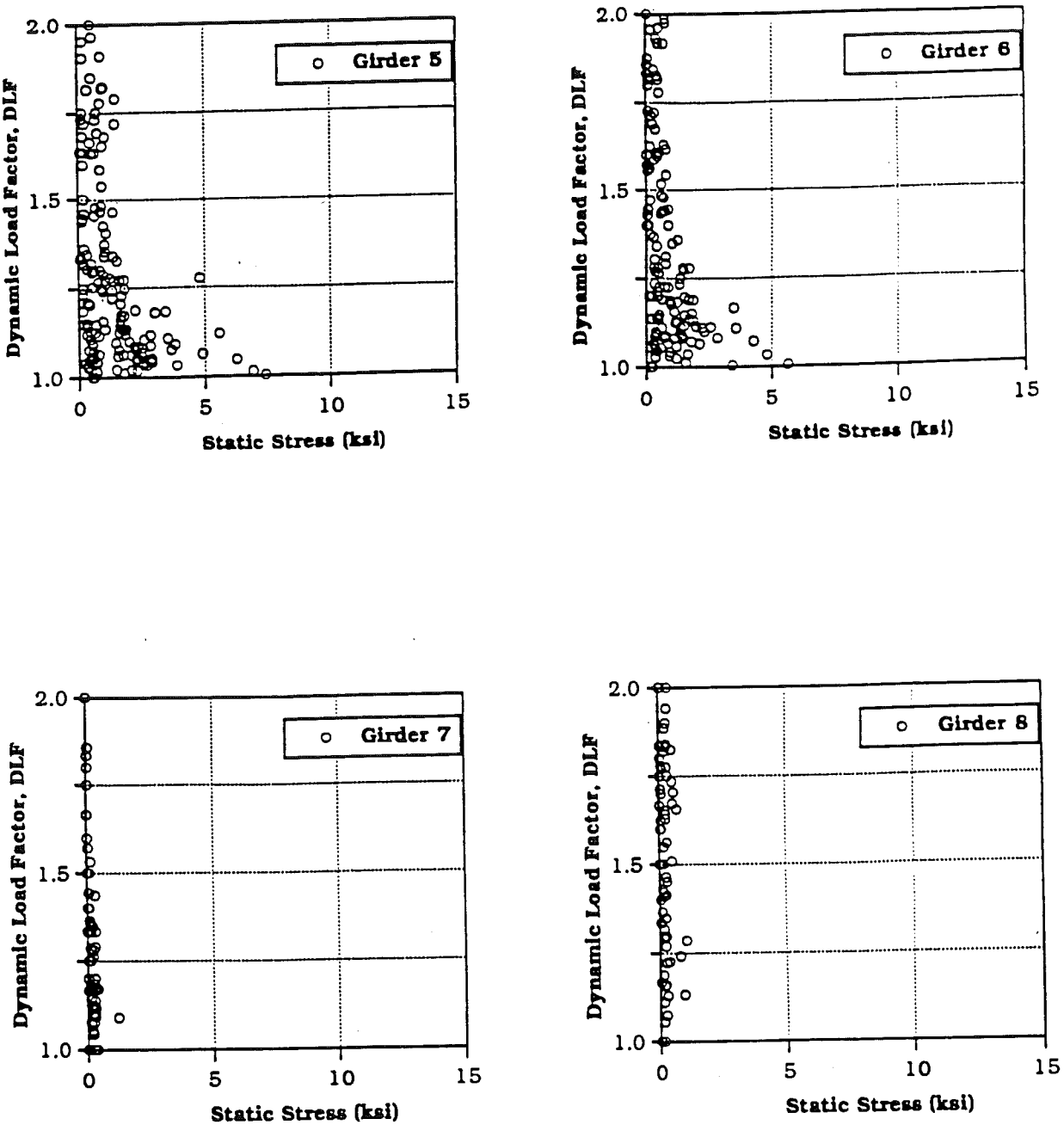

Fig. 9-25 (continued) . Dynamic Load Factor (DLF) vs. Static Stress for Girders 2-10, Bridge 4.

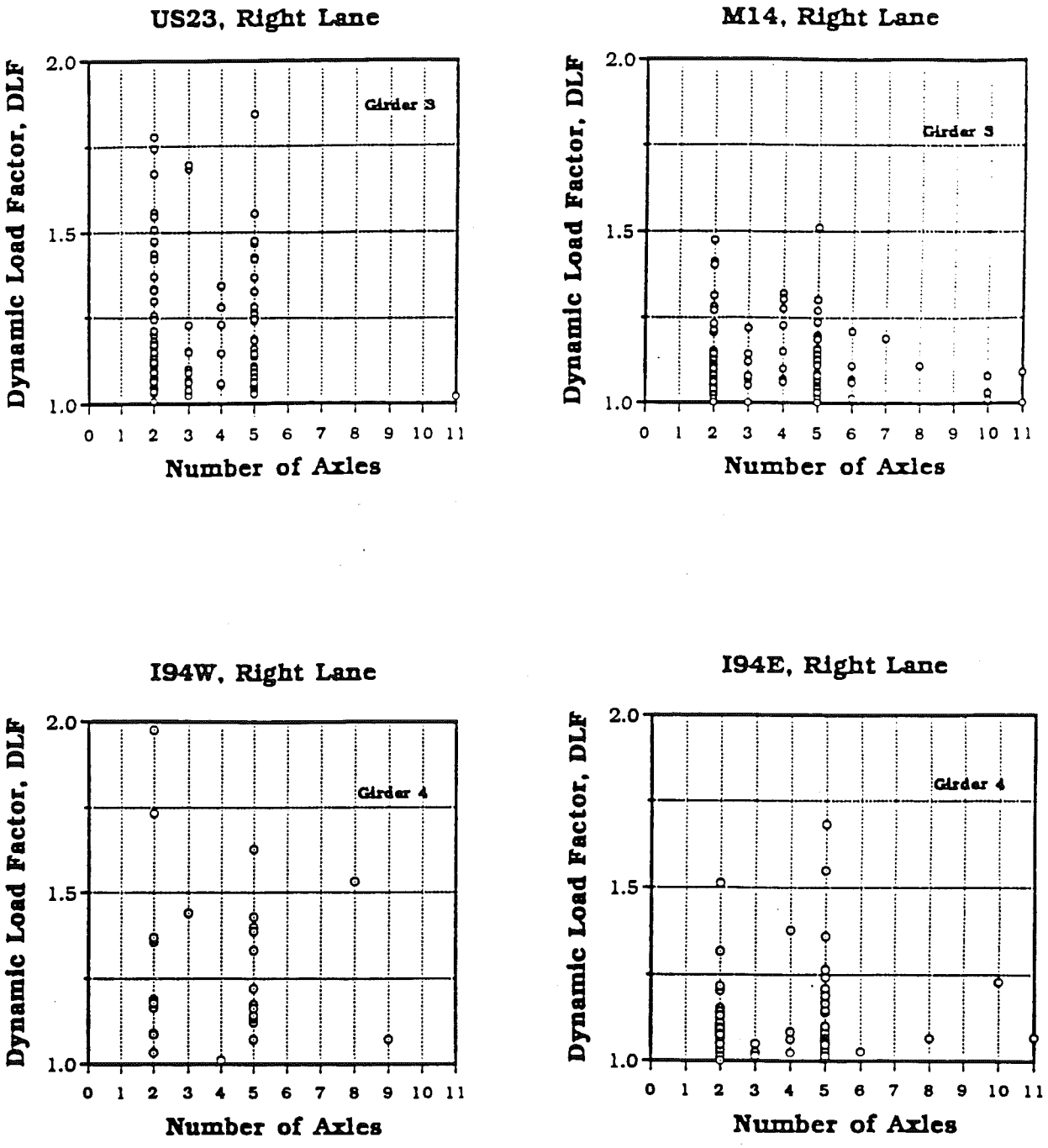

Fig. 9-26. Dynamic Load Factor (DLF) vs. Truck Type (Number of Axles).

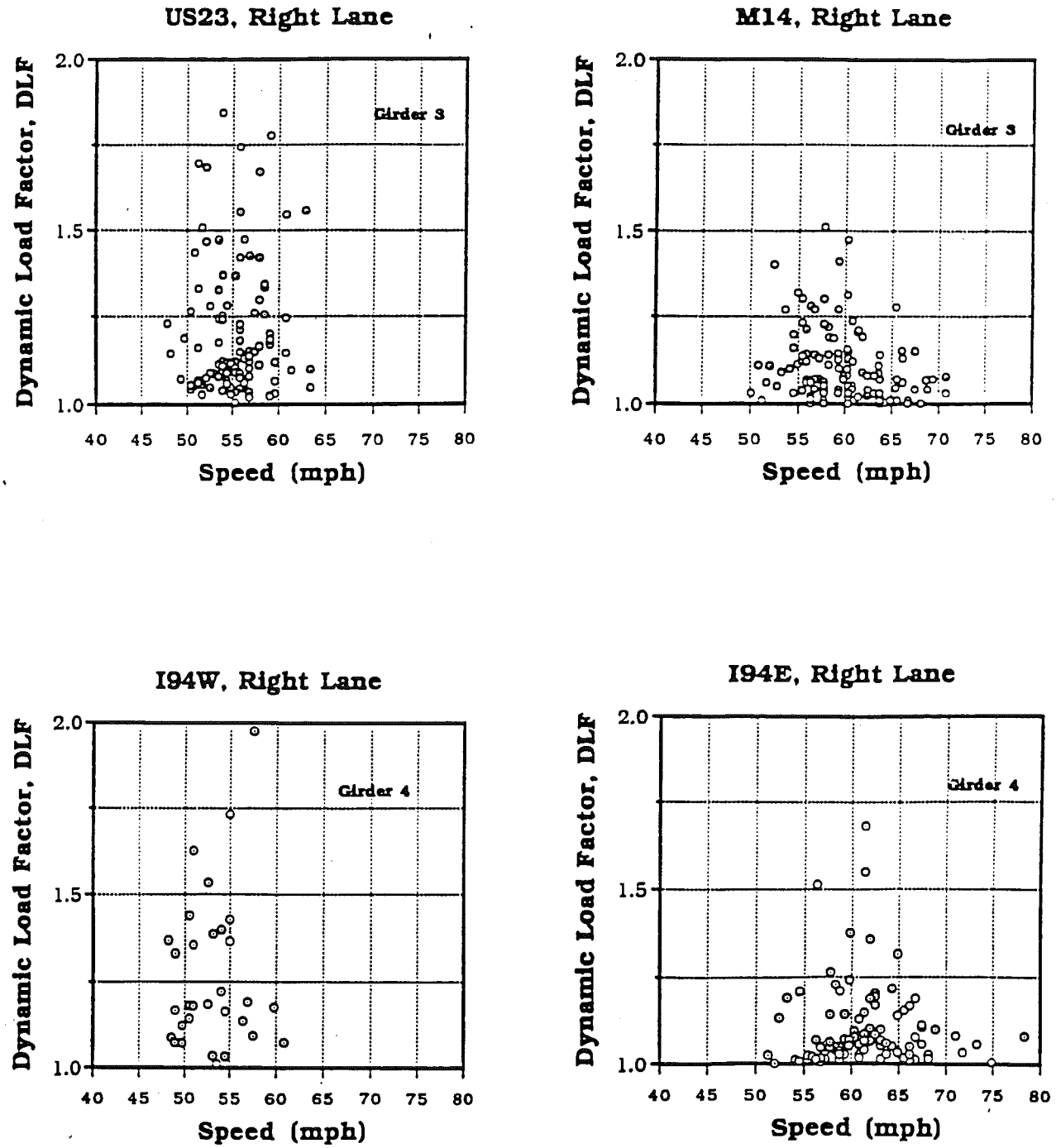

Fig. 9-27. Dynamic Load Factor (DLF) vs. Truck Speed.

9.6 Summary and Conclusions

The dynamic load is defined as the ratio of dynamic and static responses. Field measurements are performed to determine the actual truck load effects and to verify the available analytical models. The objective of this study is to present the results of these studies.

The tests are carried out on four steel girder bridges. Measurements are taken using accelerometers and a weigh-in-motion (WIM) system with strain transducers. For each truck passage, the dynamic response is monitored by recording accelerations and strain data. The truck weight, speed, axle configuration, and lane occupancy are also determined and recorded. A numerical procedure is developed to filter and process collected data. The dynamic load factor (DLF) is determined under normal truck traffic of various load ranges and axle configurations.

The dynamic loads under a normal highway traffic are measured for selected steel girder bridges. For each truck, the measured parameters include: axle loads, axle spacings, speed, strain record and acceleration record. A numerical procedure is developed for data processing, filtering and smoothing. The dynamic load factor (DLF) is calculated using strain records.

The field measurements confirm the results of the analytical study. It is observed that the dynamic component of stress is practically independent on GVW. Therefore, DLF decreases with increased GVW. For very heavy trucks, DLF does not exceed the theoretical results obtained by Hwang and Nowak (1991).

Larger values of DLF are observed in exterior girders, however, this is due to relatively smaller static load effect. Values of DLF should be based on those obtained from interior girders.

10. EVALUATION OF BRIDGES WITH REGARD TO CORROSION

Bridge evaluation requires the knowledge of load and resistance. Therefore, there is a need for information about two groups of parameters:

- Loads; actual loads, extreme expected loads, fatigue load spectra, load distribution, component loads, load combinations.
- Resistance; actual load carrying capacity, degree of deterioration, rate of deterioration, remaining life.

The measurement of truck loads and component-specific stress spectra provides a important data base for evalution. It also serves as a means for verification of the theoretical design models. However, the load carrying capacity has an equal and sometimes even more important effect on bridge performance. Therefore, it should be evaluated as accurately as possible.

Resistance (load carrying capacity) varies from structure to structure due to quality of material and workmanship, level of maintenance, and traffic parameters (volume and magnitude of truck loads). Furthermore, the resistance is a time-dependent variable due to deterioration. The accumulated damage can be estimated by inspection and measurements. However, the prediction of future performance usually involves more uncertainty. The important forms of deterioration which affect bridge resistance are corrosion and fatigue.

Corrosion is one of the most important causes of deterioration in steel bridges. Rational criteria are needed to determine the actual strength and remaining life of existing corroded structures. This Chapter, deals with the deterioration models for corroded steel girder bridges.

The primary cause of corrosion is the accumulation of water and salt (marine environment or deicing media) on bridge steel. The

source of water and salt is either from deck leakage or from the accumulation of road spray and condensation. The source of the moisture often determines the pattern of corrosion on a bridge. The rate of corrosion will depend upon the contaminants in the moisture and the ambient temperature. By combining information on the location and rate of corrosion with the structural analysis of corroded members, a model of deteriorating capacity is developed (Kayser and Nowak 1989).

10.1 Forms of Corrosion

There are six main forms of corrosion damage which can affect a steel girder bridge:

- uniform corrosion,
- pitting corrosion,
- galvanic corrosion,
- crevice corrosion,
- stress corrosion cracking,
- corrosion fatigue.

The most prevalent form is the uniform corrosion which is a general loss of surface material. This condition will lead to the gradual thinning of members. Uniform corrosion accounts for the largest percentage of corrosion damage.

Pitting corrosion also involves loss of material at the surface. However, it is restricted to a very small area. Pits can be dangerous because they extend into the metal, showing little evidence of their existance. Pit occurrence is serious in high stress regions because it can cause local stress concentrations.

Galvanic corrosion occurs when two dissimilar metals are electrochemically coupled. Such situations may occur at bolted or welded connections. Galvanic corrosion can be local, leading to pit formation.

Crevice corrosion occurs in small confined areas, such as beneath peeling paint or between faying surfaces. It is usally caused by a low concentration of dissolved oxygen in the moisture held within a crevice. Deep pits can provide locations for crevice corrosion to occur.

Stress corrosion cracking occurs when metal is subjected to tensile stress in a corrosive environment. For mild carbon steel in ordinary bridge environment, stress corrosion cracking is usually not a problem. In general, the lower the fracture resistance of a metal, the higher its susceptibility to stress corrosion cracking.

Fatigue corrosion has been identified as a corrosion phenomenon. It is actually a combination of pitting, crevice, and stress corrosion cracking. The effect of fatigue corrosion is a reduction in the fatigue life of the metal. This can result when pits cause stress concentration or when crevice or stress corrosion causes the advancement of cracks.

The rate of corrosion in different environments has been evaluated in several ongoing studies. It has been observed that corrosion loss follows an exponential function [Komp 1987];

$$C = A\, t^{B} \qquad (10\text{-}1)$$

where C represents the average corrosion penetration, in microns, t is the number of years, and A and B are the parameters determined from the regression analysis of experimental data. Test results for the parameters A and B for carbon and weathering steel were summarized by Albrecht and Naeemi [1984]. Average values for parameters A and B are listed in Table 10-1.

Table 10-1. Average Values for Corrosion Parameters A and B for Carbon Steel and Weathering Steel.

	Carbon Steel		Weathering Steel	
Environment	A	B	A	B
Rural	34.0	0.65	33.3	0.50
Urban	80.2	0.59	50.7	0.57
Marine	70.6	0.79	40.2	0.56

There are two basic changes which can occur in a steel bridge due to corrosion:

- loss of material and reduction of section parameters,
- buildup of corrosion products.

Loss of material will cause smaller net sections. This may increase the stress level for a given load or the stress range due to cyclic loading. When corrosion is localized, as in pitting, stress concentrations can occur, further increasing the stress level.

A reduction in section area will decrease the geometric properties, such as moment of intertia and/or radius of gyration. This change may occur in a nonlinear manner because the geometric properties are related to the square or cube of the dimensions. Buckling capacity of members can be critically affected by the reduction in metal thickness.

The buildup of corrosion products can also adversely affect steel bridges. Rust formation may exert pressure on adjacent elements. Brockenbrough [1983] found that the resulting stress can exceed 1,200 psi. This pressure can pry apart plates, causing stresses and eccentricities in the connected parts. The formation of "pack" rust around a bearing or hinge can lock the mechanism in place. A

nonfunctional hinge may cause unintended stresses in the structure [Bellenoit et al. 1985].

10. 2 Corrosion Patterns

Corrosion can occur wherever electrolytes (water and contaminants) can collect on the structure. On a simple span bridge, corrosion occurs usually as the result of deck joint leakage or the accumulation of road spray and dust on flat undrained surfaces. The pattern developed will be the corrosion of the webs at the ends of the girders, and the corrosion of the bottom portion of the girder, along the entire length. Fig. 10-1 illustrates the typical locations where corrosion is likely to occur assuming both joint leakage and traffic spray. The components of a bridge can be affected by more than one form of corrosion damage. In addition, the corrosion of a component can result in more than one type of deterioration. The forms of corrosion that are possible, the bridge components affected, and the types of structural damage were summarized by Kayser and Nowak [1987; 1989]. The present discussion is based on their findings.

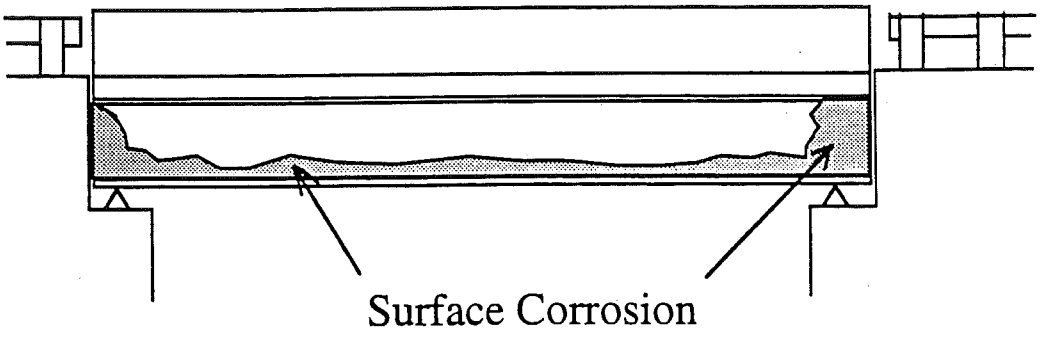

Fig. 10-1. Corrosion Pattern on a Typical Steel Bridge.

10. 3 Behavior of Corroded Bridges

To evaluate the effects of corrosion on structural performance, the various regions where corrosion will occur must be evaluated in

terms of net remaining area, structural behavior, and structural loading. In this study, the corrosion model is developed for simple span steel girder bridges.

The loss of section in a component will cause a reduction in the carrying capacity of that component. The amount of capacity reduction will depend on whether the component is in tension or compression. Tension capacity is computed as the net remaining area times the tensile strength. Compressive capacity depends upon the net area, geometry, and boundary conditions of the element.

In a steel girder, corrosion may affect the capacity in bending, shear, and bearing. Bending will be considered mainly at the midspan of a girder or above an intermediate support. At these regions, the type of corrosion most likely to occur will be section loss on the top surface of the bottom flange and on the lower portion of the web, as shown in Fig. 10-1.

10.3.1 Bending Behavior

The performance of a simply supported composite steel bridge girder in bending depends upon three basic failure modes. Failure may take place either due to excessive yielding in the steel, crushing of the concrete, or slippage in the composite connectors. The type of failure which is preferred at ultimate capacity is steel yielding. A yielding failure is ductile in nature, providing prior warning to the users. The crushing failure of concrete occurs at strain levels in the range of 0.0025-0.0040 (in ACI Code and LRFD AASHTO Code it is assumed as 0.003). For composite girders of standard design, steel reaches the yielding level before the concrete begins to crush. Also, the slippage of the composite connectors is minor and can be ignored.

For continuous girders, there is the additional possiblity of the lower flange buckling in the negative moment region. The actual capacity of the section in negative bending will depend upon the

amount of slab reinforcement above the support and the slenderness of the bottom flange.

Autostress design is a relatively new approach to designing continuous steel girders [Haaijer et al. 1983]. This method has the advantage of eliminating cover plates from the bottom flange. The method relies on the plastic rotational capacity of the girder. If corrosion were to occur on the bottom flange, either due to deck leakage or contaminant accumulation, the slenderness ratio would increase. Under such conditions, buckling could occur in the bottom flange before plastic strain levels are reached.

To evaluate the bending behavior of a composite section, an analytical model was developed. In this model, a section is treated as a collection of composite segments, Fig. 10-2. Each segment can represent a different material, and is made up of several layers. The effective width of the deck segment must be calculated, since girder spacing may be quite large. In this study the AASHTO [1983] effective width formulas are used.

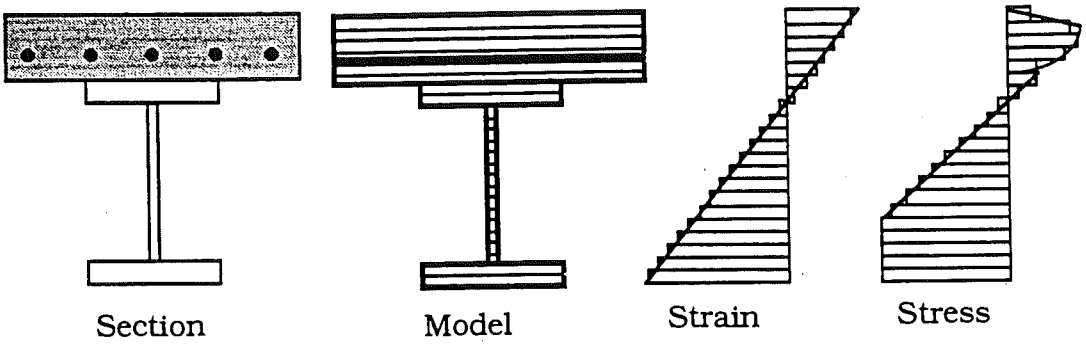

Fig. 10-2. Analytical Model of a Composite Section.

A basic assumption is made that plane sections before bending remain plane after bending. Using the linear strain distribution and the stress strain relationship for each material, the stress level can be calculated at each layer, Fig. 10-2. By iteratively finding the correct

stress distribution for each level of moment, the moment curvature relationship can be established.

The stress level for each layer depends upon the stress strain characteristics of the material, Fig. 10-3. For concrete, the stress strain distribution is modeled as a Hognestad parabola [Hognestad et al. 1955] with a linear descending portion. For steel, a tri-linear distribution is used. The elastic modulus of the strain hardening region is approximated as the initial tangent modulus at strain hardening. An example of the resulting bending moment-curvature plot is shown in Fig. 10-4.

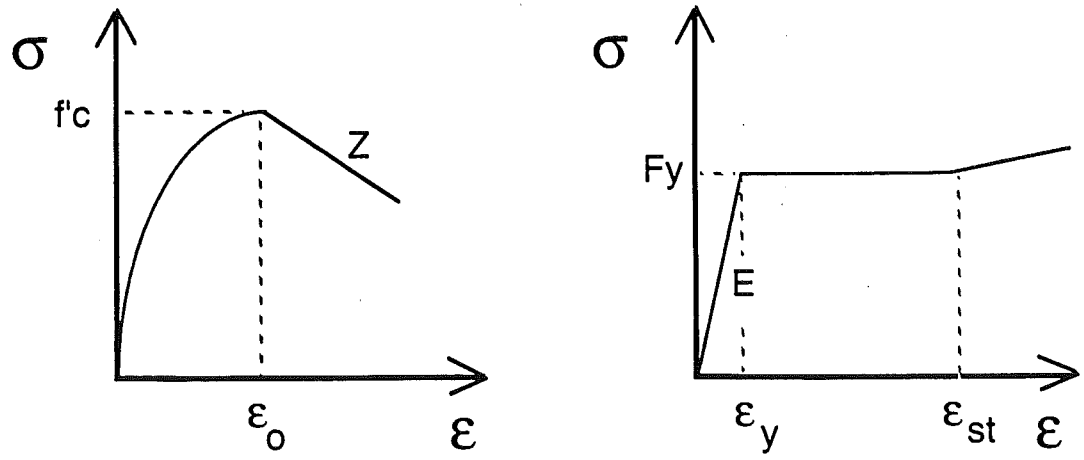

Fig. 10-3. Stress-Strain Curves for Concrete and Steel.

The effect of corrosion on the bending behavior will depend on whether the section is positive or negative moment region. For a continuous span, a reduced lower flange thickness may cause local buckling above an interior support. For the positive moment regions, corrosion loss will cause a reduction in the tensile capacity of the lower flange. There will also be a reduction in the geometric bending properties of the section. A capacity loss analysis was carried out for both composite and noncomposite wide flange girders, in positive

bending. The results are shown in Fig. 10-5. The reduction in bending capacity and stiffness is shown to be linearly proportional to the section loss.

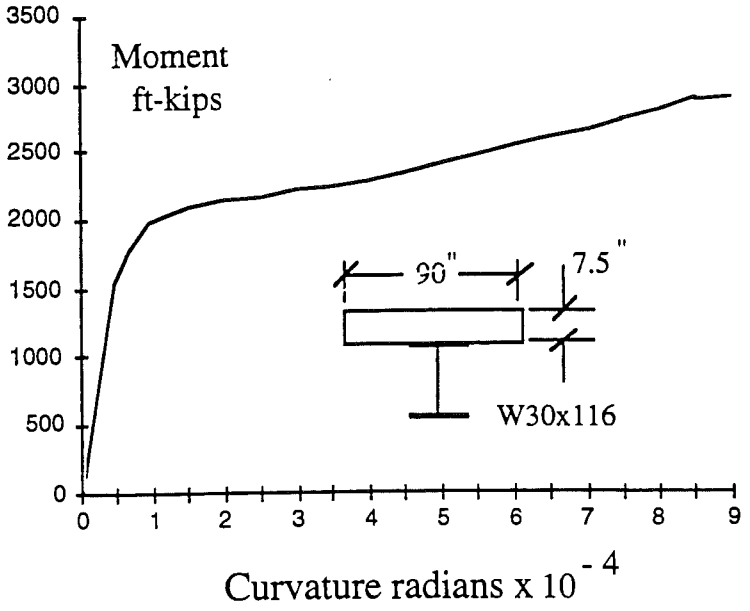

Fig. 10-4. Moment Curvature Plot for a Composite Section.

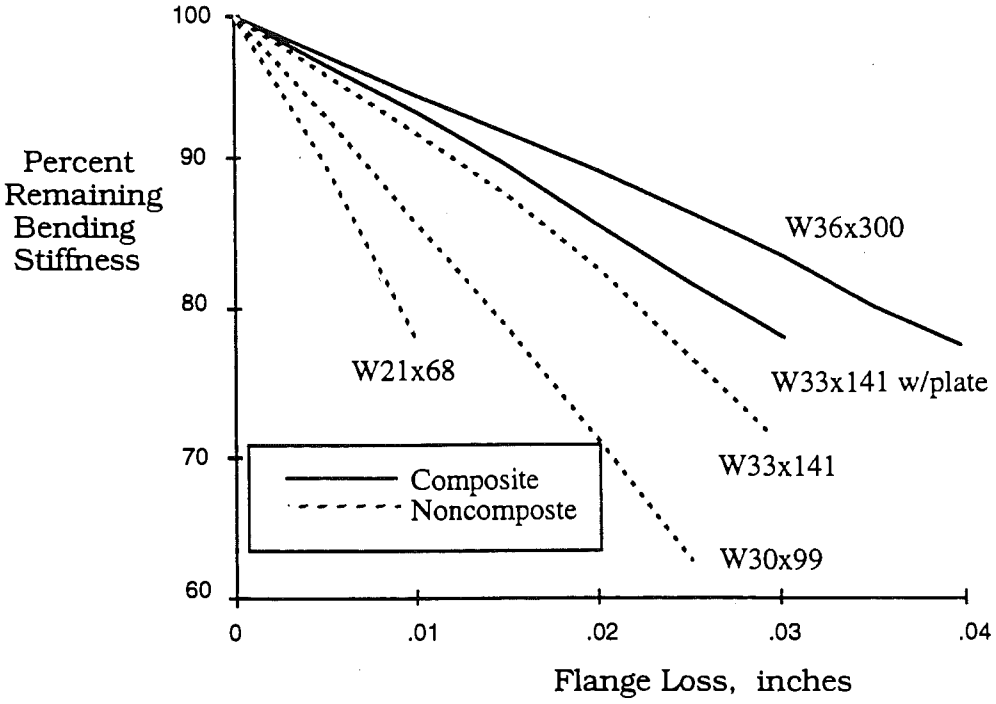

Fig. 10-5. Reduction in Bending Stiffness Due to Corrosion.

10.3.2 Shear Behavior

Corrosion may affect the resistance of shear forces, which are mainly carried by the web. Usually, the web is designed to operate at elastic nonbuckling stress levels. In order to investigate the possiblity of a thin slender web, plate buckling theory must be considered. The web panel adjacent to a support can be modeled as a rectangular plate with hinged edges all around [Johnston 1976]. The critical shear stress depends on the slenderness ratio, as shown in Fig. 10-6. The critical stress depends also on the relative dimensions of the plate and the spacing of the web stiffners.

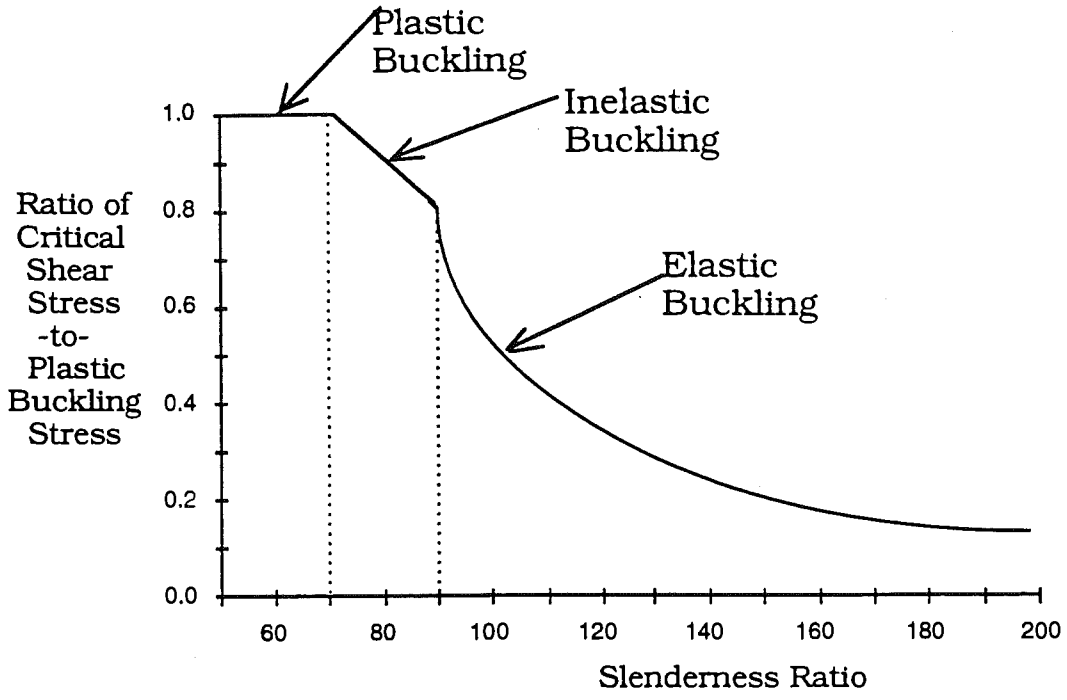

Fig. 10-6. Critical Shear Stress in Web Panel.

The maximum shear occurs near the supports. For simple span girders, this is also where the greatest amount of web corrosion will occur, Fig. 10-1. Shear load is carried by the web. The loss in web material will reduce shear capacity due to both section loss and

geometric buckling. Examples of the effect of corrosion on the shear capacity is shown in Fig. 10-7, for four types of wide flange girders. The loss of shear capacity is linear up to the point where buckling occurs. After the buckling stage is reached, shear capacity diminishes rapidly.

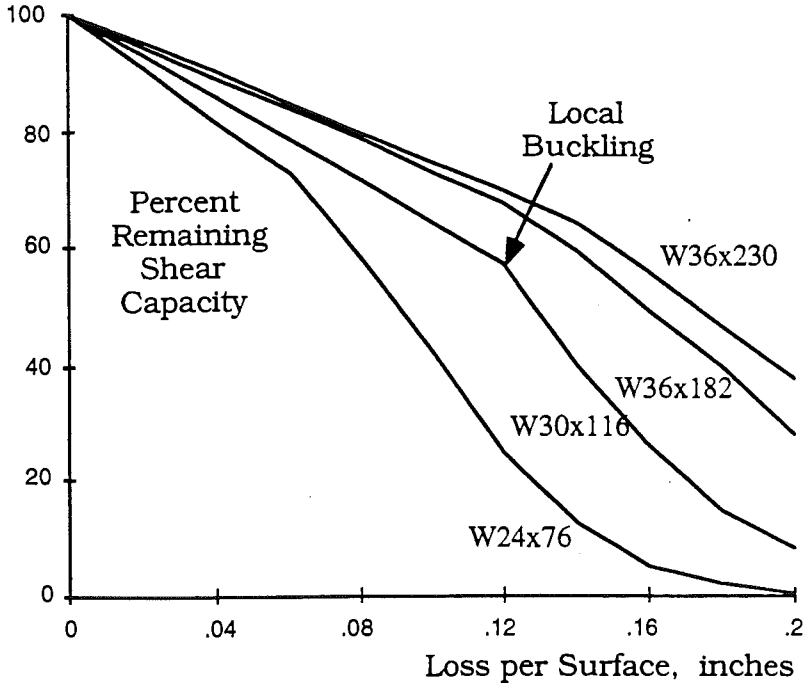

Fig. 10-7. Reduction in Shear Capacity Due to Corrosion.

10.3.3 Bearing Behavior.

The bearing capacity can also be affected by corrosion. Bearing forces are primarily resisted by the web, immediately above the supports. The strength of the web depends on the presence of stiffeners. The installation of stiffeners is mandatory for plate girders and rolled girders above intermediate supports. For rolled simple span steel girders, installation is necessary only if the nominal shear load exceeds 75 percent of the design shear capacity [AASHTO 1983a]. Although a girder may not require a stiffener at the time it is constructed, after serious corrosion a stiffener may be necessary to maintain the original design capacity.

The capacity of a stiffened web in bearing can be evaluated by treating the stiffener web combination as a column [AISC 1986]. The effective area of the column is illustrated in Fig. 10-8. The effective width of the web is approximately 12 times the web thickness [AISC 1986]. However, AASHTO [1992] allows up to 18 times the web thickness to be considered as part of the column.

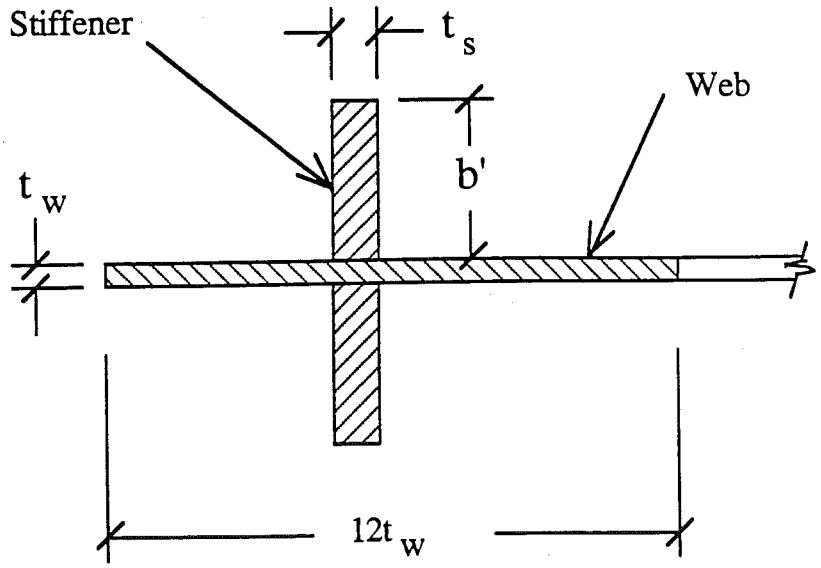

Fig. 10-8. Net Area of Bearing Stiffener Column.

The calculation of the ultimate bearing stress, F_{ult}, follows the method oulined by the Structural Stability Research Council [Johnston 1976]. The slenderness ratio is Kh/r; where K is the effective length factor, h is the height of the web, and r is the minimum radius of gyration. Then F_{ult} is:

$$F_{ult} = \begin{cases} F_y \left[1 - \dfrac{(Kh/r)^2}{2C_c^2} \right] & \text{for } Kh/r < C_c \\ \dfrac{\pi^2 E}{(Kh/r)^2} & \text{for } Kh/r \geq C_c \end{cases} \qquad (10\text{-}2)$$

where:

$$C_c = \sqrt{\frac{2\pi^2 E}{F_y}}$$

If no stiffener is present, the standard procedure [AASHTO 1992] is to allow the bearing stress in the web to be 80 percent of the yield stress. This criteria is adequate for new sections. However, if a web becomes thin, crippling may take place at lower stress levels.

There are three analysis methods available for evaluating web bearing strength. These three methods are;

- effective width approach,
- plastic hinge failure mechanism,
- plate theory.

Using the effective width approach, the post buckled strength of a thin member is calculated based on the effective width of the member resisting compression. This method, however, relies on the presence of a stiffener and therefore is not adequate for evaluating an unstiffened web.

The plastic hinge mechanism approach is used in the most recent edition of the steel design code [AISC 1986] for determining the bearing strength of a girder. This criteria, however, was developed on the basis of web crippling in a midspan section of a stiffened girder [Roberts 1981]. The application of the plastic hinge mechanism approach to end web panels may be inaccurate if no stiffeners are present.

The approach used in this study is based on plate theory. The end panel of the girder web resists the bearing stresses at the support. This panel can be idealized as a rectangular plate, supported on three sides and subjected to edge loading. The length of the web subjected to bearing stress will depend on the length of the bearing plate. In most cases, the length of the bearing plate is approximately equal to the width of the girder flange. In this study, the length of the web in bearing is assumed equal to the width of the flange plus the thickness

of the flange and the web fillet. The ultimate bearing stress, F_{ult}, is calculated using the plate equation [Johnston 1976];

$$F_{ult} = k \frac{\pi^2 E}{12(1 - \upsilon^2)(b/t_w)^2} \leq F_y \qquad (10\text{-}3)$$

where k is the plate coefficient, υ is Poisson's ratio, b is the length of the web in bearing, and t_w is the thickness of the web. The value of k depends on the boundary conditions and the stress distribution. If the supported edges of the plate are fixed and the bearing stress is uniformly distributed then k = 1.28.

Corrosion may cause a considerable reduction in bearing capacity. At the ends of a girder, section loss may take place over the entire web area, as shown in Fig. 10-1. The section loss that affects shear performance will also affect bearing performance. In order to illustrate the effect of corrosion on bearing capacity, three wide flange girders are evaluated for bearing capacity at different corrosion levels. The results are shown in Fig. 10-9. The girders are examined with and without bearing stiffeners. The stiffener sizes are; 4x1 in for the W36x230, 4x3/4 in for the W30x116, and 3x3/4 in for the W24x76.

Two observations can be made from the bearing capacity results. The first is that the reduction in bearing capacity is linear with the initial section loss, then becomes nonlinear. This is the same type of behavior exhibited by the shear capacity. The second observation is that bearing stiffeners improve the capacity at high corrosion levels. This observation also applies to cases with the same rate corrosion in the web and stiffeners.

10.3.4 Connections and Secondary Members

Connections are comprised of welded or bolted components. The capacity of a connection is directly related to the net area of the connectors, the bolt area, weld throat, or base metal dimensions.

Material loss, due to corrosion, will directly decrease the available net areas.

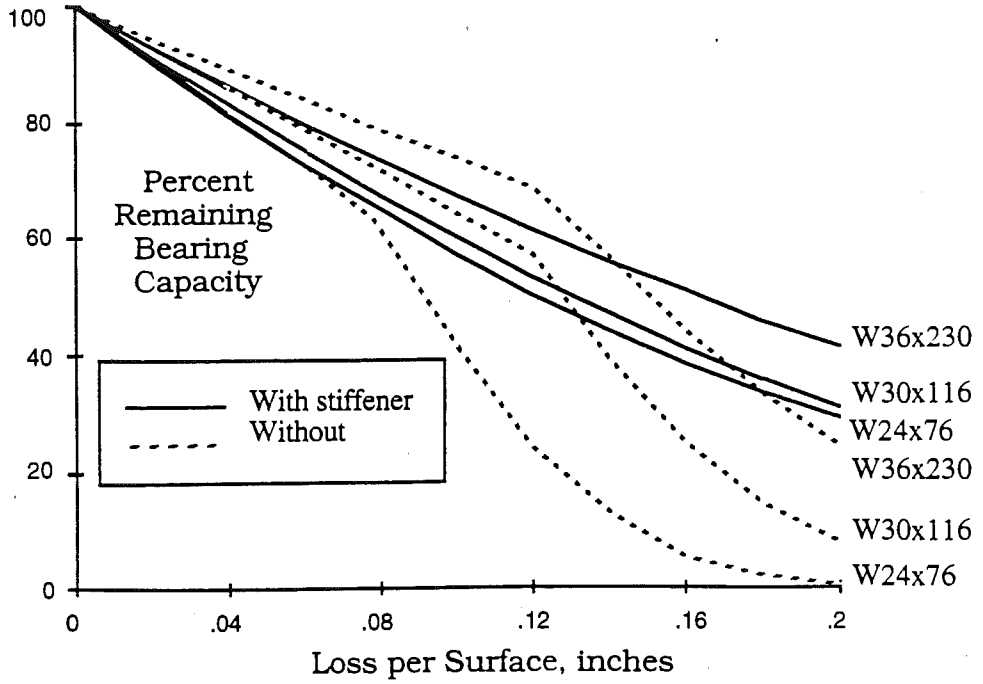

Fig. 10-9. Reduction in Bearing Capacity Due to Corrosion.

Pin-hanger supports can also be considered as connections. Because of their large size, general surface corrosion is a relatively minor problem. However, pitting corrosion can be serious because of the possibility of local stress concentrations and the difficulty of inspection. Pin-hangers are also susceptible to lockup due to rust formation. A "frozen" pin connection can induce unintended stresses by inhibiting superstructure movement.

Secondary members are typically the transverse bracing members spaced at intervals along the length of a bridge. These members serve the purpose of providing lateral support to the main elements and distributing loads transversely across the deck. The primary effect of corrosion on secondary members is the loss of section. This loss will reduce tensile and buckling capacities. The connection of transverse bracing members into the webs of longitudinal girders, is a fatigue prone area. With the additional effect

of corrosion, the brace connection will also suffer a reduction in fatigue life.

10.4 Examples of Evaluation

The effect of corrosion on load carrying capacity was evaluated for typical steel girder bridges. Two simple spans are considered, 40 ft and 60 ft. The bridges were designed using the Load Factor Design approach [AASHTO 1992]. For each span length the calculations were performed for two cases; with and without bearing stiffeners. A cross sectional view, common to both structures, is shown in Figure 10-10. The 40 ft bridge, uses composite W24x76 steel girders, with 3x4/4 in bearing stiffeners. The 60 ft bridge uses composite W30x116 girders, with 4x3/4 in bearing stiffeners. The A36 steel girders are spaced at 8 ft centers, supporting a 7.5 in thick concrete deck. The installation of bearing stiffeners is not required for either of the bridges. However, for the case of the 40 ft bridge, the web design is within 5 percent of the allowable above which a stiffener is required.

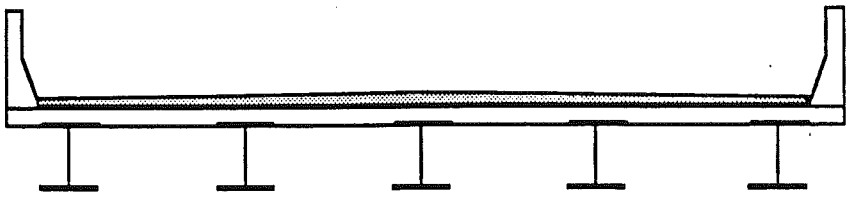

Fig. 10-10. Cross Section of a Steel Girder Bridge.

The bridges were examined for their HS rating factor in an unprotected marine environment. The evaluation is based on the AASHTO [1983b] operating rating formula, using an HS 20-44 truck as the live load vehicle;

$$\text{HS Rating Factor} = \frac{\text{Capacity - 1.3 Dead Load}}{\text{1.3 [Live Load + Impact]}} \qquad (10\text{-}4)$$

The capacity is calculated on the basis of the previously developed behavior models. The live load per girder is determined using the wheel load distribution factors for bending moment, and the assumption that the deck acts as a simple beam between girders for shear [AASHTO 1992]. The results of the calculations are illustrated in Figures 10-11 and 10-12. The HS rating factor is plotted against the number of years of exposure. The rated capacity is shown for bending, shear, and bearing modes. The bearing mode is considered with and without stiffeners.

Fig. 10-11 illustrates the rating of the 40 ft bridge. Actual rate of corrosion varies in time. In the considered example, a constant rate of corrosion of marine environment is assumed. The most notable item is the decline in shear and bearing capacity. The shear and bearing modes depend on the buckling strength of the web, which is sensitive to corrosion. For this bridge, the unstiffened bearing capacity is low and governs during the entire life of the structure. Ultimately, such a bridge would probably fail due to buckling of the web at the support. The installation of a stiffener can cause a significant increase in bearing capacity for both new and old bridges. With a stiffener present, the bending mode governs for the new bridge. Then, after several years of corrosion, the shear mode becomes critical.

The 60 ft bridge is illustrated in Fig. 10-12. As with the 40 ft span, the performance of the bridge depends greatly on whether bearing stiffeners are installed. If no bearing stiffener is present, the initial controlling mode of failure is bending. However, because the decline in bending strength is less than that for bearing, the bearing mode will dominate after approximately 15 years. The installation of a web stiffener significantly increases the bearing capacity. Under such conditions, the bending capacity would govern for the life of the structure.

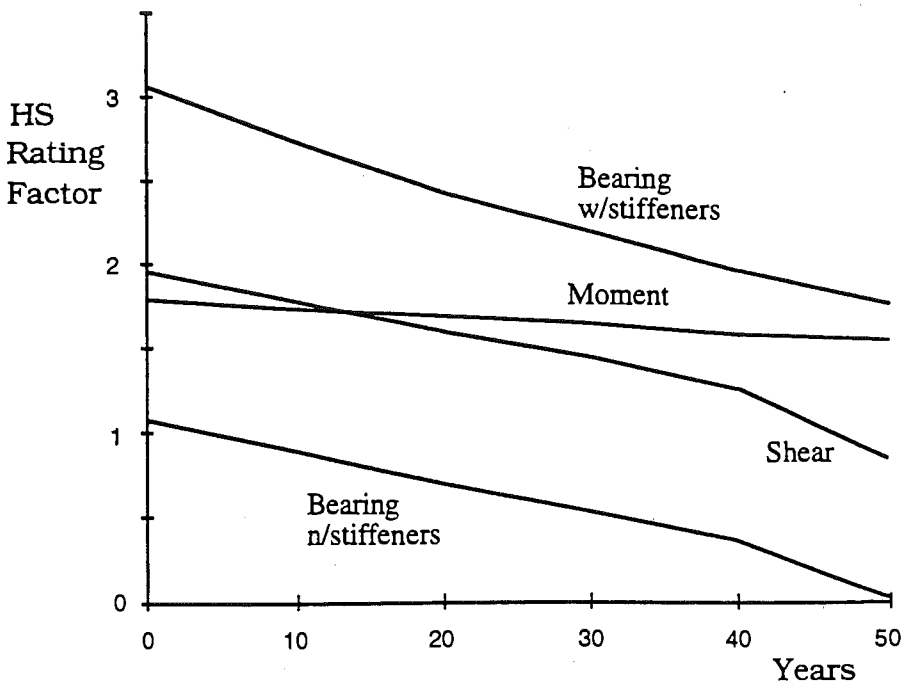

Fig. 10-11. Cross Section of a Steel Girder Bridge.

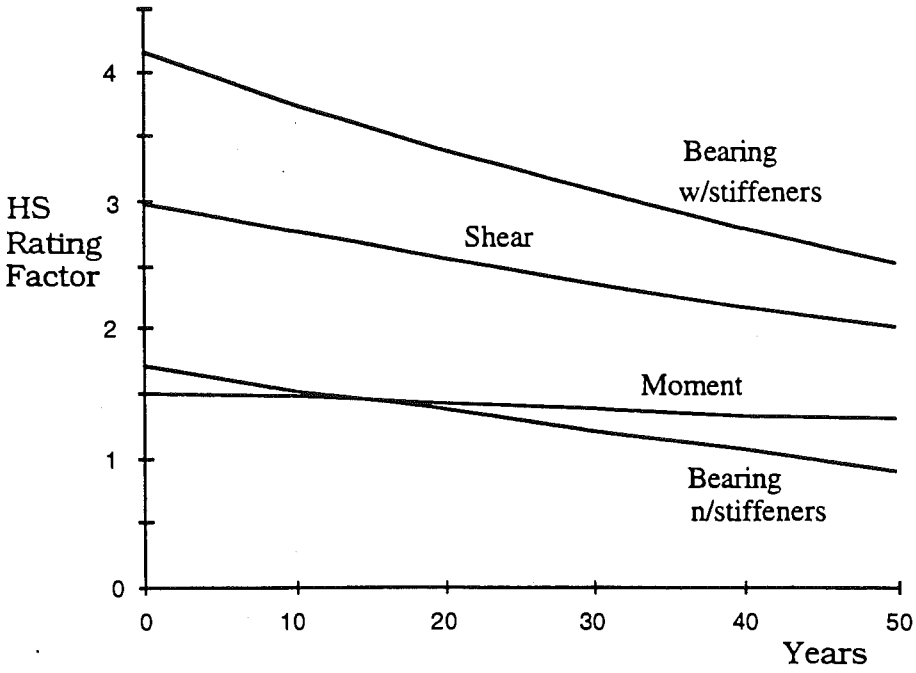

Fig. 10-12. Equivalent HS Rating vs. Time for 60 ft Span.

The deteriorated capacity of steel bridges can be modeled by combining information about the location and rate of corrosion with the structural analysis methods. Corrosion has a detrimental effect on bridge capacity. The effect of corrosion varies though, depending on the mode of resistance. Reduction of capacity occurs faster for modes which depend on thin elements, particularly those in compression. Therefore, the modes of resistance that govern the design of a new bridge may not be the same as those which govern when the bridge is old.

In order to evaluate the bearing capacity of an unstiffened web, plate theory was used. This bearing model accounted for the possibility of web buckling. It was shown that buckling of the web is the critical mode of failure for the 40 ft bridge; whereas bearing is not as important for the 60 ft bridge, because of a larger web thickness. If a steel bridge will not receive proper maintenance and painting, it should be constructed with bearing stiffeners. These stiffeners will provide for a more corrosion tolerant structure. The benefit from bearing stiffeners will be greater for shorter bridges, with lighter sections, than for longer bridges.

10. 5 Evaluation Procedure for Corroded Bridges

The evaluation procedure is based on the past experience, structural analysis and engineering judgement.

Step 1 Preparation for Field Inspection

Review of the available information: drawings, inspection reports, and calculations. Identification of corrosion-prone components and details.

Step 2 Field Inspection

Cursory inspection of structural components and details to observe corrosion patterns. Identification of visually critical

components and details. Special attention must be paid to pitting corrosion.

Thorough inspection of corrosion-prone and/or corroded components and details including in particular web at the support, stiffeners at the support, lower flange at midspan, and metal bearings.

Measurement of corrosion loss. Removal of debris may be necessary to obtain accurate results. Most accuracy is needed in the critical parts of components and details (web thickness at the support, stiffners, and flanges).

Step 3 Cursory Structural Analysis

The effect of corrosion loss on the actual strength is evaluated analytically. For given percentage of loss of thickness, the percentage loss of capacity is evaluated. The analysis is performed for the web, flanges and stiffeners. Evaluate the The results are then evaluated and it is determined whether the reduced capacity is less than the minimum acceptable level. If this is the case, then go to Step 4.

Step 4 Full Structural Analysis

Carry out structural analysis of the critical components and details. There are several levels possible depending on the required accuracy and computational capabilities. Hand calculations can be performed to verify the conformance with the current AASHTO Specifications. Linear elastic analysis (FEM) may reveal the reserves in the actual load distribution. Nonlinear analysis (FEM) can be used to estimate the actual ultimate load carrying capacity.

Step 5 Evaluation of the Actual Strength

The actual load carrying capacity is determined on the basis of the critical component and/or detail. The capacity reduction (if any) can be expressed in terms of the rating factor, RF.

Step 6 Prediction of Rate of Corrosion

Rate of corrosion depends on many factors (aggressive environment, exposure to moisture, type of material, detailing, age). Rate of corrosion observed on similar bridges in the area can be a good indication. Because of uncertainties involved in this prediction, it is convenient to give the rates with estimated probabilities, e.g. the corrosion rate is 0.002 inch/year with the probability 60%, 0.004 with the probability 30%, and 0.006 with the probability 10%.

Step 7 Prediction of the Remaining Life

Prediction of the remaining life is based on the estimated actual strength and rate of corrosion. Therefore, the prediction involves a considerable degree of uncertainty.

The uncertainty involved in calculation of the strength depends on the accuracy of input data (dimensions and material properties) and method of analysis (simple girder distribution factors from AASHTO, linear FEM and nonlinear FEM).

The calculation can be carried out for various rates of corrosion. For each corrosion rate, the loss of capacity can be calculated gradually on the annual basis. For each rate, the remaining life is obtained as the number of years to failure. The remaining life for the bridge is then given with probabilities associated with corrosion rate predictions (e.g. remaining life is 5 years with probability 10%, 8 years with probability 30% and 12 years with probability 60%).

The proposed probability-based evaluation procedure for corroded steel bridges is currently being developed at the University of Michigan. The final product will be an interactive Knowledge-Based Expert System (KBES) for use by the state bridge engineer for inspection and evalution.

10. 6 Summary

Corrosion is one of the most serious causes of deterioration in steel grider bridges. The corrosion rate varies depending on use of salt, air polution, maintenance (painting), presence of leaking joints, and other factors. Corrosion is observed mostly in the immediate vicinity of the joints and on lower flanges of the griders. The critical part of the girder is the web area close of the joint (at the abutment). Web stiffeners can considerably increase the life of the structure.

11 EVALUATION OF BRIDGES WITH REGARD TO FATIGUE

11.1 Introduction

In order to make the Bridge Weigh-in-Motion (BWIM) data and the dynamic strain data useful for fatigue analysis, load models must be developed. Development of fatigue load models is necessary for the effective application of fatigue resistance models to the problem of fatigue in steel girder highway bridges. An understanding of fatigue resistance models and fatigue load data analysis is required for the formulation of accurate reliability based fatigue load models. Following is development of each of these important aspects of a probabilistic approach to fatigue analysis in steel girder highway bridges.

11.2 Available Bridge Fatigue Analysis Models

Various fatigue models are available for the analysis of girder bridges. Some are deterministic and some are based on probabilistic methods. Probabilistic methods consider the uncertainties in the analysis, while a deterministic analysis assumes that the variables are known and relies on a factor of safety to ensure safe performance of the structure. United States code provisions for fatigue are specified in the American Association for State Highway and Transportation Officials (AASHTO) *Standard Specifications for Highway Bridges* and in Canada, the *Ontario Highway Bridge Design Code* (OHBDC). Design of members by both North American codes subject to repetitive loading is based on a calculated stress range and a fatigue stress range which is not to be exceeded. The allowable stresses are dependent upon material type and detail location described in the codes. Schilling (1977, 1982, 1984), Nyman and Moses (1985), and Raju, Moses, and Schilling (1990) have developed fatigue load models for the analysis of girder bridges, on which the AASHTO model is largely based.

Schilling Fatigue Model

Schilling (1977) developed the idea of a single fatigue truck with weight equivalent to the actual truck traffic. The equivalent weight, W_{eq} ,is calculated by equation 11.1:

$$W_{eq} = \left(\sum_{i=1}^{n} \alpha_i W_i^3 \right)^{1/3} \qquad (11.1)$$

where α_i is the fraction of vehicles at the GVW of W_i and W_i is the GVW range. Schilling (1982) proposed the a fatigue design vehicle with gross vehicle weight based on equation 11.1 and axle weights proportioned as the AASHTO HS20 truck. Schilling (1984) also studied the number of stress cycles, N_e, induced by a truck crossing various types of spans of highway bridges. Schilling asserts that 92% to 98% of the fatigue damage caused is due to 4 and 5 axle vehicles. By analyzing the moments caused by a fatigue truck in several simple and continuous spans Schilling concludes:

1. N_e = 2.0 for simple spans < 40 feet and N_e = 1.0 for simple spans > 40 feet.
2. N_e = 2.0 near supports for continuous spans < 40 feet and N_e = 1.5 near supports for continuous spans > 40 feet.
3. N_e = 2.0 between supports for continuous spans < 40 feet and N_e = 1.0 between supports for continuous spans > 40 feet.
4. N_e = 10 for all cantilever spans.
5. N_e = 1.0 for all spans of trusses.

Due to dynamic effects Schilling recommends that the primary cycle be increased by an impact factor. Schilling further concludes that the effect of additional cycles caused by the dynamics of bridge - truck interaction are small and may be ignored. Multiple presence of vehicles may also be ignored as the effect on the fatigue life is very small.

Raju, Moses and Schilling Model

Nyman and Moses (1985) developed a bridge fatigue design model based on the WIM data collected in seven states by Snyder et al. (1985). The model utilizes a reliability format with a limit state function $g = D_f - D(t)$ where D(t) is the accumulated damage at time t and D_f is the damage to cause failure.

$$D(t) = \frac{1}{c}\sum_{i=1}^{V_t} S_i^3 \qquad (11.2)$$

where c is the S-N intercept, V is truck volume per day or ADTT, t is the life in days, and S_i is the stress range due to the ith truck. The failure function becomes:

$$g = D_f - \frac{Vt}{N_D}\frac{M^3G^3I^3H^3}{S^3}L_o \qquad (11.3)$$

where M, G, I, H, and S are the ratios of variable mean to the variable design value and N_D is the number of design cycles for the component. It is assumed for this model that each truck induces a single cycle and that a linear relationship exists between the truck gross vehicle weight and the magnitude of the stress cycle.

Raju, Moses and Schilling (1990) refined the model proposed by Nyman and Moses (1985) in three ways. A factor of safety, g, a stress cycle per truck factor, C, and a random variable Z_x were included in the model (equation 11.4).

$$Z = \frac{XN_T}{365(ADTT)C}\left(\frac{\gamma Z_x S}{WGIMH}\right)^3 - Y_s \qquad (11.4)$$

W is the effective truck weight factor with a mean of 1.0 and a coefficient of variation equal to 10 percent to account for variation from site to site in W_{eq} (Moses, Schilling, and Raju (1988)). All other variables are as defined above for equation 11.3. Raju et al (1990)

recommended a GVW of 54.0 kips for the fatigue design truck as calculated by equation 11.1 and based on WIM measurements.

AASHTO Fatigue Design Specification

AASHTO *LRFD Specifications for Highway Bridges*, Section 3.6.1.4 specifies the design loads and load factors for bridge fatigue design. A fatigue truck is specified, with dynamic load allowance for fatigue equal to 1.15. Frequency of occurrence of the AASHTO fatigue design truck is to be taken as the single lane ADTT, or $ADTT_{SL}$ and is to be applied separately to each lane. AASHTO *LRFD Specifications for Highway Bridges*, Section 6.6 specifies design requirements for fatigue considerations. AASHTO considers only live load stress range since the level of total applied stress has been shown to be negligible. The fatigue stress range is considered where a net tensile stress is induced, or where the permanent compressive stress is less than twice the maximum tensile live load stress. The design criteria for fatigue is specified in equation 11.5:

$$\gamma\,(\Delta f) \le (\Delta F)_n \tag{11.5}$$

where γ is the load factor equal to 0.75, (Δf) is the force effect, and $(\Delta F)_n$ is the nominal fatigue resistance. Fatigue resistance is a function of the detail category and is specified in AASHTO by equation 11.6.

$$(\Delta F)_n = \left(\frac{A}{N}\right)^{1/3} \ge \frac{1}{2}(\Delta F)_{TH} \tag{11.6}$$

where N = (365)(75) n $(ADTT_{SL})$, A is a constant based on detail category (Table 11.1), n is the number of stress range cycles per truck based on the span length (Table 11.3), and $(\Delta F)_{TH}$ is the constant-amplitude fatigue threshold as a function of detail category (Table 11.2).

Table 11.1. AASHTO Constant, A.

Detail Category	A x 10^8
A	250
B	120
B'	61.0
C	44.0
C'	44.0
D	22.0
E	11.0
E'	3.9
A325 Bolts	17.1
A490 Bolts	31.5

Table 11.2. AASHTO Fatigue Threshold.

Detail Category	Threshold (ksi)
A	24.0
B	16.0
B'	12.0
C	10.0
C'	12.0
D	7.0
E	4.5
E'	2.6
A325 Bolts	31.0
A490 Bolts	38.0

Table 11.3. AASHTO Cycles per Truck, n.

Longitudinal Members	Span Length	
	> 40 feet	≤ 40 feet
Simple Span Girders	1.0	2.0
Continuous Girders		
1. Near interior support	1.5	2.0
2. elsewhere	1.0	2.0
Cantilever Girders	5.0	
Trusses	1.0	
Transverse Members	Spacing	
	> 20 feet	≤ 20 feet
	1.0	2.0

Summary

In each of the above fatigue load models the same vehicle is used for strength design and fatigue design. In reality, fatigue damage is accumulated from the passage of many types of vehicles, where vehicles may induce more than one strain cycle which will cause incremental damage. Criteria for strength is based on the single largest expected event in a given time period, however, fatigue is an accumulation of damage due to a wide range of loading over generally long periods of time. Since bridge live loading is a load spectra, it is reasonable to expect inaccuracies in the above described methods, particularly at sites where there may be more than one distinct truck type in the vehicle population. This effect was demonstrated by Tallin and Petreshock (1990) in their analysis of the WIM data (Snyder et al, 1985) utilized by Nyman and Moses (1985) and Raju, Moses, and Schilling (1990). Two bimodal distributions of gross vehicle weights were developed based on pairs of lognormal distributions and a lognormal and an extreme type III distribution. Tallin and Petreshock then assumed that the stress range experienced by a bridge detail is a linear function of the GVW of the truck causing the stress. Based on the developed models, Miner's rule, and ADTT of 1000, equation 11.7 was derived.

$$L = \frac{AF_D^{-m}/E[W^m]}{ADTT\,X\,365} \tag{11.7}$$

Where A and m are material constants, $ADTT$ is the average daily truck traffic, L is the detail life in years, F_D is the fatigue design stress, and $E[W^m]$ is the mth expected moment of the GVW distribution. Using this deterministic analysis the fatigue lifetimes are calculated for several AASHTO fatigue categories. Tallin and Petreshock conclude that a bimodal distribution of GVW results in a shorter detail life than a single mode distribution and that the type of bimodal distribution used causes a only a small variation in the resulting predicted life of the detail.

11.3 Fatigue Analysis

There are available three distinct theories for the evaluation and design of components to resist fatigue loadings. These are commonly known as stress-life approach, strain-life approach, and the fracture mechanics method. Stress-life was the first method developed to understand fatigue and is primarily used when stresses are within the elastic range. The strain-life approach considers the effect of component response in the plastic range and is therefore strain dependent. This is often the case at stress concentrations or notches. The fracture mechanics method makes a distinction between crack initiation and propagation, recognizing that at low strain amplitudes initiation dominates, and at high strain amplitudes propagation dominates. The fracture mechanics method is normally used to estimate the propagation life of the component.

The stress-life approach is the most suitable to this study due to the fact that the bridge components remain in the elastic range, and it is also the more flexible and analytically simple approach. Fatigue stress-life resistance test data has been shown to fit a curve of the form:

$$NS^m = K \tag{11-8}$$

Where N = the number of cycles to failure, S = the stress, K = a material constant, and m = the negative reciprocal of the slope of the S-N curve. A log-log plot of Eq. 11-8 produces a straight line which may be interpreted as the line indicating the median of failures.

K and m in Eq. 11-8 are random variables as shown by the distributions in Fig. 11-1. Researchers have found that generally there is little variation in m over the range of cycles, N, and the variability of the material resistance is generally accounted for by K.

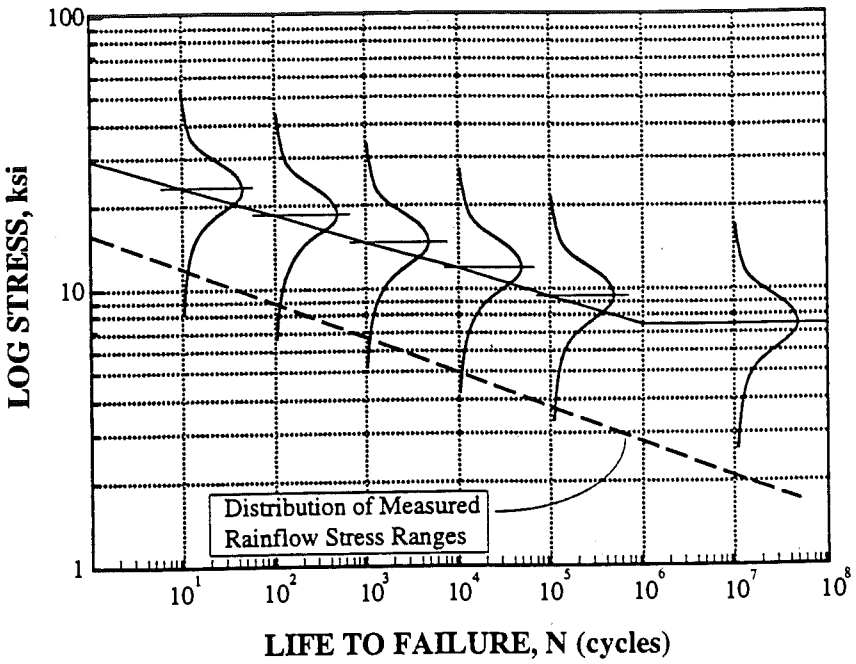

Fig. 11-1. General P-S-N Curve of Material Resistance, (Haugen, 1980).

Eq. 11-8 must also be modified to account for such factors as mean stress, size effects, type of loading, surface finish and treatments, and other factors. Effects of mean stress are plotted on a Haigh diagram (see texts for fundamental fatigue analysis such as Bannatine, et al 1990), but this is often not available. Other empirical relationships are available which estimate infinite life design region. These include the Soderberg, Goodman, Gerber, and Morrow equations (see Bannatine, et al 1990). For components subject to conditions which deviate from the standard R.R. Moore fatigue material test (see Bannatine, et al 1990), other factors which modify the endurance limit are available. For bridge structures, size effect factors may be difficult to estimate. Effects of loading type may be determined by the stresses and the volume of highly stressed material in proportion to the component. Bridge structures and components are rarely finished or surface treated, however effects of corrosion on fatigue must be considered and can be significant as shown in Fig. 11-2 (Juvinal, 1967).

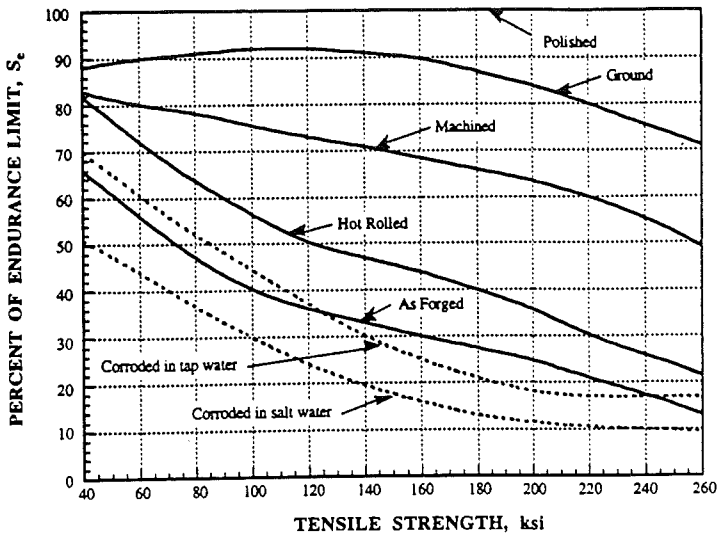

Fig. 11-2. Surface Finish Effects on the Fatigue Endurance Limit.

Development of material fatigue resistance data of bridge details and typical bridge steels is required for the application of the stress-life approach. Albrecht (1986) found that the distribution of test data points is log normal with an approximately constant standard deviation at all stress levels. Further, Albrecht found that this held true within all AASHTO categories of details. Albrecht proposes that for any stress value the fatigue resistance of a component within a category will exhibit the same log normal distribution, mean, and standard deviation. Statistics for the six AASHTO categories have been summarized by Albrecht and are shown in Table 11-4:

Table 11-4. Resistance Statistics for AASHTO Component Categories.

Category	Type of Detail	Regression Coeff		Standard Deviation
		Intercept	Slope	
A	Rolled Beam	11.121	3.178	0.2210
B	Welded Beam	10.870	3.372	0.1470
C	Stiffeners	10.085	3.097	0.1580
C'	2" Attachments	10.0384	3.250	0.0628
D	4" Attachments	9.603	3.071	0.1080
E	Cover Plate End	9.2916	3.095	0.1006
E'	Cover Plate End	9.1664	3.200	0.1943
Mean	-	10.025	3.180	0.1420

11.4 Statistical Models for Fatigue Loading

Development of a probabilistic fatigue load model requires collection of actual dynamic strain time histories of various members and components. Following the collection of time histories, data must be processed into a usable form. This section presents the characteristics of the dynamic strain time history commonly found in steel girder highway bridges as a random process, fatigue damage accumulation, and methods of counting fatigue damage.

Commonly occurring load histories in fatigue analysis often are categorized as either narrow band or wide band processes. Narrow band processes are characterized by an approximately constant period such as that shown in Fig. 11-3a. Wide band processes are characterized by higher frequently small excursions superimposed on a lower, variable frequency process such as that shown in Fig. 11-3b. For steel girder highway bridges, where the loading is both random and dynamic, the strain histories are wide band in nature.

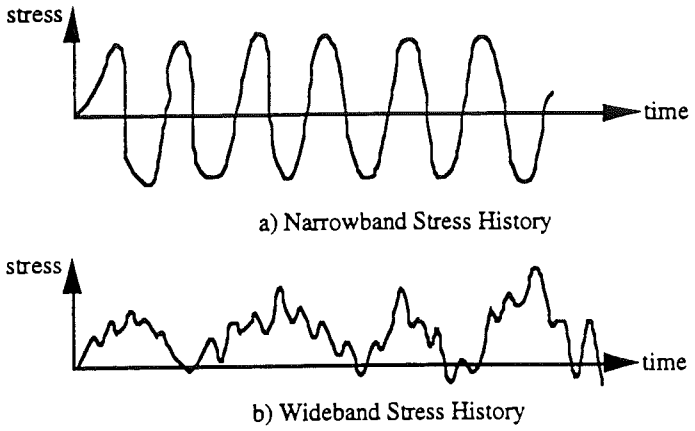

Fig. 11.3. Example of Narrow and Wide Band Stress Histories.

11.4.1 Fatigue Damage Accumulation

Wide band random fatigue load effect is generally accounted for by utilizing a cumulative damage formula. The most common and widely accepted of the cumulative damage theories is the Palmgren-Miner's hypothesis, or Miner's Rule. Miner's Rule, as does others, assumes a relationship between variable amplitude loading and results of constant amplitude fatigue testing. The damage of each cycle in the complex stress history adds incrementally to the total fatigue damage based on the assumption that the accumulation of fatigue damage proceeds linearly over time. Lutes, et al (1984) has demonstrated that the expected value of the damage function at failure is approximately 1.0 for sufficiently large sample sizes. The linear damage rule, also known as Miners's rule, for fatigue damage accumulation is as follows:

$$D = \sum_{i=1}^{n} D_i = \sum_{i=1}^{n} \frac{1}{N_i} = \frac{1}{K} \sum_{i=1}^{n} S_i^m = \frac{n}{K} E[S^m] \qquad (11\text{-}9)$$

where D = accumulated damage factor, D_i = incremental damage due to the ith stress cycle, n = total number of stress cycles in the stress history, K = a material constant, N_i = total number of cycles to failure for constant amplitude stress level S_i, and $E[S^m]$ is the expected value of the random variable, S^m. Failure is assumed to occur at $D \geq 1.0$ for a

deterministic analysis. The random variable D has a mean value of 1.0 and a coefficient of variation equal to 0.3 (Wirsching, 1980)

It is useful to express Eq. 11-9 in terms of time rather than cycles. Substituting for the cycles, $n = f\,t$, where f is a frequency of cycles and t is time, Eq. 11-9 becomes:

$$t = T_F = \frac{D\,K}{f\,E[S^m]} \tag{11-10}$$

Miner also developed the concept of an equivalent stress. An equivalent stress, for the same number of cycles, will cause the same damage as a variable amplitude loading. Miner's equivalent stress, $S_{r_{Miner}}$ is given by Eq. 11-11`:

$$S_{r_{Miner}} = \left[\sum_{i=1}^{k} \alpha_i \, S_{r_i}^n \right]^{\frac{1}{n}} \tag{11-11}$$

where, $\alpha_i = \frac{n_i}{N_T}$, n_i = cycles per bin (or stress range), N_T = total cycles, and n is a coefficient, usually 3. When n = 3 equation 11-11 is the root mean cube (RMC) of the distribution. The accuracy of this method is questionable since it is dependent on the selection of the coefficient, n, and stress ranges included, however this is the state of the art at this time. The equivalent stress is a convenient concept to be used for the comparison of stress histograms obtained by the rainflow method.

11.4.2 Rainflow Method of Cycle Counting

Stress histories which are wide band in nature do not allow for simple cycle counting. The cycles are irregular with variable frequencies and amplitudes. Several cycle counting methods are available for the case of wide band and non-stationary processes, each successful to a degree in predicting the fatigue life of a structure. The rainflow method is preferred due to the identification of strain ranges within the variable amplitude and frequency stress histogram which

are associated with closed hysteresis loops. This is important when comparing the counted cycles with established fatigue test data obtained from constant amplitude stress histories.

The rainflow method, proposed by Matsuishi and Endo in 1968, counts the number, n, of cycles in each predetermined stress range, S_i, for a given stress history. Rules of counting are applied to the stress history after orienting the trace vertically, positive time axis pointing downward. This convention facilitates the flow of "rain" due to gravity along the trace and is merely a device to aid in the understanding of the method. Following are rules for the rainflow method:

1. All positive peaks are evenly numbered.

2. A rainflow path is initiated at the inside of each strain peak and trough.

3. The "rainflow" progresses along a slope and "drips" down to the next slope.

4. The "rainflow" is permitted to continue unless the flow was initiated at a minimum more negative than the minimum opposite the flow and similarly for a rainflow initiated a maximum. For example path 1-8, 9-10, 2-3, 4-5, and 6-7.

5. A "rainflow" must stop if it meets another flow which flows from above. For example path 3-3a, 5-5a, and 7-7a.

6. A "rainflow" is not initiated until the preceding flow has stopped.

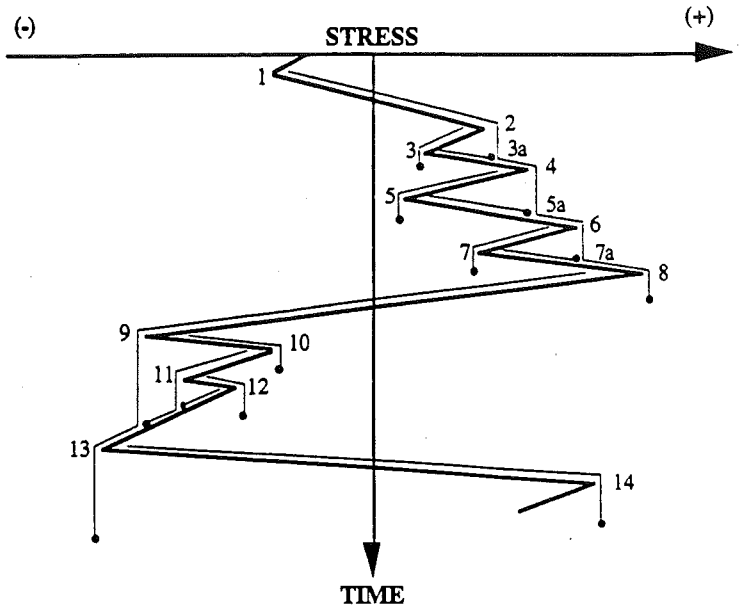

Fig. 11-4. Rainflow Counting Diagram.

Following the above procedure each segment of the history is counted only once. Half cycles are counted between the most negative minimum and positive maximum as well as the half cycles or interruptions between the maximum and minimum. As shown in Fig. 11-4, all negative trough initiated half cycles will eventually be paired with a peak initiated cycle of equal magnitude. For a more detailed explanation and discussion of the rainflow method and others see an introductory text on fatigue analysis such as Bannantine et al (1992).

11.4.3 Rainflow Load History Distribution

Load histories collected in histogram form using the rainflow method tend to reflect an irregular process which is described by stress ranges and frequency of occurrence. The data to establish the histogram is by necessity collected over a short period of time relative to the desired service life of the component. It may be assumed, however, that if extremely large records are collected a more regular process will be reflected in the histogram and the probability density function of the process can be analytically formulated. Wirsching and Light (1990) have proposed the Weibull distribution to model the long

term distribution of stress ranges. The Weibull distribution is chosen not due to an underlying physical mechanism, but because the distribution is flexible and can model many forms of observed distributions. The Weibull probability distribution function (PDF), f(x), cumulative distribution function (CDF), *F(x)*, and the expected value, *E[X]*, and variance , *Var[X]* are presented in Equations 11-12 through 11-15 respectively (See Benjamin and Cornell, 1970).

$$f(x) = \frac{\theta_2}{\theta_1}\left(\frac{x}{\theta_1}\right)^{\theta_2 - 1} e^{-(x/\theta_1)^{\theta_2}} \tag{11-12}$$

$$F(x) = 1 - e^{-(x/\theta_1)^{\theta_2}} \tag{11-13}$$

$$E[X^k] = \theta_1^k \, \Gamma\left(\frac{k}{\theta_2} + 1\right) \tag{11-14}$$

$$Var[X] = \theta_1^2 \left\{ \Gamma\left(\frac{2}{\theta_2} + 1\right) - \left[\Gamma\left(\frac{1}{\theta_2} + 1\right)\right]^2 \right\} \tag{11-15}$$

where θ_1 = the true scale parameter, θ_2 = the shape parameter, and Γ = the gamma function. Estimation of the Weibull distribution parameters requires solution of nonlinear Equations or can be found using a simple graphical procedure (Hahn and Shapiro, 1992).

Applying the Weibull distribution to the distribution of stress ranges for fatigue reliability analysis results in the expected value of S^m as in Eq. 11-9:

$$E[S^m] = \theta_1^m \, \Gamma\left(\frac{m}{\theta_2} + 1\right) \tag{11-9}$$

11.5 Reliability Analysis for Fatigue

The purpose of a reliability analysis is to determine the probability of failure due to fatigue loading of the highway girder bridge. From the probability of failure the reliability index is easily calculated. For fatigue reliability this will involve the determination of

the distance between the average fatigue load and the average material fatigue resistance. Fatigue resistance is most commonly defined by the number of constant amplitude cycles required to fail the member under consideration. The load is defined as the stress history of the bridge. It has been previously demonstrated in section 11.3 that bridge structures experience a wide band stress history, which presents a difficulty for the reliability analysis. This study develops the load models to enable a reliability analysis and determination of the probability of failure.

11.5.1 Structural Reliability Theory

The reliability of a structure can be considered as the probability that there will not be a structural failure within a prescribed period of time, or, the probability that the resistance of a structure will exceed the applied load. Since all variables considered in a structural analysis are random, this approach is more rational than traditional deterministic analysis. Analysis based on deterministic methods assumes that the resistance and load are known and relies on a prescribed safety factor to ensure that the resistance is sufficiently greater than the load. Analysis based on Structural Reliability Theory recognizes that both the resistance and the load, due to fluctuations, and are represented by a mean and a statistical distribution. The actual values affecting the analysis cannot be precisely determined. The reliability analysis evaluates the probability of failure for structural systems and members.

Failure modes can be represented in a mathematical form, or limit state function. This formulation represents the limit or boundary between survival and failure. Limit state functions are categorized by two types, serviceability limit state, (SLS) and ultimate limit state, (ULS). Serviceability refers to such concerns as deflection, cracking, or undesirable dynamic characteristics. Ultimate refers to complete collapse of a structure, which may develop due to various considerations such as bending, shear, compression, or buckling. For the simple case of the limit state equaling the resistance minus the

load, the probability of failure can be illustrated as shown in Fig. 11-5. The shaded portion of the graph represents the probability of failure, or the area where the load exceeds the resistance and the safety margin is less than zero. The limit state occurs at $g = 0$, $g < 0$ represents failure, and $g > 0$ represents the safe region.

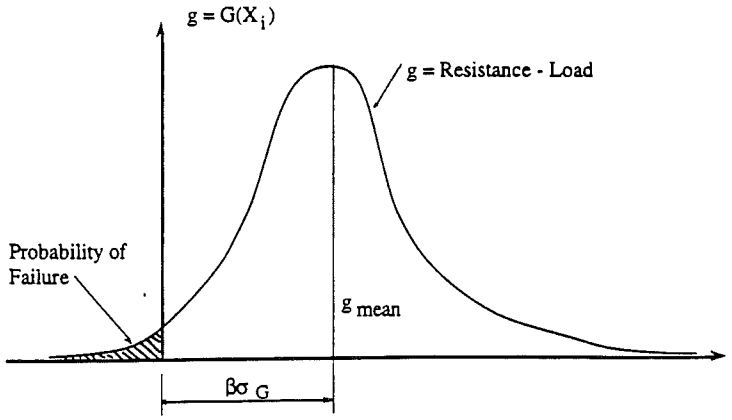

Fig. 11-5. Probability Density Function of the Safety Margin, G.

Numerically, the calculation of the shaded area is often an extremely complex multivariant integration. Nonlinearities in the limit state function can further complicate the calculation of the probability of failure. The following common technique to calculate the probability of failure, or the reliability index, β which is calculated using Eq. 11-16 is sufficiently accurate for most applications.

$$\beta = \Phi^{-1}(p_F) \tag{11-16}$$

where Φ^{-1} is the inverse normal distribution function (see appendix A) and p_F is the probability of failure. Table 11-5 illustrates some values of the reliability index and the corresponding probability of failure.

Reliability Index, β	Probability of Failure, P_F
0	0.5
1	0.159
2	0.0228
3	0.00135
4	0.0000317
5	0.000000287
6	0.000000000987

Table 11-5. Reliability Index and Probability of Failure.

Approximate methods of analysis to determine the probability of failure, or reliability index, β, have been developed by several researchers. Among these methods are the First-Order Second-Moment Reliability Index, Hasofer and Lind Reliability Index, Rackwitz and Fiessler Procedure, and a number of simulation techniques. For uncorrelated variables the reliability index becomes:

$$\beta = \frac{\overline{g}}{\sigma_g} \qquad (11\text{-}17)$$

where $\overline{g}$ is the mean value of the limit state function and σ_g is the standard deviation. Substituting the simple limit state where g equals the resistance minus the load:

$$\beta = \frac{\overline{R} - \overline{Q}}{\sqrt{\sigma_R^2 + \sigma_Q^2}} \qquad (11\text{-}18)$$

Where $\overline{R}$ = mean resistance, $\overline{Q}$ = mean load, σ_R = standard deviation of resistance and σ_Q = Standard deviation of load.

11.6 Limit State Function for Fatigue

The development of the fatigue limit state involves the mathematical formulation of the boundary between survival and failure based on fatigue. A service limit state (SLS) function which considers load characteristics developed in this study and utilizes the available resistance parameters must incorporate the time to failure, T_F and the desired service time, T_S.

$$P_F = P(T_F \geq T_S) \tag{11-19}$$

The probability of failure is then the probability that the time to failure is greater than the time of desired service. Expressing the limit state function in the form described by equation 11-19, the fatigue limit state function becomes:

$$g = T_S - T_F \tag{11-20}$$

where g must be greater than or equal to zero. Utilizing reliability methods and a lognormal format of equation 11-17, the reliability index expression becomes:

$$\beta = \frac{ln\left(\frac{\overline{T}_F}{T_S}\right)}{\sigma_{ln\,T_F}} \tag{11-21}$$

and from Eq. 11-9 the mean time to failure, $\overline{T}_F$, can be found as shown in equation 11-22 (See Laman, 1995).

$$\overline{T_F} = \frac{\overline{D}\,\overline{K}}{f\;\overline{P}\,E[S^m]} \tag{11-22}$$

$$f = 365\;\alpha\,(ADTT) \tag{11-23}$$

for f in units of cycles/year. The truck cycle factor, α, accounts for shorter spans where there will be more than one cycle per truck. It is assumed that only truck traffic will cause stress cycles of significance

to the fatigue damage calculation, therefore the average daily truck traffic factor, ADTT is used. Note that the truck cycle factor and ADTT are specific to the site and is considered to have no variation. There will, however, be variation in these factors from site to site. A Professional factor, P, is also included in Eq. 11-24 to account for uncertainty in modeling the actual stress distribution with the Weibull statistical model, errors in calculating the Weibull parameters, data collection and equipment errors, and sample errors due to the necessarily short sample times.

$$\sigma_{\ln T_f} = \left\{ \ln\left[(1 + C_D^2)(1 + C_K^2)(1 + C_P^2)^{m^2} \right] \right\}^{1/2} \qquad (11\text{-}24)$$

where C_D, C_K, and C_P are coefficients of variation for the variables D, K, and P respectively, which are defined above.

11.6 Results of Stress Spectra Testing

The following figures 11-6 through 11-101 are histograms and cummulative distribution functions (CDFs) of strain and stress testing results. The results are arranged by bridge. Each Girder was tested at the mid-span and diaphragms were tested at the ends. Each histogram corresponds to a CDF and consists of one full week of continuous testing for each component, approximately 150 components in all. The data was collected continuously and reduced using the rainflow algorithm discussed above, allowing for the collection over the longer period of time. Strain data was not collected at Wyoming Road over I-94 due to equipment security reasons.

11.6.1 Bridge US-23/Huron River (23/HR)

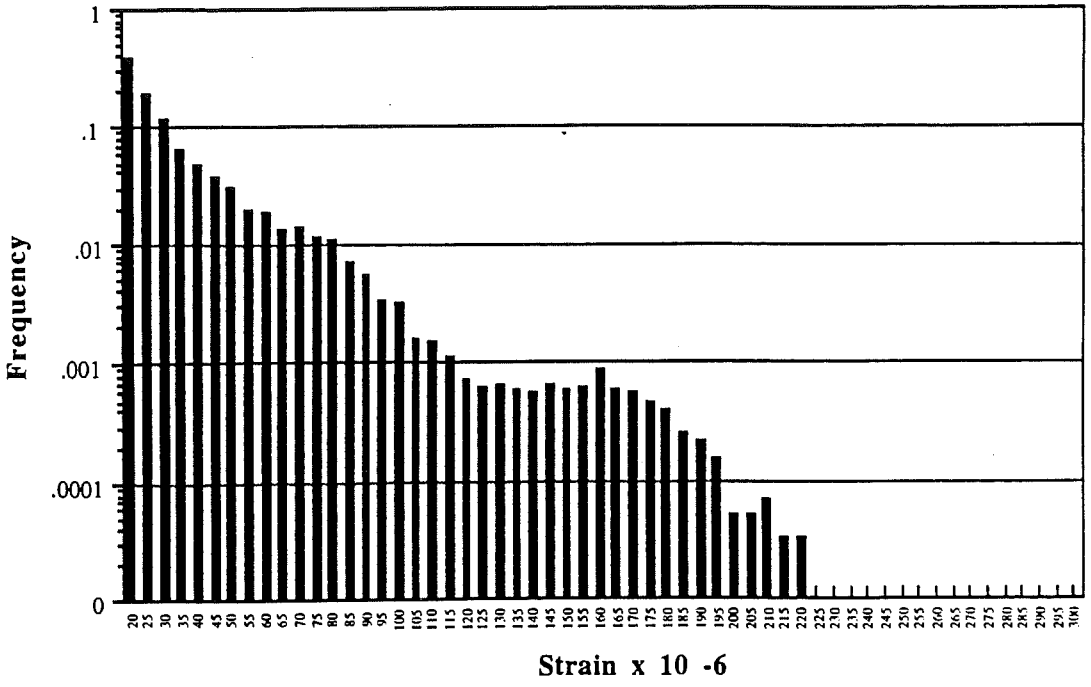

Fig. 11-6. Bridge 23/HR, Girder 1, Rainflow Strain Histogram.

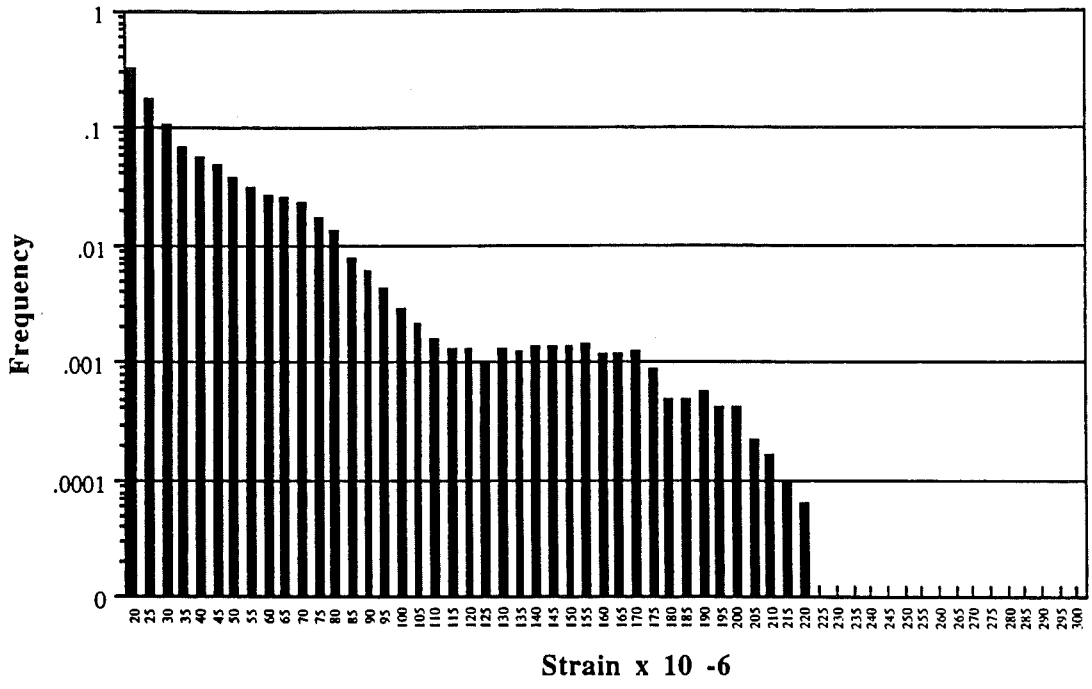

Fig. 11-7. Bridge 23/HR, Girder 2, Rainflow Strain Histogram.

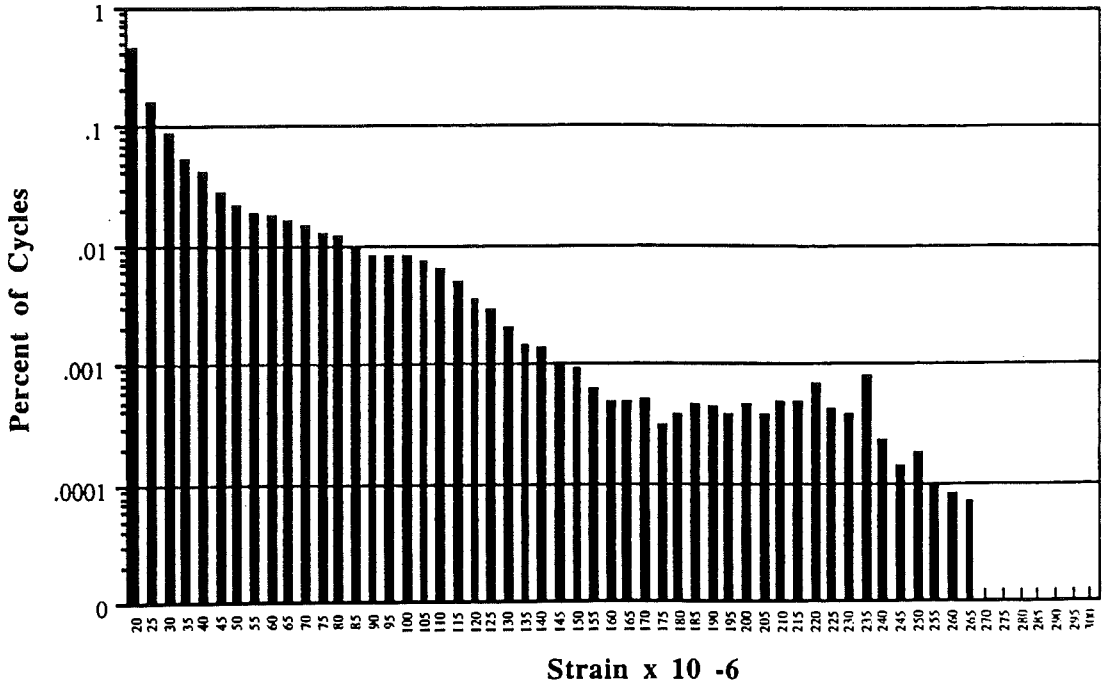

Fig. 11-8. Bridge 23/HR, Girder 3, Rainflow Strain Histogram.

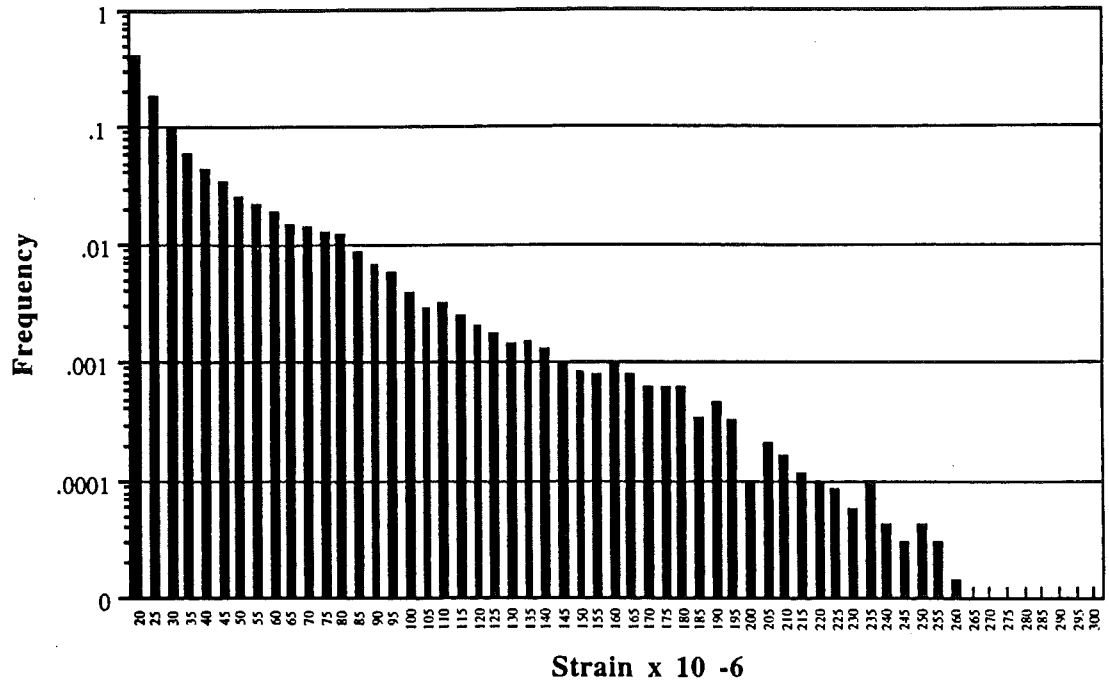

Fig. 11-9. Bridge 23/HR, Girder 4, Rainflow Strain Histogram.

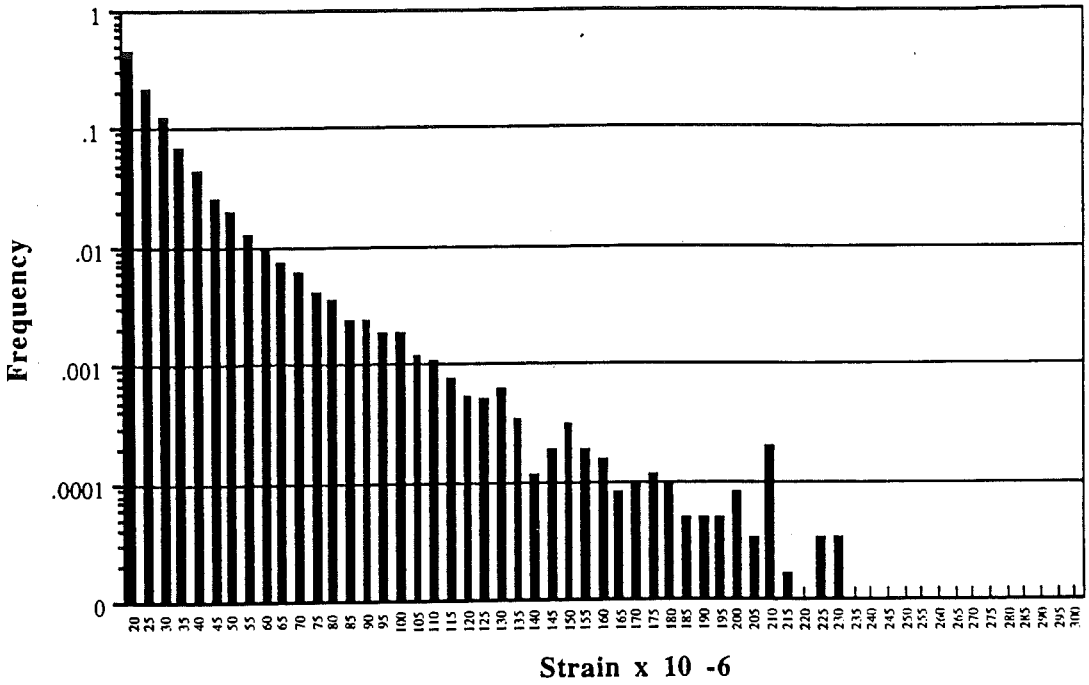

Fig. 11-10. Bridge 23/HR, Girder 5, Rainflow Strain Histogram.

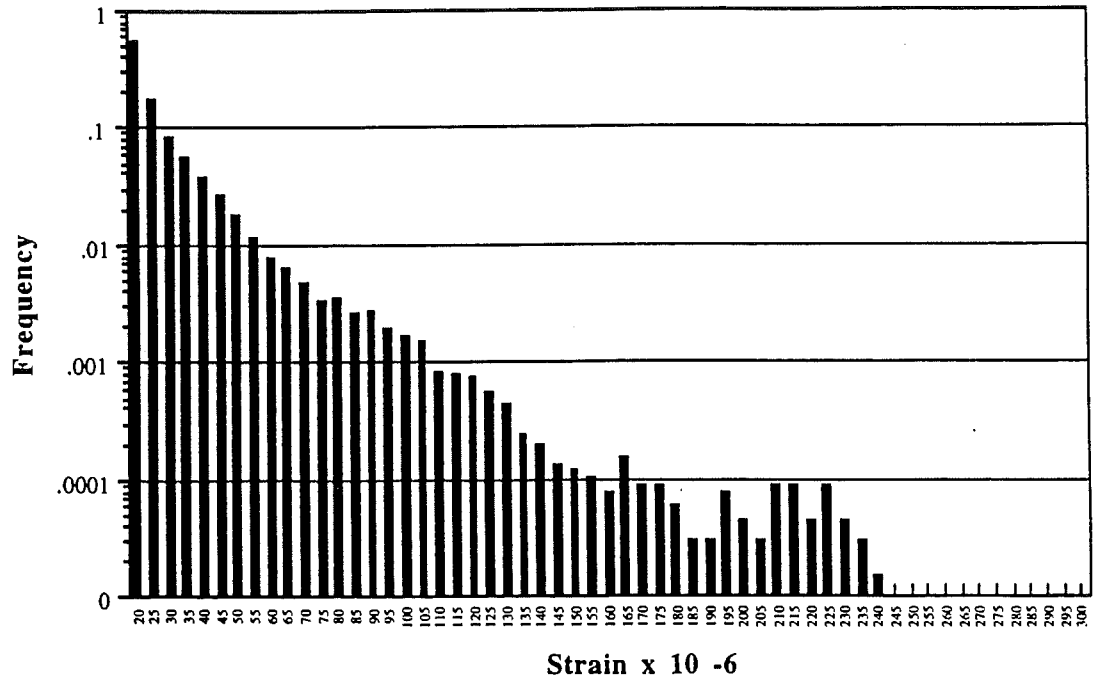

Fig. 11-11. Bridge 23/HR, Girder 6, Rainflow Strain Histogram.

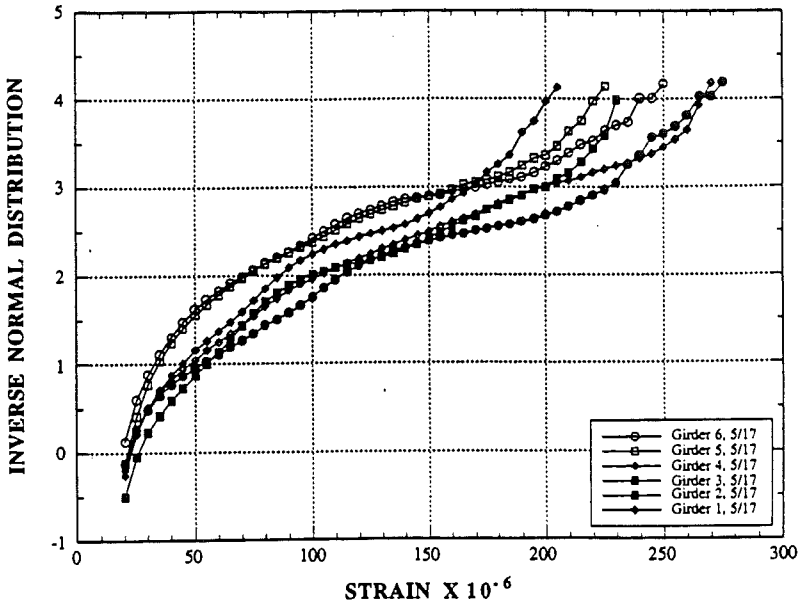

Fig. 11-12. Bridge 23/HR, NB, Rainflow Strain CDFs for 5/17/93.

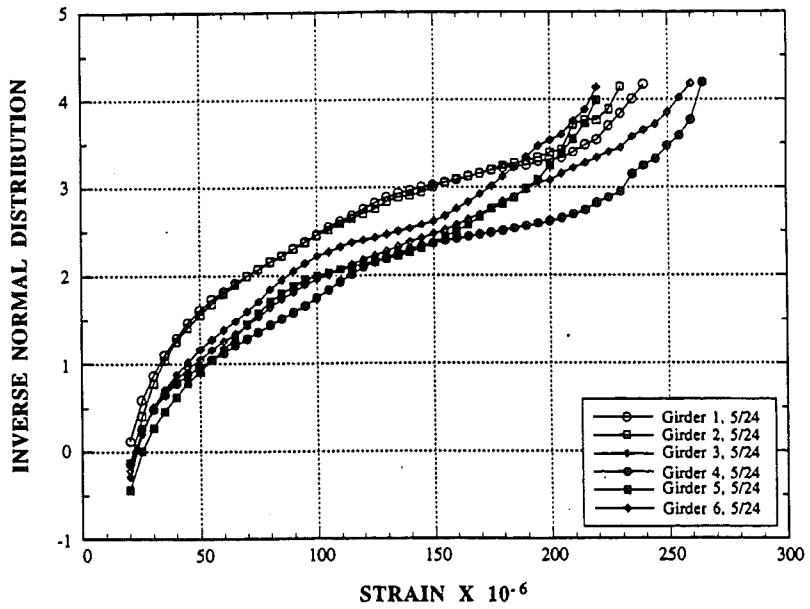

Fig. 11-13, Bridge US23/HR, NB, Rainflow Strain CDFs for 5/24/93.

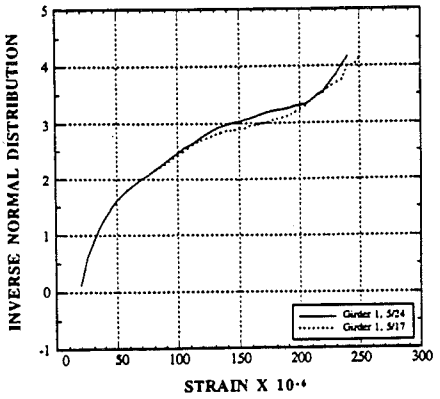

Fig. 11-14. 23/HR, G1.

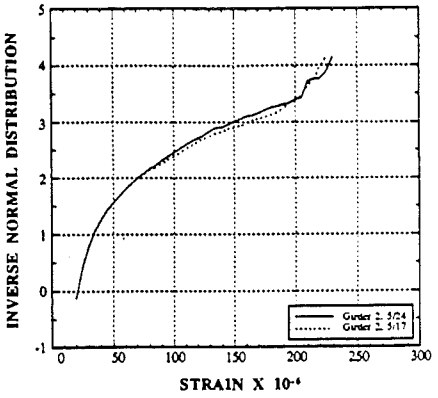

Fig. 11-15. 23/HR, G2.

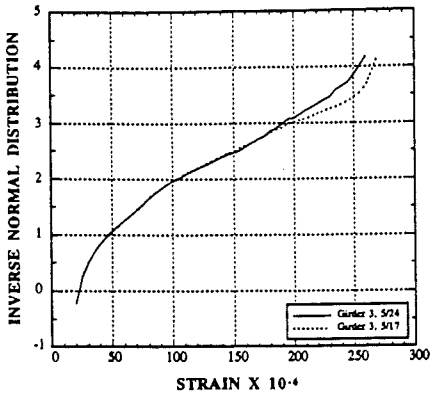

Fig. 11-16. 23/HR, G3.

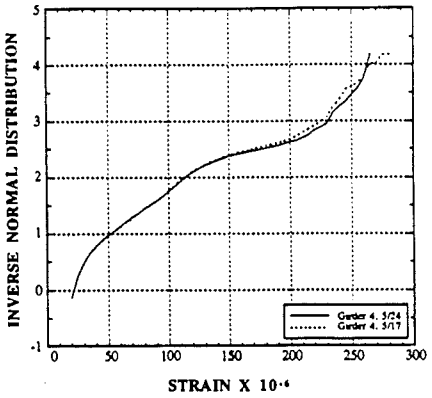

Fig. 11-17. US-23/HR, G4.

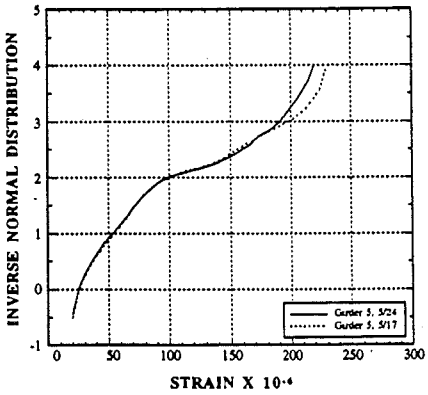

Fig. 11-18. US-23/HR, G5.

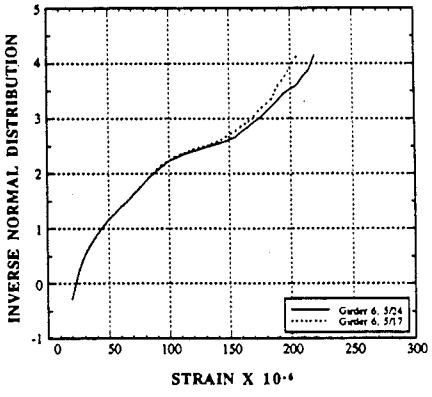

Fig. 11-19. US-23/HR, G10.

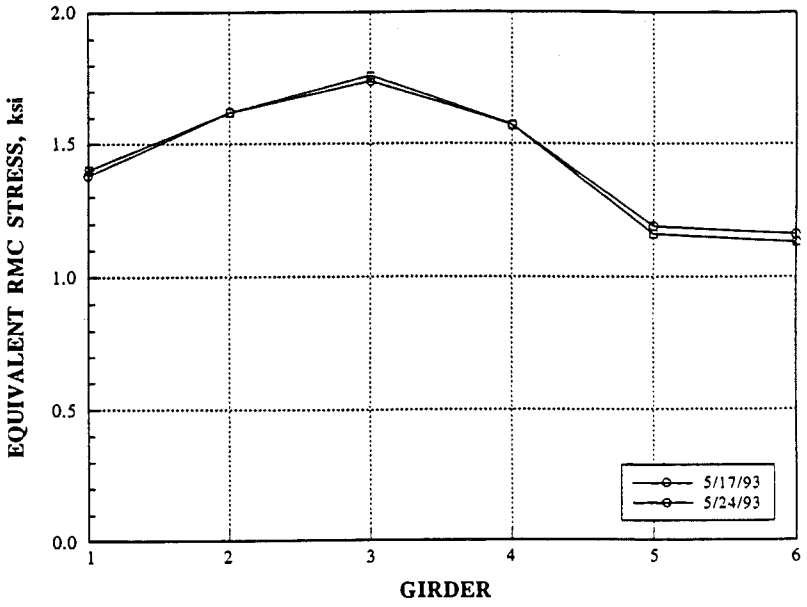

Fig. 11-20. 23/HR, NB, Equivalent RMC Stresses for Girders.

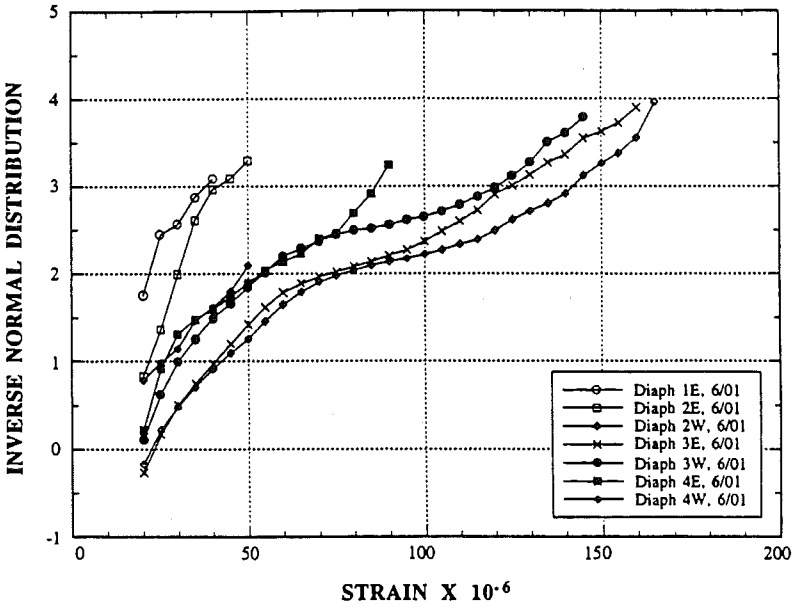

Fig. 11-21. 23/HR, NB, Strain Distribution for Diaphragms.

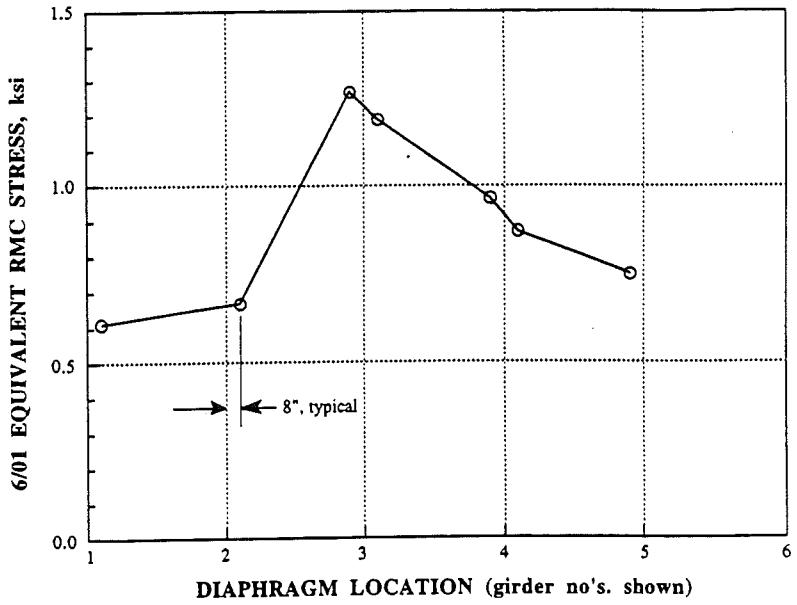

Fig. 11-22. 23/HR, NB, Equiv. RMC Stresses for Diaphragms.

11.6.2 Bridge US-23/Saline River (23/SR)

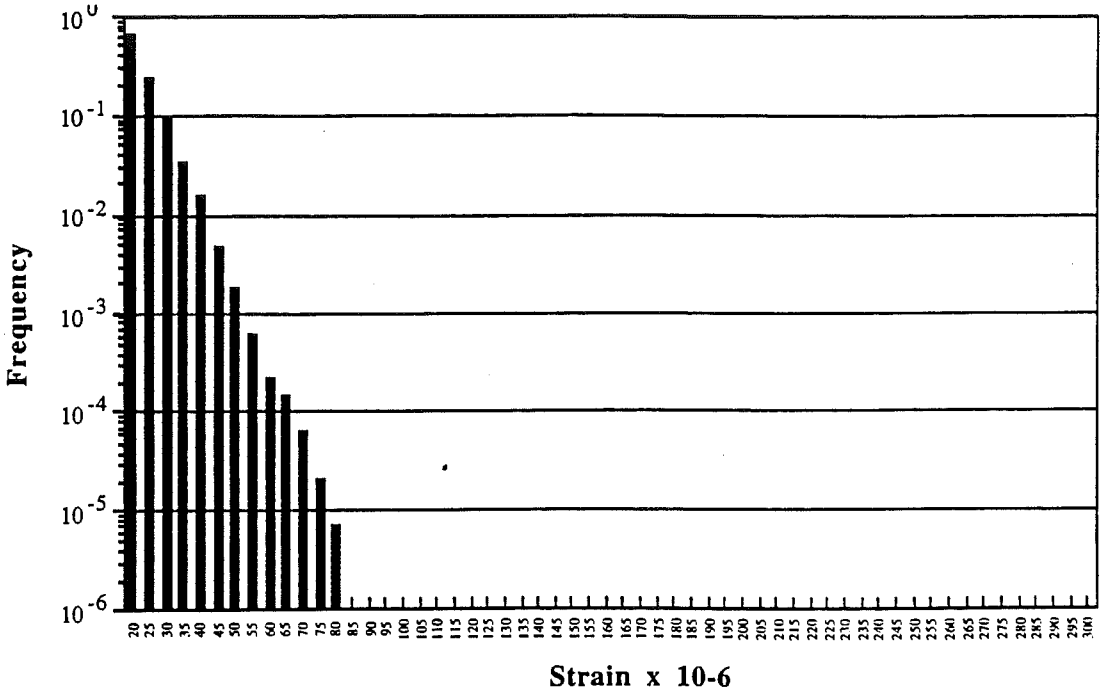

Fig. 11-23. Bridge 23/SR, Girder 1, Rainflow Strain Histogram.

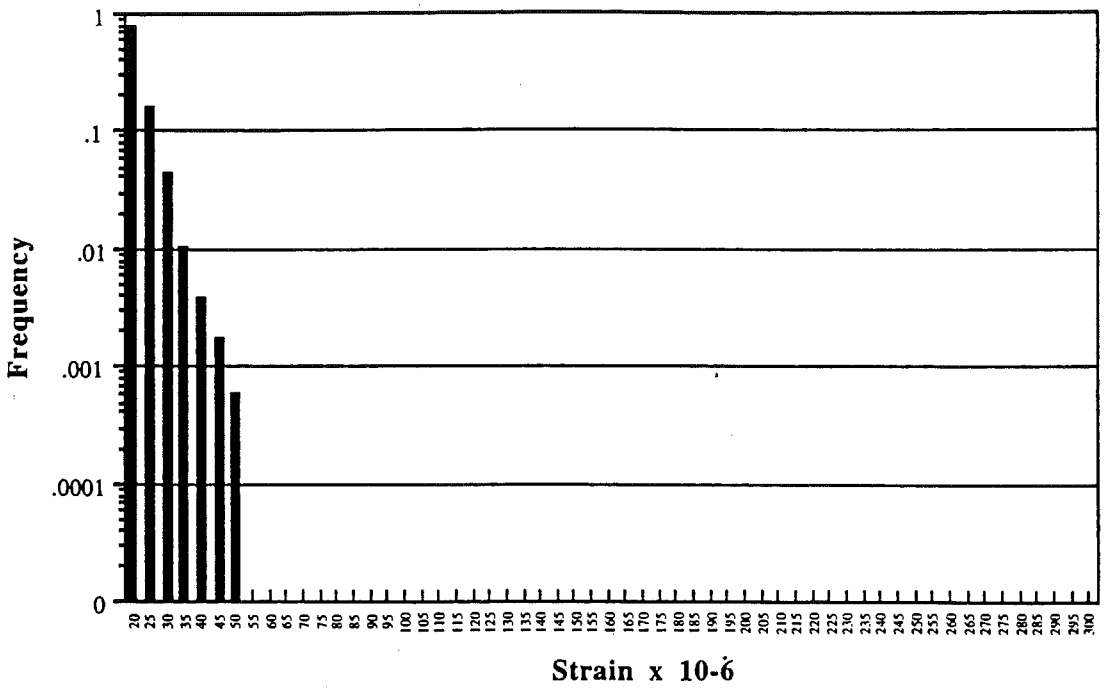

Fig. 11-24. Bridge 23/SR, Girder 2, Rainflow Strain Histogram.

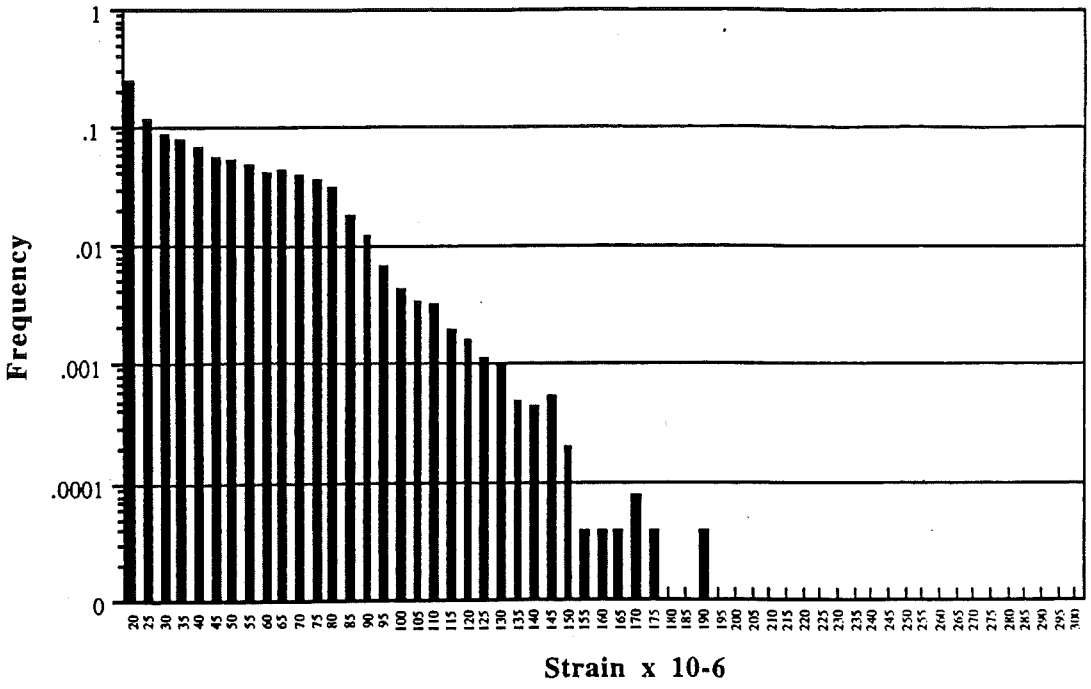

Fig. 11-25. Bridge 23/SR, Girder 3, Rainflow Strain Histogram.

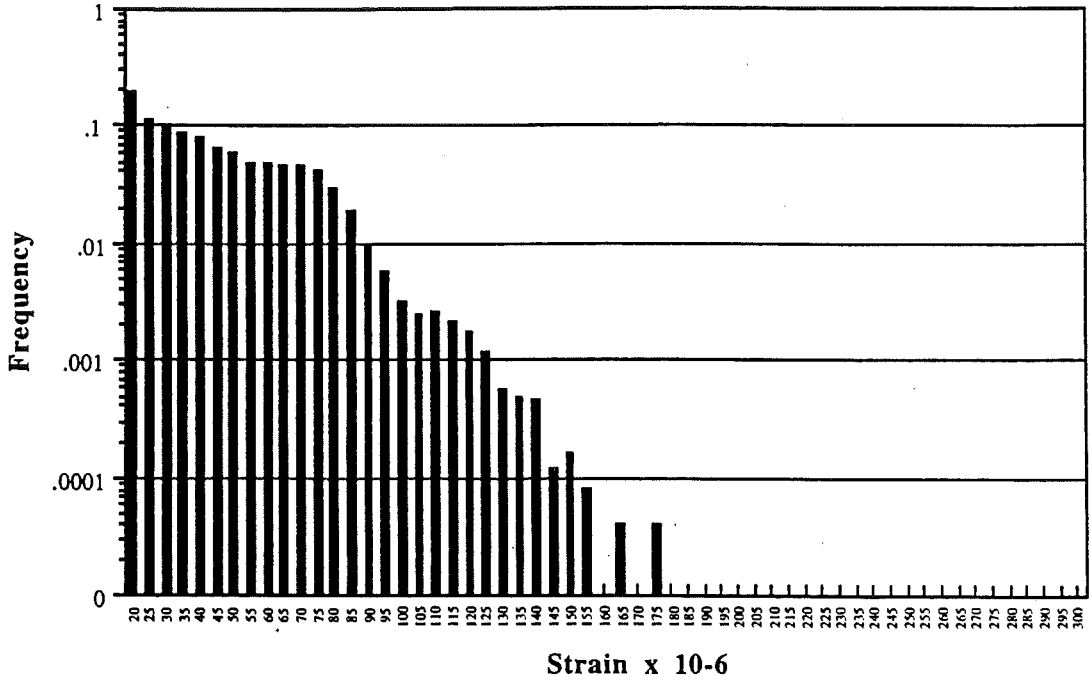

Fig. 11-26. Bridge 23/SR, Girder 4, Rainflow Strain Histogram.

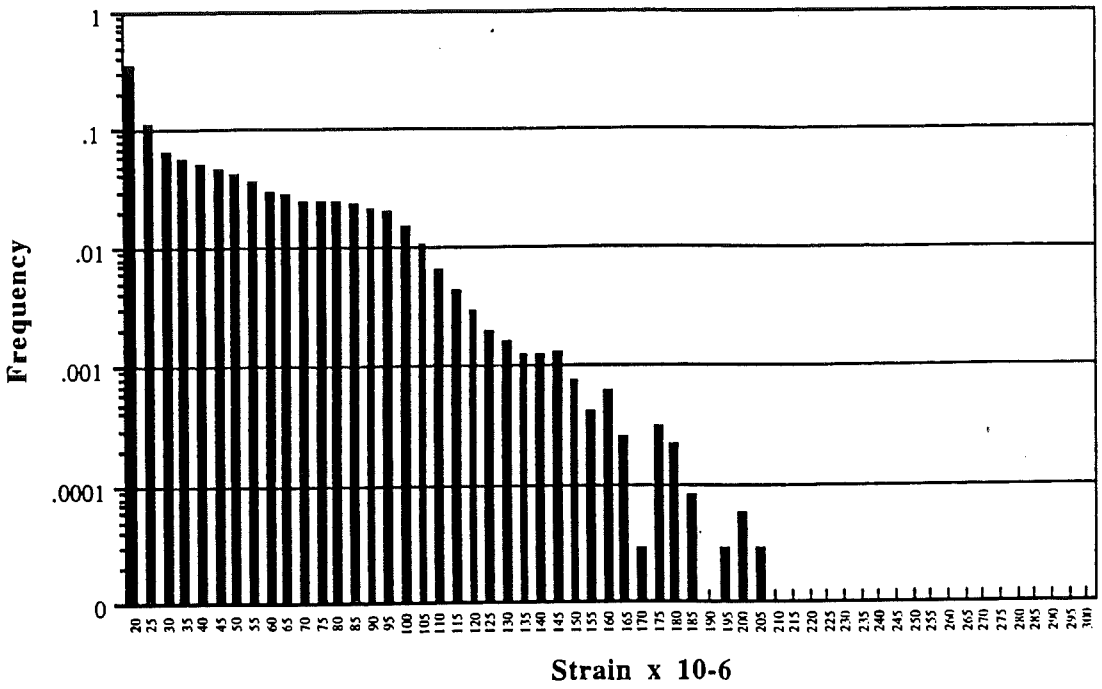

Fig. 11-27. Bridge 23/SR, Girder 5, Rainflow Strain Histogram.

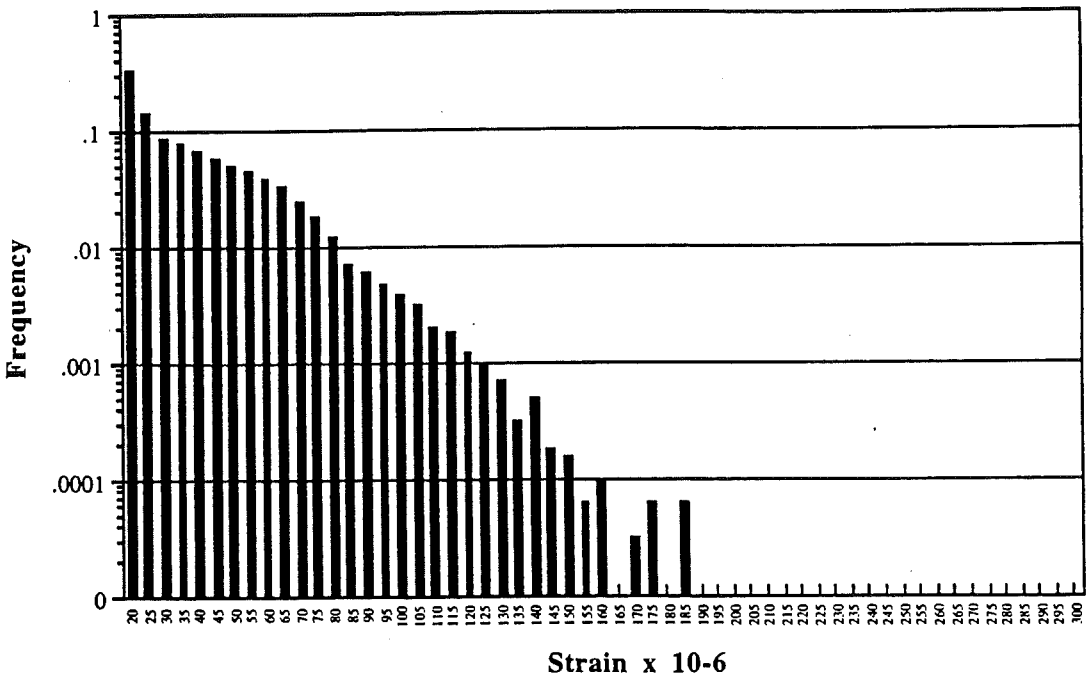

Fig. 11-28. Bridge 23/SR, Girder 6, Rainflow Strain Histogram.

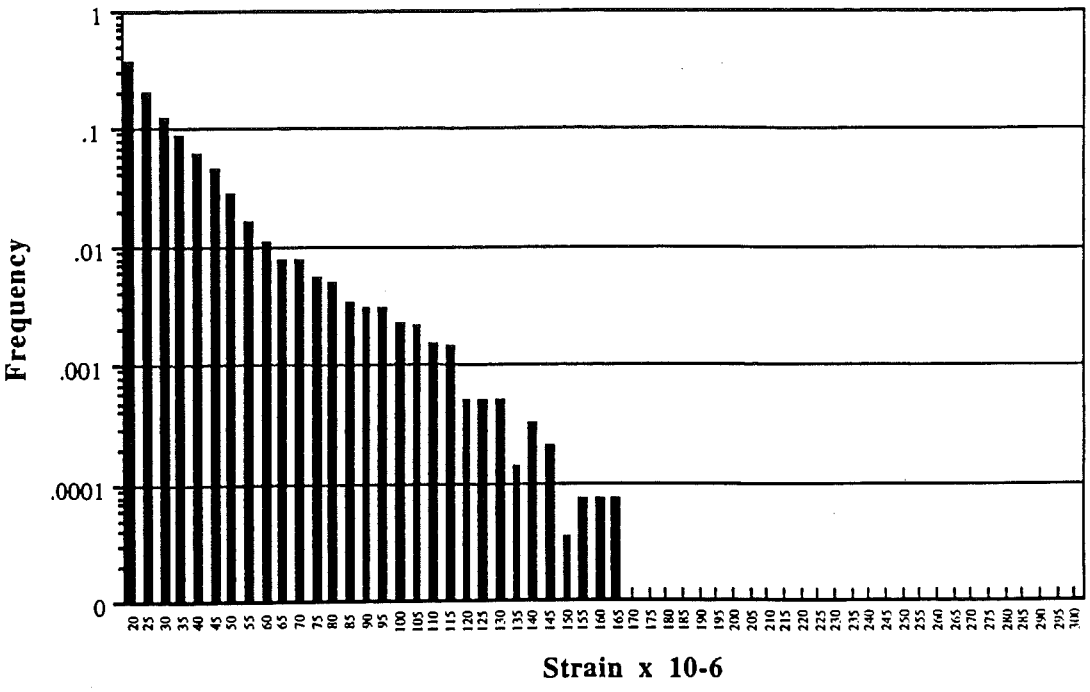

Fig. 11-29, Bridge 23/SR, ,Girder 7, Rainflow Strain Histogram.

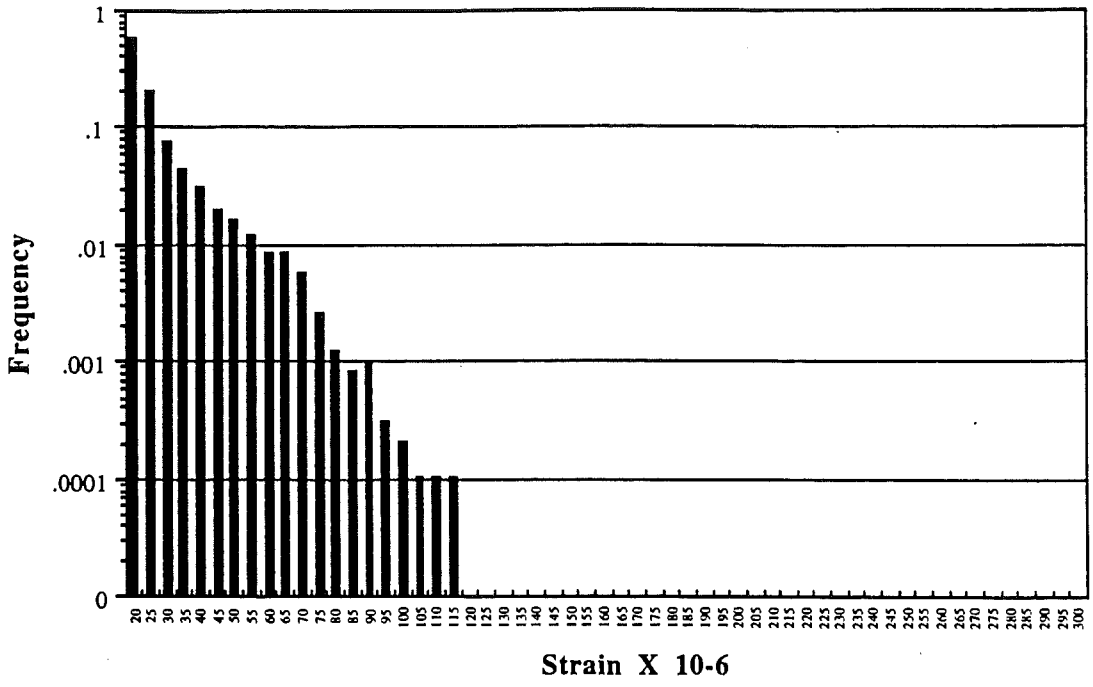

Fig. 11-30. Bridge 23/SR, Girder 8, Rainflow Strain Histogram.

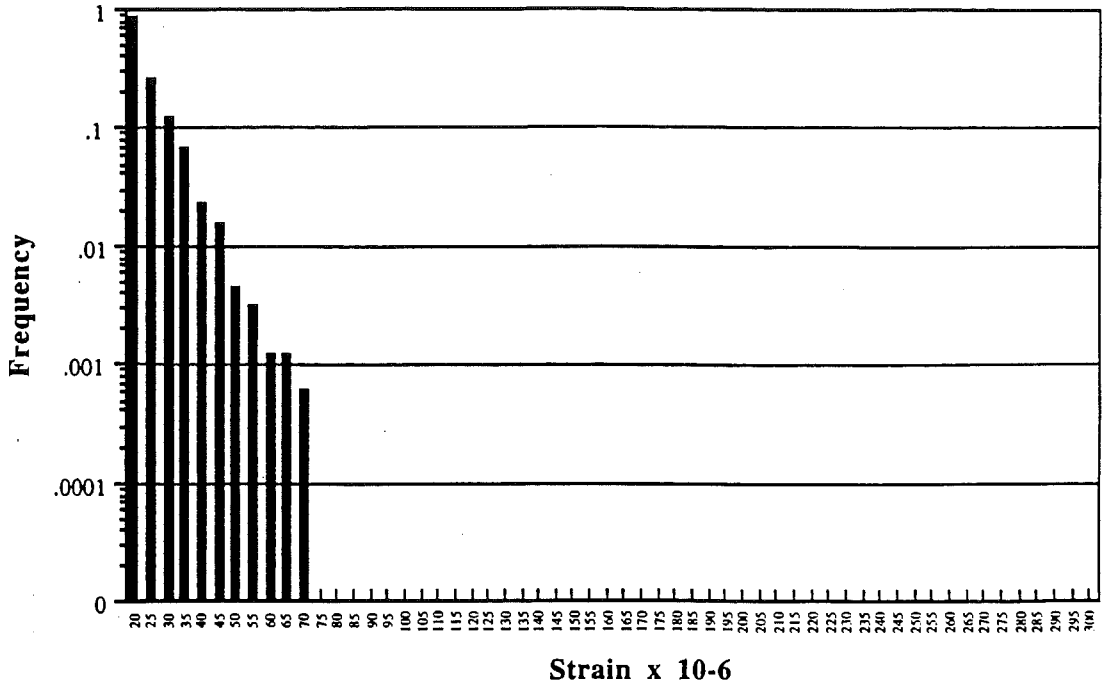

Fig. 11-31. Bridge 23/SR, Girder 9, Rainflow Strain Histogram.

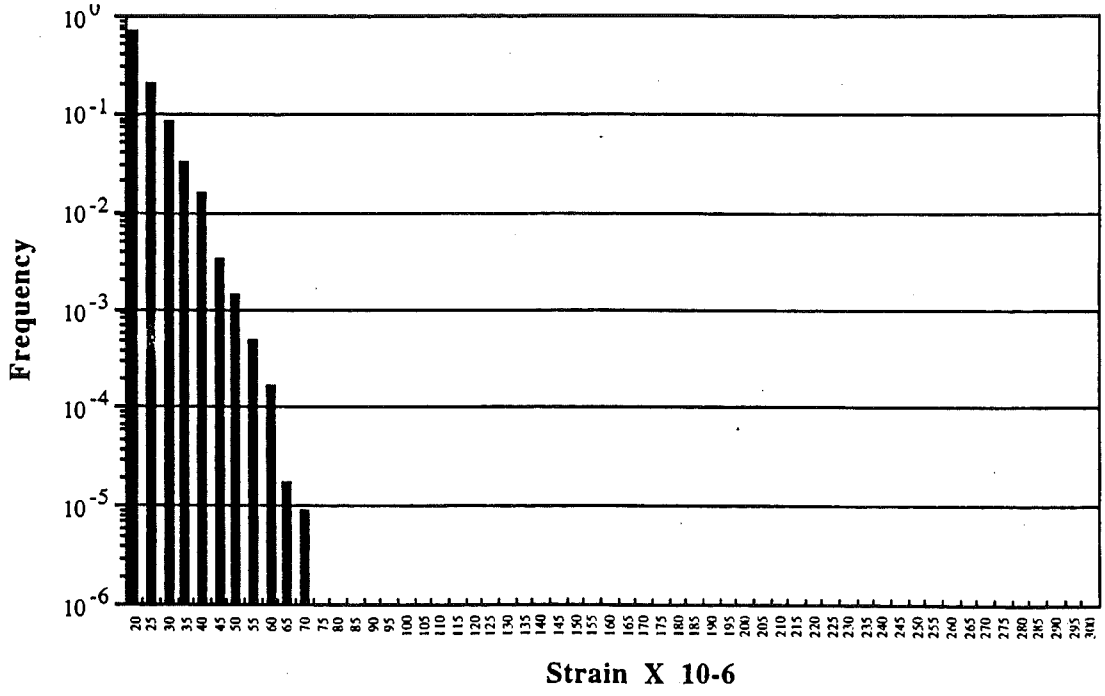

Fig. 11-32. US-23/SR, Girder 10, Rainflow Strain Histogram.

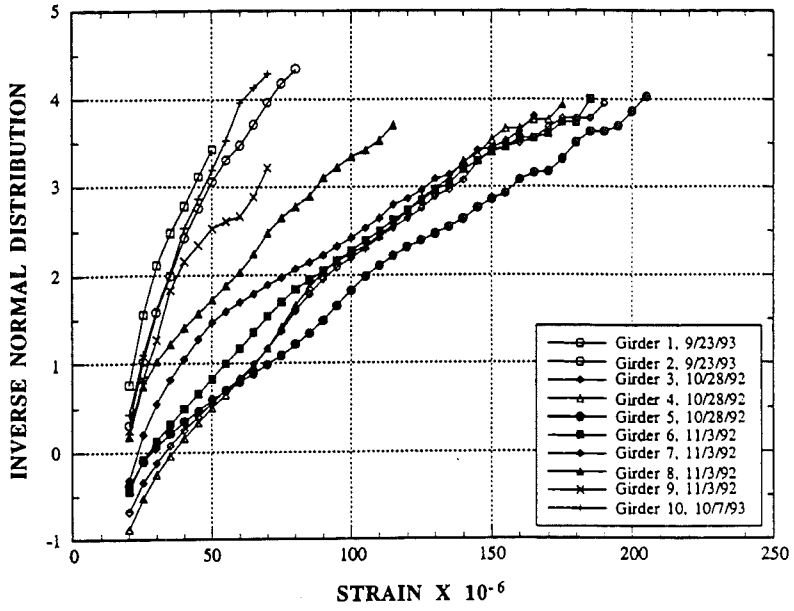

Fig. 11-33. 23/SR, SB, Rainflow Strain CDFs for Girders1 - 10.

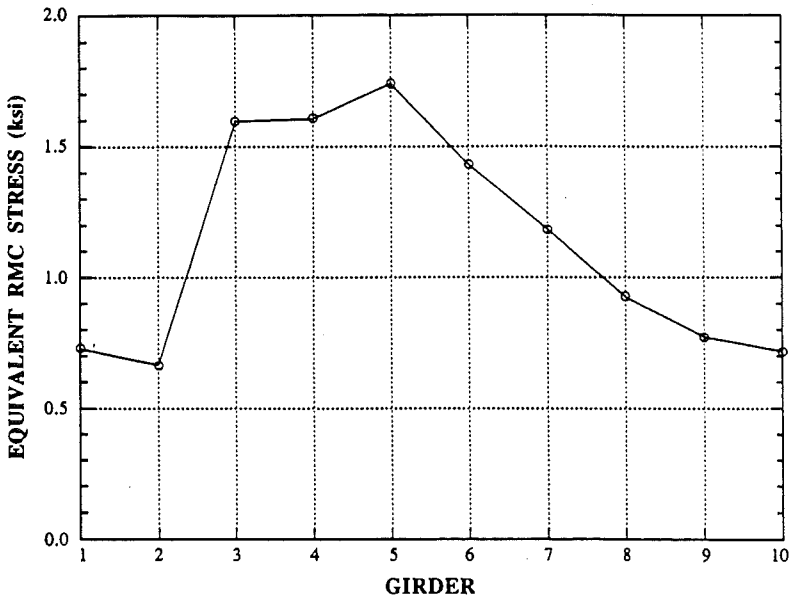

Fig. 11-34. 23/SR, SB, Equivalent RMC Stresses for Girders.

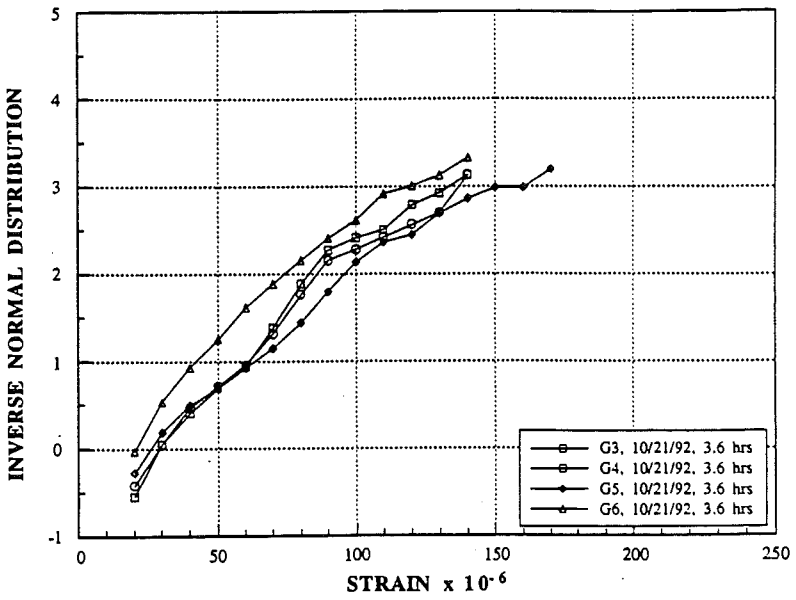

Fig. 11-35. 23/SR, Rainflow Strain CDF for Girders 3-6, 10/21/92.

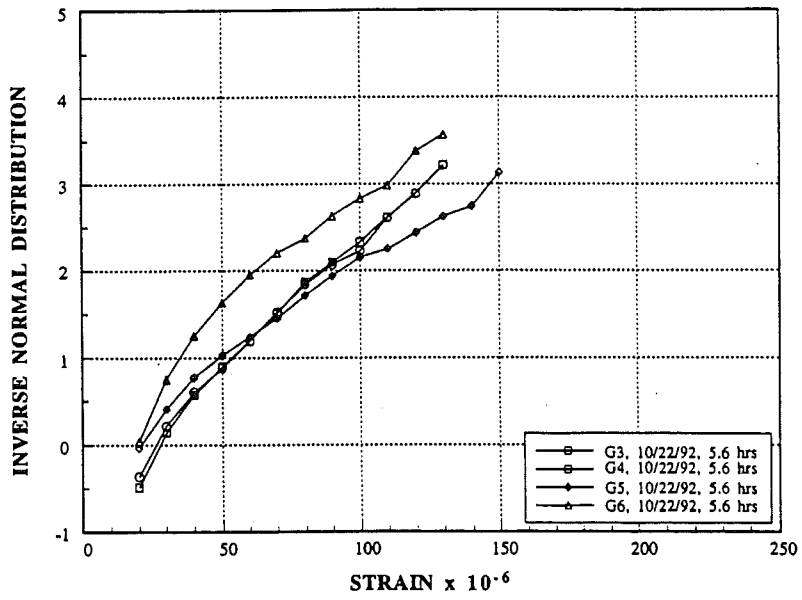

Fig. 11-36. 23/SR, Rainflow Strain CDF for Girders 3-6, 10/22/92.

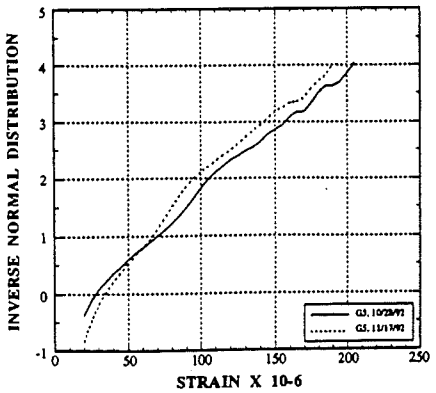

Fig. 11-37. 23/SR, G5.

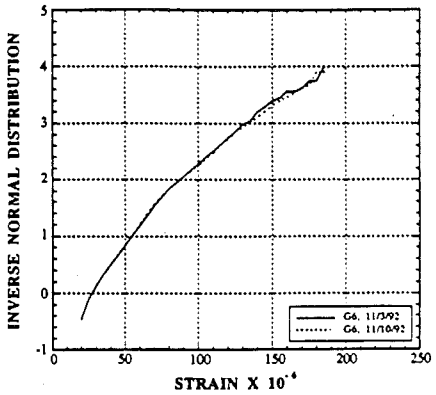

Fig. 11-38. 23/SR, G6.

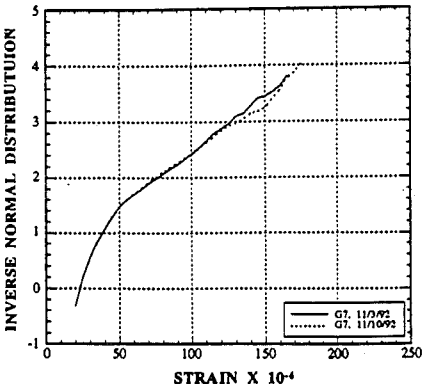

Fig. 11-39. 23/SR, G7.

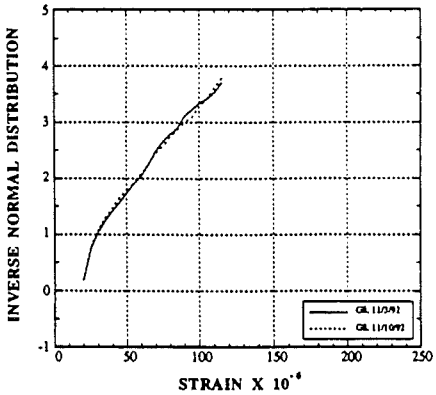

Fig. 11-40. 23/SR, G8.

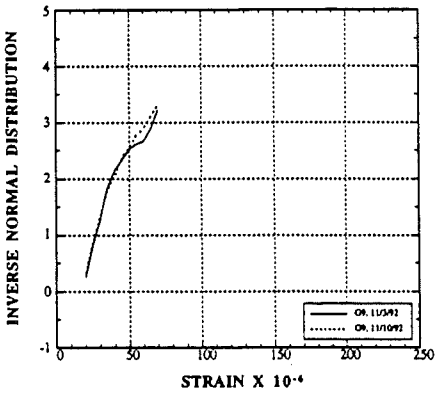

Fig. 11-41. 23/SR, Girder 9.

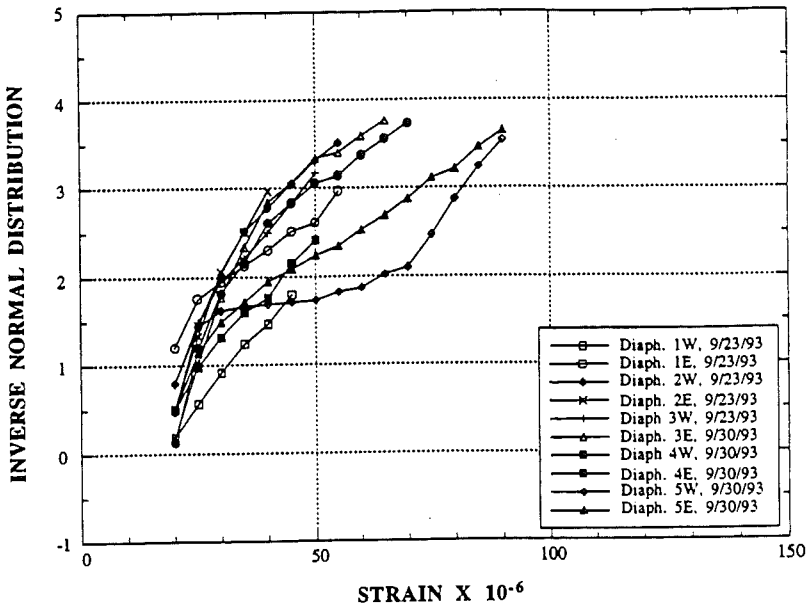

Fig. 11-42. 23/SR, Rainflow Strain CDF for Diaphragms 1 - 5.

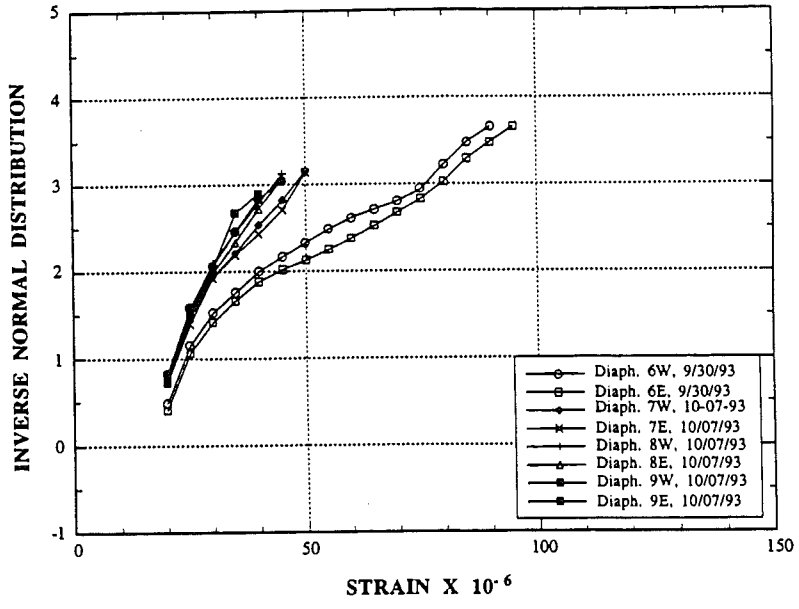

Fig. 11-43. 23/SR Rainflow Strain CDF's for Diaphragms 6 - 9.

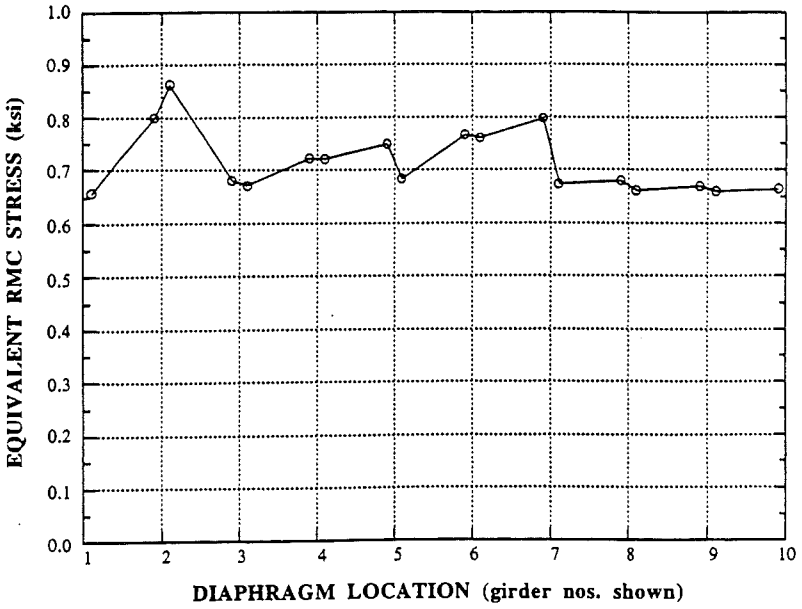

Fig. 11-44. 23/SR, SB, Equivalent RMC Stress for Diaphragms.

11.6.3 Bridge I-94/Jackson Road (94/JR)

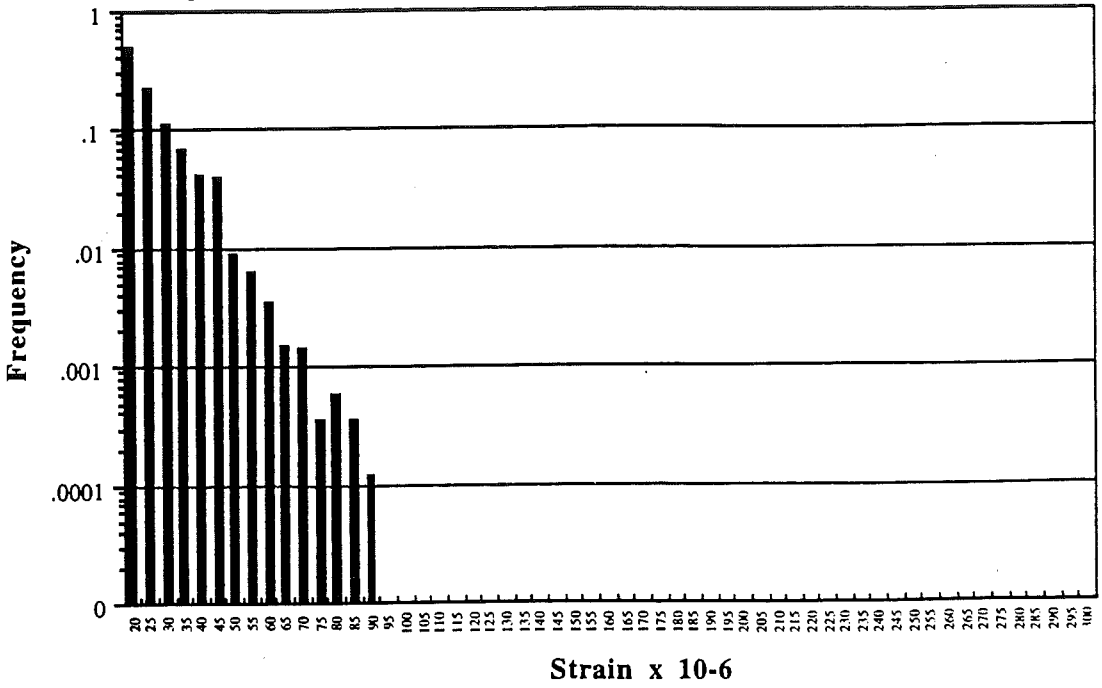

Fig. 11-45. Bridge 94/JR, WB, Girder 1, Rainflow Strain Histogram.

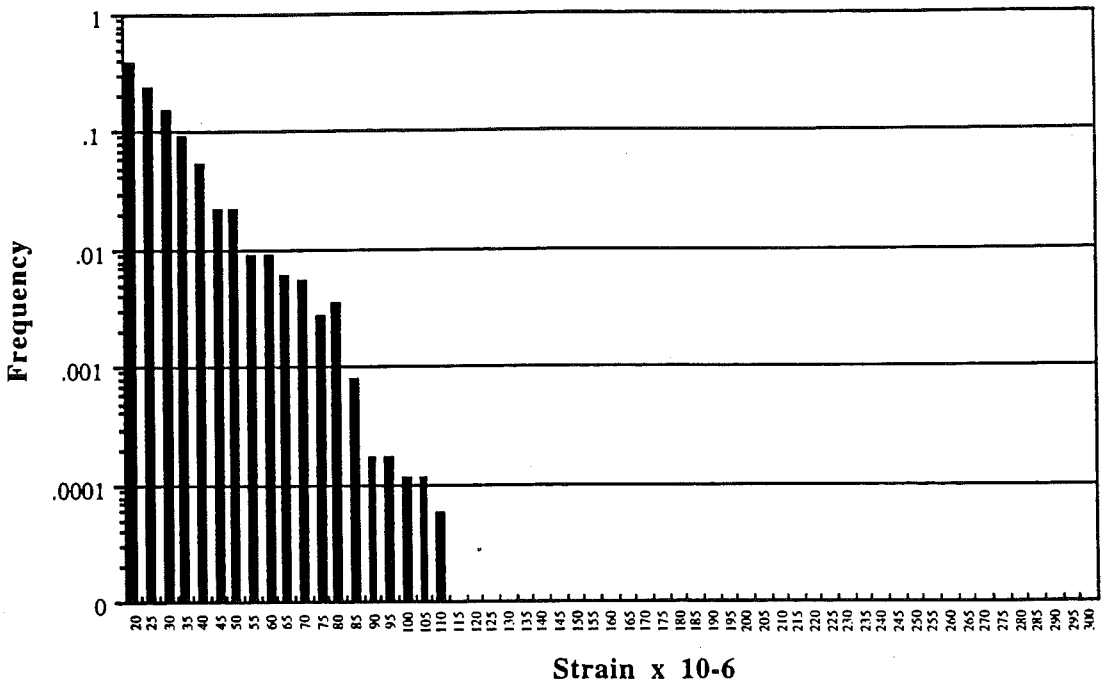

Fig. 11-46. Bridge 94/JR, WB ,Girder 2, Rainflow Strain Histogram.

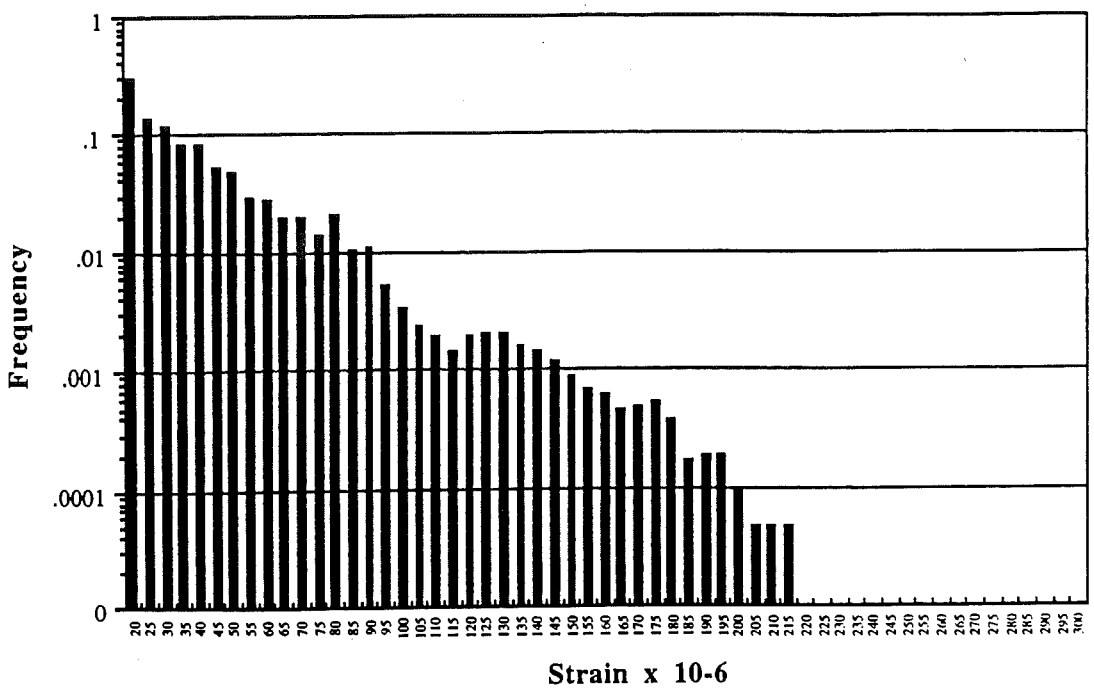

Fig. 11-47. Bridge 94/JR, WB, Girder 3, Rainflow Strain Histogram.

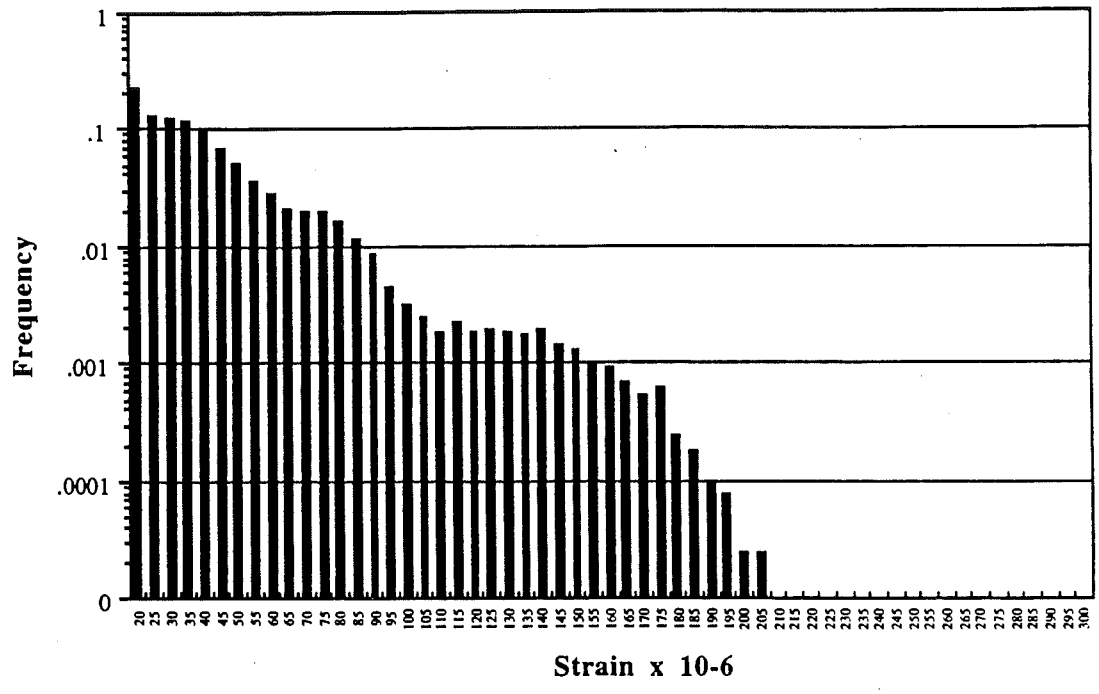

Fig. 11-48. Bridge 94/JR, WB, Girder 4, Rainflow Strain Histogram.

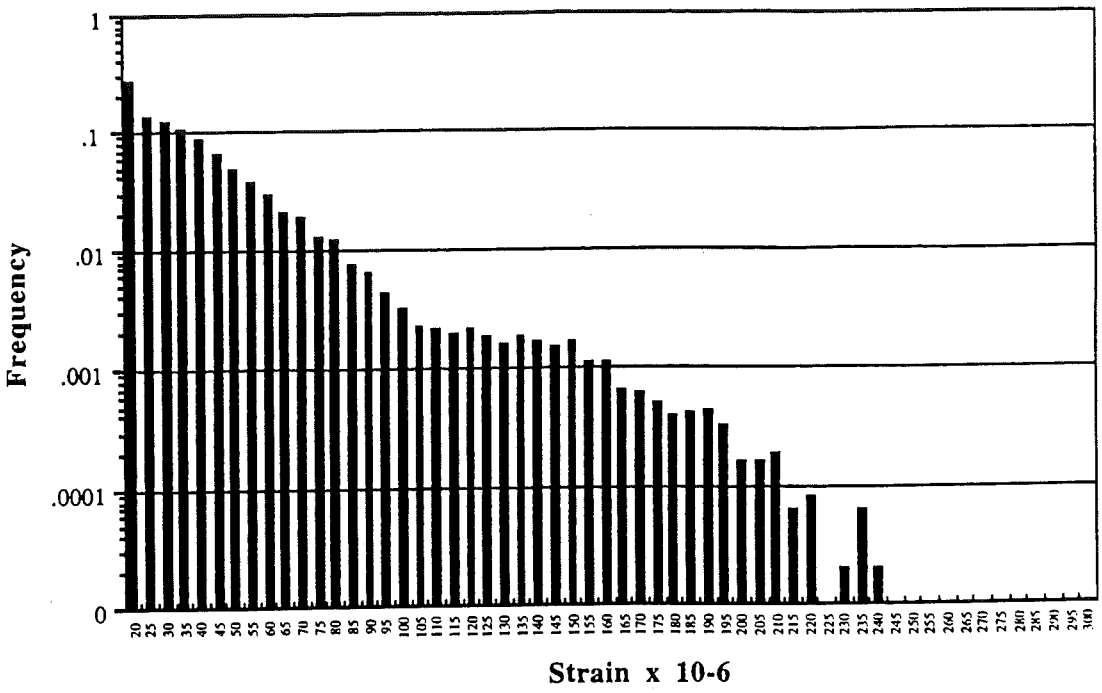

Fig. 11-49. Bridge 94/JR, WB, Girder 5, Rainflow Strain Histogram.

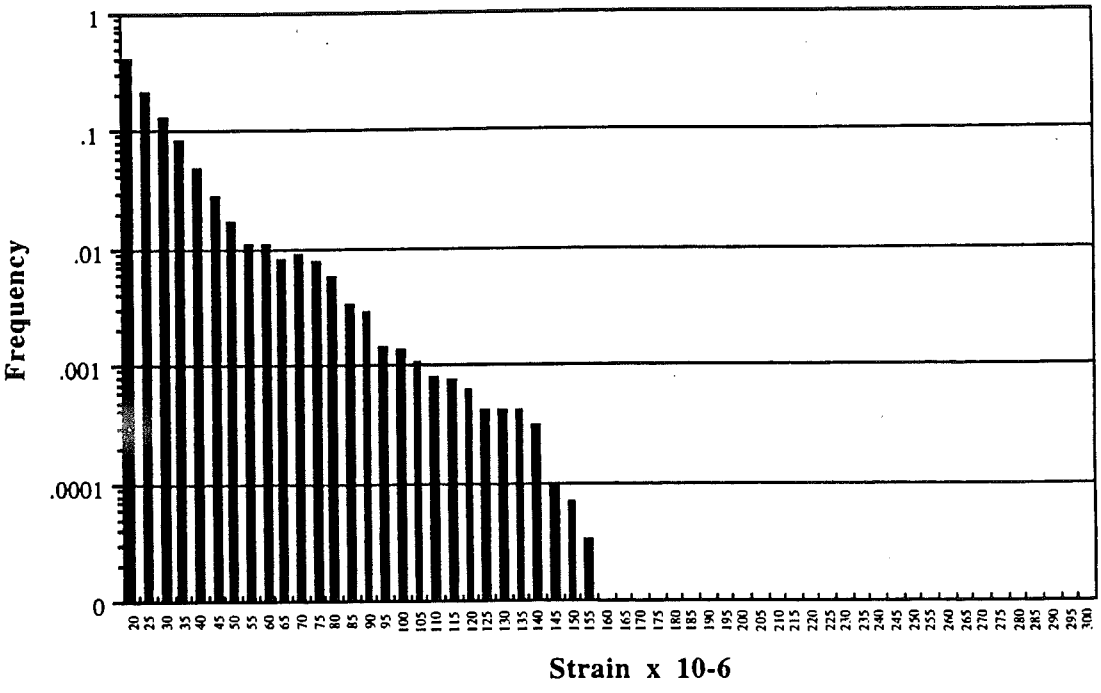

Fig. 11-50. Bridge 94/JR, WB, Girder 6, Rainflow Strain Histogram.

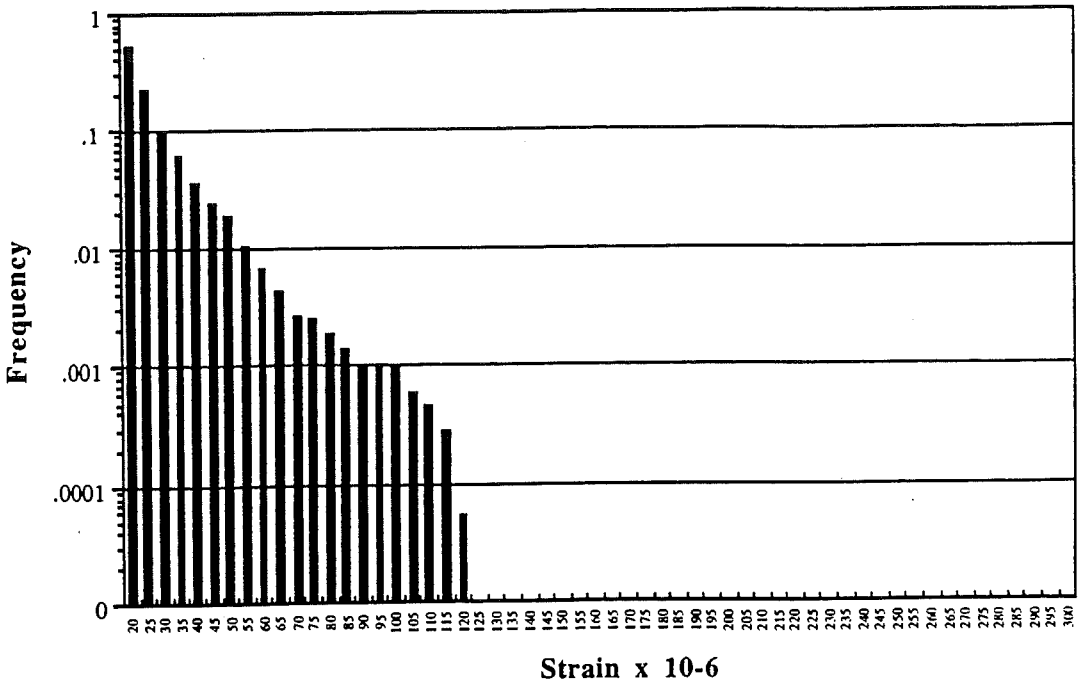

Fig. 11-51. Bridge 94/JR, WB, Girder 7, Rainflow Strain Histogram.

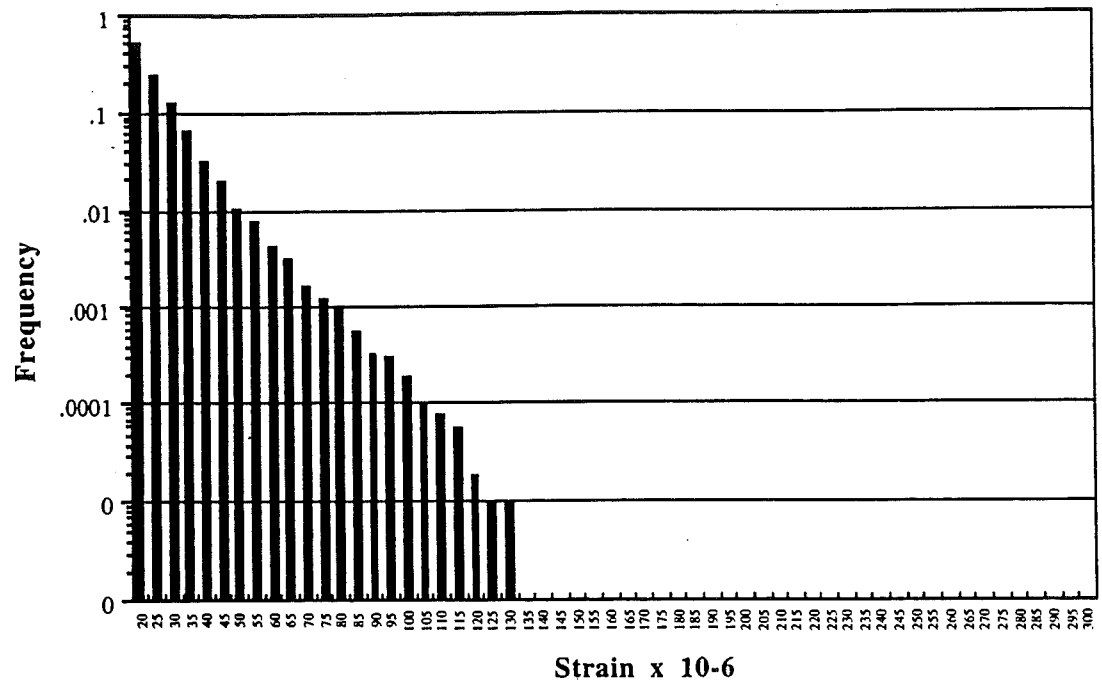

Fig. 11-52. Bridge 94/JR, WB, Girder 8, Rainflow Strain Histogram.

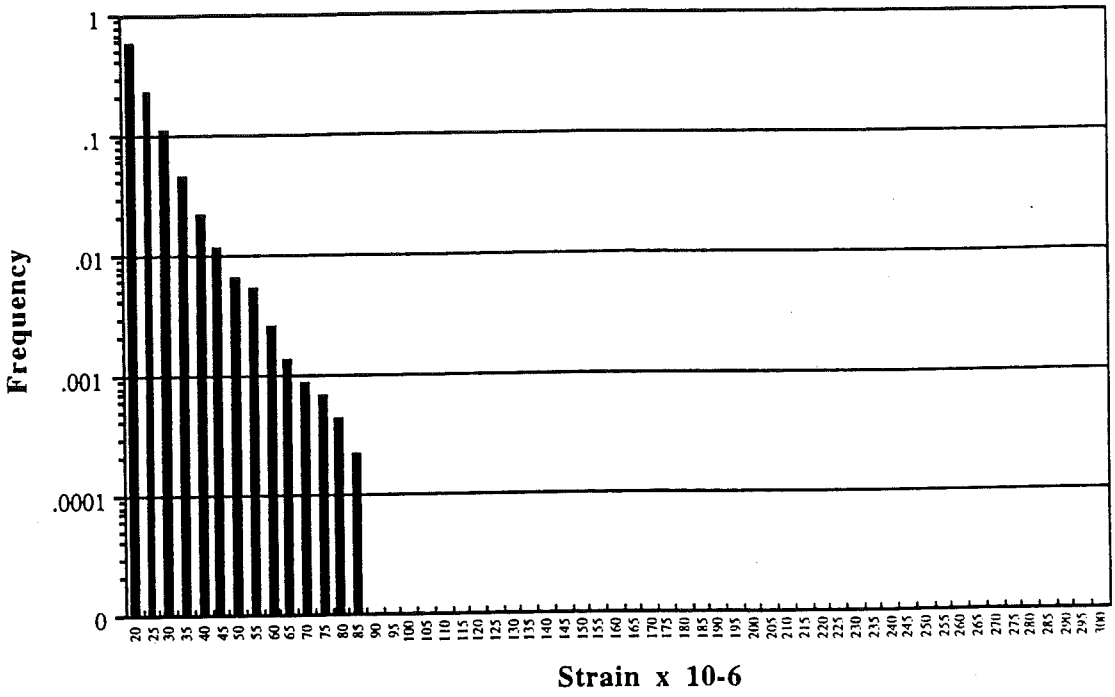

Fig. 11-53. Bridge 94/JR, WB, Girder 9, Rainflow Strain Histogram.

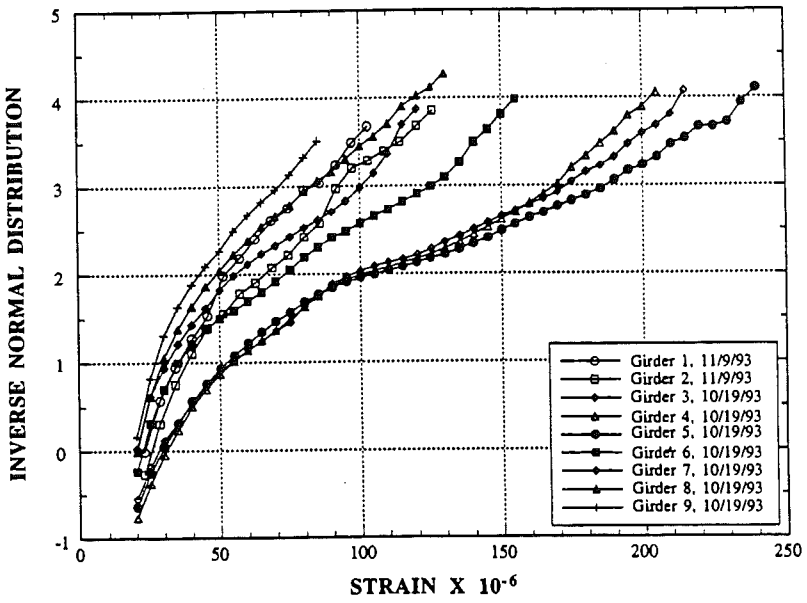

Fig. 11-54. Bridge 94/JR, WB, Rainflow Strain CDF for G1 - 9.

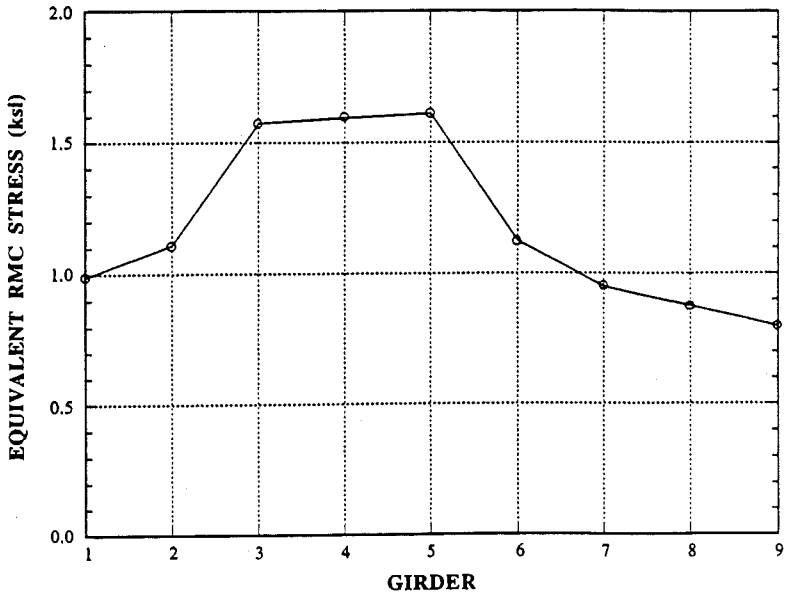

Fig. 11-55. 94/JR, Equivalent RMC Stresses for Girders.

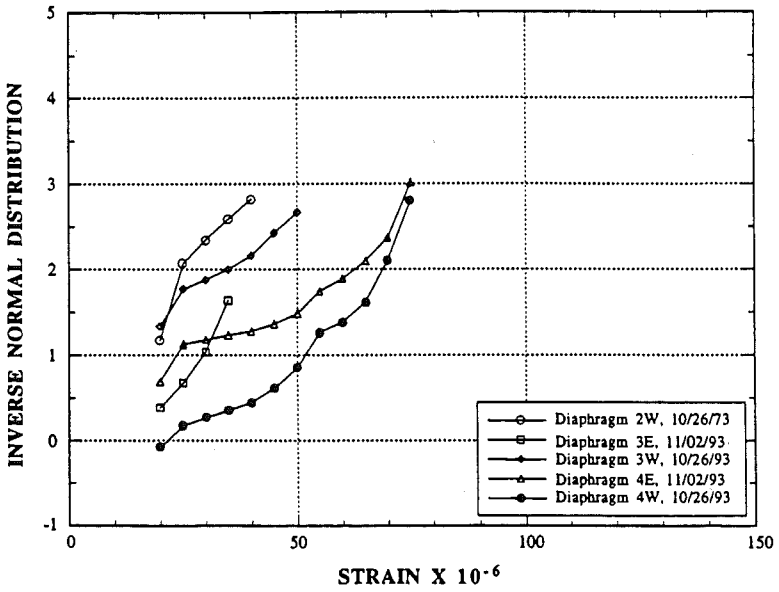

Fig. 11-56. 94/JR, Rainflow Strain CDF for Diaphragms 2 - 4.

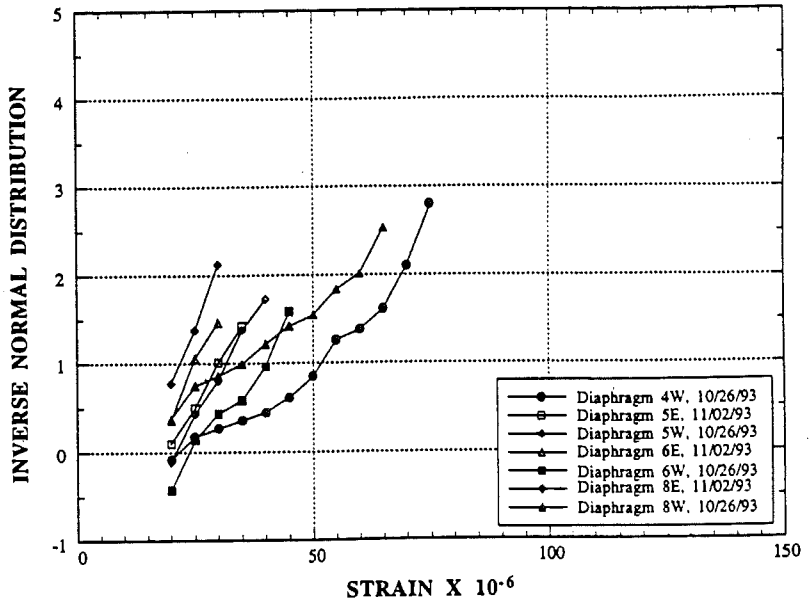

Fig. 11-57. 94/JR, Rainflow Strain CDF for Diaphragms 5 - 8.

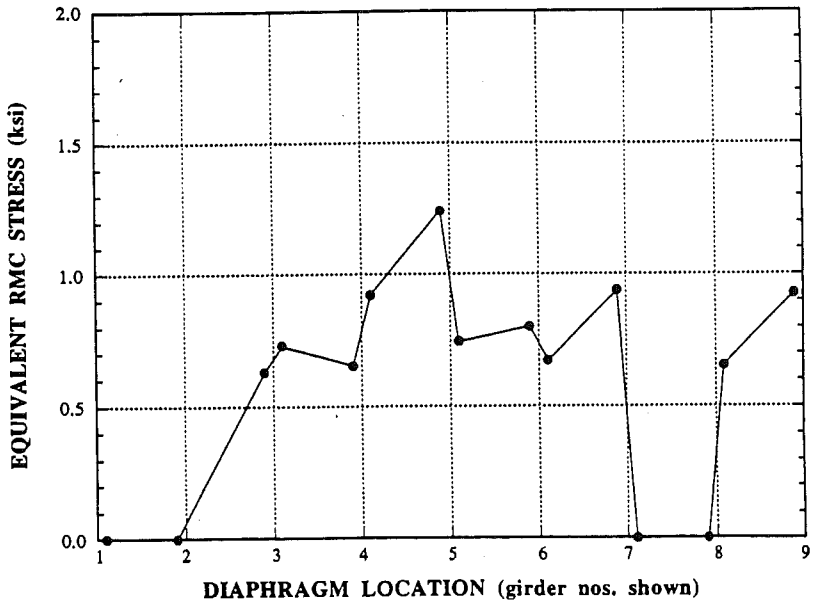

Fig. 11-58. 94/JR, Equivalent RMC Stresses for Diaphragms.

11.6.4 Bridge I-94 over Pierce Road in Grass Lake (94/PR).

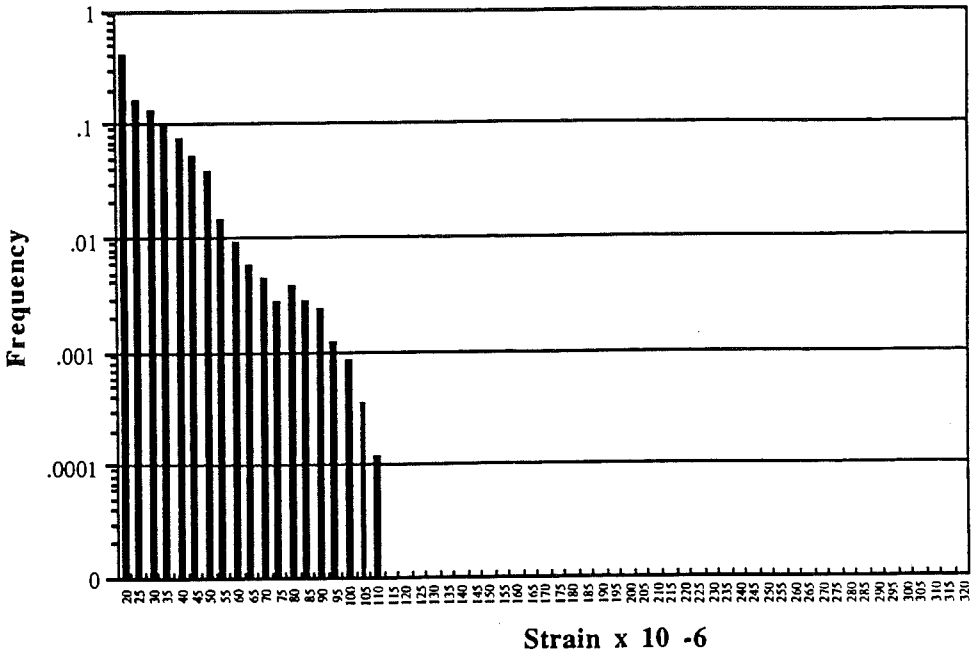

Fig. 11-59. Bridge 94/PR, EB, Girder 1, Rainflow Strain Histogram.

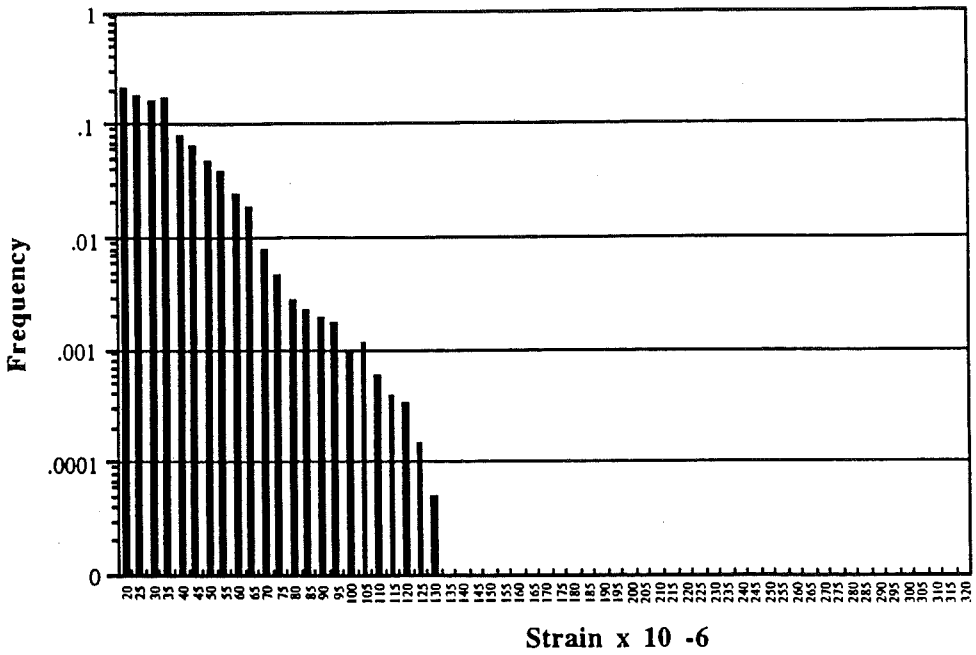

Fig. 11-60. Bridge. 94/PR, EB, Girder 2, Rainflow Strain Histogram.

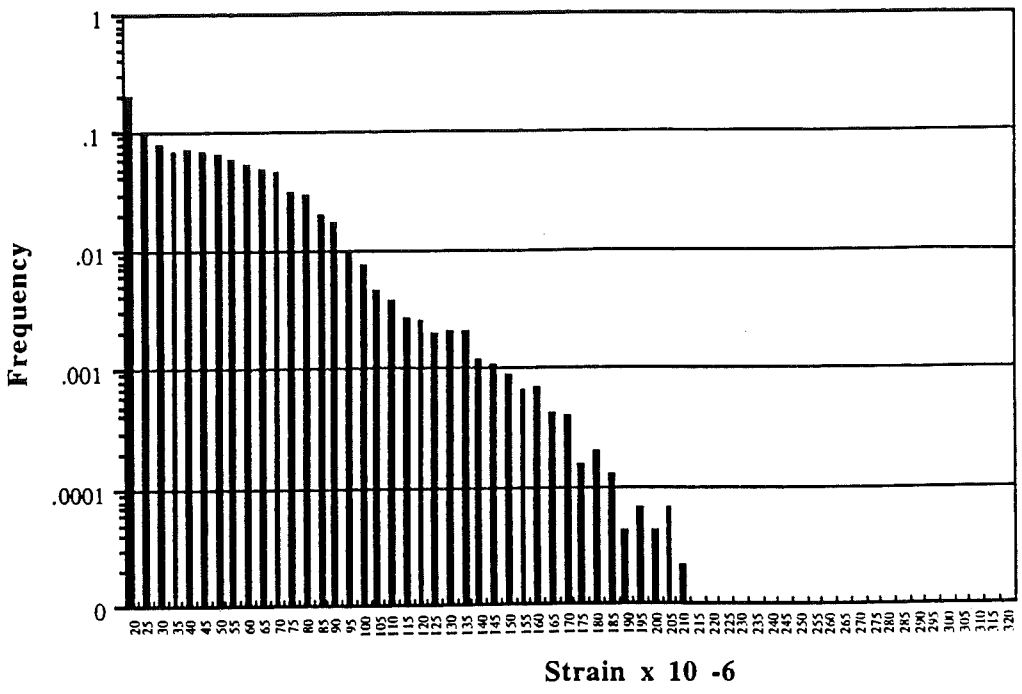

Fig. 11-61. Bridge 94/PR, EB Girder 3, Rainflow Strain Histogram.

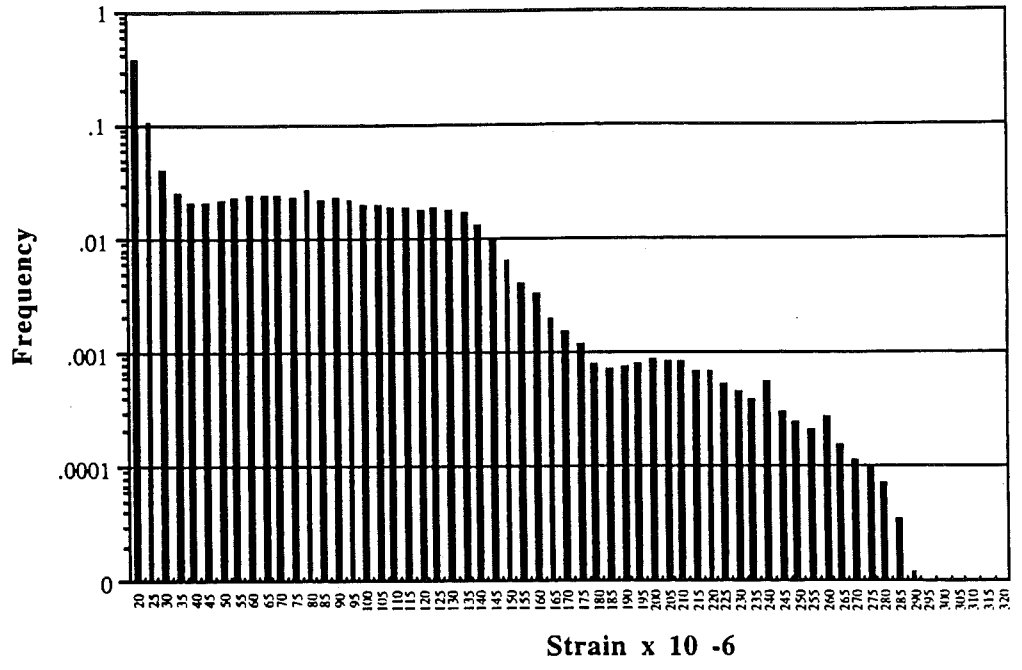

Fig. 11-62. Bridge 94/PR, EB, Girder 4, Rainflow Strain Histogram.

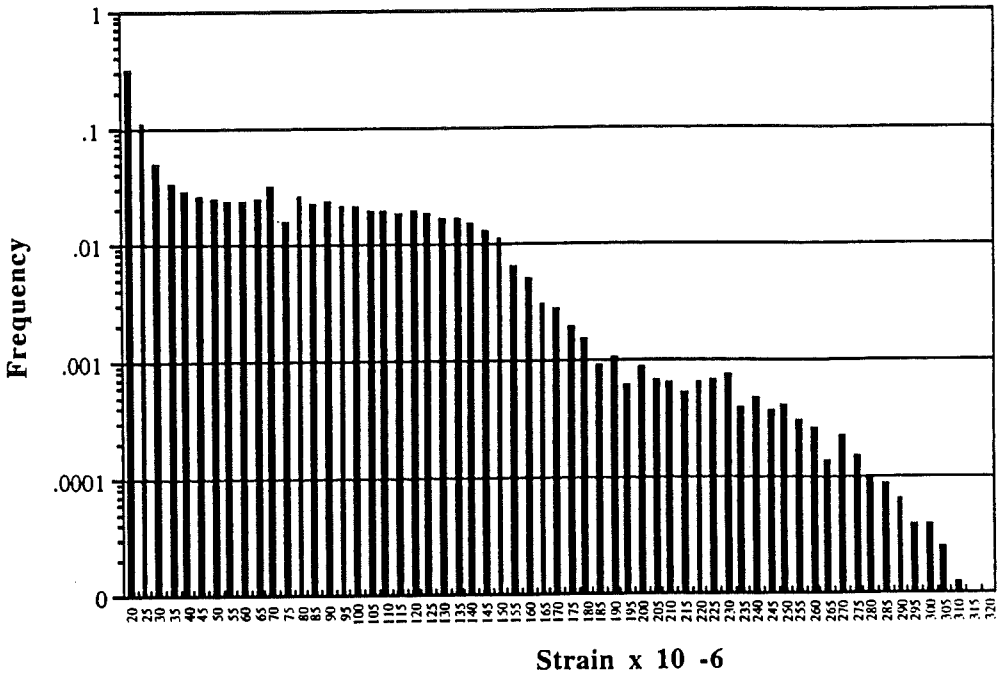

Fig. 11-63. 94/PR, EB, Girder 5, Rainflow Strain Histogram.

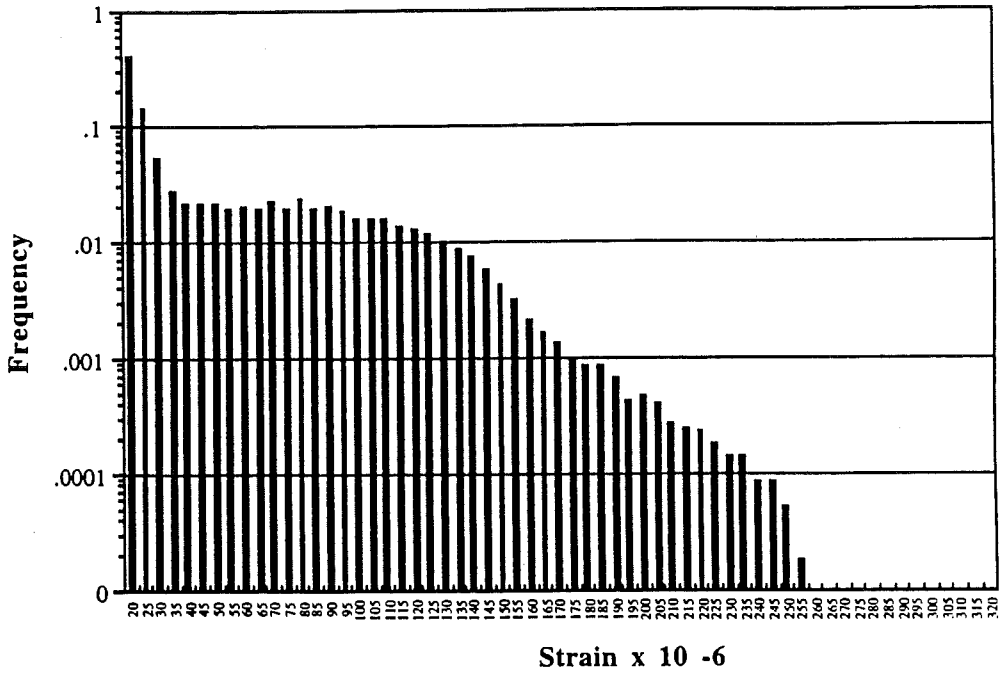

Fig. 11-64. Bridge 94/PR, EB, Girder 6, Rainflow Strain Histogram.

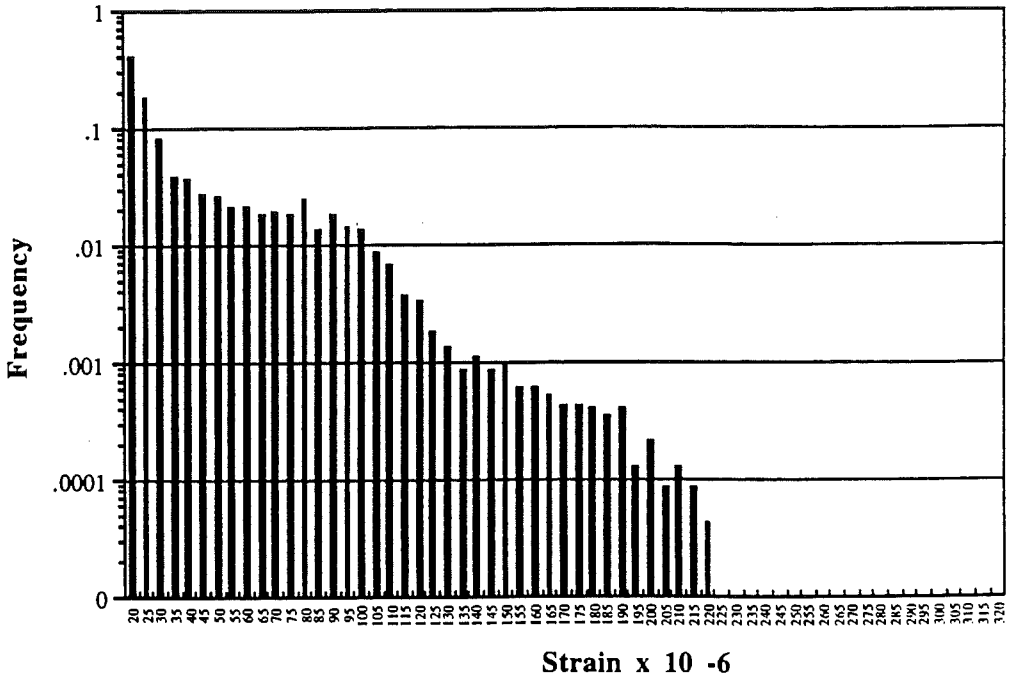

Fig. 11-65. Bridge 94/PR, EB, Girder 7 Rainflow Strain Histogram.

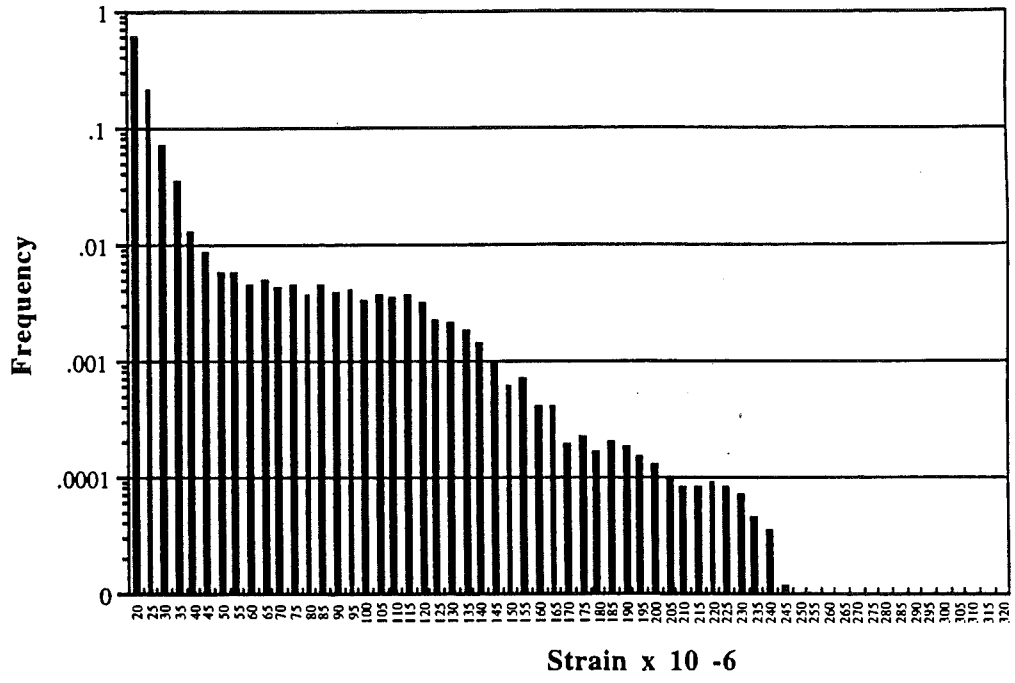

Fig. 11-66. Bridge 94/PR, EB, Girder 8, Rainflow Strain Histogram.

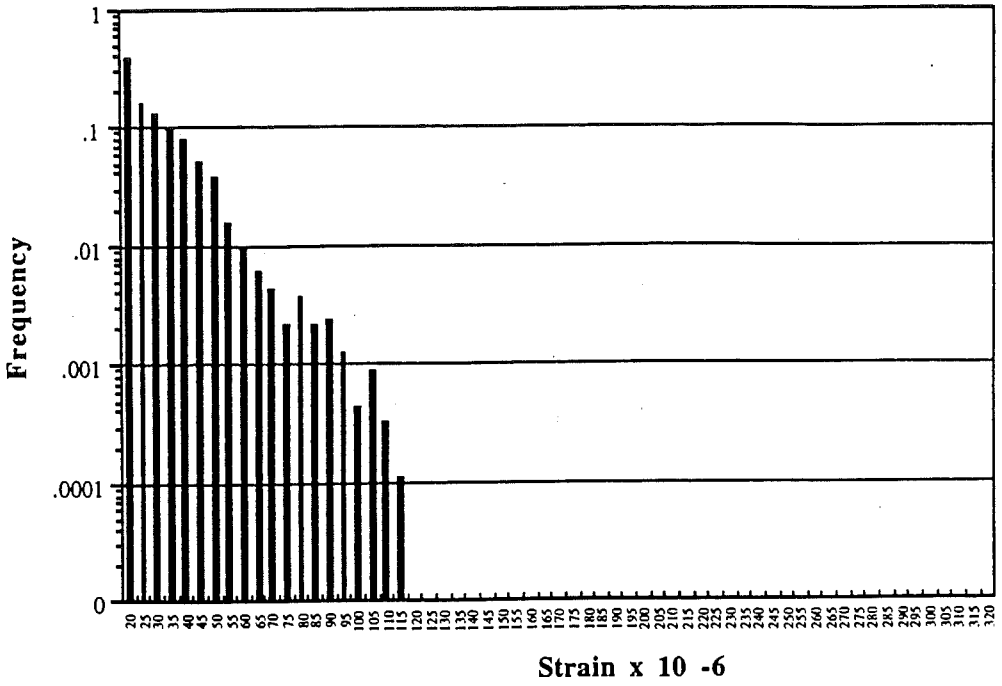

Fig. 11-67. Bridge I-94/PR, EB, Girder 9, Rainflow Strain Histogram.

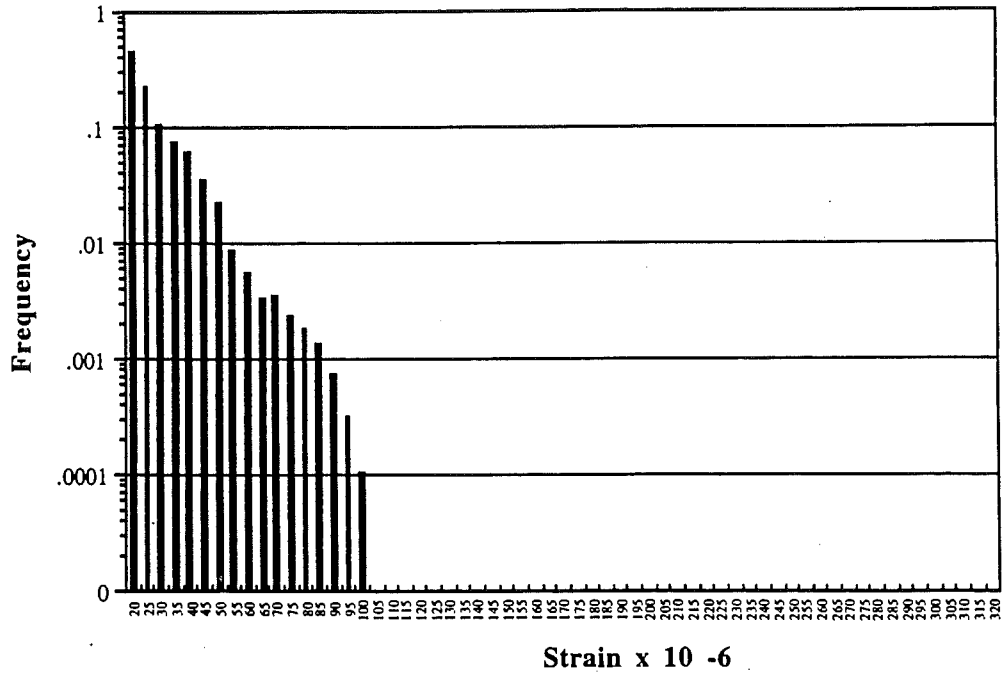

Fig. 11-68. I-94/PR, EB, Girder 10 ,Rainflow Strain Histogram.

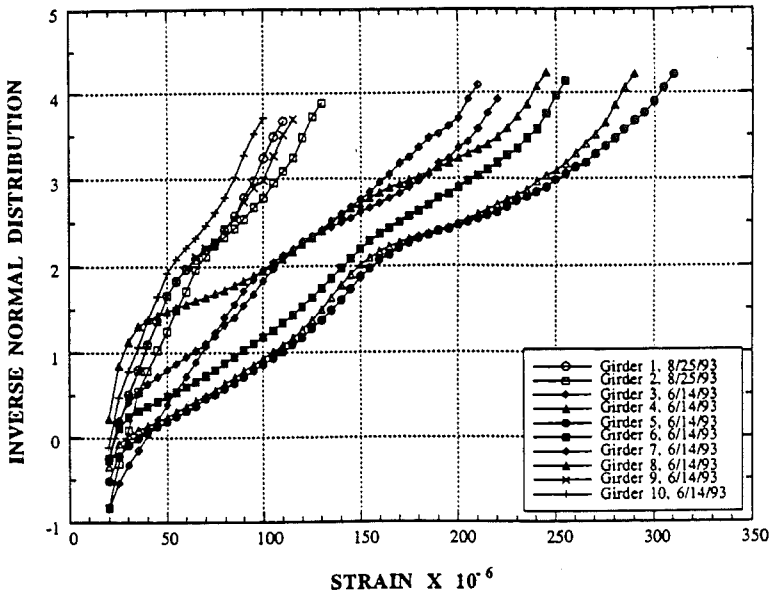

Fig. 11-69. 94/PR, EB, Rainflow Strain Distributions for Girders 1 - 10.

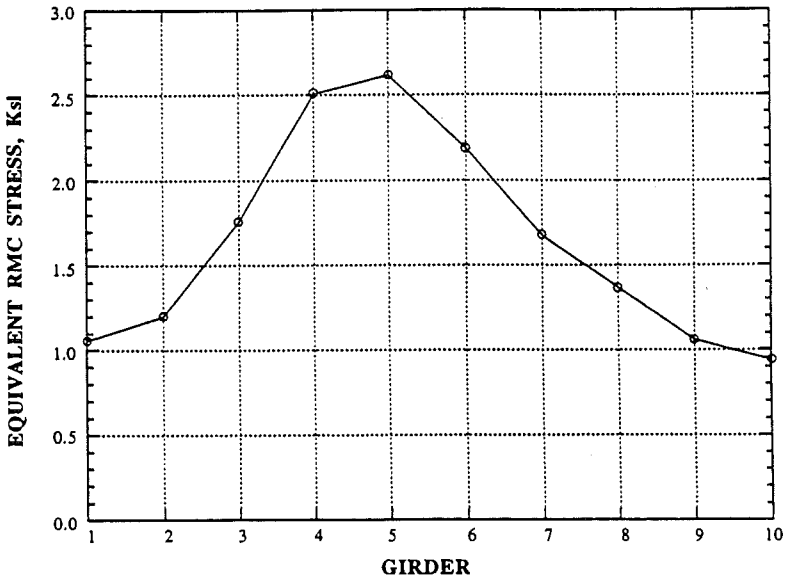

Fig. 11-70. Bridge 94/PR, EB, Equivalent RMC Stresses for Girders.

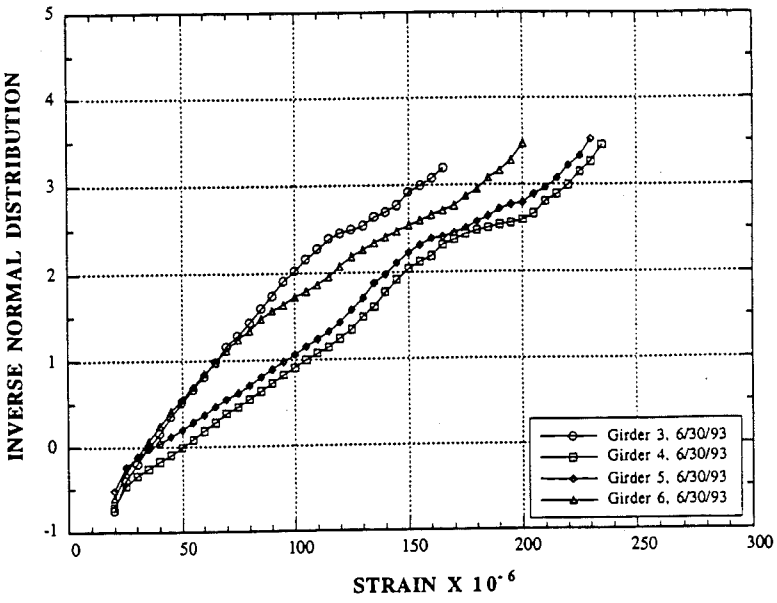

Fig. 11-71. 94/PR, Rainflow Strain Distributions for G3 - 6. 6/30/93.

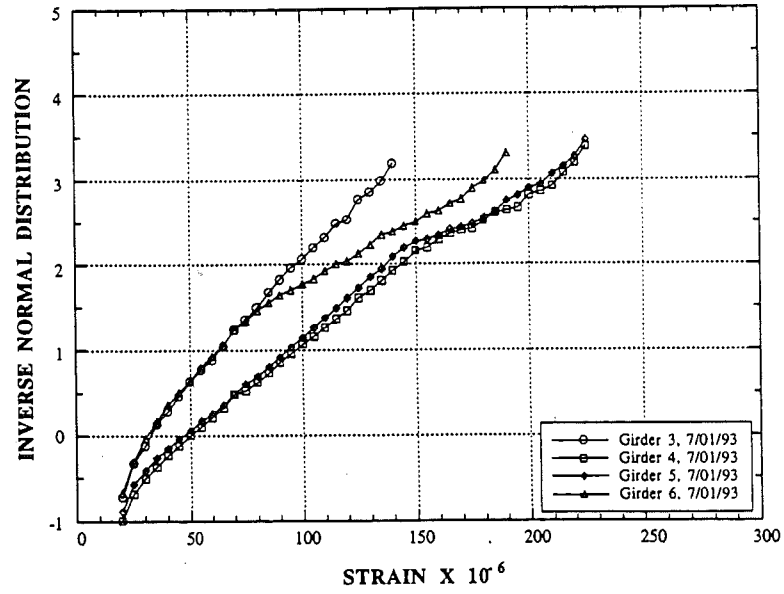

Fig. 11-72. 94/PR, Rainflow Strain Distributions for G3 - 6. 07/01/93.

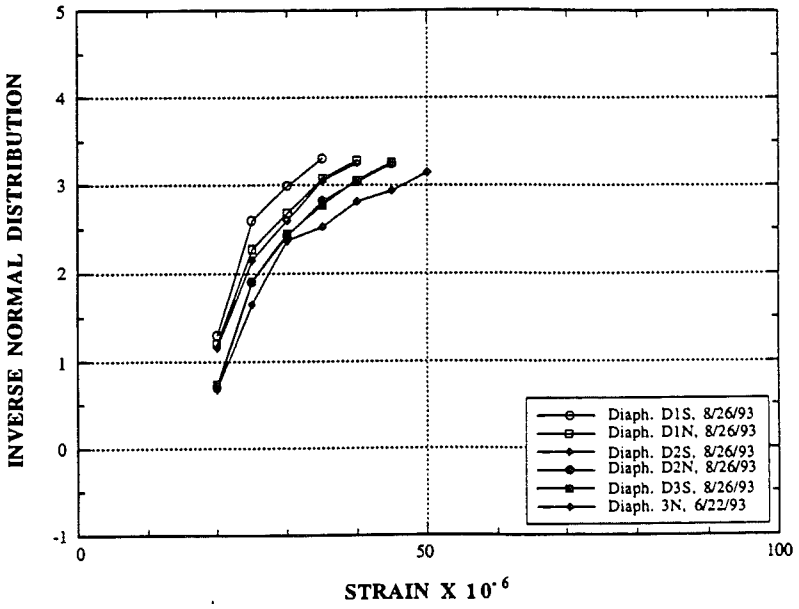

Fig. 11-73. 94/R, EB, Rainflow Strain CDF for Diaphragms 1 - 3.

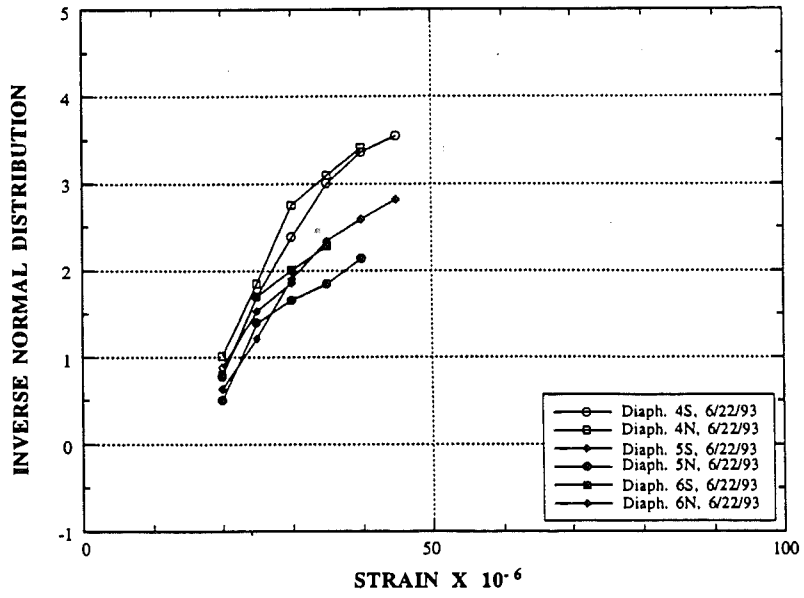

Fig. 11-74. 94/PR, EB, Rainflow Strain CDF for Diaphragms 4 - 6.

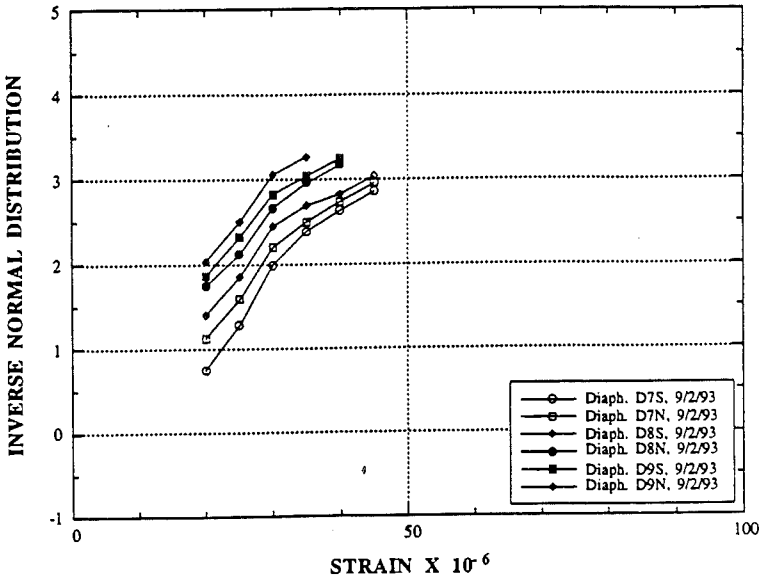

Fig. 11-75. 94/PR, EB, Rainflow Strain CDF for Diaphragms 7 - 9.

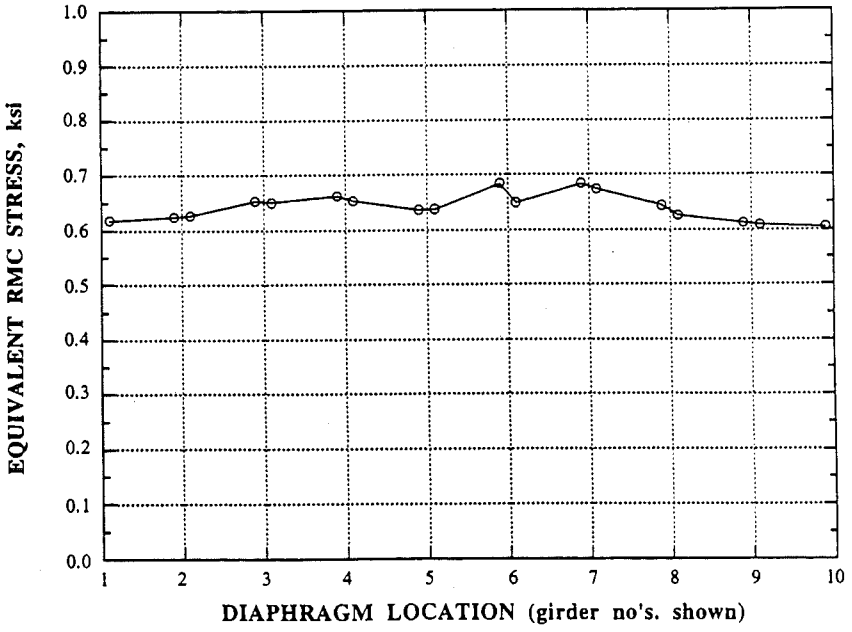

Fig. 11-76. 94/PR, EB, Equivalent RMC Stresses for Diaphragms.

11.6.5 M-14 over N.Y.C. Railroad (14/NY) in Ann Arbor

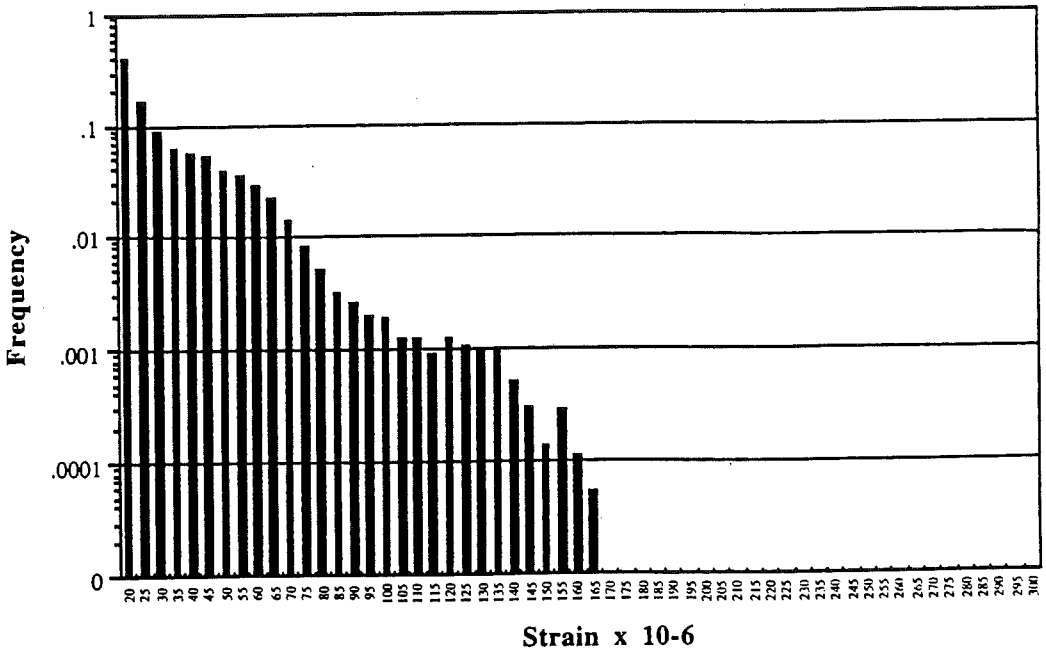

Fig. 11-77. Bridge 14/NY, EB, Girder 1, Rainflow Strain Histogram.

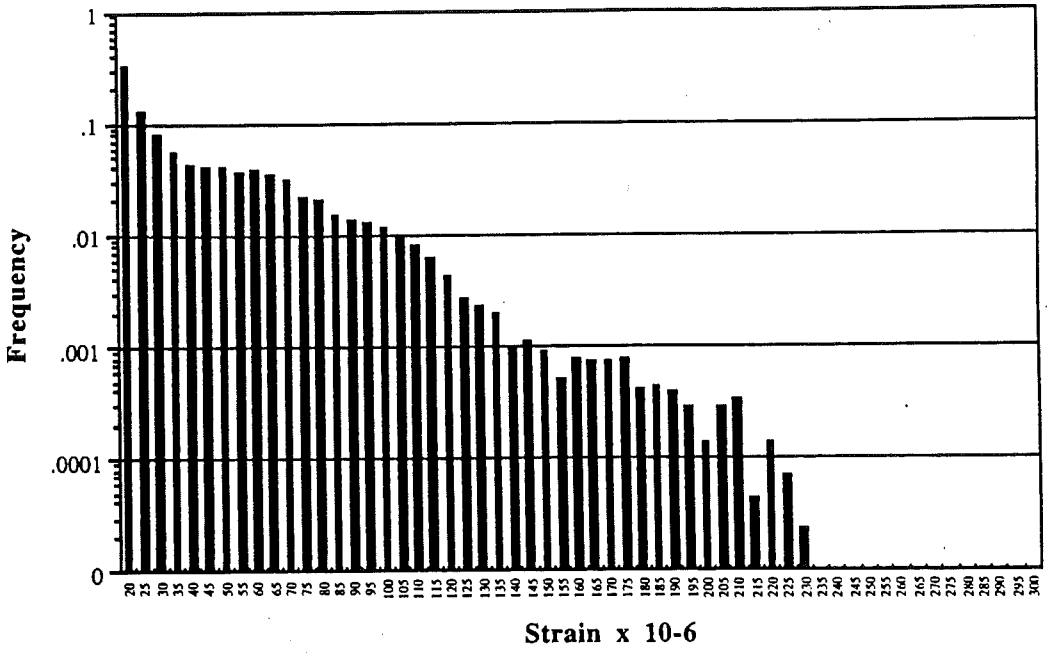

Fig. 11-78. 14/NY, EB, Girder 2, Rainflow Strain Histogram.

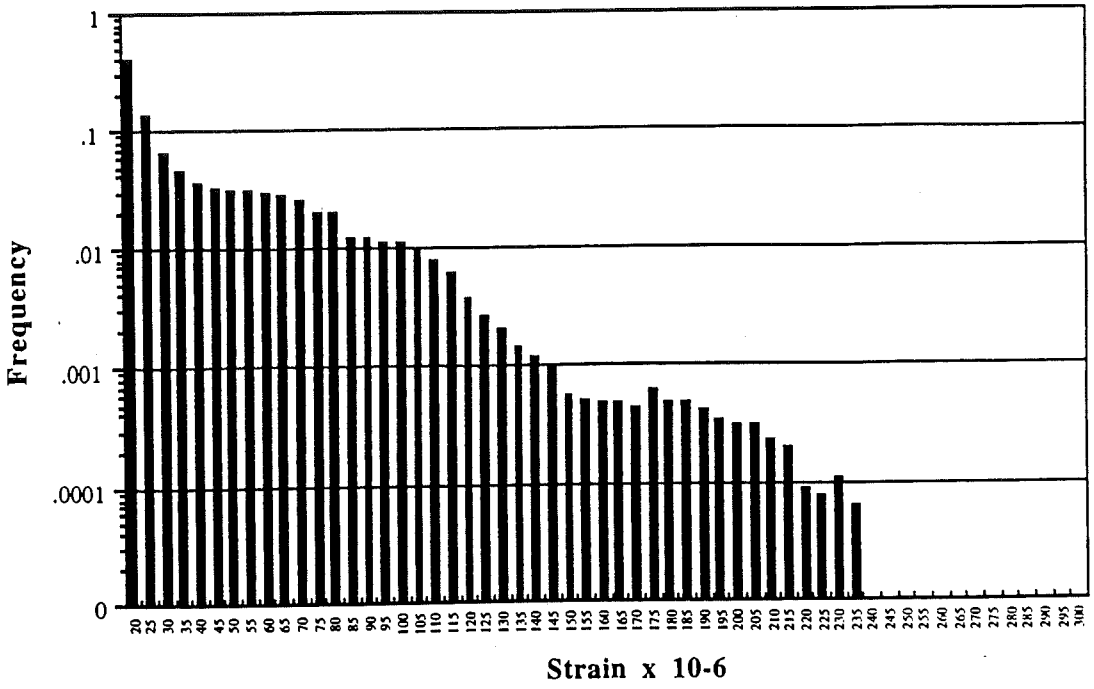

Fig. 11-79. Bridge 14/NY, EB, Girder 3, Rainflow Strain Histogram.

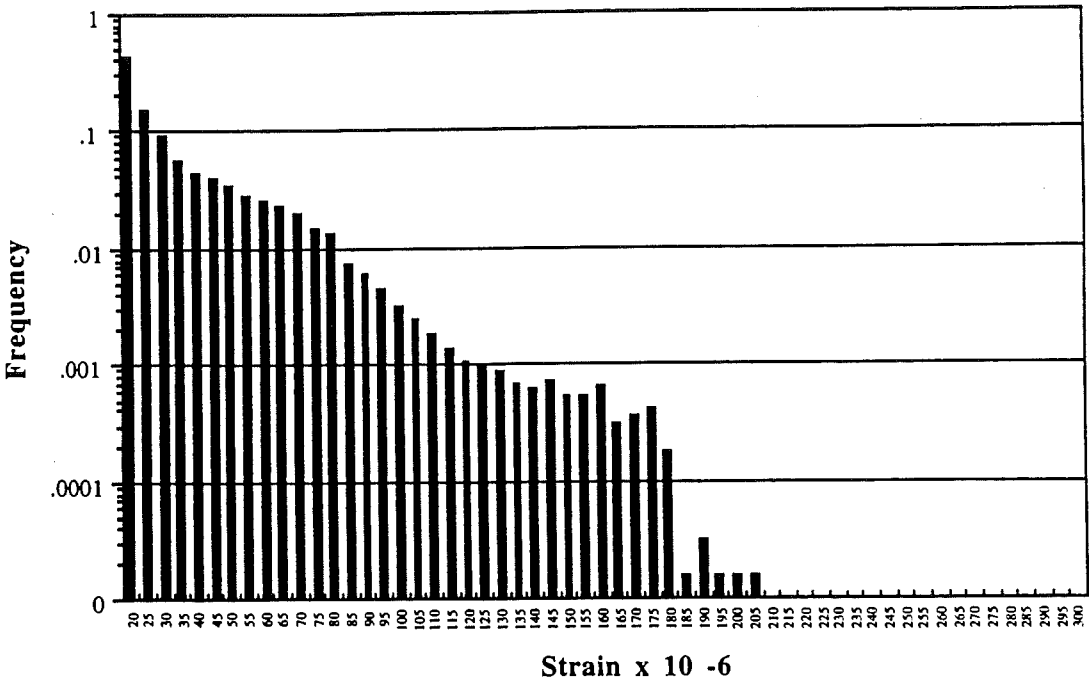

Fig. 11-80. Bridge 14/NY ,EB, Girder 4 Rainflow Strain Histogram.

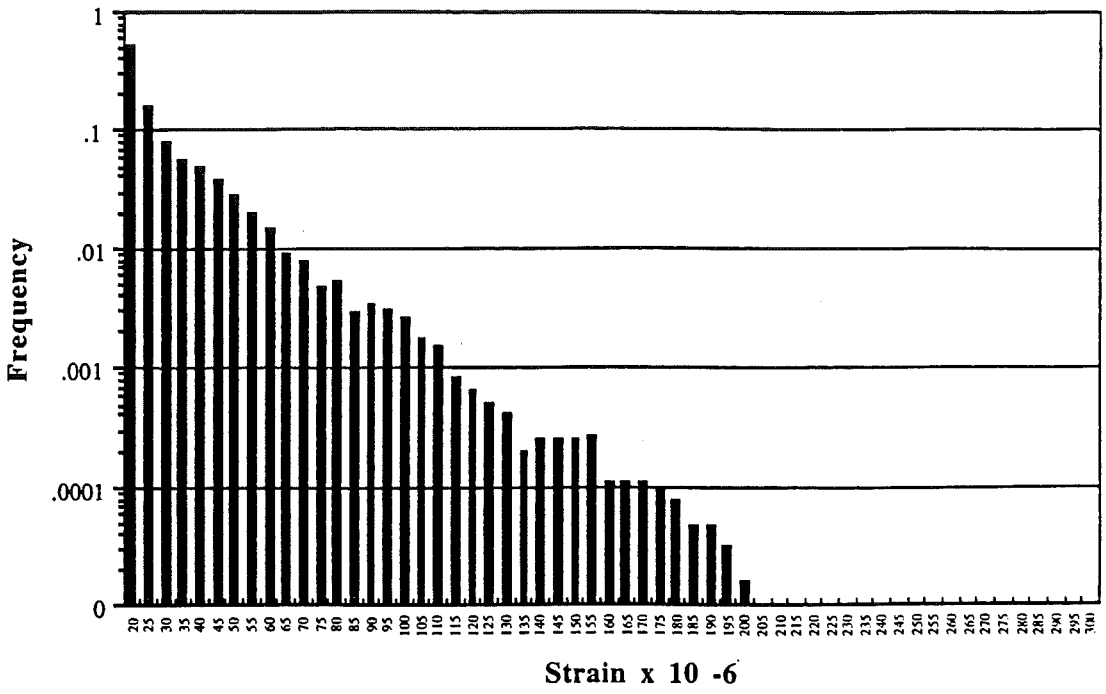

Fig. 11-81. Bridge 14/NY, EB, Girder 5, Rainflow Strain Histogram.

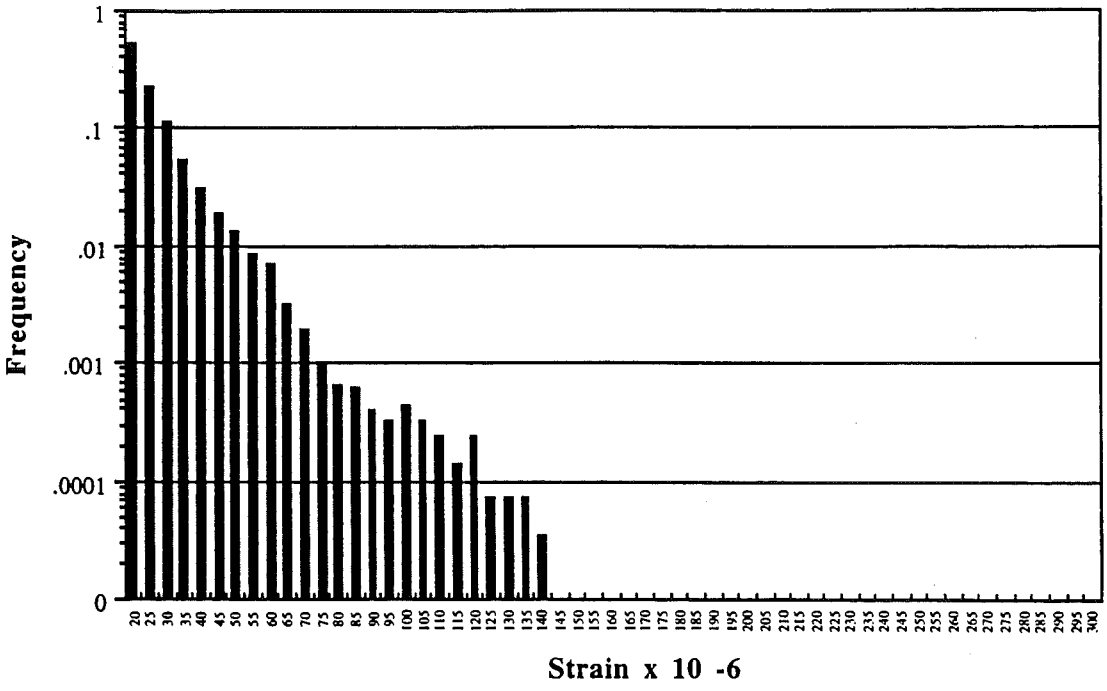

Fig. 11-82. Bridge 14/NY, EB, Girder 6, Rainflow Strain Histogram.

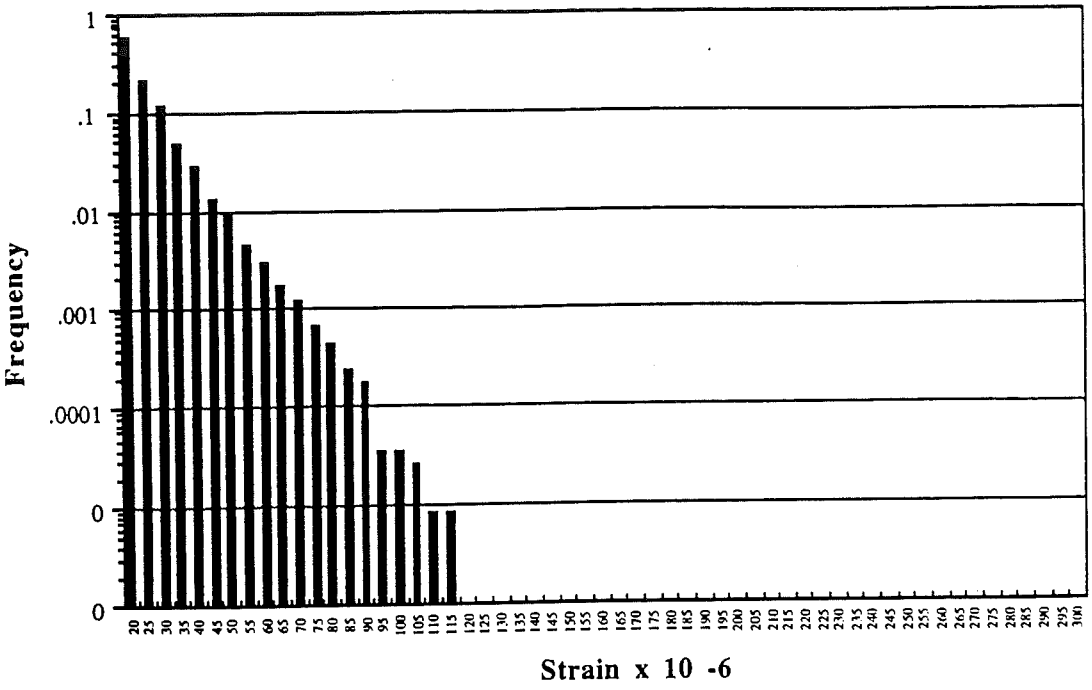

Fig. 11-83. 14/NY, EB, Girder 7, Rainflow Strain Histogram.

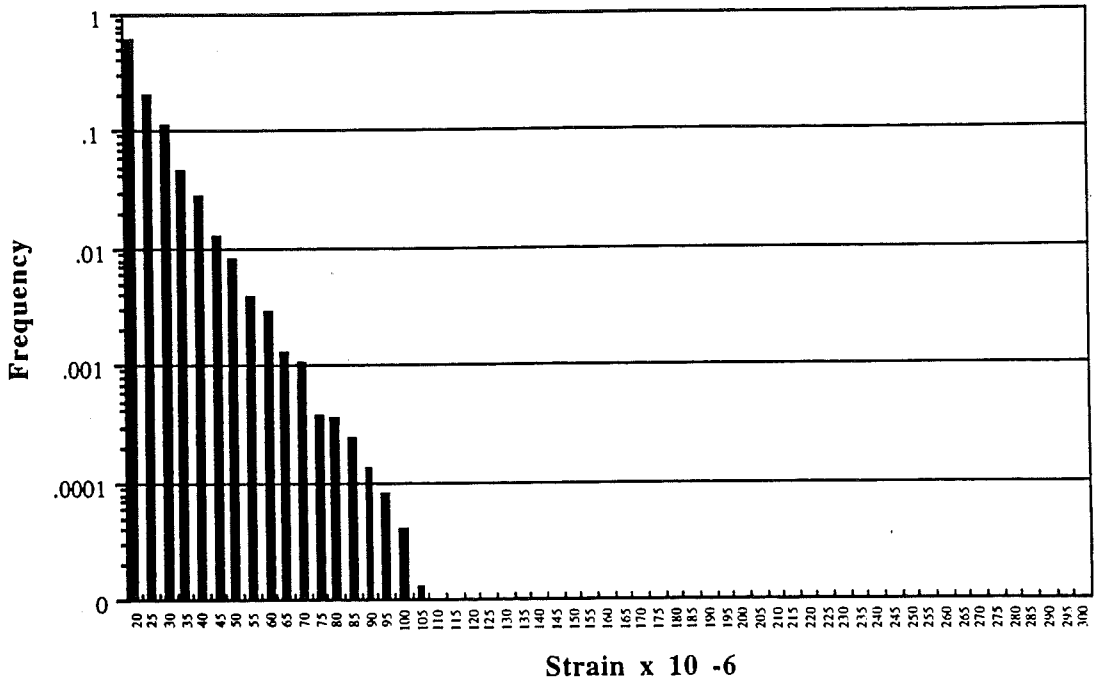

Fig. 11-84. Bridge 14/NY, EB, Girder 8, Rainflow Strain Histogram.

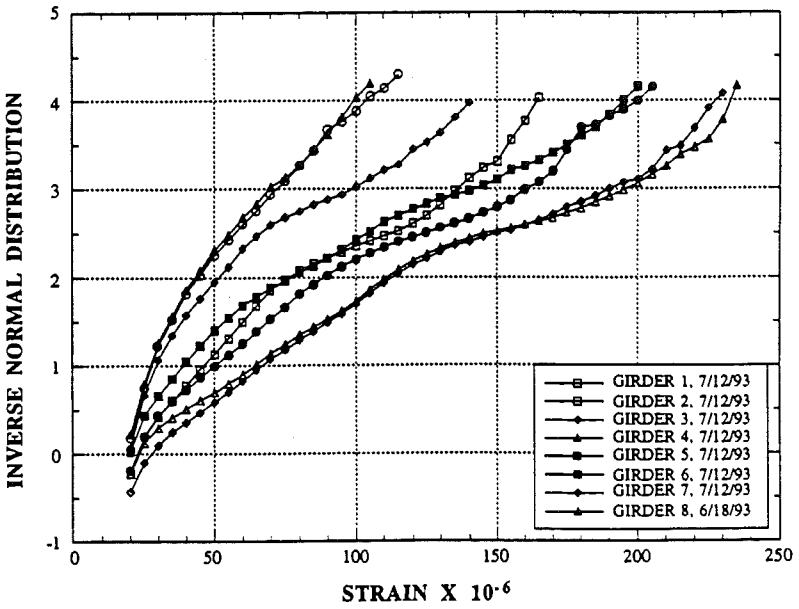

Fig. 11-85. Bridge 14/NY, EB, Rainflow Strain CDF for Girders 1 - 8.

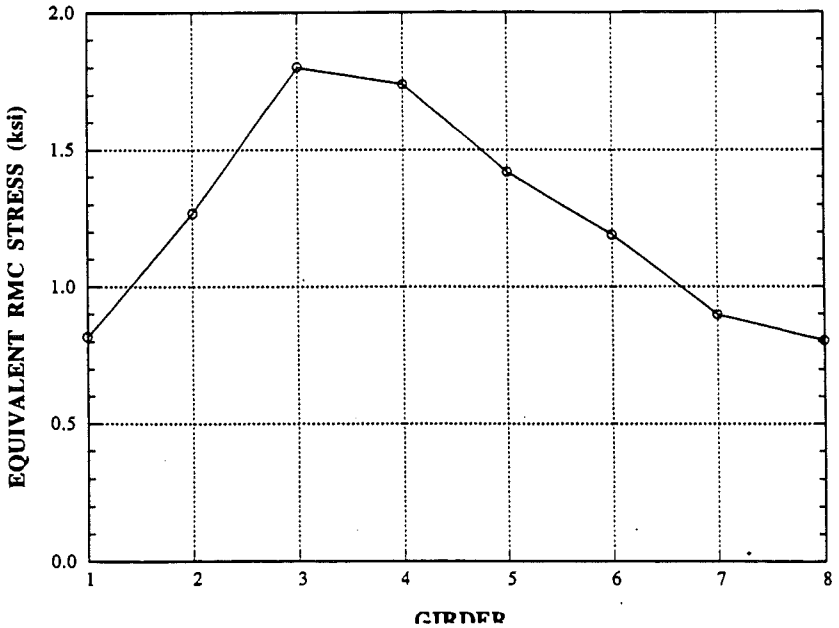

Fig. 11-86. Bridge 14/NY, Equivalent RMC Stresses for Girders.

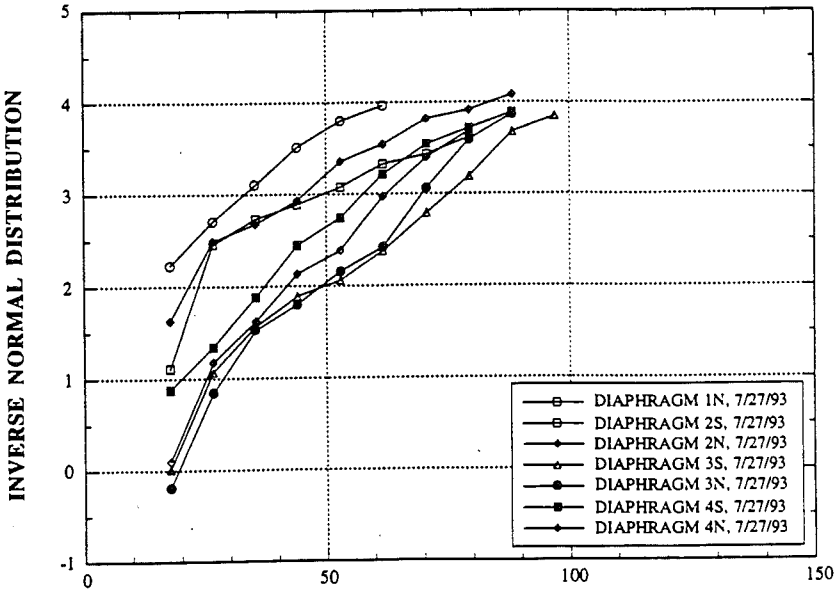

Fig. 11-87. 14/NY, EB, Rainflow Strain CDF for Diaphragms 1 - 4.

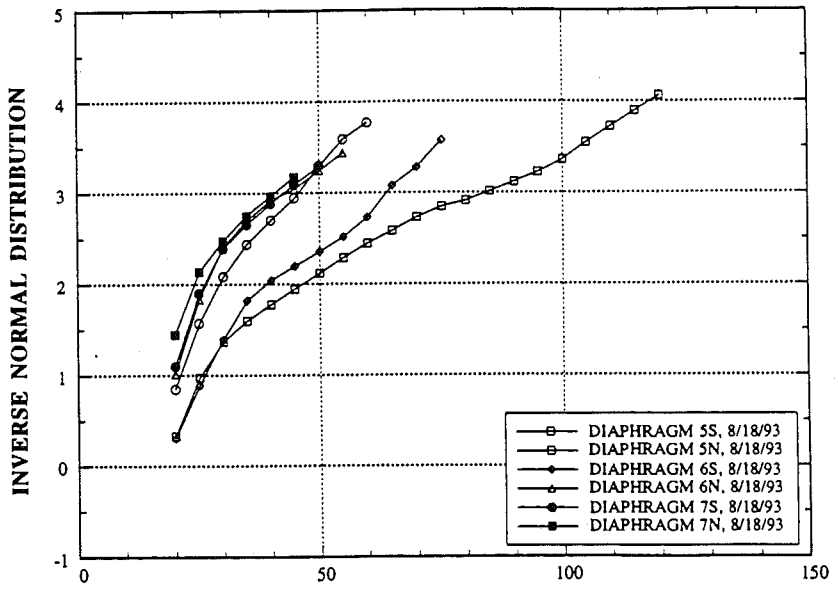

Fig. 11-88. Bridge 14/NY,EB, Rainflow Strain CDF for Diaphragms 5-7.

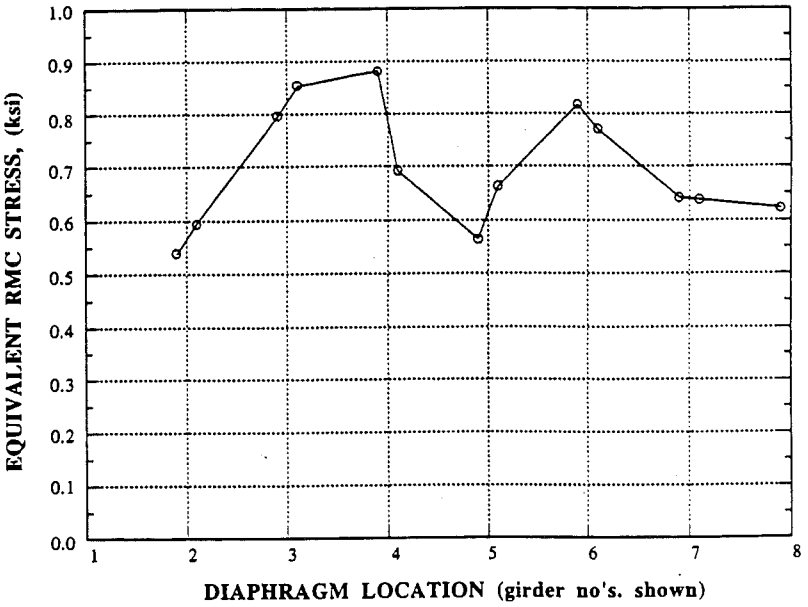

Fig. 11-89. Bridge 14/NY, Equivalent RMC Stresses for Diaphragms.

11.6.6 Bridge I-75 Over Bay Creek Rd. in Luna Pier (75/BC)

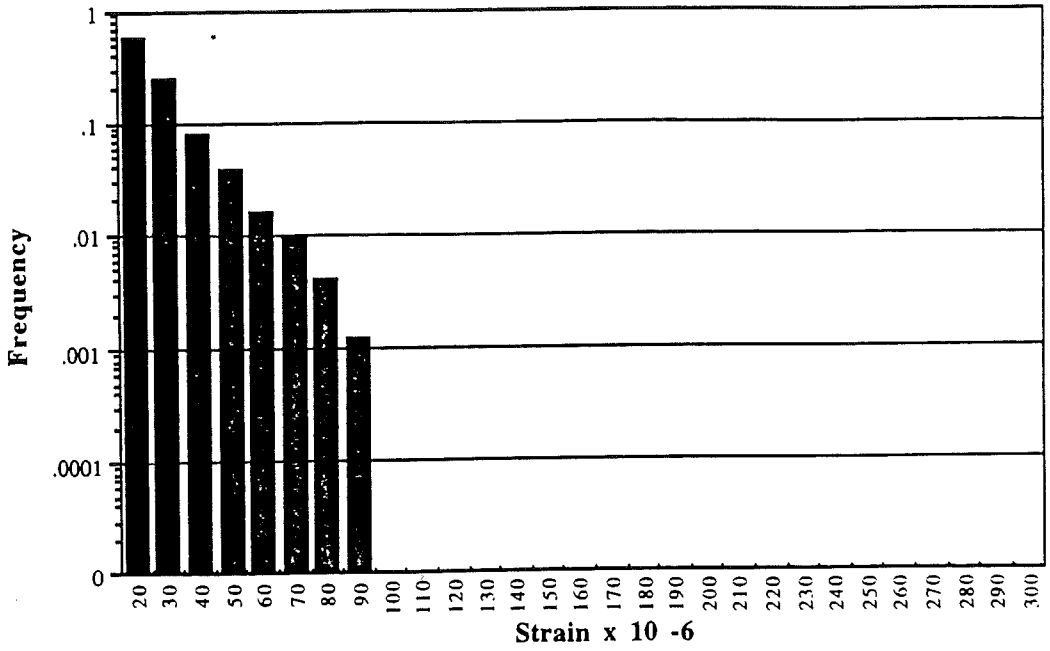

Fig. 11-90. Bridge 75/BC, NB, Girder 1 Rainflow Strain Histogram.

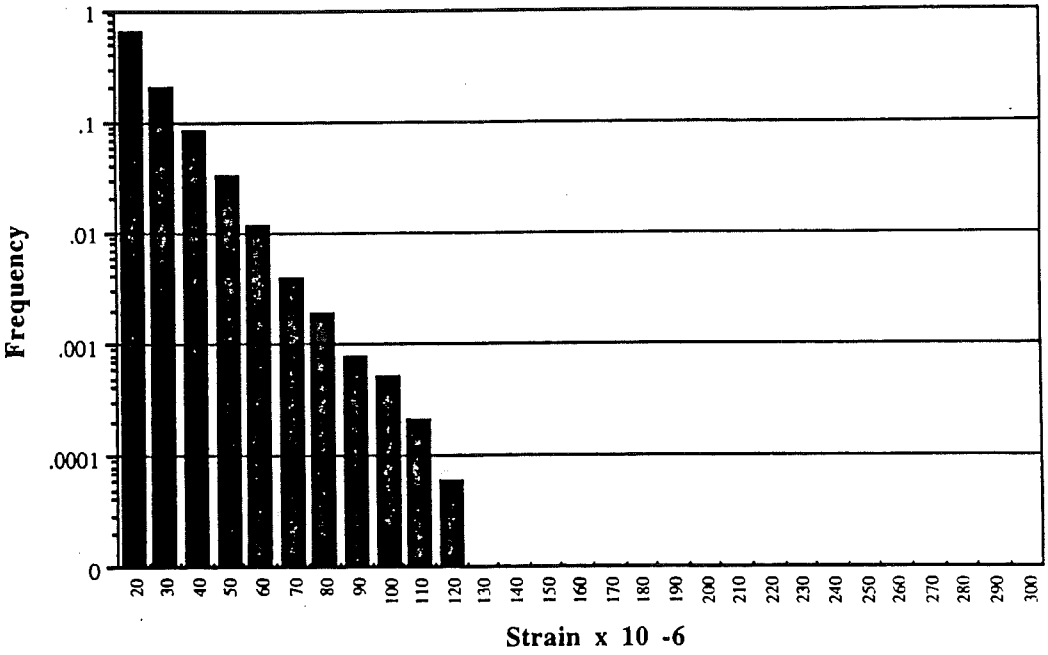

Fig. 11-91. Bridge 75/BC, NB, Girder 2 Rainflow Strain Histogram.

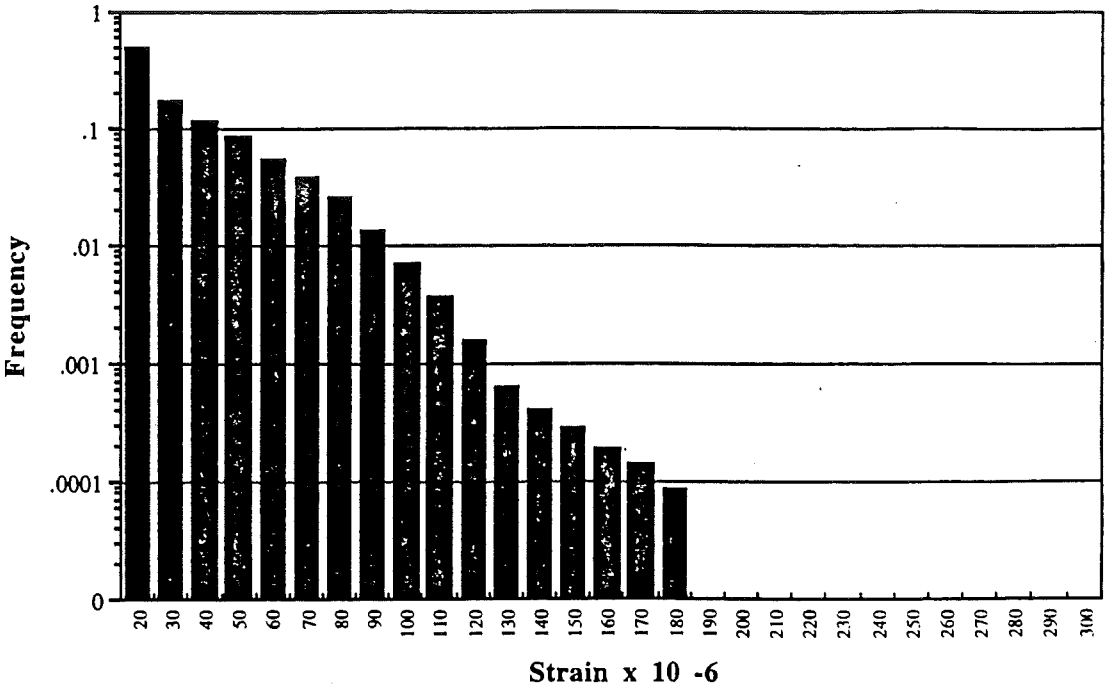

Fig. 11-92. Bridge 75/BC, NB, Girder 3, Rainflow Strain Histogram.

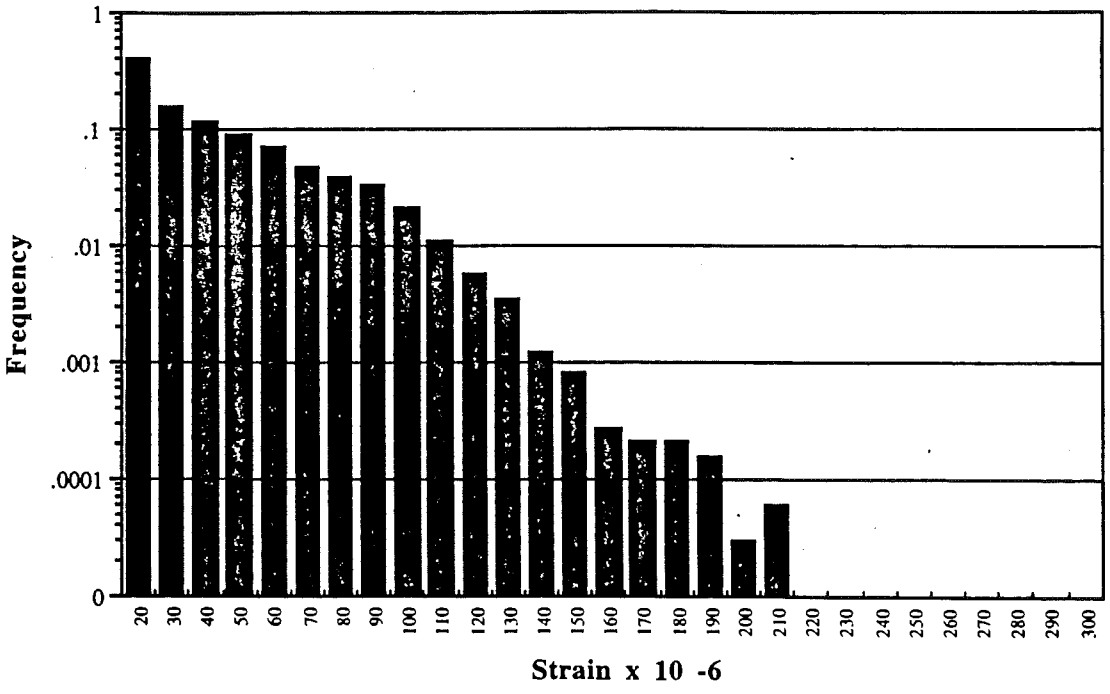

Fig. 11-93. 75/BC, NB, Girder 4, Rainflow Strain Histogram.

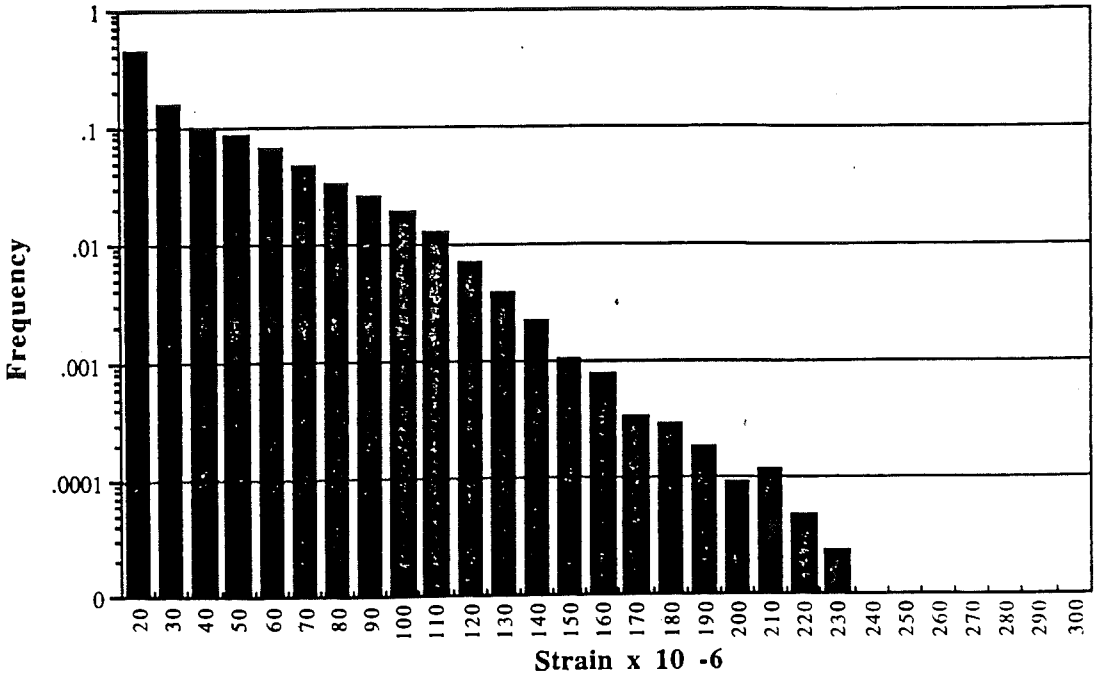

Fig. 11-94. Bridge 75/BC, NB, Girder 5, Rainflow Strain Histogram.

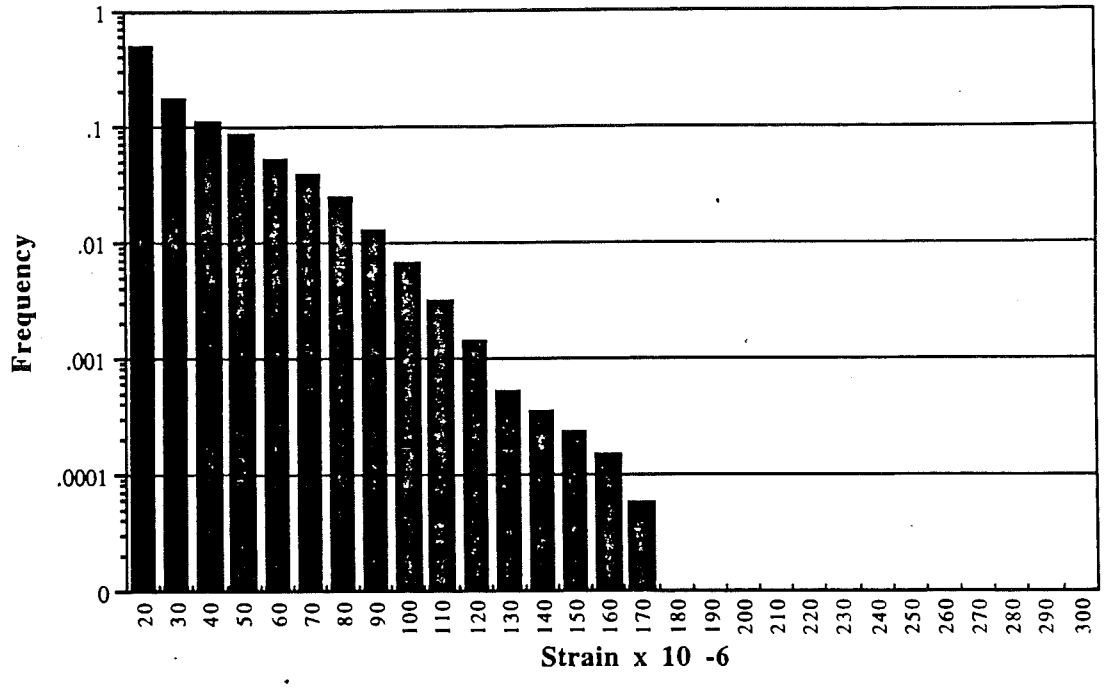

Fig. 11-95. Bridge 75/BC, NB, Girder 6, Rainflow Strain Histogram.

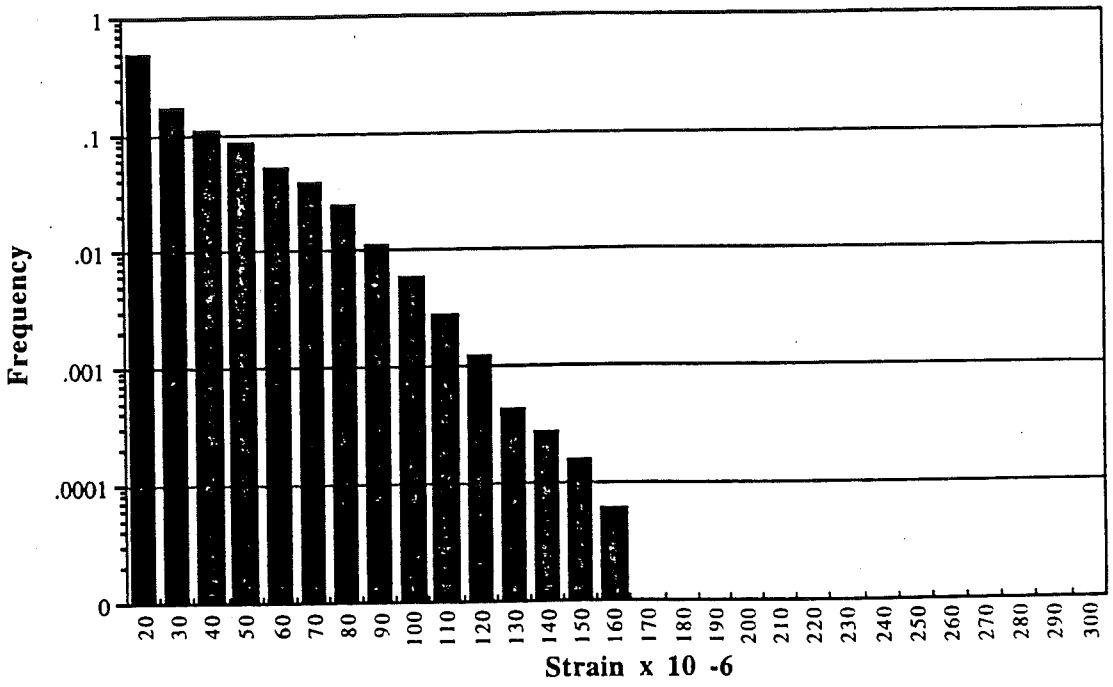

Fig. 11-96. Bridge 75/BC, NB, Girder 7, Rainflow Strain Histogram.

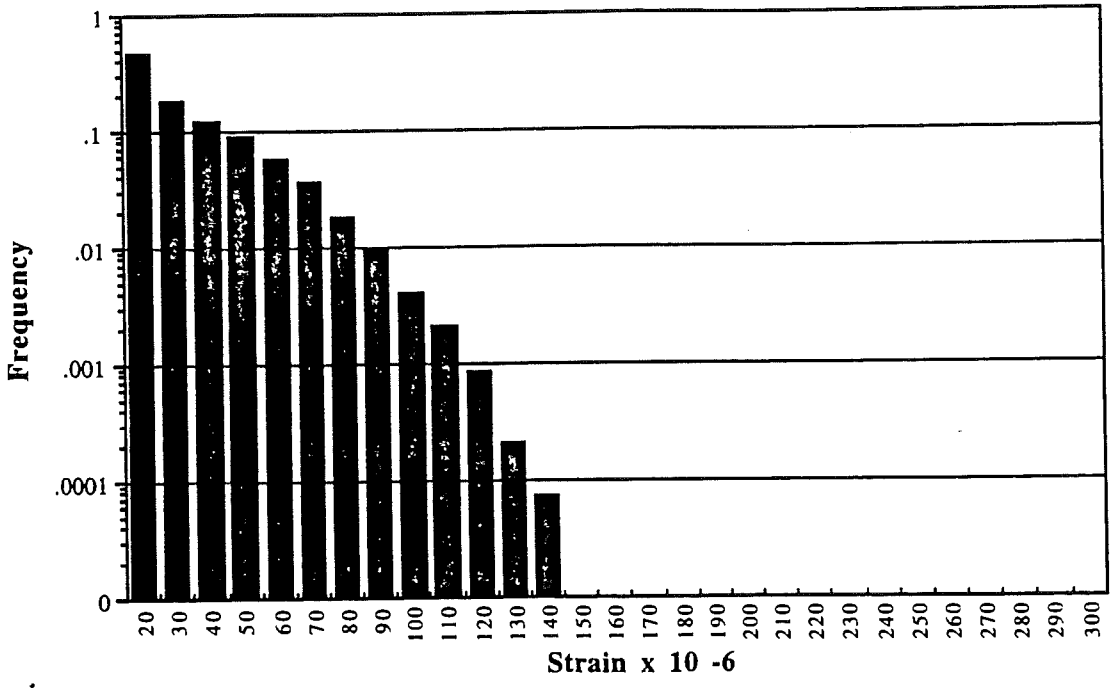

Fig. 11-97. Bridge 75/BC, NB, Girder 8 Rainflow Strain Histogram.

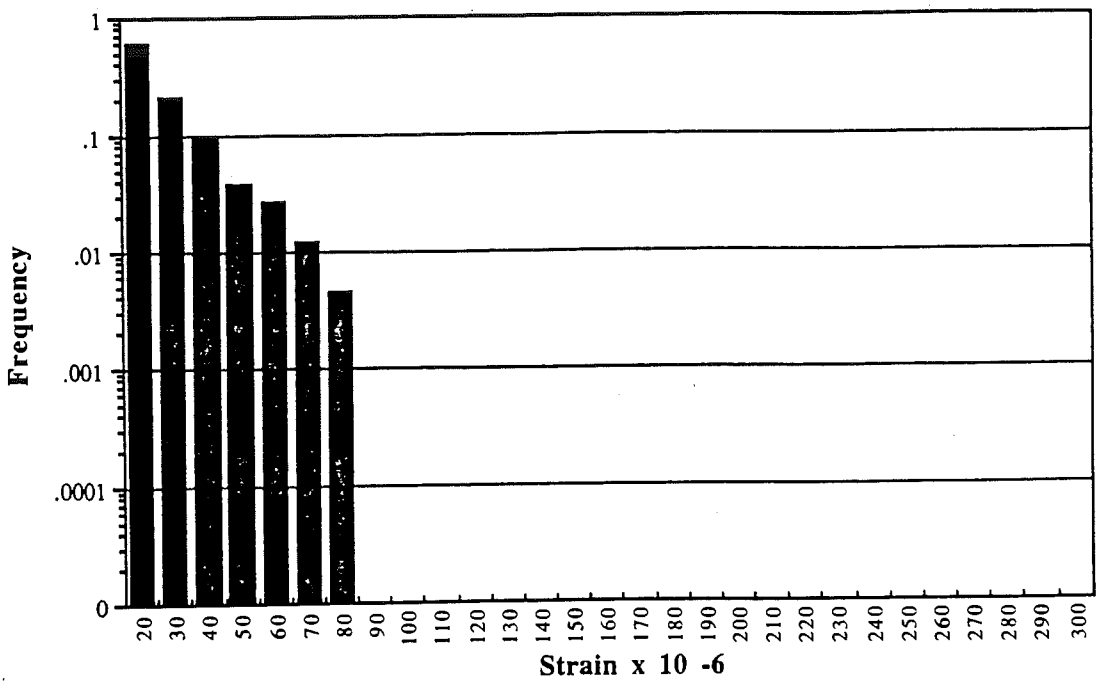

Fig. 11-98. Bridge 75/BC, NB, Girder 9, Rainflow Strain Histogram.

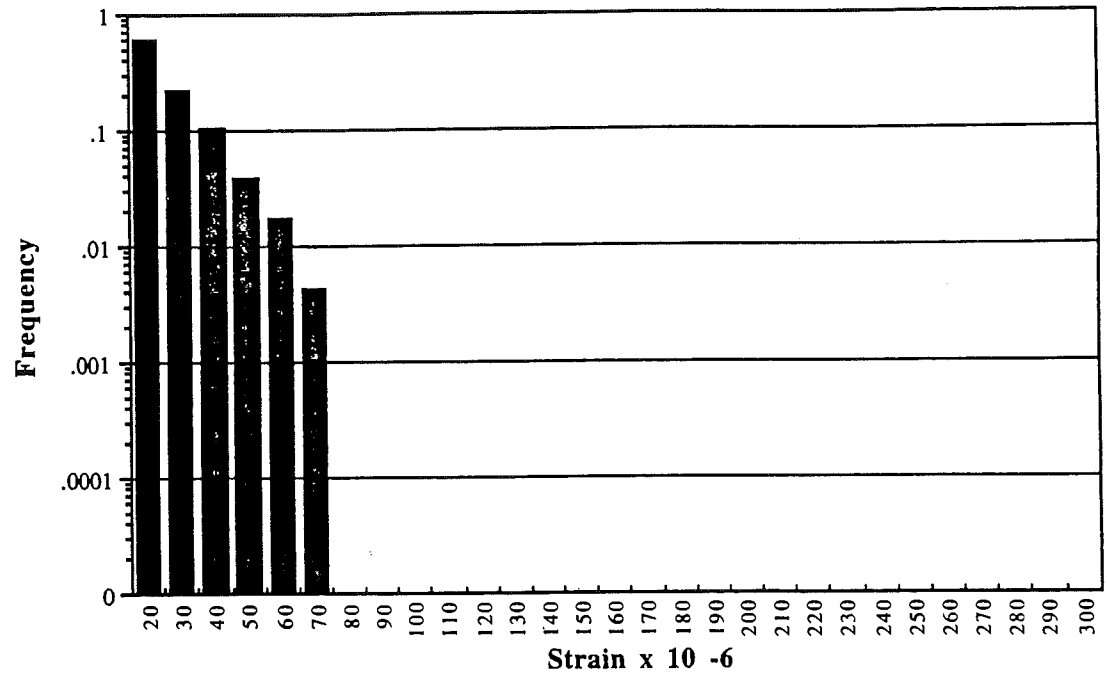

Fig. 11-99. Bridge 75/BC, NB, Girder 10, Rainflow Strain Histogram.

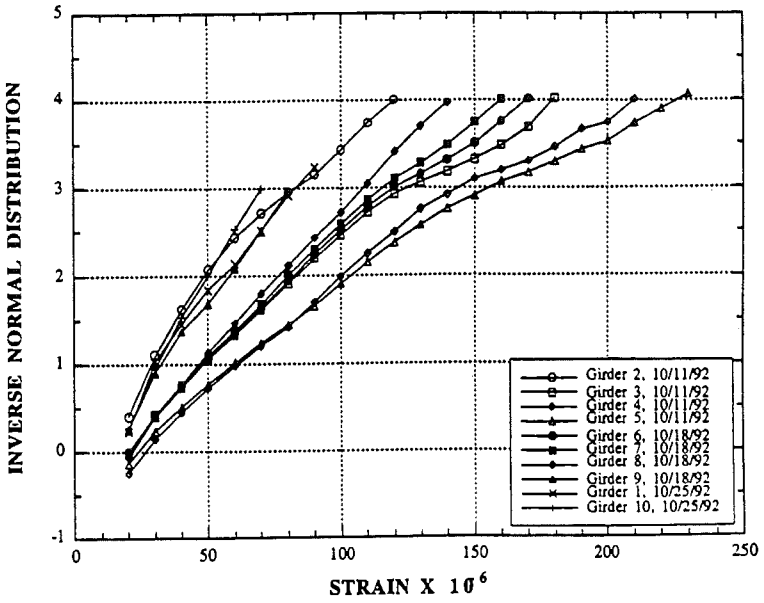

Fig. 11-100. 75/BC, NB, Rainflow Strain CDF for Girders 1 - 10.

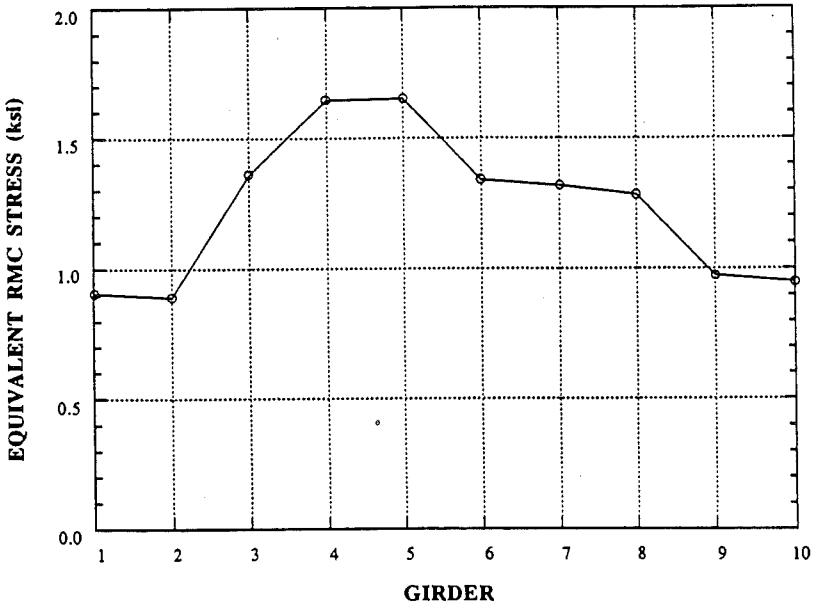

Fig. 11-101. Bridge 75/BC, NB, Equivalent RMC Stresses for Girders.

11.7 Analysis of Data for Fatigue

Research to develop fatigue load models for highway girder bridges has focused on obtaining an equivalent fatigue truck as discussed above. An equivalent vehicle which causes the same cumulative fatigue damage as the normal traffic distribution is an extremely useful tool for the practicing engineer. This chapter examines the statistics required to accurately utilize the available models.

11.7.1 Site Specific Statistics for Current Fatigue Models

Effective utilization of current fatigue load models requires accurate statistics of the load spectra. WIM data collected for this study has been analyzed to determine the required statistics of the following:

Gross vehicle weight distribution at each site.
Lane moment effect distribution for each site.
Correlation of GVW to Lane Moment
Moment effect as a function of GVW.

Effective truck weight, W_{eq}, for each WIM site in the study, headway, impact, and girder distribution are also important parameters for the current models. W_{eq} is presented in table 11-7 in addition to the equivalent moment for each of several spans. Other studies have addressed the issues of headway (Nowak and Nassif, 1991), impact (Nassif, 1992), and girder distribution and quantified statistics for these parameters.

The correlation of GVW to lane moment as a function of span length is shown in figure 11-102a through 11-102f and in table 11-6. The correlation between GVW and lane moment approaches 1.0 as the length of the span increases

The coefficient of variation (COV) of static lane moment as a function of span ranges from approximately 5% for 200 foot spans to as high as 24% for 20 foot spans. The relationship of lane moment COV to span is presented in figure 11-103a through 11-103f for each bridge. It can be observed that each site demonstrates a similar trend of lane moment COV, however this parameter is site and span dependent.

11.7.2 Fatigue Analysis of WIM Data

Schilling (1984) observed that 4 and 5 axle trucks accounted for between 92% and 98% of all truck traffic. The data obtained in this study indicates that between 40% and 80% of the truck population (table 11-8) are 5 axle vehicles. Vehicles with 3 and 4 axles are often configured similar to 5 axle vehicles, which when included accounts for between 55% and 95% of the truck population. Due to the site specific nature of the distribution of vehicle types by axle a single model for fatigue loading may not be the most accurate approach. Table 11-8 shows between 0% and 7.4% of the population is 11 axle vehicles. In Michigan, and in other states, vehicles with more than 5 axles are permitted. While these vehicles do not account for a significant portion of the population, the more important determination is the extent these vehicles contribute to the total fatigue damage.

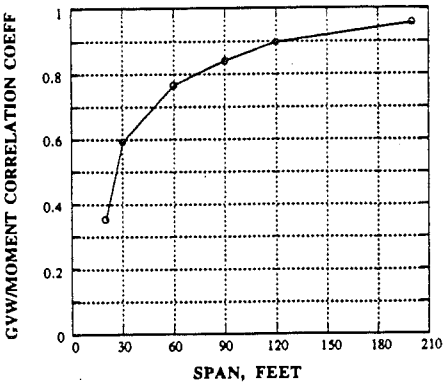

a) Correlation v Span - 23/HR(92)

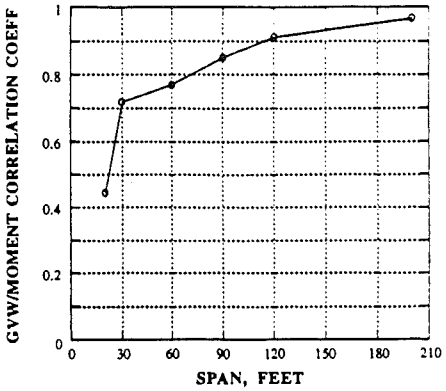

b) Correlation v Span - 23/SR

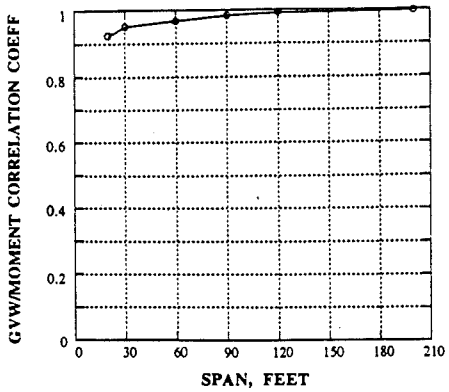

c) Correlation v Span - 94/JR

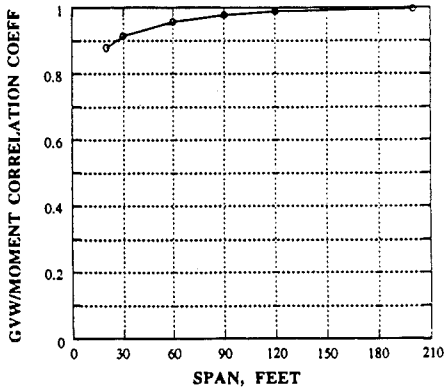

d) Correlation v Span - 94/PR(93)

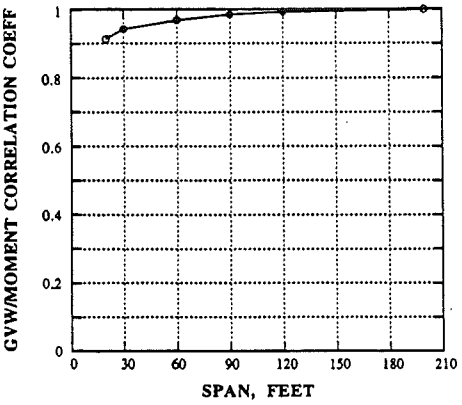

e) Correlation v Span - 14/NY

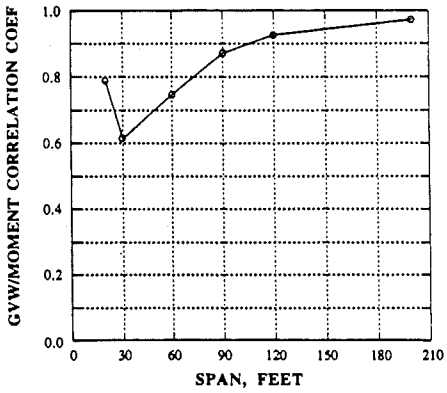

f) Correlation v Span - WY/94

Fig. 11-102. Correlation Coefficient of GVW to Lane Moment vs. Span by Bridge.

Table 11-6. Correlation Coefficient of GVW to Lane Moment by Span and Bridge.

Correlation Coefficient - GVW/Max. Lane Moment								
Span Feet	14/NY	23/HR 1991	23/HR 1992	23/SR	94/PR 1991	94/PR 1993	WY/94	94/JR
20	0.7880	0.9125	0.8786	0.3534	0.4450	0.9287	0.8793	0.9246
30	0.6140	0.9424	0.9098	0.5938	0.7186	0.9375	0.9153	0.9516
60	0.7470	0.9689	0.9516	0.7669	0.7702	0.9546	0.9576	0.9690
90	0.8720	0.9852	0.9773	0.8410	0.8497	0.9782	0.9790	0.9851
120	0.9260	0.9934	0.9900	0.8979	0.9120	0.9912	0.9900	0.9933
200	0.9730	0.9981	0.9972	0.9581	0.9679	0.9977	0.9975	0.9981

Table 11-7. Equivalent (RMC) GVW and Moments for 20 - 200 Ft Span.

Bridge	GVW_{eq}	Equivalent Moment by RMC for each Span (Ft-kip)					
	(Kips)	20 Ft	30 Ft	60 Ft	90 Ft	120 Ft	200 Ft
23/HR(92)	62.4	121.2	213.0	568.1	1004	1467	2711
23/HR(91)	68.9	116.8	205.6	566.4	1046	1561	2931
23/SR	77.2	130.3	226.2	618.2	1153	1730	3270
94/JR	76.7	125.4	227	636.6	1170	1742	3274
94/PR(93)	63.9	111.1	191.0	506.5	935.9	1413	2693
94/PR(91)	58.6	107.8	183.2	460.6	839.3	1276	2449
14/NY	78.1	128.5	226.2	644.8	1196	1783	3346
WY/94	59.5	98.4	175.4	494.4	907.8	1354	2531

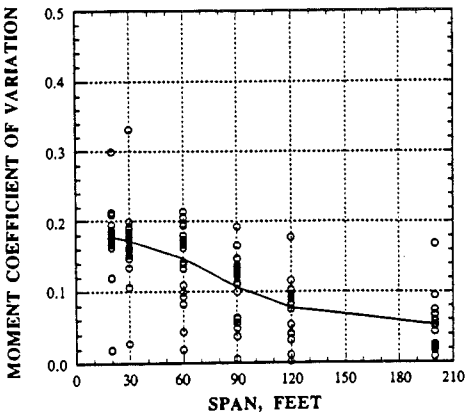

a) US-23/Huron River (92).

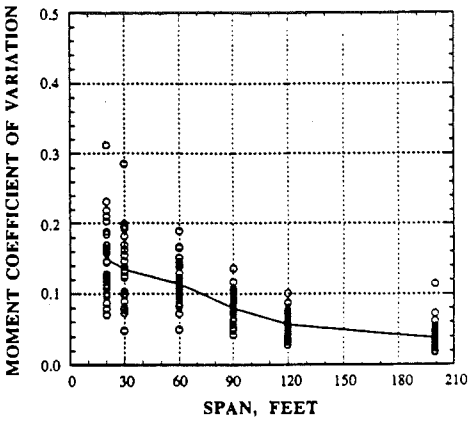

b) US-23/Saline River.

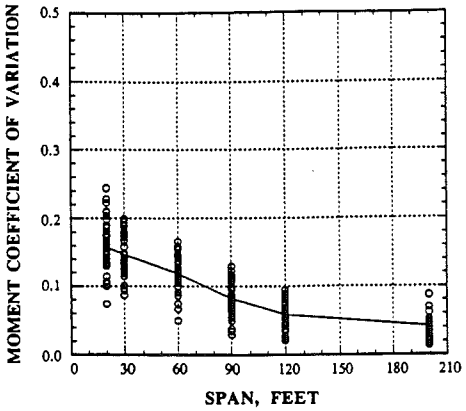

c) I-94/Jackson Road.

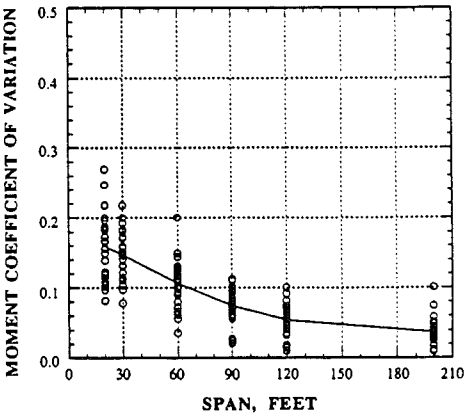

d) I-94/Pierce Road (93).

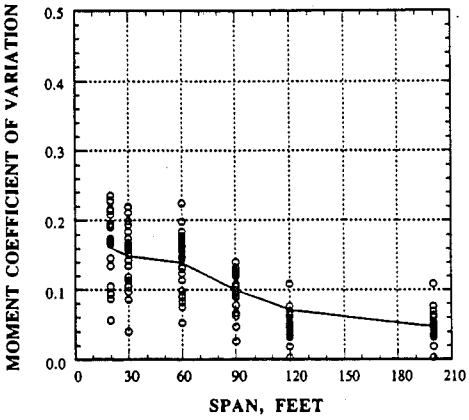

e) M-14/New York City RR.

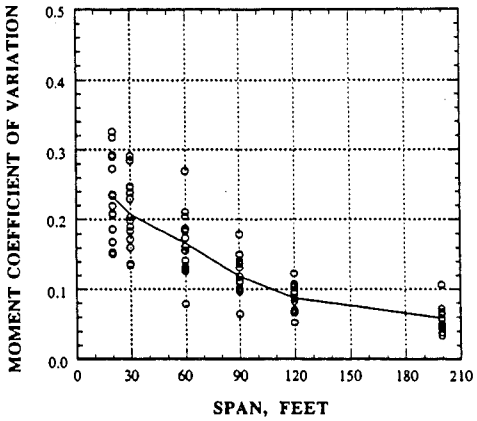

f) Wyoming Road/I-94

Fig. 11-103. Static Lane Moment Coefficient of Variation vs. Span.

Table 11-8. Distribution of Truck Types by No. of Axles and Bridge.

Distribution of Truck Types by Number of Axles (>15 kips GVW)								
	Bridge							
TRUCK AXLES	23/HR (92) %	23/HR (91) %	23/SR %	94/PR (93) %	94/PR (91) %	94/JR %	14/NY %	WY/94 %
2	9.5	8.6	9.5	7.7	4.2	8.0	8.3	20.2
3	11.0	8.7	6.0	5.2	8.4	6.2	7.7	10.3
4	14.5	8.3	6.9	5.6	7.7	5.7	11.6	6.6
5	54.3	62.9	63.5	72.6	78.9	69.1	61.2	39.3
6	3.4	4.5	3.6	3.8	0.0	2.6	4.6	6.2
7	2.0	1.0	0.8	0.9	0.0	0.8	1.3	3.5
8	1.0	1.1	1.0	1.3	0.7	1.4	2.2	5.1
9	0.0	0.1	0.8	0.7	0.0	1.2	0.7	0.3
10	1.1	0.8	1.3	0.4	0.2	0.8	0.5	1.1
11	3.2	4.2	6.6	1.7	0.0	4.1	2.0	7.4

An analysis was performed using the WIM results as a data base to determine the contribution to the total fatigue damage by each vehicle type. A FORTRAN program was developed at the University of Michigan to simulate the truck traffic flow and to calculate the static stress history of each truck as it passed over theoretical simple span bridges of 20-200 foot spans. The analytical model was calibrated using captured strain files of weighed trucks enabling accurate distribution of load to the girders in the model and accurate calculation of stresses. Following the stress analysis, a rainflow analysis was performed and damage was calculated using the stress-life approach. The damage was then accumulated by Miner's Rule in a matrix of vehicle types and span lengths.

The results of the damage analysis are presented in table 11-9 and figures 11-104a through 11-104e. The results clearly show that vehicles with greater than 5 axles account for the majority of accumulated fatigue damage. Eleven axle vehicles dominate the

calculation of accumulation of fatigue damage as seen in each of the figures 11-104 through 11-108 for each bridge site.

Each vehicle type in the WIM data base was filtered and total stress cycles were calculated for spans of 20 - 200 feet. Figure 11-105 plots the results of this analysis and demonstrates that there is a relationship between greater numbers of axles and average significant stress cycles. Also evident from figure 11-105 is the decrease in the average number of stress cycles per vehicle to 1.0 as the span increases. Therefore, the parameter of stress cycles becomes less important as the span of the bridge under consideration exceeds 60 to 70 feet, depending on the distribution of vehicle types in the normal traffic flow.

Table 11-9. % Damage by Span and Vehicle Type for Each Bridge.

	Bridge Location	% Damage Due to Vehicle Type (number of axles)									
		2	3	4	5	6	7	8	9	10	11
20'	23/HR (92)	0.0	1.7	5.9	26.1	6.2	9.1	0.6	0.0	12.6	37.7
	23/SR	0.0	1.9	1.2	61.2	6.7	1.3	3.9	2.5	2.0	18.9
	94/JR	0.3	1.0	1.6	36.0	6.9	3.1	9.0	2.8	5.9	33.4
	94/PR (93)	2.5	1.8	4.0	73.7	5.0	0.7	1.5	1.8	1.3	7.8
	14/NY	0.0	2.6	4.5	46.3	7.7	5.7	4.0	5.6	11.2	11.9
30'	23/HR (92)	0.1	1.6	4.9	22.3	5.5	9.6	0.4	0.0	11.5	44.0
	23/SR	0.2	1.6	0.7	49.9	5.8	1.3	5.5	3.2	2.9	28.9
	94/JR	0.1	0.6	0.9	21.7	4.5	2.4	9.4	3.3	8.0	48.9
	94/PR (93)	1.4	1.4	2.9	67.2	5.1	0.8	1.6	2.5	2.1	15.0
	14/NY	0.3	2.1	3.0	34.4	7.0	4.5	4.9	4.6	10.6	28.4
60'	23/HR (92)	0.0	1.1	3.6	11.5	3.1	6.6	0.4	0.0	13.3	60.4
	23/SR	0.1	0.9	0.3	18.8	5.6	1.7	6.6	5.6	4.5	55.9
	94/JR	0.0	0.3	0.4	7.5	3.1	1.8	5.6	4.1	10.1	67.1
	94/PR (93)	0.6	1.1	1.5	34.5	4.8	1.2	3.3	4.5	3.8	44.8
	14/NY	0.1	0.7	0.9	9.1	5.2	6.8	3.5	5.8	14.1	53.8
90'	23/HR (92)	0.0	0.7	2.5	10.9	2.7	5	0.5	0.0	14.1	63.5
	23/SR	0.0	0.4	0.2	16.3	5.3	1.6	5.7	5.4	4.8	60.1
	94/JR	0.0	0.2	0.3	7.3	2.8	1.7	5.1	4.2	10.5	67.9
	94/PR (93)	0.3	0.6	1.2	29.7	4.9	1.3	4.2	6.3	4.2	47.4
	14/NY	0.0	0.4	0.7	8.2	4.6	5.9	4.2	7.6	13.3	55.2
120	23/HR (92)	0.0	0.6	2.0	11.9	2.6	4.5	0.5	0.0	13.7	64.1
	23/SR	0.0	0.3	0.2	17.3	5.0	1.5	5.3	5.4	4.8	60.0
	94/JR	0.0	0.1	0.2	8.2	2.7	1.6	4.7	4.2	10.5	67.5
	94/PR (93)	0.2	0.4	1.0	30.9	4.6	1.2	4.4	6.6	4.2	46.4
	14/NY	0.0	0.3	0.6	9.1	4.3	5.7	4.5	8.1	12.6	54.8
200	23/HR (92)	0.0	0.5	1.6	12.8	2.6	3.9	0.6	0.0	13.7	64.2
	23/SR	0.0	0.2	0.2	18.9	4.8	1.5	5.1	5.4	4.9	59.0
	94/JR	0.0	0.1	0.2	9.2	2.7	1.5	4.5	4.1	10.1	67.5
	94/PR (93)	0.1	0.3	0.9	32.6	4.6	1.2	4.9	7.0	4.4	44.0
	14/NY	0.0	0.2	0.5	9.9	4.2	5.2	5.1	8.7	11.9	54.2

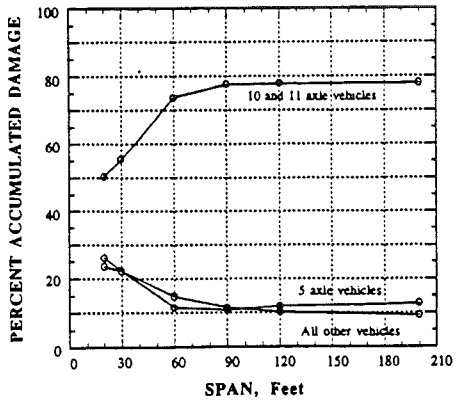

a) US-23/HR(92) % Damage.

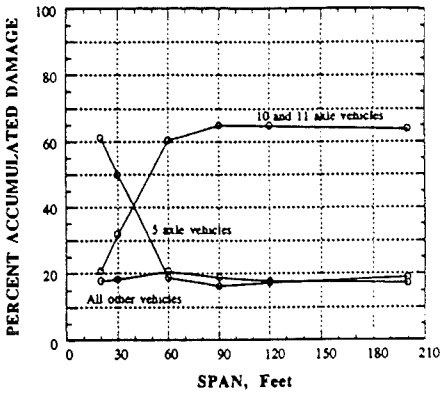

b) US-23/SR(92) % Damage.

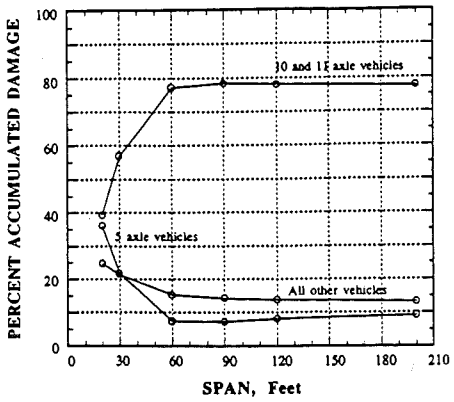

c) I-94/JR % Damage.

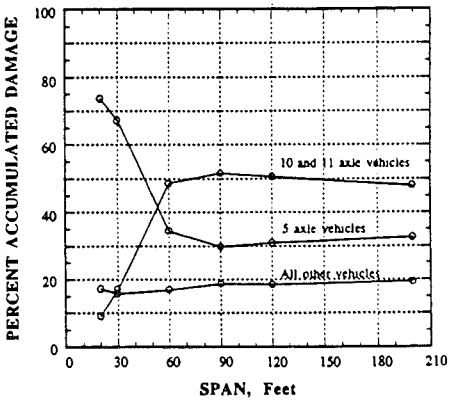

d) I-94/JR % Damage.

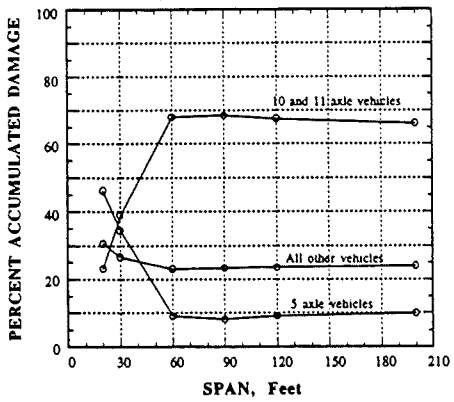

e) M-14/NYCRR % Damage.

Fig. 11-104. % Damage by Vehicle. Type vs. Span Length.

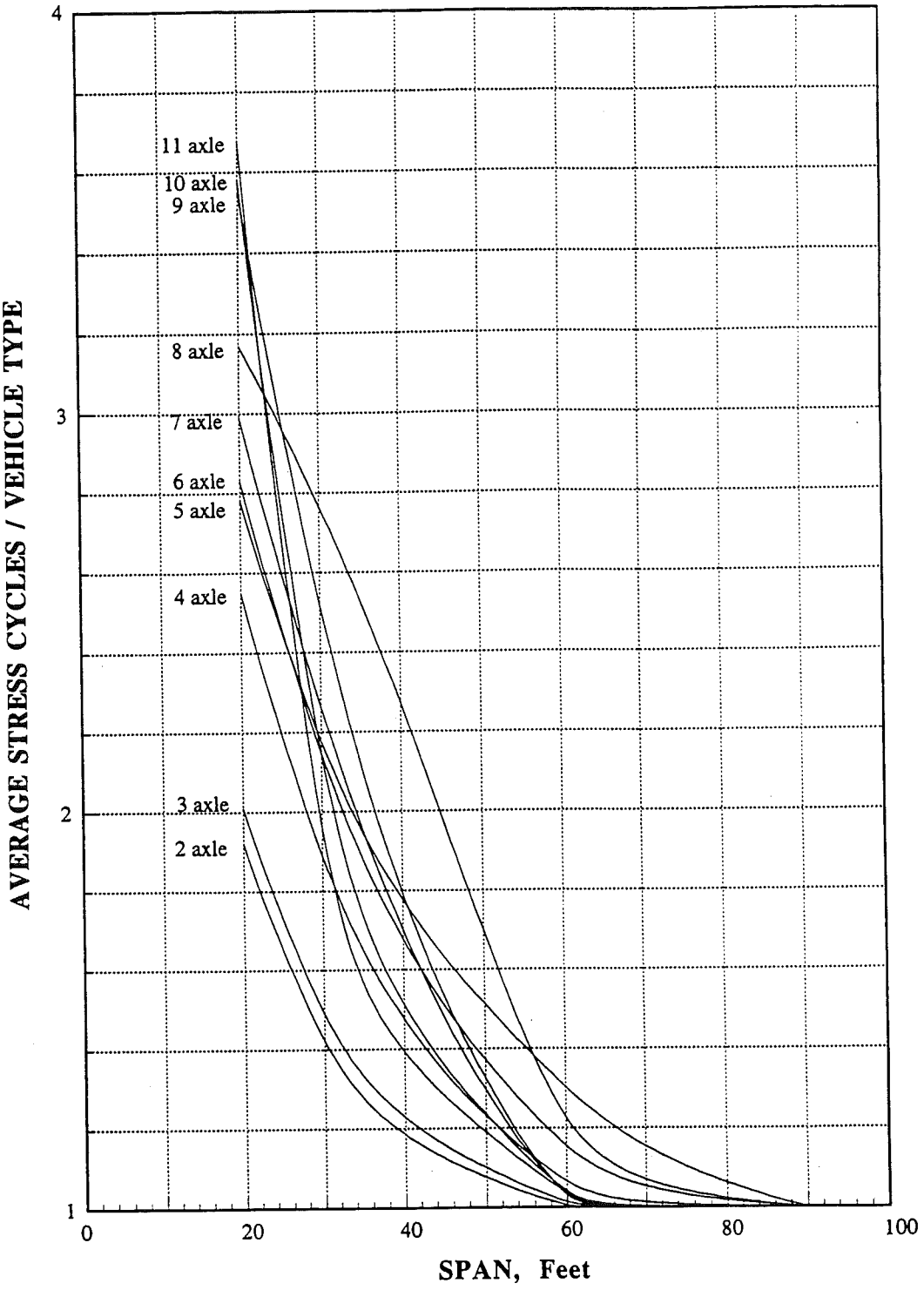

Fig. 11-105. Average Cycles/Vehicle. Type (by No. of Axles) vs. Span.

11-8 Summary

The above analysis of the WIM and strain history data provides information required to complete a fatigue lifetime analysis of the tested bridges and other bridges along the routes surveyed. More detailed strain measurements may be taken in components of concern, however the bridges tested do not appear to have fatigue susceptable details and it is not anticipated that fatigue will be a governing concern during the normal life of these bridges.

The most damaging vehicles for bridges are the eight to eleven axle vehicles, and in particular the eleven axle vehicles. This is true even when considering the relatively low percentage of eleven axle vehicles in the total truck population. Bridges with suspected fatigue prone details should be analyzed with methods other than the AASHTO fatigue truck model. The AASHTO model and others were developed based on WIM measurements which did not include the typical vehicles encountered in the State of Michigan, that is vehicles with more than 5 axles.

Note:

Intentionally left blank

12. CONCLUSIONS AND RECOMMENDATIONS

The conclusions refer to the evaluation of the actual live load on bridges, evaluation of corroded bridges and fatigue evaluation of steel bridges.

1. WIM measurements provide unbiased information about the actual live load on bridges. Truck drivers are not aware that their vehicles are being measured and, therefore, they do not make any special effort to avoid the WIM system. In the results, there is a considerable difference between the results of truck survey using weigh stations and WIM.

2. The heaviest vehicles (GVW) are 11 axle trucks with coils of steel, gravel, or asphalt.

3. The measurements taken in the vicinity of Truck Weigh Station indicate that truck weights are within the legal limits. However, on bridges further away from Weigh Stations, truck weights often exceed the legal limits. This applies to GVW and axle loads. The observation was also confirmed by measurements on I-94 over Pierce Road when the Weigh Station was open and closed. This observation confirms that overloaded trucks avoid the scales.

4. The effect of heavy trucks is larger for longer spans. Moments and shear forces are calculated for the measured trucks. The largest moments and shears are for 11 axle vehicles, in particular for spans 120-200 ft.

5. Live load varies depending on location. The difference is not only in ADTT, but also in magnitude (truck weights). The heaviest traffic occurs on bridges that are not located close to the Truck Weigh Station.

6. The major problem with the currently used WIM equipment is tape switches and infrared sensors. Both are sensitive to damage by

truck tires, both require traffic control, and depend on the weather. Therefore, effort will be made in the future to find an alternative solution.

7. The system used for fatigue load spectra performed very well. It is convenient, small size, reliable, operates using a battery, and it can be left in an unattended mode for up to 3 weeks time. Therefore, effort will be made to develop the software for this system to measure truck weights.

8. Dynamic load on bridges is a function of three parameters: bridge dynamics (natural frequency of vibration), surface roughness and truck dynamics. The field tests confirmed earlier theoretical results obtained at the University of Michigan (Hwang and Nowak 1991). Dynamic load as a percentage of live load decreases with increasing truck weight.

9. Load carrying capacity of corroded steel girder bridges depends mostly on the condition of parameters such as web thickness at the support and flange thickness at the mid-portion of the span. Excessive loss of material may lead to local buckling in the compressed part of the web. Presence of web stiffeners (bearing stiffeners) can extend the life of the structure.

10. Prediction of the remaining life of corroded steel girder bridges involves the prediction of future rate of corrosion. For given rates, material loss and corresponding reduction of the load carrying capacity can be evaluated. Remaining life is the maximum number of years until the capacity is reduced below a critical level..

11. Fatigue evaluation involves calculation of the accumulated damage and prediction of the remaining life. An important part of fatigue analysis is the evaluation of load spectra. Accumulated damage is a function of the past load cycles, ADTT's and truck weights. Prediction of remaining life involves prediction of the future loads (ADTT's and truck weights). The analysis can be based on the

available WIM results. The extrapolation of moments and shears can be performed using the normal probability paper (Nowak and Hong 1991; Nowak 1993).

12. Stress values due to traffic load recorded in the girders are rather low. The maximum observed values are about 10 ksi. However, in most cases the maximum values do not exceed 5 ksi, for the most loaded girder, with most readings being about 1 ksi.

13. Stress spectra considerably vary from girder to girder (component-specific). Therefore, the expected fatigue life is different depending on girder location. Exterior girders experience the lowest load spectra.

14. It is recommended to continue WIM studies on Michigan highways. The results will be used to establish different classes of highways with regard to ADTT (low, medium and high) and truck weights (low, medium and high). A combination of ADTT and weight class can serve as a basis for fatigue evaluation of bridges.

15. There is a need for a practical application of the corrosion evaluation procedure. The procedure will be further developed in a form of an interactive knowledge-based expert system (KBES).

16. Fatigue live load spectra can be determined by WIM measurements. Fatigue evaluation procedure will be further developed in a form of an expert system (KBES).

Note:
Intentionally left blank

13. REFERENCES

AASHTO, (1994). "LRFD Bridge Design Specification," American Association of State and Transportation Officials, Washington, D.C.

AASHTO, (1992). "Standard Specification for Highway Bridges," American Association of State and Transportation Officials, Washington, D.C.

AASHTO, (1989). *Guide Specifications for Strength Evaluation of Existing Steel and Concrete Bridges*, American Association of State and Transportation Officials, Washington, D.C.1989.

AASHTO, (1989). Standard Specifications for Highway Bridges, American Association of State Highway and Transportation Officials, Washington, DC.

AASHTO, (1983). Manual for Maintenance Inspection of Bridges, American Association of State Highway and Transportation Officials, Washington, D.C.

AASHTO, (1983b). "Manual for Maintenance Inspection of Bridges," American Association of State Highway and Transportation Officials, Washington, DC.

AISC, (1986). Manual of Steel Construction Load and Resistance Factor Design, American Institute of Steel Construction, First Edition.

Albrecht, P., and Naeemi, A.H., (1984). "Performance of Weathering Steel in Bridges," National Cooperative Highway Research Program, Report 272, July.

Albrecht, M. and Friedland, I.M., (1979). "Fatigue-Limit Effect on Variable-Amplitude Fatigue Stiffeners," *Journal of Structural Engineering*, ASCE, Vol. 105, ST12, December 1979, pp. 2657-75.

Al-Zaid, R. Z. and Nowak, A. S., "Fatigue Strength of Prestressed Concrete Girder Bridges," Canadian Journal of Civil Engineering, Vol. 15, No. 2, April 1988, pp. 199-205.

Bakht, B. and Pinjarkar, S. G. (1989). "Dynamic Testing of Highway Bridges - A Review," Transportation Research Record, No. 1223, Washington, D. C. pp. 93-100.

Bannantine, J.A., Comer, J.J., and Handrock, J.L., (1990). *Fundamentals of Metal Fatigue Analysis*, Prentice Hall, Englewood Cliffs, New Jersey.

Bellenoit, J. R., Yen, B. T., and Fisher, J. W., (1984). "Stresses in Hanger Plates of Suspended Bridge Girders," Transportation Research Record, No. 950, Vol. 2, pp. 20-23.

Benjamin, J.R., and Cornell, C.A., (1970). *Probability, Statistics, and Decision Making for Civil Engineers*, McGraw-Hill Book Company.

Billing, J. R. (1984). "Dynamic Loading and Testing of Bridges in Ontario," Canadian Journal of Civil Engineering, Vol. 11, No. 4, pp. 883-843.

Blejwas, T. E., Feng, C. C., and Ayre, R. S. (1979). "Dynamic Interaction of Moving Vehicles and Structures", Journal of Sound and Vibration, Vol. 67, No. 4, December, pp. 513-521.

Brockenbrough, R. L., (1983). "Considerations in the Design of Bolted Joints for Weathering Steel," AISC Engineering Journal, American Institute of Steel Construction, Vol. 20, No. 1, pp. 40-45.

Cantieni, R. (1983). "Dynamic Load Tests on Highway Bridges in Switzerland", Report No. 211, Swiss Federal Laboratories of Material Testing and Research (EMPA), Dubendorf, Switzerland.

Cho, H-N, Kim, D-H, and Ang, H-S, (1989). "Fatigue Reliability of Steel Structures in the Presence of Residual Stresses," Proceedings, 5th ICOSSAR, 1989, pp. 1579.

Committee on Fatigue and Fracture Reliability of the Committee on Structural Safety and Reliability of the Structural Division, (1982). "Fatigue Reliability: Variable Amplitude Loading," *Journal of the Structural Division*, ASCE, Vol. 108, No. ST1, January 1982, pp. 47-69.

Deurling, K., and Albrecht, P., (1979). "Fatigue Probability in Steel Highway Bridges," Proceedings, *Specialty Conference on Probabilistic Mechanics and Structural Reliability*, ASCE, Tucson, Ariz., Jan. 1979, pp. 186-90.

Ditlevsen, O., (1981). "Principle of Normal Tail Approximation," *Journal of Engineering Mechanics*, ASCE, Vol. 107, No. EM6.

Dowelling, N.E., (1972). "Fatigue Failure Predictions for Complicated Stress-Strain Histories," *Journal of Materials*, JMLSA, Vol. 7, No. 1, March 1972, pp. 71-87.

FHWA, *The State of the Nation's Highway and Bridges: Condition and Performance and Highway Bridge Replacement and Rehabilitation Program*. Federal Highway Administration, US. Department of Transportation, Washington D.C., 1989.

Fisher, J.W., (1984). *Fatigue and Fracture in Steel Bridges: Case Studies*, New York : Wiley, 1984.

Fisher, J.W., Mertz, D.R., and Zhong, A., (1983). "Steel Bridge Members Under Variable Amplitude Long Life Fatigue Loading," *NCHRP Report 267*, Lehigh University, TRB, December 1983.

Fisher, J.W., (1977). "Bridge Fatigue Guide - Design and Details", American Institute of Steel Construction, Chicago.

Fisher, J.W., et al, (1970). "Effect of Weldments on the Fatigue Strength of Steel Beams," National Cooperative Research Program, Report 102, 1970.

Frank, K.H., (1992). "Using Measured Stress Histories to Evaluate the Remaining Fatigue Life of Bridges," 3rd Int'l Workshop on Bridge Rehabilitation, Kluer Academic Publishers, Dordrecht, The Netherlands, June, 1992, pp. 529.

Fujino,Y. and Bhartia, B.K., (1987). "Effect of Multiple Pressence of Vehicles on Fatigue Damage of Highway Bridges," 5th ICASP, 1987, pp.1157.

Genin, J. and Chung, Y. I. (1979). "Response of Continuous Guideway on Equally Spaced Supports Traversed by a Moving Vehicle," Journal of Sound and Vibration, Vol. 67, No. 2, November, pp. 245-251.

Ghosn, M. and Moses, F. (1984). "Bridge Load Modeling and Reliability Analysis," Report No. R 84-1, Department of Civil Engineering, Case Western Reserve University.

Gupta, R. K. (1980). "Dynamic Loading of Highway Bridges", Journal of the Engineering Mechanics Division, Proceedings of ASCE, Vol. 106). No. EM2, April, pp. 377-393.

Haaijer, G., Carshaddan, M. A., and Grubb, M. A. (1983). "Autostress Design of Steel Bridge," Journal of the Structural Division, ASCE, Vol. 109, No. ST1, January, pp. 188-199.

Hahin, C, et al, (1993). "Accurate and Rapid Determination of Fatigue Damage in Steel Bridges," *Journal of Structural Engineering*, ASCE, Vol. 119, No, 1, January 1993.

Hahn and Shapiro, (1992). *Statistical Models in Engineering*, John Wiley and Sons, New York, pp 108-11, 1992.

Hanna, S.Y. and Karsan, D.I., (1991). "Fatigue Data for Reliability-Based Offshore Platform Inspection and Repair," *Journal of Structural Engineering*, ASCE, Vol. 117, No. 10, October 1991.

Hasofer, A.M. and Lind, N.C., (1974). "An Exact and Invariant First Order Reliability Format," *Journal of Structural Mechanics Division*, ASCE, Vol. 100, No. EM2, February 1974.

Haugen, E.B., (1980). *Probabilistic Mechanical Design*, John Wiley and Sons, New York, 1980.

Heavner, J.W., et al, (1985). "Measured Fatigue Stress Response of North Sea Jacket Platforms, " Proceedings of 4th ICOSSAR, 1985.

Hikosaka, H., Yoshimira, T., and Uchitani, T. (1978). "Non- Stationary Random Response of Bridges to a Series of Moving Vehicle Load," Theoretical and Applied Mechanics, Vol. 28, Proceedings of the 26th Japan National Congress for Applied Mechanics, pp. 379-386.

Hognestad, E., Hanson, N. W., and McHenry, D. (1955,). "Concrete Stress Distribution in Ultimate Strength Design," ACI Journal, Vol. 55, December, pp. 455-479.

Honda, H., Kobori, T. and Yamada, Y. (1986). "Dynamic Factor of Highway Steel Girder Bridges," International Association of Bridge and Structural Engineering, IABSE Proceedings P-98/86), May, pp. 57-75.

Huang, D., Wang, T. L., and Shahawy, M. (1992). "Impact Analysis of Continuos Multigirder Bridges Due to Moving Vehicles," Journal of Structural Engineering, ASCE, Vol. 118, No. 12, pp. 3427-3443.

Hwang, E-S. and Nowak, A.S., "Dynamic Analysis of Girder Bridges," Transportation Research Record, No. 1223, 1990, pp. 85-92.

Hwang, E.-S., and Nowak, A.S. (1991). "Simulation of Dynamic Load for Bridges," Journal of Structural Engineering, ASCE, Vol. 117 No. 5, pp. 1413-1434.

Imbsen and Associates, (1987). "Development of Site Specific Load Models for Bridge Rating," Interim Report, *NCHRP 12-28(11)*, Transportation Research Board, Washington, D. C., Nov. 1987.

Johnston, B. C. (1976). Guide to stability Design Criteria for Metal Structures, Structural Stability Research Council, 3rd Edition, John Wiley and Sons, New York.

Juvinall, R.C., (1967). *Engineering Considerations of Stress, Strain, and Strength*, McGraw Hill Book Company, New York, 1967.

Karadeniz, H., (1989). "Spectral Analysis and Fatigue Reliability Assessment for Offshore Structures," Proceedings of 5th ICOSSAR, 1989, pp. 135.

Karamchandani, A., Dalane, J.I., and Bjerager, P., (1992). "Systems Reliability Approach to Fatigue of Structures," *Journal of Structural Engineering*, ASCE, Vol. 118, No. 3, March 1992.

Karpenko, G.V. and Vasilenko, I.I. (1979). Stress Corrosion Cracking of Steel, Freund Publishing,Tel-Aviv, Israel.

Kayser, J. R. (1988). The Effects of Corrosion on the Reliability of Steel Girder Bridges, Ph.D. Thesis, Dept. of Civil Engrg., University of Michigan.

Kayser, J.R. and Nowak, A.S., "Reliability of Corroded Steel Girder Bridges," Journal of Structural Safety, No. 6, 1989, pp. 53-63.

Kayser, J. R. and Nowak, A.S. (1989). "Capacity Loss Due to Corrosion in Steel Girder Bridges," ASCE, Journal of Structural Engineering, Vol. 115, No. 6, June, pp. 1525-37.

Kayser, J. R. and Nowak, A. S. (1987). "Evaluation of Corroded Steel Bridges," Bridges and Transmission Line Structures, American Society of Civil Engineers, pp. 35-46.

Khaleel, M.A. and Itani, R.Y., (1993). "Effect of Alternative Truck Configurations and Weights on the Fatigue Life of Bridges," Transportation Research Record 1393, Transportation Research Board, Washington DC, 1993.

Komp, M. E. (1987). "Atmospheric Corrosion Ratings of Weathering Steels - Calculations and Significance," Materials Performance, Vol. 26, No. 7, July, pp. 42-44.

Konig, G. and Nowak, A.S., ed., "Bridge Rehabilitation", Ernst & Sohn, Berlin, Germany, 1992.

Konig, G., and Seifert, P., (1990). "Fatigue Loading and Design for Bridges", Proceedings of the NATO Advanced Research Workshop, *Bridge Evaluation, Repair and Rehabilitation*, Kluer Academic Publishers, Dordrecht, The Netherlands, April 1990.

Kumar, A. and Karsan, D.I., (1990). "Fatigue Reliability of Parallel Systems," *Journal of Structural Engineering*, ASCE, Vol. 116, No. 3, March 1990.

Laman, J.A. (in print). Fatigue Load Models for Girder Bridges, Doctoral Disertation, University of Michigan, Ann Arbor, Michigan.

LRFD AASHTO, (1993). "LRFD Code for Design of Bridges", American Association of State Highway and Transportation Officials, Washington, D. C. (4th Draft).

Lawrence, M., et al, (1990). "Fatigue Crack-Growth Reliability," *Journal of Engineering Mechanics*, ASCE, Vol. 116, No. 3, March 1990.

Lutes, L.D. and Larsen, C.E., (1990). "Improved Spectral Method for Variable Amplitude Fatigue Prediction," *Journal of Structural Engineering*, ASCE, Vol. 116, No. 4, April 1984.

Lutes, L.D., et al, (1984). "Stochastic Fatigue Damage Accumulation," *Journal of Structural Engineering*, ASCE, Vol. 110, No. 11, November 1984.

Moses, F., Schilling, C., and Raju, S., (1988). "Fatigue Evaluation Procedures for Steel Bridges," Final Report, *NCHRP 12-28(3)*, Transportation Research Board, 1988,

Moses, F. and Ghosn, M., (1983). "Instrumentation for Weighing Trucks-in-Motion for Highway Bridge Loads," Final Report, FHWA/OH-83/001, August 1983.

Moses, F., (1979). "Weigh-in-Motion System Using Instrumented Bridges," *Journal of the Transportation Division*, ASCE, May 1979. (TA1001.A52)

Nassif, H. H. (1993) " Live Load Spectra For Girder Bridges", Ph.D. Dissertation, University of Michigan, Ann Arbor, Michigan.

Nassif, H.H., (1992). "Live Load Spectra for Girder Bridges," Doctoral Dissertation, University of Michigan, Ann Arbor, Michigan 1992.

Nowak, A.S. (1993). " Calibration of LRFD Bridge Design Code", Report UMCEE 93-22, Department of Civil and Environmental Engineering, University of Michigan, Ann Arbor.

Nowak, A. S., Nassif, H. H., and DeFrain, L. (1993). "Effect of Truck Loads on Bridges, " ASCE Journal of Transportation Engineering, Vol. 119, No. 6, pp. 853-867.

Nowak, A.S. and Hong, Y-K, (1991). "Bridge Live Load Models," *Journal of Structural Engineering*, ASCE, Vol. 117, No. 9, pp. 2757-67, Sept. 1991.

Nowak, A.S. and Nassif, H., (1991). "Effect of Truck Loading on Bridges," Report UMCE 91-11, Department of Civil Engineering, University of Michigan, Ann Arbor, Michigan, 1991.

Nowak, A.S., (1988). "Damage Accumulation Models for Bridges," Proceedings of the 5th ASCE Specialty Conference, *Probabilistic Methods in Civil Engineering*, P. D. Spanos, (ed), Blacksburg, VA, May 1988, pp. 225-8.

Nowak, A.S., ed.,"Bridge Evaluation, Repair and Rehabilitation," NATO ASI Series E, Vol. 187, Kluwer Academic Publishers, Dordrecht, Netherlands, 1990.

Nowak, A. S. and Absi, E., ed., "Bridge Evaluation, Repair and Rehabilitation," NSF Workshop Proceedings, University of Michigan, 1987.

Nowak, A.S., Yamani, A.S. and Tabsh, S.W., 1994, "Probabilistic Models for Resistance of Concrete Bridge Girders", ACI Structural Journal, Vol. 91, No. 3, pp. 269-276.

Nowak, A.S., 1994, "Load Model for Bridge Design Code", Canadian Journal of Civil Engineering, Vol. 21, pp. 36-49.

Nowak, A.S. and Grouni, H.N., 1994, "Calibration of the OHBDC-1991", Canadian Journal of Civil Engineering, Vol. 21, pp. 25-35.

Nowak, A.S., 1993, "Live Load Model for Highway Bridges", Journal of Structural Safety, Vol. 13, Nos. 1+2, December, pp. 53-66.

Nowak, A.S., Nassif, H. and Frank, K.H., "Fatigue Load Spectra for Steel Girder Bridge", Transportation Research Record, No. 1393, pp. 154-161.

Nowak, A.S., Hong, Y-K and Hwang, E-S., "Modeling Live Load and Dynamic Load for Bridges," Transportation Research Record, No. 1289, 1991, pp. 110-118.

Nowak, A. S. and Tharmabala, T., "Bridge Reliability Evaluation using Load Tests," Journal of Structural Engineering, ASCE, Vol. 114, No. 10, October 1988, pp. 2268-2279.

Nowak, A.S., and Tharmabala, T., (1987). "Mathematical Models for Bridge Reliability," *Canadian Journal of Civil Engineering*, Vol. 14, No. 2, 1987.

Nowak, A.S., et al., (1987). "Design Loads for Future Bridges," *Report UMCE1*, Dept. of Civil Engineering, University of Michigan, Ann Arbor, MI, Feb. 1987.

Nyman, W.E. and Moses, F., (1985). "Calibration of Bridge Fatigue design Model," *Journal of Structural Engineering*, ASCE, Vol. 11:1251-66, June 1985.

O'Connor, C. and Chan, T.H.T. (1988). "Dynamic Wheel Loads From Bridge Strains", ASCE Journal of Structural Engineering, Vol. 114, No. 8, pp. 1703-1723.

O'Connor, C. and Pritchard, R. W. (1985). "Impact Studies on Small Composite Girder Bridge", ASCE Journal of Structural Engineering, Vol. 111, No. 3, pp. 641-653.

OHBDC. (1979; 1983; 1993). "Ontario Highway Bridge Design Code." Ministry of Transportation, Downsview, Ontario, Canada.

OBDC, (1991). Ontario Highway Bridge Design Code, Third Edition, Ontario Ministry of Transportation, highway Engineering Division, Ontario, Canada.

Ortiz, K. and Chen, N.K., (1987). "Fatigue Damage Prediction for Stationary Wideband Random Stresses," Proceedings of 5th ICASP, University of British Columbia, Vancouver, Canada, 1987, pp. 317.

Paultre, P., Chaallal, O. and Proulx, J., (1992). "Bridge Dynamics and Dynamic Amplification Factors - a Review of Analytical and Experimental Findings", Canadian Journal of Civil Engineering, Vol. 19, pp. 260-278.

Pavia,, A., (1975). "Reliability Approach to Fatigue Design of Highway Bridges," Doctoral Dissertation, Case Western Reserve University, Cleveland, Ohio, 1975.

Paz, Mario (1991). "Structural Dynamics - Theory and Computation", 3rd Edition, Van Nostrand Reinhold, New York, 626 p.

Press, W. H., Flannery, B. P., Teukolsky, S. A., Vetterling, W. T., (1988). "Numerical Recipes - The Art of Scientific Computing", Cambridge University Press, 818 p.

Pritchard, R.W., (1991). "Fatigue Testing of Breakfast Creek Bridge," Proceedings of AustroRoads Conf., Brisbane, Australia, R.J. Heywood ed., 1991, pp. 289-302.

Raju, S.K., Moses, F., and Schilling, C.G., (1990). "Reliability Calibration of Fatigue Evaluation and Design Procedures," *Journal of Structural Engineering*, Vol. 116:1356-69, May 1990.

Roberts, T. M. (1981)."Slender Plate Girders Subjected to Edge Loading," Proceedings of the Institute of Civil Engineers, London, Vol. 71, Part 2, Sept., pp. 805-819.

Sakano, M., Mikami, I., and Miyagawa, (1993). "Simultaneous Loading Effect of Plural Vehicles on Fatigue Damage of Highway Bridges," Proceedings of the IFIP WG7.5 Fifth Working Conference on Reliability and Optimization of Structural Systems, Takamatsu, Kagawa, Japan, March 1993.

Saunders, S.C., (1972). "On the Probabilistic Determination of Scatter Factors Using Miner's Rule in Fatigue Studies," Probabilistic Aspects of Fatigue, ASTM STP 511, American Society for Testing materials, 1972, pp. 185-203.

Schilling, C.G., (1984). "Stress Cycles for Fatigue Design of Steel Bridges," *Journal of Structural Engineering*, ASCE, Vol. 110, No. 6, June 1984.

Schilling, C.G., (1982a). "Lateral-Distribution Factors for Fatigue Design," *Journal of the Structural Division*, ASCE, Vol. 108, ST9, September 1982. pp. 2015-33.

Schilling, C.G., (1982b). "Impact Factors for Fatigue Design," *Journal of Structural Engineering*, ASCE, Vol. 108, No. ST9, September 1982.

Schilling, C.B., et al. (1978). "Fatigue of Welded Steel Bridge Members Under Variable Amplitude Loading," *NCHRP Report 188*, U.S. Steel Corp., TRB, Washington D.C.

Shin, J.C., et al, (1989). "Fatigue Reliability and Remaining Fatigue Life of Existing Steel Rail-Road Bridges," Proceedings of 5th ICOSSAR, 1989, pp. 1587-94.

SIA 160E, (1988). Einwirkungen und Tragwerke, Entwurf, Schweiz Ingenieur und Architektenverein, Zurich, Switzerland.

Snyder, R.E., Likins, G.E., and Moses, F., (1985). "Loading Spectrum Experienced by Bridge Structures in the United States," Report FHWA/RD-85/012, FHWA, US Department of Transportation, Washington DC, 1985.

Sommer, A.M., Nowak, A.S. and Thoft-Christensen, P., 1993, "Probability-based Bridge Inspection Strategy", ASCE Jnl of Structural Eng., Vol. 119, No. 12, pp. 3520-3536.

Tabsh, S.W. and Nowak, A.S., "Reliability of Highway Girder Bridges," ASCE Journal of Structural Engineering, Vol. 117, No. 8, August 1991, pp. 2373-2388.

Tallin, A.G. and Petreshock, T., (1990). *Modeling Fatigue loads for Steel Bridges*, Transportation Research Record No. 1275, Washington D.C., 1990.

Tang, J-P. and Yao, J.T.P., (1972). "Fatigue Damage Factor in Structural Design," *Journal of Structural Engineering*, ASCE, Vol. 98, No. ST1, January 1972. pp. 125-34.

Thoft-Christensen, P., and Murotsu, Y., (1982). *Application of Structural Reliability Theory* , Springer-Verlag, New York, NY, 1982.

Thoft-Christensen, P., and Baker, M.J., (1986). *Structural Reliability Theory and Its Applications*, Springer-Verlag, New York, NY, 1986.

Tilly, G.P. and Nunn, D.E., (1980). "Variable Amplitude Fatigue in Relation to Highway Bridges," Proceedings, *The Institution of Mechanical Engineers*, Applied Mechanics Group, 194(27). pp. 258-267.

Ting, S-C. and Nowak, A.S., "Effect of Rebar Area Loss on Flexural Behavior of R/C Beams," ACI Structural Journal, Vol. 88, No. 3, May-June 1991, pp. 309-314.

Ting, S-C. and Nowak, A.S., "Effect of Tendon Area Loss on Flexural Behavior of P/C Beams," ASCE Journal of Structural Engineering, Vol. 117, No. 4, April 1991, pp. 1127-1143.

Torng, T.Y, and Wirsching, P.H., (1991). "Fatigue and Fracture Reliability and Maintainability Process," *Journal of Structural Engineering*, ASCE, Vol. 117, No. 12, December 1991.

Tunna, J.M., (1985). "Random Load Fatigue: Theory and Experiment," Proceedings, *The Institution of Mechanical Engineers*, Vol. 199, N0. C3, March 1985.

Wirsching, P.H., (1984). "Fatigue Reliability for Offshore Structures," *Journal of Structural Engineering*, ASCE, Vol. 110, No. 10, October 1984.

Wirshing, P.H. and Light, M.C., (1980). "Fatigue Under Wide Band Random Stresses," *Journal of the Structural Division*, ASCE, Vol. 106, No ST7, pp. 1593-1607, July 1980.

Wirsching, P.H. and Shehata, A.M., (1977). "Fatigue Under Wide Band Random Stresses using the Rainflow Method," Journal of Materials and Technology, Trans of ASME, July 1977, pp. 205-211.

Wu, Y-T and Wirsching, P.H., (1984). "Advanced Reliability Method for Fatigue Analysis," *Journal of Structural Engineering*, ASCE, Vol. 110, No. 4, April 1984.

Wu, J. S. and Dai, C. W. (1987). "Dynamic Responses of Multispan Nonuniform Beam due to Moving Loads," ASCE Journal of Structural Engineering, Vol. 113, No. 3, pp. 458-474.

Yao, J.T.P., (1974). "Fatigue Reliability and Design," *Journal of the Structural Division*, ASCE, Vol. 100, No ST9, pp. 1827-37, September 1974.

Yazdanii, N., and Albrecht, P., (1987). "Risk Analysis of Fatigue Failure of Highway Steel Bridges", *Journal of Structural Engineering*, Vol. 113:483-500, March 1987.

Zhou, J-H. and Nowak, A. S., "Nonlinear Analysis of Highway Bridges," Transportation Research Record, No. 1118, 1988, pp. 25-28.

Zuraski, P.D., and Johnson, J.E., (1990). "Fatigue Strength of Deteriorated Steel Highway Bridges," *Journal of Structural Engineering*, ASCE, Vol. 116:2671-90. Oct. 1990.

Zwerneman, F.J. and Frank, K.H., (1988). "Fatigue Damage Under Variable Amplitude Loads," *Journal of Structural Engineering*, ASCE, Vol. 114:67-83, January 1988.

APPENDIX A - PROBABILITY PAPER

1. Introduction

WIM measurements provided a large amount of data. From the bridge evaluation point of view, it is important to calculate the maximum moments and shears. Therefore, for each measured truck, moments and shears were calculated for various spans. Random variation of moments and shears can be studied by the analysis of their cumulative distribution functions (CDF's). The most important is the upper tail which represents the largest values of moments and shears. However, because of the scale, it is not possible to examine their shapes. Therefore, the cumulative distribution function is plotted on the so called normal probability paper.

Normal probability paper is a special scale such that any normal distribution function is represented by a straight line and any straight line represents a normal distribution function. Construction of the normal probability paper is explained in the basic probability textbooks (Benjamin and Cornell 1980). Probability paper is particularly usefull for plotting the numerical data.

Construction and use of probability paper for plotting test results is presented in this Appendix.

2. Normal Random Variable

Probability density function (PDF) of a normal or Gaussian random variable is

$$f_X(x) = \frac{1}{\sigma\sqrt{2\pi}} e^{-\frac{(x-\bar{x})^2}{2\sigma^2}} \qquad \text{(A-1)}$$

where: $\bar{x}$ = mean and σ = standard deviation.

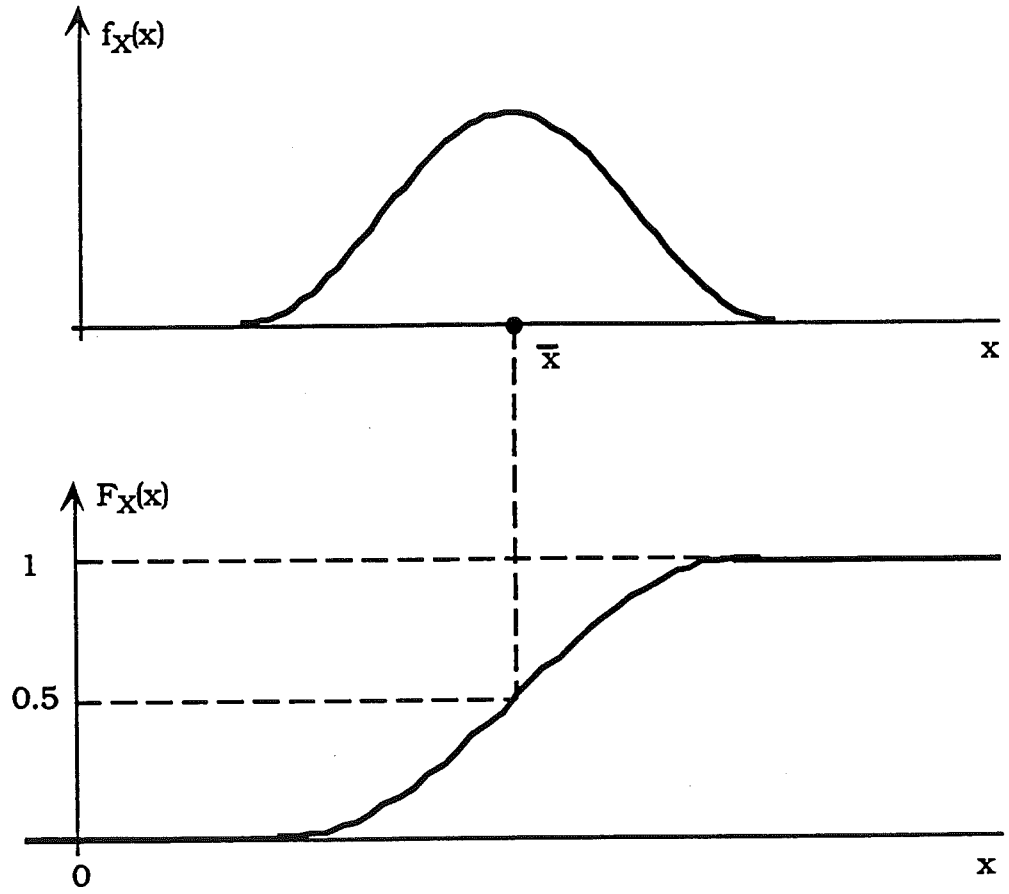

Fig. A-1. PDF and CDF of a Normal Random Variable.

Examples of cumulative distribution functions (CDF's) and PDF's for various normal random variables are shown in Fig. A-1.

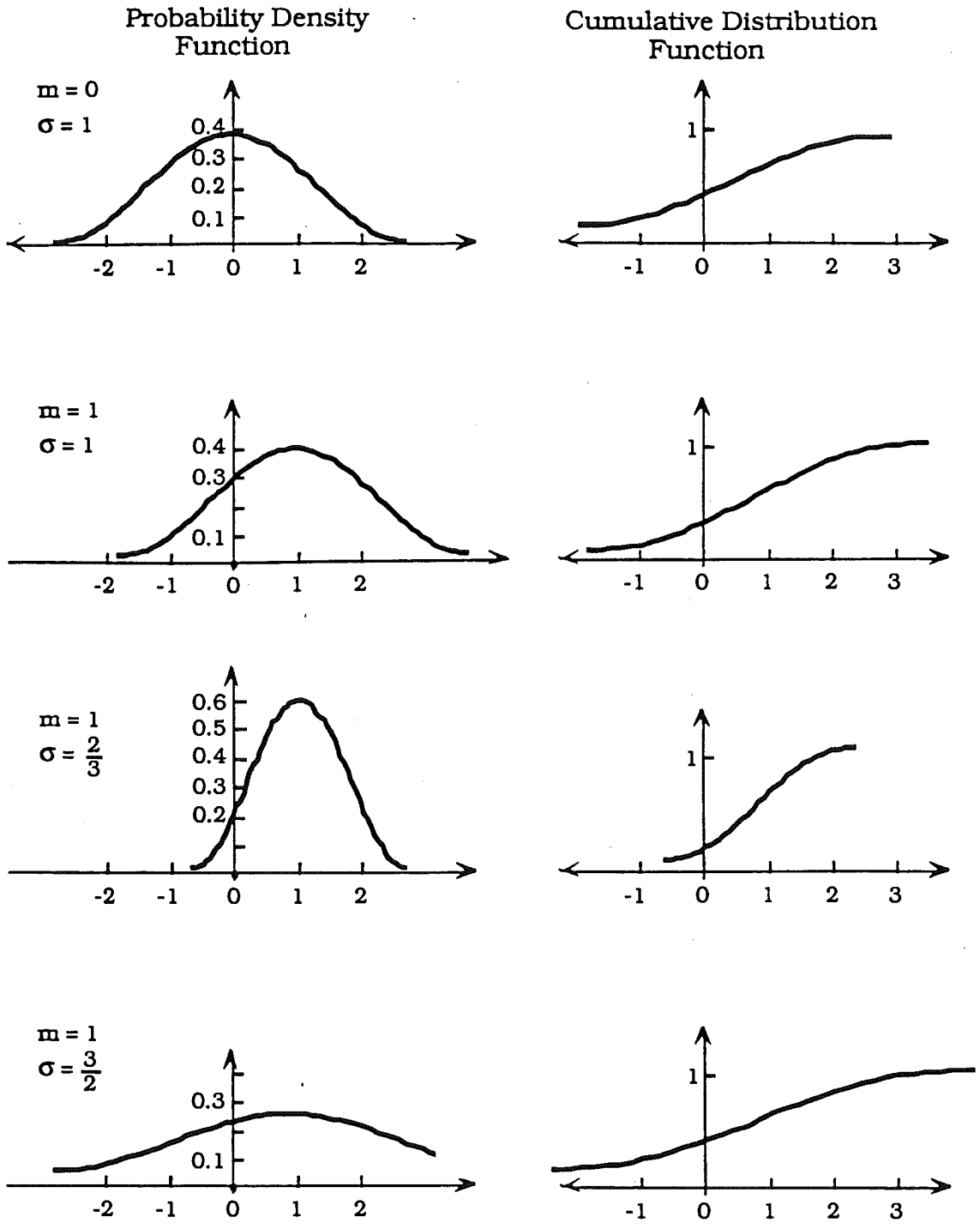

Fig. A-2. Examples of PDF's and CDF's for Normal Random Variables.

There is no closed-form solution for CDF,

$$F_X(x) = \int_{-\infty}^{x} f_X(t)\, dt \qquad \text{(A-2)}$$

Properties of $F_X(x)$ and $f_X(x)$ for a normal random variable include:

1. $f_X(x)$ is symmetrical about $\bar{x}$

$$f_X(x + \bar{x}) = f_X(-x + \bar{x}) \qquad \text{(A-3)}$$

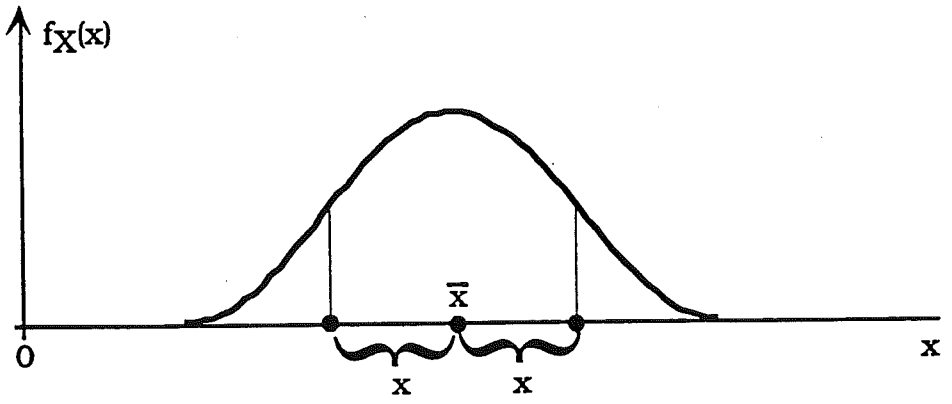

Fig. A-3. Normal Random Variable is Symmetrical about the Mean.

2. Sum of $F_X(x)$ calculated for $(x + \bar{x})$ and $(- x + \bar{x})$ is equal to 1,

$$F_X(x + \bar{x}) = 1 - F_X(-x + \bar{x}) \qquad \text{(A-4)}$$

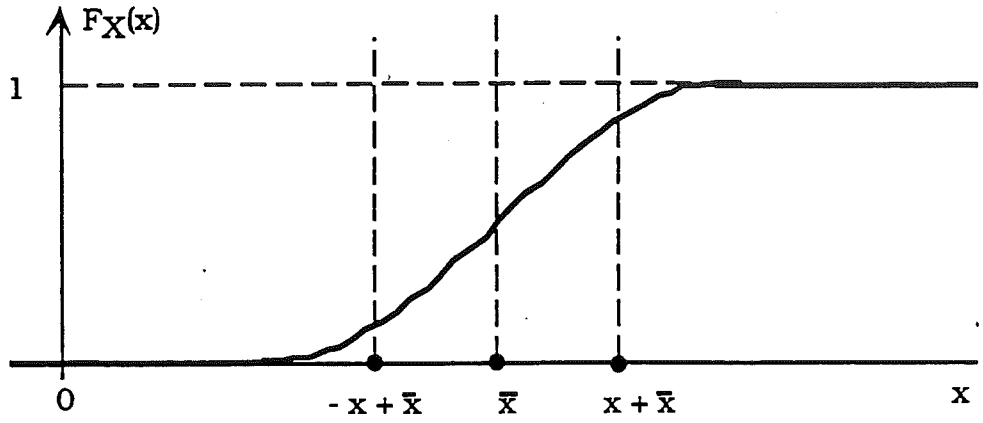

Fig. A-4. CDF for a Normal Random Variable.

3. Standard Normal Distribution

Probability density function (PDF) for a standard normal random variable can be obtained from Eq. A-1, by replacing $\bar{x}$ with 0, and σ with 1. The resulting equation is,

$$\phi(x) = \frac{1}{\sqrt{2\pi}} e^{-\frac{x^2}{2}} \qquad \text{(A-5)}$$

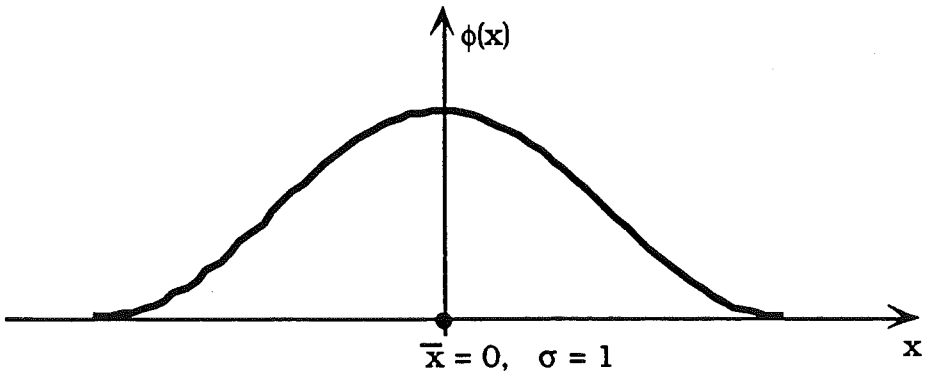

Fig. A-5. PDF for a Standard Normal Random Variable.

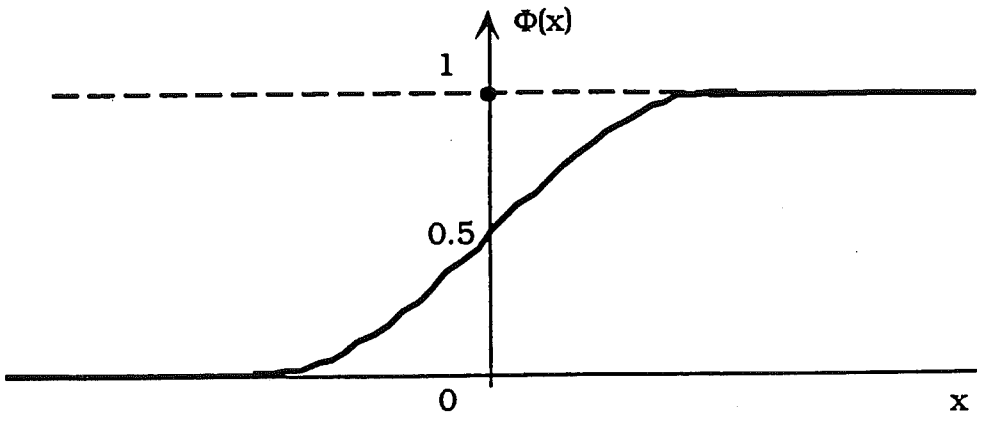

Fig. A-6. CDF for a Standard Normal Random Variable.

Let X be a normal random variable, and Z is its standard form. Then,

$$Z = \frac{X - \bar{x}}{\sigma_X}$$

and hence

$$X = \bar{x} + Z\,\sigma_X \tag{A-6}$$

Therefore,

$$F_X(x) = P\left(X \le x\right) = P\left(\bar{x} + Z\,\sigma_X \le x\right) \tag{A-7}$$

$$F_X(x) = P\left(Z \le \frac{x - \bar{x}}{\sigma_X}\right) = F_Z\left(\frac{x - \bar{x}}{\sigma_X}\right) = \Phi\left(\frac{x - \bar{x}}{\sigma_X}\right) \tag{A-8}$$

and finally,

$$F_X(x) = \Phi\left(\frac{x - \bar{x}}{\sigma_X}\right) \tag{A-9}$$

Function Φ is widely available in tables. It is also available in computers and calculators.

Similarly, a relationship can be derived for PDF of any normal random variable, $f_X(x)$, and PDF of the standard normal variable, $\phi(x)$,

$$f_X(x) = \frac{d\,F_X(x)}{dx} = \frac{d\left[\Phi\left(\frac{x - \bar{x}}{\sigma_X}\right)\right]}{dx} = \phi\left(\frac{x - \bar{x}}{\sigma_X}\right)\frac{1}{\sigma_X} \tag{A-10}$$

And for any normal random variable X,

$$f_X(x) = \phi\left(\frac{x - \bar{x}}{\sigma_X}\right)\frac{1}{\sigma_X} \tag{A-11}$$

Examples of $\Phi(x)$ for various values of x are given in Table A-1.

Table A-1. $\Phi(x)$ for Selected Values of x.

x	$\Phi(x)$
4.0	0.9999683
3.0	0.99865
2.0	0.9772
1.0	0.841
0.0	0.5
- 1.0	0.159
- 2.0	0.0228
- 3.0	0.00135
- 4.0	0.0000317

Values of $\Phi(x)$ are listed in Table A-2 for x from 0 to -15. Values of $\phi(x)$ are listed in Table A-3. Table A-2-4 provides $\Phi(x)$ for negative values of x only ($x \leq 0$). To calculate $\Phi(x)$ for $x > 0$, value of $\Phi(-x)$ is read from Table A-2-4 first, and then $\Phi(x) = 1 - \Phi(-x)$.

Example A-1.

(a) $x = 2.16$

From Table A-2,

$\Phi(x) = \Phi(-2.16) = 0.154_{10^{-1}} = 0.0154$

(b) Given $\Phi(x) = 0.80_{10^{-4}}$, determine $x = ?$

From Table A-2,

$x = -0.3775$ (by interpolation)

Table A-2. Values of Standard Normal CDF, $\Phi(x)$.

	.0	.01	.02	.03	.04	.05	.06	.07	.08	.09
0.0	.500E+00	.496E+00	.492E+00	.488E+00	.484E+00	.480E+00	.476E+00	.472E+00	.468E+00	.464E+00
0.1	.460E+00	.456E+00	.452E+00	.448E+00	.444E+00	.440E+00	.436E+00	.433E+00	.429E+00	.425E+00
0.2	.421E+00	.417E+00	.413E+00	.409E+00	.405E+00	.401E+00	.397E+00	.394E+00	.390E+00	.386E+00
0.3	.382E+00	.378E+00	.374E+00	.371E+00	.367E+00	.363E+00	.359E+00	.356E+00	.352E+00	.348E+00
0.4	.345E+00	.341E+00	.337E+00	.334E+00	.330E+00	.326E+00	.323E+00	.319E+00	.316E+00	.312E+00
0.5	.309E+00	.305E+00	.302E+00	.298E+00	.295E+00	.291E+00	.288E+00	.284E+00	.281E+00	.278E+00
0.6	.274E+00	.271E+00	.268E+00	.264E+00	.261E+00	.258E+00	.255E+00	.251E+00	.248E+00	.245E+00
0.7	.242E+00	.239E+00	.236E+00	.233E+00	.230E+00	.227E+00	.224E+00	.221E+00	.218E+00	.215E+00
0.8	.212E+00	.209E+00	.206E+00	.203E+00	.200E+00	.198E+00	.195E+00	.192E+00	.189E+00	.187E+00
0.9	.184E+00	.181E+00	.179E+00	.176E+00	.174E+00	.171E+00	.169E+00	.166E+00	.164E+00	.161E+00
1.0	.159E+00	.156E+00	.154E+00	.152E+00	.149E+00	.147E+00	.145E+00	.142E+00	.140E+00	.138E+00
1.1	.136E+00	.133E+00	.131E+00	.129E+00	.127E+00	.125E+00	.123E+00	.121E+00	.119E+00	.117E+00
1.2	.115E+00	.113E+00	.111E+00	.109E+00	.107E+00	.106E+00	.104E+00	.102E+00	.100E+00	.985E-01
1.3	.960E-01	.951E-01	.934E-01	.918E-01	.901E-01	.885E-01	.869E-01	.853E-01	.838E-01	.823E-01
1.4	.808E-01	.793E-01	.778E-01	.764E-01	.749E-01	.735E-01	.721E-01	.708E-01	.694E-01	.681E-01
1.5	.668E-01	.655E-01	.643E-01	.630E-01	.618E-01	.606E-01	.594E-01	.582E-01	.571E-01	.559E-01
1.6	.548E-01	.537E-01	.526E-01	.516E-01	.505E-01	.495E-01	.485E-01	.475E-01	.465E-01	.455E-01
1.7	.446E-01	.436E-01	.427E-01	.418E-01	.409E-01	.401E-01	.392E-01	.384E-01	.375E-01	.367E-01
1.8	.359E-01	.351E-01	.344E-01	.336E-01	.329E-01	.322E-01	.314E-01	.307E-01	.301E-01	.294E-01
1.9	.287E-01	.281E-01	.274E-01	.268E-01	.262E-01	.256E-01	.250E-01	.244E-01	.239E-01	.233E-01
2.0	.228E-01	.222E-01	.217E-01	.212E-01	.207E-01	.202E-01	.197E-01	.192E-01	.188E-01	.183E-01
2.1	.179E-01	.174E-01	.170E-01	.166E-01	.162E-01	.158E-01	.154E-01	.150E-01	.146E-01	.143E-01
2.2	.139E-01	.136E-01	.132E-01	.129E-01	.125E-01	.122E-01	.119E-01	.116E-01	.113E-01	.110E-01
2.3	.107E-01	.104E-01	.102E-01	.990E-02	.964E-02	.939E-02	.914E-02	.889E-02	.866E-02	.842E-02
2.4	.820E-02	.798E-02	.776E-02	.755E-02	.734E-02	.714E-02	.695E-02	.676E-02	.657E-02	.639E-02
2.5	.621E-02	.604E-02	.587E-02	.570E-02	.554E-02	.539E-02	.523E-02	.508E-02	.494E-02	.480E-02
2.6	.466E-02	.453E-02	.440E-02	.427E-02	.415E-02	.402E-02	.391E-02	.379E-02	.368E-02	.357E-02
2.7	.347E-02	.336E-02	.326E-02	.317E-02	.307E-02	.298E-02	.289E-02	.280E-02	.272E-02	.264E-02
2.8	.256E-02	.248E-02	.240E-02	.233E-02	.226E-02	.219E-02	.212E-02	.205E-02	.199E-02	.193E-02
2.9	.187E-02	.181E-02	.175E-02	.169E-02	.164E-02	.159E-02	.154E-02	.149E-02	.144E-02	.139E-02
3.0	.135E-02	.131E-02	.126E-02	.122E-02	.118E-02	.114E-02	.111E-02	.107E-02	.104E-02	.100E-02
3.1	.968E-03	.935E-03	.904E-03	.874E-03	.845E-03	.816E-03	.789E-03	.762E-03	.736E-03	.711E-03
3.2	.687E-03	.664E-03	.641E-03	.619E-03	.598E-03	.577E-03	.557E-03	.538E-03	.519E-03	.501E-03
3.3	.483E-03	.466E-03	.450E-03	.434E-03	.419E-03	.404E-03	.390E-03	.376E-03	.362E-03	.349E-03
3.4	.337E-03	.325E-03	.313E-03	.302E-03	.291E-03	.280E-03	.270E-03	.260E-03	.251E-03	.242E-03
3.5	.233E-03	.224E-03	.216E-03	.208E-03	.200E-03	.193E-03	.185E-03	.178E-03	.172E-03	.165E-03
3.6	.159E-03	.153E-03	.147E-03	.142E-03	.136E-03	.131E-03	.126E-03	.121E-03	.117E-03	.112E-03
3.7	.108E-03	.104E-03	.996E-04	.957E-04	.920E-04	.884E-04	.850E-04	.816E-04	.784E-04	.753E-04
3.8	.723E-04	.695E-04	.667E-04	.641E-04	.615E-04	.591E-04	.567E-04	.544E-04	.522E-04	.501E-04
3.9	.481E-04	.461E-04	.443E-04	.425E-04	.407E-04	.391E-04	.375E-04	.359E-04	.345E-04	.330E-04

Table A-2. Values of Standard Normal CDF, Φ(x) - continued.

4.0	.317E-04	.304E-04	.291E-04	.279E-04	.267E-04	.256E-04	.245E-04	.235E-04	.225E-04	.216E-04
4.1	.207E-04	.198E-04	.189E-04	.181E-04	.174E-04	.166E-04	.159E-04	.152E-04	.146E-04	.139E-04
4.2	.133E-04	.128E-04	.122E-04	.117E-04	.112E-04	.107E-04	.102E-04	.977E-05	.934E-05	.893E-05
4.3	.854E-05	.816E-05	.780E-05	.746E-05	.712E-05	.681E-05	.650E-05	.621E-05	.593E-05	.567E-05
4.4	.541E-05	.517E-05	.494E-05	.471E-05	.450E-05	.429E-05	.410E-05	.391E-05	.373E-05	.356E-05
4.5	.340E-05	.324E-05	.309E-05	.295E-05	.281E-05	.268E-05	.256E-05	.244E-05	.232E-05	.222E-05
4.6	.211E-05	.201E-05	.192E-05	.183E-05	.174E-05	.166E-05	.158E-05	.151E-05	.143E-05	.137E-05
4.7	.130E-05	.124E-05	.118E-05	.112E-05	.107E-05	.102E-05	.968E-06	.921E-06	.876E-06	.834E-06
4.8	.793E-06	.755E-06	.718E-06	.683E-06	.649E-06	.617E-06	.587E-06	.558E-06	.530E-06	.504E-06
4.9	.479E-06	.455E-06	.433E-06	.411E-06	.391E-06	.371E-06	.352E-06	.335E-06	.318E-06	.302E-06
5.0	.287E-06	.272E-06	.258E-06	.245E-06	.233E-06	.221E-06	.210E-06	.199E-06	.189E-06	.179E-06
5.1	.170E-06	.161E-06	.153E-06	.145E-06	.137E-06	.130E-06	.123E-06	.117E-06	.111E-06	.105E-06
5.2	.996E-07	.944E-07	.895E-07	.848E-07	.803E-07	.761E-07	.720E-07	.682E-07	.646E-07	.612E-07
5.3	.579E-07	.548E-07	.519E-07	.491E-07	.465E-07	.440E-07	.416E-07	.394E-07	.372E-07	.352E-07
5.4	.333E-07	.315E-07	.298E-07	.282E-07	.266E-07	.252E-07	.238E-07	.225E-07	.213E-07	.201E-07
5.5	.190E-07	.179E-07	.170E-07	.160E-07	.151E-07	.143E-07	.135E-07	.127E-07	.120E-07	.114E-07
5.6	.107E-07	.101E-07	.955E-08	.901E-08	.850E-08	.802E-08	.757E-08	.714E-08	.673E-08	.635E-08
5.7	.599E-08	.565E-08	.533E-08	.502E-08	.473E-08	.446E-08	.421E-08	.396E-08	.374E-08	.352E-08
5.8	.332E-08	.312E-08	.294E-08	.277E-08	.261E-08	.246E-08	.231E-08	.218E-08	.205E-08	.193E-08
5.9	.182E-08	.171E-08	.161E-08	.151E-08	.143E-08	.134E-08	.126E-08	.119E-08	.112E-08	.105E-08
6.0	.987E-09	.928E-09	.872E-09	.820E-09	.771E-09	.724E-09	.681E-09	.640E-09	.601E-09	.565E-09
6.1	.530E-09	.498E-09	.468E-09	.439E-09	.413E-09	.387E-09	.364E-09	.341E-09	.321E-09	.301E-09
6.2	.282E-09	.265E-09	.249E-09	.233E-09	.219E-09	.205E-09	.192E-09	.181E-09	.169E-09	.159E-09
6.3	.149E-09	.140E-09	.131E-09	.123E-09	.115E-09	.108E-09	.101E-09	.945E-10	.885E-10	.829E-10
6.4	.777E-10	.728E-10	.681E-10	.638E-10	.597E-10	.559E-10	.524E-10	.490E-10	.459E-10	.429E-10
6.5	.402E-10	.376E-10	.352E-10	.329E-10	.308E-10	.288E-10	.269E-10	.252E-10	.235E-10	.220E-10
6.6	.206E-10	.192E-10	.180E-10	.168E-10	.157E-10	.147E-10	.137E-10	.128E-10	.119E-10	.112E-10
6.7	.104E-10	.973E-11	.909E-11	.848E-11	.792E-11	.739E-11	.690E-11	.644E-11	.601E-11	.561E-11
6.8	.523E-11	.488E-11	.455E-11	.425E-11	.396E-11	.369E-11	.344E-11	.321E-11	.299E-11	.279E-11
6.9	.260E-11	.242E-11	.226E-11	.210E-11	.196E-11	.183E-11	.170E-11	.158E-11	.148E-11	.137E-11
7.0	.128E-11	.119E-11	.111E-11	.103E-11	.961E-12	.895E-12	.833E-12	.775E-12	.721E-12	.671E-12
7.1	.624E-12	.580E-12	.540E-12	.502E-12	.467E-12	.434E-12	.403E-12	.375E-12	.349E-12	.324E-12
7.2	.301E-12	.280E-12	.260E-12	.241E-12	.224E-12	.208E-12	.194E-12	.180E-12	.167E-12	.155E-12
7.3	.144E-12	.134E-12	.124E-12	.115E-12	.107E-12	.991E-13	.920E-13	.853E-13	.791E-13	.734E-13
7.4	.681E-13	.631E-13	.586E-13	.543E-13	.503E-13	.467E-13	.433E-13	.401E-13	.372E-13	.344E-13
7.5	.319E-13	.296E-13	.274E-13	.254E-13	.235E-13	.218E-13	.202E-13	.187E-13	.173E-13	.160E-13
7.6	.148E-13	.137E-13	.127E-13	.117E-13	.109E-13	.100E-13	.928E-14	.859E-14	.795E-14	.736E-14
7.7	.680E-14	.629E-14	.581E-14	.537E-14	.497E-14	.459E-14	.423E-14	.391E-14	.362E-14	.334E-14
7.8	.309E-14	.286E-14	.264E-14	.243E-14	.225E-14	.207E-14	.192E-14	.176E-14	.162E-14	.150E-14
7.9	.139E-14	.128E-14	.118E-14	.108E-14	.999E-15	.930E-15	.847E-15	.791E-15	.722E-15	.666E-15
8.0	.611E-15	.569E-15	.527E-15	.486E-15	.444E-15	.402E-15	.375E-15	.347E-15	.319E-15	.291E-15
8.1	.264E-15	.250E-15	.222E-15	.208E-15	.194E-15	.180E-15	.167E-15	.153E-15	.139E-15	.125E-15
8.2	.111E-15	.971E-16	.971E-16	.833E-16	.833E-16	.694E-16	.694E-16	.555E-16	.555E-16	.555E-16

Table A-3. Values of Standard Normal PDF, $\phi(x)$.

	.00	.01	.02	.03	.04	.05	.06	.07	.08	.09
0.0	.399E+00	.399E+00	.399E+00	.399E+00	.399E+00	.398E+00	.398E+00	.398E+00	.398E+00	.397E+00
0.1	.397E+00	.397E+00	.396E+00	.396E+00	.395E+00	.394E+00	.394E+00	.393E+00	.393E+00	.392E+00
0.2	.391E+00	.390E+00	.389E+00	.389E+00	.388E+00	.387E+00	.386E+00	.385E+00	.384E+00	.383E+00
0.3	.381E+00	.380E+00	.379E+00	.378E+00	.377E+00	.375E+00	.374E+00	.373E+00	.371E+00	.370E+00
0.4	.368E+00	.367E+00	.365E+00	.364E+00	.362E+00	.361E+00	.359E+00	.357E+00	.356E+00	.354E+00
0.5	.352E+00	.350E+00	.348E+00	.347E+00	.345E+00	.343E+00	.341E+00	.339E+00	.337E+00	.335E+00
0.6	.333E+00	.331E+00	.329E+00	.327E+00	.325E+00	.323E+00	.321E+00	.319E+00	.317E+00	.314E+00
0.7	.312E+00	.310E+00	.308E+00	.306E+00	.303E+00	.301E+00	.299E+00	.297E+00	.294E+00	.292E+00
0.8	.290E+00	.287E+00	.285E+00	.283E+00	.280E+00	.278E+00	.276E+00	.273E+00	.271E+00	.268E+00
0.9	.266E+00	.264E+00	.261E+00	.259E+00	.256E+00	.254E+00	.252E+00	.249E+00	.247E+00	.244E+00
1.0	.242E+00	.240E+00	.237E+00	.235E+00	.232E+00	.230E+00	.227E+00	.225E+00	.223E+00	.220E+00
1.1	.218E+00	.215E+00	.213E+00	.211E+00	.208E+00	.206E+00	.204E+00	.201E+00	.199E+00	.197E+00
1.2	.194E+00	.192E+00	.190E+00	.187E+00	.185E+00	.183E+00	.180E+00	.178E+00	.176E+00	.174E+00
1.3	.171E+00	.169E+00	.167E+00	.165E+00	.163E+00	.160E+00	.158E+00	.156E+00	.154E+00	.152E+00
1.4	.150E+00	.148E+00	.146E+00	.144E+00	.141E+00	.139E+00	.137E+00	.135E+00	.133E+00	.131E+00
1.5	.130E+00	.128E+00	.126E+00	.124E+00	.122E+00	.120E+00	.118E+00	.116E+00	.115E+00	.113E+00
1.6	.111E+00	.109E+00	.107E+00	.106E+00	.104E+00	.102E+00	.101E+00	.989E-01	.973E-01	.957E-01
1.7	.940E-01	.925E-01	.909E-01	.893E-01	.878E-01	.863E-01	.846E-01	.833E-01	.818E-01	.804E-01
1.8	.790E-01	.775E-01	.761E-01	.748E-01	.734E-01	.721E-01	.707E-01	.694E-01	.681E-01	.669E-01
1.9	.656E-01	.644E-01	.632E-01	.620E-01	.608E-01	.596E-01	.584E-01	.573E-01	.562E-01	.551E-01
2.0	.540E-01	.529E-01	.519E-01	.508E-01	.498E-01	.488E-01	.478E-01	.468E-01	.459E-01	.449E-01
2.1	.440E-01	.431E-01	.422E-01	.413E-01	.404E-01	.396E-01	.387E-01	.379E-01	.371E-01	.363E-01
2.2	.355E-01	.347E-01	.339E-01	.332E-01	.325E-01	.317E-01	.310E-01	.303E-01	.297E-01	.290E-01
2.3	.283E-01	.277E-01	.270E-01	.264E-01	.258E-01	.252E-01	.246E-01	.241E-01	.235E-01	.229E-01
2.4	.224E-01	.219E-01	.213E-01	.208E-01	.203E-01	.198E-01	.194E-01	.189E-01	.184E-01	.180E-01
2.5	.175E-01	.171E-01	.167E-01	.163E-01	.158E-01	.154E-01	.151E-01	.147E-01	.143E-01	.139E-01
2.6	.136E-01	.132E-01	.129E-01	.126E-01	.122E-01	.119E-01	.116E-01	.113E-01	.110E-01	.107E-01
2.7	.104E-01	.101E-01	.987E-02	.961E-02	.935E-02	.909E-02	.885E-02	.861E-02	.837E-02	.814E-02
2.8	.792E-02	.770E-02	.748E-02	.727E-02	.707E-02	.687E-02	.668E-02	.649E-02	.631E-02	.613E-02
2.9	.595E-02	.578E-02	.562E-02	.545E-02	.530E-02	.514E-02	.499E-02	.485E-02	.470E-02	.457E-02
3.0	.443E-02	.430E-02	.417E-02	.405E-02	.393E-02	.381E-02	.370E-02	.358E-02	.348E-02	.337E-02
3.1	.327E-02	.317E-02	.307E-02	.298E-02	.288E-02	.279E-02	.271E-02	.262E-02	.254E-02	.246E-02
3.2	.238E-02	.231E-02	.224E-02	.216E-02	.210E-02	.203E-02	.196E-02	.190E-02	.184E-02	.178E-02
3.3	.172E-02	.167E-02	.161E-02	.156E-02	.151E-02	.146E-02	.141E-02	.136E-02	.132E-02	.127E-02
3.4	.123E-02	.119E-02	.115E-02	.111E-02	.107E-02	.104E-02	.100E-02	.969E-03	.934E-03	.900E-03
3.5	.873E-03	.843E-03	.814E-03	.785E-03	.758E-03	.732E-03	.706E-03	.681E-03	.657E-03	.634E-03
3.6	.612E-03	.590E-03	.569E-03	.549E-03	.529E-03	.510E-03	.492E-03	.474E-03	.457E-03	.441E-03
3.7	.425E-03	.409E-03	.394E-03	.380E-03	.366E-03	.353E-03	.340E-03	.327E-03	.315E-03	.303E-03
3.8	.292E-03	.281E-03	.271E-03	.260E-03	.251E-03	.241E-03	.232E-03	.223E-03	.215E-03	.207E-03
3.9	.199E-03	.191E-03	.184E-03	.177E-03	.170E-03	.163E-03	.157E-03	.151E-03	.145E-03	.139E-03
4.0	.134E-03	.129E-03	.124E-03	.119E-03	.114E-03	.109E-03	.105E-03	.101E-03	.967E-04	.930E-04
4.1	.893E-04	.857E-04	.822E-04	.789E-04	.757E-04	.726E-04	.697E-04	.668E-04	.641E-04	.615E-04
4.2	.589E-04	.565E-04	.542E-04	.519E-04	.498E-04	.477E-04	.457E-04	.438E-04	.420E-04	.402E-04
4.3	.385E-04	.369E-04	.354E-04	.339E-04	.324E-04	.310E-04	.297E-04	.284E-04	.272E-04	.261E-04

Table A-3. Values of Standard Normal PDF, $\phi(x)$ - continued.

4.6	.101E-04	.960E-05	.925E-05	.883E-05	.843E-05	.805E-05	.760E-05	.733E-05	.700E-05	.668E-05
4.7	.637E-05	.608E-05	.580E-05	.553E-05	.527E-05	.503E-05	.480E-05	.457E-05	.436E-05	.416E-05
4.8	.396E-05	.378E-05	.360E-05	.343E-05	.327E-05	.311E-05	.296E-05	.282E-05	.269E-05	.256E-05
4.9	.244E-05	.232E-05	.221E-05	.210E-05	.200E-05	.191E-05	.181E-05	.173E-05	.164E-05	.156E-05
5.0	.149E-05	.141E-05	.134E-05	.128E-05	.122E-05	.116E-05	.110E-05	.105E-05	.993E-06	.944E-06
5.1	.897E-06	.853E-06	.810E-06	.770E-06	.731E-06	.694E-06	.660E-06	.626E-06	.595E-06	.565E-06
5.2	.536E-06	.509E-06	.483E-06	.458E-06	.435E-06	.413E-06	.392E-06	.372E-06	.353E-06	.334E-06
5.3	.317E-06	.301E-06	.285E-06	.270E-06	.256E-06	.243E-06	.230E-06	.218E-06	.207E-06	.196E-06
5.4	.186E-06	.176E-06	.167E-06	.158E-06	.150E-06	.142E-06	.134E-06	.127E-06	.120E-06	.114E-06
5.5	.100E-06	.102E-06	.965E-07	.913E-07	.864E-07	.817E-07	.773E-07	.731E-07	.691E-07	.654E-07
5.6	.410E-07	.505E-07	.553E-07	.522E-07	.494E-07	.467E-07	.441E-07	.417E-07	.394E-07	.372E-07
5.7	.351E-07	.332E-07	.313E-07	.296E-07	.280E-07	.264E-07	.249E-07	.235E-07	.222E-07	.210E-07
5.8	.190E-07	.107E-07	.176E-07	.166E-07	.157E-07	.140E-07	.139E-07	.131E-07	.124E-07	.117E-07
5.9	.110E-07	.104E-07	.979E-08	.922E-08	.869E-08	.819E-08	.772E-08	.727E-08	.685E-08	.645E-08
6.0	.600E-08	.572E-08	.539E-08	.507E-08	.470E-08	.450E-08	.423E-08	.398E-08	.375E-08	.353E-08
6.1	.332E-08	.313E-08	.294E-08	.276E-08	.260E-08	.244E-08	.230E-08	.216E-08	.203E-08	.191E-08
6.2	.179E-08	.169E-08	.158E-08	.149E-08	.140E-08	.131E-08	.123E-08	.116E-08	.109E-08	.102E-08
6.3	.960E-09	.901E-09	.846E-09	.794E-09	.746E-09	.700E-09	.657E-09	.616E-09	.578E-09	.542E-09
6.4	.509E-09	.477E-09	.448E-09	.420E-09	.394E-09	.369E-09	.346E-09	.324E-09	.304E-09	.285E-09
6.5	.267E-09	.250E-09	.234E-09	.220E-09	.206E-09	.193E-09	.180E-09	.169E-09	.158E-09	.148E-09
6.6	.139E-09	.130E-09	.121E-09	.114E-09	.106E-09	.996E-10	.932E-10	.872E-10	.815E-10	.763E-10
6.7	.713E-10	.667E-10	.624E-10	.583E-10	.545E-10	.509E-10	.476E-10	.445E-10	.416E-10	.389E-10
6.8	.363E-10	.339E-10	.317E-10	.296E-10	.276E-10	.258E-10	.241E-10	.225E-10	.210E-10	.196E-10
6.9	.183E-10	.171E-10	.159E-10	.149E-10	.139E-10	.129E-10	.121E-10	.113E-10	.105E-10	.980E-11
7.0	.913E-11	.852E-11	.794E-11	.740E-11	.690E-11	.643E-11	.599E-11	.558E-11	.520E-11	.485E-11
7.1	.451E-11	.420E-11	.392E-11	.365E-11	.339E-11	.316E-11	.294E-11	.274E-11	.255E-11	.237E-11
7.2	.221E-11	.205E-11	.191E-11	.178E-11	.165E-11	.154E-11	.143E-11	.133E-11	.124E-11	.115E-11
7.3	.107E-11	.994E-12	.924E-12	.859E-12	.798E-12	.741E-12	.689E-12	.640E-12	.594E-12	.552E-12
7.4	.513E-12	.476E-12	.442E-12	.411E-12	.381E-12	.354E-12	.328E-12	.305E-12	.283E-12	.262E-12
7.5	.243E-12	.226E-12	.209E-12	.194E-12	.180E-12	.167E-12	.155E-12	.144E-12	.133E-12	.123E-12
7.6	.114E-12	.106E-12	.983E-13	.910E-13	.844E-13	.781E-13	.724E-13	.670E-13	.621E-13	.575E-13
7.7	.532E-13	.493E-13	.456E-13	.422E-13	.391E-13	.362E-13	.335E-13	.310E-13	.287E-13	.265E-13
7.8	.245E-13	.227E-13	.210E-13	.194E-13	.179E-13	.166E-13	.153E-13	.142E-13	.131E-13	.121E-13
7.9	.112E-13	.103E-13	.955E-14	.882E-14	.815E-14	.753E-14	.695E-14	.642E-14	.593E-14	.547E-14
8.0	.505E-14	.466E-14	.430E-14	.397E-14	.367E-14	.338E-14	.312E-14	.288E-14	.266E-14	.245E-14
8.1	.226E-14	.208E-14	.192E-14	.177E-14	.163E-14	.150E-14	.139E-14	.128E-14	.118E-14	.109E-14
8.2	.100E-14	.921E-15	.848E-15	.781E-15	.720E-15	.663E-15	.610E-15	.562E-15	.517E-15	.476E-15
8.3	.438E-15	.403E-15	.371E-15	.341E-15	.314E-15	.289E-15	.266E-15	.244E-15	.225E-15	.207E-15
8.4	.190E-15	.175E-15	.161E-15	.148E-15	.136E-15	.125E-15	.115E-15	.105E-15	.968E-16	.890E-16
8.5	.817E-16	.750E-16	.689E-16	.633E-16	.581E-16	.533E-16	.490E-16	.449E-16	.412E-16	.378E-16
8.6	.347E-16	.319E-16	.292E-16	.268E-16	.246E-16	.226E-16	.207E-16	.190E-16	.174E-16	.160E-16
8.7	.146E-16	.134E-16	.123E-16	.113E-16	.103E-16	.945E-17	.866E-17	.793E-17	.727E-17	.666E-17
8.8	.610E-17	.558E-17	.511E-17	.468E-17	.428E-17	.392E-17	.359E-17	.328E-17	.301E-17	.275E-17
8.9	.252E-17	.230E-17	.211E-17	.193E-17	.176E-17	.161E-17	.147E-17	.135E-17	.123E-17	.113E-17
9.0	.103E-17	.939E-18	.858E-18	.784E-18	.717E-18	.655E-18	.598E-18	.546E-18	.498E-18	.455E-18

Example A-2.

X is a normal random variable with $\bar{x}$ = 1500 psi, σ_x = 200 psi.

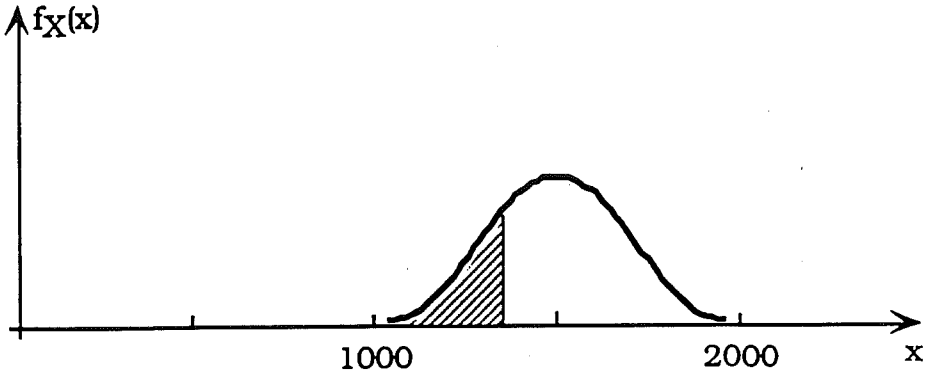

Fig. A-7. PDF of Random Variable in Example A-2.

(a) Calculate F_X (1,300) =

$$F_X(1300) = \Phi\left(\frac{1300 - \bar{x}}{\sigma_x}\right) = \Phi\left(\frac{1300 - 1500}{200}\right) =$$
$$= \Phi\left(\frac{-200}{200}\right) = \Phi(-1) = 0.159$$

(b) Calculate F_X (1,900) = ?

$$F_X(1900) = \Phi\left(\frac{1900 - \bar{x}}{\sigma_x}\right) = \Phi\left(\frac{1900 - 1500}{200}\right) =$$
$$= \Phi\left(\frac{400}{200}\right) = \Phi(2) = 0.977$$

because

$$\Phi(2) = 1 - \Phi(-2) = 1 - 0.0228 = 0.977$$

(c) Calculate F_X (1,700) = ?

$$F_X(1700) = 1 - F_X(1300) = 0.841$$

because

$$F_X(x + \bar{x}) = 1 - F_X(-x + \bar{x}))$$

(d) Calculate $f_X(x)$ for x = 1,300 psi

$$f_X(1300) = \phi\left(\frac{1300 - 1500}{200}\right)\frac{1}{200} = \frac{\phi(1)}{200} =$$
$$= \frac{1}{\sqrt{2\pi}}\frac{1}{200}e^{-\frac{1}{2}} = \frac{0.242}{200} = 0.00121$$

(e) Calculate f_X (1,500) = ?

$$f_X(1500) = \phi\left(\frac{1500 - 1500}{200}\right)\frac{1}{200} = \frac{\phi(0)}{200} =$$
$$= \frac{1}{\sqrt{2\pi}}\frac{1}{200}e^{0} = \frac{0.398}{200} = 0.00199$$

4. Inverse Normal Distribution

Inverse normal distribution function can be calculated using a closed-form formula. The formula gives very accurate results, even though it is an approximation. Most computer procedures use this formula too.

Let $p = \Phi(x)$. Most of practical applications require the calculation of x, for a given value of p,

$$x = \Phi^{-1}(p) \qquad \text{(A-12)}$$

The following formula is available for calculation of x, for $p \leq 0.5$,

$$x = \Phi^{-1}(p) = -t + \frac{c_0 + c_1 t + c_2 t^2}{1 + d_1 t + d_2 t^2 + d_3 t^3} \qquad \text{(A-13)}$$

where: $c_0 = 2.515517$
$c_1 = 0.802853$
$c_2 = 0.010328$
$d_1 = 1.432788$
$d_2 = 0.189269$
$d_3 = 0.001308$
$t = \sqrt{-\ln p^2}$ (A-14)

For $p > 0.5$, Φ^{-1} is calculated for $(1 - p)$, and then for p, as shown

$$\Phi^{-1}(p) = -\Phi^{-1}(1 - p) \quad \text{(A-15)}$$

5. Normal Probability Paper

It is a special scale, so that a normal distribution is represented by a straight line:

- any normal distribution is represented by a straight line.
- any straight line represents a normal distribution.

Construction of normal probability paper

Let X be a random variable. The cumulative distribution function (CDF) of X, is $F_X(x)$, and PDF is $f_X(x)$.

Normal probability paper is obtained by modification of the vertical scale for CDF. Examples of CDF are shown in Fig. A-2 . All CDF's are contained between 0 and 1. Let the horizontal scale be the same as in Fig. A-1. However, the vertical scale is modified so that any normal distribution function is represented by a straight line. There is no 0.0 or 1.0 on the modified vertical scale: 0.0 is at negative infinity and 1.0 is at plus infinity. The mean corresponds to 0.5 on the vertical scale. Actually, 0.5 is the only point in common for the regular and normal probability scale.

The vertical scale can be developed as follows.

(a) Using Standard Normal Distribution

Set a regular horizontal scale for variable X (e.g. bending moment). Identify the mean value and standard deviation of X, $\overline{X}$ and σ_X. Plot a non-vertical straight line passing through x = 0.0 on the horizontal scale, Fig. A-8. Using an existing CDF of the standard normal variable, the normal probability scale can be determined graphically. For a given value of probability p on the regular scale, the new point p (normal probability paper) can be found at the intersection of the dashed line and vertical line passing through x corresponding to p, as shown in Fig. A-8.

The location of various probabilities p on the vertical scale can also be determined using inverse $\Phi(x)$ function. For example, to find where p is, calculate x from the equation

$$p = \Phi_X(x) \tag{A-16}$$

and hence

$$x = \Phi_X^{-1}(p) \tag{A-17}$$

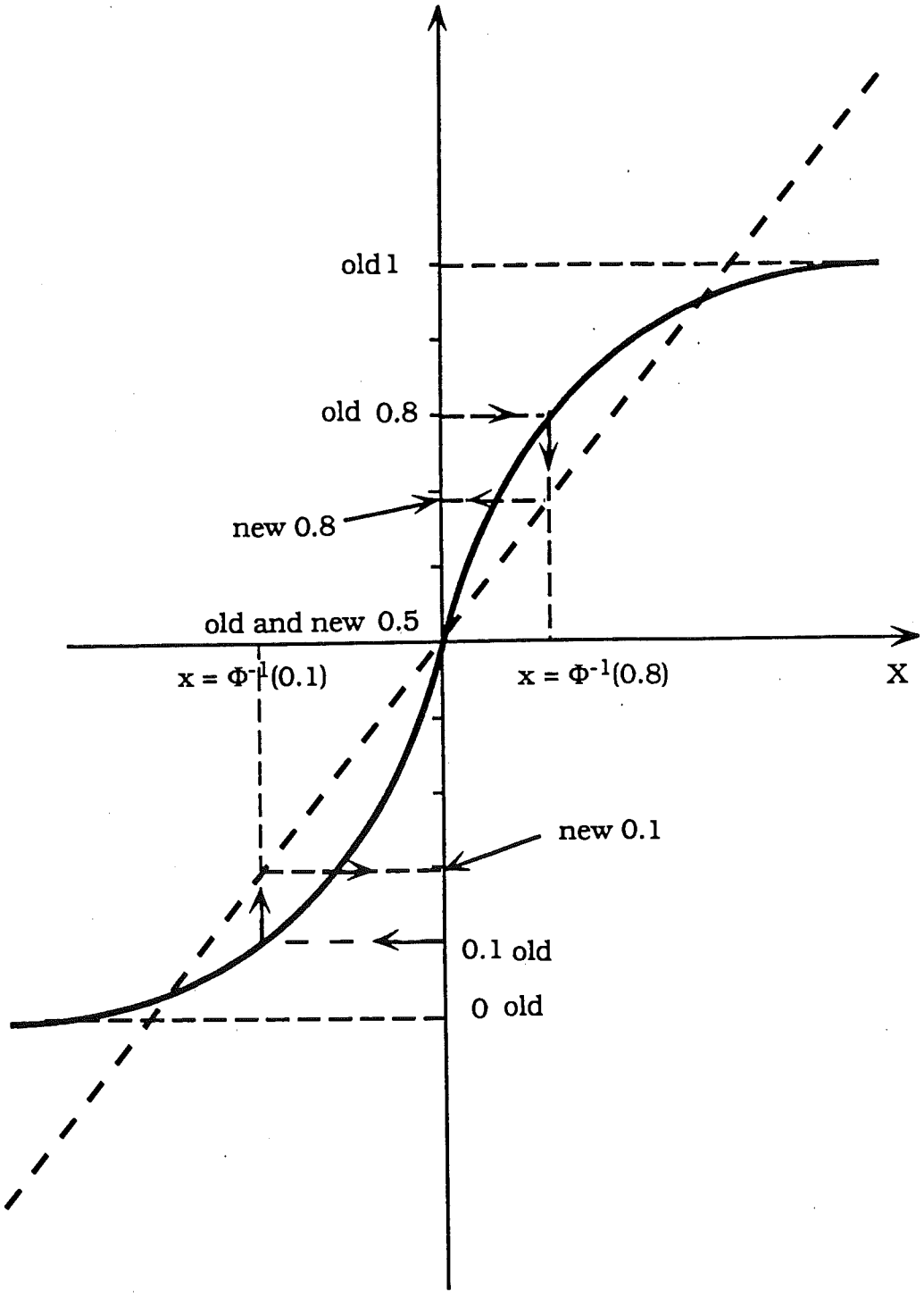

Fig. A-8. Development of Probability Paper using Standard Normal Distribution.

(b) Using Any Normal Distribution

Analytically, the normal probability scale can be developed using any normal distribution function, $F_X(x)$. The horizontal scale corresponds to X. The CDF of X is represented by a straight line passing through the mean value ($x = \bar{x}$). The slope can be chosen depending on the maximum and minimum values of probability to be shown. For a given value of probability p, the corresponding x can be calculated using Eq. 9,

$$x = \bar{x} + \sigma_X \Phi_X^{-1}(p) \qquad \text{(A-18)}$$

Values of $\Phi_X^{-1}(p)$ can be calculated using Table A- 2. Once x is found, the location of p on the vertical scale is determined as shown in Fig. A-9.

An example of the normal probability paper is shown in Fig. A-10. Normal probability paper is also commercially available, however the vertical scale is multiplied by 100 (percentage).

Properties of a Normal Probability Paper

(a) Any normal distribution function (CDF) is represented by a straight line on the normal probability paper. A straight line is determined by the coordinates of two points. For example, let X be a normal random variable, with $\bar{x} = 5.0$ and $\sigma_X = 1.5$. The mean corresponds to 0.5 on the vertical scale. The second point is determined for $x = \bar{x} + \sigma_X = 6.5$, which corresponds to 0.841 on the vertical scale, because

$$\Phi_X [(\bar{x} + \sigma_X - \bar{x}) / \sigma_X] = \Phi_X(1) = 0.841 \qquad \text{(A-19)}$$

The location of these two points is shown on Fig. A-11.

(b) Any straight line on normal probability paper represents a normal distribution function. The mean, $\bar{x}$, is equal to the horizontal coordinate corresponding to 0.5 on the vertical scale, and the standard deviation can be calculated as shown in Fig. A-11.

The vertical scale (normal distribution function) is irregular. In practical applications it is convenient to use a regular vertical scale; the inverse of the standard normal distribution Φ^{-1}. The standard normal distribution is a normal distribution with the mean = 0 and standard deviation = 1. Value of $\Phi^{-1}(0.5) = 0$ and $\Phi^{-1}(0.841) = 1$ (see Table A-1). The inverse normal scale is also shown in Fig. A-11.

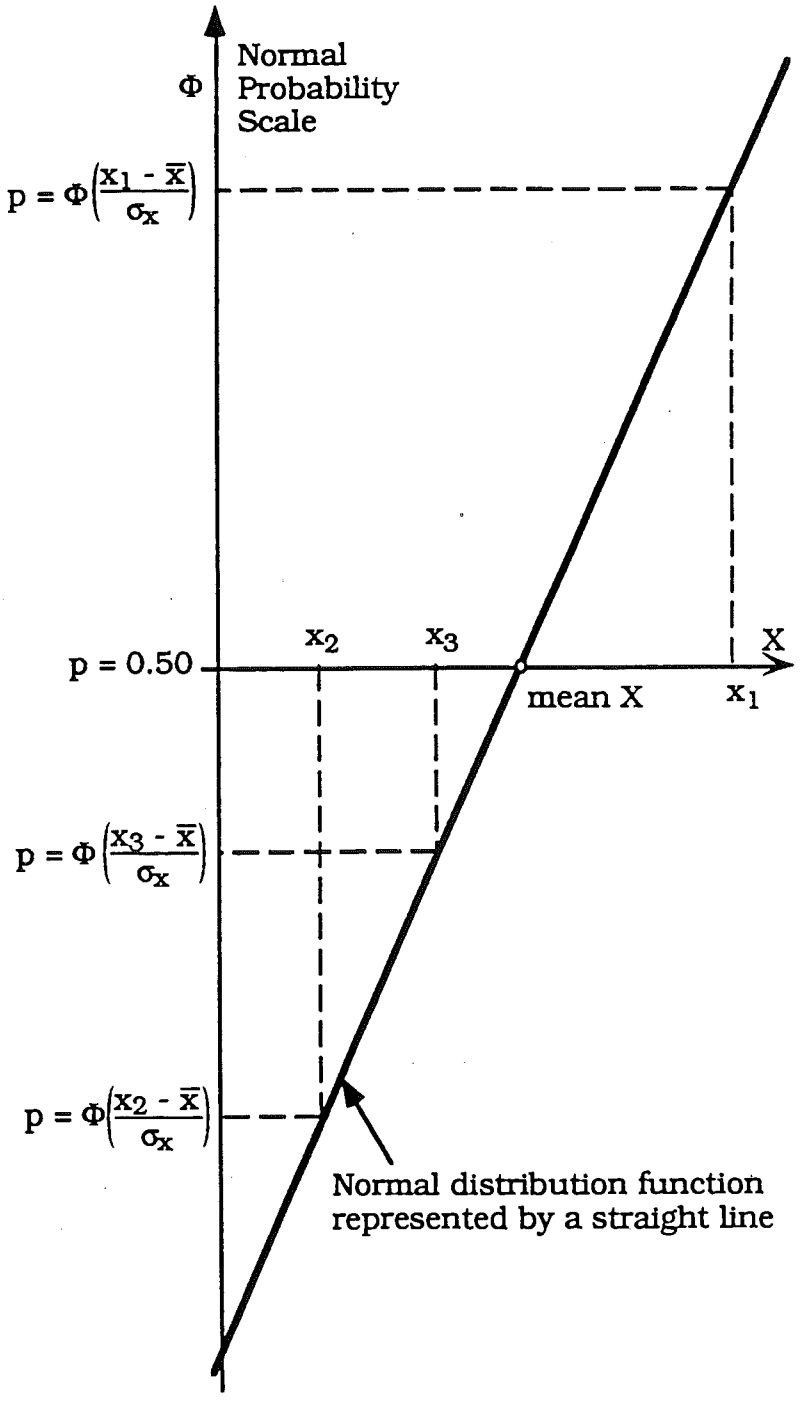

Fig. A-9. Development of Probability Paper using any Normal Distribution.

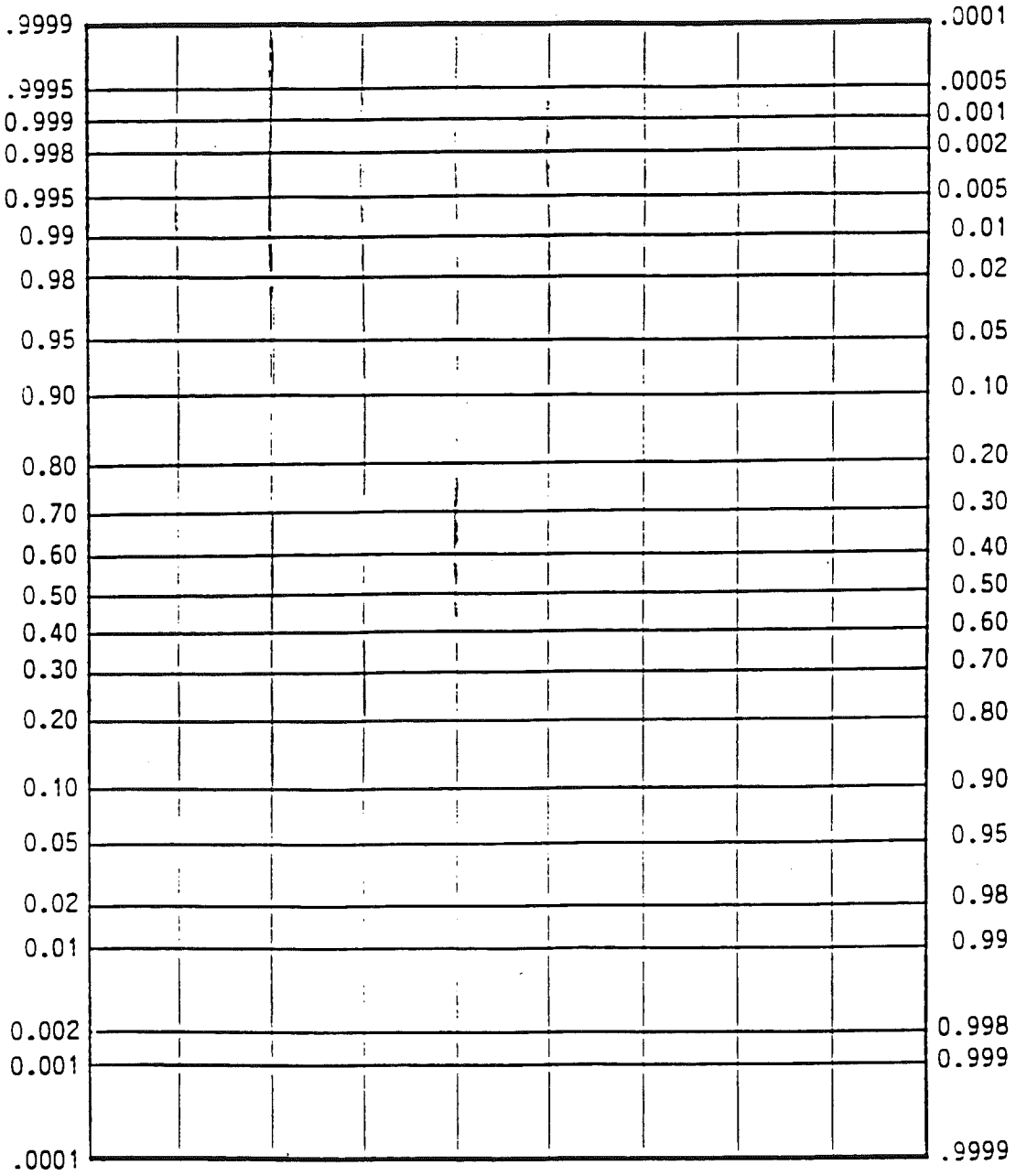

Fig. A-10. Normal Probability Paper.

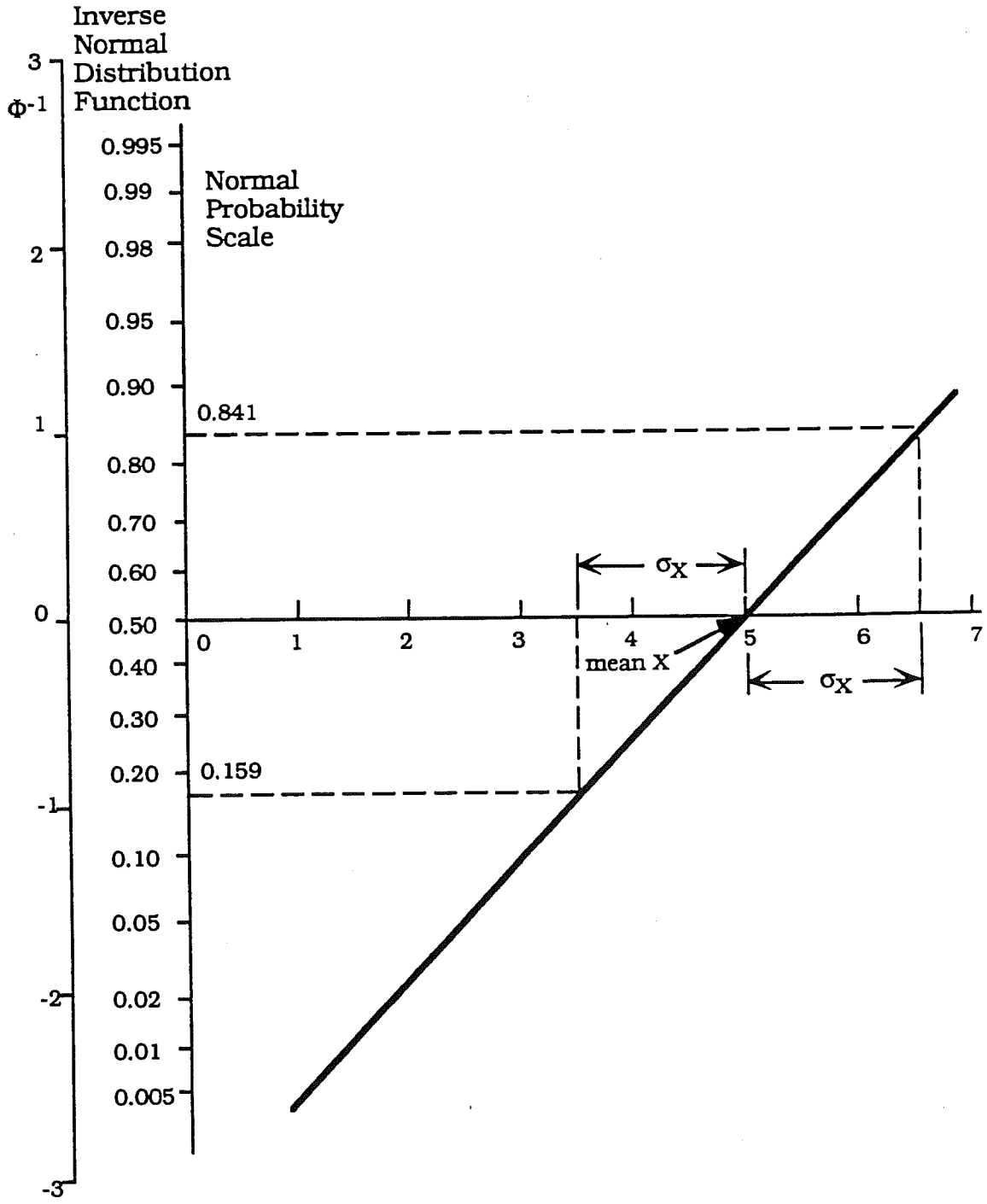

Fig. A-11. Mean and Standard Deviation of a Normal Random Variable on Normal Probability Paper.

Plotting Test Data on Normal Probability Paper

Let the test data be $a_1, a_2, \ldots, a_n$. To plot these test results on the normal probability paper, a_i's are ranked first, from the minimum to the maximum value. Let $b_1, b_2, \ldots, b_n$ represent a rearranged a_i's, so that

$$b_1 \leq b_2 \leq \ldots \leq b_n$$

Then b_1 (on the horizontal scale) is plotted vs. 1/n on the vertical scale, b_2 is plotted vs. 2/n, b_3 vs. 3/n and so on. The maximum value, b_n, cannot be plotted as it corresponds to n/n = 1 on the vertical scale and $\Phi = 1$ is not shown on normal probability paper. Therefore, instead of denominator (n), (n -1) is often used.

Example A-3.

Let the ranked data points be: 5.3, 5.5, 5.9, 5.9, 6.4, 6.5, 6.5, 6.8, 7.2 (9 points). The corresponding distribution is plotted in Fig. A-12. The normality of the resulting distribution can be evaluated by visual inspection of the plot. If the points are located on a straight line, then the distribution is normal.

Table A- 4. Test Data Considered in Example A-3.

Number	1	2	3	4	5	6	7	8	9
Test Result	5.3	5.5	5.9	5.9	6.4	6.5	6.5	6.8	7.2
Probability= = i / (1 + n)	0.1	0.2	0.3	0.4	0.5	0.6	0.7	0.8	0.9

Other Examples of Normal Probability Paper

Examples of actual data plotted on normal probability paper are shown in Fig. A-13 and 14.

An example of a special probability paper is shown in Fig. A-15. The vertical scales extends to 10^{-6}. Only the probabilities less than 0.5 are shown. Values of the inverse normal distribution are given on the left side.

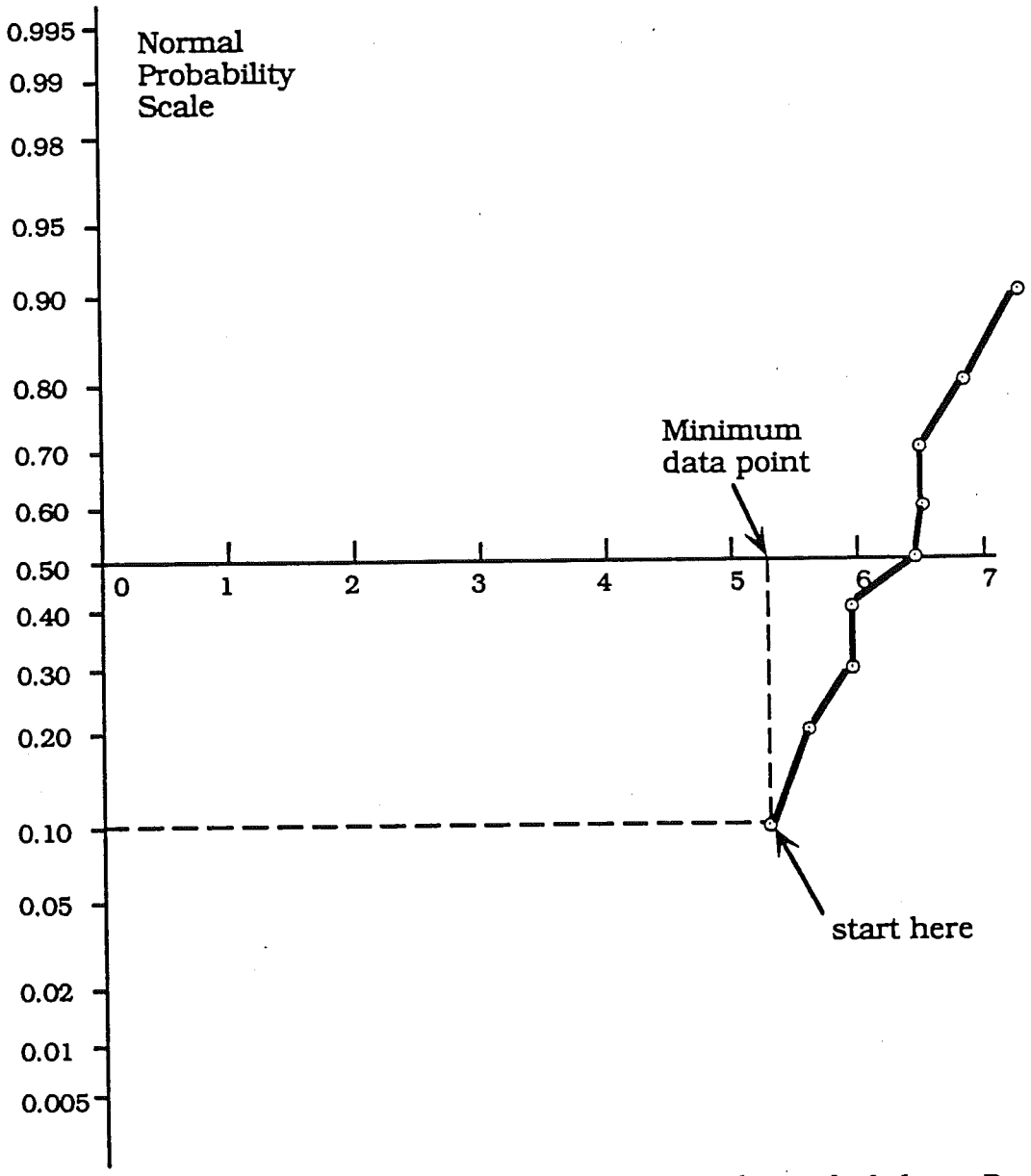

Fig. A-12. Test Data Plotted on Normal Probability Paper.

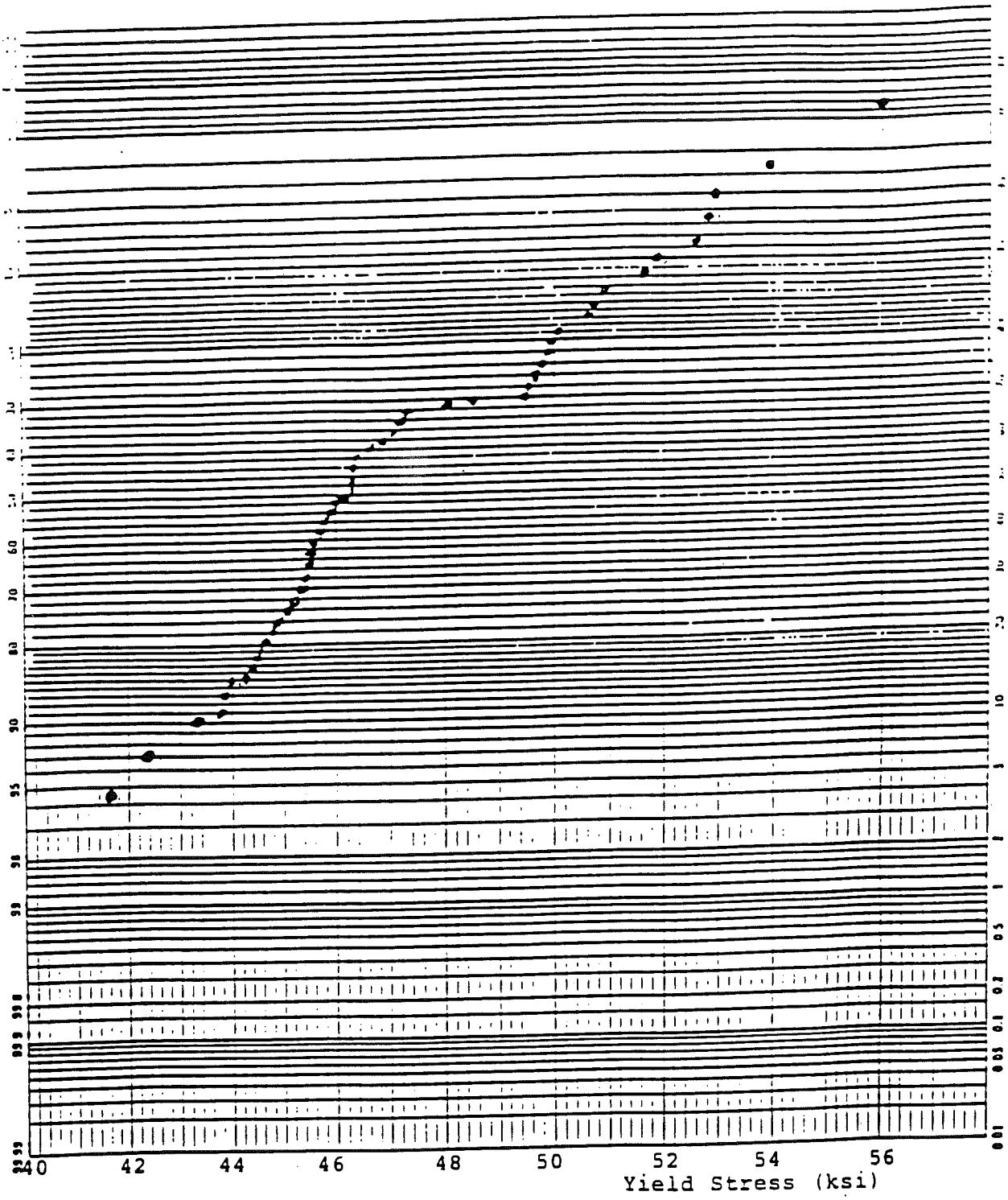

Fig. A-13. Test Results of Yield Stress of Steel on Normal Probability Paper.

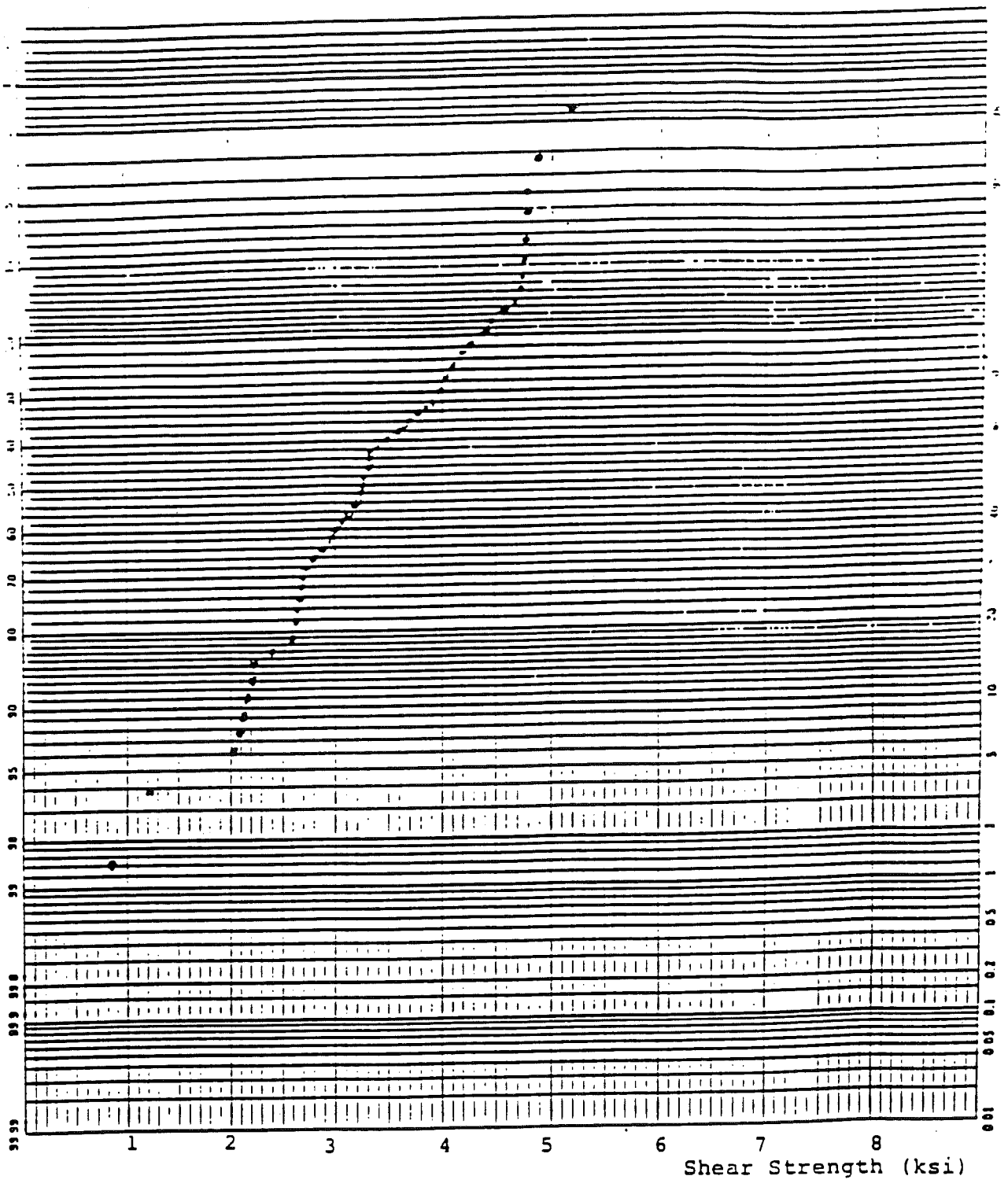

Fig. A-14. Test Results of Shear Strength of Spot Welds on Normal Probability Paper.

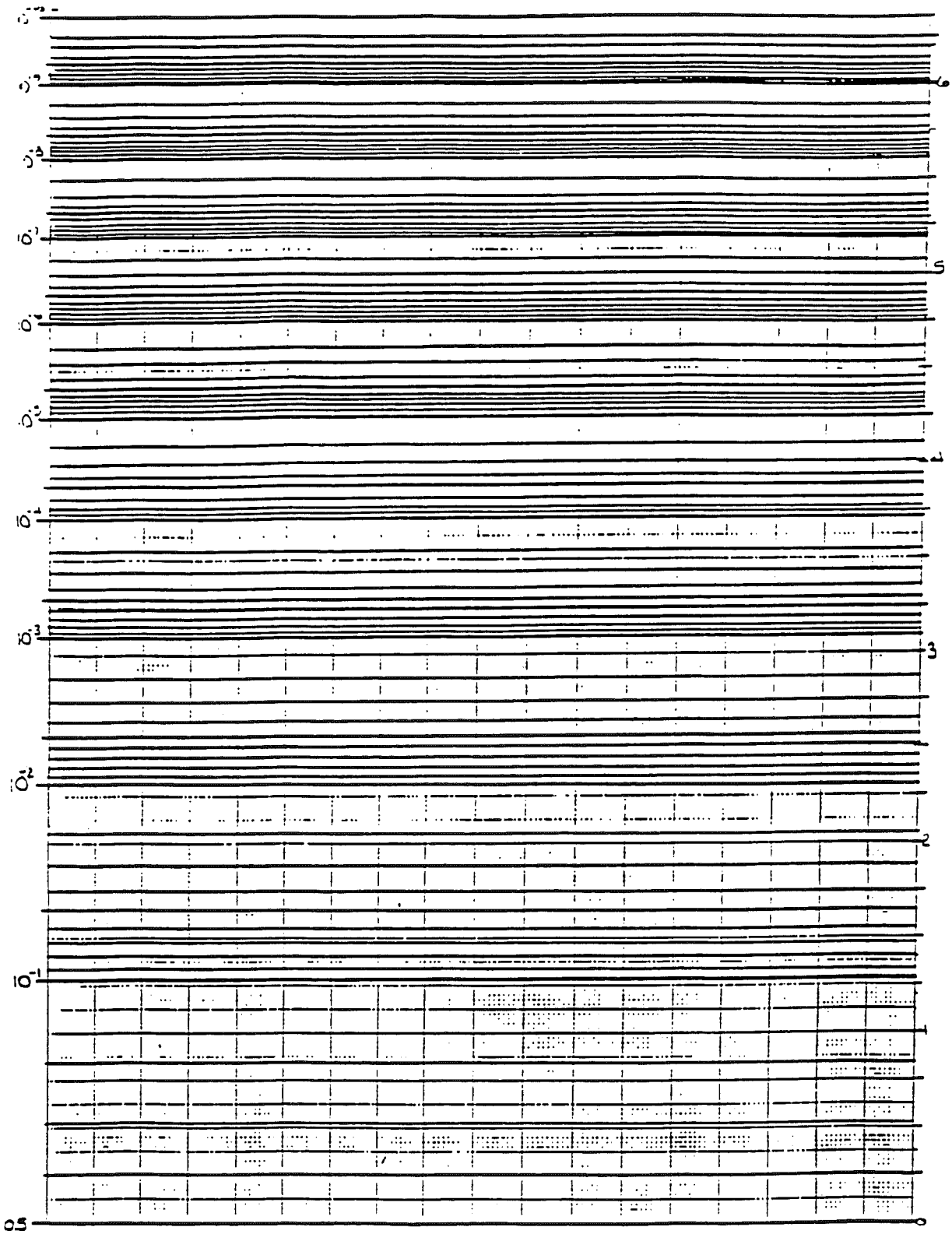

Fig. A-15. Special Normal Probability Paper.

APPENDIX B

FEDERAL HIGHWAY ADMINISTRATION (FHWA)
AXLE CONFIGURATION CLASS

DESCRIPTION	CLASS	SPACINGS (FT)	TOTAL LENGTH (FT)
2-axle vehicles:			
Motorcycle	10	0.0 - 6.7	6.7
Car	20	6.7 - 10.0	10.0
Pick-up/Van	30	10.0 - 13.3	13.3
Bus	40	20.0 - 40.0	40.0
2-axle/6-tire	50	13.3 - 20.0	20.0
3-axle vehicles:			
Car with 1-axle trailer	21	6.7 - 10.0 6.7 - 16.7	26.7
Pick-up/Van with 1-axle trailer	31	10.0 - 13.3 6.7 - 16.7	30.0
Bus	41	20.0 - 40.0 0.0 - 6.7	46.7
3-axle single unit	60	6.7 - 20.0 0.0 - 6.7	26.7
2S1	80	6.7 - 16.7 16.7 - 40.0	53.3

DESCRIPTION	CLASS	SPACINGS (FT)	TOTAL LENGTH (FT)
4-axle vehicles:			
Car with 2-axle trailer	22	6.7 - 10.0 6.7 - 13.3 0.0 - 6.7	30.0
Pick-up/Van with 2-axle trailer	32	10.0 - 13.3 6.7 - 16.7 0.0 - 3.0	33.0
4-axle single unit	70	6.7 - 20.0 0.0 - 6.7 0.0 - 6.7	33.3
3S1	81	6.7 - 20.0 0.0 - 6.7 10.0 - 40.0	66.7
2S2	82	7.6 - 16.7 13.3 - 40.0 0.0 - 6.7	66.7

DESCRIPTION	CLASS	SPACINGS (FT)	TOTAL LENGTH (FT)
5-axle vehicles:			
3S2	90	6.7 - 20.0	
		0.0 - 6.7	
		10.0 - 40.0	
		0.0 - 13.3	66.7
3-axle with trailer	91	6.7 - 20.0	
		0.0 - 6.7	
		6.7 - 26.7	
		10.0 - 26.7	66.7
5-axle with trailer	110	6.7 - 16.7	
		13.3 - 26.7	
		6.7 - 16.7	
		10.0 - 26.7	66.7
6-axle vehicles:			
6-axle single unit	100	6.7 - 16.7	
		0.0 - 6.7	
		10.0 - 40.0	
		0.0 - 10.0	
		0.0 - 10.0	80.0
6-axle multi-trailer	120	6.7 - 16.7	
		0.0 - 6.7	
		13.3 - 26.7	
		6.7 - 13.3	
		10.0 - 26.7	80.0

DESCRIPTION	CLASS	SPACINGS (FT)	TOTAL LENGTH (FT)
7-axle vehicles:			
7-axle (or more) single trailer	101	6.7 - 16.7 0.0 - 6.7 13.3 - 40.0 0.0 - 13.3 0.0 - 13.3 0.0 - 13.3	80.0
7-axle	130	6.7 - 16.7 0.0 - 6.7 10.0 - 26.7 6.7 - 13.3 0.0 - 40.0 0.0 - 6.7	80.0
Any vehicles not meeting any of the criteria above.	140		